



PACIFIC EARTHQUAKE ENGINEERING RESEARCH CENTER

Cover-Plate and Flange-Plate Reinforced Steel Moment-Resisting Connections

Taejin Kim
Andrew S. Whittaker
Amir S. J. Gilani
Vitelmo V. Bertero
Shakhzod M. Takhirov
University of California, Berkeley

Report to sponsor SAC Joint Venture
Sacramento, California

Cover-Plate and Flange-Plate Reinforced Steel Moment-Resisting Connections

**Taejin Kim
Andrew S. Whittaker
Amir S. J. Gilani
Vitelmo V. Bertero
Shakhzod M. Takhirov**

**Report to sponsor SAC Joint Venture
Sacramento, California**

**PEER Report 2000/07
Pacific Earthquake Engineering Research Center
College of Engineering
University of California, Berkeley
September 2000**

ABSTRACT

Five 230-kV disconnect switches were selected for testing and evaluation. Switches of this rating were known to be vulnerable to the effects of earthquake shaking. The class of the switches selected included two horizontal-break and three vertical-break switches. Switches with both porcelain and composite polymer insulators, and switches with both cast aluminum and welded steel base hardware were tested. First, an individual pole (out of three) of each switch was mounted directly on the simulator platform. Static and resonance search tests were conducted to determine the dynamic properties of the posts and to assist in preparing simple analytical models of the posts. Earthquake tests were then conducted to see if the poles were robust. Following these tests, three-pole (phase) switches were mounted on a stiff, low-profile frame, similar to a frame proposed by PG&E for new construction, and tested. Static and resonance search tests were conducted to determine the dynamic properties of the switch posts.

Triaxial earthquake tests were used to qualify the switches on the frame. Two sets of part spectrum-compatible ground motion records were derived from the near-field motions recorded during the 1978 Tabas, Iran, earthquake for the earthquake-simulator studies. Neither of the horizontal-break switches was qualified to the High Level on the stiff frame. The vertical-break switches were qualified to the High Level on a stiff frame provided that welded steel spacers were used at the base of the insulators. The most vulnerable components in the switches were the cast aluminum spacers at the base of the switch posts, the welded post-blade connection, and the bolted connections at the base of the posts.

Single-degree-of-freedom models of the switch insulator posts were developed using experimental data. These models predicted reasonably well the displacement response of the switches mounted on the test frame. These models were then used to evaluate the likely amplification of response of switches when mounted on frames of different heights and stiffnesses. Four frames were selected for study: two in-service (one tall and one short), and two proposed for new construction (one tall and one short). The short braced frame proposed for new construction was stiff and did not amplify the response of the switches significantly. For the other three frames, amplification factors of greater than 2 were recorded. The tall braced frame proposed for new construction produced the largest amplification factors, and consideration should be given to stiffening this frame.

ACKNOWLEDGMENTS

The work described in this report was funded by the SAC Joint Venture through a contract with the Pacific Earthquake Engineering Research (PEER) Center. This financial support is gratefully acknowledged.

Rolled steel sections were supplied at no cost to the University by Nucor Yamato, Inc., of Blytheville, Arkansas. The ten test specimens were fabricated and shipped to the University at no cost by Gayle Manufacturing Company, Woodland, California. Fabrication inspection services and testing services were also provided at no cost to the University by Signet Testing Laboratories, Inc., of Hayward, California. The research described in this report could not have been undertaken without this generous support.

Many individuals made significant technical contributions to this research program. Special thanks are due to Mr. Rick Wilkinson of the Gayle Manufacturing Company, Mr. Michael Engestom of Nucor Yamato, Inc., Mr. Robert Tongson of Signet Testing Services; Messrs. Don Clyde and Wesley Neighbour and Ms. Janine Hannel of PEER; Mr. Jim Malley of Degenkolb Engineers; Mr. Ron Hamburger of EQE International; Professor Stephen Mahin of the University of California, Berkeley; Professor Helmut Krawinkler of Stanford University; Professor Charles Roeder of the University of Washington; and Professor Chia-Ming Uang of the University of California, San Diego.

This work was supported in part by the Pacific Earthquake Engineering Research Center through the Earthquake Engineering Research Centers Program of the National Science Foundation under Award Number EEC-9701568.

CONTENTS

Abstract.....	iii
Acknowledgments	v
Table of Contents.....	vii
List of Tables	xi
List of Figures.....	xiii
1 Reinforced Steel Connections.....	1
1.1 Introduction.....	1
1.2 Objectives of the Berkeley Study.....	2
1.3 Report Organization	2
2 Literature Review	5
2.1 Overview.....	5
2.2 Cover-Plate Connections.....	5
2.3 Flange-Plate Connections.....	9
3 Experimental Program	25
3.1 General	25
3.2 Test Specimen Design and Detailing	26
3.2.1 Specimen design.....	26
3.2.2 Specimen details.....	27
3.2.3 Restraint to lateral-torsional buckling.....	29
3.3 Test Specimen Fabrication and Data.....	29
3.3.1 Supply and fabrication	29
3.3.2 Mechanical properties of materials	29
3.3.3 Welding procedures and inspection	30
3.4 Experimental Program	30
3.4.1 Test fixture	30
3.4.2 Loading protocol	30
3.4.3 Instrumentation	31
3.4.4 Data acquisition.....	37
4 Finite Element Analysis of Reinforced Connections.....	53
4.1 Introduction.....	53
4.2 Material Properties	54
4.3 Finite Element Models of the Connections	55
4.3.1 General	55
4.3.2 Finite element models Type SOL	55
4.3.2.1 Finite element mesh.....	55
4.3.3 Finite element models Type SH.....	57
4.3.3.1 Finite element mesh.....	57

4.3.3.2	Buckled shape of Type SH models.....	57
4.3.4	Boundary conditions and applied loading.....	58
4.4	Damage and Response Indices.....	58
4.5	Unreinforced Connection RC00 (Model Type SOL).....	60
4.5.1	General.....	60
4.5.2	Beam-column shear force transfer.....	61
4.5.3	Response indices.....	61
4.6	Cover-Plate Reinforced Connections (Model Type SOL).....	63
4.6.1	Connection RC01.....	63
4.6.2	Connection RC03.....	64
4.6.3	Connection RC05.....	65
4.7	Flange-Plate Reinforced Connections (Model Type SOL).....	66
4.7.1	Connection RC06.....	66
4.7.2	Connection RC08.....	67
4.7.3	Connection RC09.....	67
4.8	Model Type SOL Results Summary.....	68
4.8.1	Summary results.....	68
4.9	Shell Element Models of Reinforced Connections.....	72
4.9.1	Introduction.....	72
4.9.2	Force versus displacement relations.....	72
4.9.3	Fillet weld geometry.....	72
4.9.4	Flange- and web-local buckling.....	72
4.9.5	Lateral-torsional buckling.....	74
5	Experimental Results.....	109
5.1	Introduction and Summary Data.....	109
5.2	Specimen RC01.....	115
5.2.1	Response summary.....	115
5.2.2	Global response.....	115
5.2.3	Local response.....	116
5.3	Specimen RC02.....	117
5.3.1	Specimen response.....	117
5.3.2	Global response.....	118
5.3.3	Local response.....	118
5.4	Specimen RC03.....	119
5.4.1	Specimen response.....	119
5.4.2	Global response.....	120
5.4.3	Local response.....	120
5.5	Specimen RC04.....	121
5.5.1	Specimen response.....	121
5.5.2	Global response.....	121
5.5.3	Local response.....	122
5.6	Specimen RC05.....	122
5.6.1	Specimen response.....	122
5.6.2	Global response.....	123
5.6.3	Local response.....	124
5.7	Specimen RC06.....	124
5.7.1	Specimen response.....	124
5.7.2	Global response.....	125

5.7.3	Local response.....	126
5.8	Specimen RC07.....	126
5.9	Specimen RC08.....	127
5.9.1	Specimen response	127
5.9.2	Global response.....	127
5.9.3	Local response.....	128
5.10	Specimen RC09.....	128
5.10.1	Specimen response	128
5.10.2	Global response.....	129
5.10.3	Local response.....	129
5.11	Specimen UCB-RC10	130
5.11.1	Specimen response	130
5.11.2	Global response.....	131
5.11.3	Local response.....	131
6	Evaluation of Analytical and Experimental Response Data	179
6.1	Introduction	179
6.2	Plate Type Reinforcement.....	179
6.3	Reinforcement Plate Geometry	181
6.4	Fillet Weld Geometry.....	183
6.5	Restraint of Lateral-Torsional Buckling	187
6.6	Loading History	188
6.7	Web Local Buckling	189
6.8	Reinforcing Plate Strain	190
6.9	Panel Zone Strength	190
6.10	Reinforced Shear Tabs	192
6.11	Load Transfer to Column from Beam in Reinforced Connections	194
6.11.1	Cover-plate connections.....	194
6.11.2	Flange-plate connections.....	196
6.11.3	Summary remarks	197
7	Design Guidelines and Prequalified Reinforced Connections.....	231
7.1	Introduction	231
7.2	Design Guidelines for Cover-Plate Connections	231
7.2.1	Introduction	231
7.2.2	Cover-plate design	232
7.2.3	Cover-plate joining.....	233
7.2.4	Beam web connection	234
7.2.5	Panel zone design.....	234
7.2.6	Column-beam flexural strength ratio	236
7.3	Design Guidelines for Flange-Plate Connections	236
7.3.1	Introduction	236
7.3.2	Flange-plate design	237
7.3.3	Flange-plate joining	237
7.3.4	Beam web connection	237
7.3.5	Panel zone design.....	238
7.3.6	Column-beam flexural strength ratio	238
7.4	Prequalified Cover- and Flange-Plate Connections	238

8	Summary and Conclusions	245
8.1	Summary	245
8.1.1	Introduction	245
8.1.2	Plate-reinforced connections and test specimens	245
8.1.3	Analytical studies	247
8.1.4	Experimental studies	250
8.1.5	Response evaluation	254
8.1.6	Guidelines	257
8.2	Conclusions	257
	References.....	259
	Appendix A Fabrication Details	263
A.1	Mill Certificate Data	264
A.2	Welding Procedure Specifications	265
A.3	Stress-Strain Relations from Coupon Tests	276
A.4	Charpy Test Data.....	288
	Appendix B Summary of Test Data.....	289

LIST OF TABLES

Table 2-1	Cover-plate connection test summary	7
Table 2-2	Flange-plate literature review summary	11
Table 3-1	Summary information on test specimens	26
Table 3-2	Mechanical properties of test specimens, U.S. units	30
Table 3-3	Typical instrumentation for RC01 through RC05	32
Table 3-4	Non-typical instrumentation for RC04	34
Table 3-5	Non-typical instrumentation for RC05	34
Table 3-6	Instrumentation for RC06 through RC10	35
Table 4-1	Material properties used for the analytical models	54
Table 4-2	Elastic distribution of shear force in beam flanges and beam web of RC00	61
Table 4-3	Maxima of indices at 0.5-percent story drift at column flange	68
Table 4-4	Maxima of indices at 0.5-percent story drift at nose of reinforcing plate	69
Table 4-5	Maxima of indices at 1-percent story drift at column flange	70
Table 4-6	Maxima of indices at 1-percent story drift at nose of reinforcing plate	70
Table 4-7	Maxima of indices at 2-percent story drift at column flange	71
Table 4-8	Maxima of indices at 2-percent story drift at nose of reinforcing plate	71
Table 4-9	Buckle amplitudes in RC03	73
Table 5-1	Summary information for RC01 through RC10 (US units)	112
Table 5-2	Summary information for RC01 through RC10 (SI units)	113
Table 5-3	Summary beam plastic rotation information for RC01 through RC10	114
Table 6-1	Shear force transfer from RC00 W30x99 into W14x176 column	193
Table 6-2	RC00 beam web reinforcement effectiveness at 0.5- and 2-percent story drift	194
Table 6-3	Shear force transfer in cover-plate connection at 0.5- and 2-percent story drift	195
Table 6-4	Shear force transfer in flange-plate connection at 0.5- and 2-percent story drift	196
Table 7-1	Prequalified cover-plate connections, U.S. units	239
Table 7-2	Prequalified flange-plate connections, U.S. units	240
Table 7-3	Definition of symbols for prequalified connections	241
Table 8-1	Summary information on test specimens (SI units)	246
Table 8-2	Cover-plate response indices at 2-percent story drift using Type SOL models	248
Table 8-3	Flange-plate response indices at 2-percent story drift using Type SOL models	249
Table 8-4	Summary information for reinforced connections (SI units)	251

Table B-1	Experimental results for specimen RC01	290
Table B-2	Experimental results for specimen RC02	292
Table B-3	Experimental results for specimen RC03	294
Table B-4	Experimental results for specimen RC04	296
Table B-5	Experimental results for specimen RC05	298
Table B-6	Experimental results for specimen RC06	300
Table B-7	Experimental results for specimen RC08	302
Table B-8	Experimental results for specimen RC09	304
Table B-9	Experimental results for specimen RC10	306

LIST OF FIGURES

Figure 1-1	Flat-plate reinforced connections.....	3
Figure 2-1	Details of cover-plate connections tested by Engelhardt and Sabol (1995).....	12
Figure 2-2	Construction details for cover-plate connection of Blackman and Popov (1995)	13
Figure 2-3	Construction details for cover-plate connection of Popov et al. (1996)	13
Figure 2-4	Cover-plate details for specimen AN1 (Whittaker et al. 1996)	14
Figure 2-5	Hysteretic response of cover-plate specimen AN1 (Whittaker et al. 1996).....	15
Figure 2-6	Longitudinal fillet weld tear in cover-plate specimen AN1 (Whittaker et al. 1996)	16
Figure 2-7	Net section fracture of bottom flange of specimen AN1 (Whittaker et al. 1996).....	16
Figure 2-8	Test fixture for the RiverPark II cover-plate specimen.....	17
Figure 2-9	RiverPark II cover-plate details	17
Figure 2-10	Hysteresis for RiverPark II specimen	18
Figure 2-11	Fracture of RiverPark II specimen	19
Figure 2-12	Test fixture for FUSD flange-plate specimens (Whittaker and Gilani 1996)	20
Figure 2-13	Hysteretic response of flange-plate specimen FUSD-1 (Whittaker and Gilani 1996)...	20
Figure 2-14	Hysteretic response of flange-plate specimen FUSD-3 (Whittaker and Gilani 1996)...	21
Figure 2-15	Fractured column flange in specimen FUSD-3 (Whittaker and Gilani 1996)	22
Figure 2-16	Construction details of flange-plate connection tested by Lee et al. (1997).....	23
Figure 2-17	Double-sided flange-plate test specimen (Noel and Uang 1996).....	24
Figure 3-1	SAC Phase II test fixture.....	38
Figure 3-2	Photograph of SAC Phase II test fixture	38
Figure 3-3	Typical SAC Phase II cover-plate connection details.....	39
Figure 3-4	Typical SAC Phase II flange-plate connection details.....	39
Figure 3-5	Construction details for RC01 and RC02	40
Figure 3-6	Construction details for RC03.....	40
Figure 3-7	Construction details for RC04.....	41
Figure 3-8	Construction details for RC05.....	41
Figure 3-9	Construction details for RC06 and RC07	42
Figure 3-10	Construction details for RC08 and RC09	42
Figure 3-11	Construction details for RC10.....	43
Figure 3-12	Restraint to lateral-torsional buckling of RC02 at 35 in. from the face of column.....	43
Figure 3-13	Loading histories for SAC Phase II specimens.....	44

Figure 3-14 Instrumentation for specimens RC01, RC02, and RC03	45
Figure 3-15 Instrumentation for specimen RC04	46
Figure 3-16 Instrumentation for specimen RC05	47
Figure 3-17 Instrumentation of panel zone for Specimen RC02	48
Figure 3-18 Instrumentation of top cover plate and beam flange for specimen RC02.....	48
Figure 3-19 Instrumentation for specimens RC06, RC07, RC08, and RC09	49
Figure 3-20 Instrumentation for specimen RC10	50
Figure 3-21 Instrumentation of specimen RC06.....	51
Figure 3-22 Instrumentation of specimen RC10.....	51
Figure 4-1 Assumed trilinear stress-strain relationship for ABAQUS models.....	75
Figure 4-2 ABAQUS Type SOL models and symmetry conditions	76
Figure 4-3 Element meshing for beam and column of Type SOL models	77
Figure 4-4 Solid element meshing for reinforcing plates of Type SOL models.....	78
Figure 4-5 ABAQUS Type SH models	78
Figure 4-6 Buckled shapes of RC03 for first eigenvector	79
Figure 4-7 Deformed shape of the RC03 beam cross section at flange buckle	79
Figure 4-8 Distribution of shear stress in beam of RC00	80
Figure 4-9 Distribution of normal stress S22 in RC00 at story drifts of 0.5, 1, and 2 percent	80
Figure 4-10 Stress distributions in RC00 beam at story drifts of 0.5, 1, and 2 percent.....	81
Figure 4-11 Fracture indices in RC00 beam at story drifts of 0.5, 1, and 2 percent.....	82
Figure 4-12 Contour plots of Rupture Index at 2-percent story drift.....	83
Figure 4-13 Stress and fracture indices in RC00 beam flange at toe of weld access hole.....	84
Figure 4-14 Stress and strain distribution on RC00 beam web centerline at 2-percent story drift ...	85
Figure 4-15 Stress and fracture indices in RC01 cover plate at face of column.....	86
Figure 4-16 Stress and fracture indices in RC01 beam flange at face of column.....	87
Figure 4-17 Stress and fracture indices in RC01 beam flange at nose of cover plate	88
Figure 4-18 Stress and fracture indices in RC03 cover plate at face of column.....	89
Figure 4-19 Stress and fracture indices in RC03 beam flange at face of column.....	90
Figure 4-20 Stress and fracture indices in RC03 beam flange at edge of transverse fillet weld	91
Figure 4-21 Stress and fracture indices in RC05 cover plate at face of column.....	92
Figure 4-22 Stress and fracture indices in RC05 beam flange at face of column.....	93
Figure 4-23 Stress and fracture indices in RC05 beam flange at edge of transverse fillet weld	94
Figure 4-24 Stress and fracture indices in RC06 flange plate at face of column.....	95

Figure 4-25	Stress and fracture indices in RC06 beam flange at edge of transverse fillet weld	96
Figure 4-26	Stress and fracture indices in RC08 flange plate at face of column.....	97
Figure 4-27	Stress and fracture indices in RC08 beam flange at edge of transverse fillet weld	98
Figure 4-28	Stress and fracture indices in RC09 flange plate at face of column.....	99
Figure 4-29	Stress and fracture indices in RC09 beam flange at edge of transverse fillet weld	100
Figure 4-30	Shell element meshes in vicinity of bottom reinforcement plate.....	101
Figure 4-31	Force-displacement relations for RC01, RC03, and RC06	102
Figure 4-32	Deformed shapes of RC01 and RC03 at 5-percent story drift	102
Figure 4-33	Force-displacement relation for specimen RC03.....	103
Figure 4-34	Deformed shape of RC03 beam cross section as a function of displacement for points on force-displacement relation of Figure 4-33	104
Figure 4-35	Isometric view of deformed shape of RC03 beam section at 5-percent story drift.....	105
Figure 4-36	Flange- and web-local buckling in specimen RC03 (sheet 1 of 2)	106
Figure 4-37	Flange- and web-local buckling in specimen RC03 (sheet 2 of 2)	107
Figure 4-38	Effect of lateral-torsional buckling on force-displacement relations	108
Figure 5-1	Calculation of maximum beam plastic rotations.....	132
Figure 5-2	Rectangular cover plate of RC01	133
Figure 5-3	Beam FLB and WLB in RC01 at a drift angle of 0.04h	133
Figure 5-4	Tearing of the beam top flange in RC01	134
Figure 5-5	Actuator force versus drift angle for RC01.....	134
Figure 5-6	Moment at the column face versus panel zone plastic rotation for RC01	135
Figure 5-7	Moment at the column face versus beam plastic rotation for RC01	135
Figure 5-8	Components of drift angle for RC01.....	136
Figure 5-9	Beam and cover-plate strains for RC01	136
Figure 5-10	Cover-plate and continuity-plate strains for RC01	137
Figure 5-11	Column-web and the doubler-plate shear strains for RC01	137
Figure 5-12	Strain response along line b for RC01	138
Figure 5-13	Beam FLB and WLB in RC02 at a drift angle of 0.03h	138
Figure 5-14	Fractured lateral brace web tabs in RC02	139
Figure 5-15	Actuator force versus drift angle for RC02.....	139
Figure 5-16	Moment at the column face versus panel zone plastic rotation for RC02	140
Figure 5-17	Moment at the column face versus beam plastic rotation for RC02	140
Figure 5-18	Components of drift angle for RC02.....	141

Figure 5-19	Column-web and the doubler-plate shear strains for RC02	141
Figure 5-20	Normalized force history in lateral braces for RC02	142
Figure 5-21	Beam FLB and WLB in RC03 at a drift angle of 0.03h	142
Figure 5-22	Flange local buckling at nose of cover plate in RC03	143
Figure 5-23	Tearing of k-line and beam bottom flange in RC03	143
Figure 5-24	Actuator force versus drift angle for RC03.....	144
Figure 5-25	Moment at the column face versus panel zone plastic rotation for RC03	144
Figure 5-26	Moment at the column face versus beam plastic rotation for RC03	145
Figure 5-27	Components of drift angle for RC03.....	145
Figure 5-28	Column-web and the doubler-plate strains for RC03	146
Figure 5-29	Swallowtail flange plate for RC04.....	146
Figure 5-30	Beam FLB and WLB in RC04 at a drift angle of 0.03h	147
Figure 5-31	Beam top flange and flange plate in RC04 at a drift angle of 0.02h.....	147
Figure 5-32	Fracture in bottom flange of beam in RC04	148
Figure 5-33	Actuator force versus drift angle for RC04.....	148
Figure 5-34	Moment at the column face versus panel zone plastic rotation for RC04	149
Figure 5-35	Moment at the column face versus beam plastic rotation for RC04	149
Figure 5-36	Components of drift angle for RC04.....	150
Figure 5-37	Beam and flange plate strains for RC04	150
Figure 5-38	Flange plate and continuity plate strains for RC04.....	151
Figure 5-39	Trapezoidal cover plate of RC05	151
Figure 5-40	Beam FLB and WLB in RC05 at a drift angle of 0.05h	152
Figure 5-41	Tear in bottom flange of beam in RC05	152
Figure 5-42	Actuator force versus drift angle for RC05.....	153
Figure 5-43	Moment at the column face versus panel zone plastic rotation for RC05	153
Figure 5-44	Moment at the column face versus beam plastic rotation for RC05	154
Figure 5-45	Components of drift angle for RC05.....	154
Figure 5-46	Beam and cover-plate strains for RC05	155
Figure 5-47	Cover-plate and continuity-plate strains for RC05	155
Figure 5-48	Strain response along line b for RC05	156
Figure 5-49	Rectangular flange plate of RC06.....	156
Figure 5-50	Beam FLB and WLB in RC06 at a drift angle of 0.04h	157
Figure 5-51	Ductile tears in the beam top flange of RC06	157

Figure 5-52	Fracture in the beam top flange k-line of RC06.....	158
Figure 5-53	Actuator force versus drift angle for RC06.....	158
Figure 5-54	Moment at the column face versus panel zone plastic rotation for RC06	159
Figure 5-55	Moment at the column face versus beam plastic rotation for RC06.....	159
Figure 5-56	Components of drift angle for RC06.....	160
Figure 5-57	Beam and flange-plate strains for RC06.....	160
Figure 5-58	Strain response along line b for RC06	161
Figure 5-59	Near-field displacement history for RC07	161
Figure 5-60	Beam FLB and WLB in RC07 at a drift angle of 0.04h	162
Figure 5-61	Tearing of beam top flange in RC07.....	162
Figure 5-62	Actuator force versus drift angle for RC07.....	163
Figure 5-63	Moment at the column face versus panel zone plastic rotation for RC07	163
Figure 5-64	Moment at the column face versus beam plastic rotation for RC07	164
Figure 5-65	Beam FLB and WLB in RC08 at a drift angle of 0.05h	164
Figure 5-66	Fracture in the beam top flange of RC08.....	165
Figure 5-67	Yielding of flange plate in RC08 at a drift angle of 0.04h.....	165
Figure 5-68	Actuator force versus drift angle for RC08.....	166
Figure 5-69	Moment at the column face versus panel zone plastic rotation for RC08	166
Figure 5-70	Moment at the column face versus beam plastic rotation for RC08	167
Figure 5-71	Components of drift angle for RC08.....	167
Figure 5-72	Beam and flange-plate strains for RC08	168
Figure 5-73	Strain response along line b for RC08	168
Figure 5-74	Yielding of the panel zone in RC09 at a drift angle of 0.015h	169
Figure 5-75	Beam FLB and WLB in RC09 at a drift angle of 0.05h	169
Figure 5-76	Fracture of beam bottom flange in RC09.....	170
Figure 5-77	Yielding of top flange plate in RC09 at a drift angle of 0.03h	170
Figure 5-78	Actuator force versus drift angle for RC09.....	171
Figure 5-79	Moment at the column face versus panel zone plastic rotation for RC09	171
Figure 5-80	Moment at the column face versus beam plastic rotation for RC09	172
Figure 5-81	Components of drift angle for RC09.....	172
Figure 5-82	Beam and flange-plate strains in RC09.....	173
Figure 5-83	Column-web strains in panel zone of RC09	173
Figure 5-84	Strain response along line b in RC09.....	174

Figure 5-85	Horizontal stiffeners on RC10 to delay web local buckling	174
Figure 5-86	Beam flange local buckling in RC10 at a drift angle of 0.03h.....	175
Figure 5-87	Fracture of top flange of RC10 outside horizontal stiffeners.....	175
Figure 5-88	Actuator force versus drift angle for RC10.....	176
Figure 5-89	Moment at the column face versus panel zone plastic rotation for RC10	176
Figure 5-90	Moment at the column face versus beam plastic rotation for RC10.....	177
Figure 5-91	Components of drift angle for RC10.....	177
Figure 5-92	Beam and cover-plate strains for RC10	178
Figure 6-1	Reinforcement-plate groove weld geometries	198
Figure 6-2	Comparison of response of cover-plated (RC03) and flange-plated (RC06) specimens.....	198
Figure 6-3	Deformed shape of cover plate and beam flange near face of column	199
Figure 6-4	Mises and hydrostatic pressure distributions at column face in RC03 at 1-percent story drift	200
Figure 6-5	Mises and hydrostatic pressure distributions at column face in RC06 at 1-percent story drift	201
Figure 6-6	Equivalent plastic strain distribution at column face in RC03 and RC06 at 2-percent story drift	202
Figure 6-7	Moment at column face versus beam plastic rotation for RC03 and RC05.....	203
Figure 6-8	Strain response of cover plates in RC03 and RC05 as a function of story drift	203
Figure 6-9	Mises stress distribution at column face in RC05 at 1-percent story drift.....	204
Figure 6-10	Stress S22 distribution along the cover plates of RC03 and RC05 at 1-percent story drift	205
Figure 6-11	Stress S22 distribution along the beam flanges of RC03 and RC05 at 1-percent story drift	206
Figure 6-12	Mises stress distribution along the beam flanges of RC03 and RC05 at 1-percent story drift	207
Figure 6-13	Equivalent plastic strain distributions on the beam flanges of RC03 and RC06 at 2-percent story drift	208
Figure 6-14	Photograph of SAC Phase I cover-plate specimen AN1 (Whittaker et al. 1996)	209
Figure 6-15	Measured longitudinal (2-2) strains in cover-plate specimens RC01 and RC03 at 13 in. (330 mm) from the column face	209
Figure 6-16	Deformations in cover plates and flanges of RC01 and RC03 at 4-percent story drift	210
Figure 6-17	Mises stress distribution along the beam flanges of RC01 and RC03 at 1-percent story drift	211

Figure 6-18	Hydrostatic pressure distribution along the beam flanges of RC01 and RC03 at 1-percent story drift	212
Figure 6-19	Equivalent plastic strain distribution along the beam flanges of RC01 and RC03 at 2-percent story drift	213
Figure 6-20	Stress S22 distribution along the cover plates of RC01 and RC03 at 1-percent story drift	214
Figure 6-21	Stress S22 and Mises distributions along the beam flange of RC05 at 1-percent story drift	215
Figure 6-22	Hydrostatic pressure distribution along the upper surface of the beam flange of RC05 at 1-percent story drift.....	216
Figure 6-23	Normal stress distributions along the upper surface of the beam flanges for RC01, RC03, and RC05, at 2-percent story drift.....	217
Figure 6-24	Response distributions along the upper surface of the beam flanges for RC01, RC03, and RC05, at 2-percent story drift.....	218
Figure 6-25	Distributions on Pressure Index, Triaxiality Ratio, and Rupture Index along the upper surface of the beam flanges for RC01, RC03, and RC05, at 2-percent story drift	219
Figure 6-26	Backbone curves for RC01 and RC02 and forces in Braces B1 and B2 of RC02.....	220
Figure 6-27	Backbone curves for RC06 and RC07	220
Figure 6-28	Normalized moment versus beam plastic rotation for RC03 and RC10.....	221
Figure 6-29	Comparison of global responses of RC06 and RC08	221
Figure 6-30	Measured strains in the flange plates of RC06 and RC08 at different story drift levels	222
Figure 6-31	Moment versus story drift index relationships for RC06 and RC09.....	223
Figure 6-32	Moment versus panel zone plastic rotation relationships for RC06 and RC09	224
Figure 6-33	Stress (S23) distribution in panel zone of RC09 at 1-percent story drift.....	225
Figure 6-34	Mises stress distribution in panel zone of RC09 at 1-percent story drift	225
Figure 6-35	Mises stress distribution on upper surface of flange plates of RC09 and RC06 at 1-percent story drift	226
Figure 6-36	Deformations in RC09 at 2-percent story drift	227
Figure 6-37	Equivalent plastic strain distribution in RC09 panel zone and beam web at 2-percent story drift	227
Figure 6-38	Equivalent plastic strain distributions in flange plate and beam flange of RC09 at 2-percent story drift	228
Figure 6-39	Equivalent plastic strain distributions in flange plate and beam flange of RC06 at 2-percent story drift	229
Figure 6-40	RC00 beam web reinforcement study	230

Figure 6-41	Normalized load transfer into cover plate of Configuration 3	230
Figure 7-1	Reinforced steel moment connections	242
Figure 7-2	Typical details for cover-plate connection	243
Figure 7-3	Preferred access hole and CJP groove weld details for cover-plate connections	243
Figure 7-4	Typical details for flange-plate connection	244
Figure 7-5	Preferred access hole and CJP groove weld details for flange-plate connections	244

1 Reinforced Steel Connections

1.1 Introduction

The January 1994, Northridge earthquake caused widespread damage to steel moment-frame buildings sited in the epicentral region. Much of the damage was concentrated in the beam-column moment-resisting connections at the face of the column. In mid-1994, a joint venture of the Structural Engineers Association of California (SEAOC), the Applied Technology Council (ATC), and the California Universities for Research in Earthquake Engineering (CUREe) was formed with the specific goal of investigating the damage to welded steel moment-frame buildings and developing repair techniques and new design approaches to minimize damage to steel moment-frame buildings in future earthquakes. The joint venture is known by the acronym SAC. SAC initially embarked on a Phase I, 24-month problem-focused study to develop interim solutions for the identification, evaluation, repair, and modification of damaged welded steel moment-frame buildings. Some effort was also devoted to new approaches to design and construction of steel moment-resisting frames. The SAC Phase I project was funded by the Federal Emergency Management Agency (FEMA) and the California Office of Emergency Services (OES). The results of the SAC Phase I project were published as FEMA 267, *Interim Guidelines: Evaluation, Repair, Modification, and Design of Welded Steel Moment Frame Structures* (FEMA 1995a) in August 1995 and in numerous other technical reports. Key experimental data from the SAC Phase I project were published in SAC (1996).

Following the completion of the SAC Phase I project, FEMA funded the SAC Phase II project that focused on new steel moment-frame construction. Six topical areas were identified for study: Materials and Fracture, Joining and Inspection, Connection Performance (Analytical Studies and Large-Scale Testing), System Performance, and Performance of Steel Buildings in Past Earthquakes. The Connection Performance topical area involved a total of ten large-scale beam-column connection testing programs. Such tests studied reduced beam sections, welded cover plates and flange plates, alternate weld details, bolted connections, retrofit strategies, strain-rate effects, and load-history effects, among others. The research program described in this report was funded in the Connection Performance topical area and focused on the response of steel moment-resisting connections reinforced with flat steel plates that served to relocate the plastic hinge away from the face of the column. The investigation described in the following chapters built on previous work undertaken by the authors on steel moment-resisting connections reinforced with flat steel plates (Whittaker, Gilani, and Bertero 1996; Whittaker and Gilani 1996).

Two plate-reinforced connections are described in this report, namely, the cover-plate and flange-plate connections. Sketches of both details are provided in Figure 1-1. The major difference between the connection details is the joining of the beam flange to the column flange. For the cover-plate connection, the cover plate and the beam flange are welded to the column flange, whereas only the flange plate is welded to the column flange in the flange-plate connection.

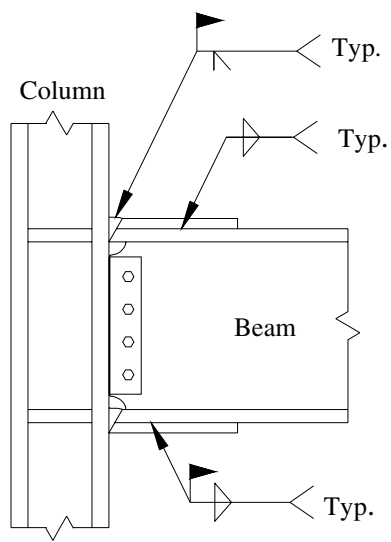
1.2 Objectives of the Berkeley Study

The goal of the studies described in this report was to understand the seismic response of modest and large-scale steel moment-resisting connections reinforced with flat steel plates. The key objectives of the research program were five-fold, namely,

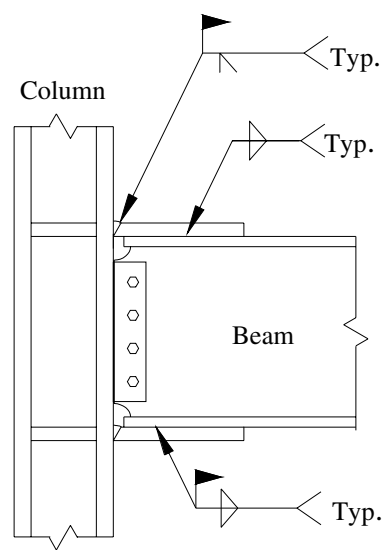
1. Identify the key design variables for reinforced steel moment-resisting connections and develop an experimental program to study such variables.
2. Design, detail, and construct ten full-size, single-sided specimens using the procedures of FEMA 267A (FEMA 1995b) for the purpose of static cyclic testing.
3. Prepare nonlinear finite element analysis models of each of the specimens to study the effect of weld and plate geometry on important elastic stress, plastic strain, and fracture-mechanics parameters prior to the construction of the specimens.
4. Test each single-sided specimen and report data in accordance with the procedures set forth by the SAC Joint Venture.
5. Interpret the analytical and experimental data for the purposes of (a) developing prequalified plate-reinforced steel moment-resisting connections and (b) writing guidelines for the design, detailing, and construction of plate-reinforced steel moment-resisting connections.

1.3 Report Organization

This report is divided into eight chapters, a list of references, and two appendices. Chapter 2 provides summary information on previous studies of steel moment-resisting connections reinforced with flat plates. Chapter 3 describes the design of the ten test specimens, the test fixture, material data collected following the test program, and a list of the transducers used to monitor the response of the test specimens. Chapter 4 presents the results of the nonlinear finite element analysis of each of the test specimens and identifies key findings. Chapter 5 summarizes the results of the experimental program. An evaluation of the analytical and experimental data is presented in Chapter 6. Chapter 7 provides design guidelines for reinforced connections and information on prequalified connections. A summary and conclusions are presented in Chapter 8. References are listed following Chapter 8. Mill-certificate data, coupon-test data, and fabrication reports are presented in Appendix A. Experimental data for each primary loading cycles for each test specimen are tabulated in Appendix B; such data reporting was a requirement of the SAC Joint Venture.



a. cover-plate connection



b. flange-plate connection

Figure 1-1 Flat-plate reinforced connections

2 Literature Review

2.1 Overview

Prior to developing the test program described in Chapter 3, the results of previous tests on steel moment-resisting connections reinforced with flat steel plates were carefully reviewed. The results of this literature review guided the development of the testing program and the selection of the design variables for reinforced connections. The following two sections summarize work completed before the current project on connections reinforced with flat steel plates. Section 2.2 presents summary information on cover-plate connections and Section 2.3 presents information on flange-plate connections.

Most of the studies described below were experimental and included no pretest finite element analysis (including the tests by the authors on the SAC Phase I project). Despite the relatively large number of tests of cover-plate and flange-plate connections, the key design variables for such connections were not systematically identified and evaluated. This is not a criticism of the previous work but recognition that much of the work was industry driven to provide information for specific projects.

The SAC Phase II project provided the opportunity to systematically study steel moment-resisting connections reinforced with flat steel plates. The work described in the remaining chapters of the report builds on the studies presented in the following two sections. Emphasis is placed on work conducted by the authors that directly impacted the SAC Phase II test program that is described in this report.

2.2 Cover-Plate Connections

Table 2-1 lists the results of studies of 37 tests of single-sided cover-plate connections. All cover-plate and beam flange assemblies were groove welded to the column flange. Summarized in the table are beam sizes, column sizes, geometry of the top and bottom cover plates, geometry of the fillet welds joining the cover plates to the beam flanges, the connection of the beam web to the column flange, and maximum plastic rotation of the joint (beam plus panel zone). The shaded cells in the last column of the table indicate undesirable failures (e.g., column fracture). Also indicated in the second-to-last column of the table is whether finite element analysis was undertaken as part of the research program. The data in the last column that was extracted from the literature should be used with caution because in some cases the authors did not specify

whether (a) the maximum rotation included a contribution for the panel zone, (b) the maximum rotation was the largest recorded value or that value at which the maximum resistance dropped below a percentage of the peak resistance, and (c) the value was computed at the column face, the center of the plastic hinge, or the centerline of the column.

Shortly after the 1994 Northridge earthquake, Engelhardt and Sabol (1995) tested 12 single-sided steel moment-resisting connections reinforced with trapezoidal and rectangular cover plates. The typical beam size was W36x150 of A36 steel. Beam flange yield strengths ranged between 292 and 340 MPa. Columns ranged in size from W14x257 to W14x455; Grade 50 steel was used for all columns. Details of two of the 12 specimens are presented in Figure 2-1. Ten of the 12 test specimens developed large plastic rotations under cyclic loading but two (AISC-3A and AISC-5B) performed poorly. In specimen AISC-3A (see Figure 2-1a), the groove weld joining the beam top flange and cover plate fractured in a brittle manner, likely due to low toughness of the weld metal. In AISC-5B, a brittle fracture occurred at the bottom flange, causing a complete separation of the beam bottom flange and cover plate from the column flange. Fractographic and metallographic examination by Engelhardt and Sabol suggested that higher yield strength, heavy and long cover plates, high heat input during welding, and the presence of an initial crack contributed to the observed failures. Parenthetically, these two failures of cover-plate connections called into question the reliability of such connections that led to the research program described below.

Blackman and Popov (1995) tested one beam-column connection reinforced with trapezoidal cover plates. This specimen was constructed with a W36x150 A36 steel beam and a W14x211 Grade 50 column. Construction details for this specimen are shown in Figure 2-2. Four continuity plates were placed opposite each flange as seen in the figure to "...prevent the build-up of residual stress in the heat-affected zones of the column flange." A dumbbell-shaped slot was drilled and cut in the column web opposite each beam flange to "...soften..." and "...add flexibility..." to the connection. This specimen failed prematurely due to brittle fracture of the column flange. Blackman and Popov report that the crack initiated at the "relief" hole, which was drilled to reduce stresses, and propagated into the column flange.

Popov, Blondet, and Stepanov (1996) tested three identical beam-column connections (ADP-1, ADP-2, and ADP-3) that were reinforced with trapezoidal top cover plates and rectangular bottom cover plates as shown in Figure 2-3. The specimens were constructed using a W36x245 A36 beam and a W14x398 Grade 50 column. Doubler plates were added to strengthen the beam-to-column panel zone. Specimens ADP-2 and ADP-3 failed prematurely due to fracture of the column flange at the level of the underside of the beam flange. In ADP-2, the top (trapezoidal) cover plate, both column flanges, and the column web fractured. The maximum plastic rotation in this connection exceeded 0.04 radian. In ADP-3, the column flange and column web inside the panel zone fractured at a lower maximum plastic rotation of 0.02 radian.

Anderson and Duan (1998) tested three pre-Northridge beam-column connections that were reinforced with rectangular top and bottom cover plates. Rectangular mini-plates were used for one of the three connections. The specimens were fabricated from W21x68 A36 beams and W12x106 Grade 50 columns—substantially smaller beams and columns than those tested by Engelhardt and Popov. Each specimen developed plastic rotations in excess of 0.03 radian.

Table 2-1 Cover-plate connection test summary

Researcher	Beam	Column	Top Cover Plate ¹	Bottom Cover Plate ¹	Top Plate Weld Geometry ²	Bottom Plate Weld Geometry ²	Web Connection ³	FE Analysis ⁴	Max plastic rotation ⁵
Engelhardt and Sabol	W36x150	W14x455	T	R	FW-T	FW-L	B+SW	None	0.015
	W36x150	W14x455	T	R	FW-T	FW-L	B+SW	None	0.025
	W36x150	W14x426	T	R	FW-T	FW-L	B+SW	None	0.025
	W36x150	W14x426	T	R	FW-T	FW-L	B+SW	None	0.005
	W36x150	W14x426	T	R	FW-T	FW-L	B+SW	None	0.035+
	W36x150	W14x426	T	R	FW-T	FW-L	B+SW	None	0.050+
	W36x150	W14x426	T	R	FW-T	FW-L	B+SW	None	0.035+
	W36x150	W14x426	T	R	FW-T	FW-L	B+SW	None	0.035+
	W36x150	W14x257	T	R	FW-T	FW-L	B+SW	None	0.037+
	W36x150	W14x426	T	R	FW-T	FW-L	W	None	0.033+
	W30x148	W14x257	T	R	FW-T	FW-L	W	None	0.038+
W36x150	W14x455	T	R	FW-T	FW-L	W	None	0.038+	
Blackman and Popov	W36x150	W14x211	T	T	FW-T	FW-T	W	None	0.010 ⁶
Popov, Blondet, and Stepanov	W36x245	W14x398	T	R	FW-T	FW-L	B	None	0.043
	W36x245	W14x398	T	R	FW-T	FW-L	B	None	0.044
	W36x245	W14x398	T	R	FW-T	FW-L	B	None	0.019
Anderson and Duan	W21x68	W12x106	R	R	PP	PP	B	NL-Sh, KH	0.040
	W21x68	W12x106	R	R	PP	PP	B	NL-Sh, KH	0.065
	W21x68	W12x106	MR	MR	PP	PP	B	NL-Sh, KH	0.060
Whittaker, Bertero, and Gilani	W30x99	W14x176	T	R	FW-T FW-N	FW-L	B+SW	None	0.043+
Whittaker, and Gilani	W36x359	BW36x670	T	R	FW-T	FW-L FW-N	W	NL-So, KH	0.008

Table 2-1 Cover-plate connection test summary

Bjorhovde, Goland, and Benac	W21x122	W14x176	T	T	FW-T	FW-T	B	None	0.027
	W21x122	W14x176	T	T	FW-T	FW-T	B	None	0.027
	W21x122	W14x176	T	T	FW-T	FW-T	B	None	0.017
	W21x122	W14x176	T	T	FW-T	FW-T	B	None	0.029
	W21x122	W14x176	T	T	FW-T	FW-T	B	None	0.018
	W21x122	W14x176	T	T	FW-T	FW-T	B	None	0.028
	W21x122	W14x176	T	T	FW-T	FW-T	B	None	0.028
	W21x122	W14x176	T	T	FW-T	FW-T	B	None	0.028
	W21x122	W14x176	T	T	FW-T	FW-T	B	None	0.043
	W21x122	W14x176	T	T	FW-T	FW-T	B	None	0.027
	W21x122	W14x176	T	T	FW-T	FW-T	B	None	0.027
	W21x122	W14x176	T	T	FW-T	FW-T	B	None	0.031
	W21x122	W14x176	T	T	FW-T	FW-T	B	None	0.031
	W21x122	W14x176	T	T	FW-T	FW-T	B	None	0.027
	W21x122	W14x176	T	T	FW-T	FW-T	B	None	0.038
	W21x122	W14x176	T	T	FW-T	FW-T	B	None	0.038

1. T = trapezoidal; R = rectangular; MR = mini-rectangular
2. FW-T = fillet weld on tapered edges; FW-N = fillet weld on nose; FW-L = fillet weld on longitudinal edges; PP = partial penetration.
3. W = welded; B = bolted; B+SW = bolted plus supplemental web tab welds
4. NL = nonlinear; Sh = shell elements; So = solid elements; KH = kinematic hardening
5. Values reported by research team, in radians
6. Failure initiated in column adjacent drilled (relief) holes in web.

Whittaker et al. (1996) tested one single-sided cover-plate connection as part of the SAC Phase I project using the ATC-24 loading protocol (ATC 1992). A trapezoidal top cover plate and a rectangular bottom cover plate were used. The top plate was narrower than the beam flange to permit downhand welding of the cover plate to the beam. The bottom plate was used as an erection seat and was groove welded to the column in the shop. This plate was wider than the beam flange to permit downhand fillet welding to the beam bottom flange. Details of the connection are shown in Figure 2-4. The connection of the beam web to the column flange utilized bolts and supplemental web tab welds. The connection represented the state-of-the-art in 1996 and was designed by industry representatives from the SAC Joint Venture and the research team. Two bolts can be seen in part *b* of the figure. These bolts were added to delay separation of the beam bottom flange and the rectangular plate. No doubler plate was welded to the column web in this connection even though the panel zone thickness would not have met the requirements of the *AISC Seismic Provisions for Structural Steel Buildings* (AISC 1997). The response of the connection is summarized in Figure 2-5. Part *a* of the figure shows the relationship between the moment at the column face and beam plastic rotation, where the beam plastic rotation is calculated as the plastic deformation of the beam divided by the distance between the centerline

of the actuator and the centerline of the plastic hinge that was assumed to be located 15 inches from the nose (front) of the cover plate. Part *b.* of the figure shows the relation between the moment at the column face and panel zone plastic rotation. In this specimen, the panel zone yielded prior to the beam. Only after substantial strain hardening in the panel zone did the beam yield beyond the nose of the cover plate. Yielding of the beam was followed by flange local buckling and web local buckling in the beam at the nose of the cover plate. Flange buckling at the nose of the bottom cover plate led to tearing of the longitudinal fillet weld joining the plate to the beam flange (see Figure 2-6). The tear in the fillet weld propagated with repeated cycling of the test specimen back to the line of the two bolts seen in Figure 2-4b. The bottom flange of the connection then suffered a net section fracture as seen in Figure 2-7. The maximum beam plastic rotation was 0.023 radian.

In 1998, Whittaker and Gilani tested a single-sided cover-plate specimen composed of a W36x359 Grade 50 beam and a BW36x670 column fabricated from Grade 50 plate. Figure 2-8 shows the test fixture. A trapezoidal top cover plate and a rectangular bottom cover plate, both of Grade 50 plate were used (see Figure 2-9). The beam web was groove welded to the column flange. A doubler plate was welded to the column web to increase the strength of the panel zone and substantially eliminate plastic deformation in the panel zone. The hysteretic response of the connection is shown in Figure 2-10. The beam fractured immediately beyond the nose of the top cover plate. The fracture propagated through the beam top flange, the beam web, and the beam bottom flange, and was arrested by the bottom cover plate. Photographs of the failed specimen are shown in Figure 2-11. Fractographic analysis of the failure surface showed laminations and imperfections in the parent metal, and indicated that fracture initiated immediately below the end of the fillet weld joining the top trapezoidal cover plate and the beam top flange. Subsequent finite element analysis of this connection showed high triaxial stresses at the fracture initiation site.

Bjorhovde, Golland, and Benac (1999) tested 17 full-scale, beam-column connections reinforced with cover plates. All specimens were constructed with W14x176 columns and W21x122 beams of ASTM A572 Grade 50 steel. The variables considered by the authors included cover-plate thickness, column-straightening protocol, strain rate, continuity plate location and weld details, and cover plate-column flange weld geometry. Thirteen of the 17 specimens achieved a maximum plastic rotation of 0.025 radian or greater. Bjorhovde et al. (1999) concluded that there was no significant difference in response between assemblies using rotary straightened, gag straightened, or unstraightened columns and that the loading protocol was unimportant, although dynamic testing appeared to be a more severe loading condition than static testing.

2.3 Flange-Plate Connections

Table 2-2 lists the results of studies of 13 tests of single-sided flange-plate connections. All flange plates were groove welded to the column flange. Summarized in the table are the beam sizes, column sizes, geometry of the top and bottom cover plates, geometry of the fillet welds joining the cover plates to the beam flanges, connection of the beam web to the column flange, and maximum plastic rotation of the joint (beam plus panel zone). The shaded cells in the last column of the table indicate undesirable failures. Also indicated in the second-to-last column of the table is whether finite element analysis was undertaken as part of the research program.

Popov and Jokerst (1995) tested two flange plate connections for the Lawrence Berkeley National Laboratory. Both connections were composed of W30x99 beams and W14x283 columns of ASTM A572 Grade 50 steel. The connections were reinforced with 267-mm wide, 610-mm long trapezoidal cover plates. Popov reported maximum beam plastic rotations of 0.034 radian for both specimens.

Whittaker and Gilani (1996) tested three flange plate connections for the Fremont Unified School District (FUSD). Specimen FUSD-1 was composed of a W21x50 beam and a W21x111 column. FUSD-2 was composed of a W24x62 beam and a W21x111 column. FUSD-3 was composed of a W24x76 beam and a W21x101 column. All beams and columns were of Grade 50 steel. Rectangular flange plates were used in all instances. The test fixture for the three flange-plate connection tests is shown in Figure 2-12. FUSD-1 failed due to horizontal fracture of the beam web immediately adjacent to the top flange during the second loading cycle to seven times the nominal yield displacement. The contribution of the panel zone plastic rotation to the joint rotation was negligible. Figure 2-13 shows the hysteretic response for FUSD-1. FUSD-3 failed by complete fracture of the column flange immediately above the top flange plate during the third cycle to five times the yield displacement. The fracture propagated approximately 1 inch (25 mm) into the web of the column. The flexibility and weakness of the FUSD-3 panel zone contributed substantially to the failure of the specimen. Figure 2-14 shows the relation between the moment at the column face and beam plastic rotation (Figure 2-14a) and panel zone plastic rotation (Figure 2-14b). The large distortions in the panel zone led to kinking of the column flanges and a state of high triaxial tension at the fracture initiation site (when the top flange was in tension) and likely was a key contributor to the failure. Figure 2-15 is a photograph of the fractured column flange in FUSD-3. For information on the response of FUSD-2, which was similar to that of FUSD-1, refer to Whittaker and Gilani (1996).

Lee, Goel and Stojadinovic (1997) proposed a new design procedure for steel beam-column moment connections based on a truss analogy. The adequacy of the procedure was checked by nonlinear finite element analysis and testing of a moderate-scale specimen. Figure 2-16 shows the construction details for the specimen, which was composed of a W21x50 A36 beam and a W12x152 Grade 50 column. In this connection, the beam is joined to the column via flange plates and vertical ribs attached to the top and bottom of each flange. (For information, the lack of a positive beam web-to-column connection was first tested by Popov and Stephen (1970) on a specimen of a similar size to that tested by Lee et al.) A maximum joint (panel zone plus beam) plastic rotation of 0.045 radian was reported by Lee.

Noel and Uang (1996) tested three double-sided and one single-sided steel moment connections reinforced with welded flange plates. Figure 2-17 shows construction details for one double-sided connection. ASTM A572 Grade 50 steel was used for all beams, column, and flange plates. The beams ranged from W24x94 through W18x86. The columns for the double-sided connection were W24x279. A box column of 20x20x2 was used for the single-sided connection. Maximum beam plastic rotations ranged between 0.013 radian and 0.046 radian. Two of the key findings of this research plan were (1) that tearing of the fillet welds joining the beam flange to the flange plate was the typical failure mode and (2) that the groove welded joints between the column and the flange plate performed well regardless of whether the backup bars were removed, left in place, or left in place but reinforced with fillet welds.

Table 2-2 Flange-plate literature review summary

Researcher	Beam	Column	Top Flange Plate ¹	Bottom Flange Plate ¹	Top Plate Weld Geometry ²	Bottom Plate Weld Geometry ²	Web Connection ³	FE Analysis ⁴	Max plastic rotation ⁵
Popov	W30x99	W14x283	T	T	FW-T	FW-T	W	None	0.034
	W30x99	W14x283	T	T	FW-T	FW-T	W	None	0.034
Whittaker and Gilani	W21x50	W12x111	R	R	FW-L	FW-L	W	None	0.028+
	W24x62	W21x111	R	R	FW-L	FW-L	W	None	0.045+
	W24x76	W21x101	R	R	FW-L	FW-L	W	None	0.030 ⁶
Lee, Goel and Stojadinovic	W21x50	W12x152	R ⁷	R ⁷	FW-L	FW-L	None	Yes	0.045
Noel and Uang	W24x94	W24x279	T	T	FW-T	FW-T	W	None	0.034
	W24x94	W24x279	T	T	FW-T	FW-T	W	None	0.046
	W24x94	BX20x20x2	T	T	FW-T	FW-T	W	None	0.022
	W16x89	W24x279	R	R	FW-L	FW-L	B	None	0.030
	W18x86	W24x279	R	R	FW-L	FW-L	B	None	0.013
	W24x94	W24x279	T	T	FW-T	FW-T	B	None	0.030
	W24x94	W24x279	T	T	FW-T	FW-T	B	None	0.030

1. T = trapezoidal; R = rectangular;

2. FW-T = fillet weld on tapered edges; FW-N = fillet weld on nose; FW-L = fillet weld on longitudinal edges;

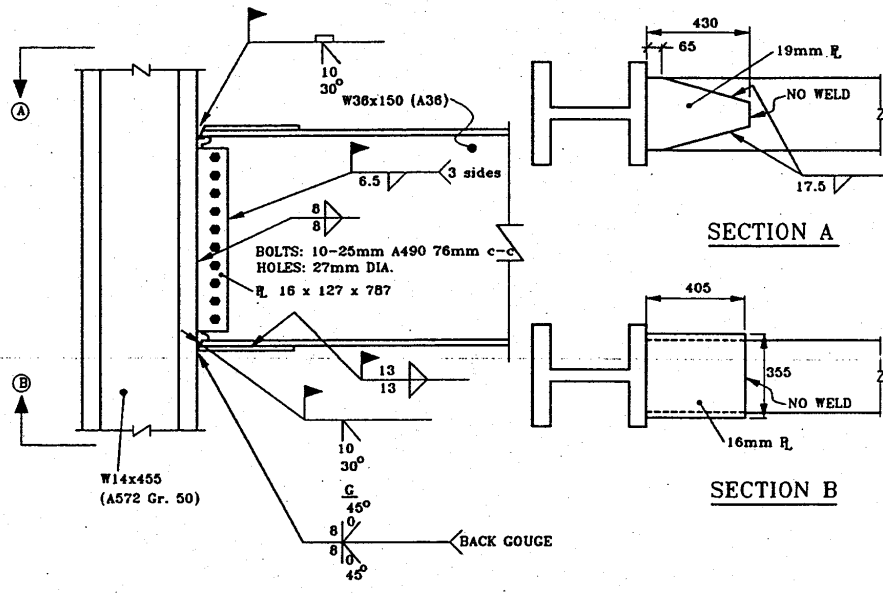
3. W = welded; B = bolted; B+SW = bolted plus supplemental web tab welds

4. NL = nonlinear; Sh = shell elements; So = solid elements; KH = kinematic hardening

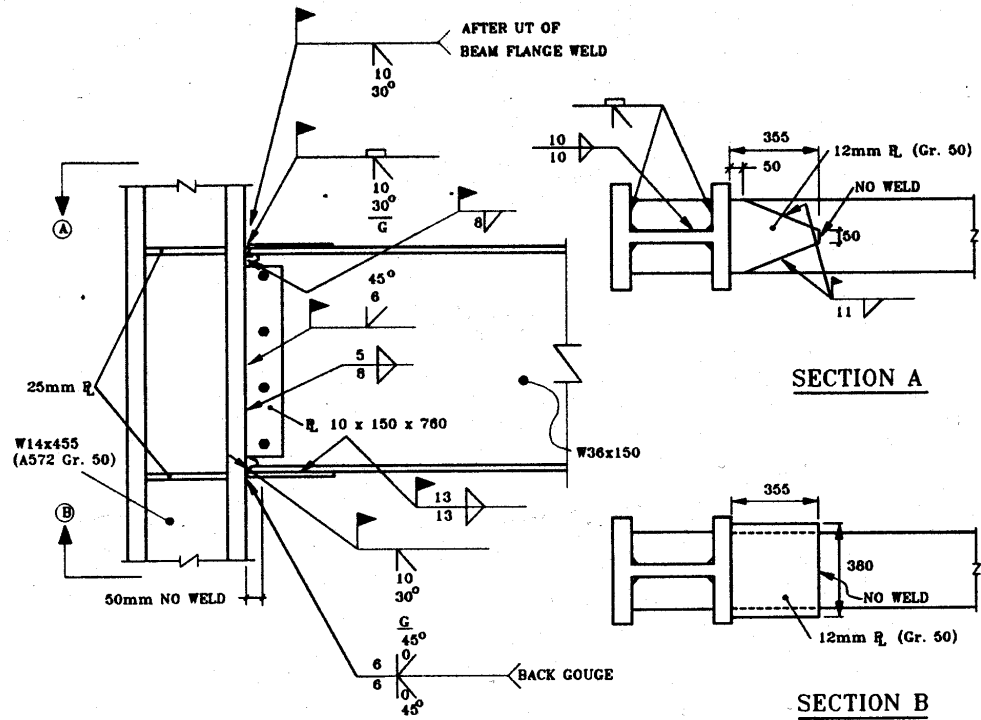
5. Values reported by research team, in radians

6. Plastic rotation in panel zone; minimal beam rotation; column flange fracture

7. Connection at face of column strengthened with two vertical ribs welded to each flange plate



a. specimen AISC-3A construction details



b. specimen NSF-7 construction details

Figure 2-1 Details of cover-plate connections tested by Engelhardt and Sabol (1995)

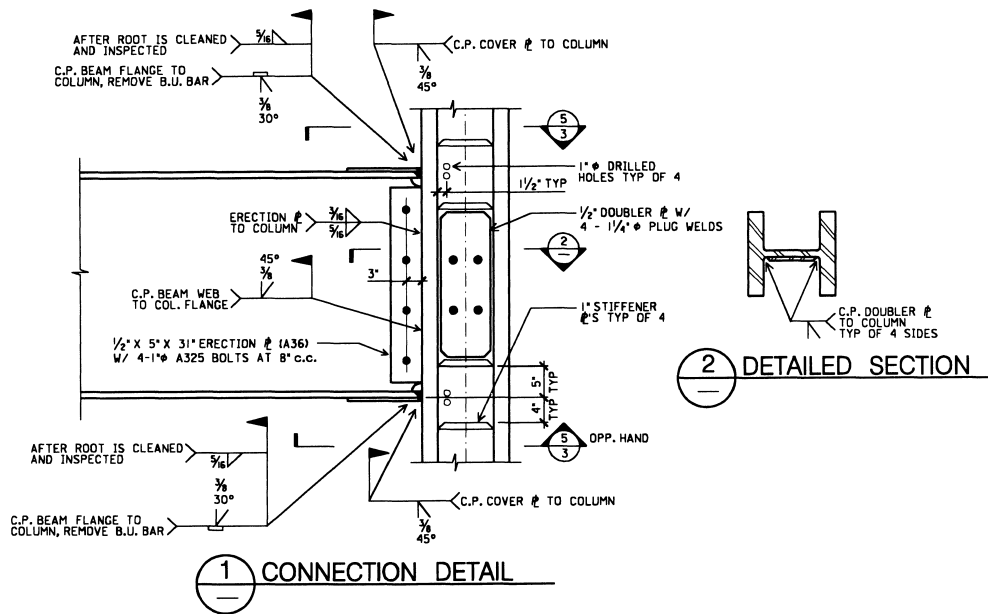


Figure 2-2 Construction details for cover-plate connection of Blackman and Popov (1995)

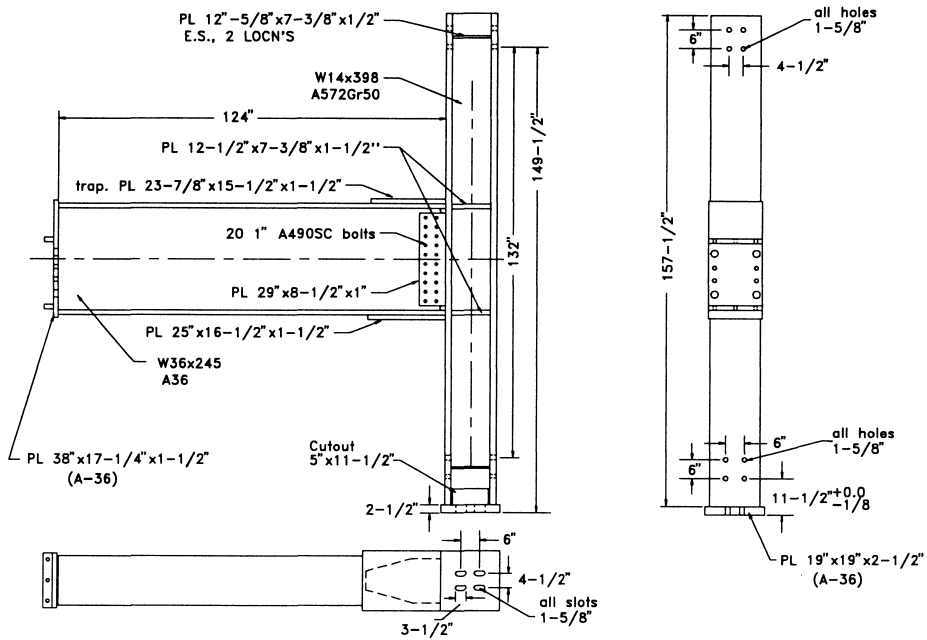
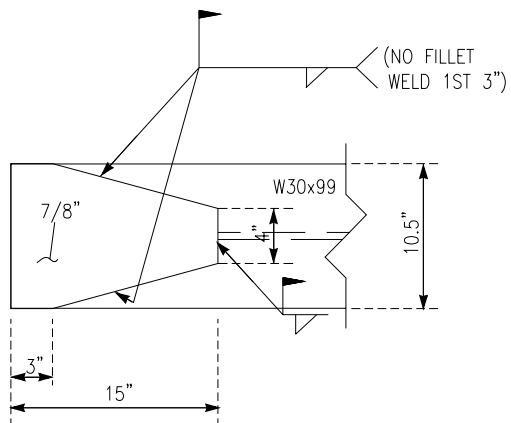
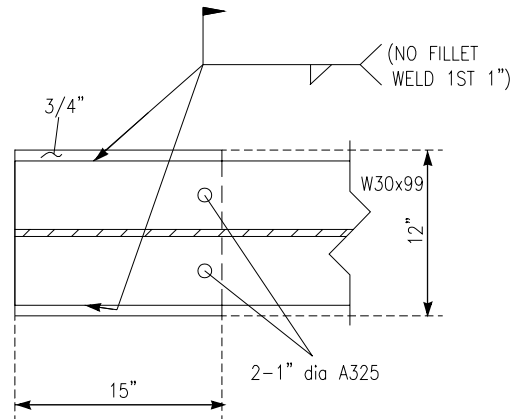


Figure 2-3 Construction details for cover-plate connection of Popov et al. (1996)



a. top cover plate



b. bottom cover plate

Figure 2-4 Cover-plate details for specimen AN1 (Whittaker et al. 1996)

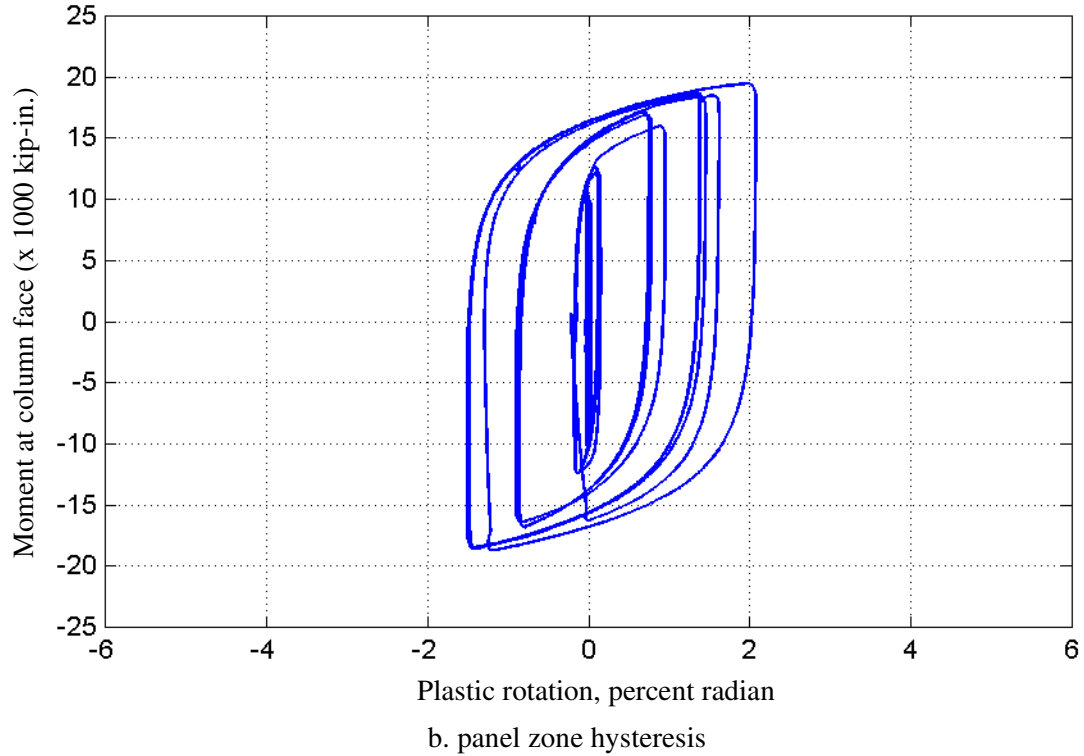
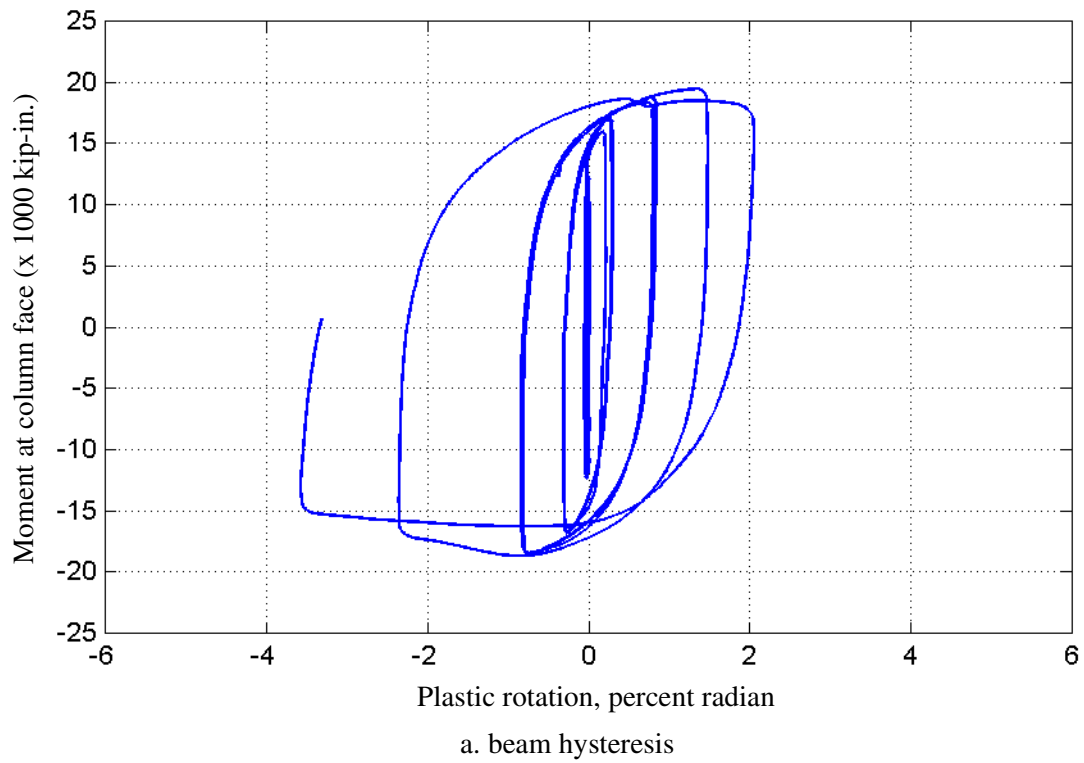


Figure 2-5 Hysteretic response of cover-plate specimen AN1 (Whittaker et al. 1996)

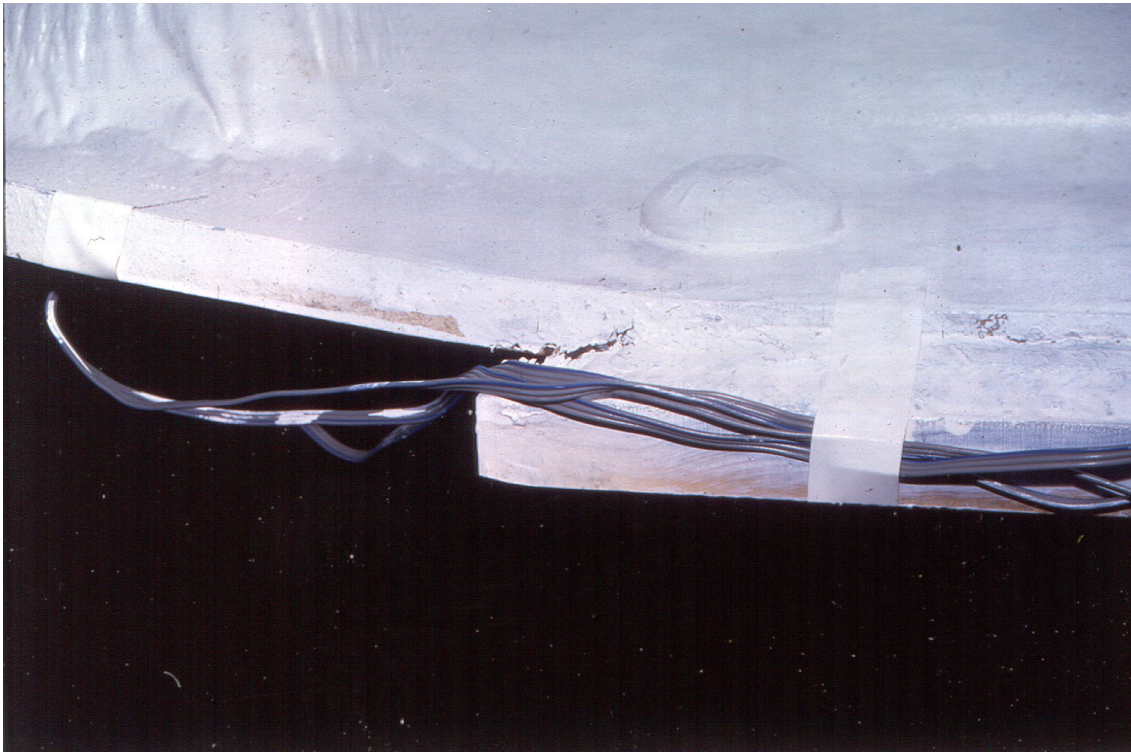


Figure 2-6 Longitudinal fillet weld tear in cover-plate specimen AN1 (Whittaker et al. 1996)

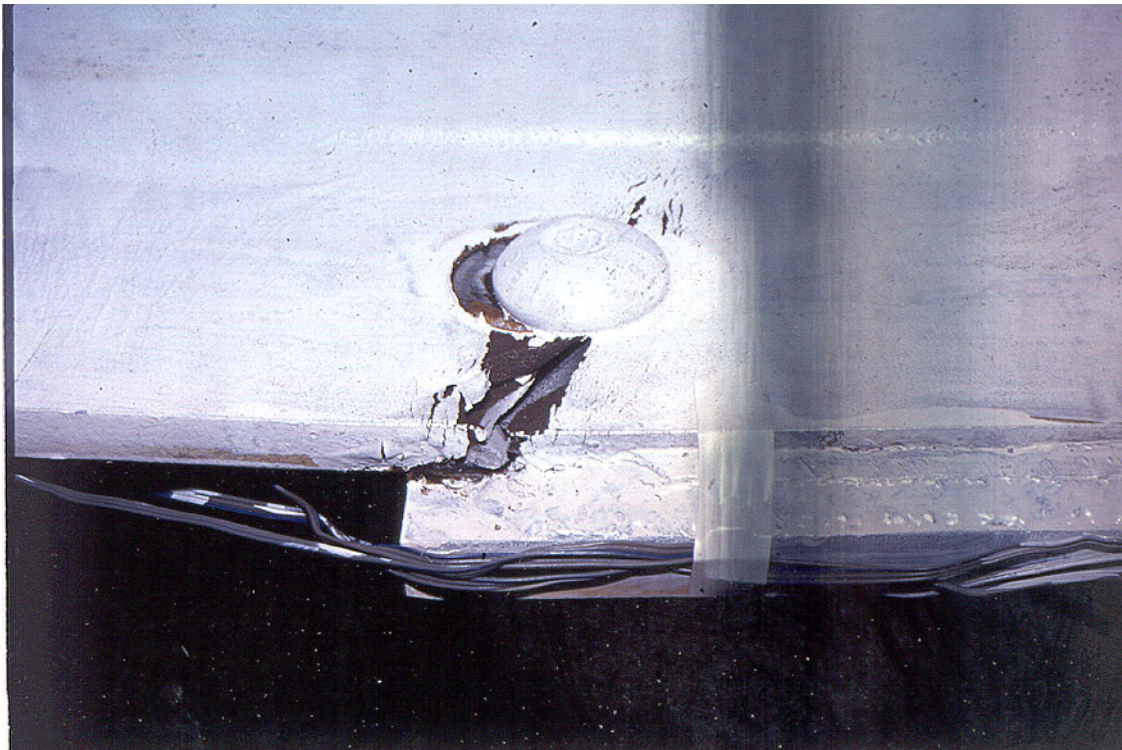
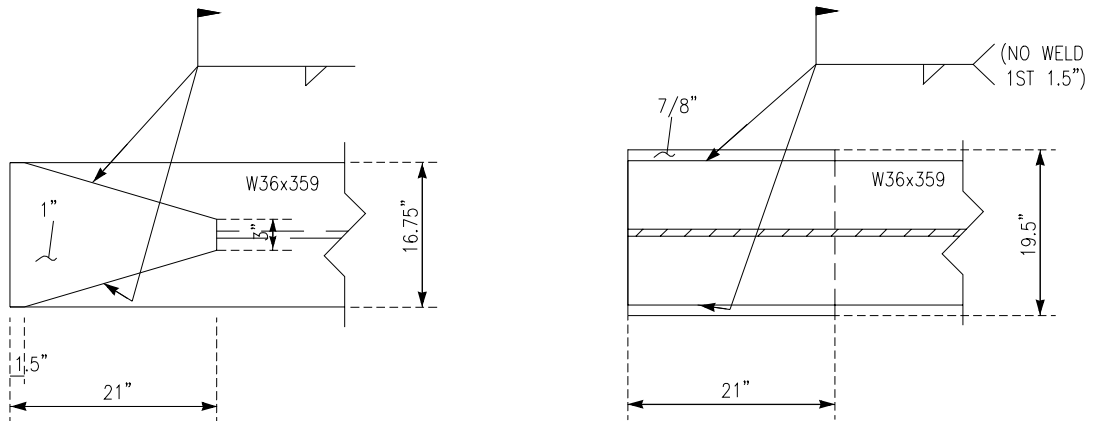


Figure 2-7 Net section fracture of bottom flange of specimen AN1 (Whittaker et al. 1996)



Figure 2-8 Test fixture for the RiverPark II cover-plate specimen



a. top cover plate

b. bottom cover plate

Figure 2-9 RiverPark II cover-plate details

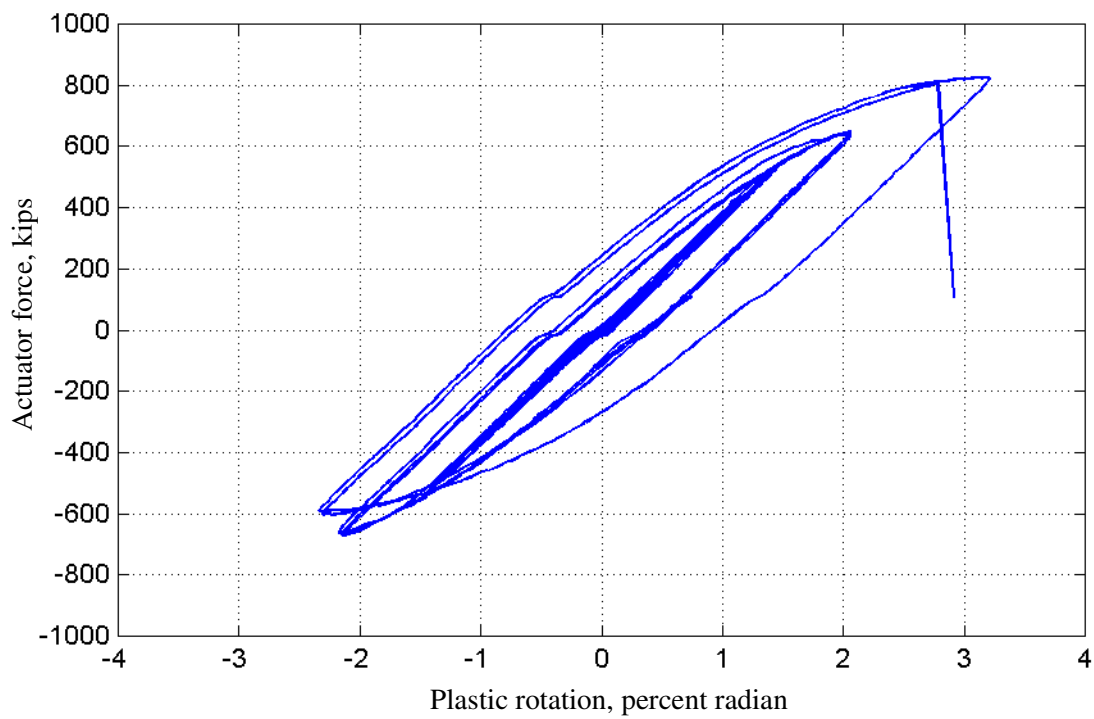
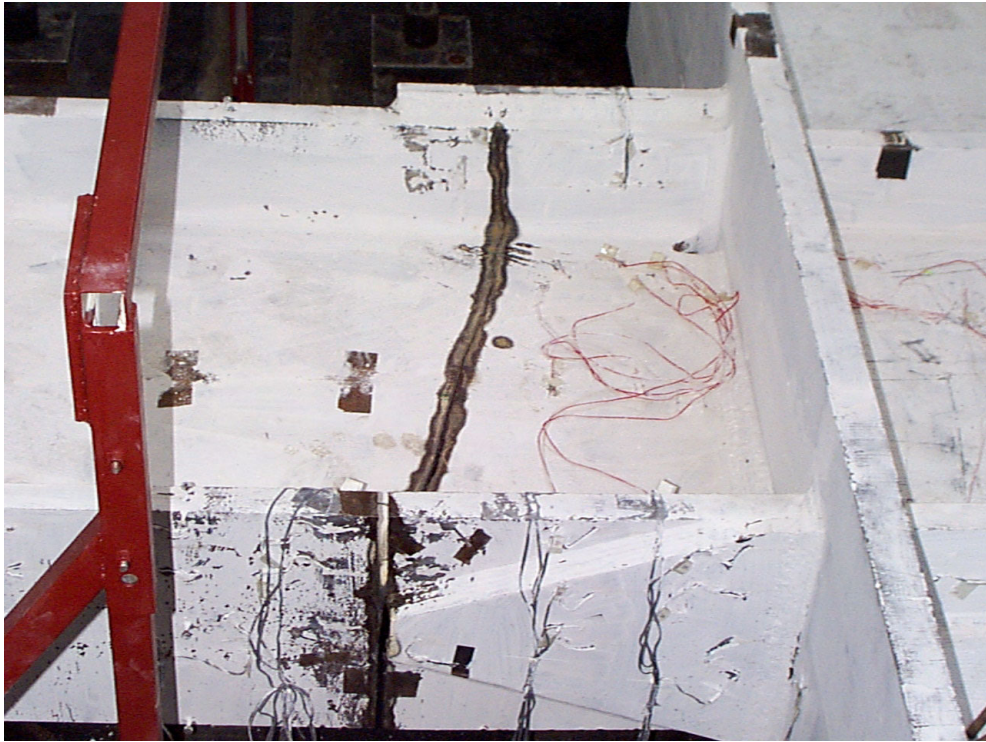


Figure 2-10 Hysteresis for RiverPark II specimen



a. elevation of beam showing line of fracture



b. view of top flange of beam showing line of fracture

Figure 2-11 Fracture of RiverPark II specimen



Figure 2-12 Test fixture for FUSD flange-plate specimens (Whittaker and Gilani 1996)

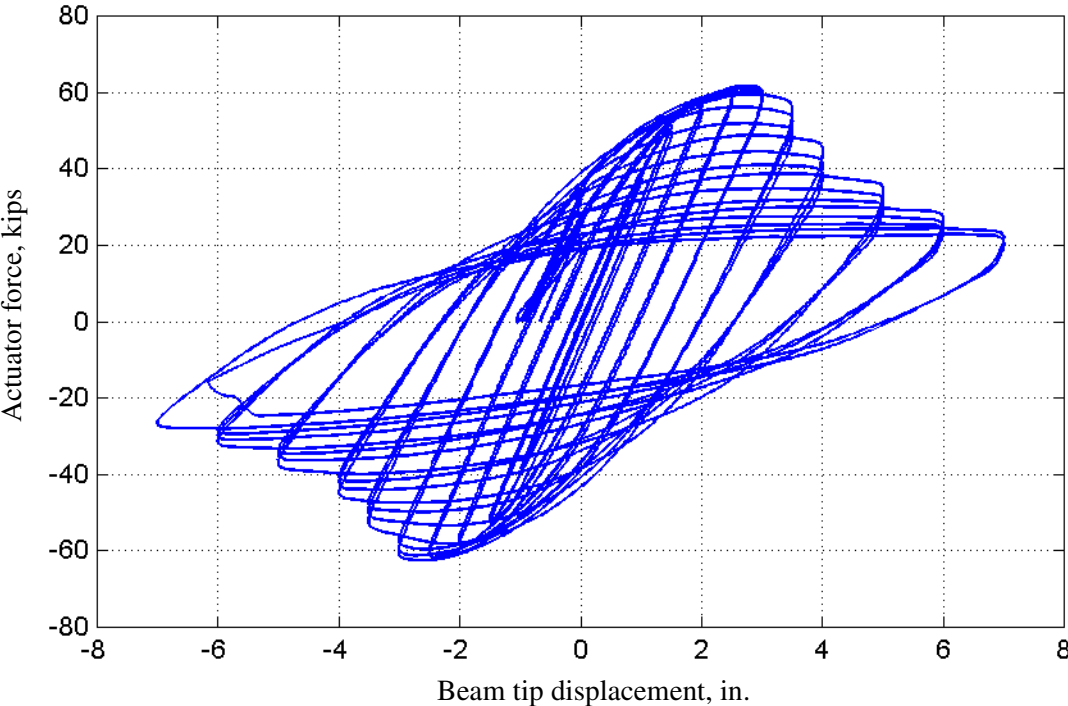
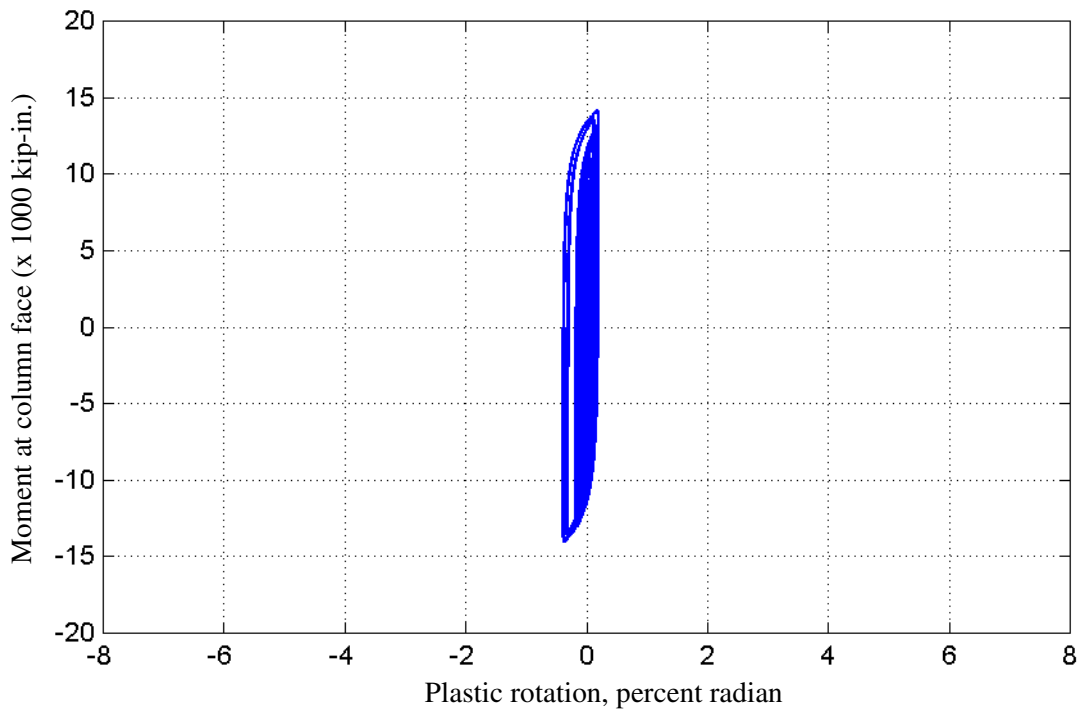
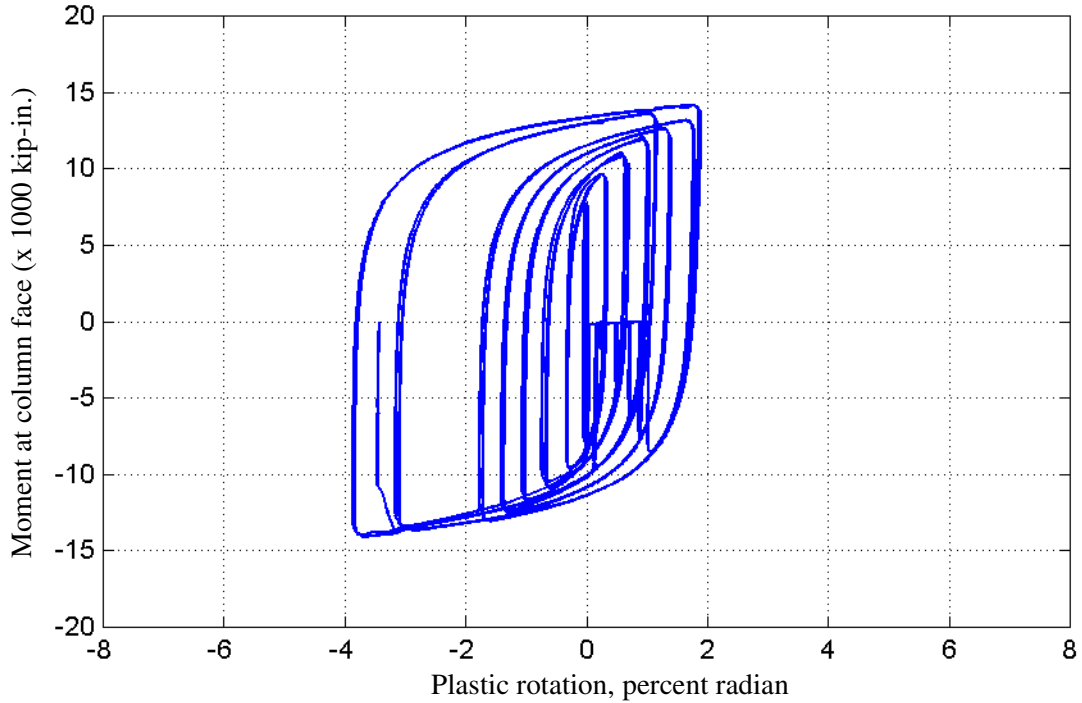


Figure 2-13 Hysteretic response of flange-plate specimen FUSD-1 (Whittaker and Gilani 1996)



a. beam hysteresis



b. panel zone hysteresis

Figure 2-14 Hysteretic response of flange-plate specimen FUSD-3 (Whittaker and Gilani 1996)

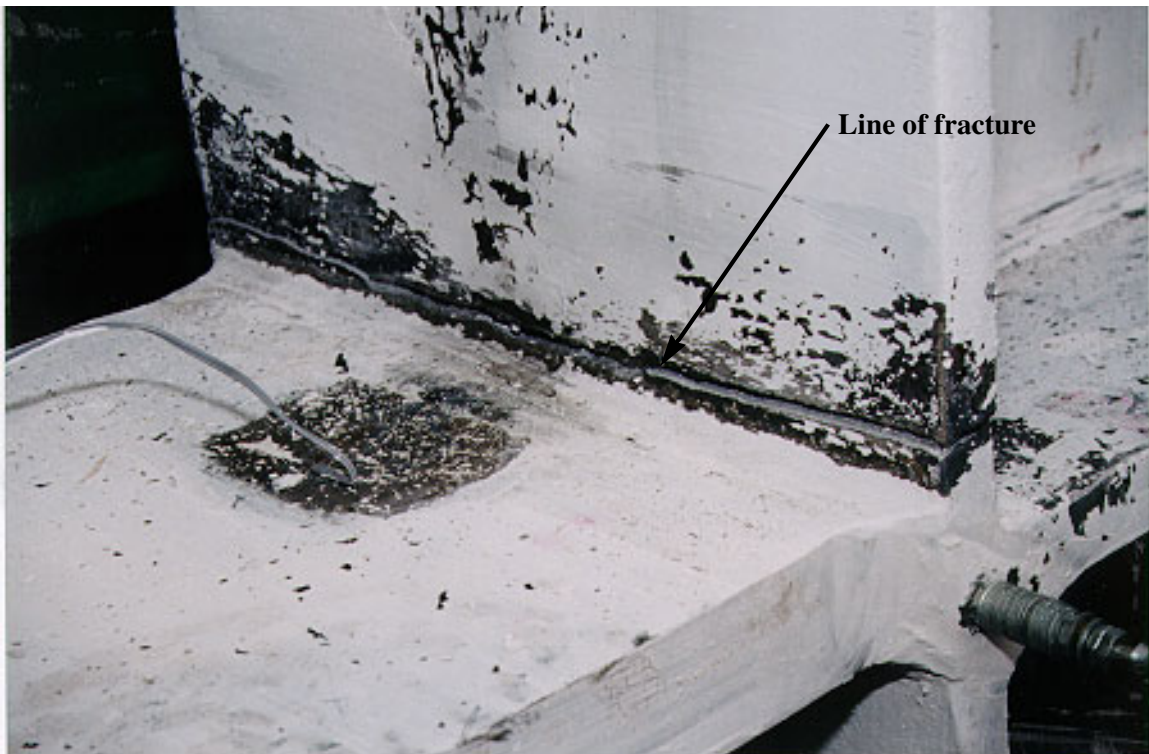
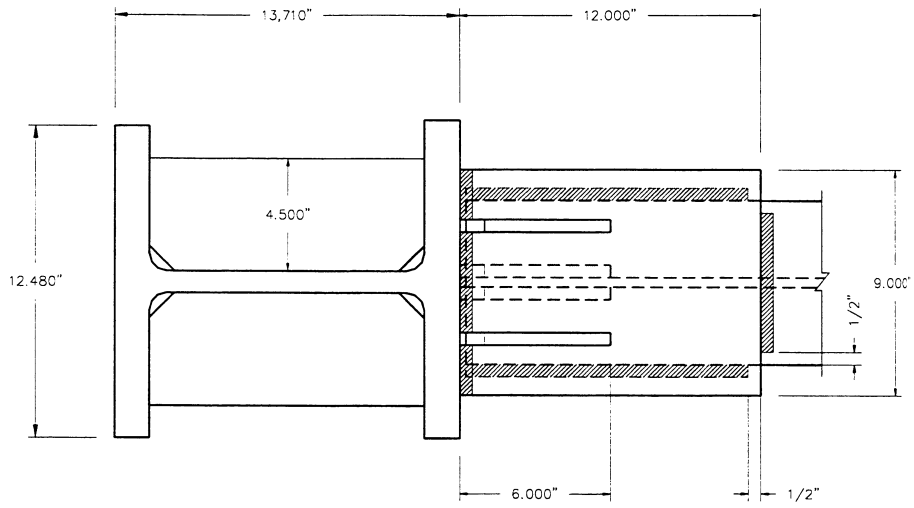
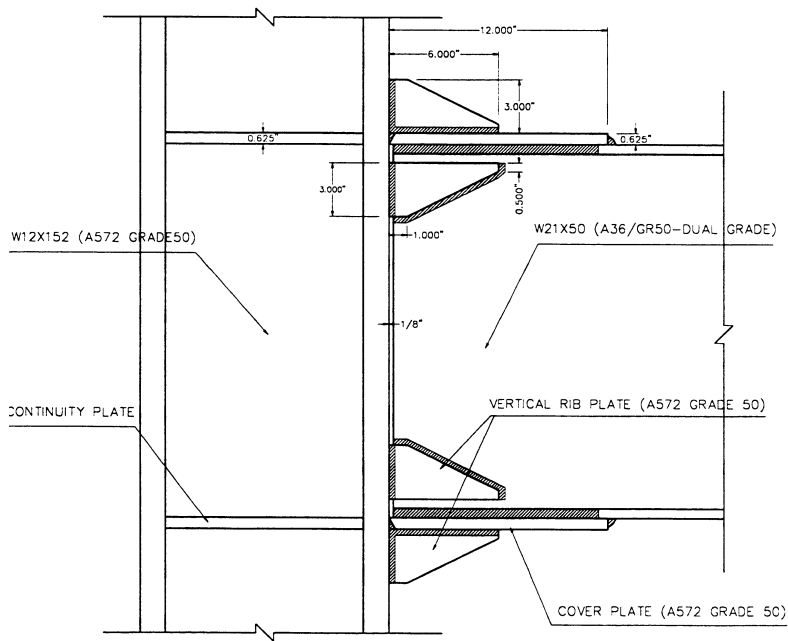


Figure 2-15 Fractured column flange in specimen FUSD-3 (Whittaker and Gilani 1996)



a. plan view



b. elevation

Figure 2-16 Construction details of flange-plate connection tested by Lee et al. (1997)

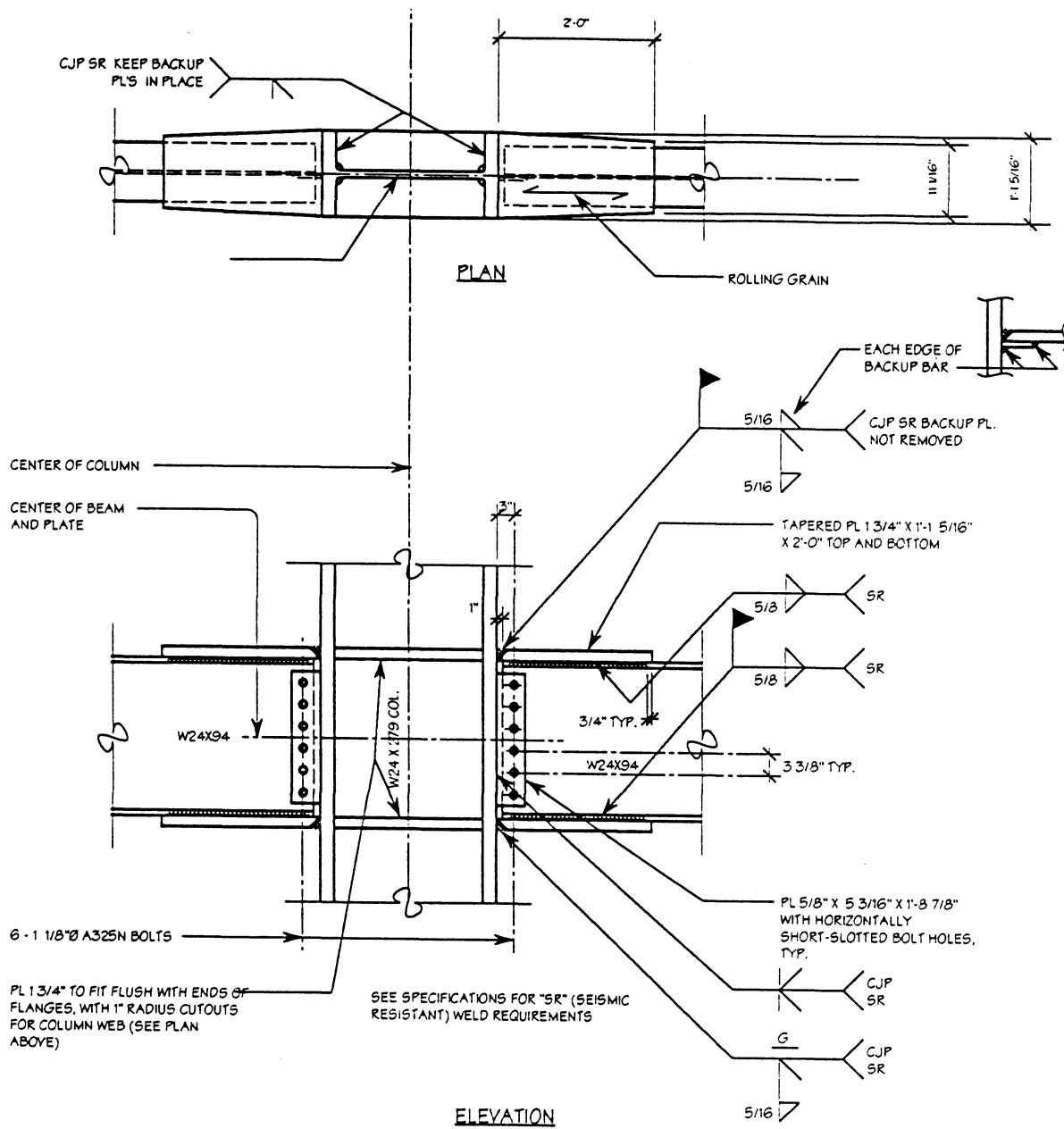


Figure 2-17 Double-sided flange-plate test specimen (Noel and Uang 1996)

3 Experimental Program

3.1 General

The experimental portion of the SAC Phase II project described in this report included full-scale testing of five single-sided cover-plate and five single-sided flange-plate specimens. The SAC Phase I project completed by Whittaker, Gilani, and Bertero (1996) involved testing of unreinforced and reinforced steel moment-resisting connections. All specimens tested in that program were constructed using W14x176 Grade 50 columns and dual certified W30x99 Grade A36 beams. (The mechanical properties of the A36 beams were similar to those of the Grade 50 columns.) One SAC Phase I specimen, AN1, was detailed and tested as a cover-plate connection.

To take advantage of the SAC Phase I data and other information on connections composed of W14x176 columns and W30x99 beams, the authors and the SAC Joint Venture decided to continue the use of these sections for the SAC Phase II project. Grade 50 steel was specified for both the beams and the columns. All 10 beams and 10 columns were specified to be of the same heats. The specimens were fabricated from W14x176 Grade 50 columns and W30x99 Grade 50 beams. Grade 50 flat plate was used to reinforce both the cover-plate and flange-plate specimens.

Design variables for flat-plate reinforced connections were identified to aid the design of the 10 test specimens. The key design variables were (a) reinforcing plate geometry, (b) maximum reinforcement-plate strain, (c) plate-to-flange fillet weld geometry, (d) loading history, (e) restraint to lateral-torsional buckling (LTB) at the plastic hinge, (f) panel zone strength and stiffness, and (g) restraint to web local buckling (WLB).

The remainder of this chapter summarizes the procedures used to design the test specimens, the mechanical properties of the rolled sections and pertinent aspects of their fabrication, and the experimental program, including the test fixture, test parameters, instrumentation, and data acquisition.

3.2 Test Specimen Design and Detailing

3.2.1 Specimen design

The ten specimens were designed using the procedures set forth in FEMA 267A, *Interim Guidelines* (FEMA 1995b). Specimens RC01 and RC06 were designated as the benchmark cover-plate and flange-plate specimens, respectively. Specimens RC01, RC02, RC03, RC05, and RC10 were cover-plate specimens. The remaining specimens, RC04, RC06, RC07, RC08, and RC09 were flange-plate specimens. The following paragraphs describe the key features of each specimen. Summary information on each specimen is presented in Table 3-1. For each specimen, restraint to lateral-torsional buckling (LTB) of the beam was provided near the actuator to protect it from damage. Figure 3-1 is a drawing of the test fixture showing the orientation of the specimen and the location of the LTB restraint. Figure 3-2 is a photograph of the test fixture. Figure 3-3 presents typical connection details for the cover-plate test specimens. Figure 3-4 presents typical details for the flange-plate test specimens. The length of all cover plates and flange plates was set equal to 15 in. (380 mm) to facilitate comparison of specimen responses.

Table 3-1 Summary information on test specimens

	<i>Specimen RC</i>									
	<i>01</i>	<i>02</i>	<i>03</i>	<i>04</i>	<i>05</i>	<i>06</i>	<i>07</i>	<i>08</i>	<i>09</i>	<i>10</i>
<i>Reinforcing plate</i> ¹	CP	CP	CP	FP	CP	FP	FP	FP	FP	CP
<i>Plate geometry</i> ²	R	R	R	S	Tr	R	R	R	R	R
<i>Width (mm)</i>	305	305	305	330	267	337	337	337	337	305
<i>Thickness (mm)</i>	16	16	16	29	17	25	25	22	22	16
<i>Fillet weld size</i> ³										
<i>Longitudinal (mm)</i>	14	14	11	14	16	16	16	14	14	11
<i>Transverse (mm)</i>	-	-	11	19	16	16	16	14	14	11
<i>Doubler plate (mm)</i>	10	10	10	10	10	10	10	10	0	10
<i>Continuity plate (mm)</i>	29	29	29	29	29	25	25	22	16	29
<i>Loading history</i> ⁴	Cy	Cy	Cy	Cy	Cy	Cy	Nf	Cy	Cy	Cy
<i>Restraint to LTB</i> ⁵	N	Y	N	N	N	N	N	N	N	N

1. CP = cover plate; FP = flange plate.

2. R = rectangular; S = swallowtail; Tr = trapezoidal.

3. Fillet welds joining the reinforcing plate to the beam flange.

4. Cy = cyclic; Nf = near-field.

5. Restraint to lateral torsional buckling in the plastic hinge zone; N = no; Y = yes.

The reinforcement plates for Specimen RC01 were designed to relocate the plastic hinge beyond the nose of the cover plate and away from the face of the column. The following steps were followed to design this connection:

1. *Maximum beam moment:* Estimate the maximum beam moment (M_{pr}) at the plastic hinge per FEMA 267A as equal to $1.1Z_bF_{ya}$, where Z_b is the plastic section modulus and F_{ya} is expected yield strength. Calculate the corresponding shear force at the plastic hinge that was assumed to form at $d_b/4$ beyond the nose of the cover plate, where d_b is the depth of the beam. Calculate the moment at the column face (M_{col}). *Results:* $M_{pr} = 19,905$ kip-in. (2,247 kN-m); $M_{col} = 23,920$ kip-in (2,700 kN-m).
2. *Strong-column weak-beam:* Check that the reinforced connection satisfies the strong-column weak-beam requirements of FEMA 267A. *Result:* Connection satisfactory.
3. *Size reinforcement plates:* Size the reinforcement plates at the face of the column using the elastic section modulus of the composite plate-beam. Limit the through-thickness stress at the column face to F_{yc} , where F_{yc} is the yield strength of the column-flange material. (Note that this assumption does not conform to FEMA 267A, which writes that the through-thickness stress shall not exceed $0.9F_{yc}$. Assuming an all-welded web connection and ignoring the cope holes, calculate the required area of each of the reinforcing plates (A_{pl}). Select plate width (b_{pl}) and thickness (t_{pl}). *Result:* $F_{yc} = 50$ ksi (345 MPa); $A_{pl} = 7.10$ in² (4,580 mm²); $b_{pl} = 12$ in. (305 mm); $t_{pl} = 0.63$ in. (16 mm).
4. *Connection of reinforcement plate to beam flange:* Design the fillet weld connection of the reinforcing plate to the beam for the tensile yield strength of the reinforcing plate. Assume that no fillet weld is placed within 1 in. (25 mm) of the column face and that only longitudinal fillet welds are used. *Result:* 9/16 in. (14 mm) fillet weld.
5. *Panel zone strength:* Check the strength of the panel zone against the requirements of FEMA 267. *Result:* One-quarter in. (6 mm) doubler plates added per FEMA 267. The fabricator increased the thickness of the doubler plates so that the plates could serve as backing for the complete joint penetration (CJP) welds of the continuity plates to the column web. Doubler plug welded to column web in field with 4 No. 1 in. (25 mm) diameter welds.
6. *Size continuity plates:* Size the continuity plates subject to the restrictions set forth on page 7-25 of FEMA 267. Design continuity plates for the tensile yield strength of the beam flange and cover plate. *Result:* Full width, 1.125 in. (29 mm) thick plates.

3.2.2 Specimen details

Summary information on the RC01 beam-column connection is presented in Figure 3-5. Note that the use of cover plates that were wider than the beam flange required that the beam be rotated 180 degrees to place the second set of cover plate to beam flange fillet welds.

Specimen RC02 was identical to RC01 except for tabs welded to the beam web-flange junction to connect the braces that were used to delay lateral-torsional buckling of the beam at the end of the plastic hinge. Data from this specimen were used to study the effect of lateral-torsional buckling on stiffness and strength degradation in the plastic hinge zone.

Specimen RC03 was identical to RC01 except for differences in the fillet welding of the cover plate to the beam flange. Specifically, 0.44-in. (11 mm) longitudinal and transverse fillet welds were used in RC03 to better mobilize the cover plate. The total volume of fillet weld metal in the RC03 cover-plate to beam flange connection was approximately equal to that used in RC01. Figure 3-6 presents details of the RC03 cover plate to beam flange fillet welds. This specimen was tested to investigate the effect of fillet weld geometry on the response of the reinforcing plate.

Specimen RC04 was the first flange-plate specimen. The design procedure followed that described above for the cover-plate specimens except that the beam flanges were not included in the calculation of the elastic section modulus of Step 3. The flange plate was cut to a swallowtail profile (1) to increase the length of fillet weld that could be placed to join the beam flange and the flange plate and (2) to assess whether yield penetration over part of the length of the flange plate was detrimental or beneficial to the response of the specimen. Figure 3-7 presents the profile of the flange plate and information on the flange plate to beam flange fillet welds.

Cover-plate specimen RC05 was similar to RC01 except for differences in the profile of the cover plate and the geometry of the cover plate to beam flange fillet welds. The maximum width of the cover plate was equal to the width of the beam flange, namely, 10.5 in. (267 mm). The cover plate was trapezoidal in shape and similar to the top cover plate of specimen AN1 (see Section 2.2). The cover plate was fillet welded to the beam top flange along the taper cut and across the nose of the cover plate. Details of the plate shape and fillet welds are shown in Figure 3-8.

Specimen RC06 served as the benchmark flange-plate specimen. The flange plates were rectangular in shape and were designed using the six-step procedure outlined above except that the beam flanges were not included in the calculation of the elastic section modulus of Step 3. Longitudinal and transverse fillet welds were used to join the flange plate to the beam flange. Figure 3-9 shows the profile of the flange plates and the fillet welds joining the flange plate to the beam flange.

Specimen RC07 was identical to RC06 but was tested with the SAC monotonic displacement history to judge the effects of loading history on the response of flat-plate reinforced connections.

Specimen RC08 was similar to specimen RC06 except that the flange plate thickness was reduced from 25 mm to 22 mm to promote yield penetration into the flange plate. The plate thickness was selected by moving the assumed location of the plastic hinge to the nose of the flange plate (Step 1). The remainder of the design followed the procedure presented for RC06. Moving the assumed location of the plastic hinge closer to the column face reduced the calculated moment at the face of the column and thus the thickness of the flange plates. Details of the flange plates and the fillet welds to the beam flanges are shown in Figure 3-10.

Specimen RC09 was identical to RC08 except that the doubler plate in the beam-column panel zone was deleted to investigate the effect of panel zone flexibility on the global response of the connection and the local responses of the flange plates and the groove welds joining the flange plates to the column flange.

Specimen RC10 was a cover-plate connection and most similar to RC03. Horizontal stiffeners were added to RC10 to delay beam web local buckling that was identified following testing of RC01 and RC02 as the likely cause of early stiffness and strength degradation of the connection. The horizontal stiffeners were designed using the AASHTO procedures for longitudinal web stiffening that are presented in Gaylord et al. (1992). Details of the horizontal stiffeners are presented in Figure 3-11.

3.2.3 Restraint to lateral-torsional buckling

To investigate the effect of lateral-torsional buckling (LTB) on the response of reinforced connections, a frame was designed and constructed that would simulate the stiffness and strength of a field-installed lateral brace. The bracing was to be placed 35 in. (890 mm) from the column face to prevent LTB at the far end of the plastic hinge.

A prototype fly-brace stiffness of 700 kips/in. (123 kN/mm) was calculated assuming W30x99 beams at 120 in. (3050 mm). The required axial strength of the brace and its connections was 24 kips (110 kN) that was equal to 6 percent of the axial strength of the beam flange. The stiffness of 700 kips/in. was achieved using the test fixture of Figure 3-12.

3.3 Test Specimen Fabrication and Data

3.3.1 Supply and fabrication

The steel used to fabricate the test specimens was supplied by Nucor-Yamato Steel Company. The ten specimens were fabricated by the Gayle Manufacturing Company of Woodland, California, to details prepared by the authors but with substantial input from both Mr. Rick Wilkinson of Gayle and the SAC Joint Venture.

3.3.2 Mechanical properties of materials

Nucor-Yamato provided mill test reports (MTRs) with the rolled steel sections. Pertinent data taken from the MTRs are listed in Table 3-2. The MTRs are reproduced in Appendix A. Following completion of the testing program, coupons were extracted from RC10 and tested per ASTM standards by Signet Testing Laboratories. Because all beam sections were from one heat and all column sections were from one heat, data from one beam and column were considered to be representative of all beams and columns, respectively.

Data from some of these tests are also presented in Table 3-2. The Signet report on material strengths is reproduced in Appendix A. The design variables of greatest interest were beam and column flange yield strength and column (panel zone) web yield strength, and the Charpy toughness of the material in the beam flange and the beam flange-to-web k-line.

The MTR values were similar to those computed from coupon testing and all values of yield stress exceeded the nominal value of 50 ksi (345 MPa). Charpy impact values for the beam flange and k-line were 128 ft-lb (174 kN-mm) at 70 degrees F (21 degrees C). The Signet report on the Charpy tests is reproduced in Appendix A.

Table 3-2 Mechanical properties of test specimens, U.S. units

Member	Size	Location	Yield Stress (ksi)		Ultimate Stress (ksi)	
			MTR ¹	Coupon	MTR	Coupon
Beam	W30x99	flange	52.5	53.5	68.5	71.6
		web	52.5	62.0	68.5	73.4
Column	W14x176	flange	53.5	50.8	71.5	73.0
		web	53.5	56.0	71.5	72.2

1. MTR = mill test report

3.3.3 Welding procedures and inspection

All complete joint penetration (CJP) and fillet welding was performed in accordance with SAC-approved welding procedure specifications (WPSs). Welding- and fabrication-inspection services were provided by Signet Testing Laboratories. All ten specimens passed ultrasonic testing prior to shipment to the university for testing. Welder qualification test records and weld procedure specifications are reproduced in Appendix A.

3.4 Experimental Program

3.4.1 Test fixture

The test fixture of Figure 3-1 was most similar to that used for the SAC Phase I project undertaken by the authors. As evident in the figure, axial loads were not imposed on the column, and the composite slab that is most common in the field was not present for the experiments. Modest axial loads on columns in the field likely have little influence on the response of the beam-to-column connections, but the absence of the composite slab will accelerate the formation of flange and web local buckles and permit the consequent shortening of the beam in the laboratory experiments that is not physically possible in the field.

The columns in the test specimens were attached to the strong floor and the reaction frame using short segments of W14x311 to achieve near pinned boundary conditions. Displacements were imposed on the beam by a 400-kip (1,800-kN) actuator at a distance of 134 in. (3.4 m) from the column face.

3.4.2 Loading protocol

The SAC cyclic and near-field displacement histories were used for the testing program (Krawinkler 1988). Both histories were run under displacement control and both histories use story drift as the control variable. Figure 3-13 shows the two displacement histories. As indicated in Table 3-1, the cyclic history was used for all specimens except for RC07 for which the near-field history was used. Testing using both displacement histories continued until the connection fractured.

The cyclic displacement history of Figure 3-13a consisted of symmetric, stepwise-increasing displacements that were imposed by the actuator at the tip of the beam (see Figure 3-1). Story drift was used as the displacement parameter rather than yield displacement, which was used for the SAC Phase I experimental program. The complete displacement history consisted of 34 cycles: six cycles at target displacements of 0.375 percent, 0.500 percent, and 0.750 percent story drift, four cycles at a target displacement 1.0-percent story drift, two cycles at target displacements of 1.5-percent, 2.0-percent, 3.0-percent, 4.0-percent, 5.0-percent, and 5.5-percent story drift. For the test specimens, 1.0-percent story drift corresponds to 1.42 in. (36 mm). The maximum displacement was limited to 5.5-percent story drift (± 8 in. or 203 mm) because of actuator stroke limitations.

The near-field displacement history of Figure 3-13b that was imposed by the actuator at the tip of the beam included an initial displacement excursion to minus 2.0-percent story drift followed by an excursion to +5.5-percent story drift. A number of smaller displacement cycles followed the 5.5 percent drift cycle. (Note that the maximum positive displacement was specified to be 6.0 percent drift but this could not be achieved with the test fixture of Figure 3-1.) The entire sequence was then repeated if the specimen had not fractured.

3.4.3 Instrumentation

The instrumentation for the various specimens consisted of an LVDT on the actuator centerline measuring the imposed displacement; a load cell in-line with the actuator measuring axial force; and uniaxial and rosette strain gages placed at strategic locations measuring local strains; displacement transducers placed on the panel zone and column measuring deformations; and displacement transducers placed on the beam (RC06 through RC10 only) measuring amplitudes of lateral-torsional buckling, flange local buckling, and web local buckling.

The instrumentation scheme for RC01 through RC05 consisted of 60 data channels. Tables 3-3, 3-4, and 3-5 list the channel number, instrument type, response quantity, and location for each transducer. Table 3-3 lists typical information; the other two tables list variations from the information in this table. Figures 3-14, 3-15, and 3-16 present information on the instrumentation of RC01 through RC03, RC04, and RC05, respectively. Figure 3-17 shows the instrumentation of the panel zone for RC02. Figure 3-18 is a photograph of the instrumentation of the top flange of the RC02 beam. Four displacement transducers measured the absolute horizontal displacements of the reaction frame (DCDT-7 through -10). Data from these transducers were used to remove contributions to the beam tip displacement from rigid body displacements of the reaction frame that developed during testing.

Table 3-3 Typical instrumentation for RC01 through RC05¹

<i>No</i>	<i>Transducer</i> ²	<i>Response</i>	<i>Transducer location</i> ³
1	-	date	-
2	-	time	-
3	LC-1	force	actuator
4	LVDT-1	displacement	tip of beam
5	DCDT-1	deformation	panel zone deformation
6	DCDT-2	deformation	panel zone deformation
7	DCDT-3	deformation	doubler plate deformation
8	DCDT-4	deformation	doubler plate deformation
9	DCDT-5	deformation	column deformation, level of bottom continuity plate
10	DCDT-6	deformation	column deformation, level of top continuity plate
11	DCDT-7	deformation	reaction frame displ., level of bottom support
12	DCDT-8	deformation	reaction frame displ., level of bottom continuity plate
13	DCDT-9	deformation	reaction frame displ., level of top continuity plate
14	DCDT-10	deformation	reaction frame displ., level of top support
15	R-1	doubler plate shear	bottom right corner of the doubler plate
16	R-2	doubler plate shear	center of the doubler plate
17	R-3	panel zone shear	bottom right corner of the panel zone
18	R-4	panel zone shear	center of the panel zone
19	R-5	panel zone shear	top left corner of the panel zone
20	R-6	beam web shear	2 in. above bottom flange, 7 in. from column face
21	R-7	beam web shear	web centerline, 7 in. from column face
22	R-8	beam web shear	2 in. below top flange, 7 in. from column face
23	R-9	beam web shear	2 in. above bottom flange, 15 in. from column face
24	R-10	beam web shear	web centerline, 15 in. from column face
25	R-11	beam web shear	2 in. below top flange, 15 in. from column face
26	SG-1	col. flange strain	0.75 in. above top continuity plate, web centerline
27	SG-2	col. flange strain	0.75 in. above top continuity plate, 2.75 in. from web centerline
28	SG-3	col. flange strain	0.75 in. below bottom continuity plate, web centerline
29	SG-4	col. flange strain	0.75 in. below bottom continuity plate, 2.75 in. from web centerline
30	SG-5	cont. plate strain	top continuity plate, 2 in. from column far flange, line b

Table 3-3 Typical instrumentation for RC01 through RC05¹

<i>No</i>	<i>Transducer</i> ²	<i>Response</i>	<i>Transducer location</i> ³
31	SG-6	cont. plate strain	top continuity plate, 2 in. from column near flange, line d
32	SG-7	cont. plate strain	top continuity plate, 2 in. from column near flange, line b
33	SG-8	reinf. plate strain	top plate, 2 in. from column face, line d
34	SG-9	reinf. plate strain	top plate, 2 in. from column face, line b
35	SG-10	reinf. plate strain	top plate, 2 in. from column face, line a
36	SG-11	reinf. plate strain	top plate, 13 in. from column face, line d
37	SG-12	reinf. plate strain	top plate, 13 in. from column face, line b
38	SG-13	reinf. plate strain	top plate, 13 in. from column face, line a
39	SG-14	reinf. plate strain	bottom plate, 2 in. from column face, line d
40	SG-15	reinf. plate strain	bottom plate, 2 in. from column face, line b
41	SG-16	reinf. plate strain	bottom plate, 2 in. from column face, line a
42	SG-17	reinf. plate strain	bottom plate, 13 in. from column face, line d
43	SG-18	reinf. plate strain	bottom plate, 13 in. from column face, line b
44	SG-19	reinf. plate strain	bottom plate, 13 in. from column face, line a
45	SG-20	beam flange strain	underside of top flange, 2 in. from column face, line c
46	SG-21	beam flange strain	underside of top flange, 2 in. from column face, line b
47	SG-22	beam flange strain	underside of top flange, 13 in. from column face, line c
48	SG-23	beam flange strain	underside of top flange, 13 in. from column face, line b
49	SG-24	beam flange strain	topside of top flange, 17 in. from column face, line c
50	SG-25	beam flange strain	topside of top flange, 17 in. from column face, line b
51	SG-26	beam flange strain	topside of top flange, 17 in. from column face, line a
52	SG-27	beam flange strain	topside of top flange, 30 in. from column face, line b
53	SG-28	beam flange strain	topside of top flange, 30 in. from column face, line a
54	SG-29	beam flange strain	topside of bottom flange, 2 in. from column face, line c
55	SG-30	beam flange strain	topside of bottom flange, 2 in. from column face, line b
56	SG-31	beam flange strain	topside of bottom flange, 13 in. from column face, line c
57	SG-32	beam flange strain	topside of bottom flange, 13 in. from column face, line b
58	SG-33	beam flange strain	underside of bottom flange, 17 in. from column face, line c
59	SG-34	beam flange strain	underside of bottom flange, 17 in. from column face, line b
60	SG-35	beam flange strain	underside of bottom flange, 17 in. from column face, line a
61	SG-36	beam flange strain	underside of bottom flange, 30 in. from column face, line b

Table 3-3 Typical instrumentation for RC01 through RC05¹

<i>No</i>	<i>Transducer</i> ²	<i>Response</i>	<i>Transducer location</i> ³
62	SG-37	beam flange strain	underside of bottom flange, 30 in. from column face, line a

1. See following tables for variations for RC04 and RC05
2. LC = load cell; LVDT = linear voltage displacement transducer; R = rosette (shear) gage; SG = uniaxial strain gage, DCDT = direct current displacement transducer.
3. See Figure 3-14 for locations of lines a, b, c, and d.

Table 3-4 Non-typical instrumentation for RC04

<i>No</i>	<i>Transducer</i>	<i>Response</i>	<i>Transducer location</i> ³
36	SG-11	reinf. plate strain	top plate, 12 in. from column face, line c
37	SG-12	reinf. plate strain	top plate, 7 in. from column face, line c
38	SG-13	beam flange strain	beam top flange, 7 in. from column face, line a
42	SG-17	reinf. plate strain	bottom plate, 12 in. from column face, line c
43	SG-18	reinf. plate strain	bottom plate, 7 in. from column face, line c
44	SG-19	beam flange strain	beam bottom flange, 7 in. from column face, line a

1. See Table 3-3 for information not shown.

Table 3-5 Non-typical instrumentation for RC05

<i>No</i>	<i>Transducer</i>	<i>Response</i>	<i>Transducer location</i> ³
36	SG-11	beam flange strain	beam top flange, 13 in. from column face, line c
37	SG-12	reinf. plate strain	top plate, 13 in. from column face, line c
38	SG-13	reinf. plate strain	top plate, 13 in. from column face, line a
42	SG-17	beam flange strain	beam bottom flange, 13 in. from column face, line c
43	SG-18	reinf. plate strain	bottom plate, 13 in. from column face, line c
44	SG-19	reinf. plate strain	bottom plate, 13 in. from column face, line a

1. See Table 3-3 for information not shown.

Fifty-eight channels of data were collected for RC06 through RC10. Table 3-6 lists the channel number, instrument type, response quantity, and location for each transducer. Figure 3-19 presents information on the instrumentation of the beam, column, reinforcing plate, continuity plate, and panel zone for RC06 through RC09; Figure 3-20 shows similar information for RC10. Figure 3-21 shows the displacement transducers measuring buckling of Specimen UCB-RC06. Figure 3-22 is a photograph of the instrumentation for Specimen UCB-RC10, showing rosette gages on the beam web and the panel zone.

Table 3-6 Instrumentation for RC06 through RC10

<i>No</i>	<i>Transducer</i> ¹	<i>Response</i> ²	<i>Transducer location</i>
1	-	date	-
2	-	time	-
3	LC-1	force	actuator
4	LVDT-1	displacement	tip of beam
5	WP-0	displacement	actuator
6	DCDT-1	deformation	panel zone deformation
7	DCDT-2	deformation	panel zone deformation
8	DCDT-3	deformation	doubler plate deformation
9	DCDT-4	deformation	doubler plate deformation
10	DCDT-5	deformation	column deformation, level of bottom continuity plate
11	DCDT-6	deformation	column deformation, level of top continuity plate
12	DCDT-7	deformation	reaction frame displ., level of bottom support
13	DCDT-8	deformation	reaction frame displ., level of bottom continuity plate
14	DCDT-9	deformation	reaction frame displ., level of top continuity plate
15	DCDT-10	deformation	reaction frame displ., level of top support
16	WP-4	LTB ⁴	beam top flange, 22 in. from column face
17	WP-5	LTB	beam bottom flange, 22 in. from column face
18	WP-6	flange buckling	top flange, left edge of flange, 22 in. from column face
19	WP-7	flange buckling	top flange, flange centerline, 22 in. from column face
20	WP-8	flange buckling	top flange, right edge of flange, 22 in. from column face
21	DCDT-11	beam rotation	beam top flange, 22 in. from column face
22	DCDT-12	hinge rotation	beam bottom flange, 22 in. from column face
23	WP-1	web buckling	beam web, 2 in. below top flange, 22 in. from column face
24	WP-2	web buckling	beam web, web centerline, 22 in. from column face
25	WP-3	web buckling	beam web, 2 in. above bottom flange, 22 in. from col. face
26	R-1	panel zone shear	bottom right corner of the panel zone
27	R-2	panel zone shear	center of the panel zone
28	R-3	panel zone shear	top left corner of the panel zone
29	R-4	beam web shear	2 in. above bottom flange, 9 in. from column face ³
30	R-5	beam web shear	6 in. above bottom flange, 9 in. from column face ³
31	R-6	beam web shear	web centerline, 9 in. from column face ³
32	R-7	beam web shear	6 in. below top flange, 9 in. from column face ³

Table 3-6 Instrumentation for RC06 through RC10

<i>No</i>	<i>Transducer</i> ¹	<i>Response</i> ²	<i>Transducer location</i>
33	R-8	beam web shear	2 in. below top flange, 9 in. from column face ³
34	SG-1	cont. plate strain	top continuity plate, 2 in. from column far flange, line b
35	SG-2	cont. plate strain	top continuity plate, 2 in. from column near flange, line d
36	SG-3	cont. plate strain	top continuity plate, 2 in. from column near flange, line b
37	SG-4	reinf. plate strain	top plate, 2 in. from column face, line d
38	SG-5	reinf. plate strain	top plate, 2 in. from column face, line b
39	SG-6	reinf. plate strain	top plate, 2 in. from column face, line a
40	SG-7	reinf. plate strain	top plate, 13 in. from column face, line d
41	SG-8	reinf. plate strain	top plate, 13 in. from column face, line b
42	SG-9	reinf. plate strain	top plate, 13 in. from column face, line a
43	SG-10	reinf. plate strain	bottom plate, 2 in. from column face, line d
44	SG-11	reinf. plate strain	bottom plate, 2 in. from column face, line b
45	SG-12	reinf. plate strain	bottom plate, 2 in. from column face, line a
46	SG-13	reinf. plate strain	bottom plate, 13 in. from column face, line d
47	SG-14	reinf. plate strain	bottom plate, 13 in. from column face, line b
48	SG-15	reinf. plate strain	bottom plate, 13 in. from column face, line a
49	SG-16	beam flange strain	underside of top flange, 2 in. from column face, line c
50	SG-17	beam flange strain	underside of top flange, 2 in. from column face, line b
51	SG-18	beam flange strain	underside of top flange, 13 in. from column face, line c
52	SG-19	beam flange strain	underside of top flange, 13 in. from column face, line b
53	SG-20	beam flange strain	topside of top flange, 17 in. from column face, line c
54	SG-21	beam flange strain	topside of top flange, 17 in. from column face, line b
55	SG-22	beam flange strain	topside of top flange, 17 in. from column face, line a
56	SG-23	beam flange strain	topside of top flange, 30 in. from column face, line b
57	SG-24	beam flange strain	topside of top flange, 30 in. from column face, line a
58	SG-25	beam flange strain	underside of bottom flange, 17 in. from column face, line c
59	SG-26	beam flange strain	underside of bottom flange, 17 in. from column face, line b
60	SG-27	beam flange strain	underside of bottom flange, 17 in. from column face, line a

1. LC = load cell; LVDT =linear voltage displacement transducer; R = rosette (shear) gage; SG = uniaxial

2. See Figure 3-19 for locations of lines a, b, c, and d.

3. 7 in. from column face for RC06

4. LTB = lateral-torsional buckling

3.4.4 Data acquisition

The test control and the data acquisition system were run by a PC Windows-based control and acquisition program called Automated Testing System (ATS) developed by SHRP Equipment Corporation of Walnut Creek, California. This program is capable of signal generation, four channel servo-actuator command, and sixteen-channel data acquisition. For the tests described in the Chapter 5, the ATS system was used to monitor and control the displacement and force-feedback signals.

Other data were monitored and recorded using an AutoNet data acquisition system with a capacity of 64 channels. Pacific signal conditioners were used to amplify the transducer signals and to remove frequencies above 100 Hz from the analog signal.

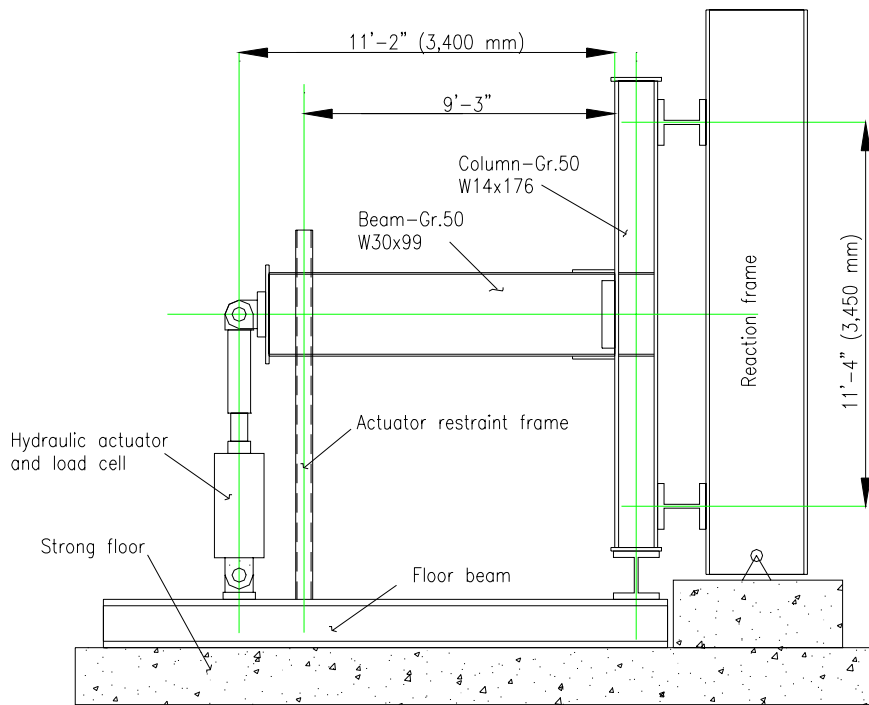


Figure 3-1 SAC Phase II test fixture

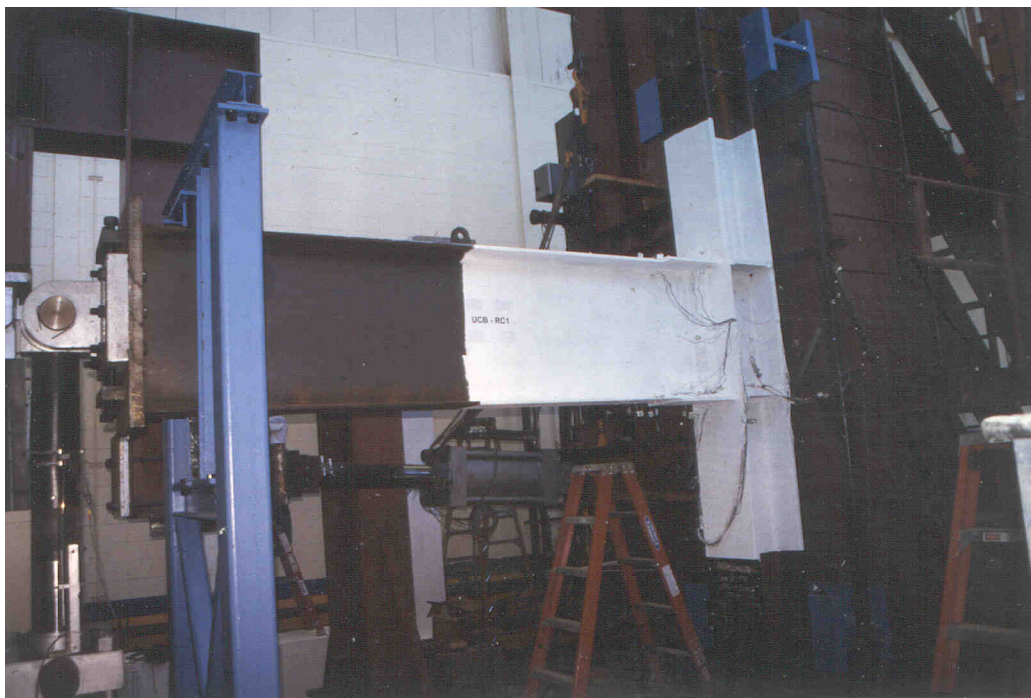


Figure 3-2 Photograph of SAC Phase II test fixture

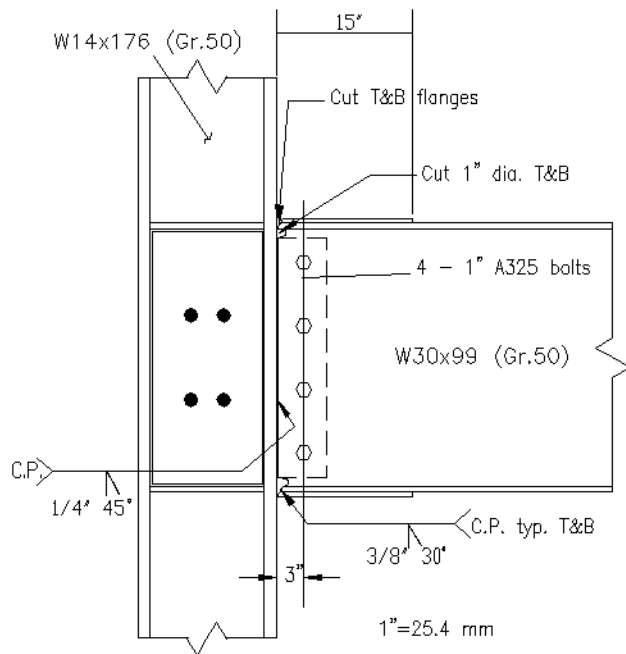


Figure 3-3 Typical SAC Phase II cover-plate connection details

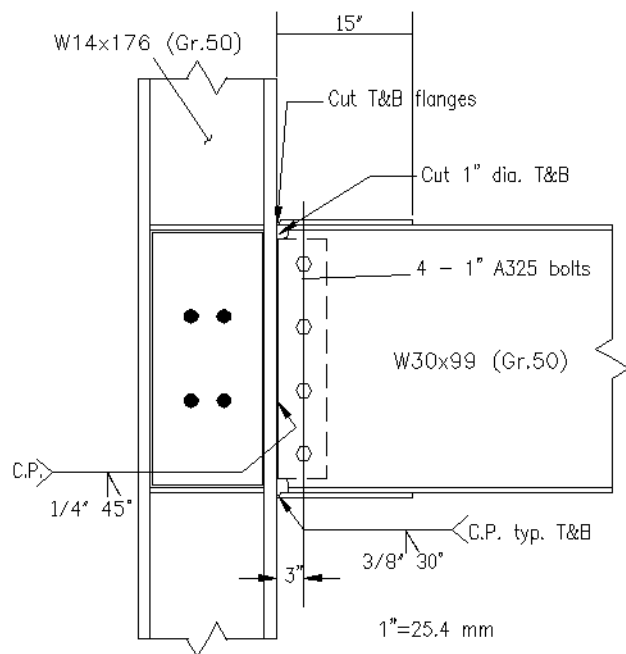


Figure 3-4 Typical SAC Phase II flange-plate connection details

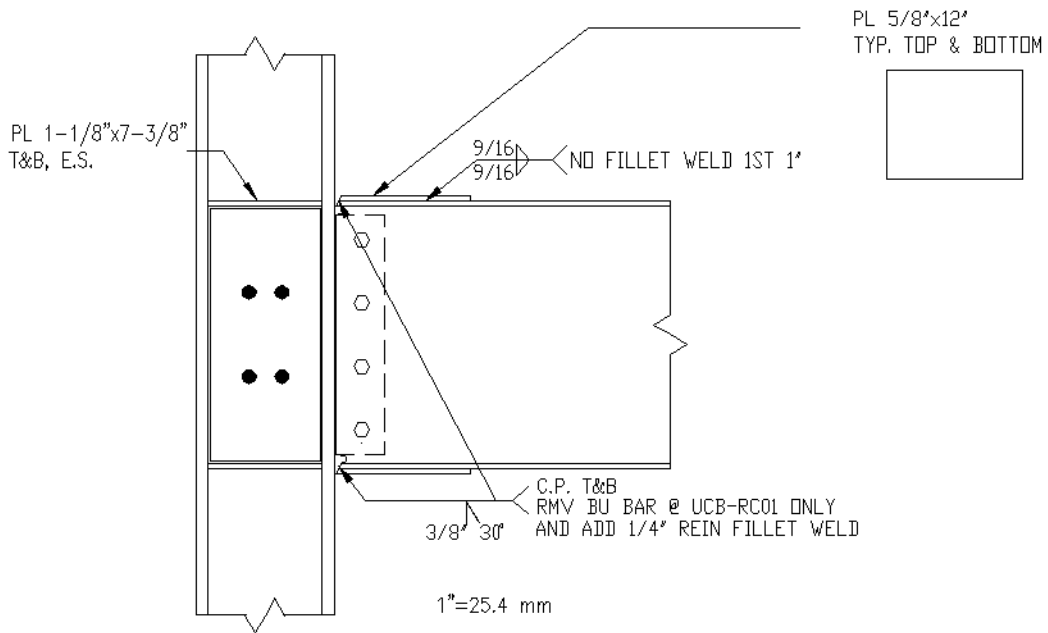


Figure 3-5 Construction details for RC01 and RC02

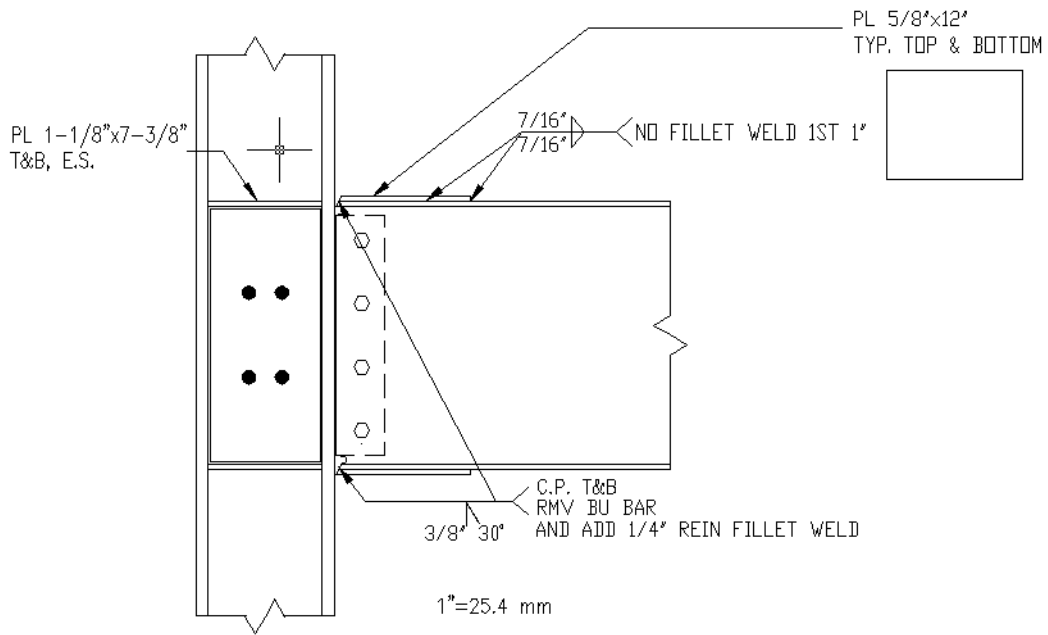


Figure 3-6 Construction details for RC03

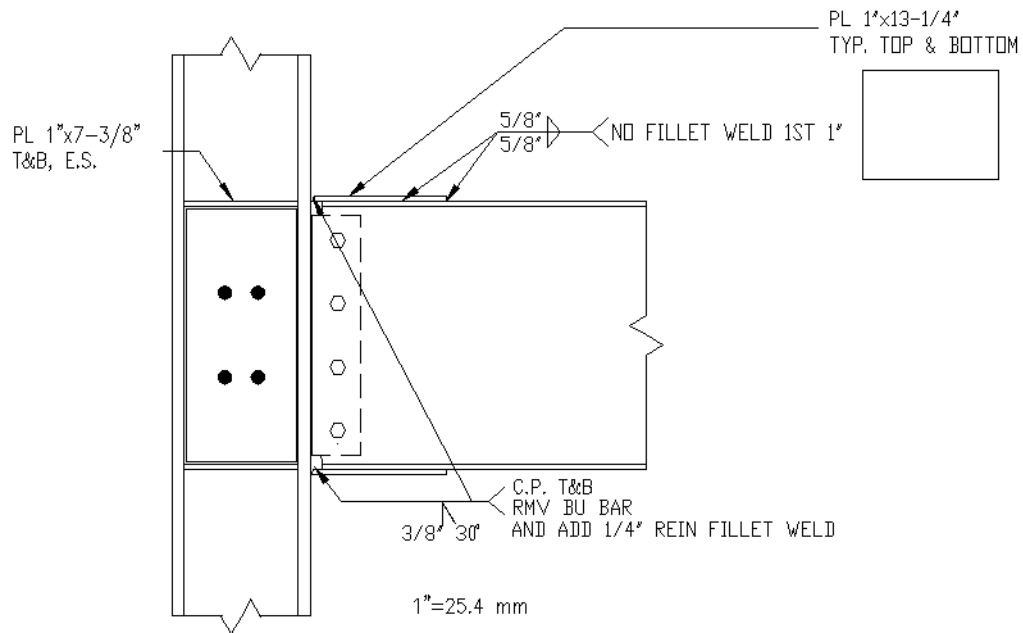


Figure 3-9 Construction details for RC06 and RC07

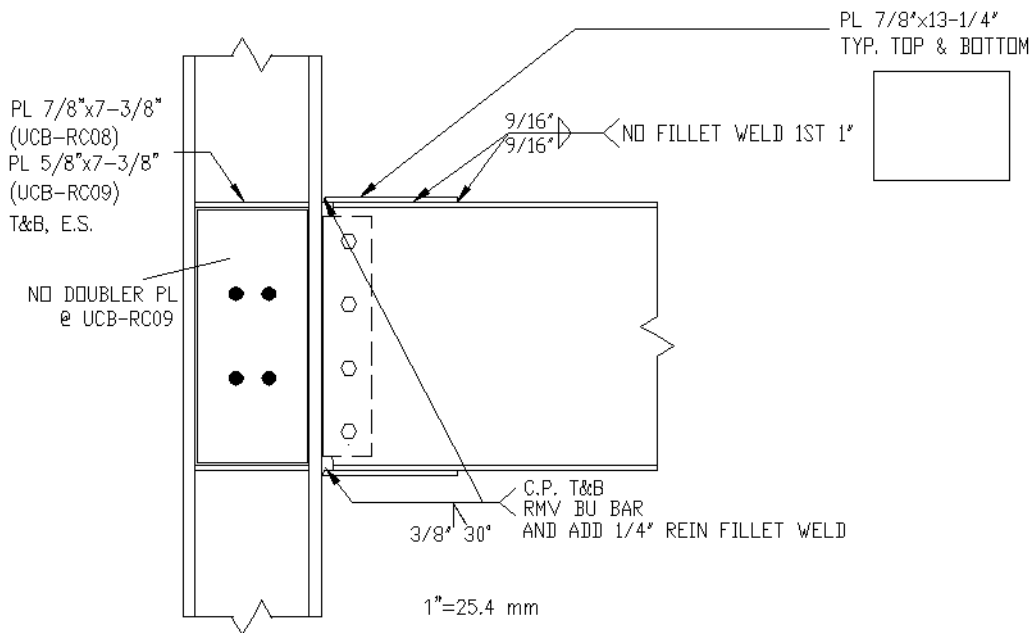


Figure 3-10 Construction details for RC08 and RC09

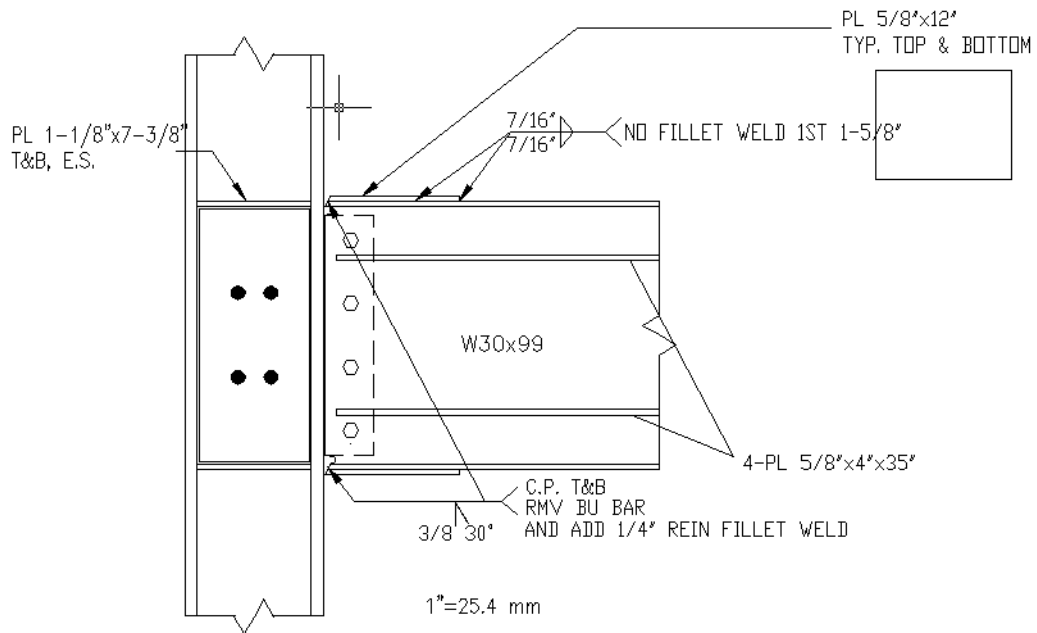


Figure 3-11 Construction details for RC10

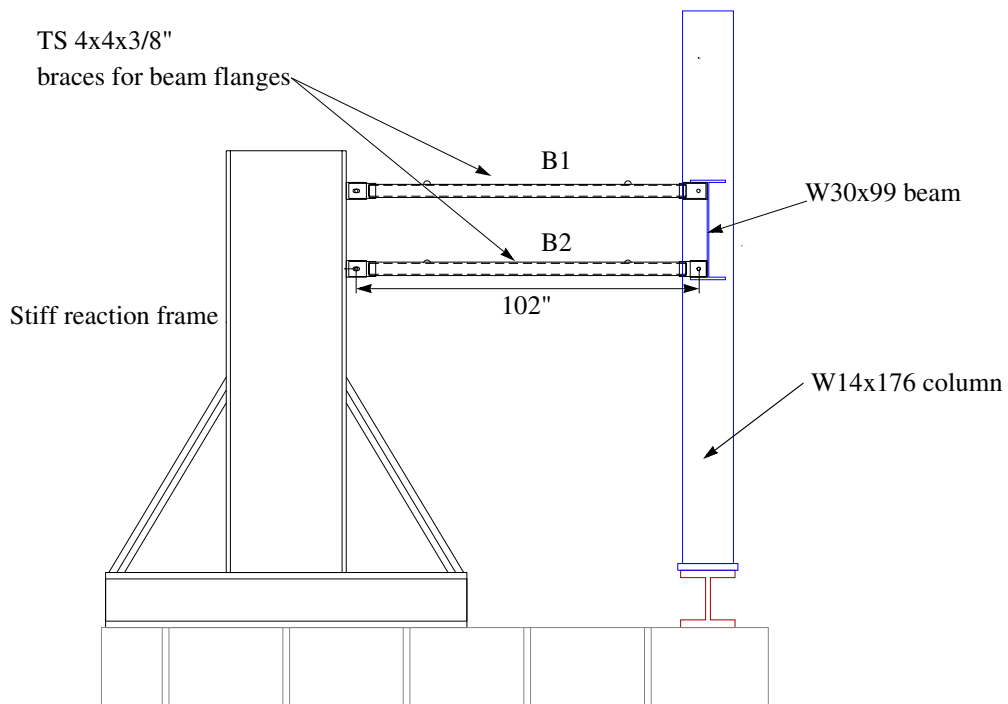
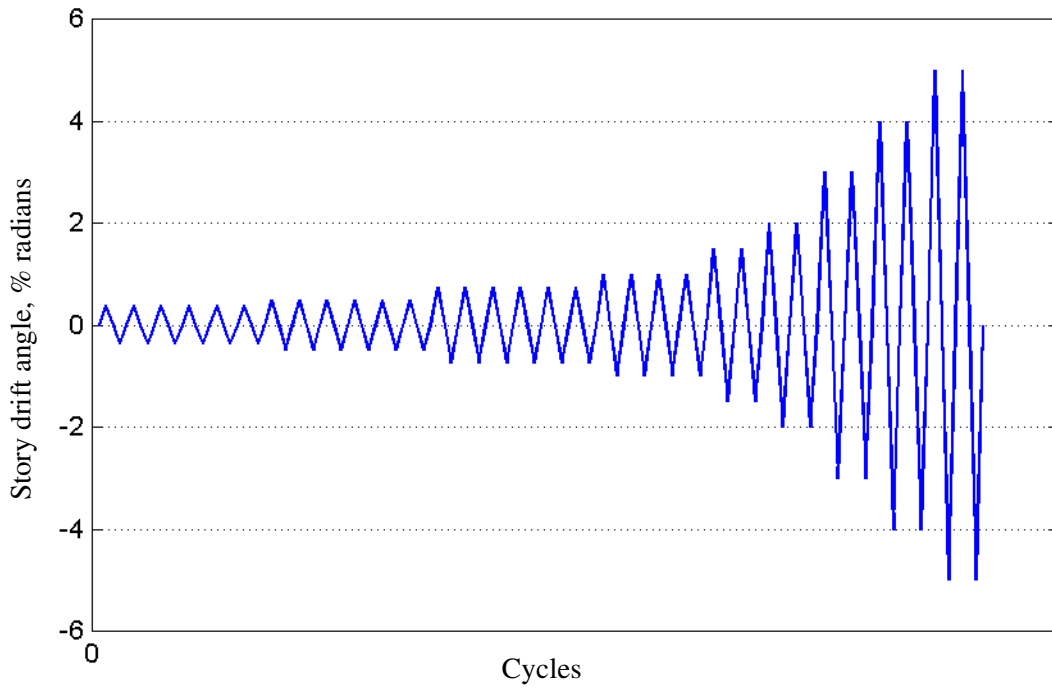
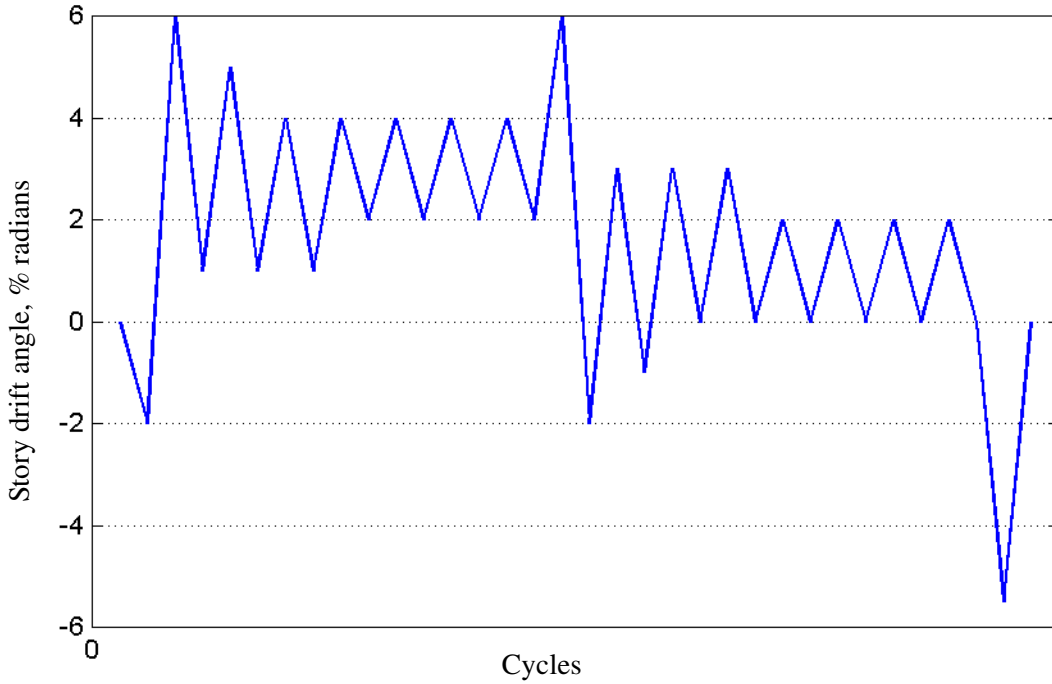


Figure 3-12 Restraint to lateral-torsional buckling of RC02 at 35 in. from the face of column



a. cyclic displacement history for RC01-RC06 and RC08-RC10



b. near-field displacement history for RC07

Figure 3-13 Loading histories for SAC Phase II specimens

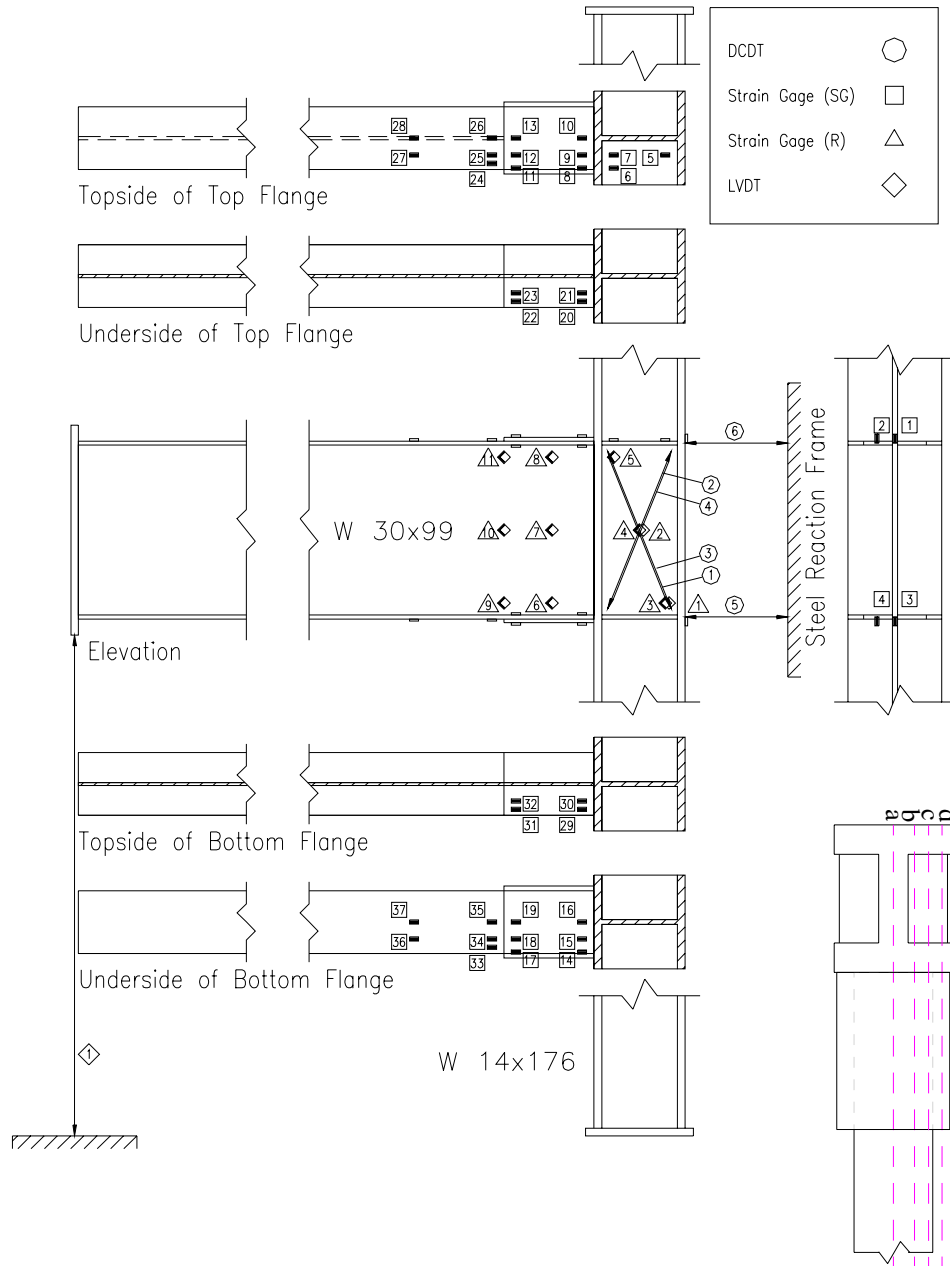


Figure 3-14 Instrumentation for specimens RC01, RC02, and RC03

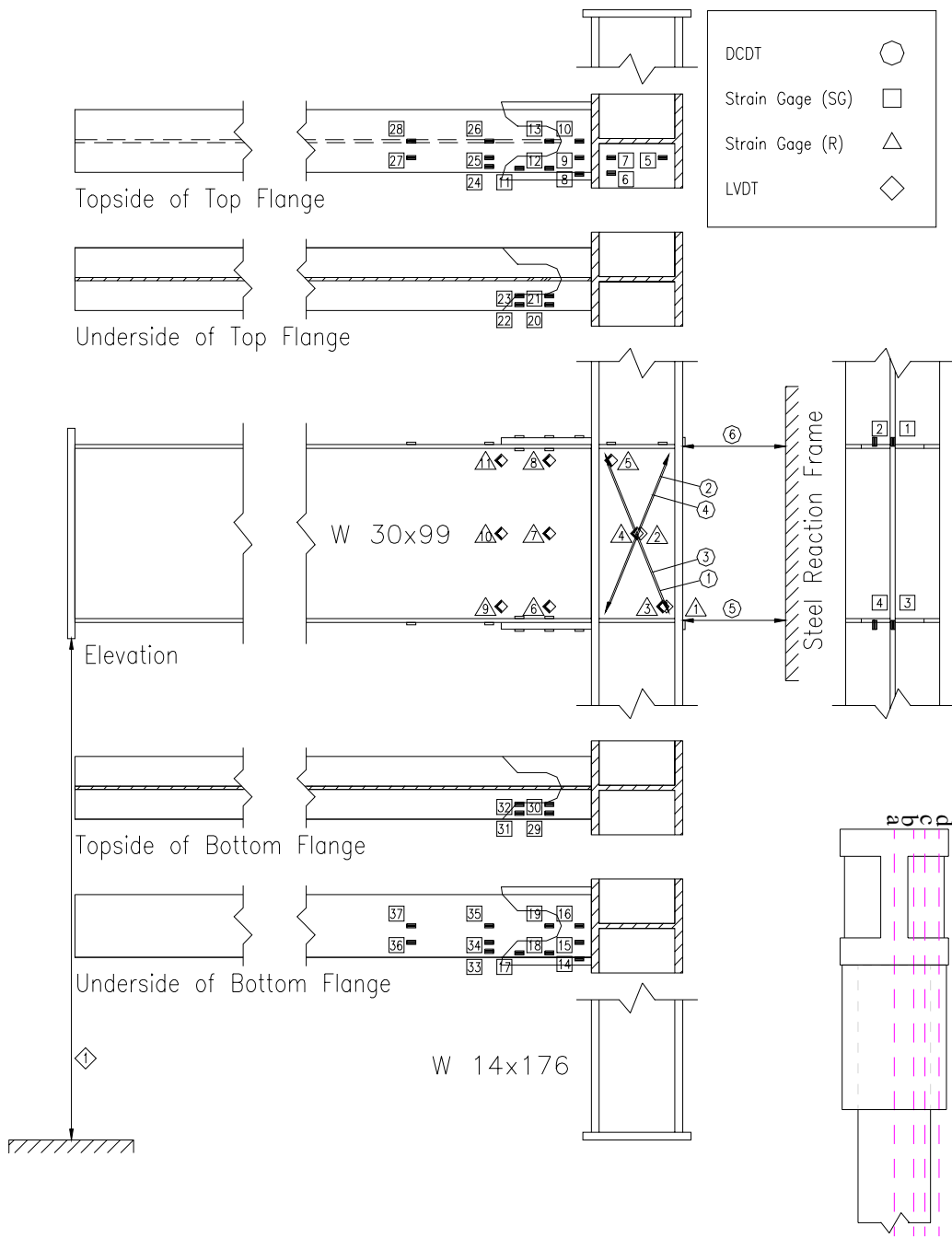


Figure 3-15 Instrumentation for specimen RC04

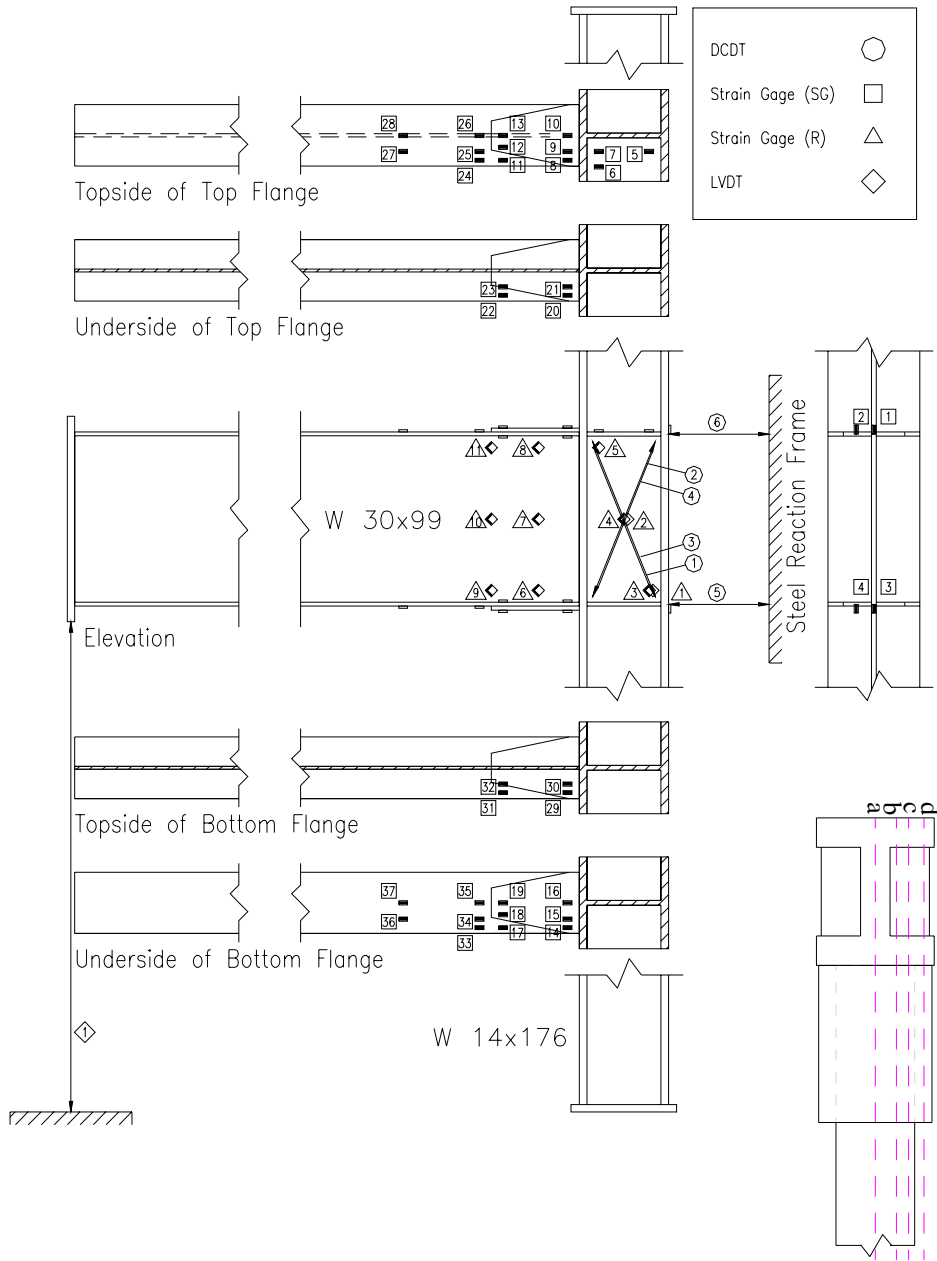


Figure 3-16 Instrumentation for specimen RC05

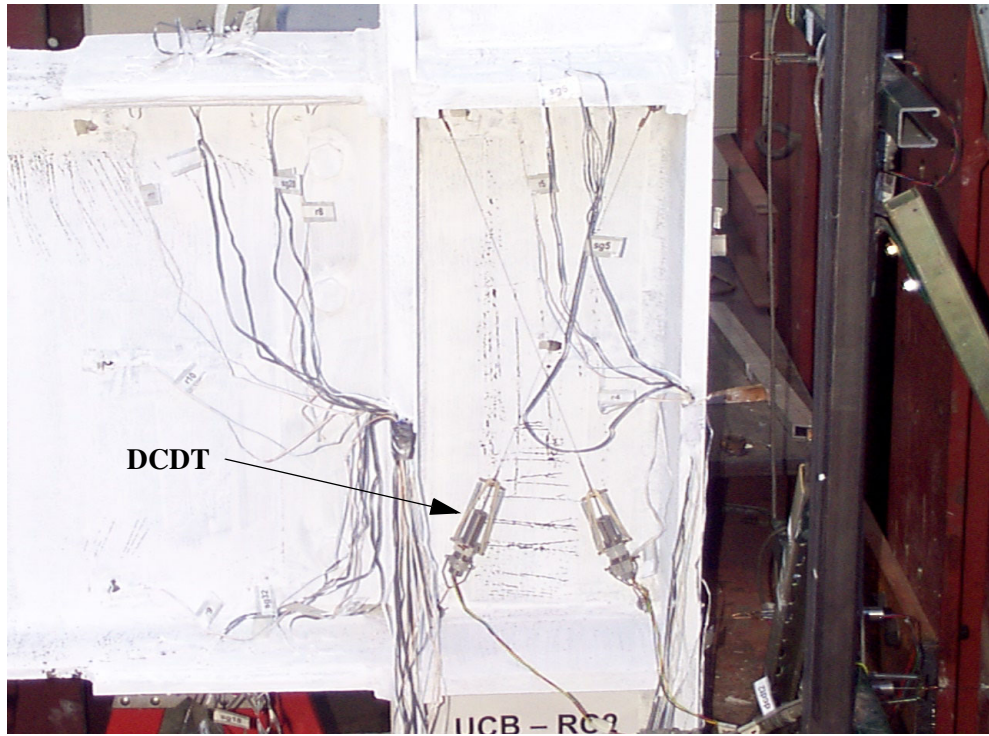


Figure 3-17 Instrumentation of panel zone for Specimen RC02

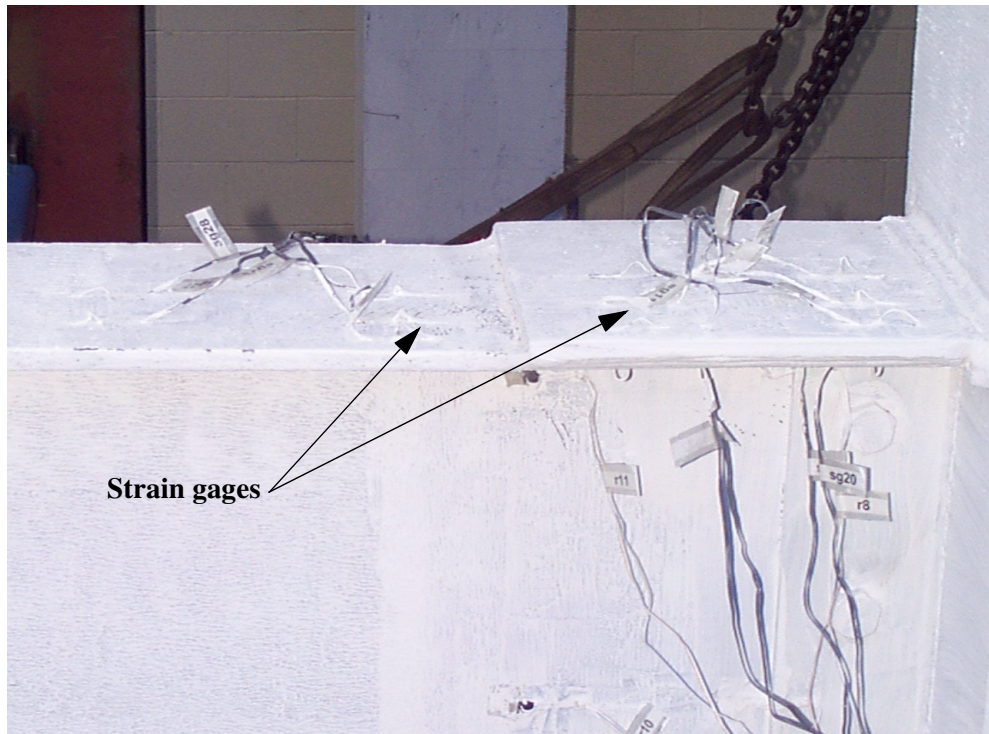


Figure 3-18 Instrumentation of top cover plate and beam flange for specimen RC02

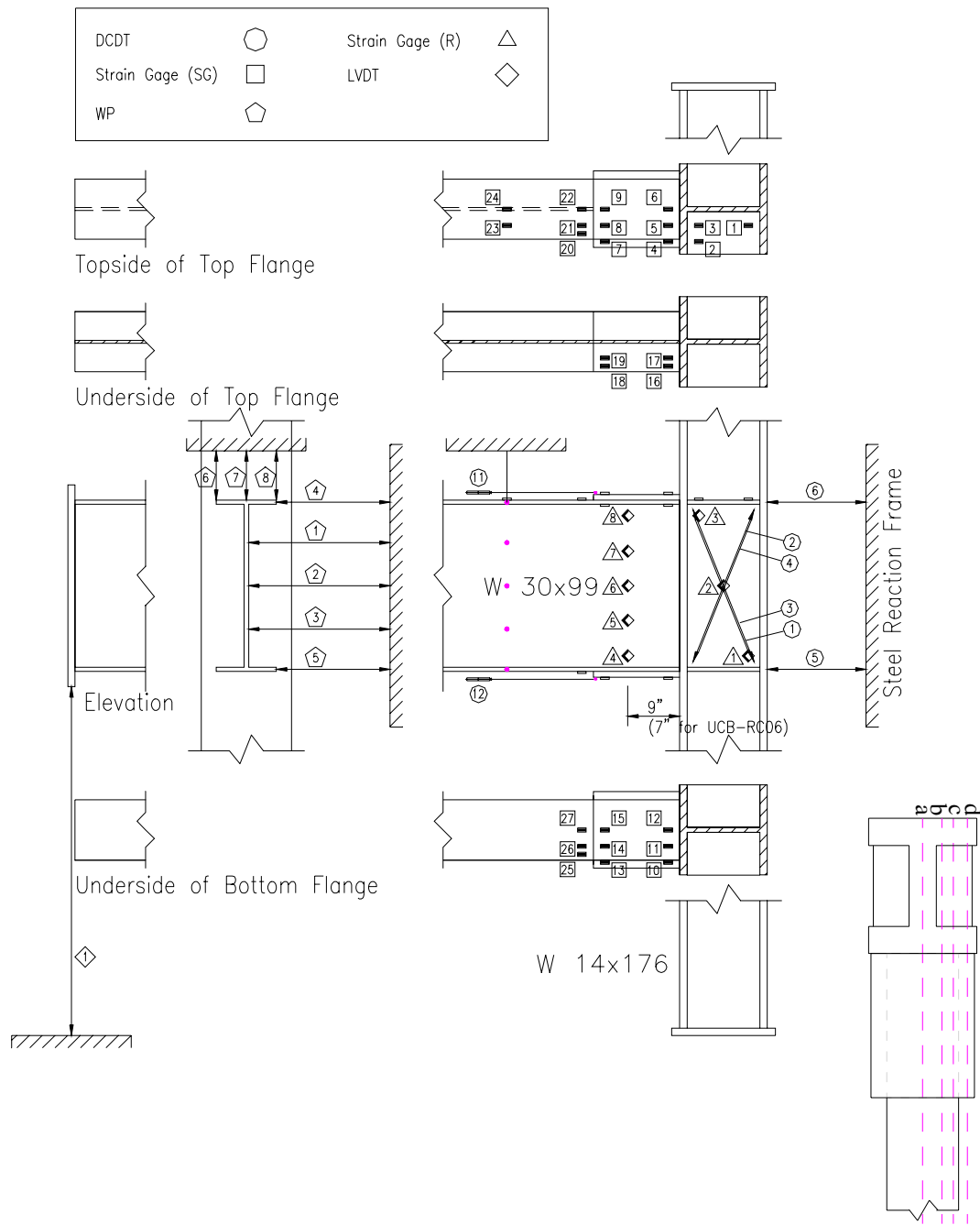


Figure 3-19 Instrumentation for specimens RC06, RC07, RC08, and RC09

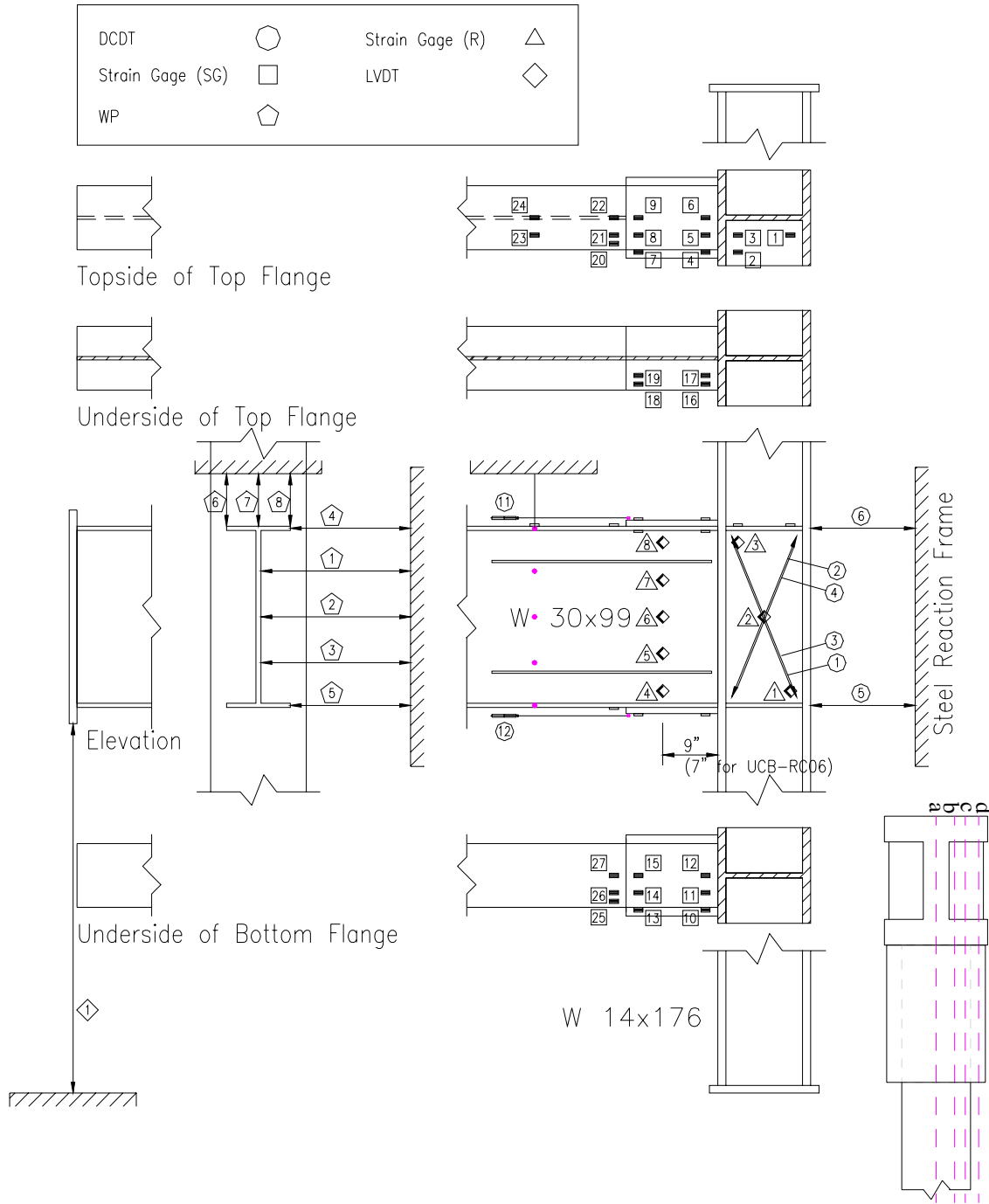


Figure 3-20 Instrumentation for specimen RC10

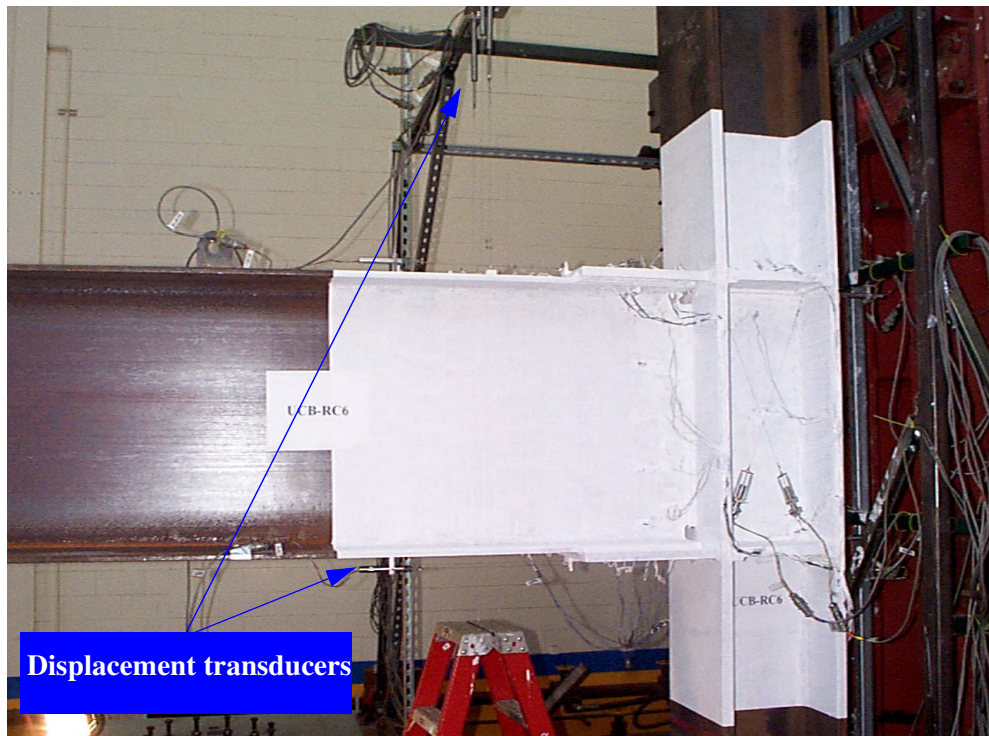


Figure 3-21 Instrumentation of specimen RC06

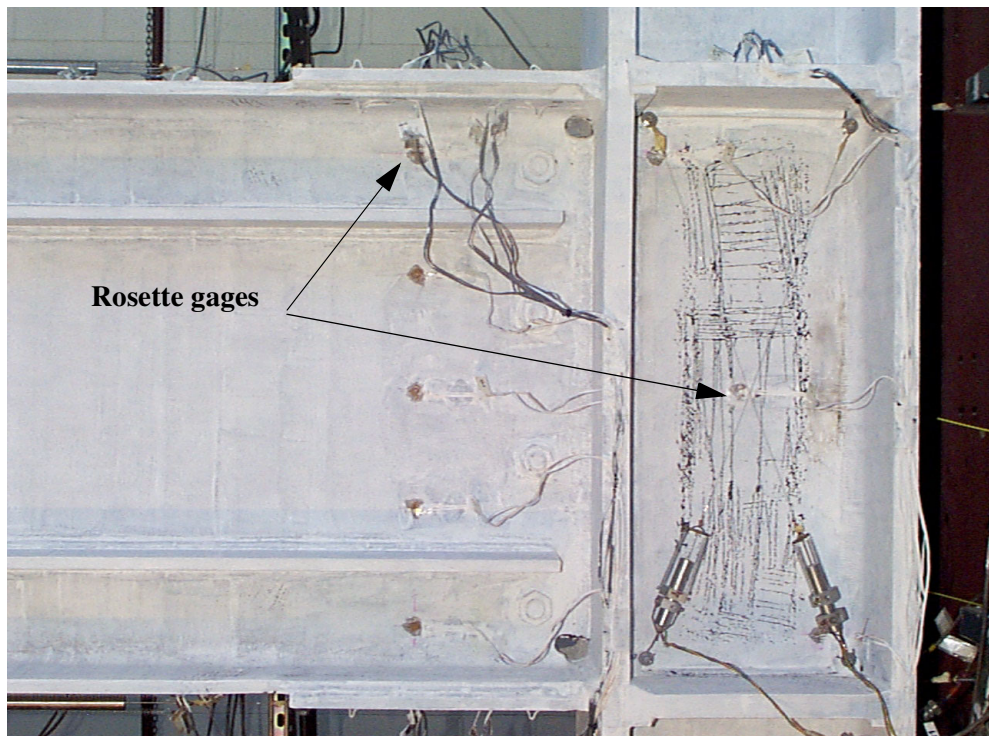


Figure 3-22 Instrumentation of specimen RC10

4 Finite Element Analysis of Reinforced Connections

4.1 Introduction

Version 5.8 of the general purpose nonlinear finite element program ABAQUS (HKS 1998) was used to model eight of the ten beam-column reinforced connections described in Chapter 3: RC01, RC03, RC04, RC05, RC06, RC08, RC09, and RC10. These *preliminary* models were prepared and analyzed prior to fabrication of the test specimens. Expected material properties were used because mill and coupon data were unavailable at that time. The primary objectives of the preliminary analyses were to (1) identify zones of high stress and strain in the test specimens, (2) understand the likely sequence of yielding in the test specimens, (3) ascertain whether the design procedures of FEMA 267A (FEMA 1995b) were appropriate for reinforced connections, and (4) determine if the strain conditions in reinforced connections were substantially better than those in unreinforced (pre-Northridge) connections. To address item (4), a mathematical model of an unreinforced connection, termed RC00, was also prepared and analyzed.

At the completion of the testing program described in Chapter 5, coupons were extracted from specimen RC10, and accurate estimates of the beam and column material properties were established. Seven (RC01, RC03, RC05, RC06, RC08, RC09, and RC00) of the eight mathematical models were updated and reanalyzed. Only the results of the reanalysis work are presented in this chapter.

The procedures used to prepare the two finite element (one solid-element and one shell-element) models are described in Section 4.3. The damage and response indices used to evaluate the behavior of the specimens are described in Section 4.4.

Nonlinear finite element analysis can provide considerable insight into the likely behavior of complex connections such as those discussed in this report, but such analysis has significant limitations because material imperfections, geometric imperfections, residual stresses and strains, and flaws or defects cannot be modeled a priori. These limitations may substantially impact the global behavior of a reinforced connection. However, limitations aside, nonlinear finite element analysis can be used to both better understand states of stress and strain in reinforced connections and to compare the effectiveness of alternate reinforcement plate geometries, fillet welds geometries, panel zone strengths, enhanced beam web connections, and alternate weld-access-hole details. Such information cannot be cost-effectively gathered from full-scale testing. Benchmark data on the response of the unreinforced connection are presented in Section 4.5.

Sections 4.6 through 4.8 present information on the states of stress and strain in the reinforced connections obtained using the solid-element models. (Comparisons of alternate reinforcement plate geometries, fillet welds geometries, panel zone strengths, and enhanced beam web connections, based on nonlinear finite element analysis are presented in Chapter 6.) The results of the shell-element modeling of some of the reinforced connections are presented Section 4.9.

4.2 Material Properties

Data from tests of coupons extracted from the beam and column of RC10 were used to establish the stress-strain relationships for the beam and column elements. Fillet welds composed of E70xx filler metal were modeled using the test data of Kaufmann (1997). For all materials, Young modulus was set equal to 29,000 ksi (200,000 MPa), Poisson's ratio was set equal to 0.3, and kinematic strain hardening was assumed. Table 4-1 presents the material properties adopted for the analytical studies reported in this chapter and Chapter 6.

Table 4-1 Material properties used for the analytical models

<i>Component</i>	<i>Yield Point¹</i>		<i>Ultimate Point¹</i>		<i>Rupture Point¹</i>	
	<i>Stress (ksi)</i> σ_y	<i>Strain (%)</i> ϵ_y	<i>Stress (ksi)</i> σ_u	<i>Strain (%)</i> ϵ_u	<i>Stress (ksi)</i> σ_r	<i>Strain (%)</i> ϵ_r
Beam flange ²	53.5	0.18	71.6	12	53.0	39
Beam web ²	62.0	0.22	73.4	12	63.1	39
Column flange ²	50.8	0.18	73.0	12	53.5	39
Column web ²	56.0	0.18	72.2	12	53.5	39
Reinforcing plates ³	53.0	0.18	72.0	12	53.0	39
Continuity plates ³	53.0	0.18	72.0	12	53.0	39
Fillet welds ³	75.0	0.26	80.0	12	75.0	39

1. See Figure 4-1 for definitions.
2. Data from coupon tests.
3. Assumed values

A trilinear stress-strain relationship was assumed for each of the components identified in Table 4-1. Figure 4-1 shows the assumed trilinear stress-strain relationship.

4.3 Finite Element Models of the Connections

4.3.1 General

Solid-element (Type SOL) models were prepared for RC00, RC01, RC03, RC05, RC06, RC08, and RC09. The beam, column, plates, and fillet welds in these connections were discretized using three-dimensional solid (brick) elements. The groove welds joining the beam to the column, the reinforcing plates to the column flange, and the continuity plates to the column flanges and web were not modeled explicitly. The weld access hole was included in the Type SOL models. The shear tab was not modeled because it served primarily as backing for the groove weld of the beam web to the column flange, and was not fillet welded around its perimeter to the beam web. The SOL models were used to study the stress and strain distributions in these connections at different levels of story drift, and to evaluate selected indices at different levels of story drift. The SOL models were not used to capture local and global instabilities such as flange- and web-local buckling, and lateral-torsional buckling. Because flange and web local buckling were observed in the beams of all ten test specimens at story drift angles greater than 2-percent radian, the results of the analyses using the SOL models are not presented for story drift angles greater than 2-percent radian.

Shell-element (Type SH) models were prepared to study local and global instabilities in the connections because such models are computationally more efficient than solid-element models for this purpose. Type SH models were prepared for RC01, RC02, RC03, and RC06. The beam, column, and plates in these connections were discretized using three-dimensional shell elements. These components were joined by constraining the nodes at common locations to have identical displacements. The weld access hole was included in the Type SH models.

4.3.2 Finite element models Type SOL

4.3.2.1 Finite element mesh

To reduce the computational effort, only one quarter of each specimen was modeled, taking advantage of symmetry and asymmetry in the model. The full model of RC00 is presented in Figure 4-2a. The half model of RC00 is shown in Figure 4-2b; this model takes advantage of symmetry about the x_2 - x_3 plane (y - y axis) of the RC00 beam. The quarter model of RC00 is shown in Figure 4-2c. This model takes advantage of asymmetry about the x_1 - x_2 plane that coincides with the x - x axis of the RC00 beam. Also shown in these figures is the global coordinate system ($1, 2, 3$) used for the analysis. The 2-direction (also referred to as x_2 or y -direction in this chapter) coincides with the longitudinal axis of the beam; the 3-direction (also referred to as x_3 or z -direction in this chapter) coincides with the longitudinal axis of the column. The 1-direction (also referred to as x_1 or x -direction in this chapter) is defined by the right-hand-screw rule, and is parallel to the beam and column flanges.

The ABAQUS *symmetric* boundary condition about the plane x_2 - x_3 constrains the displacement along the x_1 -axis and rotations (first derivative of the displacement) about the x_2 - and x_3 -axes to be zero. The ABAQUS *asymmetric* boundary condition about the x_1 - x_2 plane constrains the displacements along the x_1 -axis and x_2 -axis and rotations about the x_3 -axis to be zero. Figure 4-2d shows the quarter model of the beam in the (1, 2, 3) coordinate system. The constraints on the x_2 - x_3 and x_1 - x_2 planes are also shown in this figure.

Following the approach adopted by El-Tawil et al. (1998), a reduced integration algorithm was used to compute the tangent stiffness matrix of the eight-node solid elements. El-Tawil noted that this method reduced substantially the computational effort with no loss of accuracy. To avoid uncontrolled mesh distortion that is associated with the use of this algorithm, the feature in ABAQUS that controls hourglass (zero stiffness) modes was used for the Type SOL model studies.

The size of the finite element mesh varied over the length and height of the specimen. A fine mesh was used near the connection of the beam to the column and the beam flange to the reinforcing plate. A coarser mesh was used elsewhere. Most of the solid elements were right-angle prisms. The smallest element dimension was 1/4 in. (6 mm). The largest element dimension was 8 in. (203 mm) at the end of the column. Several transition zones were used. In the quarter model, only half of the height and width of the column and half of the depth and width of the beam were modeled. The discussion below is for the quarter model only.

Beam flanges were modeled using 4 layers of elements through the flange depth and 10 elements across the flange half-width. This choice of element size was based on the studies of El-Tawil et al. (1998). The beam web was modeled using 1 element through the (half) thickness and fourteen elements along the (half) height (from the underside of the flange). The beam k-line region was modeled with 2 layers of elements (one six-node and one eight-node) to provide a smooth transition between beam web and beam flange elements. Eight-node rectangular and six-node triangular solid prisms were used to transition the beam mesh near the column face and to model the shape of the weld access (cope) hole. Figure 4-3a is a cross section through the beam showing the discretization of the flange, web, and k-line regions. Figures 4-3b and 4-3c show the mesh in the vicinity of the weld access hole (elevation) and the nose of the reinforcing plate (plan), respectively.

The column flange near the beam was discretized into 15 elements across its (half) width and 4 elements through its thickness. The column flange remote from the beam was discretized into 14 elements across its (half) width and 2 elements through its thickness. The column web was modeled using 1 element through its (half) thickness and 22 elements along its depth. The doubler plate was included in the model by adding one layer of elements over the depth of the column web with a thickness equal to one-half the thickness of the doubler plate. Figure 4-3d is a cross section through the (half) column at the level of the beam flange. The continuity plates in the column opposite the beam flange-reinforcing plate assembly were modeled using 7 layers of elements per plate for specimen RC03 (the number of layers varied for different specimens), but are not shown in the figure.

The reinforcing plate was modeled with 4 elements through the thickness; the mesh across the width of the plates matched that of the beam flange. The fillet welds that joined the plate to the flange were modeled using 1 layer of six-node and 1 layer of eight-node solid elements. Figure 4-4a is a cross section through the reinforcing plate, longitudinal fillet weld, and beam flange; the plate and the fillet weld are shown shaded. Figure 4-4b is a cross section through the reinforcing plate parallel to the longitudinal axis of the beam. The reinforcing plate, transverse fillet weld (for RC03) and beam flange are shown in this figure. Surface contact between the beam flange and the reinforcing plate was ignored for the studies reported herein to substantially improve the computational efficiency of the analysis. Trial studies accounting for such surface contact showed little change in the key stress and strain results.

4.3.3 *Finite element models Type SH*

4.3.3.1 Finite element mesh

The Type SH models used for these studies described below consisted of 4-node reduced-integration shell elements (S4R5 elements in ABAQUS). Such elements were successfully employed by El-Tawil et al. (1998) for a related study funded by the SAC Joint Venture. The lengths of the shell elements varied over the height and length of the specimen. A relatively fine mesh was used near the connection of the beam to the column and the beam flange to the reinforcing plate. The smallest element dimension was 1.25 in. (31 mm) and the smallest element measured 1.25 in. by 1.25 in. (in plane). The largest element dimension was 8 in. (203 mm) at the end of the column.

The beam flanges and web were modeled using 8 elements across the width and 22 elements over the depth, respectively. (Inelastic mesh convergence studies by El-Tawil et al. showed that the use of 6 S4R5 elements across the width of the beam flange produced similar global results to meshes with 8 and 12 elements across the width of the beam flange. El-Tawil et al. used 6 elements across the width of the beam flange for their studies.) The column flanges and web were modeled with 12 elements across the width and 10 elements over the depth, respectively. The thickness of the column web elements in the panel zone was increased to account for the doubler plate. The mesh for the continuity plates matched the meshes for the beam flanges and the column web. The reinforcement-plate meshes also matched the meshes used for the beam flanges. The fillet welds joining the plates to the flanges were not modeled explicitly. Rather, the nodes of common location to the reinforcement plates and the beam flanges were constrained to have identical displacements. Figure 4-5a is an isometric view of the complete shell model. Figure 4-5b is an end view of the beam and the reinforcing plates.

4.3.3.2 Buckled shape of Type SH models

Geometric nonlinearity can substantially affect the load-displacement relationship for steel wide-flange components. To evaluate these effects, eigenvalue analysis was used to (1) compute the critical buckling load of the specimen, and (2) characterize the buckled mode shapes of the specimen. Meshing studies in the vicinity of the buckled zone are typically required to ensure that the estimate of the buckling load has converged. Such studies were performed as part of this

analysis. Following convergence of the buckling load, imperfections were introduced in the refined mesh at locations determined from the elastic analysis. The second stage of the analysis involved the calculation of a load-displacement curve for the specimen, using the Riks method (HKS 1998) to handle possible instabilities.

The distribution of geometric imperfections in the Type SH models matched the first eigenvector of the loaded connection configuration. The maximum imperfection was chosen as 1 percent of the flange thickness. (The studies of El-Tawil et al. showed that the results were not particularly sensitive to the magnitude of the imperfections.)

The elastic buckled shape of RC03 corresponding to the first eigenvector is shown in Figure 4-6. An isometric view of the deformed shape of the beam cross section showing inelastic buckling of the beam flange and web is presented in Figure 4-7.

4.3.4 *Boundary conditions and applied loading*

Two lines of nodes at each end of the column were restrained against translation only (i.e., a pinned connection) to approximately replicate the support conditions used for the laboratory tests described in the following chapter. Use of the pin-roller connections of El-Tawil et al. (1998) was not possible because of the symmetry conditions associated with the use of the quarter Type SOL model. A vertical displacement history was imposed at the free end of the beam using the displacement-control feature in ABAQUS. The corresponding history of the applied load was back-calculated from the support-reaction histories.

Restraint of lateral movement of the beam and column webs and flanges was provided for the Type SOL models by virtue of the fact that displacements of the beam web centerline in the *I*-direction were set equal to zero. For all Type SH models, lateral movement (*I*-direction) of the flanges of the beam was prevented at the free end of the beam, replicating approximately the lateral restraint provided by the frame near the actuator. For the Type SH model of specimen RC02, three conditions of lateral restraint of the beam flanges were considered to study the effect of lateral-torsional buckling on the response of reinforced steel moment-resisting connections.

4.4 **Damage and Response Indices**

In a text entitled *A Course on Damage Mechanics*, Lemaitre (1996) identified five different manifestations of damage: (1) brittle damage, (2) ductile damage, (3) creep damage, (4) low-cycle fatigue damage, and (5) high-cycle fatigue damage. Because brittle, ductile, and low-cycle fatigue damage can affect the seismic behavior of steel beam-column connections in buildings, each is introduced below, reproducing much of the text of Lemaitre (1996).

Brittle damage: Damage is called *brittle* when a crack is initiated at the mesoscale without a large amount of plastic strain, say if the ratio of plastic strain to elastic strain is below unity. This means that the cleavage forces are below the forces that could produce slips (plastic strain) but are higher than the debonding forces. The degree of localization is high.

Ductile damage: Damage is termed *ductile* when it occurs simultaneously with plastic deformations larger than a damage threshold plastic strain. Such damage results from the nucleation of cavities (microvoids) due to decohesions between inclusions and the matrix followed by their growth and coalescence through plastic instability. The degree of localization is comparable to that of plastic strain.

Low-cycle fatigue damage: When a material is subjected to cyclic loading at high values of stress or strain, damage develops together with cyclic plastic strain after a period of incubation preceding the phases of nucleation and propagation of microcracks. The degree of localization is higher than for ductile damage. Low-cycle fatigue is characterized by low values of the number of cycles to rupture. If the material is loaded under strain control, the damage induces a drop in the stress amplitude.

Five response indices are used in the studies reported in this chapter and in Chapter 6 to identify potential sites of *brittle* and *ductile* fracture: Pressure Index, Mises Index, Equivalent Plastic Strain Index, Triaxiality Index, and Rupture Index. These indices were used by El-Tawil et al. (1998) for finite element studies of the strength and ductility of fully restrained steel beam-column connections. Information on each of these indices follows. No robust indices are available for predicting low-cycle fatigue damage.

Pressure Index: The Pressure Index (*PI*) is defined as the ratio of the hydrostatic stress (σ_m) divided by the yield stress (σ_y), where the hydrostatic stress is defined as the negative of one-third of the first invariant (trace) of the stress tensor (σ_{ij}):

$$\sigma_m = \mathbb{D}\frac{1}{3}\text{trace}(\sigma_{ij}) = \mathbb{D}\frac{1}{3}\sigma_{ii} \quad (4-1)$$

where i and j represent the global directions ($1, 2, 3$). A large *tensile* (negative) hydrostatic stress is often accompanied by large principal stresses and generally implies a greater potential for either *brittle* or *ductile* fracture. In the presence of a crack or defect, large *tensile* hydrostatic stress (or pressures) can produce large stress intensity factors at the tip of the crack or defect, and increase the likelihood of *brittle* fracture. A large *tensile* hydrostatic stress can lead to rapid damage accumulation in metals due to microvoid nucleation, growth, and coalescence (*ductile* fracture) and a substantial reduction in component ductility. For information, a large compressive hydrostatic stress can produce large increases in the ductility of tension specimens (Hancock and Mackenzie 1976; Thomason 1990).

Mises Index: The Mises Index (*MI*) is defined as the Mises stress ($\bar{\sigma}$) divided by the yield stress (σ_y), where the Mises stress is defined as the second invariant of the deviatoric stress tensor:

$$\bar{\sigma} = \sqrt{\frac{3}{2}S_{ij}S_{ij}} \quad (4-2)$$

where S_{ij} are the deviatoric stress components, which are calculated as $S_{ij} = \sigma_{ij} + \sigma_m \delta_{ij}$.

PEEQ Index: The equivalent plastic strain index (PEEQI) is defined as the equivalent plastic strain (PEEQ in ABAQUS) divided by the yield strain (= 0.0018). The equivalent plastic strain is the second invariant of the plastic strain tensor and is calculated as

$$PEEQ = \sqrt{\frac{2}{3} \varepsilon_{ij}^p \varepsilon_{ij}^p} \quad (4-3)$$

where ε_{ij}^p are the plastic strain components. The index is a measure of ductility at the local level (El-Tawil et al. 1998).

Triaxiality Index: The Triaxiality Index (*TI*) is defined as the hydrostatic stress (σ_m) divided by the Mises stress ($\bar{\sigma}$), that is,

$$TI = \frac{PI}{MI} \quad (4-4)$$

Lemaitre (1996) describes the important effect that this index has on the *ductile* rupture of metals. El-Tawil et al. (1998) report that (1) values of *TI* between 0.75 and 1.5 can cause large reductions in the rupture strain of metals and (2) values of *TI* greater than 1.5 can trigger *brittle* fracture.

Rupture Index: The definition of the Rupture Index (*RI*) used in this study is identical to that adopted by El-Tawil et al. (1998), namely,

$$RI = a \frac{PEEQ}{\varepsilon_r} = \frac{PEEQ}{\exp\left(1.5 \frac{\sigma_m}{\bar{\sigma}}\right)} \quad (4-5)$$

where a is a material constant, ε_r is the rupture strain (see Figure 4-1), and other terms are defined above. In this equation, hydrostatic compression is positive. The strain at *ductile* fracture (rupture) given by Hancock and Mackenzie (1976) and adopted by El-Tawil et al. is

$$\varepsilon_r = a \exp\left(1.5 \frac{\sigma_m}{\bar{\sigma}}\right) \quad (4-6)$$

where hydrostatic compression increases the rupture strain and hydrostatic tension decreases the rupture strain. El-Tawil et al. note that (4-5) can be used to compare the likelihood of ductile fracture either in a single specimen at several critical locations or between different specimens.

4.5 Unreinforced Connection RC00 (Model Type SOL)

4.5.1 General

For each connection discussed in this section and the following two sections, response data are presented at three levels of story drift index, which is defined as the displacement of the beam tip divided by the distance between the beam tip and the column centerline (=141 in or 3.6 m). The three story drift indices are: 0.5 percent (elastic response); 1 percent (minor inelastic response), and 2 percent (substantial inelastic response). Data are not presented for story drift indices greater than 2 percent because flange- and web-local buckling at story drift indices slightly greater than 2 percent render the Type SOL models inaccurate. Direct comparisons between the responses of the

unreinforced (RC00) and reinforced connections can be made at each drift level because the addition of the reinforcement plates add only modest stiffness to the specimens, and the deformations and displacements in the reinforced connections are likely most similar to those of the unreinforced connection (assuming that RC00 could develop significant plastic deformation). The quarter beam of RC00 was loaded in the plus 3-direction (see Figure 4-2) to introduce tension in the beam top flange.

4.5.2 Beam-column shear force transfer

It is well documented that the transfer of shear force from the beam to the column in steel moment-resisting connections does not follow elementary beam theory. Table 4-2 shows the distribution of shear force in the web and flange of the beam as a function of distance from the column face. Figure 4-8 shows the distribution over the beam depth at $D/60$, $D/10$, and $D/2$ from column face, where D is the beam depth. At the face of the column, approximately one half of the shear force in the beam is transferred to the column via the beam flanges. Such shear forces in the flanges produce local bending effects that cannot be captured by simple elastic analysis. The distribution of shear force in the beam approaches that predicted by beam theory at a distance of approximately $D/4$ from the face of the column.

The subject of shear-force transfer from reinforced W30x99 beams to W14x176 columns is further discussed in Chapter 6 wherein the influence of added plate reinforcement to the beam web (to improve the shear-force transfer) and the beam flanges (to protect the beam-column connection) on the distribution of shear force in the beam at the face of the column are presented.

Table 4-2 Elastic distribution of shear force in beam flanges and beam web of RC00

<i>Location</i> ¹	<i>% Shear in Web</i>	<i>% Shear in Flanges</i>
$D/60$	54	46
$D/10$	87	13
$D/4$	97	3
$D/2$	97	3
$3D/2$	97	3
Beam Theory	97	3

1. Distance from column face; D = beam depth

4.5.3 Response indices

The response of specimen RC00 is described below using the stress and strain indices of Section 4.4. ABAQUS data are reported for the top surface of the (half) beam flange at the face of the column. The maximum values of stress and strain along this line were not necessarily the maximum values in the specimen, but this line was chosen to facilitate a comparison of results for different specimens. Maximum values of the Pressure Index, Mises Index, Triaxiality Index, and Rupture Index at story drifts of 0.5, 1, and 2 percent for RC00 are presented in Section 4.8.

Figure 4-9 presents the distribution of normal stress S_{22} near the top surface of the beam flange as a function of distance from the face of the column, at story drifts of 0.5, 1, and 2 percent. Figure 4-9a shows the distribution along the beam web centerline. Figure 4-9b shows the distribution 1 in. (25 mm) from the edge of the flange. At 0.5-percent story drift, the distributions are linear and follow elementary beam theory beyond 10 in. (254 mm) from the face of the column. Near the face of the column, the values of S_{22} rise sharply due to secondary flexural stresses that result from the transfer of shear force in the beam to the column via the beam flange.

Figure 4-10 presents the distributions of normal stresses S_{11} , S_{22} , and S_{33} , and the distribution of Mises Index across the half width of the top of the beam flange, at the face of the column, at story drifts of 0.5, 1, and 2 percent. Figure 4-11 presents the corresponding distributions of Equivalent Plastic Strain Index, Pressure Index, Triaxiality Index, and Rupture Index. Normal stress S_{22} is maximized at the centerline of the beam. Localized yielding is evident near the beam web centerline at 0.5-percent story drift. Normal stresses S_{11} and S_{33} are approximately one-half and one-quarter of the normal stress S_{22} , respectively, at a story drift of 2 percent. The Equivalent Plastic Strain Index is large, with a maximum value of 20, at a story drift of 2 percent. The peak value is recorded at the edge of the beam flange; the maximum value at the beam web centerline is approximately 13. The maximum value of the Triaxiality Index is approximately 0.8: such a value may cause a reduction in the rupture strain according to El-Tawil et al. (1998). Because the Triaxiality Index is essentially constant across the width of the beam flange, the Rupture Index distribution is similar in profile to that of the Equivalent Plastic Strain Index. The maximum value of the Rupture Index is 0.1 at 2-percent story drift.

Figure 4-12 presents contour plots of the Rupture Index at 2-percent story drift on two planes through the beam (half) flange: immediately above the toe of the weld access hole (Figure 4-12a) and at the beam flange-column flange interface (Figure 4-12b). The axes in this figure are Rupture Index, distance from the centerline of the beam web, and distance from the top surface of the beam flange. The inset in each figure provides additional locator information. Near the toe of the weld access hole, the Rupture Index approaches 0.2: a value twice as large as the maximum value in the beam flange at the face of the column. Large values of the Index are recorded in the immediate vicinity of the weld access hole; much smaller values are recorded in the beam flange on this plane more than 2 in. (51 mm) from the beam web centerline. These data suggest that careful preparation of the weld access hole is required to avoid the introduction of defects or flaws into the cross section that could serve as crack initiation sites. At the face of the column, the maximum values of the Rupture Index occur on the top surface of the beam; see Figure 4-11d for more information.

The distribution of normal stress S_{22} normalized by an assumed yield strength of 53.5 ksi (369 MPa), Mises Index, Equivalent Plastic Strain Index, Pressure Index, Triaxiality Index, and Rupture Index on the underside of the beam (half) flange at the toe of the weld access hole are shown in Figure 4-13. The maximum values of S_{22} , Mises Index, Equivalent Plastic Strain Index, and Rupture Index were greater at the toe of the weld access hole than at the face of the column.

Figure 4-14 shows the distributions of Mises stress (Figure 4-14a), Hydrostatic pressure (Figure 4-14b), and Equivalent Plastic Strain Index (Figure 4-14c) on the beam web centerline, over the first 17 in. (432 mm) of the beam depth, at 2-percent story drift. The values of Mises stress are large (and similar to those recorded in the beam flange) around the weld access hole. The hydrostatic pressure in the beam web below the weld access hole ranges between -30 ksi (-206 MPa) and -40 ksi (-276 MPa): lower than the maximum values recorded in the beam flange (see Figure 4-11b). The Triaxiality Index in the beam web beneath the weld access hole is approximately 0.60: lower than the maximum value recorded in the beam flange (see Figure 4-11c). The maximum value of Equivalent Plastic Strain Index in the beam web immediately below the weld access hole is approximately 36 ($= 0.065/0.0018$): a value substantially greater than the peak value on the top surface of the beam flange. The maximum value of the Rupture Index in the beam web immediately below the weld access hole is approximately 0.025, which is substantially smaller than the maximum value of 0.10 recorded at the edge of the beam-flange outstand. Clearly the geometry of the weld access hole can give rise to large concentrations of strain in the immediate vicinity of the hole, but peak values of the two of the three fracture indices occur in the beam flange. For this unreinforced connection, the critical site for fracture initiation is likely in the beam flange. Nonetheless, improved weld access hole details such as that proposed by Ricles et al. (2000), coupled with robust beam web welding procedures that guarantee high-quality filler metal at each end of the groove-welded web connection, should be adopted for construction.

4.6 Cover-Plate Reinforced Connections (Model Type SOL)

4.6.1 Connection RC01

The response of specimen RC01 is described below using the stress and strain indices of Section 4.4. ABAQUS data are reported at three locations, two on the top surface of the (half) beam flange: face of column; and nose of cover plate. ABAQUS data are also reported on the top surface of the (half width) cover plate. The maximum values of stress and strain along these lines were not necessarily the maximum values in the components, but these lines were chosen to facilitate a comparison of results for different specimens. The maximum values of the Pressure Index, Mises Index, Triaxiality Index, and Rupture Index at story drifts of 0.5, 1, and 2 percent for the cover plate and beam flange of RC01 are presented in Section 4.8. The quarter beam of RC01 was loaded in the plus 3-direction (see Figure 4-2) to introduce tension in the beam top flange and cover plate.

Figures 4-15, 4-16, and 4-17 report the distributions of normal stress S_{22} normalized by an assumed yield strength of 53.5 ksi (369 MPa), Mises Index, Equivalent Plastic Strain Index, Pressure Index, Triaxiality Index, and Rupture Index, at story drifts of 0.5, 1, and 2 percent, for the cover plate at the face of the column, the beam flange at the face of the column, and the beam flange at the nose of the cover plate, respectively. At the face of the column, the values of the Equivalent Plastic Strain Index, Pressure Index, Triaxiality Index, and Rupture Index are greatest at the top of the beam flange, beneath the cover plate. The maximum values of the Equivalent Plastic Strain Index and the Rupture Index in the beam flange are greatest at the nose of the cover

plate, near the end of the longitudinal fillet weld. The maximum value of the Triaxiality Index is recorded on the top surface of the beam above the beam web at the face of the column. In the beam flange at the nose of the cover plate, the Triaxiality Index is greatest at the end of the longitudinal fillet weld.

The utility of adding cover plates to steel moment-resisting connections to delay *brittle* and *ductile* fracture can be measured by comparing the peak values of the Equivalent Plastic Strain Index, Pressure Index, Triaxiality Index, and Rupture Index in the unreinforced and reinforced connections. The peak values of Equivalent Plastic Strain Index and Rupture Index in RC01 are less than one-half of the peak values in the unreinforced connection RC00. The maximum value of the Triaxiality Index in RC01 (= 0.82) is similar to the maximum value recorded in RC00; both maxima were located on the top of the beam flange at the face of the column. These data indicate that the use of cover reinforcing plates in steel moment-resisting connections reduces the likelihood of ductile fracture at the face of the column.

4.6.2 Connection RC03

The response of specimen RC03 is described below using the stress and strain indices of Section 4.4. ABAQUS data are reported at three locations, two on the top surface of the (half) beam flange: face of column; and the edge of the transverse fillet weld at the nose of the cover plate. ABAQUS data are also reported on the top surface of the (half) cover plate. The maximum values of the Pressure Index, Mises Index, Triaxiality Index, and Rupture Index at story drifts of 0.5, 1, and 2 percent for the cover plate and beam flange of RC03 are presented in Section 4.8. The quarter beam of RC03 was loaded in the plus 3-direction to introduce tension in the beam top flange and cover plate.

Figures 4-18, 4-19, and 4-20 report the distributions of normal stress S_{22} normalized by an assumed yield stress of 53.5 ksi (369 MPa), Mises Index, Equivalent Plastic Strain Index, Pressure Index, Triaxiality Index, and Rupture Index, at story drifts of 0.5, 1, and 2 percent, for the cover plate at the face of the column, the beam flange at the face of the column, and the beam flange at the nose of the cover plate, respectively. The Pressure Index in the beam flange, at the edge of the transverse fillet weld above the beam web, is less than 0.6 at 2-percent story drift. The probability of brittle fracture at this location in RC03 is small. Of the three locations considered, the maximum values of Pressure Index, Triaxiality Index, and Rupture Index at 2-percent story drift were measured on the top surface of the beam at the face of the column. The maximum value of the Equivalent Plastic Strain Index at 2-percent story drift was measured on the top surface of the beam, at the edge of the transverse fillet weld, beyond the end of the longitudinal fillet weld. Brittle and ductile fracture of the beam flange are more likely at the face of the column than at the nose of the cover plate (putting aside the likely differences in the sizes and locations of flaws and defects at these two sites).

A comparison of the maximum values of the fracture indices at the same locations in RC01 and RC03 shows that there is a smaller likelihood of fracture in RC03 (with three-sided fillet welds joining the cover plate to the beam flange). As expected, the distributions and values of the fracture indices in the cover plate and beam flange at the face of the column are similar in RC01 and RC03.

The maximum values of the Equivalent Plastic Strain Index, Pressure Index, and Rupture Index, at 2-percent story drift are significantly larger in the unreinforced connection (RC00) than in RC03. Ductile fracture is substantially less likely in RC03. The maximum values of the Triaxiality Index on the top surface of the beam at the column face in RC00 and RC03 are similar.

4.6.3 Connection RC05

The response of specimen RC05 is described below using the stress and strain indices of Section 4.4. ABAQUS data are reported at three locations, two on the top surface of the (half) beam flange: face of column; and the edge of the transverse fillet weld at the nose of the trapezoidal cover plate. ABAQUS data are also reported on the top surface of the (half) cover plate. The maximum values of the Pressure Index, Mises Index, Triaxiality Index, and Rupture Index at story drifts of 0.5, 1, and 2 percent for the cover plate and beam flange of RC03 are presented in Section 4.8. The quarter beam of RC05 was loaded in the plus 3-direction to introduce tension in the beam top flange and cover plate.

Figures 4-21, 4-22, and 4-23 report the distributions of normal stress S_{22} normalized by an assumed yield stress of 53.5 ksi (369 MPa), Mises Index, Equivalent Plastic Strain Index, Pressure Index, Triaxiality Index, and Rupture Index, at story drifts of 0.5, 1, and 2 percent, for the cover plate at the face of the column, the beam flange at the face of the column, and the beam flange at the nose of the trapezoidal cover plate, respectively. Of these three locations, the maximum values of Pressure Index, Triaxiality Index, and Rupture Index at 2-percent story drift were recorded on the top surface of the beam at the face of the column. The maximum value of the Equivalent Plastic Strain Index at 2-percent story drift was measured on the top surface of the beam, at the edge of the transverse fillet weld, beyond the end of the (raking) longitudinal fillet weld. Brittle and ductile fracture of the RC05 beam flange are more likely at the face of the column than at the nose of the trapezoidal cover plate. The Pressure Index in the beam flange, at the edge of the transverse fillet weld above the beam web, is less than 0.7 at 2-percent story drift. The probability of brittle fracture at this location in RC05 is small. (Other, as yet unpublished studies, have indicated that the Triaxiality Index increases as the width of the nose of the trapezoidal cover plate is decreased. As such, the above results should not be used to judge the likely behavior of all steel moment-resisting connections that are reinforced with trapezoidal cover plates.)

A comparison of the maximum values of the fracture indices at the same locations in RC03 and RC05 indicates that there is a smaller likelihood of fracture in RC03 (with three-sided fillet welds joining the cover plates to the beam flanges). The maximum values of Equivalent Plastic Strain Index, Pressure Index, Triaxiality Index, and Rupture Index at 2-percent story drift on the top surface of the beam, at the edge of the transverse fillet weld, are larger in RC05 than RC03. The values and profiles of the fracture indices across the beam flange at the face of the column are similar in RC03 and RC05. The values of these indices are slightly larger in the trapezoidal cover plate of RC05 than in the rectangular cover plate of RC03. Some of these small differences are likely due to the difference in the cross-sectional shape of the two cover plates.

The maximum values of the Equivalent Plastic Strain Index, Pressure Index, and Rupture Index, at 2-percent story drift are significantly larger in the unreinforced connection (RC00) than in RC03. Ductile fracture is substantially less likely in RC05. The maximum values of the Triaxiality Index on the top surface of the beam at the column face in RC00 and RC05 are most similar.

4.7 Flange-Plate Reinforced Connections (Model Type SOL)

4.7.1 Connection RC06

The response of specimen RC06 is described below using the stress and strain indices of section 4.4. ABAQUS data are reported at two locations: the top surface of the (half) beam flange at the edge of the transverse fillet weld at the nose of the flange plate; the top surface of the (half) flange plate at the face of the column. The maximum values of stress and strain along these line were not necessarily the maximum values in the components, but these lines were chosen to facilitate a comparison of results for different specimens. The maximum values of the Pressure Index, Mises Index, Triaxiality Index, and Rupture Index at story drifts of 0.5, 1, and 2 percent for the flange plate and beam flange of RC06 are presented in Section 4.8. The quarter beam of RC06 was loaded in the plus 3-direction (see Figure 4-2) to introduce tension in the beam top flange and flange plate.

Figures 4-24 and 4-25 report the distributions of normal stress S_{22} normalized by an assumed yield stress of 53.5 ksi (369 MPa), Mises Index, Equivalent Plastic Strain Index, Pressure Index, Triaxiality Index, and Rupture Index, at story drifts of 0.5, 1, and 2 percent, for the flange plate at the face of the column, and the beam flange at the edge of the transverse fillet weld, respectively. The maximum values of Pressure Index and Triaxiality Index at 2-percent story drift at these two locations were recorded on the top surface of the flange plate at the face of the column. The maximum values of Equivalent Plastic Strain Index and Rupture Index at 2-percent story drift were recorded on the top surface of the beam, at the edge of the transverse fillet weld, beyond the end of the longitudinal fillet weld. The Pressure Index and Triaxiality Index in the beam flange, at the edge of the transverse fillet weld above the beam web, at 2-percent story drift, are both less than -0.6. The probability of brittle fracture at this location in RC06 is small at modest levels of story drift.

The maximum values of Equivalent Plastic Strain Index and Rupture Index in RC06 are substantially smaller than the maximum values in the unreinforced connection (RC00), but larger than the maximum values in the similar cover-plate connection (RC03). The maximum value of the Pressure Index in the flange plate at the face of the column is greater than the maximum value in the beam flange of RC00 because the cross-sectional area of the flange plate in RC06 is greater than that of the beam flange in RC00.

4.7.2 Connection RC08

The response of specimen RC08 is described below using the stress and strain indices of Section 4.4. ABAQUS data are reported at two locations: the top surface of the (half) beam flange at the edge of the transverse fillet weld at the nose of the flange plate; and the top surface of the (half) flange plate at the face of the column. The maximum values of the Pressure Index, Mises Index, Triaxiality Index, and Rupture Index at story drifts of 0.5, 1, and 2 percent for the flange plate and beam flange of RC08 are presented in Section 4.8. The quarter beam of RC08 was loaded in the plus 3-direction to introduce tension in the beam top flange and flange plate.

Figures 4-26 and 4-27 report the distributions of normal stress S_{22} normalized by an assumed yield stress of 53.5 ksi (369 MPa), Mises Index, Equivalent Plastic Strain Index, Pressure Index, Triaxiality Index, and Rupture Index, at story drifts of 0.5, 1, and 2 percent, for the flange plate at the face of the column, and the beam flange at the edge of the transverse fillet weld, respectively. The maximum values of Pressure Index and Triaxiality Index at 2-percent story drift at these two locations were recorded on the top surface of the flange plate at the face of the column. The maximum values of Equivalent Plastic Strain Index and Rupture Index at 2-percent story drift were recorded on the top surface of the beam, at the edge of the transverse fillet weld, beyond the end of the longitudinal fillet weld. The Pressure Index and Triaxiality Index in the beam flange, at the edge of the transverse fillet weld above the beam web, at 2-percent story drift, are both less than -0.5. The likelihood of brittle fracture at this location in RC08 is small at modest levels of story drift.

The values of the four fracture indices discussed in the previous paragraph in the flange plates of RC06 and RC08 at the face of the column are similar, although marginally thinner flanges were used in the fabrication of RC08. The values of these indices at the edge of the transverse fillet weld were approximately equal or greater in RC08 at 2-percent story drift.

4.7.3 Connection RC09

The response of specimen RC09 is described below using the stress and strain indices of Section 4.4. ABAQUS data are reported at two locations: the top surface of the (half) beam flange at the edge of the transverse fillet weld at the nose of the flange plate; and the top surface of the (half) flange plate at the face of the column. The maximum values of the Pressure Index, Mises Index, Triaxiality Index, and Rupture Index at story drifts of 0.5, 1, and 2 percent for the flange plate and beam flange of RC09 are presented in Section 4.8. The quarter beam of RC09 was loaded in the plus 3-direction to introduce tension in the beam top flange and flange plate.

Figures 4-28 and 4-29 report the distributions of normal stress S_{22} normalized by an assumed yield stress of 53.5 ksi (369 MPa), Mises Index, Equivalent Plastic Strain Index, Pressure Index, Triaxiality Index, and Rupture Index, at story drifts of 0.5, 1, and 2 percent, for the flange plate at the face of the column, and the beam flange at the edge of the transverse fillet weld, respectively. The maximum values of the Equivalent Plastic Strain Index, Pressure Index, Triaxiality Index, and Rupture Index at 2-percent story drift at these two locations were recorded on the top surface of the flange plate at the face of the column. The maximum values of these indices in the beam flange at the edge of the transverse fillet weld were substantially smaller than those in the flange

plate at the face of the column. These values in the beam flange are small at 2-percent story drift because the plastic deformations in the beam are substantially reduced from RC08 due to yielding of the panel zone in RC09. The likelihood of fracture of the beam flange beyond the nose of the flange plate in RC09 is remote at 2-percent story drift. In the absence of flange- and web-local buckling, the critical section in RC09 is the flange plate at the face of the column.

The influence of panel zone yielding on the strain response of flange plates can be assessed by comparing data from Figures 4-26 (RC08) and 4-28 (RC09). (For reference, the doubler plate of RC08 was eliminated from RC09 and thinner continuity plates were installed in RC09. See Table 3-1 for further details.) The data presented in these figures indicate that the influence of panel zone yielding on plate response is modest for columns with relatively thick column flanges. This conclusion should not be extrapolated to beam-column connections for which the column flanges are thin.

4.8 Model Type SOL Results Summary

4.8.1 Summary results

Maximum responses were computed in nearly all cases at points on vertical planes at the face of the column and nose of the reinforcement plate. (Weld-access-hole data are not reported because the values, although large, are highly dependent on the shape of the hole, which will not follow the assumed shape in future construction. However, the shape and size of the weld-access hole can influence the maximum responses at the face of the column.) Accordingly, data are listed for these two planes only. Tables 4-3 through 4-8 present summary information on the response of the specimens at 0.5-, 1-, and 2-percent story drift. Tables 4-3 and 4-4 present response information for the beam and reinforcing plate at 0.5-percent story drift. Tables 4-5 and 4-6 present response information for the beam and reinforcing plate at 1-percent story drift. Tables 4-7 and 4-8 present response information for the beam and reinforcing plate at 2-percent story drift.

Table 4-3 Maxima of indices at 0.5-percent story drift at column flange

<i>Specimen</i>	<i>Beam Flange</i>				<i>Reinforcing Plate</i>			
	<i>PI</i> ¹	<i>MI</i> ¹	<i>TI</i> ¹	<i>RI</i> ¹	<i>PI</i> ¹	<i>MI</i> ¹	<i>TI</i> ¹	<i>RI</i> ¹
RC00	-0.63	1.00	-0.93	0.0017	-	-	-	-
RC01	-0.44	0.80	-0.85	0	-0.32	0.68	-0.87	0
RC03	-0.40	0.73	-0.82	0	-0.29	0.57	-0.92	0
RC05	-0.40	0.70	-0.81	0	-0.38	0.71	-0.92	0
RC06	-	-	-	-	-0.37	0.69	-0.84	0
RC08	-	-	-	-	-0.39	0.73	-0.83	0
RC09	-	-	-	-	-0.38	0.68	-0.85	0

1. *PI* = Pressure Index; *MI* = Mises Index; *TI* = Triaxiality Index; *RI* = Rupture Index

Table 4-4 Maxima of indices at 0.5-percent story drift at nose of reinforcing plate

Specimen	Beam Flange				Reinforcing Plate			
	PI^1	MI^1	TI^1	RI^1	PI^1	MI^1	TI^1	RI^1
RC00	-	-	-	-	-	-	-	-
RC01	-0.35	0.82	-0.60	0	-	-	-	-
RC03	-0.29	0.58	-0.61	0	-	-	-	-
RC05	-0.33	0.63	-0.54	0	-	-	-	-
RC06	-0.33	0.64	-0.76	0	-	-	-	-
RC08	-0.29	0.65	-0.74	0	-	-	-	-
RC09	-0.28	0.61	-0.74	0	-	-	-	-

1. PI = Pressure Index; MI = Mises Index; TI = Triaxiality Index; RI = Rupture Index

At 0.5-percent story drift, the maximum values of Pressure Index, Mises Index, Triaxiality Index, and Rupture Index are greater in the beam flange of the unreinforced connection RC00 than in the beam flange and reinforcing plates of any other connection studied (RC01, RC03, RC05, RC06, RC08, and RC09).

At 1-percent story drift, the maximum values of Pressure Index and Rupture Index are greater in the beam flange of the unreinforced connection RC00 than in the beam flange and reinforcing plates of any other connection studied (RC01, RC03, RC05, RC06, RC08, and RC09). In particular, the Rupture Index of RC00 in the beam flange at the column face is 2 to 15 times greater than the maximum value of the Index in the other connections at all three locations considered (beam flange at column face, reinforcing plate at column face, and beam flange immediately beyond the nose of the reinforcing plate, and 10 times greater than the maximum value in RC00 at 0.5-percent story drift. Putting aside issues related to defect size and location, the values of the fracture indices reported above clearly indicate that the addition of reinforcement plates to a steel moment-resisting connection substantially reduces the likelihood of brittle and ductile fractures at modest levels of story drift. Using the fracture indices presented in the tables, RC03 (cover-plate connection with three-sided fillet weld) and RC06 (flange-plate connection with three-sided fillet weld) appear to be the most promising of the six reinforced connections presented in the table. The values of the Rupture Index in RC01 at 1-percent story drift are significantly higher than those of RC03, which indicates that the three-sided fillet welds joining the reinforcement plates to the beam flanges are preferable to the two-sided fillet welds that were adopted for RC01.

At 2-percent story drift, the maximum value of the Rupture Index is recorded in the beam flange of RC00 at the face of the column. The RC00 value is more than three times greater than the maximum value of the Index in any of the other six specimens considered, at the face of the column. The maximum values of the Pressure Index range between 0.66 and 0.90 for all seven specimens considered. For the cover-plate connections RC01, RC03, and RC05, the smallest maximum value of the Rupture Index at the face of the column is recorded in RC03 and RC05; the differences between the values are relatively small. In these connections, the Pressure,

Table 4-5 Maxima of indices at 1-percent story drift at column flange

Specimen	Beam Flange				Reinforcing Plate			
	PI^1	MI^1	TI^1	RI^1	PI^1	MI^1	TI^1	RI^1
RC00	-0.76	1.02	-0.88	0.0170	-	-	-	-
RC01	-0.73	1.01	-0.85	0.0057	-0.57	1.00	-0.87	0.0029
RC03	-0.70	1.00	-0.83	0.0042	-0.55	1.00	-0.93	0.0012
RC05	-0.69	0.98	-0.81	0.0038	-0.67	0.98	-0.93	0.0038
RC06	-	-	-	-	-0.68	1.00	-0.84	0.0034
RC08	-	-	-	-	-0.74	0.99	-0.84	0.0046
RC09	-	-	-	-	-0.67	0.98	-0.87	0.0039

1. PI = Pressure Index; MI = Mises Index; TI = Triaxiality Index; RI = Rupture Index

Table 4-6 Maxima of indices at 1-percent story drift at nose of reinforcing plate

Specimen	Beam Flange				Reinforcing Plate			
	PI^1	MI^1	TI^1	RI^1	PI^1	MI^1	TI^1	RI^1
RC00	-	-	-	-	-	-	-	-
RC01	-0.56	1.05	-0.63	0.0087	-	-	-	-
RC03	-0.56	1.04	-0.68	0.0012	-	-	-	-
RC05	-0.61	0.98	-0.62	0.0029	-	-	-	-
RC06	-0.59	1.00	-0.79	0.0018	-	-	-	-
RC08	-0.59	1.03	-0.75	0.0030	-	-	-	-
RC09	-0.57	0.98	-0.76	0.0018	-	-	-	-

1. PI = Pressure Index; MI = Mises Index; TI = Triaxiality Index; RI = Rupture Index

Triaxiality, and Rupture Indices are greater in the beam flange than in the cover plate at the face of the column. Of these three cover-plate connections, RC03 appears to be the superior connection. Of the flange-plate connections listed in the tables, RC06, RC08, and RC09, specimen RC06 appears to be the superior connection. In RC06 and RC08, the maximum value of the Rupture Index is recorded in the beam at the nose of the reinforcing plate. Such a result is desirable because the objective of the flange-plate connection is to force inelastic action in the beam away from the column face. For RC09, the maximum value of the Rupture Index is recorded in the reinforcing plate at the face of the column; the maximum value in the plate is approximately 3.5 times larger than that in the beam. Such a result is undesirable. The large contribution of panel zone deformation to the drift of this specimen, reduced the plastic deformation demand on the beam, and consequently reduced the plastic strain demands on the beam at the nose of the cover plate.

Table 4-7 Maxima of indices at 2-percent story drift at column flange

Specimen	Beam Flange				Reinforcing Plate			
	PI^1	MI^1	TI^1	RI^1	PI^1	MI^1	TI^1	RI^1
RC00	-0.82	1.11	-0.77	0.099	-	-	-	-
RC01	-0.86	1.02	-0.84	0.029	-0.75	1.02	-0.74	0.020
RC03	-0.86	1.02	-0.84	0.025	-0.73	1.02	-0.76	0.015
RC05	-0.84	1.00	-0.84	0.025	-0.80	1.00	-0.80	0.024
RC06	-	-	-	-	-0.89	1.02	-0.88	0.025
RC08	-	-	-	-	-0.86	1.00	-0.87	0.023
RC09	-	-	-	-	-0.90	1.00	-0.90	0.028

1. PI = Pressure Index; MI = Mises Index; TI = Triaxiality Index; RI = Rupture Index

Table 4-8 Maxima of indices at 2-percent story drift at nose of reinforcing plate

Specimen	Beam Flange				Reinforcing Plate			
	PI^1	MI^1	TI^1	RI^1	PI^1	MI^1	TI^1	RI^1
RC00	-	-	-	-	-	-	-	-
RC01	-0.71	1.20	-0.66	0.052	-	-	-	-
RC03	-0.66	1.14	-0.69	0.026	-	-	-	-
RC05	-0.68	1.01	-0.68	0.024	-	-	-	-
RC06	-0.75	1.06	-0.81	0.035	-	-	-	-
RC08	-0.71	1.14	-0.78	0.046	-	-	-	-
RC09	-0.68	1.08	-0.88	0.0084	-	-	-	-

1. PI = Pressure Index; MI = Mises Index; TI = Triaxiality Index; RI = Rupture Index

On the basis of the results presented in these six tables, the use of any of the six reinforced connections listed in the tables will reduce the likelihood of ductile and brittle fracture of steel moment-resisting connections with respect to the unreinforced connection, RC00.

Specimens RC03 and RC06 are the superior reinforced connections of the six listed in the tables for story drift angles of 2-percent radian and less. The maximum values of the Rupture Index at the face of the column for RC03 and RC06 were identical (0.025 and 0.015 [RC03] versus 0.025 [RC06]) at 2-percent story drift. Larger values of the Rupture Index were recorded at the nose of the reinforcing plate of RC06 (0.026 [RC03] and 0.035 [RC06]) at 2-percent story drift.

4.9 Shell Element Models of Reinforced Connections

4.9.1 Introduction

Type SH models were prepared for RC01, RC02, RC03, and RC06. Figure 4-30 shows the meshing of the four specimens in the vicinity of the bottom reinforcing plate. The Type SH models were prepared to study (a) the influence on global response (lateral force versus story drift) of flange- and web-local buckling and lateral-torsional buckling, (b) the effect of the geometry of the fillet welds that join the reinforcing plates to the beam flanges on the buckled shapes of the specimens, (c) the relationship between flange- and web-local buckling, and (d) the role lateral-torsional buckling plays in the response of steel moment-resisting connections.

Unless noted otherwise below, the beam was loaded in the minus 3-direction (see Figure 4-2) to introduce compression in the beam top flange.

4.9.2 Force versus displacement relations

Figure 4-31 shows the beam load-beam tip displacement relations for RC01, RC03, and RC06 calculated using the Type SH models. (Data for RC02 are presented below.) These relationships were normalized by the maximum resistance of the Type SH model of RC03. The beam load-beam tip displacement relation for RC03 calculated using the Type SOL model is also shown for the purpose of comparison.

The differences between the responses of the Type SH models is small because the beam load-beam tip relationships are controlled by flange- and web-local buckling in the beam immediately beyond the nose of the reinforcing plate. The responses of the Type SH and Type SOL models of specimen RC03 are virtually identical for story drift angles up to 2-percent radian. Beyond this drift angle, local buckling of the beam flange and web result in a loss of strength and stiffness in RC03. Such buckling is accounted for in the Type SH models only.

4.9.3 Fillet weld geometry

Two key geometries of fillet weld were considered in this research program, the two-sided fillet weld of RC01 and RC02, and the three-sided fillet weld of RC03, RC05, and RC06 through RC10. The influence of fillet weld geometry on flange- and web-local buckling was studied using RC01 and RC03. Figure 4-32 shows the deformed shape of these two specimens at 5-percent story drift. The transverse fillet weld of RC03 is effective in preventing flange buckling from penetrating back beyond the nose of the reinforcing plate.

4.9.4 Flange- and web-local buckling

Figure 4-33 shows the beam load-beam tip displacement relation for RC03. Shown on this figure are points A through H that represent different stages in the response of the specimen. Point A corresponds to elastic response. Point B corresponds to maximum resistance of RC03. Figure 4-34 shows the deformed shape of the beam cross section at each of these eight points, 7.25 in. (184 mm) from the nose of the cover plate.

An isometric view of the deformed shape of the beam cross section at 5-percent story drift is shown in Figure 4-35. The buckles in the flange and web are clearly evident. The amplitudes of the flange and web buckles at this drift angle are approximately 2.7 in. (68 mm) and 2.1 in. (53 mm), respectively. Note that the location of the maximum amplitude flange and web local buckles do not necessarily occur on the same x_1 - x_3 plane. Table 4-9 lists the maximum deformations of the beam flange and web at each of the points of Figure 4-33.

The resistance of RC03 drops at story drift angles greater than 1.9-percent radian (point B in Figure 4-33) due to flange- and web-local buckling as seen in the deformed cross sections of Figure 4-34 for points C through H. The link between flange- and web-local buckling is clearly evident in the deformed cross sections of Figure 4-34 and Table 4-9: increases in the amplitude of flange buckles are accompanied by increases in the amplitude of the web buckles. The rate of strength loss in RC03 (points B to E in Figure 4-33) is greatest when the rates of increase in the amplitude of the flange and web buckles are greatest (see Table 4-9).

Table 4-9 Buckle amplitudes in RC03

<i>Point</i>	<i>Drift Angle %</i>	<i>Maximum deformation (mm)</i>	
		<i>Flange</i>	<i>Web</i>
A	1.12	0.1	0.1
B	1.85	1.6	2.4
C	1.98	6.7	10.5
D	2.08	11.3	15.3
E	2.18	16.3	19.1
F	3.08	42.9	26.0
G	4.18	57.7	46.7
H	5.11	68.6	53.9

1. See Figure 4-33 for details.

Figures 4-36 and 4-37 present views of the beam web and the underside of the beam top flange at 6 of the 8 points identified in Figure 4-33. (The view is of the beam web and the underside of beam top flange, near the face of the column) The deformed shapes of the web and flange are shown in these views together with contours of equivalent plastic strain. Each figure contains a legend showing values of equivalent plastic strain. The increment of equivalent plastic strain in these figures ($=0.020$) is approximately 10 times the yield strain ($=0.018$). The full wavelength of the local buckle for drift angles greater than 3-percent radian is equal to the yielded length of the flange as first proposed by Lay (1965). The flange-buckle wavelength increases as the plasticity spreads in the flange with increasing story drift angle. Plasticity spreads into the beam web at a story drift angle of approximately 2-percent radian (Figure 4-36) and penetrates back beyond the nose of the reinforcing plate at a story drift angle of approximately 3-percent radian. At a story drift angle of 5-percent radian, large equivalent plastic strains of approximately 0.20 and 0.30 develop in the k-line at the junction of the beam flange and beam web, and the beam flange, respectively. (For information, the rupture strain is approximately 0.40.)

4.9.5 Lateral-torsional buckling

The Type SH model of RC02 was prepared to assess the effect of lateral-torsional buckling on the force-displacement response of reinforced connections. RC02 was identical to RC01 except lateral restraint was provided to RC02.

Four conditions of lateral restraint were considered; all three conditions included lateral restraint to the beam flanges at the beam tip. The beam was loaded in the minus 3-direction (see Figure 4-2) to produce compression in the beam top flange.

1. No restraint at the end of the plastic hinge (condition 1: replicating RC01).
2. Infinitely stiff lateral restraint to the beam flanges, 20 in. (508 mm) from the nose of the reinforcement plate (condition 2: approximately replicating RC02 except that the braces shown in Figure 3-12 were not infinitely stiff).
3. Continuous lateral (*I*-direction) restraint and rotational restraint (around *I*-axis) to the centerline of the beam top flange; infinitely stiff lateral restraint to the beam bottom flange, 20 in. (508 mm) from the nose of the cover plate (condition 3: similar to condition 2 but including the restraint that would be offered by a composite slab).

The force-displacement relations for each of these conditions are presented in Figure 4-38. Also shown in this figure is the force-displacement relation for condition 3 but with the load applied in the plus 3-direction (termed condition 4). The restraint condition for each curve is identified in parenthesis in the legend. For each analysis, new eigenvectors were extracted as described in Section 4.3.3.2, and new geometric imperfections were included in the mathematical model.

Compare first the responses for conditions 1 (no restraint), and 2 (restraint), and 3 (restraint). The addition of lateral bracing at the end of the plastic hinge zone (condition 2) to delay lateral-torsional buckling of the beam has minimal effect on the beam load-beam tip displacement relationship. Likewise, the restraint of condition 3 had virtually no effect on the load-displacement relation. A substantial improvement in response is evident for condition 4, where the beam top flange is in compression and lateral and rotational restraint is provided along the centerline of this flange. Flange-local buckling (symmetric about the beam web producing a saddle-type shape) is substantially delayed by the restraint. The loss of strength for condition 4 follows web local-buckling that accompanies the shortening of the beam due to flange-local buckling. Such shortening would be difficult, but not impossible, to realize in the field.

Substantial forces develop in the braces providing the lateral restraint. For condition 2, the maximum brace force is 26.0 kips (116 kN) at a story drift angle of 5.07-percent radian. For condition 3, the maximum brace force is 26.3 kips (118 kN) at a story drift angle of 5.14-percent radian. Note that these braces were modeled as rigid components for the Type SH analysis.

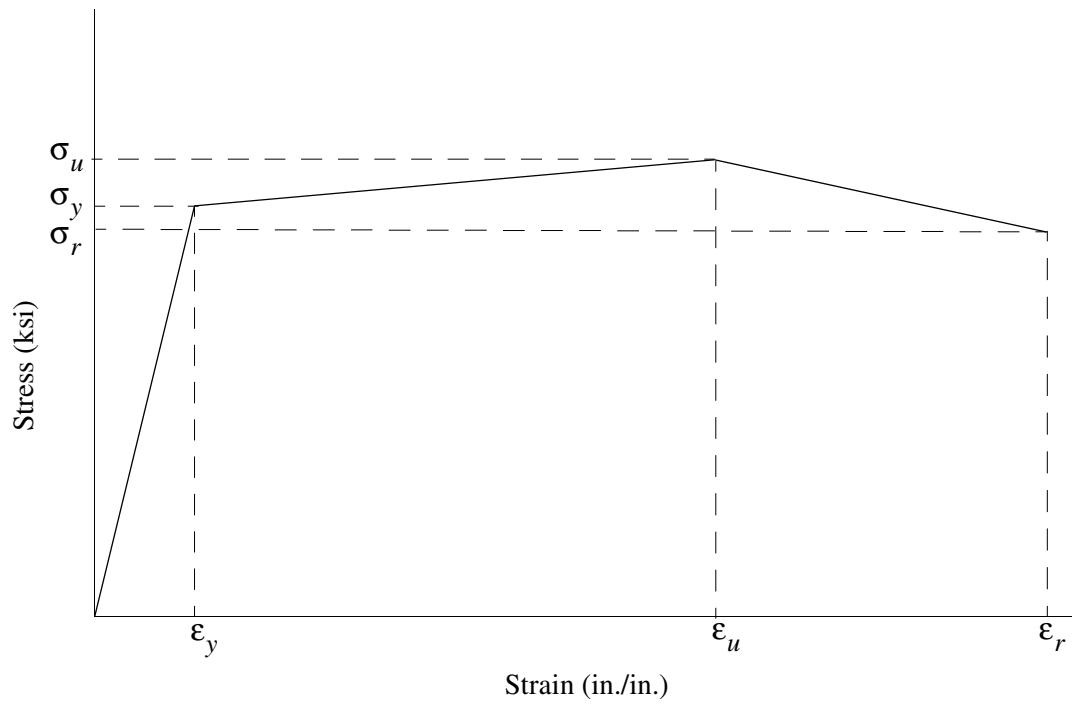
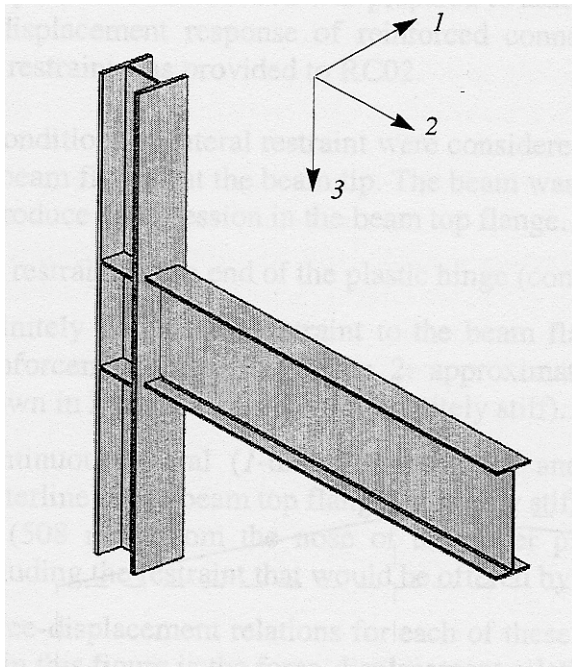
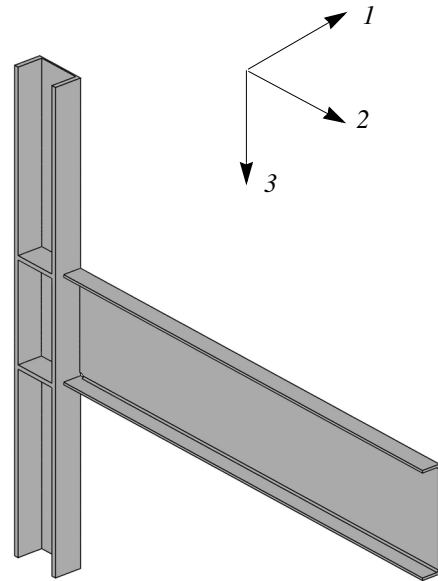


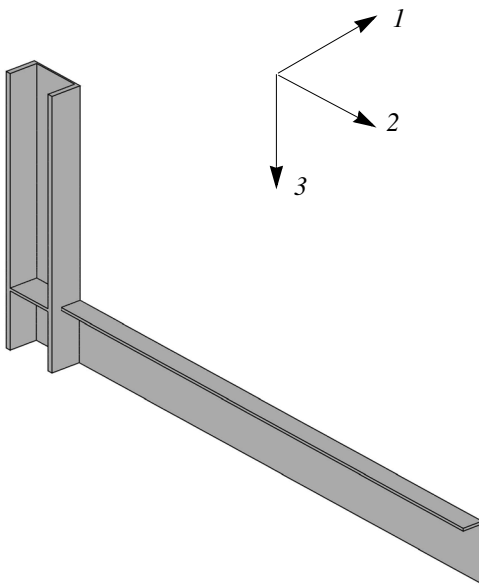
Figure 4-1 Assumed trilinear stress-strain relationship for ABAQUS models



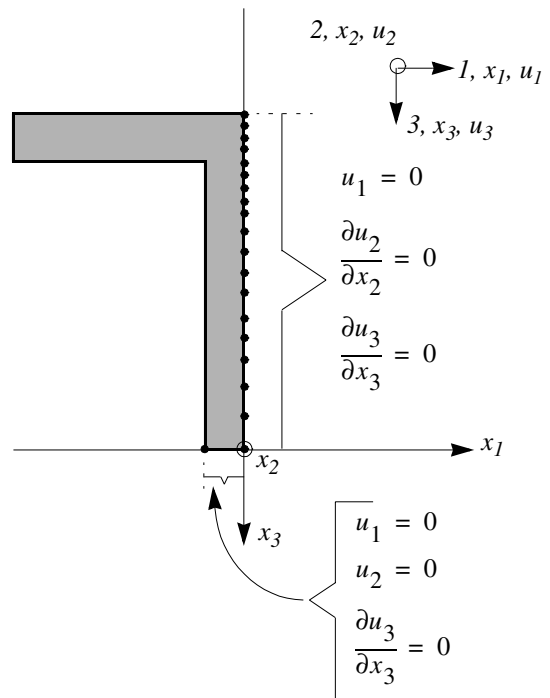
a. full model



b. half model

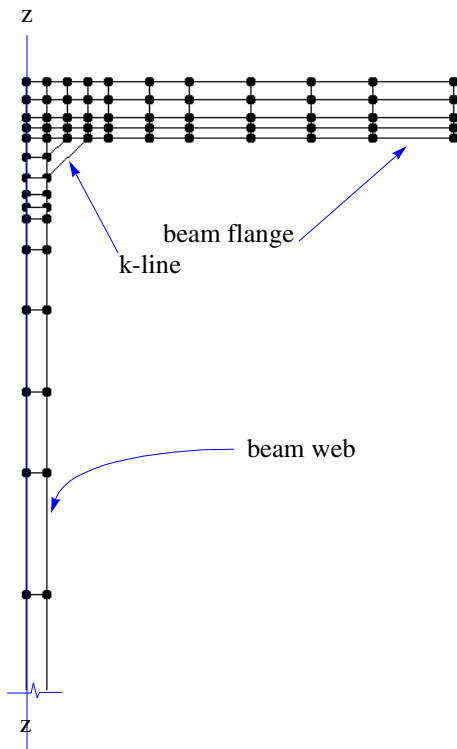


c. quarter model

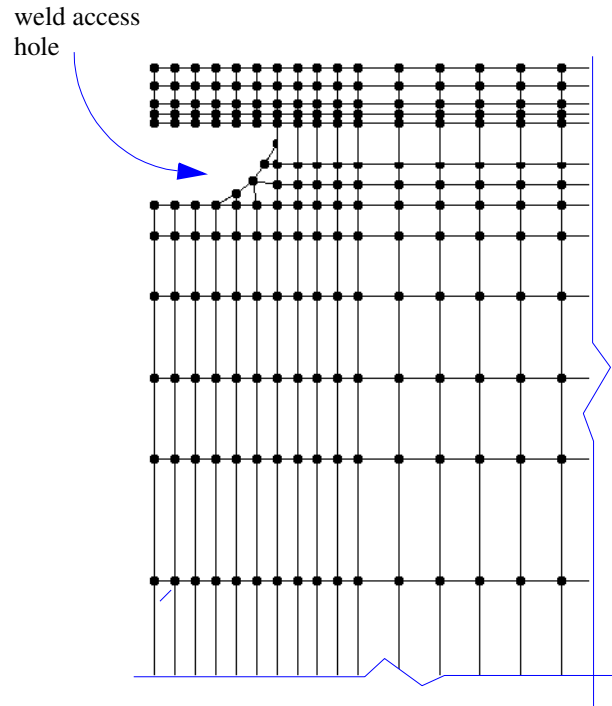


d. symmetry conditions

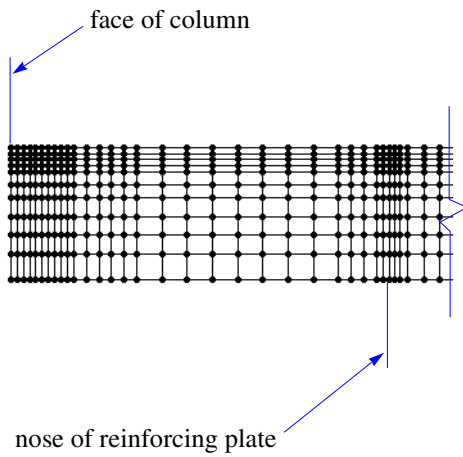
Figure 4-2 ABAQUS Type SOL models and symmetry conditions



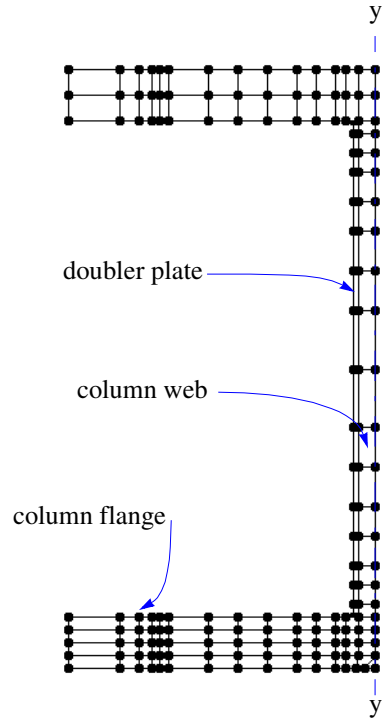
a. beam cross section



b. beam adjacent weld access hole



c. beam at nose of reinforcing plate



d. column cross section

Figure 4-3 Element meshing for beam and column of Type SOL models

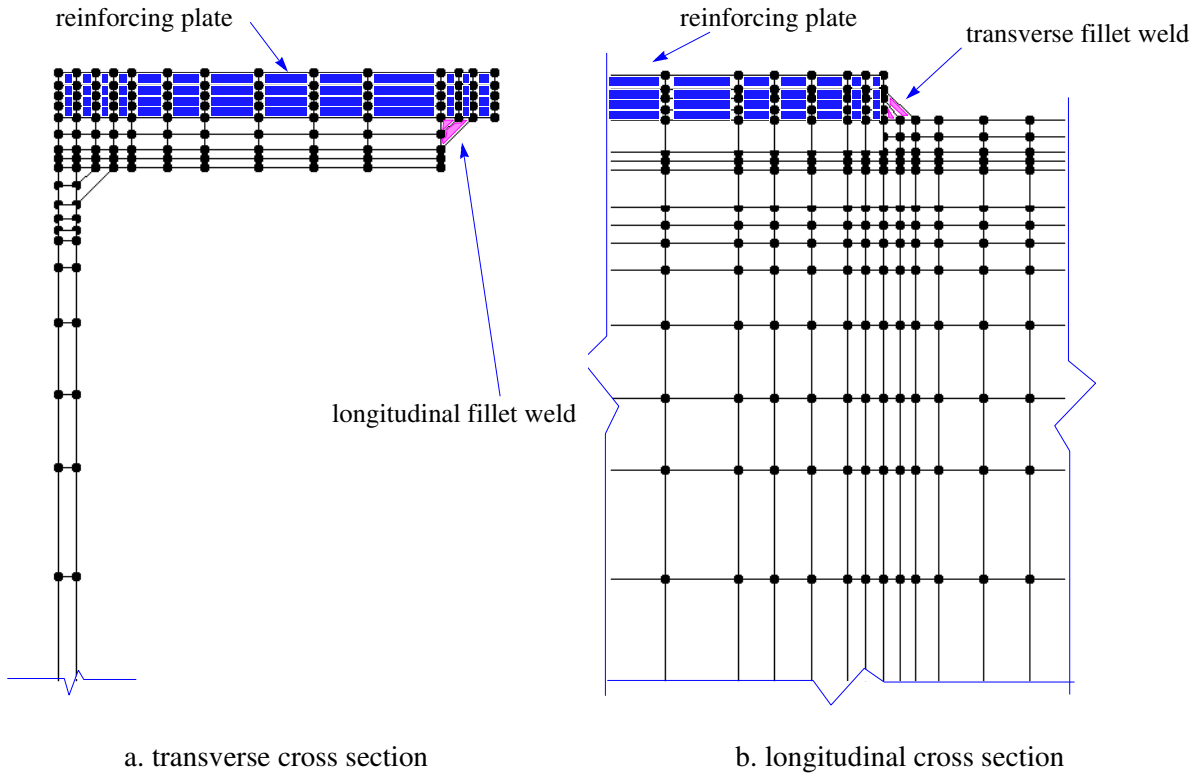


Figure 4-4 Solid element meshing for reinforcing plates of Type SOL models

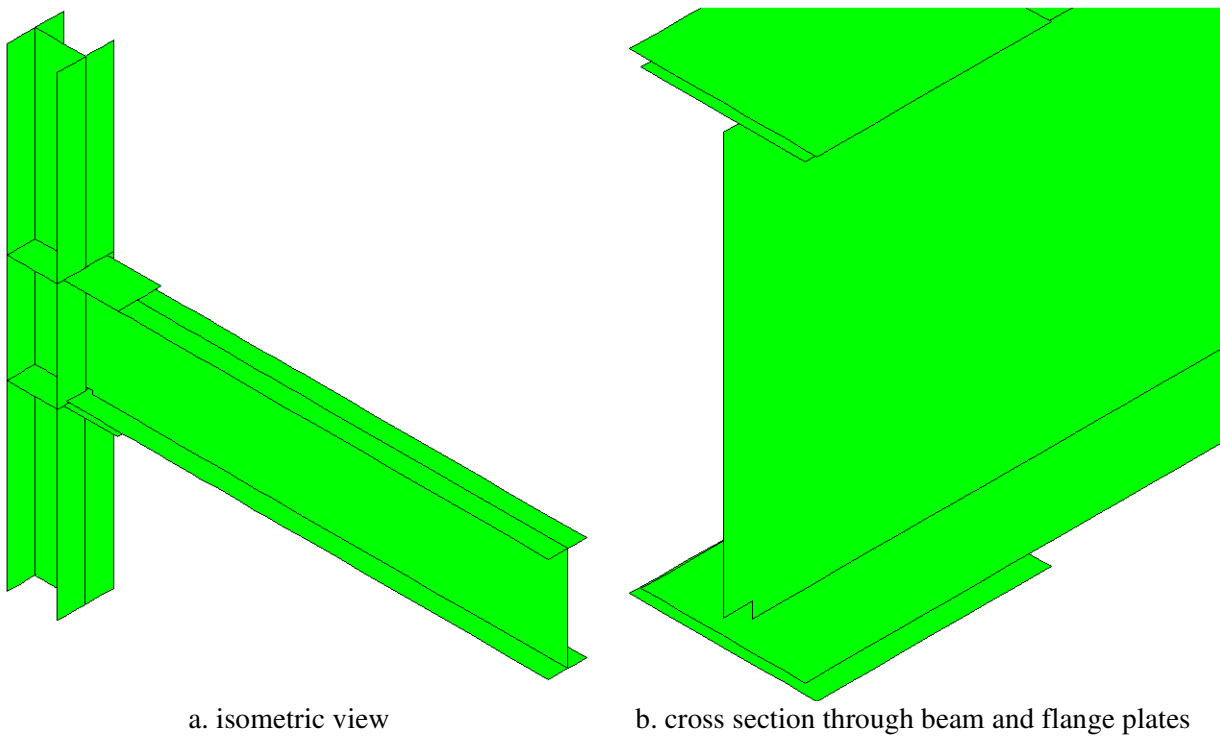


Figure 4-5 ABAQUS Type SH models

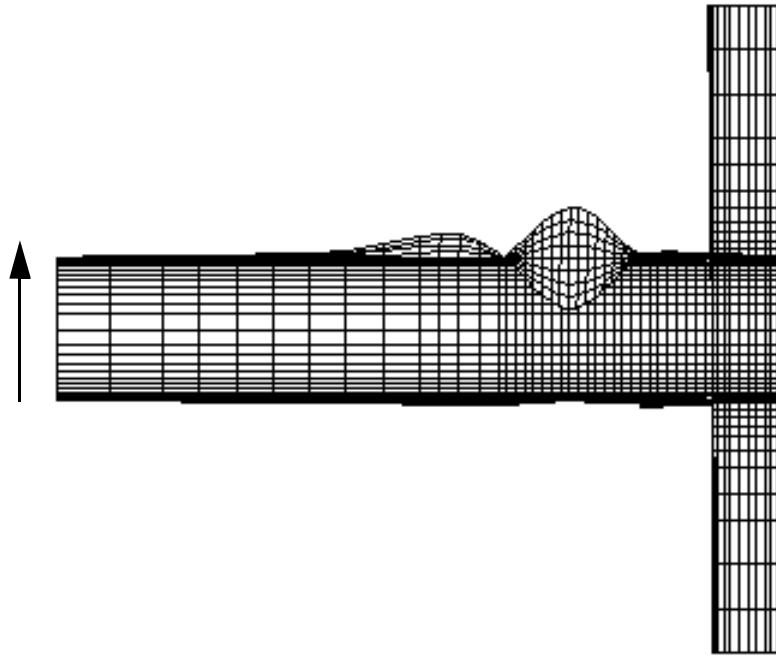


Figure 4-6 Buckled shapes of RC03 for first eigenvector

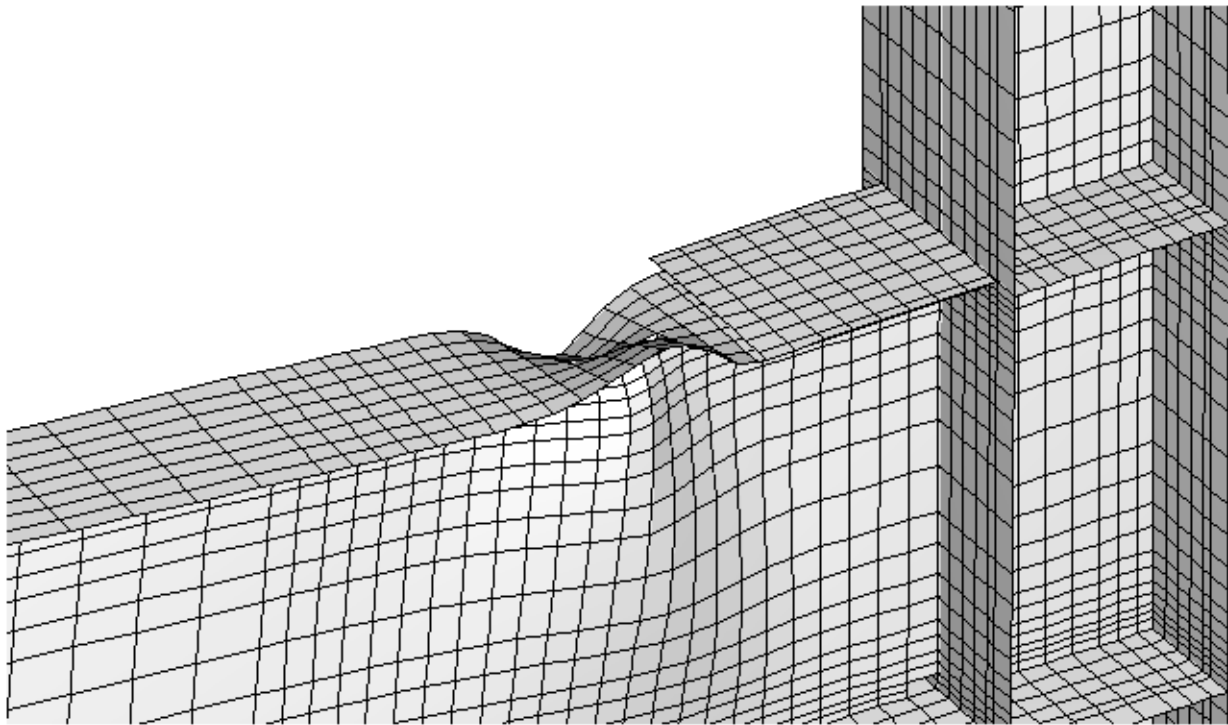


Figure 4-7 Deformed shape of the RC03 beam cross section at flange buckle

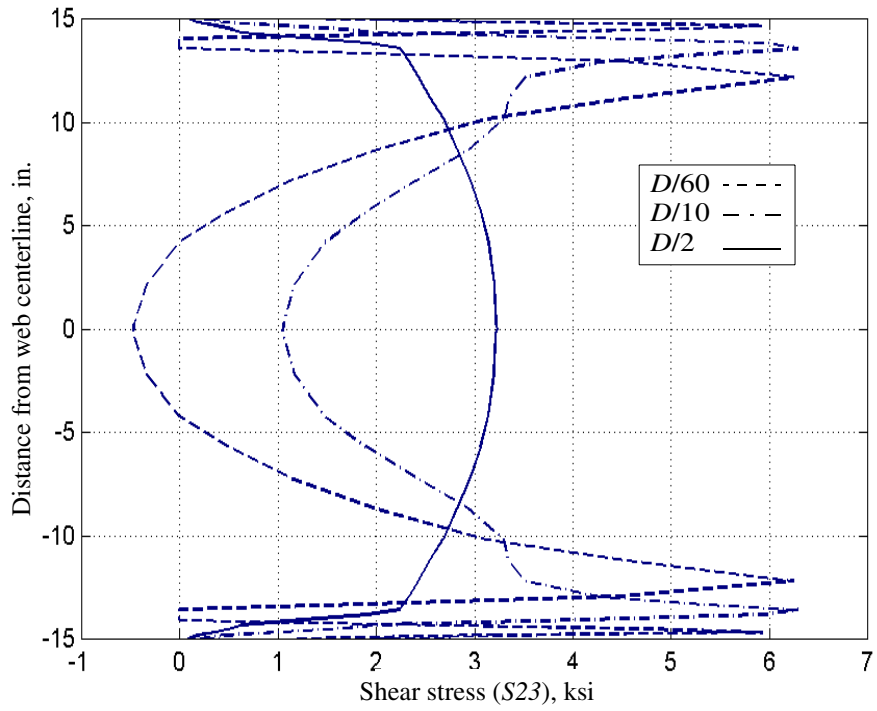


Figure 4-8 Distribution of shear stress in beam of RC00

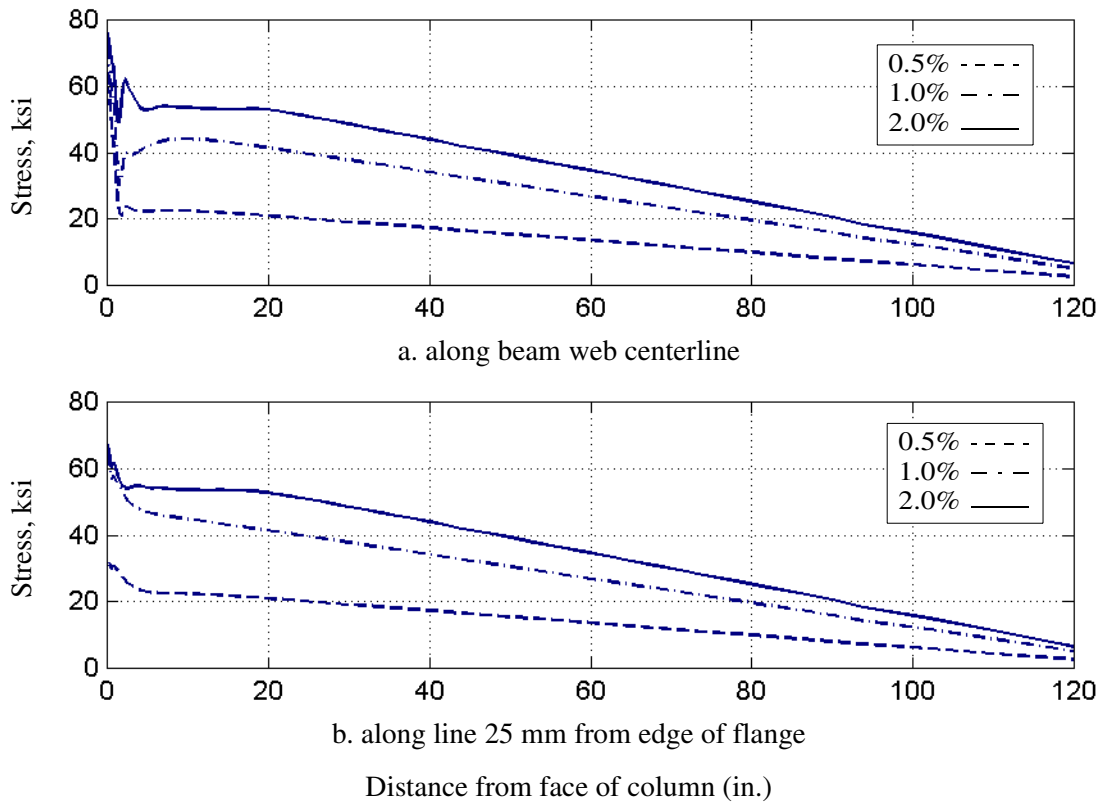
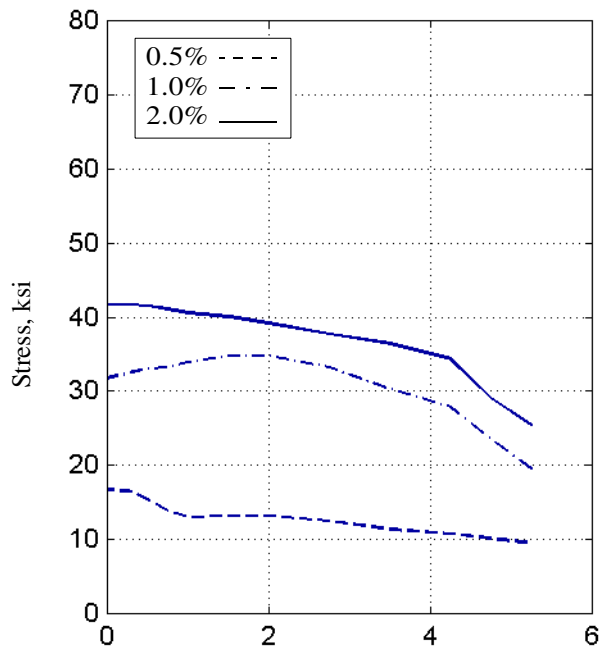
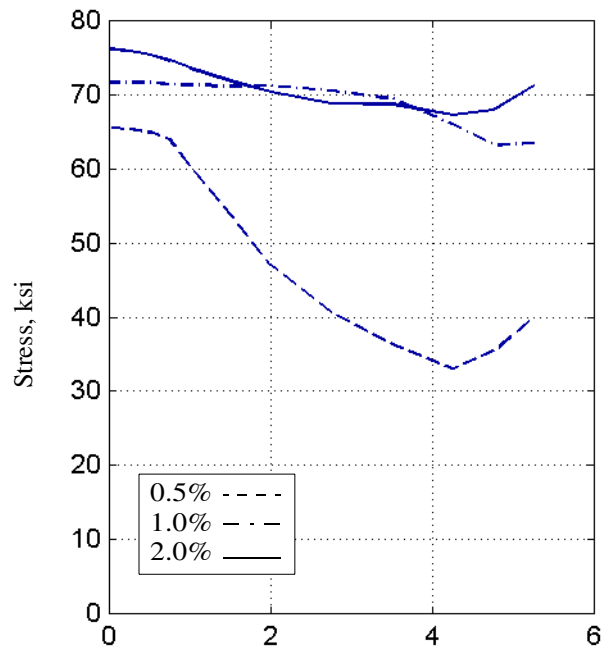


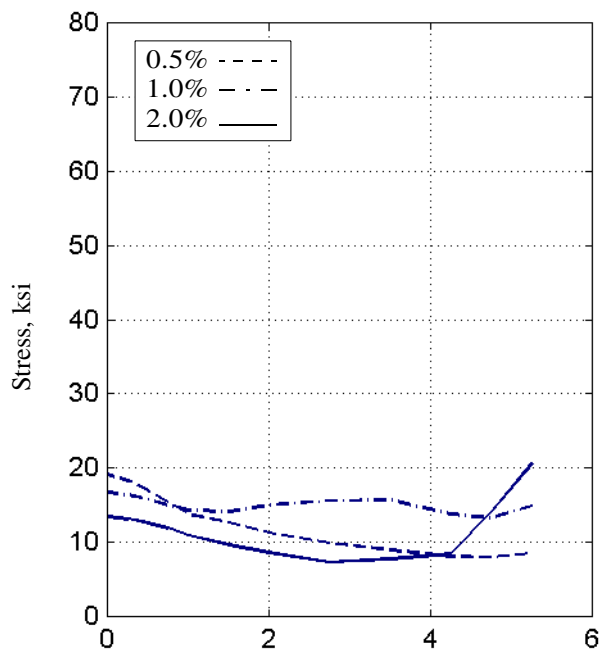
Figure 4-9 Distribution of normal stress S_{22} in RC00 at story drifts of 0.5, 1, and 2 percent



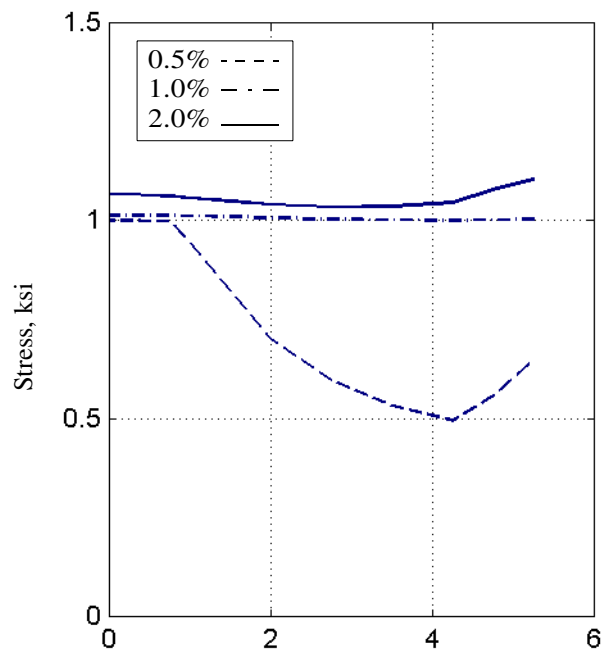
a. normal stress S_{11}



b. normal stress S_{22}



c. normal stress S_{33}

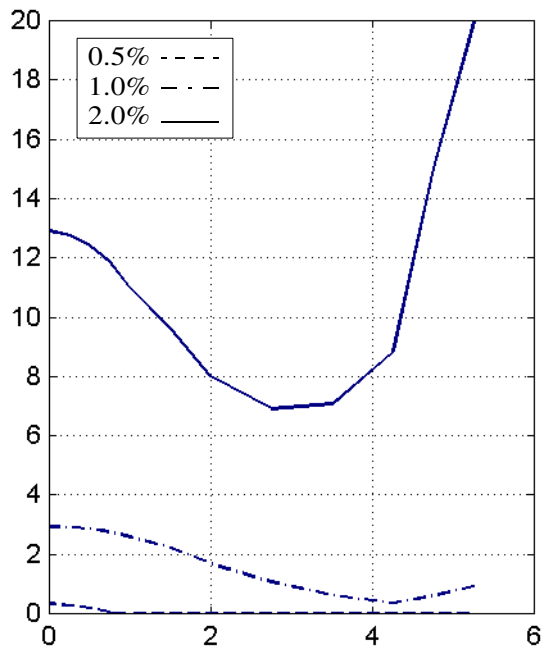


d. Mises Index

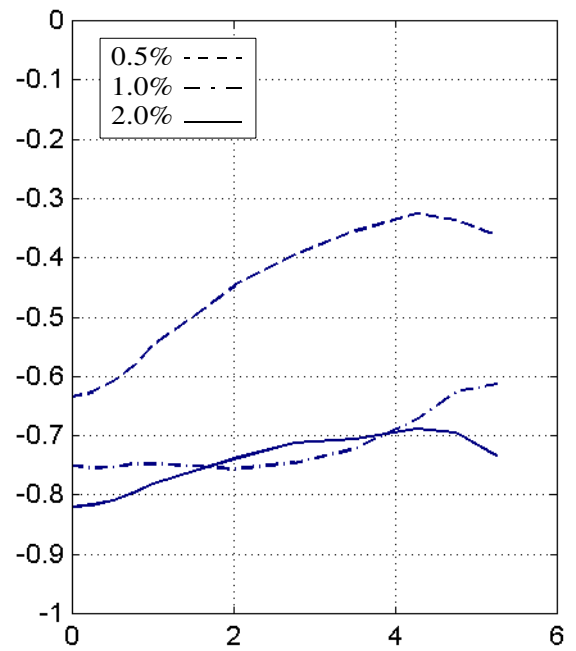
Distance from beam web centerline (in.)

Distance from beam web centerline (in.)

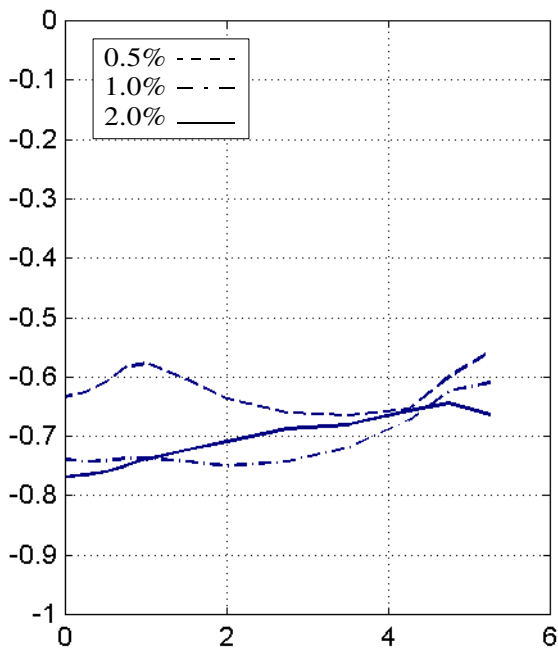
Figure 4-10 Stress distributions in RC00 beam at story drifts of 0.5, 1, and 2 percent



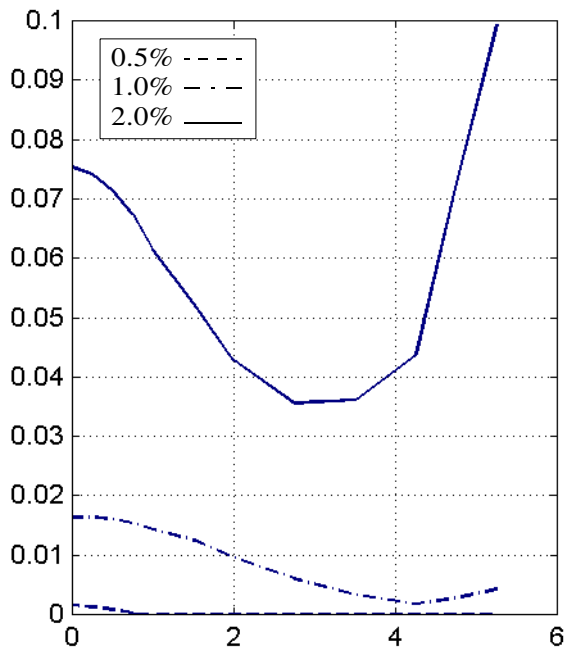
a. Equivalent Plastic Strain Index



b. Pressure Index



c. Triaxiality Index

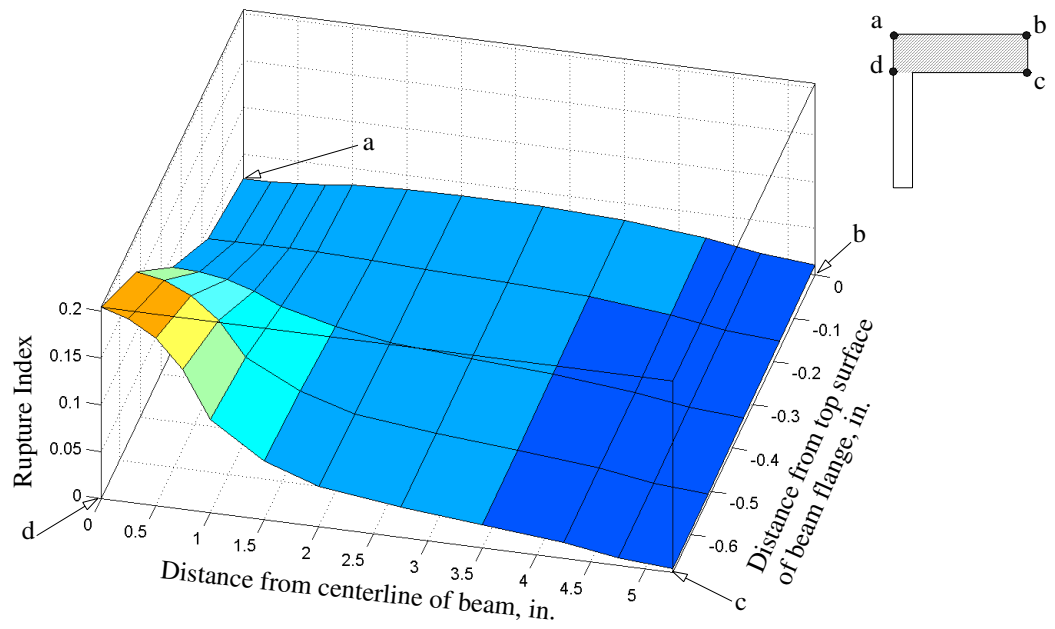


d. Rupture Index

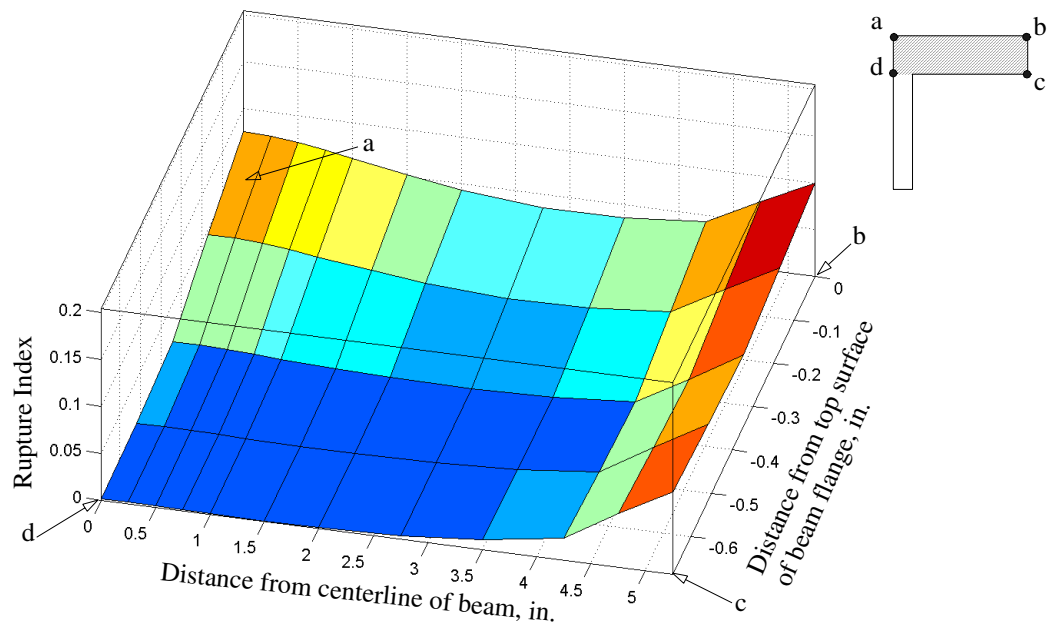
Distance from beam centerline (in.)

Distance from beam centerline (in.)

Figure 4-11 Fracture indices in RC00 beam at story drifts of 0.5, 1, and 2 percent

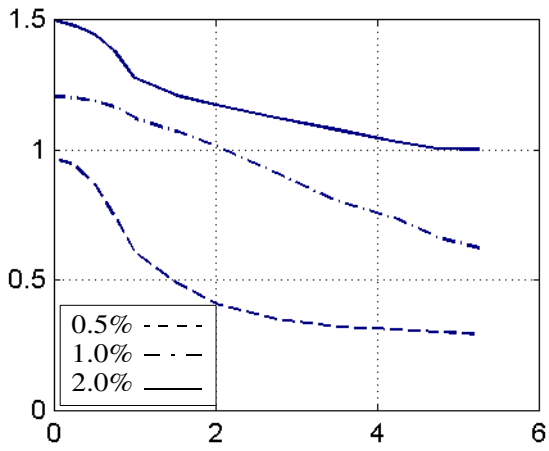


a. above toe of weld access hole

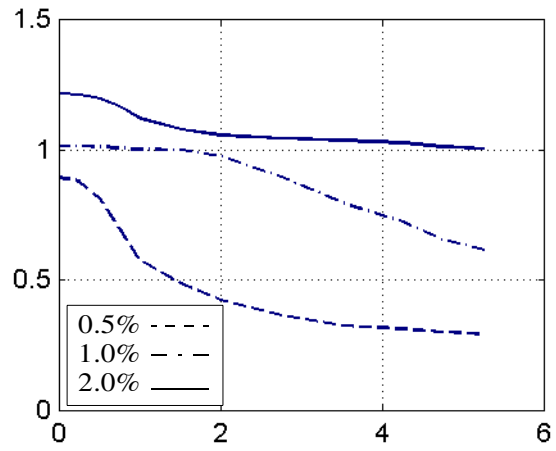


b. at beam-column interface

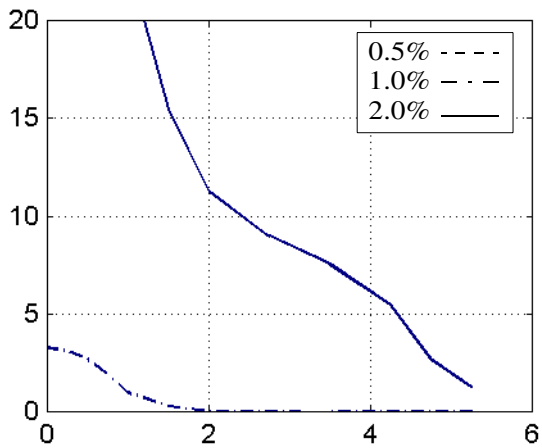
Figure 4-12 Contour plots of Rupture Index at 2-percent story drift



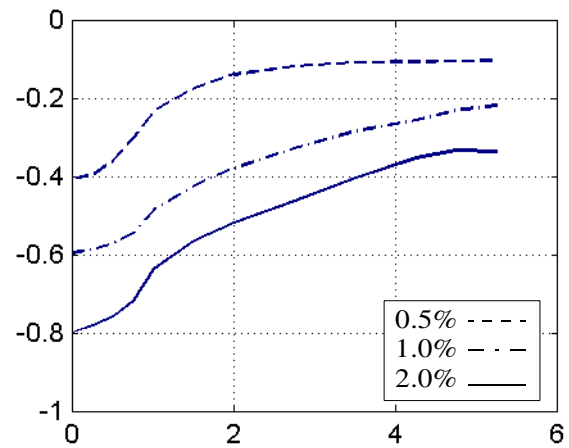
a. normal stress S_{22} normalized by σ_y



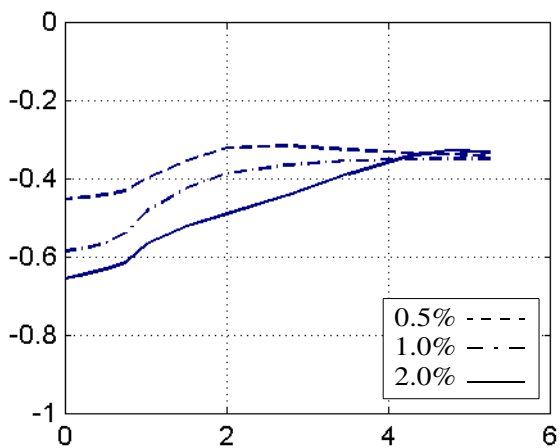
b. Mises Index



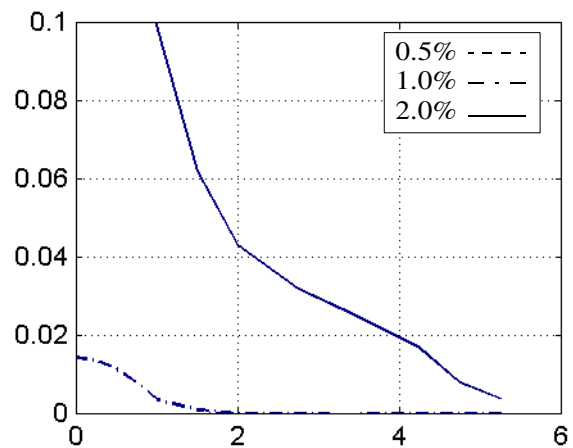
c. Equivalent Plastic Strain Index



d. Pressure Index



e. Triaxiality Index

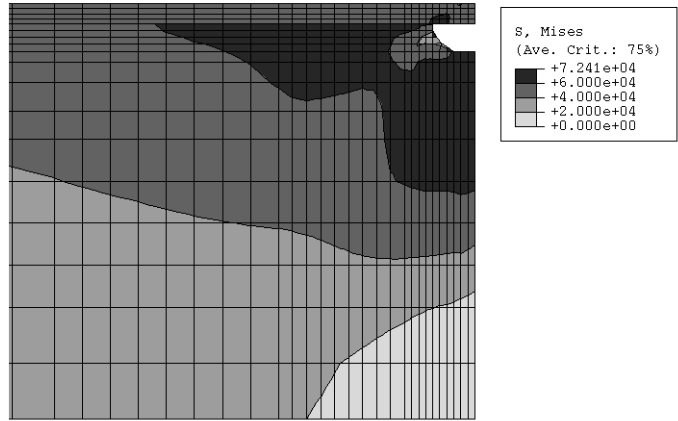


f. Rupture Index

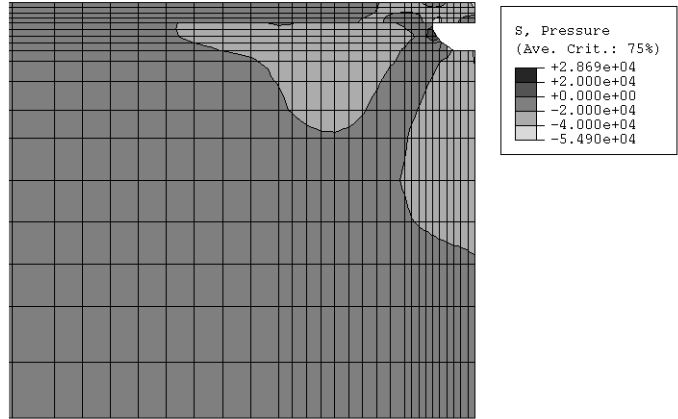
Distance from beam web centerline (in.)

Distance from beam web centerline (in.)

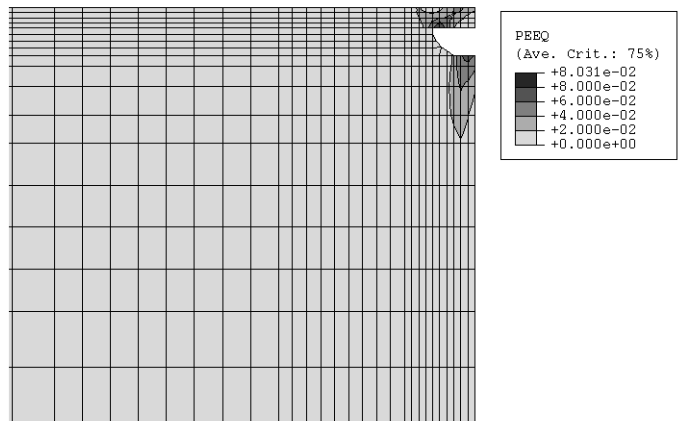
Figure 4-13 Stress and fracture indices in RC00 beam flange at toe of weld access hole



a. Mises stress

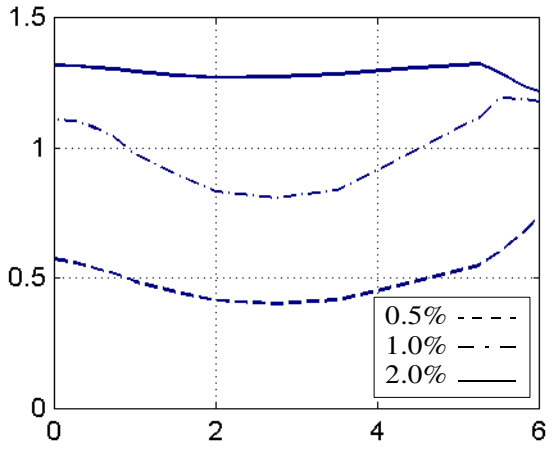


b. Hydrostatic pressure

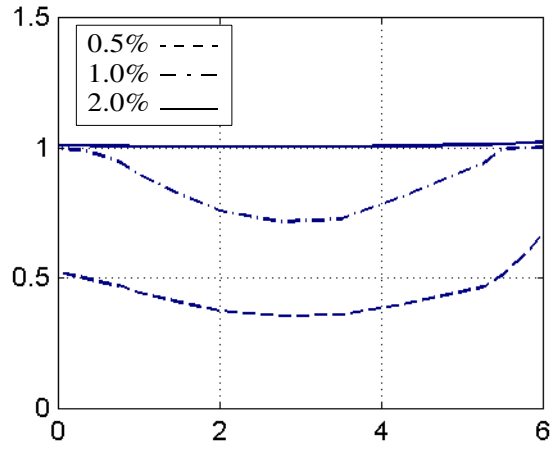


c. Equivalent Plastic Strain

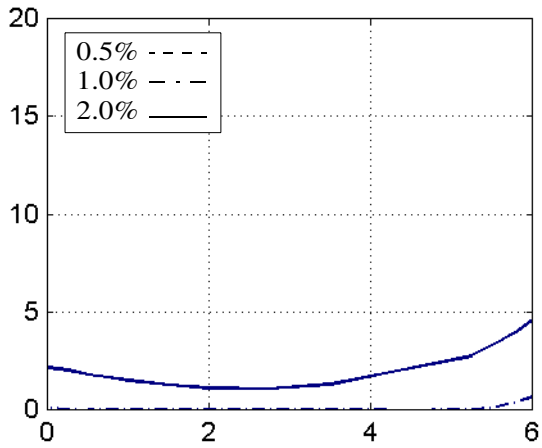
Figure 4-14 Stress and strain distribution on RC00 beam web centerline at 2-percent story drift



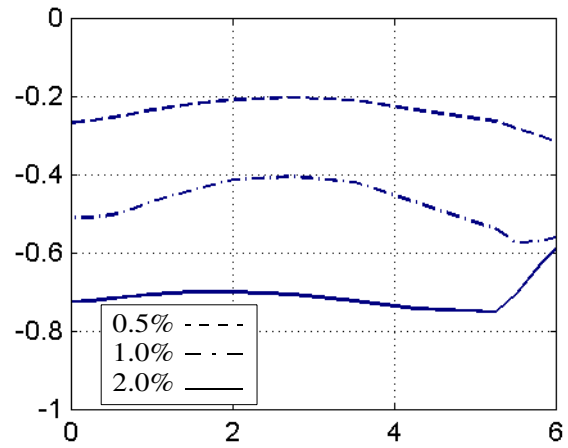
a. normal stress S_{22} normalized by σ_y



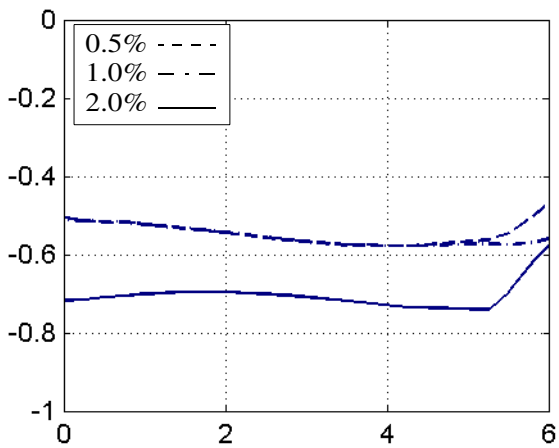
b. Mises Index



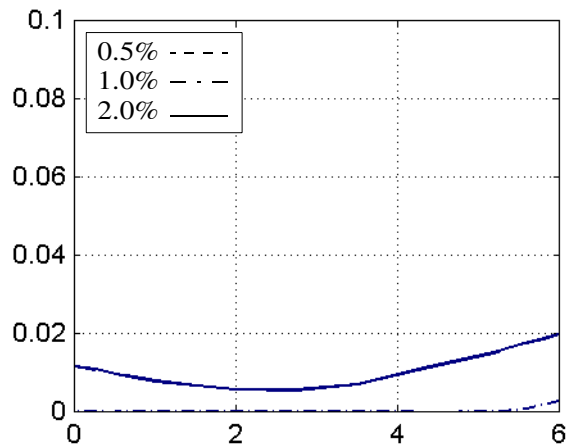
c. Equivalent Plastic Strain Index



d. Pressure Index



e. Triaxiality Index

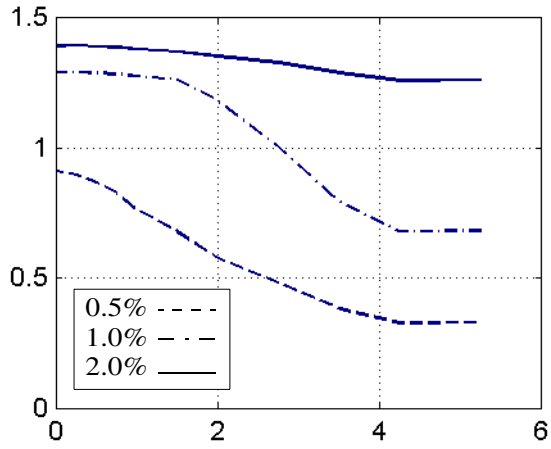


f. Rupture Index

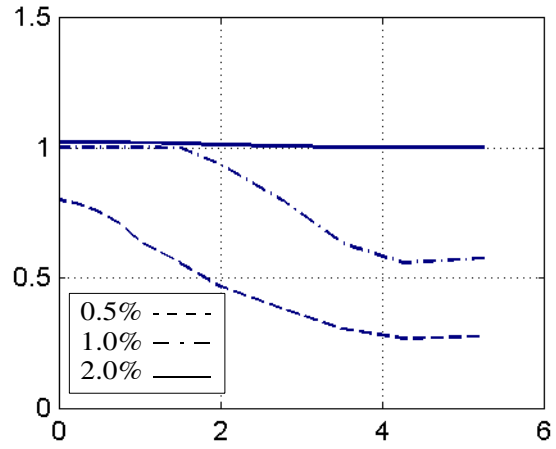
Distance from beam web centerline (in.)

Distance from beam web centerline (in.)

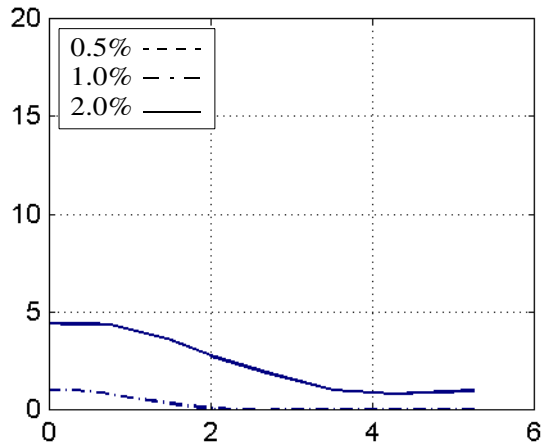
Figure 4-15 Stress and fracture indices in RC01 cover plate at face of column



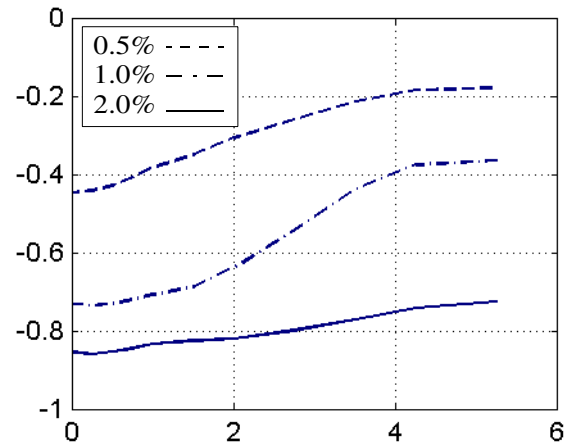
a. normal stress S_{22} normalized by σ_y



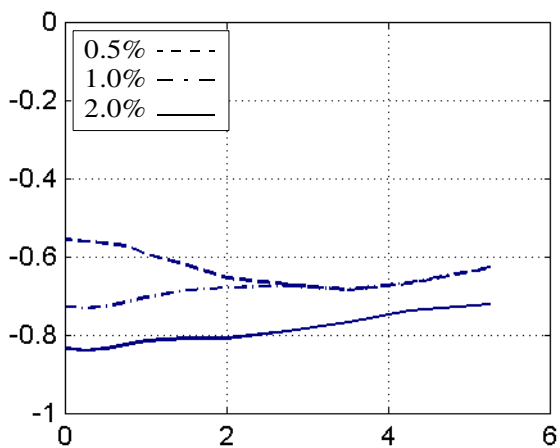
b. Mises Index



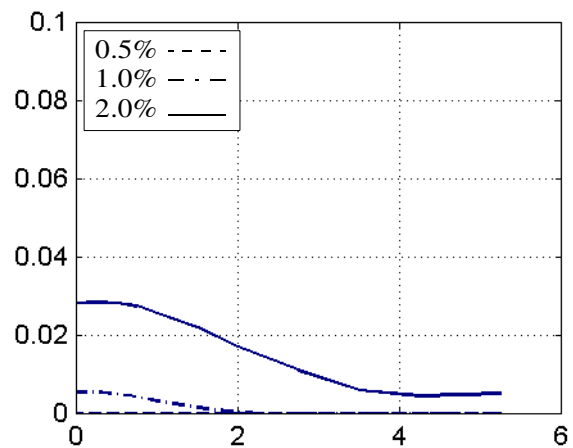
c. Equivalent Plastic Strain Index



d. Pressure Index



e. Triaxiality Index

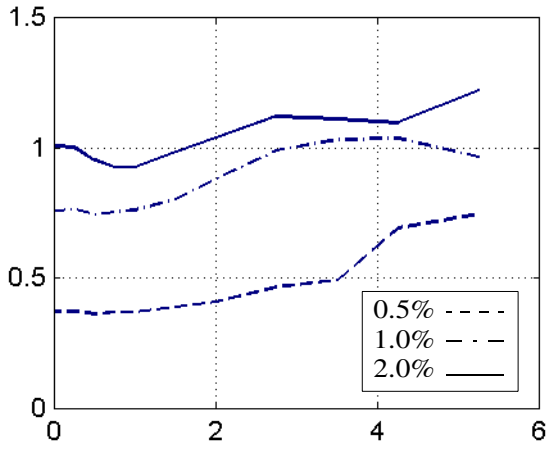


f. Rupture Index

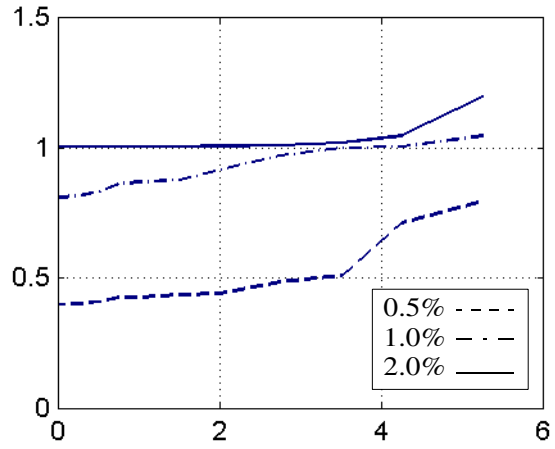
Distance from beam web centerline (in.)

Distance from beam web centerline (in.)

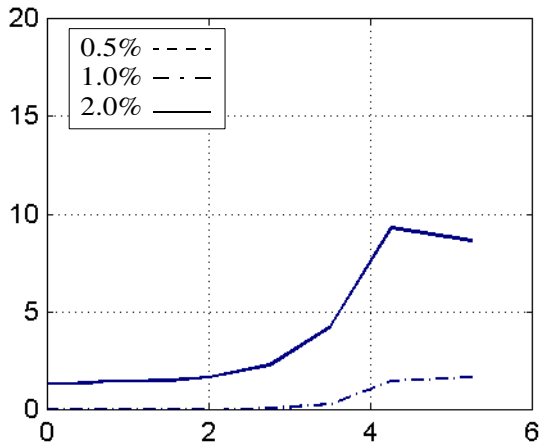
Figure 4-16 Stress and fracture indices in RC01 beam flange at face of column



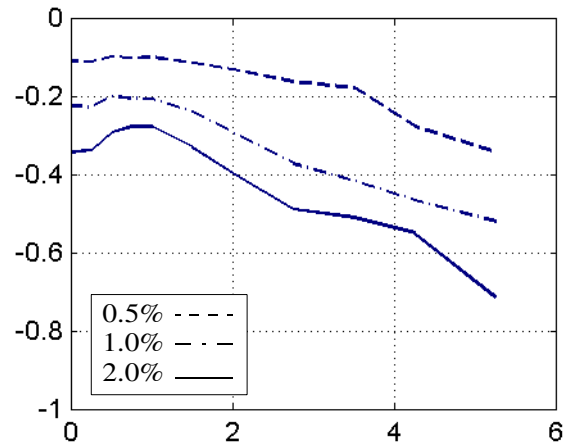
a. normal stress S_{22} normalized by σ_y



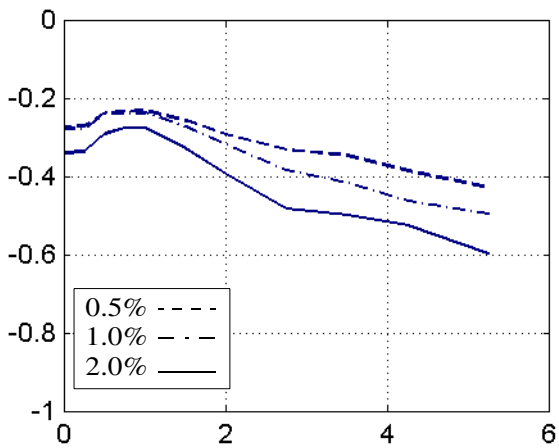
b. Mises Index



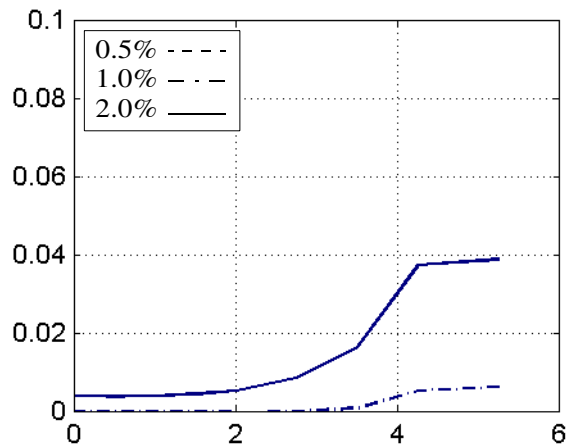
c. Equivalent Plastic Strain Index



d. Pressure Index



e. Triaxiality Index

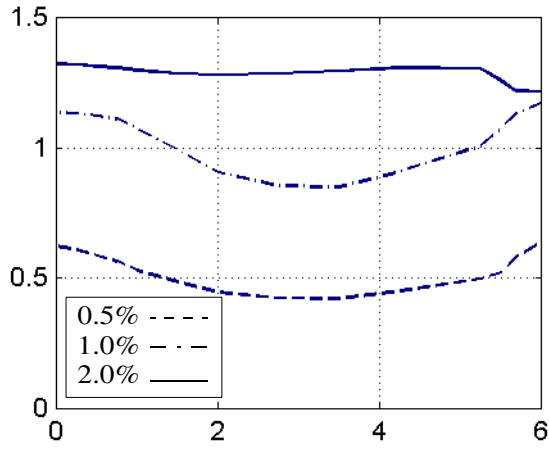


f. Rupture Index

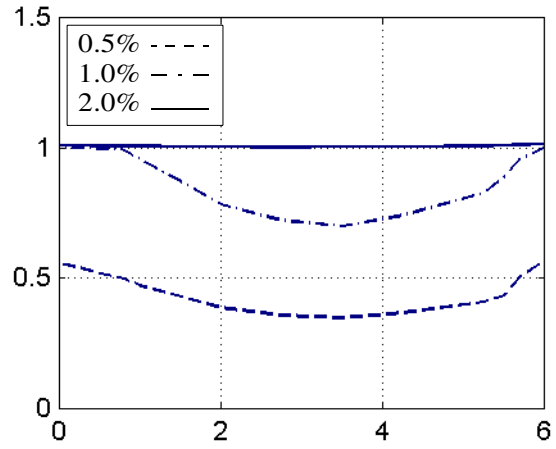
Distance from beam web centerline (in.)

Distance from beam web centerline (in.)

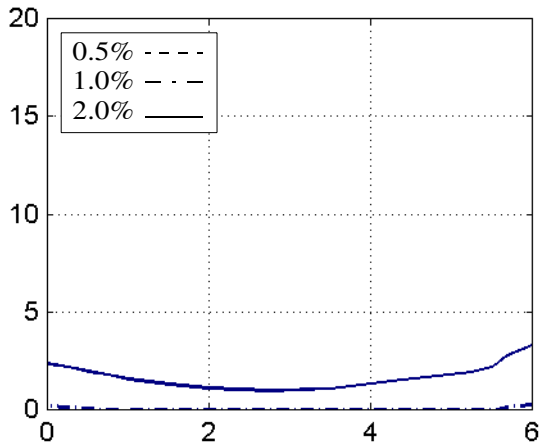
Figure 4-17 Stress and fracture indices in RC01 beam flange at nose of cover plate



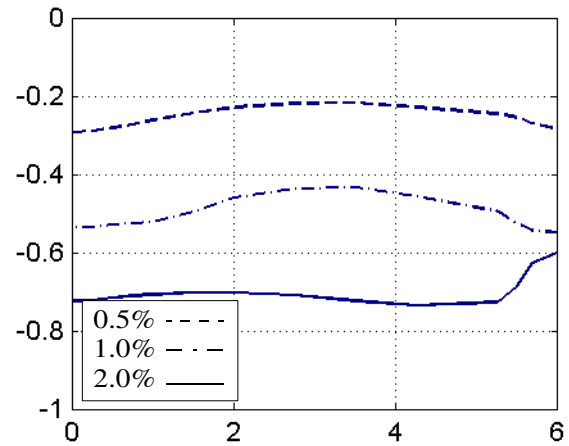
a. normal stress S_{22} normalized by σ_y



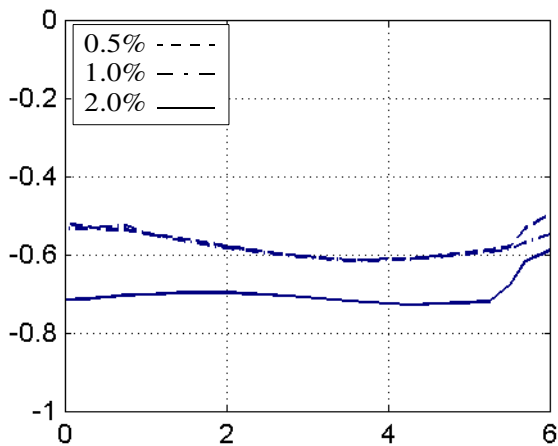
b. Mises Index



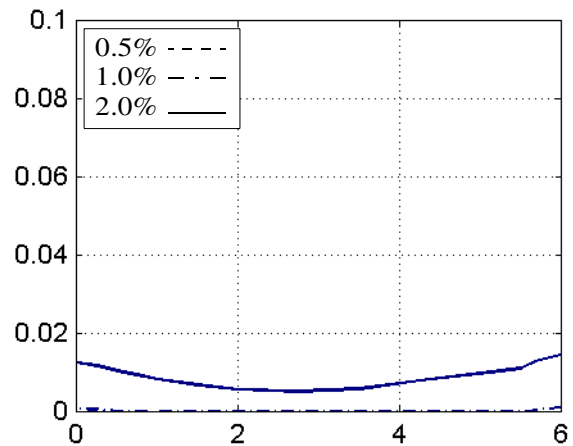
c. Equivalent Plastic Strain Index



d. Pressure Index



e. Triaxiality Index

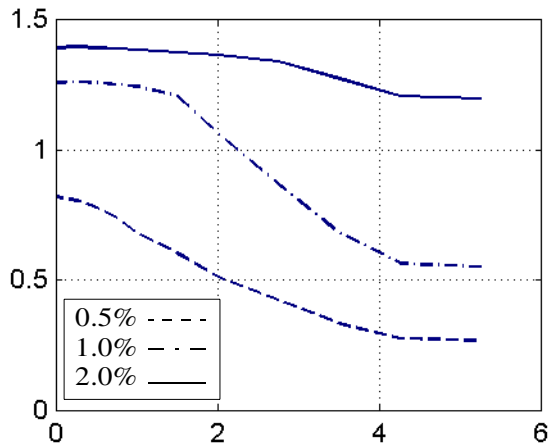


f. Rupture Index

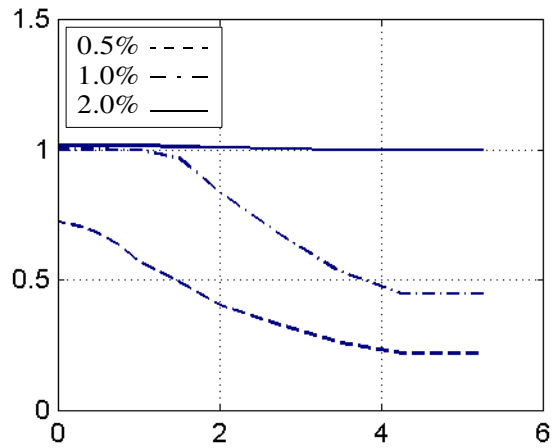
Distance from beam web centerline (in.)

Distance from beam web centerline (in.)

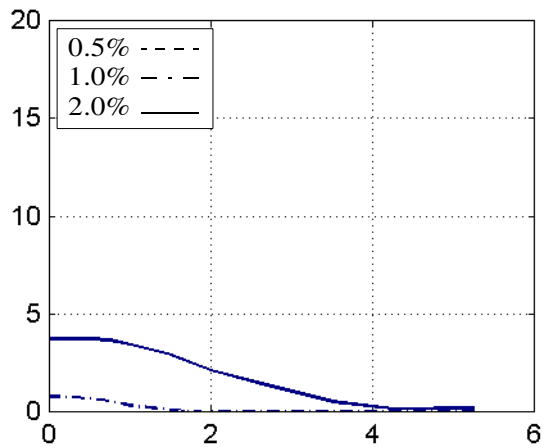
Figure 4-18 Stress and fracture indices in RC03 cover plate at face of column



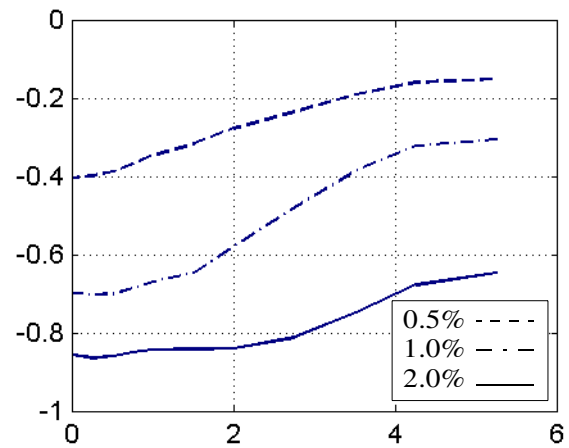
a. normal stress S22 normalized by σ_y



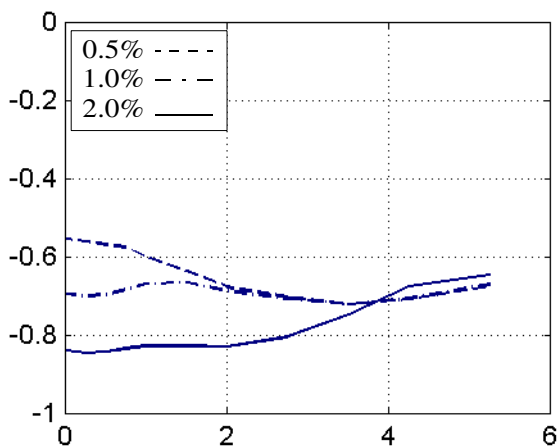
b. Mises Index



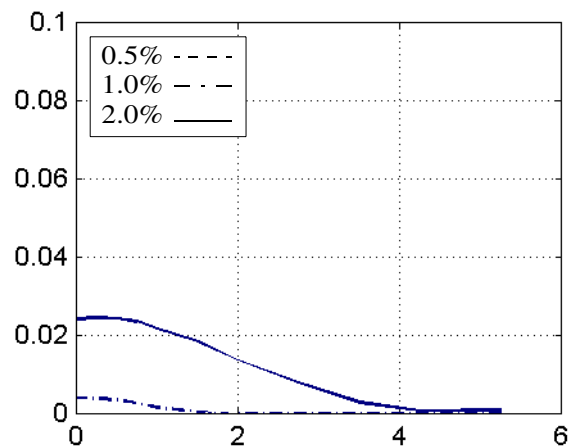
c. Equivalent Plastic Strain Index



d. Pressure Index



e. Triaxiality Index

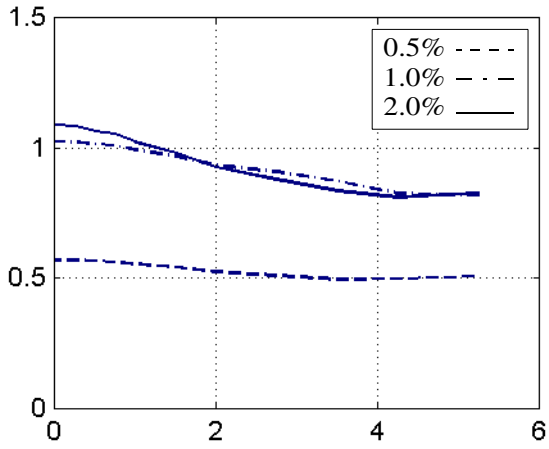


f. Rupture Index

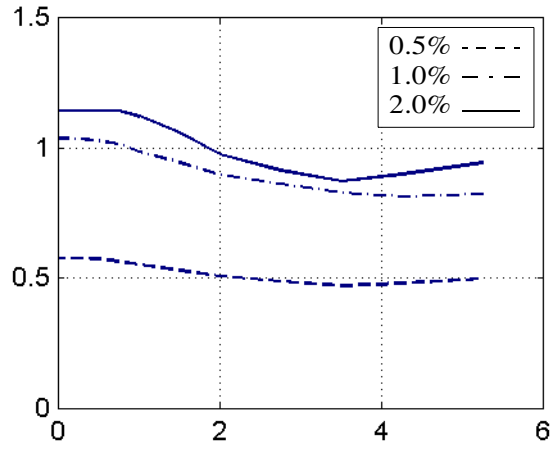
Distance from beam web centerline (in.)

Distance from beam web centerline (in.)

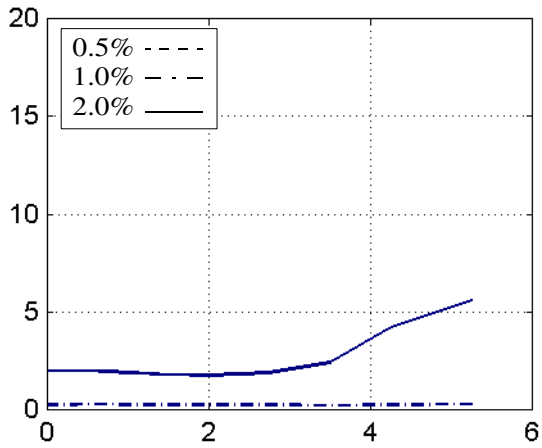
Figure 4-19 Stress and fracture indices in RC03 beam flange at face of column



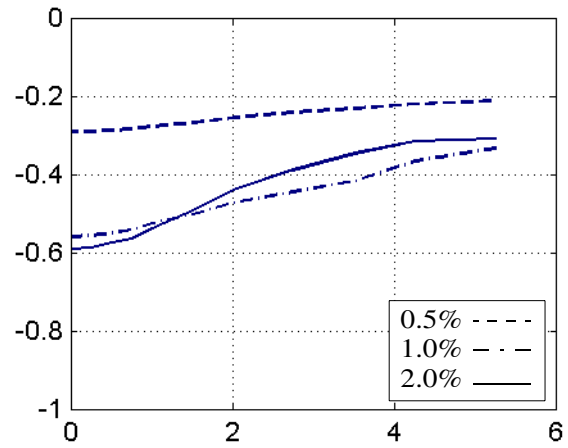
a. normal stress S_{22} normalized by σ_y



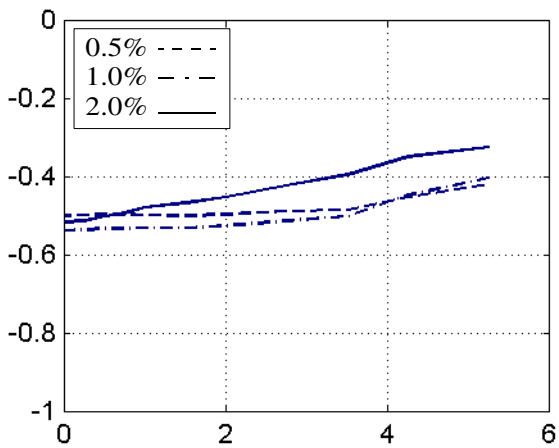
b. Mises Index



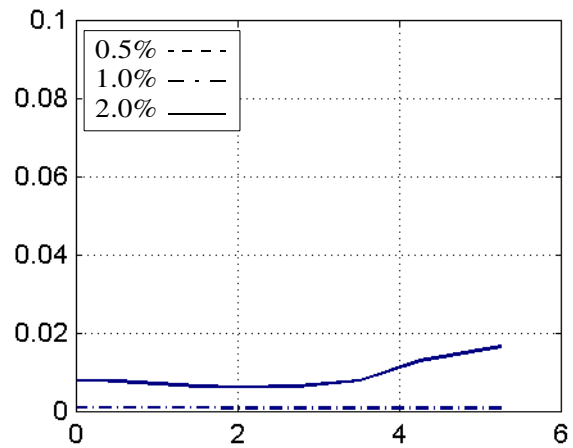
c. Equivalent Plastic Strain Index



d. Pressure Index



e. Triaxiality Index

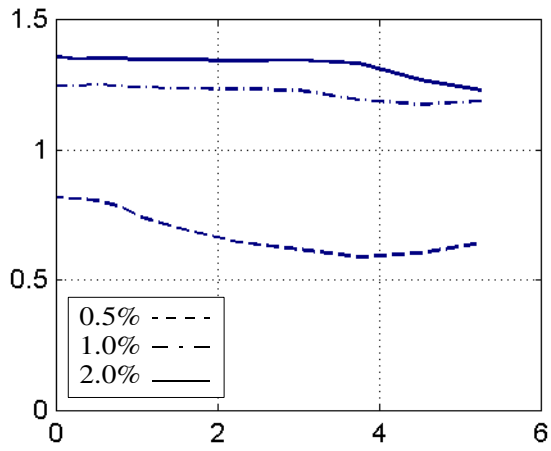


f. Rupture Index

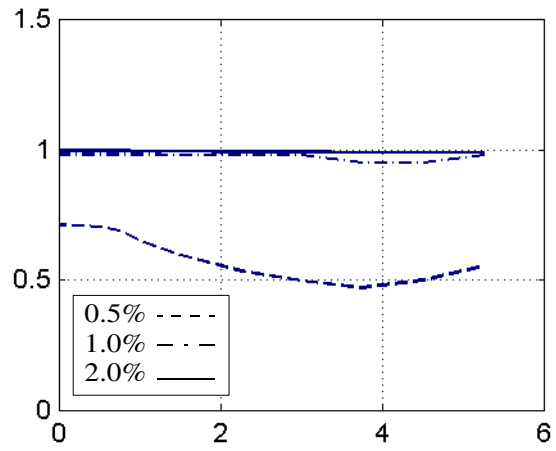
Distance from beam web centerline (in.)

Distance from beam web centerline (in.)

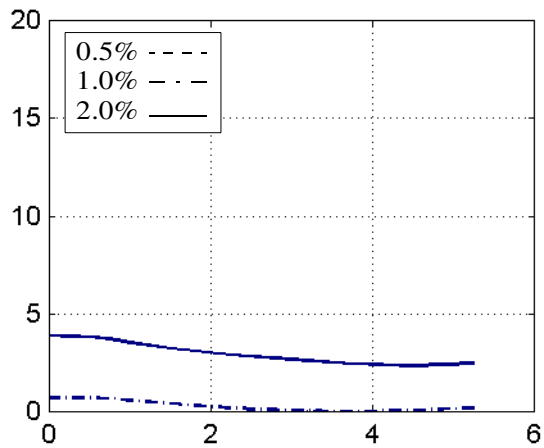
Figure 4-20 Stress and fracture indices in RC03 beam flange at edge of transverse fillet weld



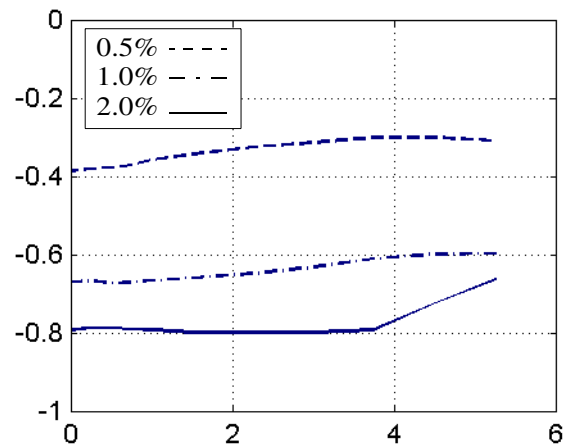
a. normal stress S22 normalized by σ_y



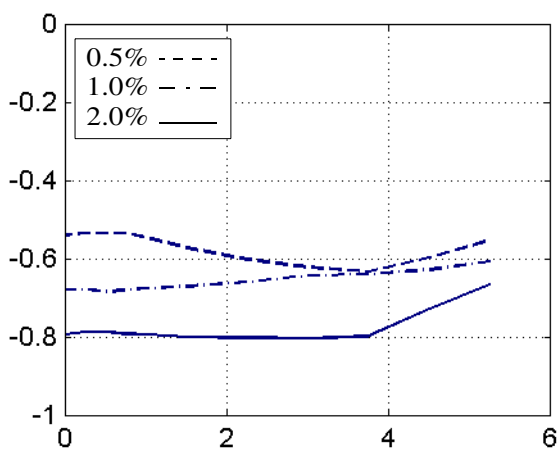
b. Mises Index



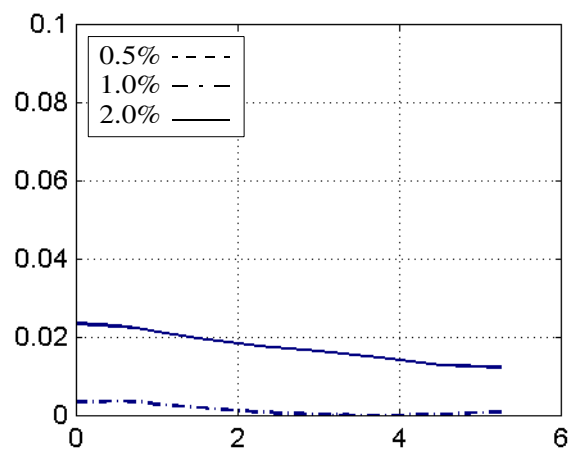
c. Equivalent Plastic Strain Index



d. Pressure Index



e. Triaxiality Index

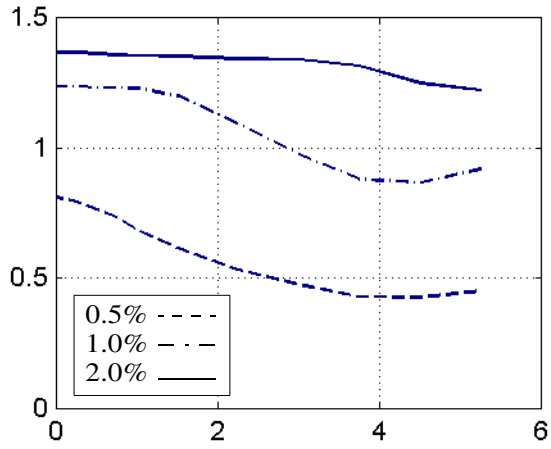


f. Rupture Index

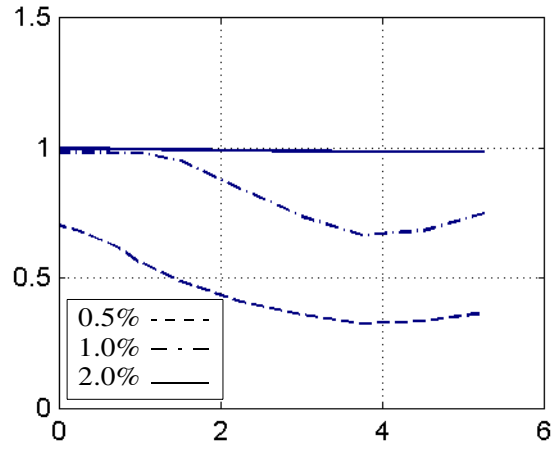
Distance from beam web centerline (in.)

Distance from beam web centerline (in.)

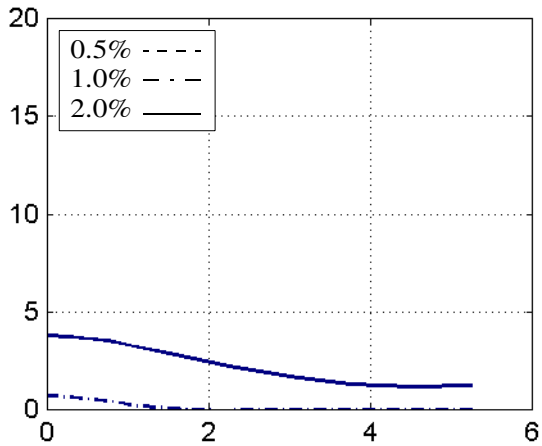
Figure 4-21 Stress and fracture indices in RC05 cover plate at face of column



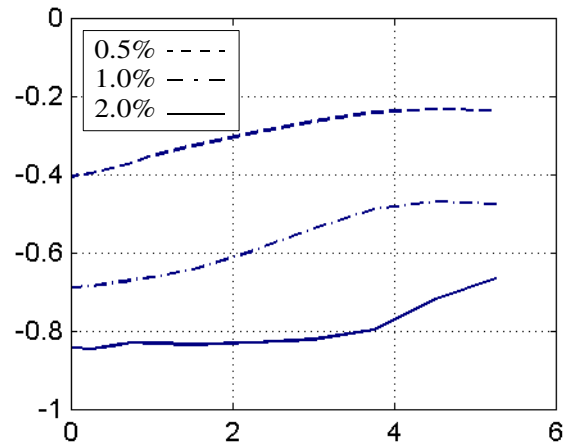
a. normal stress S_{22} normalized by σ_y



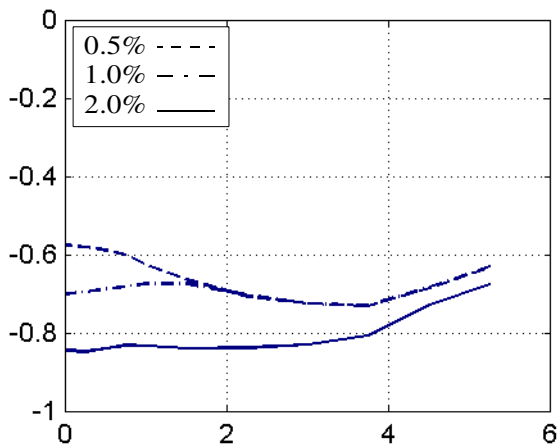
b. Mises Index



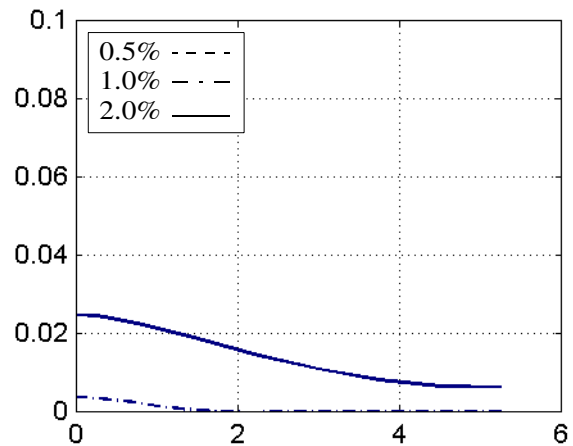
c. Equivalent Plastic Strain Index



d. Pressure Index



e. Triaxiality Index

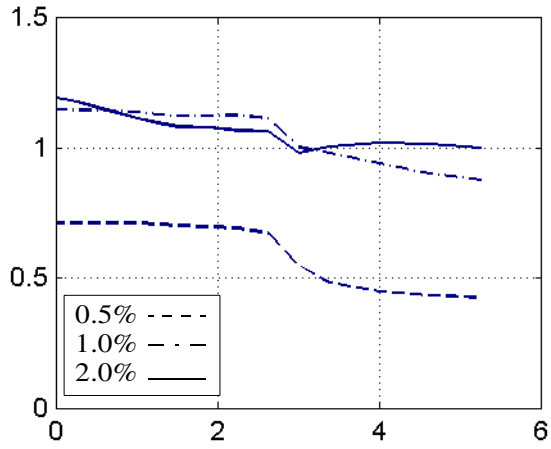


f. Rupture Index

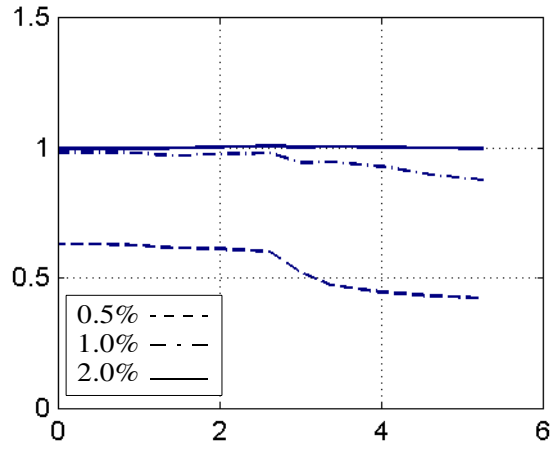
Distance from beam web centerline (in.)

Distance from beam web centerline (in.)

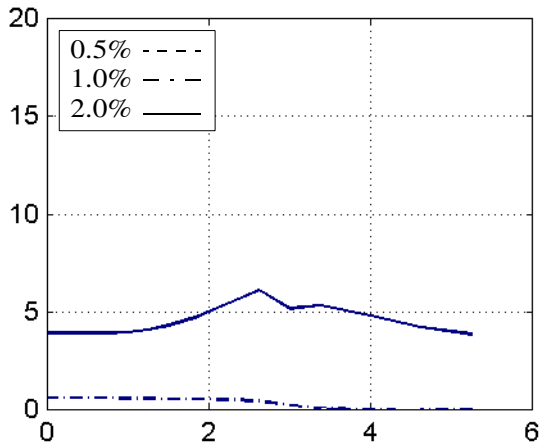
Figure 4-22 Stress and fracture indices in RC05 beam flange at face of column



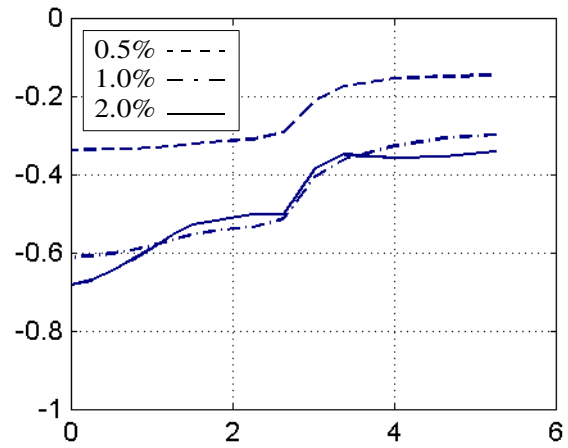
a. normal stress S22 normalized by σ_y



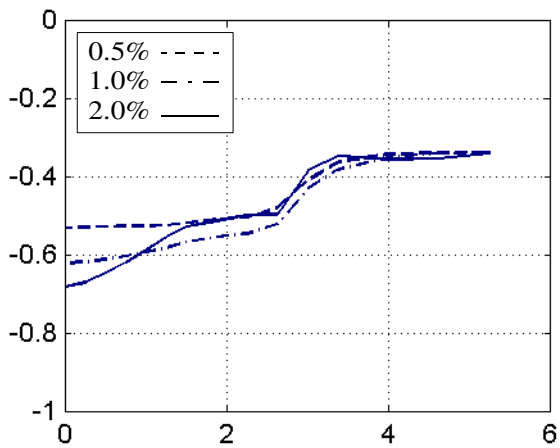
b. Mises Index



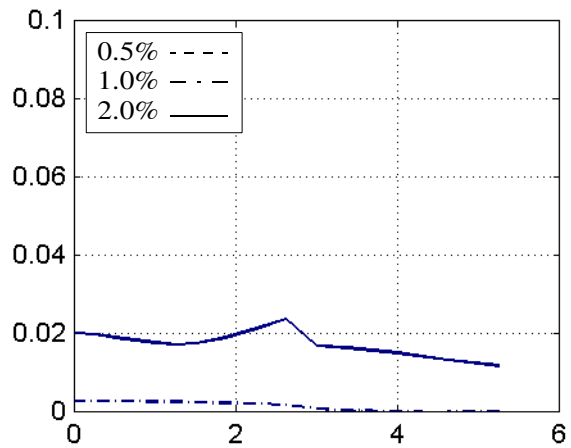
c. Equivalent Plastic Strain Index



d. Pressure Index



e. Triaxiality Index

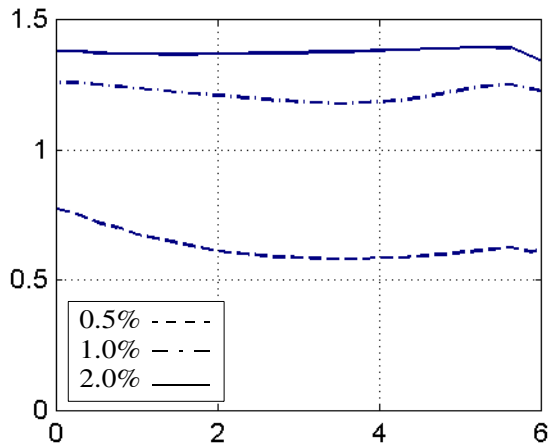


f. Rupture Index

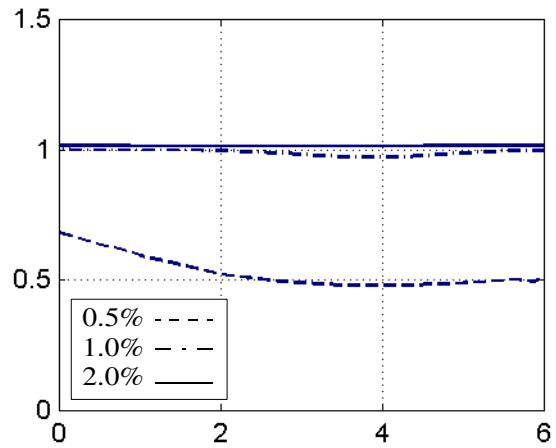
Distance from beam web centerline (in.)

Distance from beam web centerline (in.)

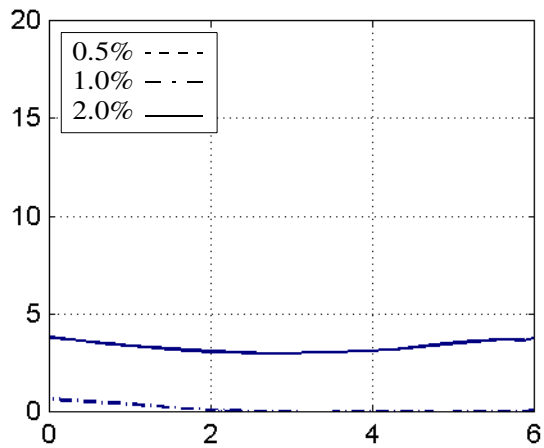
Figure 4-23 Stress and fracture indices in RC05 beam flange at edge of transverse fillet weld



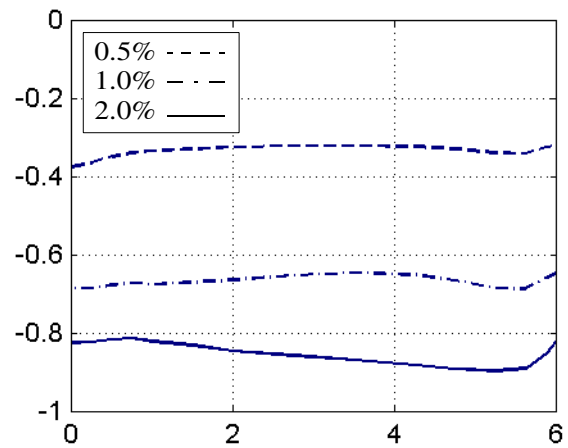
a. normal stress S_{22} normalized by σ_y



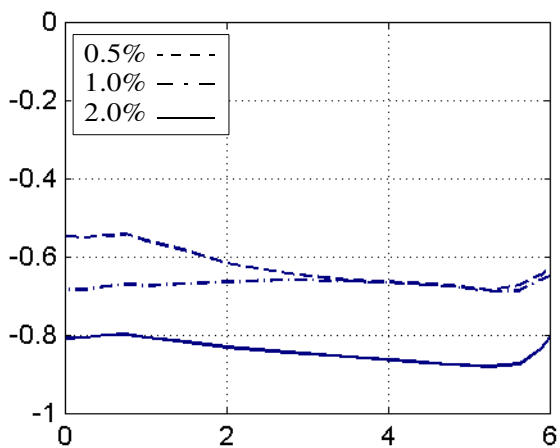
b. Mises Index



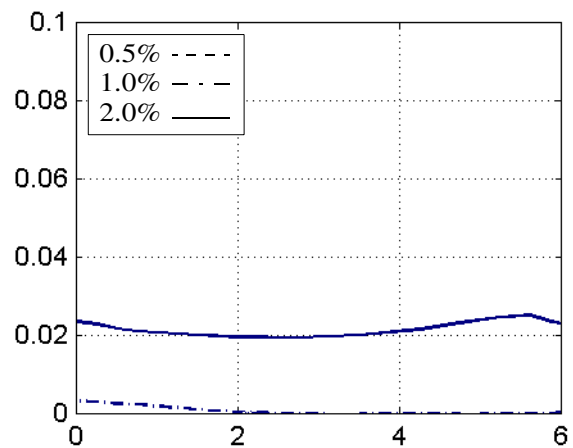
c. Equivalent Plastic Strain Index



d. Pressure Index



e. Triaxiality Index

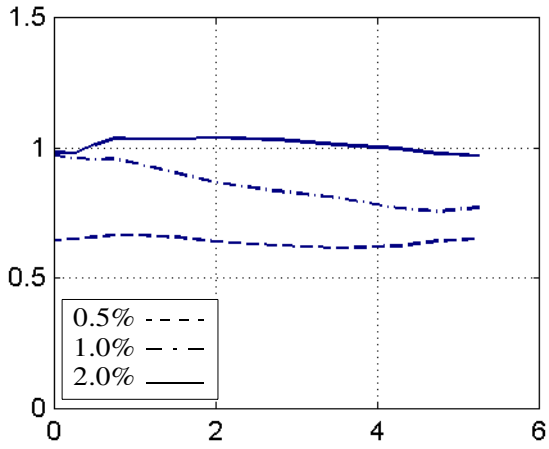


f. Rupture Index

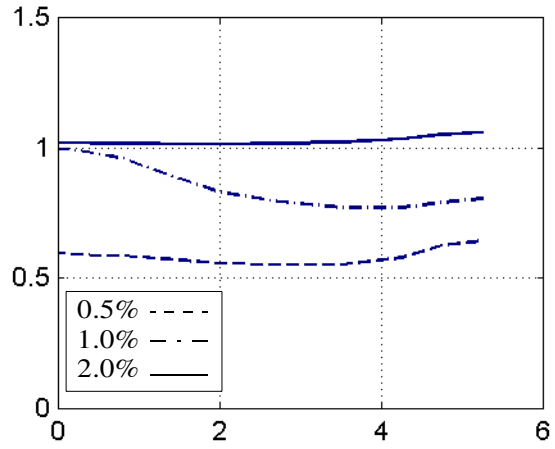
Distance from beam web centerline (in.)

Distance from beam web centerline (in.)

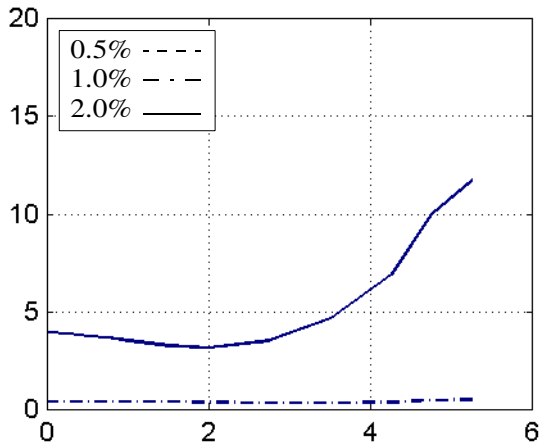
Figure 4-24 Stress and fracture indices in RC06 flange plate at face of column



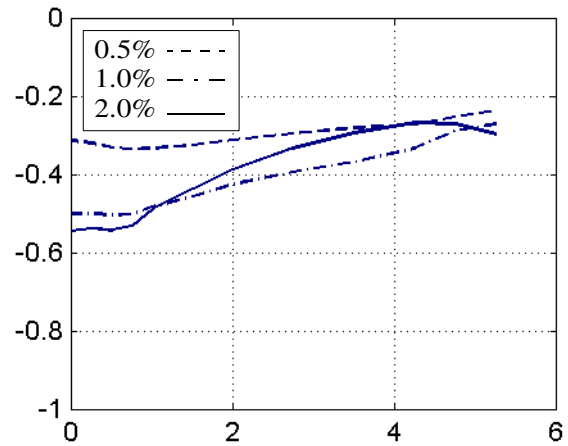
a. normal stress S_{22} normalized by σ_y



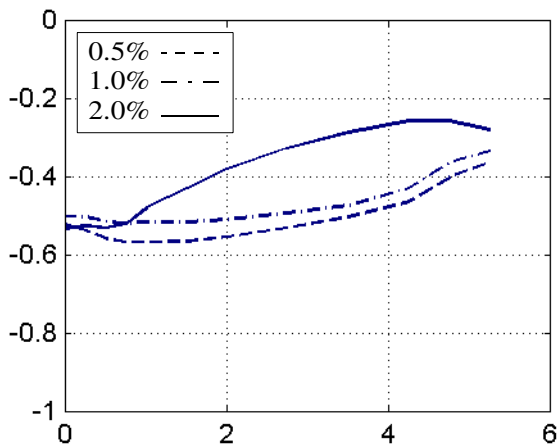
b. Mises Index



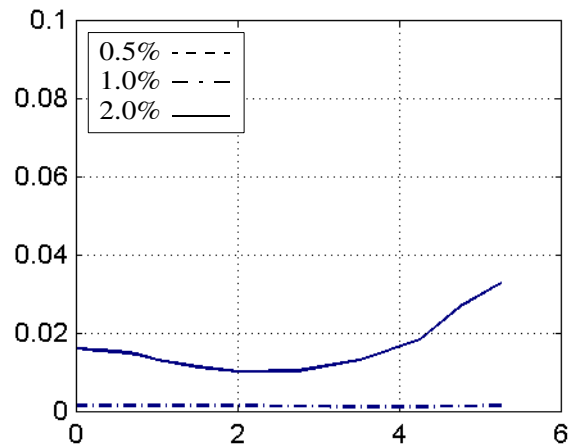
c. Equivalent Plastic Strain Index



d. Pressure Index



e. Triaxiality Index

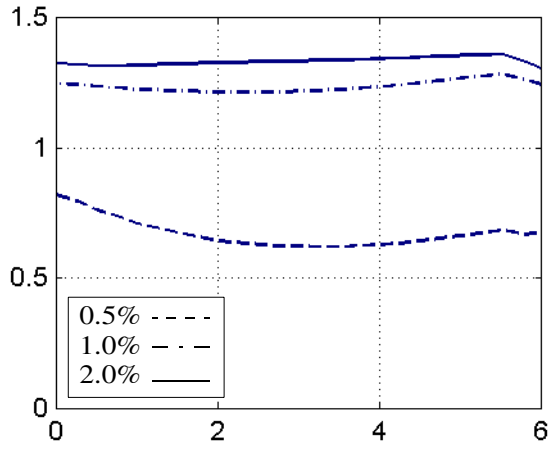


f. Rupture Index

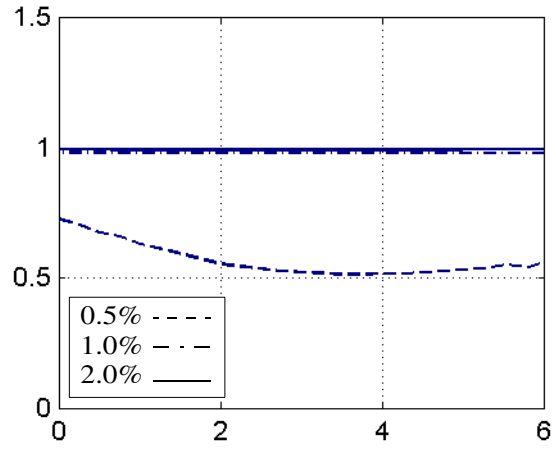
Distance from beam web centerline (in.)

Distance from beam web centerline (in.)

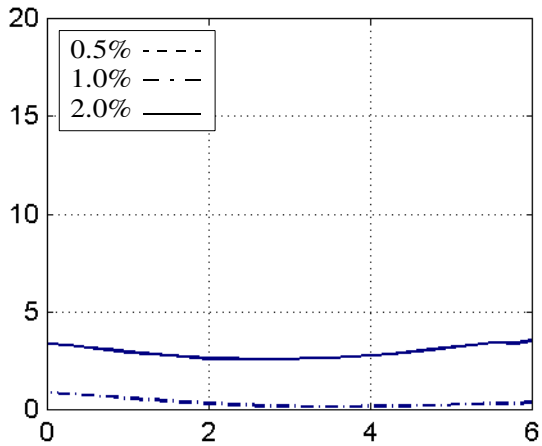
Figure 4-25 Stress and fracture indices in RC06 beam flange at edge of transverse fillet weld



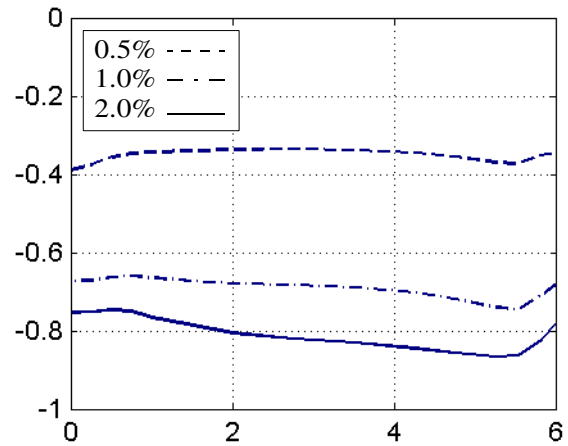
a. normal stress S22 normalized by σ_y



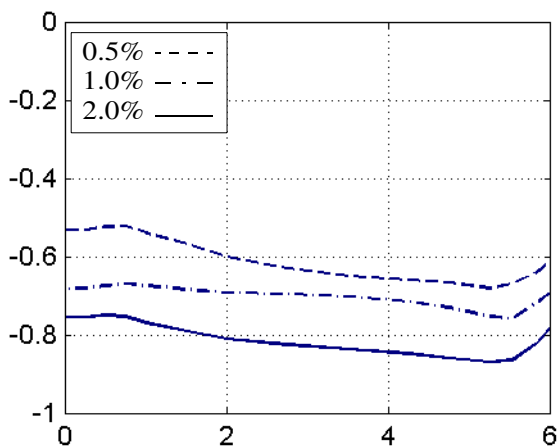
b. Mises Index



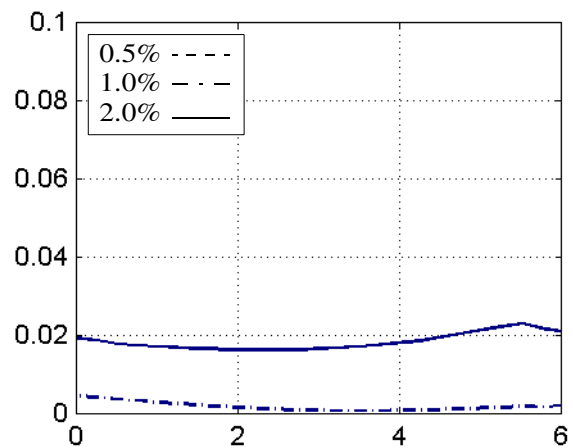
c. Equivalent Plastic Strain Index



d. Pressure Index



e. Triaxiality Index

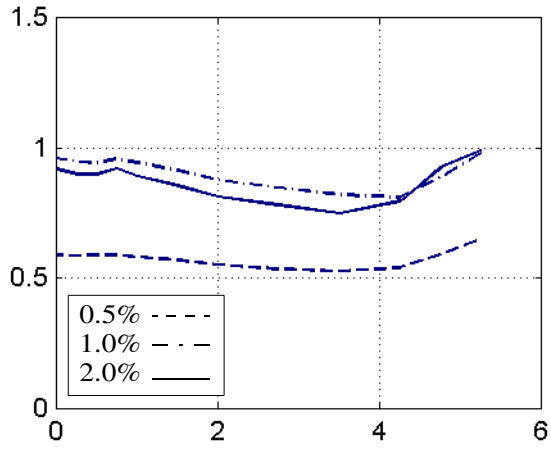


f. Rupture Index

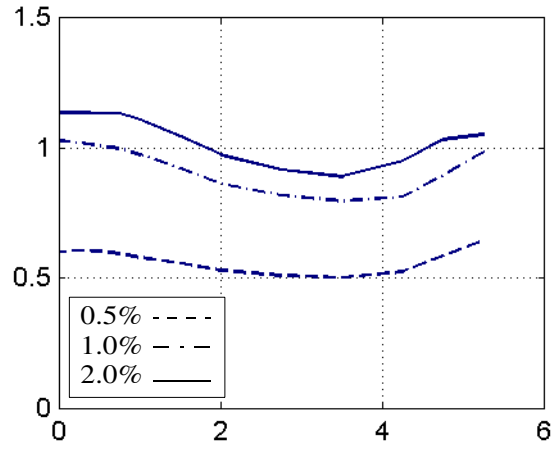
Distance from beam web centerline (in.)

Distance from beam web centerline (in.)

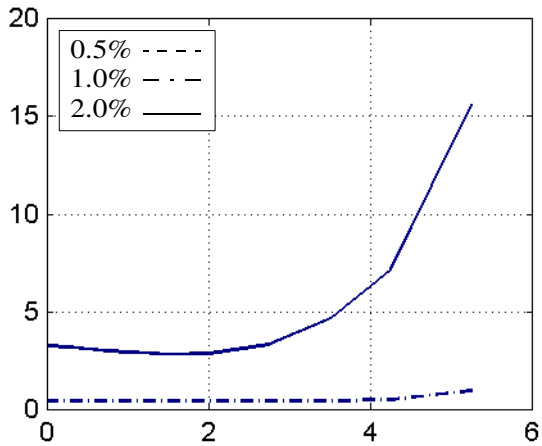
Figure 4-26 Stress and fracture indices in RC08 flange plate at face of column



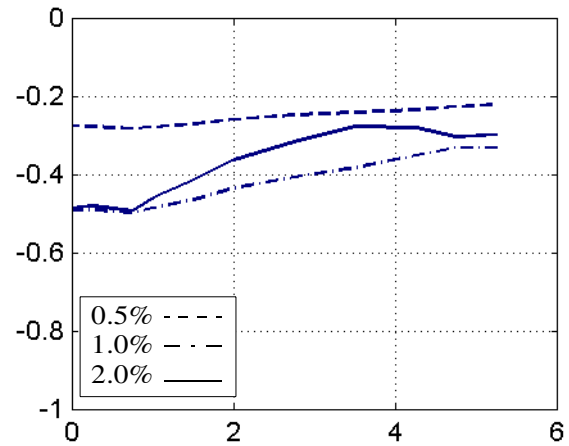
a. normal stress S_{22} normalized by σ_y



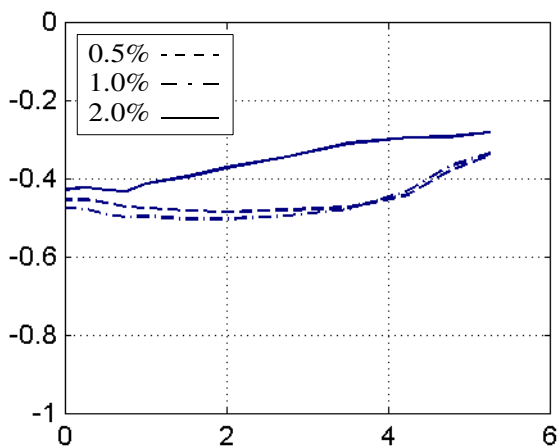
b. Mises Index



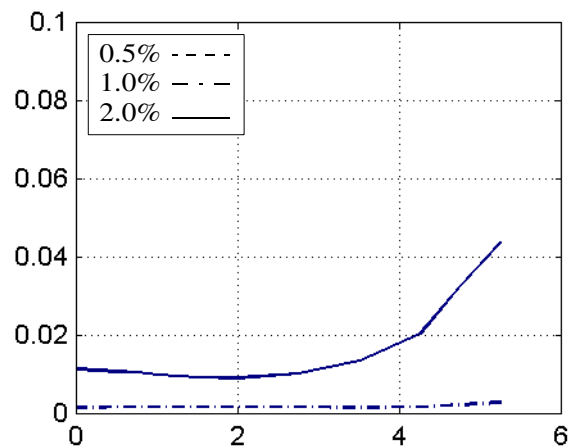
c. Equivalent Plastic Strain Index



d. Pressure Index



e. Triaxiality Index

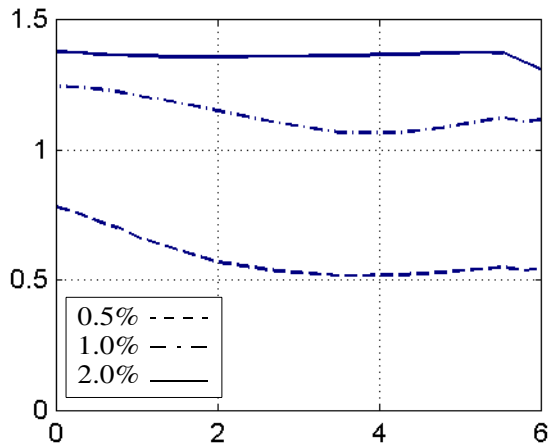


f. Rupture Index

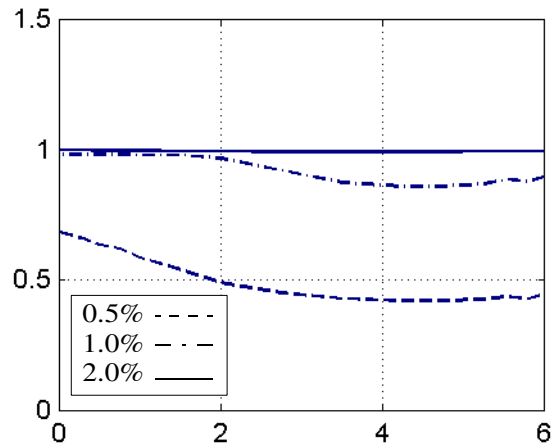
Distance from beam web centerline (in.)

Distance from beam web centerline (in.)

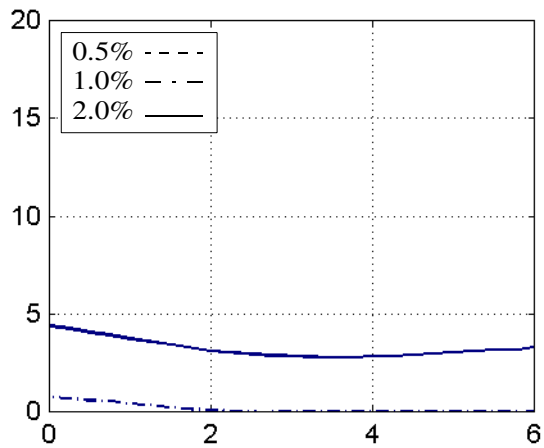
Figure 4-27 Stress and fracture indices in RC08 beam flange at edge of transverse fillet weld



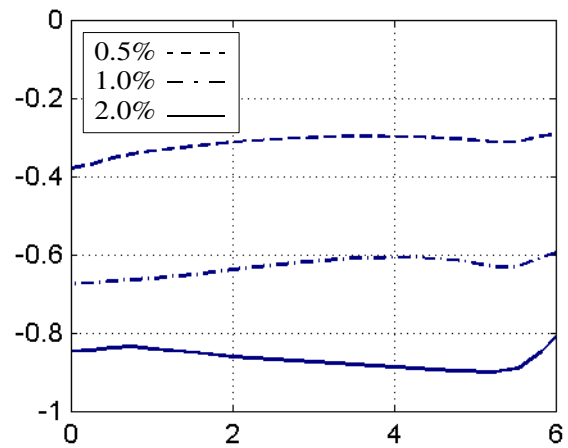
a. normal stress S_{22} normalized by σ_y



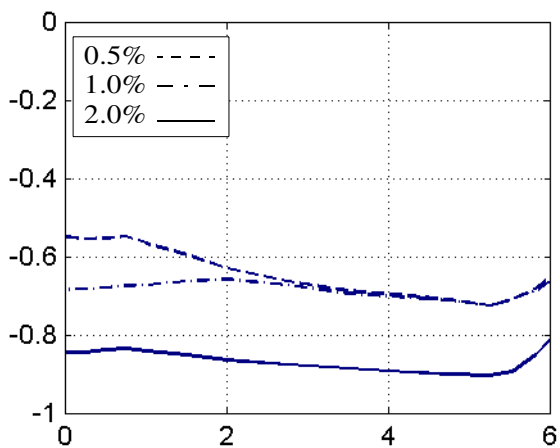
b. Mises Index



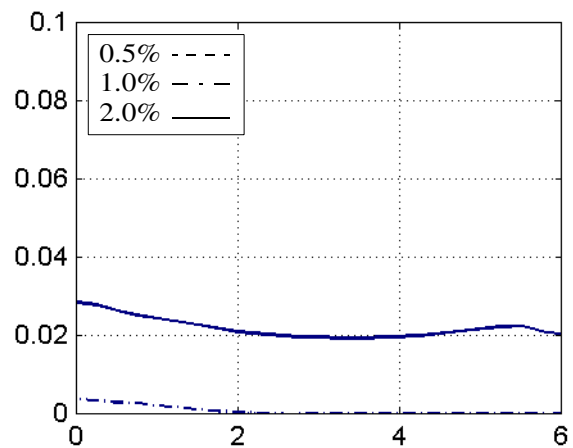
c. Equivalent Plastic Strain Index



d. Pressure Index



e. Triaxiality Index

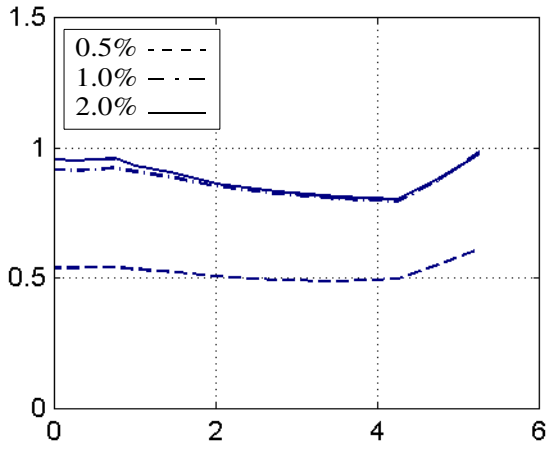


f. Rupture Index

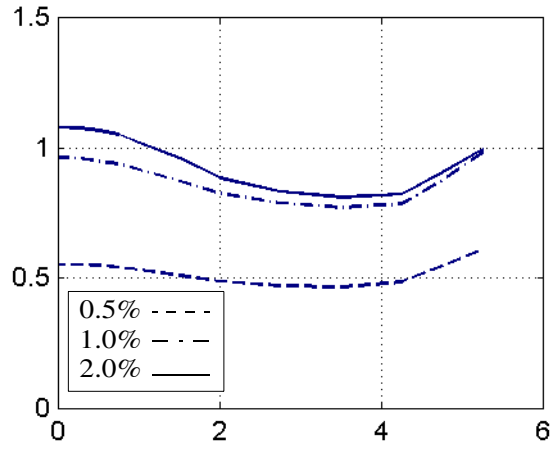
Distance from beam web centerline (in.)

Distance from beam web centerline (in.)

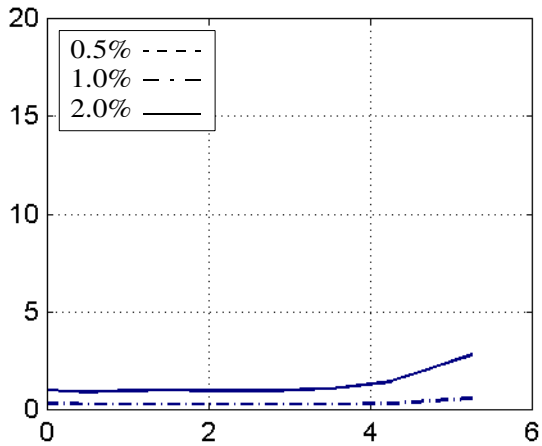
Figure 4-28 Stress and fracture indices in RC09 flange plate at face of column



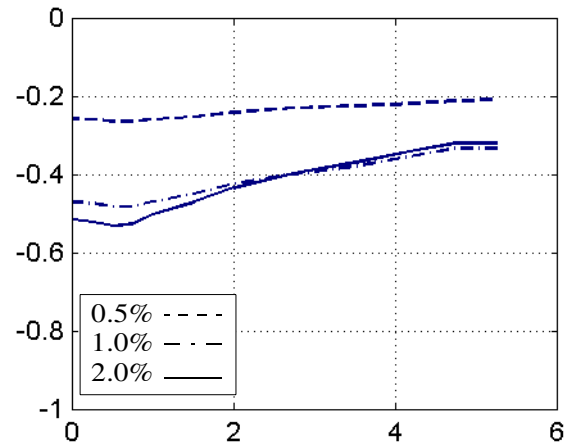
a. normal stress S_{22} normalized by σ_y



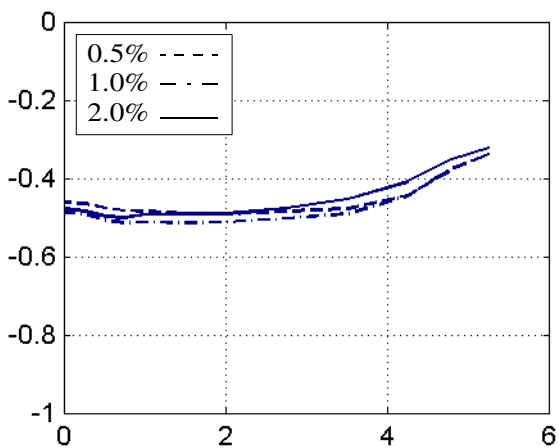
b. Mises Index



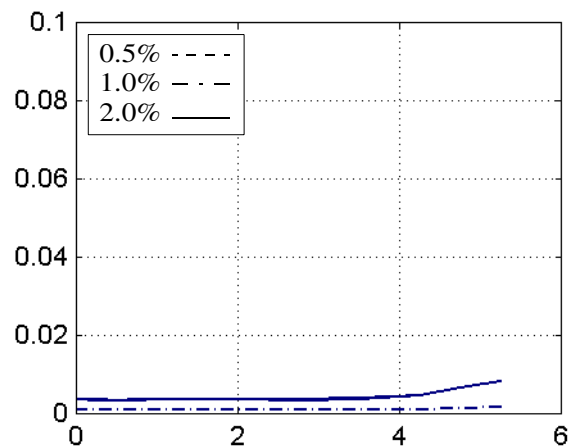
c. Equivalent Plastic Strain Index



d. Pressure Index



e. Triaxiality Index

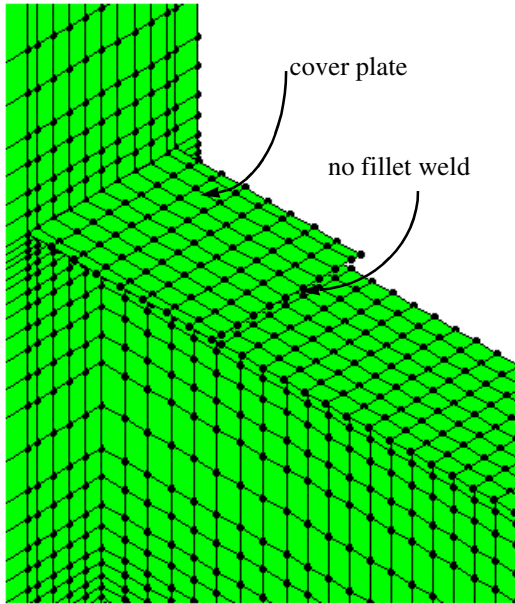


f. Rupture Index

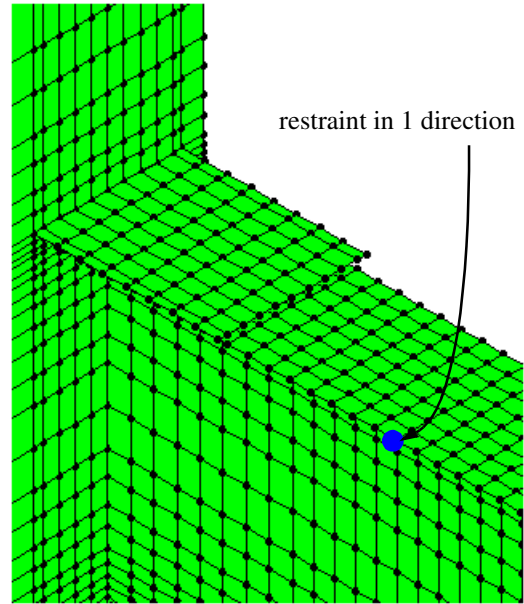
Distance from beam web centerline (in.)

Distance from beam web centerline (in.)

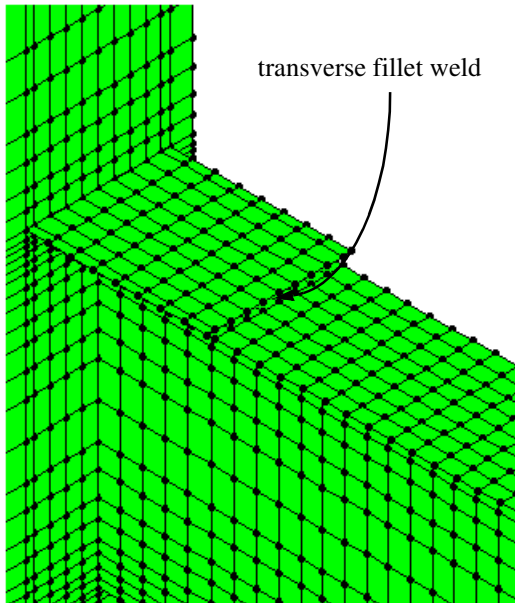
Figure 4-29 Stress and fracture indices in RC09 beam flange at edge of transverse fillet weld



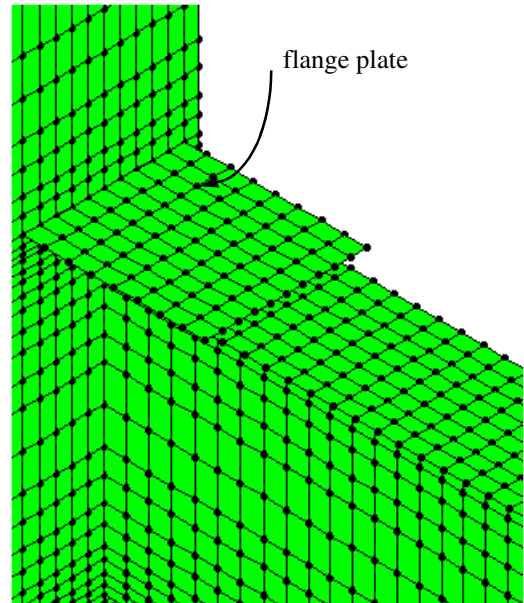
a. mesh for RC01



b. mesh for RC02



c. mesh for RC03



d. mesh for RC06

Figure 4-30 Shell element meshes in vicinity of bottom reinforcement plate

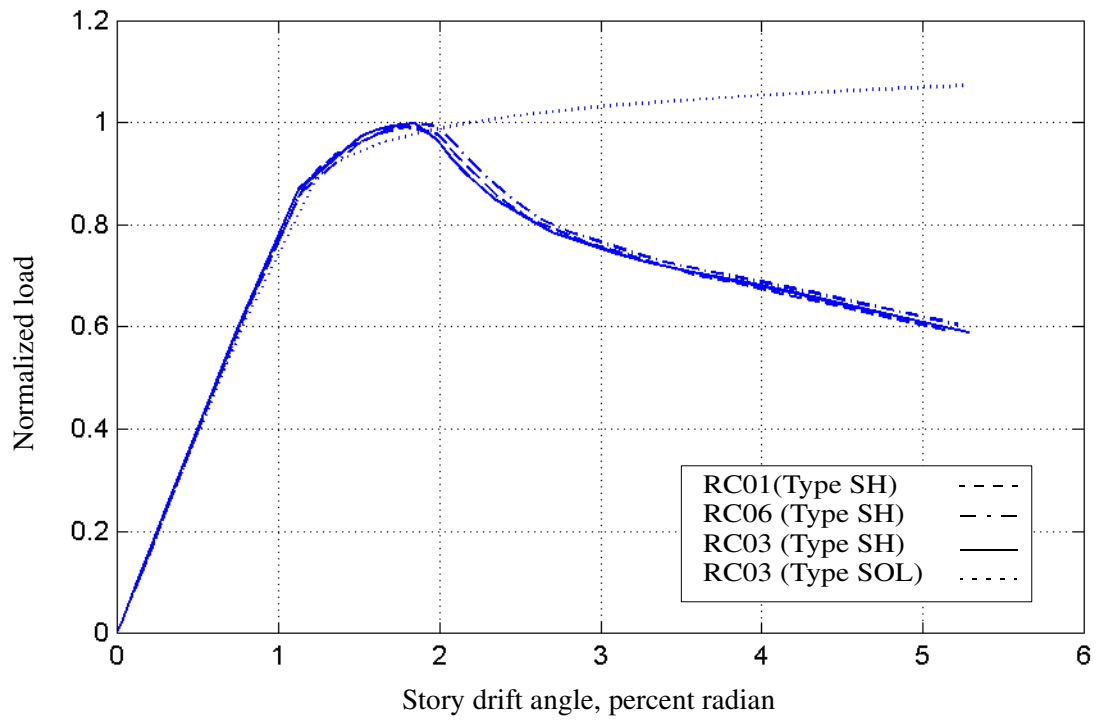


Figure 4-31 Force-displacement relations for RC01, RC03, and RC06

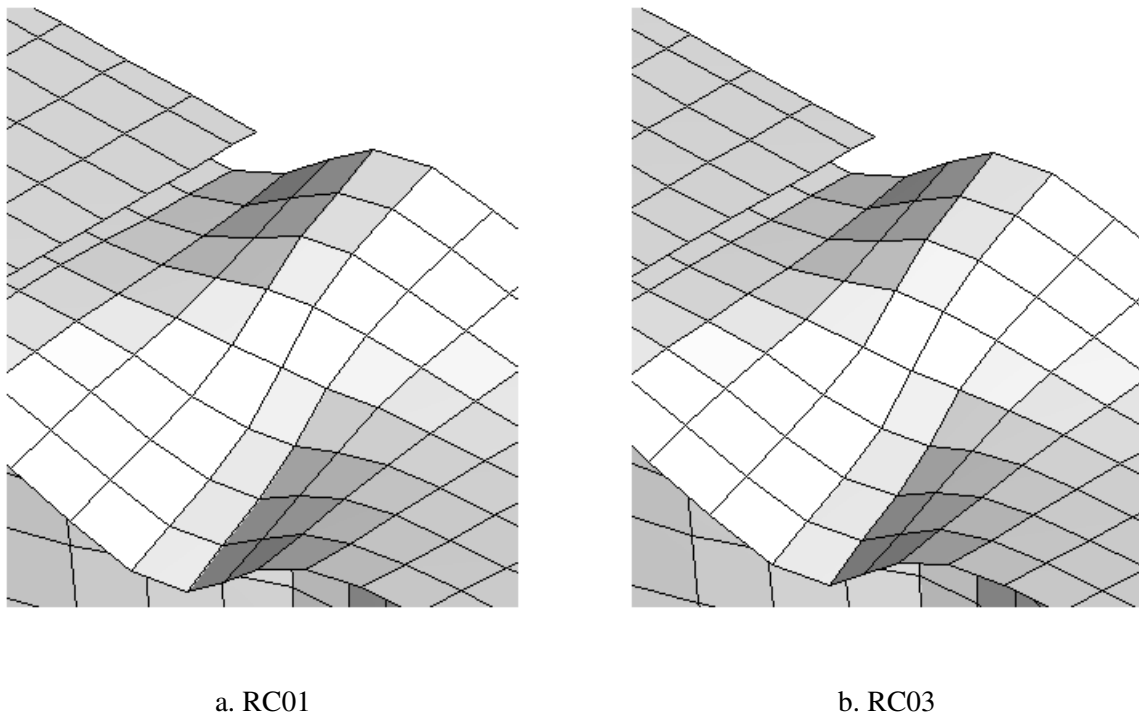


Figure 4-32 Deformed shapes of RC01 and RC03 at 5-percent story drift

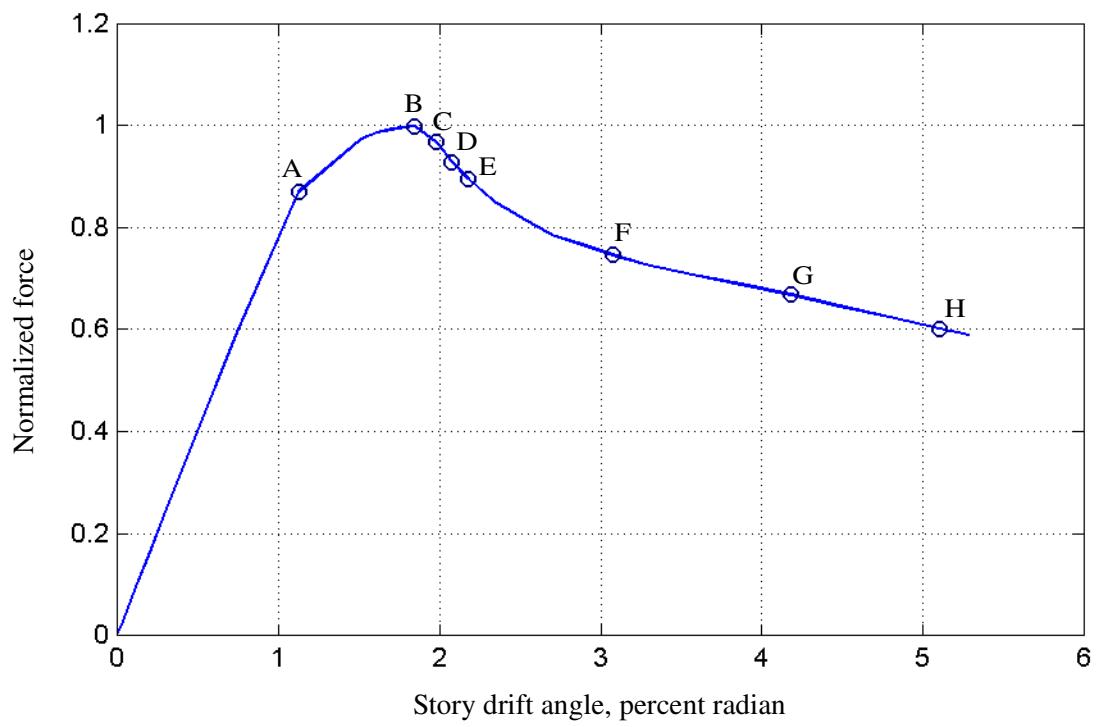


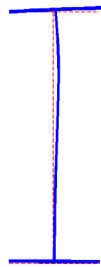
Figure 4-33 Force-displacement relation for specimen RC03



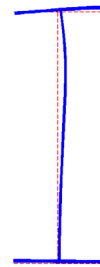
a. point A (story drift angle = 1.12% rad)



b. point B (story drift angle = 1.85% rad)



c. point C (story drift angle = 1.98% rad)



d. point D (story drift angle = 2.08% rad)



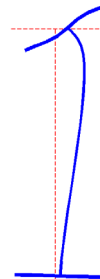
e. point E (story drift angle = 2.18% rad)



f. point F (story drift angle = 3.08% rad)



g. point G (story drift angle = 4.18% rad)



h. point H (story drift angle = 5.11% rad)

Figure 4-34 Deformed shape of RC03 beam cross section as a function of displacement for points on force-displacement relation of Figure 4-33

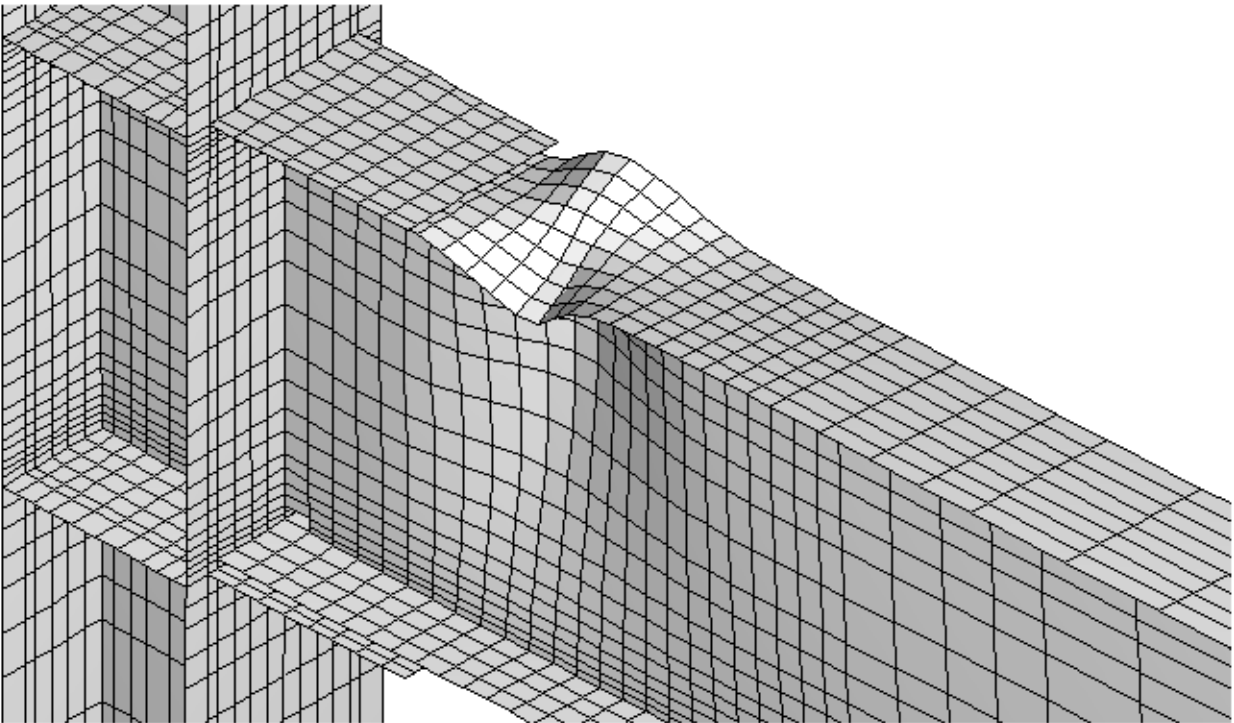
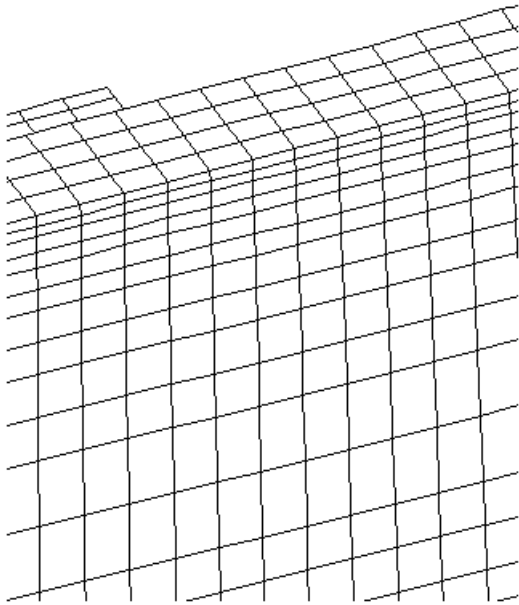
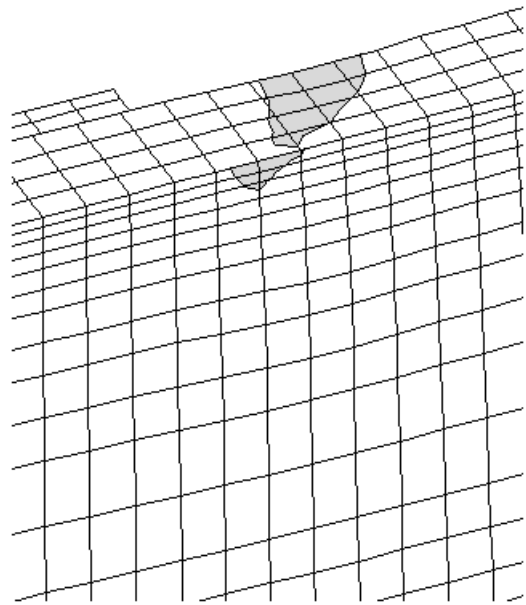


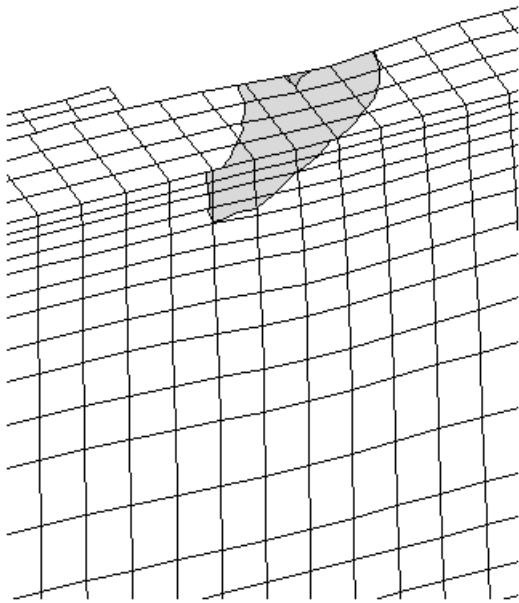
Figure 4-35 Isometric view of deformed shape of RC03 beam section at 5-percent story drift



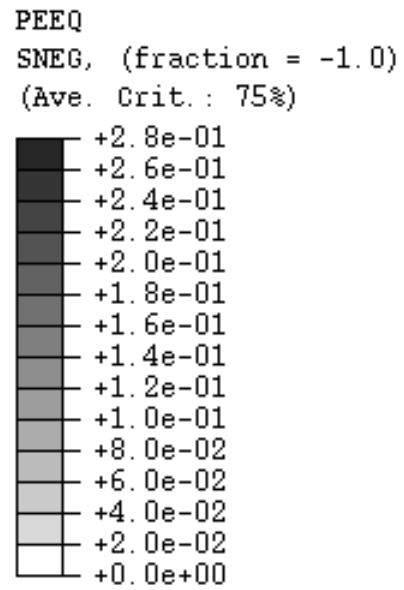
a. point B (story drift angle = 1.85% rad)



b. point C (story drift angle = 1.98% rad)

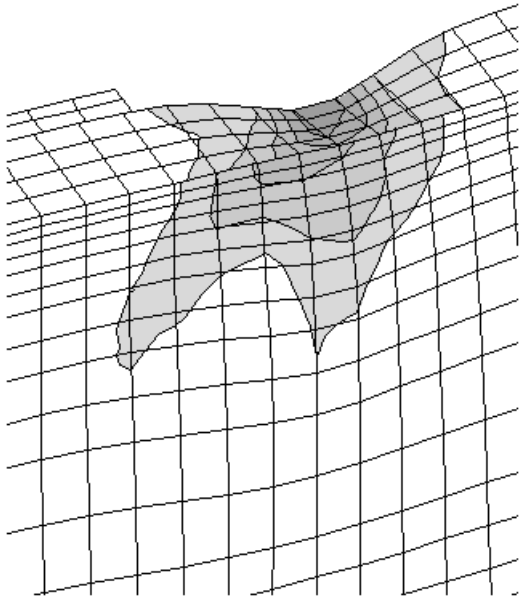


c. point D (story drift angle = 2.08% rad)

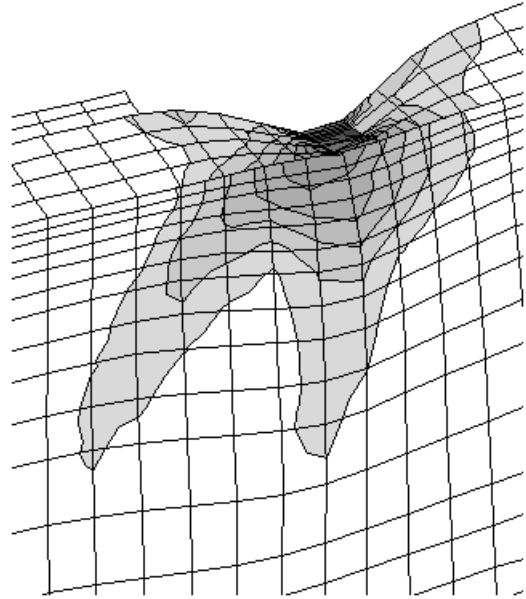


d. PEEQ values

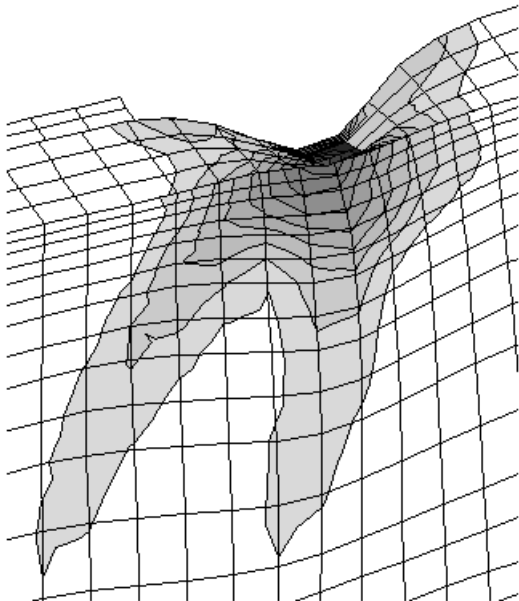
Figure 4-36 Flange- and web-local buckling in specimen RC03 (sheet 1 of 2)



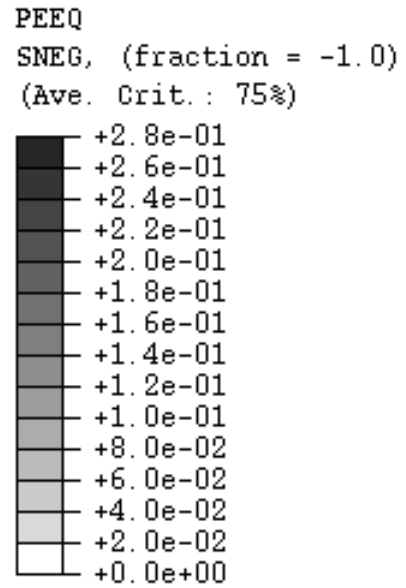
a. point F (story drift angle = 3.08% rad)



b. point G (story drift angle = 4.18% rad)



c. point H (story drift angle = 5.11% rad)



d. PEEQ values

Figure 4-37 Flange- and web-local buckling in specimen RC03 (sheet 2 of 2)

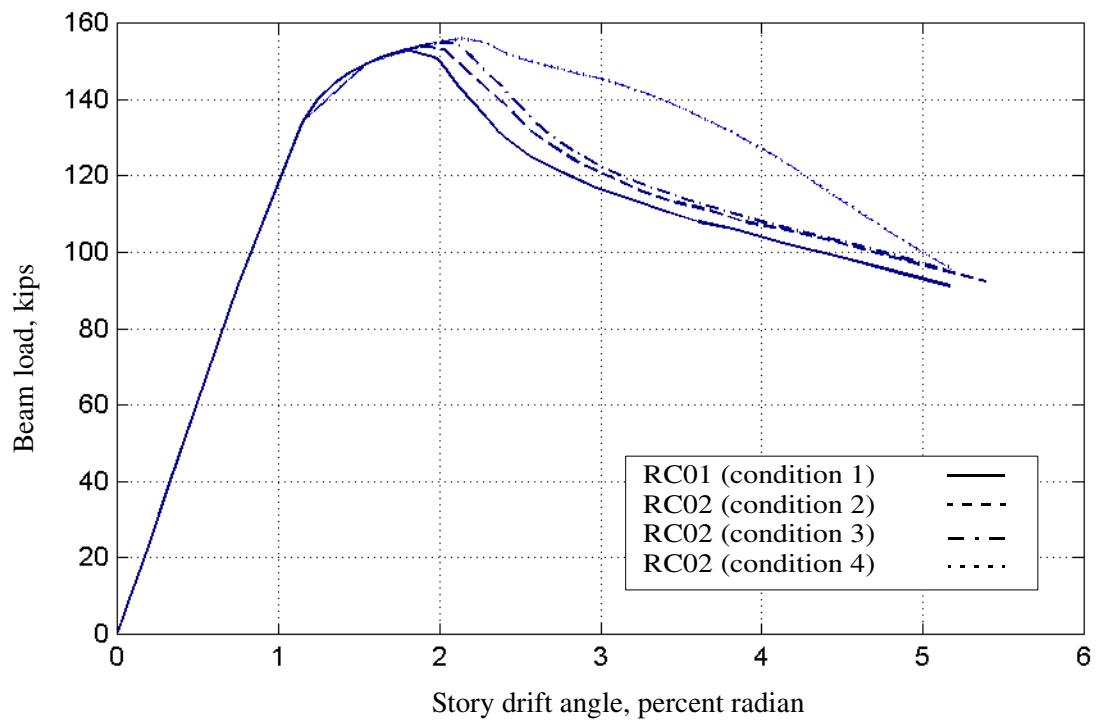


Figure 4-38 Effect of lateral-torsional buckling on force-displacement relations

5 Experimental Results

5.1 Introduction and Summary Data

The following ten sections report the results of the tests of five cover-plate (RC01, RC02, RC03, RC05, and RC10) and five flange-plate (RC04, RC06, RC07, RC08, and RC09) assemblies or specimens. The first five specimens (RC01 through RC05) were tested in the period July 13 through August 19, 1999. The data from these tests were carefully evaluated; lessons learned from the response of these specimens were included in the design and detailing of the last five specimens (RC06 through RC10). The last five specimens were tested between November 10 and December 9, 1999.

Global and local response information is presented in each of the following ten sections. Global response data in the form of actuator force versus beam tip displacement (measured in terms of story drift angle); moment at the column face versus panel zone plastic rotation; moment at the column face versus beam plastic rotation; and actuator force versus beam, panel zone, and column deformations are presented. Because the deformations of the reaction frame were significant and of the order of the column deformations, the first step in the data reduction process involved the removal of the reaction-frame displacement contributions from the beam tip displacements. As such, the displacement of the beam tip due to deformations in the specimen were always less, albeit not significantly at large tip displacements, than the target displacement or story drift angle.

Local responses were measured in terms of strains in the beam and column flanges and webs and reinforcing plates. In the following presentations, the strains are normalized with respect to a nominal yield strain that was calculated as 0.0018. The maximum normalized strain was computed as the largest peak (positive or negative) value during all cycles to a given target displacement.

Matlab (Mathworks 1999) was used to process the experimental data. The data was filtered to eliminate noise and then zero corrected. Drift in the strain gage channels was eliminated as appropriate.

The SAC Joint Venture wrote requirements that researchers studying connection performance by experimentation prepare tables listing force and displacement responses for each primary cycle of each test. Such data could be used to develop mathematical models of steel moment-resisting connections. Appendix B presents this data for all specimens except RC07 that was tested using the SAC near-field history because the reporting format specified by the Joint Venture is appropriate for cyclic test data only.

Key parameters describing the response of the ten specimens follow in Tables 5-1, 5-2, and 5-3. The component of the beam tip displacement that is due to the deformation of the reaction frame was removed from the value of deformation parameters listed below. For the purpose of reporting the displacement ductility ratio and the normalized energy dissipation, the nominal yield force was assumed to equal the maximum actuator force and the yield displacement for the specimen was computed by dividing the maximum actuator force by the initial elastic stiffness of the specimen. As defined by the Joint Venture, beam plastic rotations were computed by dividing the plastic component of the beam displacement (computed by subtracting the rigid displacement, and contributions from the column and panel zone deformation from the measured beam tip displacement) by the 141-in. (3.6-m) distance between the centerline of the column and centerline of the actuator. Three maximum and three cumulative beam plastic rotations are reported in these three tables:

1. The *maximum* beam plastic rotation (θ_p^m) recorded at the end of the test immediately prior to the fracture of the test specimen.
2. The *maximum* beam plastic rotation (θ_p^{80}) corresponding to the resistance of the specimen dropping below 80 percent of the peak resistance.
3. The *maximum* beam plastic rotation (θ_p^{80b}) corresponding to the resistance in the beam at the nose of the reinforcing plate dropping below 80 percent of the plastic moment of the beam alone, calculated as $Z\sigma_y = 312 \times 53.5 = 16,692$ kip-in. (1,900 kN-m). The moment at the column face (equal to 1.13 [=134/119] times the moment at the nose of the plate) corresponding to 80 percent of the plastic moment is 15,036 kip-in. (1,711 kN-m), that is, $15,036 = 1.13 \times 0.8 \times 16,692$.
4. The cumulative beam plastic rotation corresponding to θ_p^m .
5. The cumulative beam plastic rotation corresponding to θ_p^{80} .
6. The cumulative beam plastic rotation corresponding to θ_p^{80b} .

These calculations are explained further using Figure 5-1 that presents a generic relationship between the moment at the face of the W14x176 column and beam plastic rotation. Some cycles of response have been removed from this figure. The solid lines in this figure correspond to ± 80 of the peak resistance (positive or negative) of the specimen. The dashed lines correspond to a moment at the column face of $\pm 15,036$ kip-in. ($\pm 1,711$ kN-m).

Consider first the two beam plastic rotations, θ_p^{m+} and θ_p^{m-} , shown in the figure. The maximum beam plastic rotation θ_p^m is the larger of the absolute values of these two beam plastic rotations. The cumulative beam plastic rotation $\Sigma\theta_p^m$ is the cumulative rotation corresponding to θ_p^m .

Consider now the solid lines that are associated with 80 percent of the peak resistance of the specimen. Two crossing points are identified in the figure, one positive (θ_p^{80+}) and one negative (θ_p^{80-}). Each of these points corresponds to the largest value of beam plastic rotation at a specimen resistance equal to 80 percent of the peak resistance. The *maximum* beam plastic rotation (θ_p^{80}) is defined as the larger of the absolute values of θ_p^{80+} and θ_p^{80-} . The cumulative beam plastic rotation ($\Sigma\theta_p^{80}$) is the cumulative rotation corresponding to the rotation θ_p^{80} .

Consider finally the dashed lines that are associated with a moment at the column face of 15,036 kip-in. Two crossing points are identified in the figure, one positive (θ_p^{80b+}) and one negative (θ_p^{80b-}). Each of these points corresponds to the largest value of beam plastic rotation at a beam resistance equal to 80 percent of the beam plastic moment at the nose of the reinforcing plate. The *maximum* beam plastic rotation (θ_p^{80b}) is defined as the larger of the absolute values of θ_p^{80b+} and θ_p^{80b-} . The cumulative beam plastic rotation ($\Sigma\theta_p^{80b}$) is the cumulative rotation corresponding to the rotation θ_p^{80b} .

Table 5-1 Summary information for RC01 through RC10 (US units)

Response Quantity ¹	Specimen RC									
	01	02	03	04	05	06	07 ²	08	09	10
Q_m kips	164	168	168	158	162	165	159	168	161	192
Δ_m in.	6.7	6.7	7.1	7.5	7.7	6.7	7.6	7.8	7.4	7.3
Δ_y in.	1.8	1.9	1.9	1.8	1.9	2.0	1.8	1.9	1.9	2.1
μ	3.6	3.5	3.8	4.2	4.0	3.9	4.3	4.2	3.8	3.6
K_i kip/in.	89	87	90	88	84	84	89	91	83	93
M_m kip-ft	1,831	1,876	1,876	1,764	1,809	1,842	1,775	1,876	1,797	2,144
$\Sigma A_i / (Q_y \Delta_y)$	35.4	26.8	32.0	38.3	51.5	36.2	30.6	38.0	52.8	31.1
θ_p^m % rad	4.1	4.2	4.3	4.9	5.2	4.2	5.0	5.0	5.6	4.5
θ_p^{80} % rad	1.5	1.6	1.8	1.6	1.9	1.1	3.3	1.4	1.7	1.8
$\Sigma \theta_p^m$ % rad	37.0	32.3	38	50.9	90.4	53.3	NA	52.1	51.6	41.0
$\Sigma \theta_p^{80}$ % rad	11.0	13.0	10.5	7.3	8.9	8.5	NA	6.9	10.0	6.1

1. Q_m = maximum actuator force, Δ_m = maximum beam displacement, Δ_y = yield displacement, μ = displacement ductility ratio, K_i = initial stiffness, M_m = maximum moment at the face of column, ΣA_i = cumulative dissipated energy, $\Sigma A_i / (Q_y \Delta_y)$ = normalized dissipated energy, θ_p^m = maximum beam plastic rotation, θ_p^{80} = maximum beam plastic rotation at 80 percent maximum resistance, $\Sigma \theta_p^m$ = cumulative beam plastic rotation, $\Sigma \theta_p^{80}$ = cumulative beam plastic rotation at 80 percent of maximum resistance.

2. Near-field displacement history was used for Specimen RC07.

Table 5-2 Summary information for RC01 through RC10 (SI units)

Response Quantity ¹	Specimen RC									
	01	02	03	04	05	06	07 ²	08	09	10
Q_m kN	729	747	747	703	721	734	707	747	716	854
Δ_m mm	170	170	180	191	196	170	193	198	188	185
Δ_y mm	47	49	47	47	48	51	46	47	49	53
μ	3.6	3.5	3.8	4.2	4.0	3.9	4.3	4.2	3.8	3.6
K_i kN/m	15	16	16	16	15	15	16	16	15	16
M_m kN-m	2,481	2,542	2,542	2,372	2,453	2,497	2,409	2,542	2,436	2,906
$\Sigma A_i / (Q_y \Delta_y)$	35.4	26.8	32.0	38.3	51.5	36.2	30.6	38.0	52.8	31.1
θ_p^m % rad	4.1	4.2	4.3	4.9	5.2	4.2	5.0	5.0	5.6	4.5
θ_p^{80} % rad	1.5	1.6	1.8	1.6	1.9	1.1	3.3	1.4	1.7	1.8
$\Sigma \theta_p^m$ % rad	37.0	32.3	38	50.9	90.4	53.3	NA	52.1	51.6	41.0
$\Sigma \theta_p^{80}$ % rad	11.0	13.0	10.5	7.3	8.9	8.5	NA	6.9	10.0	6.1

1. Q_m = maximum actuator force, Δ_m = maximum beam displacement, Δ_y = yield displacement, μ = displacement ductility ratio, K_i = initial stiffness, M_m = maximum moment at the face of column, ΣA_i = cumulative dissipated energy, $\Sigma A_i / (Q_y \Delta_y)$ = normalized dissipated energy, θ_p^m = maximum beam plastic rotation, θ_p^{80} = maximum beam plastic rotation at 80 percent maximum resistance, $\Sigma \theta_p^m$ = cumulative beam plastic rotation, $\Sigma \theta_p^{80}$ = cumulative beam plastic rotation at 80 percent of maximum resistance.

2. Near-field displacement history was used for Specimen RC07.

Table 5-3 Summary beam plastic rotation information for RC01 through RC10

Response Quantity ¹	Specimen RC									
	01	02	03	04	05	06	07 ²	08	09	10
θ_p^m % rad	4.1	4.2	4.3	4.9	5.2	4.2	5.0	5.0	5.6	4.5
θ_p^{80} % rad	1.5	1.6	1.8	1.6	1.9	1.1	3.3	1.4	1.7	1.8
θ_p^{80b} % rad	2.7	2.8	2.8	2.4	2.4	2.8	3.9	2.8	2.7	NA
$\Sigma\theta_p^m$ % rad	37.0	32.3	38	50.9	90.4	53.3	NA ³	52.1	51.6	41.0
$\Sigma\theta_p^{80}$ % rad	11.0	13.0	10.5	7.3	8.9	8.5	NA	6.9	10.0	6.1
$\Sigma\theta_p^{80b}$ % rad	14.9	18.4	11.5	13.6	19.3	14.8	NA	14.3	15.3	NA

1. θ_p^m = maximum beam plastic rotation; θ_p^{80} = maximum beam plastic rotation at 80 percent maximum resistance; θ_p^{80b} = maximum beam plastic rotation at 80 percent of beam plastic moment; $\Sigma\theta_p^m$ = cumulative beam plastic rotation, $\Sigma\theta_p^{80}$ = cumulative beam plastic rotation at 80 percent of maximum resistance; $\Sigma\theta_p^{80b}$ = cumulative plastic rotation at 80 percent of beam plastic moment.

2. Near-field displacement history was used for Specimen RC07.

3. NA = not applicable.

5.2 Specimen RC01

5.2.1 Response summary

Specimen RC01 was designed as the benchmark cover-plate connection. Rectangular cover plates were used to reinforce the connection and these plates were joined to the beam flanges with longitudinal fillet welds only. Figure 5-2 is a photograph of the top cover plate.

RC01 failed during the second negative displacement excursion to $0.05h$, where h is the story height of 141 in. (3.6 m), that is equal to the distance between the actuator and the column centerlines. The beam top flange of RC01 fractured near the tip of the cover plate due to severe flange local buckling and the resulting low cycle fatigue of the beam flange. Figure 5-3 shows the degree of flange local buckling (FLB) and web local buckling (WLB) present in the beam following the displacement cycles to $0.04h$. The extent of the WLB is given by the dark zone to the right of the column face. This zone shows the extent to which the whitewash paint flaked off the surface of the beam that is indicative of yielding. The WLB penetrated back beyond the nose of the cover plate toward the face of the column.

Yielding of the panel zone and beam flange beyond the nose of the cover plate was first observed during the cycles to $0.0075h$. Local buckling of the beam flanges commenced during the cycles to $0.015h$, although the amplitude of the buckles was very small. During the cycles to $0.03h$, local buckling of the web was detected. A tear in the parent metal at the end of the fillet weld joining the beam top flange to the cover plate was observed following the first $0.03h$ cycle. This crack propagated slowly toward the beam web with subsequent cycles at $0.03h$. The amplitude of the flange and web buckles grew rapidly with cycles to $0.04h$ and $0.05h$, and the crack at the end of the fillet weld continued to grow until flange fracture. Figure 5-4 shows the tear in the beam top flange at the nose of the cover plate and the separation of the beam top flange from the cover plate. The penetration of the local buckling of the flanges back beyond the nose of the cover plate that is evident in the figure introduces additional strains in the longitudinal fillet welds that were not captured by the Type SOL finite element analysis of Chapter 4.

5.2.2 Global response

Specimen RC01 was subjected to 32 cycles of imposed displacements or drift levels up to and including $0.05h$. Figure 5-5 shows the relation between actuator force and drift angle. The maximum drift angles in this figure do not equal the target values because of deformations in the reaction frame that contributed to the beam tip displacement during testing. At the drift of approximately $0.05h$, which corresponded to a beam tip displacement of 6.7 in. (170 mm) after subtracting the reaction-frame displacements, the maximum joint plastic rotation was 4.1 percent radians. Due to the degradation of the stiffness and strength of the beam due to WLB and FLB, and the consequent unloading of the panel zone, nearly all of this plastic deformation was in the beam. The loss of strength and stiffness that is evident in the second of the two cycles to $0.03h$ was a result of WLB and FLB. Following buckling of the web, the amplitude of the flange buckles increased rapidly, which in turn increased the amplitude and extent of the web buckles.

The maximum measured moment at the nose of the cover plate, which is 15 in. (380 mm) from the face of the column, was 19,500 kip-in. (2,200 kN-m): 1.17 times the plastic moment of 16,692 kip-in (1,890 kN-m) calculated using the measured yield stress of 53.5 ksi (see Table 3-2). The inelastic behavior seen in Figure 5-5 is composed of plastic deformation in the panel zone (Figure 5-6) and the beam (Figure 5-7). The maximum plastic rotation in the panel zone was 0.0045 radian that occurred prior to loss of strength and stiffness in the beam due to FLB and WLB. Figure 5-8 presents the actuator load and drift angle relations for the beam (solid line), panel zone (dashed line), and column (dotted line). At drift angles exceeding 2 percent, the deformations in the beam comprise nearly all of the beam tip displacement or story drift.

Two of the response limit states described in Section 5.1, namely *80-percent-peak* and *80-percent-beam*, are used below and in the following nine sections to judge the performance of the reinforced connections. The horizontal solid lines in Figures 5-6 and 5-7 represent the *80-percent-peak* limit state; the dashed lines in Figure 5-7 represent the *80-percent-beam* limit state. For RC01, $\theta_p^m = 0.041$ radian, $\theta_p^{80} = 0.015$ radian, and $\theta_p^{80b} = 0.027$ radian.

5.2.3 Local response

Figure 5-9 presents the recorded strain profiles across the beam top flange at the nose of the cover plate and top cover plate at a distance of 2 in. (51 mm) from the face of the column, as a function of drift angle. The drift angle shown in this figure includes the drift contribution from the reaction frame. The strain values shown in the figure are the maximum values at each drift angle, normalized to the yield strain calculated using nominal values of yield stress and Young's modulus. For drift angles less than 0.01 radian, the strains in the cover plate and the beam flange are similar in magnitude. Following yielding in the beam flange, the strains in the beam increased rapidly but the strain in the cover plate increased at a more modest rate. At drift angles greater than 0.03 radian, the strains in the cover plate are reduced due to degradation of strength in the beam due to FLB and WLB. Strain data for the beam flange are shown for drift angles of 0.03 radian and less because at higher drift angles the gages were over-ranged. Differences in the beam gage values for drift angles larger than 0.01 radian were expected due to FLB. The maximum measured strains in the cover plate ranged between 1 and 2 times the yield strain. Such an observation is consistent with the strain data presented in Chapter 4 but conflicts with the strains calculated using beam theory, which was used to design the experiments. Modest yielding of the cover plate had no detrimental effect on either the global or local response of the specimen.

Figure 5-10 shows the recorded strain profiles along the top cover plate and continuity plate as a function of drift angle. The normalized strain values shown in the figure are the maximum values at each drift angle divided by the yield strain (assumed equal to 0.0018). The maximum strain in the 1.125-in. (29 mm) thick continuity plate immediately adjacent to the column flange that was welded to the beam flange and cover plate was 82 percent of the yield strain. The strains measured in the gage remote from the beam-to-column connection (shown by the diamond in the figure) were less than 14 percent of the yield strain indicating that much of cover-plate-flange force had been transferred to the column web.

Questions have been raised regarding the efficacy of doubler plates in resisting the shear forces that develop in panel zones of beam-column connections. For design it is assumed that the shear strains in the column web and doubler plate of the panel zone are identical. Figure 5-11 shows the recorded strain profiles for two locations in the column web and doubler plate of the panel zone as a function of story drift angle. For drift angles less than or equal to 0.01 radian, the maximum strains in the panel zone and doubler plate were identical. For drift angles greater than 0.01 radian, the strains in the corner of the panel zone and doubler plate were identical. The strains in the center of the panel zone-doubler plate were greater than those in the corner, but the values of the strains differed for drift angles between 0.01 and 0.03. For drift angles greater than or equal to 0.03, the strains were identical.

Figure 5-12 presents the distribution of the normalized axial strain along the line b (that corresponds to the center of beam flange outstand) as a function of drift angle. Data from the strain gage at the nose of the cover plate shows only modest values of strain at all drift angles, which correlates well with the Type SOL model analysis data of Chapter 4.

5.3 Specimen RC02

5.3.1 Specimen response

Specimen RC02 was identical to RC01 except that horizontal braces were attached to the beam flanges, 20 in. (508 mm) from the nose of the cover plate, to delay lateral-torsional buckling of the beam. As described in Section 3.2, the lateral braces were designed for an axial force of 25 kips (110 kN) that corresponds to $0.06A_fF_y$, where A_f is the area of the beam flange and F_y is the nominal yield stress of the beam of 50 ksi (345 MPa).

Testing of RC02 was terminated due to net section fracture of the tab plates connecting the horizontal braces to the beam flanges during the first negative displacement excursion to $0.05h$. Figure 5-13 shows the flange local buckling (FLB) and web local buckling (WLB) in the beam at an drift of $0.03h$. The extent of the WLB is given by the dark zone to the left of the column face. The WLB penetrated back beyond the nose of the cover plate toward the face of the column. Yielding of the panel zone is also evident in this photograph. A photograph of the fractured tab plates is presented in Figure 5-14.

Yielding of the panel zone was first observed during the cycles to $0.0075h$. The beam beyond the nose of the cover plate yielded during the cycles to $0.01h$. Local buckling of the beam flanges commenced during the cycles to $0.015h$, although the amplitude of the buckles was very small. Local buckling of the web commenced during the cycles to $0.03h$. The bolts connecting the web tabs to the horizontal braces slipped during the cycles to $0.04h$ and were re-tightened at the end of the $0.04h$ displacement cycles. The amplitude of the flange and web buckles grew rapidly with cycles to $0.04h$ and $0.05h$. Although the flange and web buckles in RC02 were not identical to those of RC01, the flange buckles penetrated back beyond the nose of the cover plate and likely produced high local strains in the longitudinal fillet welds and the beam flanges.

5.3.2 Global response

Specimen RC02 was subjected to 31 cycles of imposed displacements or drift levels up to and including $0.05h$. Figure 5-15 shows the relation between actuator force and drift angle. The maximum drift angles in this figure do not equal the target values because of deformations in the reaction frame that contributed to the beam tip displacement during testing. At the drift of approximately $0.05h$, which corresponded to a beam tip displacement of 6.7 in. (170 mm) after subtracting the reaction-frame displacements, the maximum joint plastic rotation was 4.2 percent radians. Due to the degradation of the stiffness and strength of the beam due to WLB and FLB, and the consequent unloading of the panel zone, nearly all of this plastic deformation was in the beam. The loss of strength and stiffness that is evident in the second of the two cycles to approximately $0.03h$ was a result of FLB and WLB. Following buckling of the web, the amplitude of the flange buckles increased rapidly, which in turn increased the amplitude and extent of the web buckles—an observation identical to RC01.

The maximum measured moment at the nose of the cover plate was 20,000 kip-in. (2,260 kN-m): 1.20 times the plastic moment of 16,692 kip-in. (1,890 kN-m) calculated using the measured yield stress of 53.5 ksi (see Table 3-2). The inelastic behavior seen in Figure 5-15 is composed of plastic deformation in the panel zone (Figure 5-16) and the beam (Figure 5-17). The horizontal solid lines in Figures 5-16 and 5-17 represent the *80-percent-peak* limit state; the dashed lines in Figure 5-17 represent the *80-percent-beam* limit state. For RC02, $\theta_p^m = 0.042$ radian, $\theta_p^{80} = 0.016$ radian, and $\theta_p^{80b} = 0.028$ radian. The maximum plastic rotation in the panel zone was 0.006 radian that occurred prior to loss of strength and stiffness in the beam. Figure 5-18 presents the relation between actuator load and drift angle relations for the beam (solid line), panel zone (dashed line), and column (dotted line). At drift angles exceeding 2 percent, the deformations in the beam comprised nearly all of the beam tip displacement or story drift.

A comparison of the global response data from RC01 and RC02 indicated that little benefit was gained from bracing the beam flanges against lateral movement at the end of the plastic hinge. Consequently, the lateral braces were not installed for the tests of the remaining specimens (RC03 through RC10).

5.3.3 Local response

The strain profiles across the width of the flange and cover plate, and over the length of the continuity plate were most similar to those reported for RC01 and are not shown here. Modest yielding was recorded in the cover plate at the face of the column but such yielding had no apparent detrimental affect on the response of the connection.

Figure 5-19 shows the recorded strain profiles for two locations in the column web and doubler plate of the panel zone as a function of drift angle. The results are most similar to those reported for RC01. For drift angles less than or equal to 0.01 radian, the maximum strains in the column web and doubler plate were identical. For drift angles greater than 0.01 radian, the strains in the

corner of the column web and doubler plate were approximately equal to all drift angles. The strains in the center of the column web and doubler plate were greater than those in the corner, but the values of the strains in each of the panel zone and doubler differed for drift angles between 0.01 and 0.03. For drift angles greater than or equal to 0.03, the strains were identical.

The axial force histories for the upper (B1) and lower (B2) horizontal braces of Figure 3-12 are presented in Figure 5-20. Force data in this figure are normalized to the yield force of the flange. The design force of $0.06A_f F_y$ is also shown in the figure. The axial forces in the braces are due to (a) the elongation of the brace as the beam displaces vertically and (b) the restraint of lateral displacement of the beam flange. At drift angles exceeding 0.03 radian, the measured forces exceeded the design forces. The maximum brace force was approximately twice the design force. Because the bottom lateral brace installation of Figure 3-12 is somewhat representative of field installations, and because the measured force in the braces substantially exceeded the design force, a review of the AISC design requirements for lateral bracing (AISC 1997) is warranted.

5.4 Specimen RC03

5.4.1 Specimen response

Specimen RC03 was identical to RC01 except that each cover plate was joined to the beam flange using two longitudinal fillet welds (per RC01 and RC02) and one transverse fillet weld. The lateral braces that were attached to RC02 to delay lateral-torsional buckling were not used for RC03 and subsequent specimens (RC04 through RC10).

Specimen RC03 failed during the second negative displacement excursion to $0.05h$ due to tearing in the k-line at the beam bottom flange that was a result of severe flange local buckling and web local buckling. Figure 5-21 shows flange local buckling (FLB) and web local buckling (WLB) in the beam following the displacement cycles to $0.03h$. The WLB penetrated back beyond the nose of the cover plate toward the face of the column. Figure 5-22 is a view of the flange buckles at the nose of the cover plate. The transverse fillet weld forced the flange local buckle away from the nose of the cover plate and eliminated the tearing of the longitudinal fillet welds at the end of the cover plate that was observed in RC01.

Flaking of the whitewash paint on the underside of the beam flanges approximately 6 in. (150 mm) from the face of the column was observed during the cycles to $0.0075h$. Likely this unexpected yielding was a result of residual stresses due to fillet welding of the cover plate to the beam flange and local stresses due to transfer of shear forces from the beam web to the plate-flange assembly. Yielding of the panel zone was first observed during the cycles to $0.01h$. Beam flange yielding outside the cover plate commenced during the cycles to $0.01h$. Local buckling of the beam flanges was detected during the cycles to $0.015h$, although the amplitude of the buckles was very small. During the cycles to $0.03h$, local buckling of the web was detected. A tear in the bottom flange k-line formed during the cycles to a drift angle of $0.04h$ and propagated during the cycles to $0.05h$. Figure 5-23 shows the tear in the bottom flange k-line and the subsequent fracture of the beam flange. The amplitude of the flange and web buckles substantially increased during the $0.04h$ cycles. Lateral-torsional buckling was observed during the $0.04h$ and $0.05h$ displacement cycles.

5.4.2 Global response

Specimen RC03 sustained 32 cycles of imposed displacements or drift levels up to and including $0.05h$. Figure 5-24 shows the relation between actuator force and drift angle. The maximum drift angles in this figure do not equal the target values because of deformations in the reaction frame that contributed to the beam tip displacement during testing. At the drift of approximately $0.05h$, which corresponded to a beam tip displacement of 7.1 in. (180 mm) after subtracting the reaction-frame displacements, the maximum joint plastic rotation was 0.044 radian. Nearly all of this plastic deformation was in the beam for the reasons cited above for RC02. The loss of strength and stiffness that is evident in the second of the two cycles to approximately $0.03h$ was a result of WLB and FLB. The amplitude of the flange buckles increased rapidly following web local buckling similar to RC01 and RC02.

The maximum measured moment at the nose of the cover plate was 20,000 kip-in. (2,260 kN-m): 1.20 times the plastic moment of 16,692 kip-in. (1,890 kN-m). The inelastic response seen in Figure 5-24 is composed of plastic deformation in the panel zone (Figure 5-25) and the beam (Figure 5-26). The horizontal solid lines in Figures 5-25 and 5-26 represent the *80-percent-peak* limit state; the dashed lines in Figure 5-26 represent the *80-percent-beam* limit state. For RC03, $\theta_p^m = 0.043$ radian, $\theta_p^{80} = 0.018$ radian, and $\theta_p^{80b} = 0.028$ radian. The maximum plastic rotation in the panel zone was 0.005 radian that occurred prior to loss of strength and stiffness in the beam due to WLB. Figure 5-27 presents the relation between actuator load and drift angle relations for the beam (solid line), panel zone (dashed line), and column (dotted line). At drift angles exceeding 2 percent, the deformations in the beam comprised nearly all of the beam tip displacement or story drift.

5.4.3 Local response

The strain profiles across the width of the flange and cover plate, and over the length of the continuity plate were most similar to those reported for RC01 and measured for RC02 and are not shown here. Modest yielding was recorded in the cover plate at the face of the column but such yielding had no apparent detrimental effect on the response of the connection. The maximum strain in the cover plates was twice the yield strain that was measured at an story drift angle of 0.03 radian. At larger drift angles, the strength of the beam degraded, which resulted in smaller strains in the cover plates.

Figure 5-28 shows the recorded strain profiles for two locations in the column web and doubler plate of the panel zone as a function of drift angle. The results are most similar to those reported for RC02. For drift angles less than or equal to 0.01 radian, the maximum strains in the column web and doubler plate at identical locations were equal. For drift angles greater than 0.01 radian, the strains in the corner of the column web and doubler plate were approximately equal at all drift angles. The strains in the center of the column web and doubler plate were greater than those in the corner, but the values of the strains in each of the column web and doubler plate differed for drift angles between 0.01 and 0.03. For drift angles greater than or equal to 0.03 radian, the strains were identical.

5.5 Specimen RC04

5.5.1 Specimen response

Specimen RC04 was the first flange-plate connection tested as part of the SAC Phase II project. A photograph of the swallowtail-shaped plate is shown in Figure 5-29. Each flange plate was welded to the beam flange using two longitudinal fillet welds and a U-shaped transverse fillet weld that followed the profile of the flange plate. The transverse weld can be seen in the figure. The lateral braces that were attached to the beam flanges of RC02 at the far end of the plastic hinge to delay lateral-torsional buckling were not used for RC04.

Specimen RC04 failed during the first negative displacement excursion to $0.055h$ due to fracture of the beam bottom flange that was a result of severe flange local buckling and web local buckling. Figure 5-30 shows flange local buckling (FLB) and web local buckling (WLB) in the beam following the displacement cycles to $0.03h$. The WLB penetrated back beyond the nose of the flange plate toward the face of the column. Figure 5-31 is a photograph of the beam top flange and flange plate at a drift of $0.02h$. Flaking of whitewash paint on the beam flange within the depth of the swallowtail plate is evident in the figure, indicating that yielding of the beam flange penetrated toward the face of the column from the nose of the flange plate.

Yielding of the panel zone, the beam flange outside the flange plate, and the back flange of the column opposite the continuity plates was first observed during the cycles to $0.01h$. Local buckling of the beam flanges commenced during the cycles to $0.020h$, although the amplitude of the buckles was very small. Local buckling of the web commenced during the cycles to $0.03h$. Tears formed in the beam flanges during the cycles to $0.04h$ due to large amplitude flange buckling. These cracks grew with the amplitude of the flange and web buckles during the cycles to drift angles of $0.05h$ and $0.055h$. Figure 5-32 shows the tear in the bottom flange that led to the fracture of the flange.

5.5.2 Global response

Specimen RC04 sustained 33 cycles of imposed displacements or drift levels up to and including $0.055h$. Figure 5-33 shows the relation between actuator force and drift angle. The maximum drift angles in this figure do not equal the target values because of deformations in the reaction frame that contributed to the beam tip displacement during testing. At the drift of approximately $0.055h$, which corresponded to a beam tip displacement of 7.5 in. (190 mm) after subtracting the reaction-frame displacements, the maximum joint plastic rotation was 0.049 radian. Nearly all of this plastic deformation was in the beam. The loss of strength and stiffness that is evident in the second of the two cycles to approximately $0.03h$ was a result of WLB and FLB. The amplitude of the flange buckles increased rapidly following web local buckling similar to RC01 through RC03.

The maximum measured moment at the nose of the flange plate was 18,800 kip-in. (2,100 kN-m): 1.13 times the plastic moment of 16,692 kip-in. (1,890 kN-m). The inelastic response seen in Figure 5-33 is composed of plastic deformation in the panel zone (Figure 5-34) and the beam (Figure 5-35).

The horizontal solid lines in Figures 5-34 and 5-35 represent the *80-percent-peak* limit state; the dashed lines in Figure 5-35 represent the *80-percent-beam* limit state. For RC04, $\theta_p^m = 0.049$ radian, $\theta_p^{80} = 0.016$ radian, and $\theta_p^{80b} = 0.024$ radian. The maximum plastic rotation in the panel zone was 0.003 radian that occurred prior to loss of strength and stiffness in the beam due to WLB. Figure 5-36 presents the relation between actuator load and drift angle relations for the beam (solid line), panel zone (dashed line), and column (dotted line). At drift angles exceeding 2 percent, the deformations in the beam comprised nearly all of the beam tip displacement or story drift.

5.5.3 Local response

Figure 5-37 presents the recorded strain profiles across the beam top flange at the nose of the flange plate and top flange plate at a distance of 2 in. (51 mm) from the face of the column, as a function of drift angle. The drift angle shown in this figure includes the drift contribution from the reaction frame. The normalized strain values shown in the figure are the maximum values at each drift angle divided by the yield strain (assumed equal to 0.0018). For drift angles less than 0.01 radian, the strains in the flange plate and the beam flange were similar in magnitude. Following yielding in the beam flange, the strains in the beam increased rapidly but the strain in the flange plate increased at a more modest rate. At drift angles greater than 0.03 radian, the strains in the flange plate reduced due to degradation of strength in the beam due to FLB and WLB. Strain data for the beam flange are shown for drift angles of 0.02 radian and less because at higher drift angles the gages were over-ranged. Differences in the beam gage values for drifts larger than 0.01 radian were expected due to FLB. The maximum measured strains in the flange plate were approximately 150 percent of the yield strain. Modest yielding of the flange plate appeared to have no detrimental effect on either the global or local response of the specimen.

Figure 5-38 shows the recorded strain profiles along the top flange plate and continuity plate as a function of drift angle. The normalized strain values shown in the figure are the maximum values at each drift angle divided by the yield strain (assumed equal to 0.0018). The maximum strain in the 1.125 in. (29 mm) thick continuity plate immediately adjacent to the column flange that was welded to the flange plate was 67 percent of the yield strain.

Shear strains at identical locations in the column web and doubler plate of the panel zone were compared at different levels of story drift angle. The recorded data are most similar to that reported for RC01 through RC03 and are not reported here.

5.6 Specimen RC05

5.6.1 Specimen response

Specimen RC05 was constructed with trapezoidal cover plates similar to that used to reinforce the top flange of specimen AN1 of the SAC Phase I project (Whittaker et al. 1996). In all other aspects, RC05 was identical to RC03. A photograph of the trapezoidal plate of RC05 is shown in Figure 5-39. Each cover plate was welded to the beam flange using two longitudinal fillet welds and a transverse fillet weld across the nose of the cover plate. These fillet welds can be seen in the figure.

Specimen RC05 failed during the second negative displacement excursion to $0.055h$ due to tearing of the beam bottom flange that was a result of severe flange local buckling and web local buckling. Figure 5-40 shows flange local buckling (FLB) and web local buckling (WLB) in the beam following the displacement cycles to $0.05h$. The WLB penetrated back beyond the nose of the cover plate toward the face of the column.

Yielding of the panel zone was first observed during the cycles to $0.0075h$. The beam beyond the nose of the cover plate yielded during the cycles to $0.01h$. Local buckling of the beam flanges commenced during the cycles to $0.02h$, although the amplitude of the buckles was very small. Local buckling of the web commenced during the cycles to $0.03h$. The amplitude of the flange and web buckles grew rapidly with cycles to $0.04h$ and $0.05h$. Small tears formed in the top and bottom flanges of the beam at the apices of the flange buckles of greatest amplitude during the first displacement cycle to $0.05h$ and propagated during the remaining cycles to $0.05h$ and the cycles to $0.055h$. Figure 5-41 shows the tear in the bottom flange that led to the failure of the specimen.

5.6.2 Global response

Specimen RC05 sustained 37 cycles of imposed displacements or drift levels up to $0.055h$, including 5 complete cycles at a drift of $0.055h$. Figure 5-42 shows the relation between actuator force and story drift angle. The maximum drift angles in this figure do not equal the target values because of deformations in the reaction frame that contributed to the beam tip displacement during testing. At the drift of approximately $0.055h$, which corresponded to a beam tip displacement of 7.7 in. (196 mm) after subtracting the reaction-frame displacements, the maximum joint plastic rotation was 0.052 radian. All of this plastic deformation was in the beam. The loss of strength and stiffness that is evident in the first of the two cycles to approximately $0.03h$ was a result of WLB and FLB. The amplitude of the flange buckles increased rapidly following web local buckling similar to RC01 through RC04.

The maximum measured moment at the nose of the cover plate was 19,300 kip-in. (2,180 kN-m): 1.16 times the plastic moment of 16,692 kip-in. (1,890 kN-m). The inelastic response seen in Figure 5-42 is composed of plastic deformation in the panel zone (Figure 5-43) and the beam (Figure 5-44).

The horizontal solid lines in Figures 5-43 and 5-44 represent the *80-percent-peak* limit state; the dashed lines in Figure 5-44 represent the *80-percent-beam* limit state. For RC05, $\theta_p^m = 0.052$ radian, $\theta_p^{80} = 0.019$ radian, and $\theta_p^{80b} = 0.024$ radian. The maximum plastic rotation in the panel zone was 0.004 radian that occurred prior to loss of strength and stiffness in the beam due to WLB and FLB. Figure 5-45 presents the relation between actuator load and drift angle relations for the beam (solid line), panel zone (dashed line), and column (dotted line). At drift angles exceeding 2 percent, the deformations in the beam comprised nearly all of the beam tip displacement or story drift.

5.6.3 Local response

Figure 5-46 presents the recorded strain profiles across the beam top flange at the nose of the cover plate and top cover plate at a distance of 2 in. (51 mm) from the face of the column, as a function of drift angle. The drift angle shown in this figure includes the drift contribution from the reaction frame. The normalized strain values shown in the figure are the maximum values at each drift angle divided by the yield strain (assumed equal to 0.0018). For drift angles less than 0.01 radian, the strains in the cover plate were similar across the half width of plate and less than those in the beam flange. Following yielding in the beam flange, the strains in the beam increased rapidly but the strains in the cover plate increased at a more modest rate. At drift angles greater than 0.03 radian, the strains in the cover plate reduced because of degradation of strength in the beam due to FLB and WLB. Strain data for the beam flange are shown for drift angles of 0.03 radian and less because some of the gages were over-ranged at larger drift angles. Differences in the beam gage values for drifts larger than 0.01 radian were expected due to FLB. The maximum measured strains in the cover plate ranged between 2 and 2.5 times the yield strain. Yielding of the cover plate appeared to have no detrimental effect on either the global or local response of the specimen.

Figure 5-47 shows the recorded strain profiles along the top cover plate and continuity plate as a function of story drift angle. The normalized strain values shown in the figure are the maximum values at each drift angle divided by the yield strain (assumed equal to 0.0018). The maximum strain in the 1.125 in. (29 mm) thick continuity plate immediately adjacent to the column flange that was welded to the flange plate was 86 percent of the yield strain.

Shear strains at identical locations in the column web and doubler plate of the panel zone were compared at different story drift angles. The recorded data are most similar to that reported for RC01 through RC04 and are not reported here.

Figure 5-48 presents the distribution of the normalized axial strain along the line *b* (that corresponds to the center of beam flange outstand) as a function of drift angle. Data from the strain gage at the nose of the cover plate shows only modest values of strain at all drift angles.

5.7 Specimen RC06

5.7.1 Specimen response

Specimen RC06 was designed as the benchmark flange-plate connection. Rectangular flange plates were used to reinforce the connection and these plates were joined to the beam flanges with two longitudinal fillet welds and one transverse fillet weld. The weld geometry of RC06 was similar to that of RC03 but larger fillet welds were used. See Table 3-1 for fillet weld details. Figure 5-49 is a photograph of the bottom flange plate.

RC06 failed during the second negative displacement excursion to $0.055h$. The beam top flange of RC06 tore beyond the nose of the flange plate due to severe flange local buckling and the resulting low cycle fatigue of the beam flange but the tears did not completely penetrate the flange. Figure 5-50 shows the degree of flange local buckling (FLB) and web local buckling (WLB) present in the beam following the displacement cycles to $0.04h$. Figure 5-51 shows the tears in the beam top flange. RC06 failed due to fracture at the k-line near the beam top flange. Figure 5-52 shows the k-line fracture.

Yielding of the panel zone was first observed during the cycles to $0.0075h$. The beam flanges beyond the reinforcing plates yielded during the cycles to $0.01h$. Local buckling of the beam flanges commenced during the cycles to $0.02h$, although the amplitude of the buckles was very small. During the cycles to $0.03h$, local buckling of the web was detected and modest lateral-torsional buckling was observed. The amplitude of the flange and web buckles grew rapidly with cycles to $0.04h$ and $0.05h$. Small ductile tears formed during the cycles to $0.04h$ due to large local strains at the apices of the flange local buckles and grew substantially in size during the cycles to $0.05h$. During the first cycle to $0.055h$, a crack formed in the k-line of the beam top flange due to large plastic deformations induced by FLB and WLB. This crack propagated quickly and led to the failure of RC06 during the second cycle to $0.055h$.

5.7.2 Global response

Specimen RC06 sustained 34 cycles of imposed displacements or drift levels up to $0.055h$, including 2 cycles at a drift of $0.055h$. Figure 5-53 shows the relation between actuator force and drift angle. The maximum drift angles in this figure do not equal the target values because of deformations in the reaction frame that contributed to the beam tip displacement during testing. At the drift of approximately $0.055h$, the maximum joint plastic rotation was 0.043 radian. Nearly all of this plastic deformation was in the beam. The loss of strength and stiffness that is evident in the first of the two cycles to approximately $0.03h$ was a result of WLB and FLB. The amplitude of the flange buckles increased rapidly following web local buckling similar to RC01 through RC05.

The maximum measured moment at the nose of the flange plate was 19,600 kip-in. (2,180 kN-m): 1.17 times the plastic moment of 16,692 kip-in. (1,890 kN-m). The inelastic response seen in Figure 5-53 is composed of plastic deformation in the panel zone (Figure 5-54) and the beam (Figure 5-55).

The horizontal solid lines in Figures 5-54 and 5-55 represent the *80-percent-peak* limit state; the dashed lines in Figure 5-55 represent the *80-percent-beam* limit state. For RC06, $\theta_p^m = 0.042$ radian, $\theta_p^{80} = 0.011$ radian, and $\theta_p^{80b} = 0.028$ radian. The maximum plastic rotation in the panel zone was 0.005 radian that occurred prior to loss of strength and stiffness in the beam due to FLB and WLB. Figure 5-56 presents the relation between actuator load and drift angle relations for the beam (solid line), panel zone (dashed line), and column (dotted line). At drift angles exceeding 2 percent, the deformations in the beam comprised nearly all of the beam tip displacement or story drift.

5.7.3 Local response

Figure 5-57 presents the recorded strain profiles across the beam top flange at the nose of the cover plate and top flange plate at a distance of 2 in. (51 mm) from the face of the column, as a function of drift angle. The drift angle shown in this figure includes the drift contribution from the reaction frame. The normalized strain values shown in the figure are the maximum values at each drift angle divided by the yield strain (assumed equal to 0.0018). For drift angles less than 0.01 radian, the strains in the flange plate were similar across the half width of plate and less than those in the beam flange. Following yielding in the beam flange, the strains in the beam increased rapidly but the strains in the flange plate increased at a more modest rate. At drift angles greater than 0.03 radian, the strains in the flange plate reduced because of degradation of strength in the beam due to FLB and WLB. Strain data for the beam flange are shown for drift angles of 0.02 radian and less because some of the gages were over-ranged at larger drift angles. The maximum measured strains in the flange plate ranged between 2 and 3 times the yield strain. Modest yielding of the flange plate appeared to have no detrimental effect on either the global or local response of the specimen.

Figure 5-58 presents the distribution of the normalized axial strain along the line b as a function of drift angle. Data from the strain gages are similar to those of RC05.

5.8 Specimen RC07

Specimen RC07 was identical to RC06 but was tested using the near-field displacement history of Figure 3-13b rather than the cyclic displacement history of Figure 3-13a that was used for RC01 through RC06. The objective of this test was to investigate load-history effects on the response of reinforced steel connections.

The displacement history for RC07 is presented in Figure 5-59. Point A in this figure marks the end of the SAC near-field history. Additional cycles to $0.055h$ were imposed on the specimen until fracture. The maximum positive drift imposed on RC07 was $0.055h$ rather than the $0.06h$ of the SAC history because of stroke limitations in the test fixture.

RC07 failed during the third fully reversed displacement cycle to $0.055h$, that followed the completion of the SAC near-field history. The beam top flange of RC07 tore beyond the nose of the flange plate due to severe flange local buckling and the resulting low cycle fatigue of the beam flange. Figure 5-60 shows the degree of flange local buckling (FLB) and web local buckling (WLB) present in the beam following the displacement cycles to $0.04h$. Figure 5-61 shows the tears in the beam top flange.

During the first excursion to $-0.02h$, yielding was observed in the panel zone, the beam beyond the nose of the flange plate, and the flange plate at the face of the column. Minor buckling of the beam flange was also observed during this displacement excursion. In the subsequent excursion to $+0.055h$, additional yielding was observed in the beam and the flange plates, the beam bottom flange buckled, the beam web buckled, and the beam underwent lateral-torsional buckling. Tearing was also observed at the apices of the bottom flange buckles. During the final cycle to $0.055h$, a tear formed in the k-line of the beam top flange but this tear did not lead to the fracture of the flange.

Specimen RC07 survived the SAC near-field history and 2.5 subsequent cycles to a drift of $0.055h$. The rate of degradation in RC07 was much smaller than that of RC06 that was tested with the SAC cyclic history. A comparison of data from RC06 and RC07 is presented in Chapter 6. The maximum plastic rotation in the beam was 0.050 radian. Figure 5-62 shows the relation between actuator force and drift angle. The maximum drift angles in this figure do not equal the target values because of deformations in the reaction frame that contributed to the beam tip displacement during testing.

The maximum measured moment at the nose of the flange plate was 18,900 kip-in. (2,140 kN-m): 1.14 times the plastic moment of 16,692 kip-in. (1,890 kN-m). The inelastic response seen in Figure 5-62 is composed of plastic deformation in the panel zone (Figure 5-63) and the beam (Figure 5-64). The horizontal solid lines in Figures 5-63 and 5-64 represent the *80-percent-peak* limit state; the dashed lines in Figure 5-64 represent the *80-percent-beam* limit state. For RC07, $\theta_p^m = 0.050$ radian, $\theta_p^{80} = 0.033$ radian, and $\theta_p^{80b} = 0.039$ radian.

5.9 Specimen RC08

5.9.1 Specimen response

Specimen RC08 was similar to RC06 with the key exception being the thickness of the flange plate, which was thinner than that of RC06. The objective of this test was to investigate the response of flange-plate connections with yielding flange plates.

RC08 failed during the second negative displacement excursion to $0.055h$. The beam top flange of RC08 tore beyond the nose of the flange plate due to severe flange local buckling and the resulting low cycle fatigue of the beam flange. Figure 5-65 shows the degree of flange local buckling (FLB) and web local buckling (WLB) present in the beam following the displacement cycles to $0.05h$.

Yielding of the panel zone was first observed during the cycles to $0.0075h$. The beam flanges beyond the reinforcing plates yielded during the cycles to $0.01h$. Yielding of the flange plate at the face of the column was observed during the cycles to $0.015h$. Local buckling of the beam flanges commenced during the cycles to $0.02h$, although the amplitude of the buckles was very small. During the cycles to $0.03h$, local buckling of the web was detected and modest lateral-torsional buckling was observed. The amplitude of the flange and web buckles grew rapidly with cycles to $0.04h$ and $0.05h$. During the first cycle to $0.055h$, a crack formed in the k-line of the beam top flange due to large plastic rotations induced by WLB and FLB. This crack propagated quickly into the flange and led to the failure of RC08 during the second cycle to $0.055h$. Figure 5-66 shows the fracture in the beam top flange. Yielding of the top flange plate near the face of the column at a drift angle of $0.04h$ is shown in Figure 5-67.

5.9.2 Global response

Specimen RC08 sustained 34 cycles of imposed displacements or drift levels up to $0.055h$, including 2 cycles at a drift of $0.055h$. Figure 5-68 shows the relation between actuator force and drift angle. The maximum drift angles in this figure do not equal the target values because of deformations in the reaction frame that contributed to the beam tip displacement during testing.

At the drift of approximately $0.055h$, the maximum joint plastic rotation was 0.051 radian. Nearly all of this plastic deformation was in the beam. The loss of strength and stiffness that is evident in the first of the two cycles to approximately $0.03h$ followed local buckling of the web. The amplitude of the flange buckles increased rapidly following web local buckling similar to RC01 through RC07.

The maximum measured moment at the nose of the flange plate was 20,000 kip-in. (2,260 kN-m): 1.20 times the plastic moment of 16,692 kip-in. (1,890 kN-m). The inelastic response seen in Figure 5-68 is composed of plastic deformation in the panel zone (Figure 5-69) and the beam (Figure 5-70).

The horizontal solid lines in Figures 5-69 and 5-70 represent the *80-percent-peak* limit state; the dashed lines in Figure 5-70 represent the *80-percent-beam* limit state. For RC08, $\theta_p^m = 0.050$ radian, $\theta_p^{80} = 0.014$ radian, and $\theta_p^{80b} = 0.028$ radian. Figure 5-71 presents the relation between actuator load and drift angle relations for the beam (solid line), panel zone (dashed line), and column (dotted line).

5.9.3 Local response

Figure 5-72 presents the recorded strain profiles across the beam top flange at the nose of the flange plate and across the top flange plate at a distance of 2 in. (51 mm) from the face of the column, as a function of drift angle. The drift angle shown in this figure includes the drift contribution from the reaction frame. The normalized strain values shown in the figure are the maximum values at each drift angle divided by the yield strain (assumed equal to 0.0018). For drift angles less than 0.01 radian, the strains in the flange plate were similar across the half width of plate and less than those in the beam flange. Following yielding in the beam flange, the strains in the beam increased rapidly but the strains in the cover plate increased at a more modest rate. At drift angles greater than 0.03 radian, the strains in the flange plate reduced because of the degradation of strength in the beam due to FLB and WLB. The maximum measured strains in the flange plate ranged between 2 and 3 times the yield strain. Such yielding of the flange plate appeared to have no detrimental effect on either the global or local response of the specimen.

Figure 5-73 presents the distribution of the normalized axial strain along the line *b* as a function of story drift angle. Data from the strain gages along line *b* show similar trends to those reported for RC01, RC05, and RC06.

5.10 Specimen RC09

5.10.1 Specimen response

The objectives of the test were two-fold, namely, (a) to investigate the response of flange-plate connections with yielding flange plate and (b) to study the influence of a weak panel zone on the response of reinforced connections. Specimen RC09 was similar to RC08 with the key exception being the thickness of the continuity plates that was thinner in RC09 and the absence of a doubler plate in RC09. The panel zone alone of RC09 did not comply with current AISC and SAC requirements for panel zone strength.

RC09 failed during the second positive displacement excursion to $0.055h$. Testing was continued for another two cycles to a drift of $0.055h$ to investigate the post-fracture response of reinforced connections. The beam bottom flange of RC09 fractured beyond the nose of the flange plate due to the propagation of a crack that formed in the k-line of the bottom flange. Yielding of the panel zone following displacement cycles to $0.015h$ is shown in Figure 5-74. Figure 5-75 shows the flange local buckling (FLB) and web local buckling (WLB) present in the beam following the displacement cycles to $0.05h$.

Yielding of the panel zone was first observed during the cycles to $0.0075h$. The beam flanges beyond the reinforcing plates yielded during the cycles to $0.01h$. Yielding of the flange plate at the face of the column and the back column flange opposite the continuity plate was observed during the cycles to $0.015h$. During the cycles to $0.03h$, local buckling of the beam flange and web, and yielding of the continuity plates was observed. The amplitude of the flange and web buckles grew rapidly with cycles to $0.04h$ and $0.05h$. During the first cycle to $0.055h$, a crack formed in the k-line of the beam bottom flange due to large plastic rotations induced by web buckling. This crack propagated quickly into the flange and led to the failure of RC09 during the second cycle to $0.055h$. Figure 5-76 shows the fracture in the beam top flange. Yielding of the top flange plate at a drift angle of $0.03h$ is shown in Figure 5-77.

5.10.2 Global response

Specimen RC09 sustained 34 cycles of imposed displacements or drift levels up to $0.055h$, including 2 cycles at a drift angle of $0.055h$. Figure 5-78 shows the relation between actuator force and drift angle. The maximum drift angles in this figure do not equal the target values because of deformations in the reaction frame that contributed to the beam tip displacement during testing. At the drift of approximately $0.055h$, the maximum joint plastic rotation was 0.056 radian. The loss of strength and stiffness that is evident in the second of the two cycles to approximately $0.04h$ followed FLB and WLB. The effect of the fracture of the beam bottom flange on the hysteretic response of the specimen can be clearly seen in the figure.

The maximum measured moment at the nose of the flange plate was $19,200$ kip-in. ($2,170$ kN-m): 1.15 times the plastic moment of $16,692$ kip-in. ($1,890$ kN-m). The inelastic response seen in Figure 5-78 is composed of plastic deformation in the panel zone (Figure 5-79) and the beam (Figure 5-80). The horizontal solid lines in Figures 5-79 and 5-80 represent the *80-percent-peak* limit state; the dashed lines in Figure 5-80 represent the *80-percent-beam* limit state. For RC09, $\theta_p^m = 0.056$ radian, $\theta_p^{80} = 0.017$ radian, and $\theta_p^{80b} = 0.027$ radian. Figure 5-81 presents the relation between actuator load and drift angle for the beam (solid line), panel zone (dashed line), and column (dotted line).

5.10.3 Local response

Figure 5-82 presents the recorded strain profiles across the beam top flange at the nose of the flange plate and across the top flange plate at a distance of 2 in. (51 mm) from the face of the column, as a function of drift angle. The drift angle shown in this figure includes the drift contribution from the reaction frame. The normalized strain values shown in the figure are the maximum values at each drift angle divided by the yield strain (assumed equal to 0.0018). For

drift angles less than 0.01 radian, the strains in the flange plate were similar across the half width of plate and less than those in the beam flange. The strains in the flange plate and the beam flange increased rapidly following yielding in the plate and flange. At drift angles greater than 0.04 radian, the strains in the flange plate reduced because of degradation of strength in the beam due to FLB and WLB. The maximum measured strains in the flange plate ranged between 4 and 6 times the yield strain. Such yielding of the flange plate appeared to have no detrimental effect on either the global or local response of the specimen.

Normalized shear strains in the panel zone are shown in Figure 5-83 as a function of drift angle. The strains in the middle of the panel zone exceed those in the corner of the panel zone at all levels of drift angle. The strains in the panel zone decrease at drift angles larger than 0.04 radian due to loss of strength in the beam due to FLB and WLB.

Figure 5-84 presents the distribution of the normalized axial strain along the line b as a function of drift angle. The maximum strain in the continuity plate exceeded 150 percent of the yield strain with no adverse effect on the response of the specimen. Data from the strain gage at the nose of the flange plate shows only modest values of strain at all drift angles.

5.11 Specimen UCB-RC10

5.11.1 Specimen response

In the tests of the first five specimens, RC01 through RC05, web local buckling (WLB) was identified as a trigger for degradation of stiffness and strength in the reinforced connections. Specimen RC10 was designed to study the effect of delaying WLB on the global response of a reinforced connection. RC10 was identical to cover-plate specimen RC03 except for the addition of two pairs of horizontal stiffeners to RC10 that were designed to delay web local buckling rather than increase the strength of the specimen. Details on the design of the stiffeners are provided in Section 3.2. Figure 5-85 is a photograph of the horizontal stiffeners on one side of the beam web.

Specimen RC10 failed during the second negative displacement excursion to $0.055h$ due to fracture of the beam top flange due to severe flange local buckling and web local buckling. Figure 5-86 shows flange local buckling (FLB) in the beam following the displacement cycles to a drift of $0.03h$.

Yielding of the panel zone and the beam flanges beyond the nose of the cover plates was first observed during the cycles to $0.01h$. During the cycles to a drift of $0.03h$, minor yielding of the web near the k-line regions and of the beam flanges, immediately beyond the end of the horizontal stiffeners, was observed. Local buckling of the beam flanges commenced during the cycles to $0.030h$. Although the amplitude of the flange buckles was small, the wavelength was 30 in. (762 mm) commencing at the nose of the cover plate. During the second cycle to a drift of $0.03h$, WLB was detected. The amplitude of the flange and web buckles increased during the cycles to drift of $0.04h$ and $0.05h$. In the first cycle to a drift of $0.055h$, substantial deformation was observed in the top cover plate, and tears formed in the beam top flange at the apices of the flange buckles immediately beyond the end of the longitudinal stiffeners (i.e., at a distance of 35 in. (889 mm) from the column face). These tears propagated through and across the flange during the following cycle. Figure 5-87 shows the fracture in the beam top flange.

5.11.2 Global response

Specimen RC10 sustained 32 cycles of imposed displacements or drift levels up to $0.055h$, including 2 cycles at a drift of $0.055h$. Figure 5-88 shows the relation between actuator force and drift angle. The maximum drift angles in this figure do not equal the target values because of deformations in the reaction frame that contributed to the beam tip displacement during testing. At the drift of approximately $0.055h$, the maximum joint plastic rotation was 4.7 percent radians. The loss of strength and stiffness that is evident in the first of the two cycles to approximately $0.04h$ was a result of FLB and WLB.

The maximum measured moment at the nose of the cover plate was 22,800 kip-in. (2,580 kN-m) and substantially larger than the maximum moment in RC03 of 20,000 kip-in. This increase in strength was due to the addition of the pair of longitudinal stiffeners to the beam web that increased the modulus of the beam cross section. The inelastic response seen in Figure 5-88 is composed of plastic deformation in the panel zone (Figure 5-89) the beam (Figure 5-90), and the column.

The horizontal solid lines in Figures 5-89 and 5-90 represent the *80-percent-peak* limit state. For RC10, $\theta_p^m = 0.045$ radian and $\theta_p^{80} = 0.018$ radian. Figure 5-91 presents the relationship between actuator load and drift angle for the beam (solid line), panel zone (dashed line), and column (dotted line).

5.11.3 Local response

Figure 5-92 presents the recorded strain profiles across the beam top flange at the nose of the flange plate and across the top flange plate at a distance of 2 in. (51 mm) from the face of the column, as a function of drift angle. The drift angle shown in this figure includes the drift contribution from the reaction frame. The normalized strain values shown in the figure are the maximum values at each drift angle divided by the yield strain (assumed equal to 0.0018). For drift angles less than 0.01 radian, the strains in the cover plate were similar across the half width of the plate and less than those in the beam flange. The strains in the beam flange increased rapidly with drift angle following yielding in the flange. At drift angles greater than 0.04 radian, the strains in the cover plate decreased because of degradation of strength in the beam due to FLB and WLB. Strain data for the beam flange are only shown for drift angles of 0.03 radian and less. The maximum measured strains in the flange plate ranged between 4 and 8 times the yield strain. Such yielding of the cover plate appeared to have no detrimental effect on either the global or local response of the specimen.

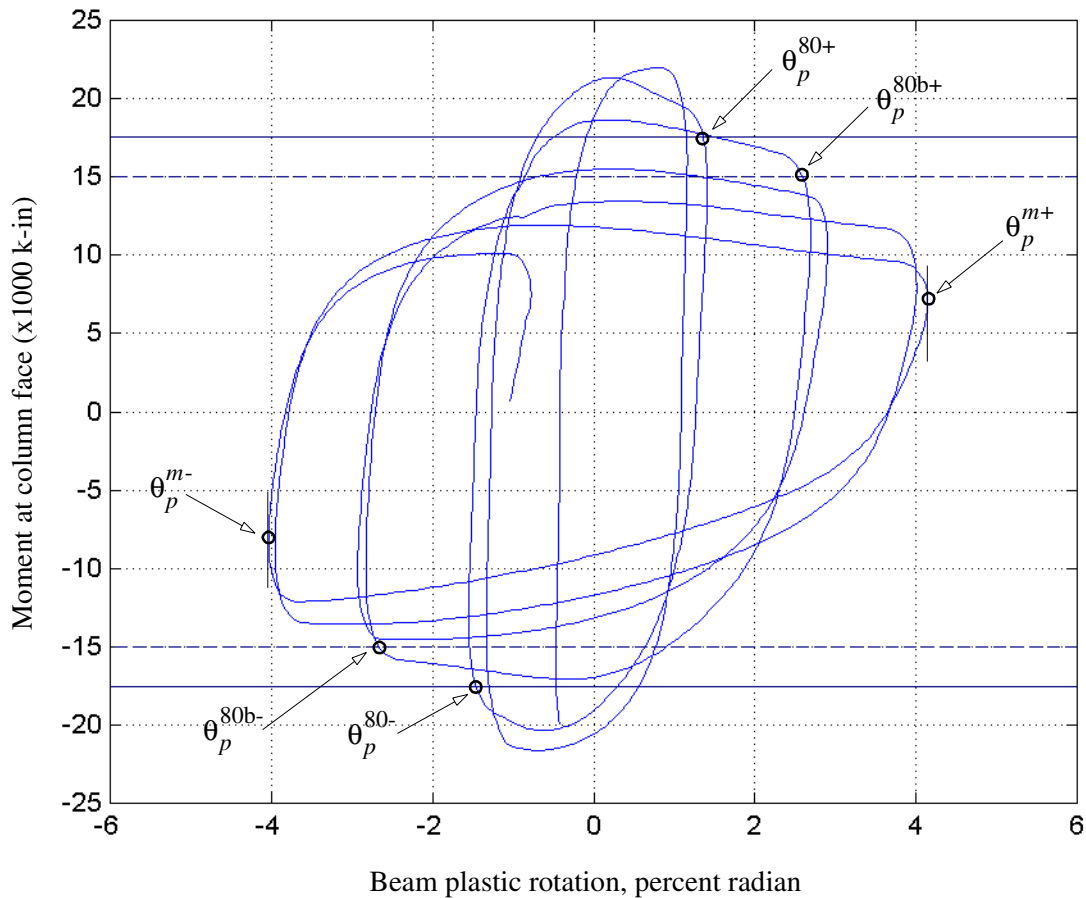


Figure 5-1 Calculation of maximum beam plastic rotations



Figure 5-2 Rectangular cover plate of RC01



Figure 5-3 Beam FLB and WLB in RC01 at a drift angle of $0.04h$

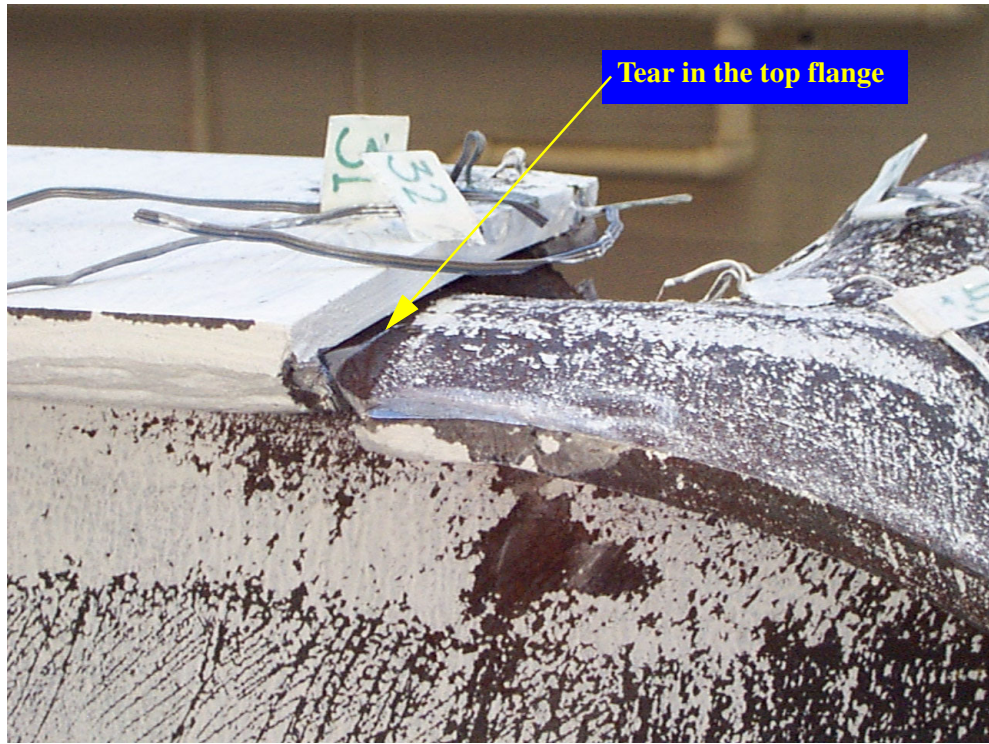


Figure 5-4 Tearing of the beam top flange in RC01

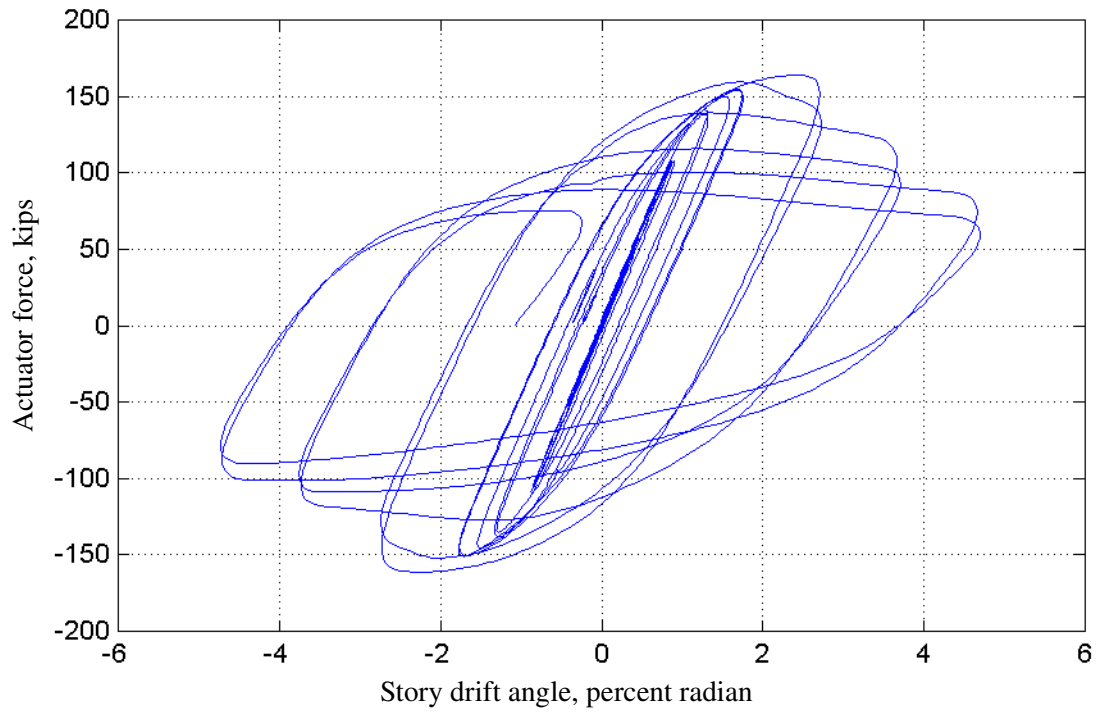


Figure 5-5 Actuator force versus drift angle for RC01

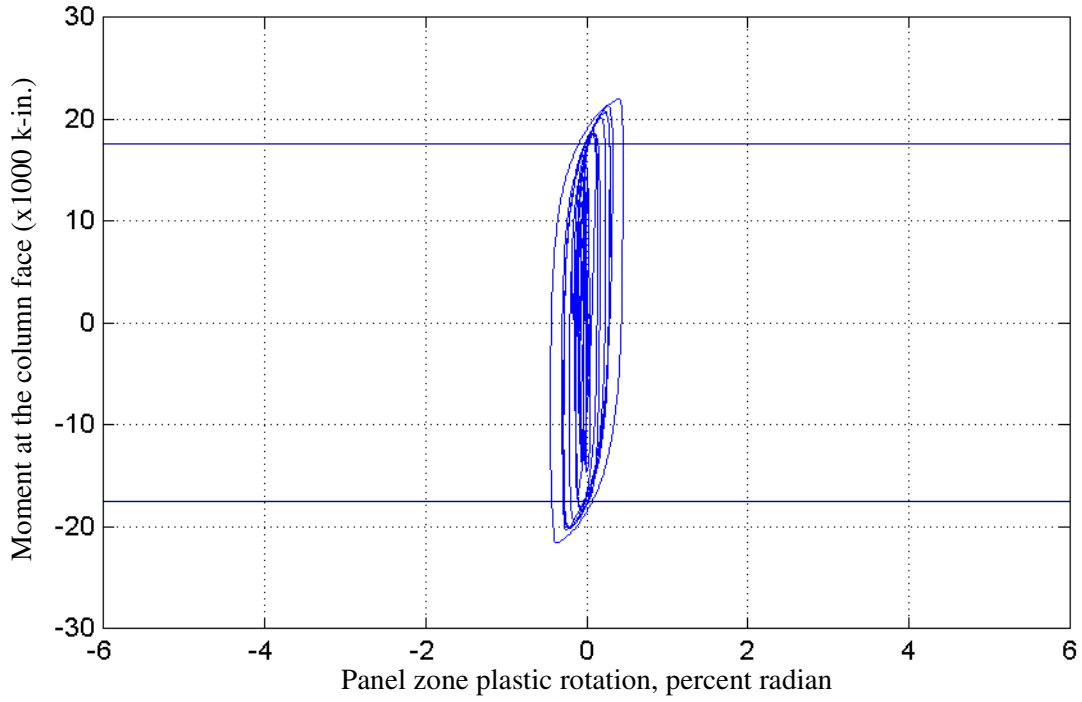


Figure 5-6 Moment at the column face versus panel zone plastic rotation for RC01

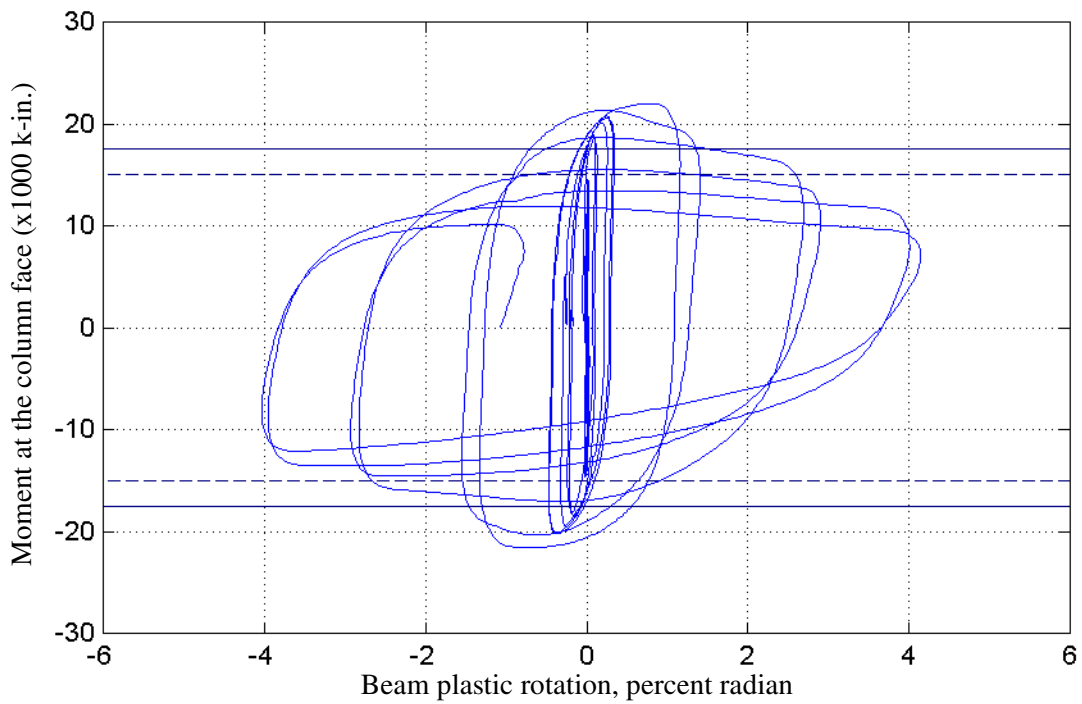


Figure 5-7 Moment at the column face versus beam plastic rotation for RC01

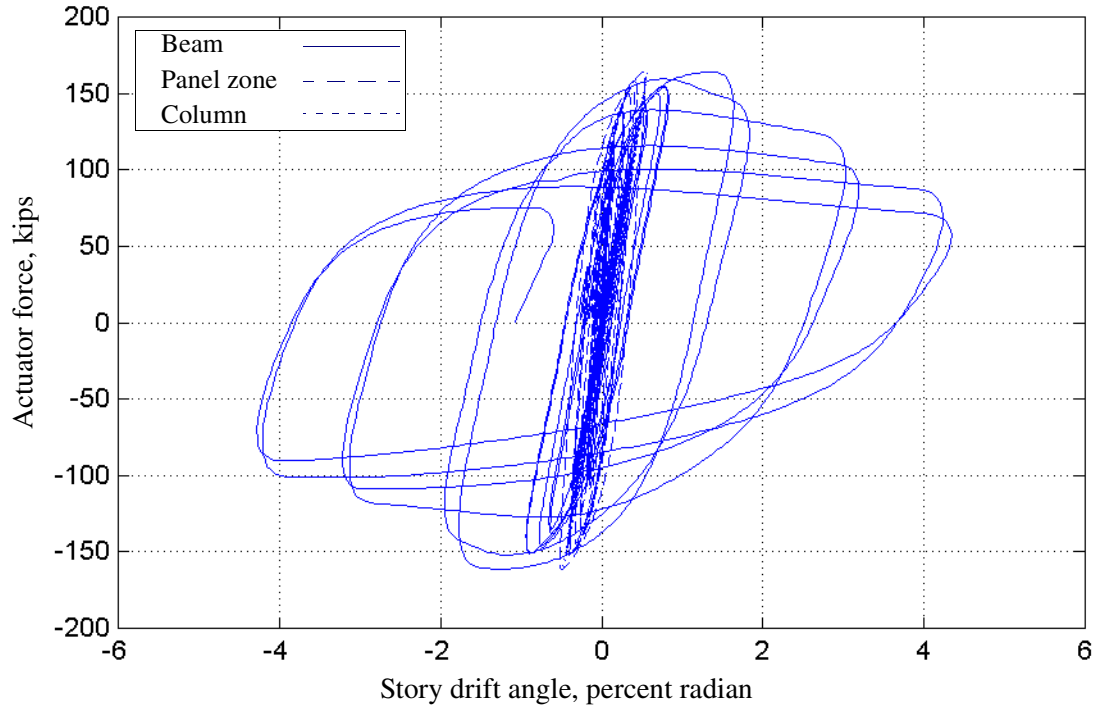


Figure 5-8 Components of drift angle for RC01

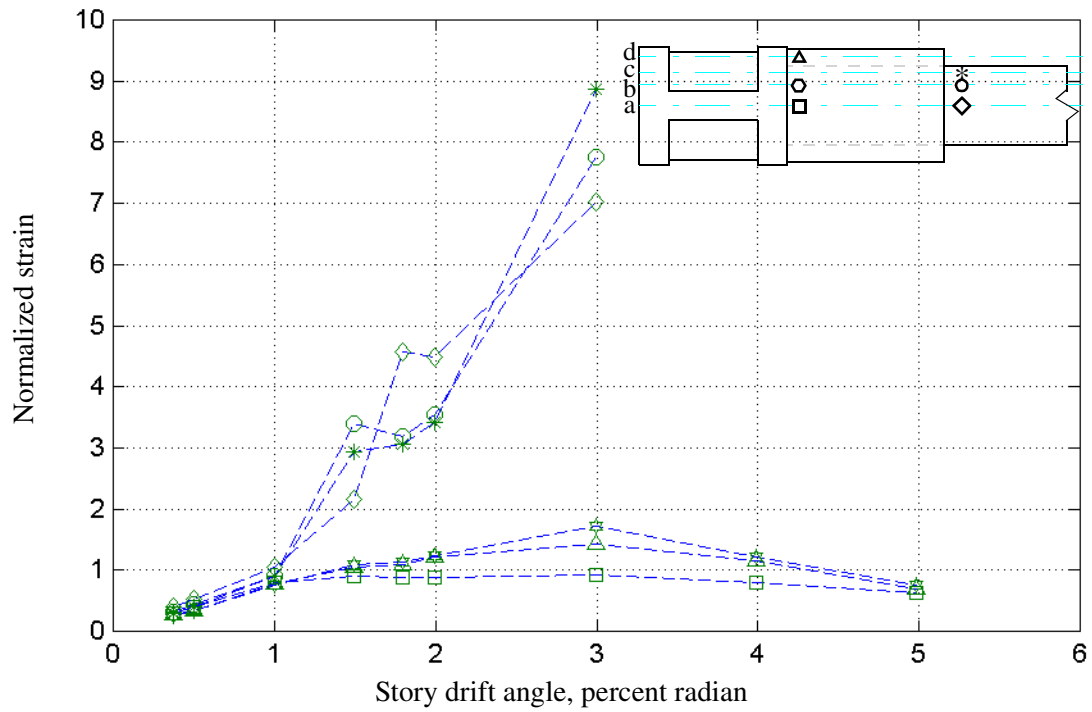


Figure 5-9 Beam and cover-plate strains for RC01

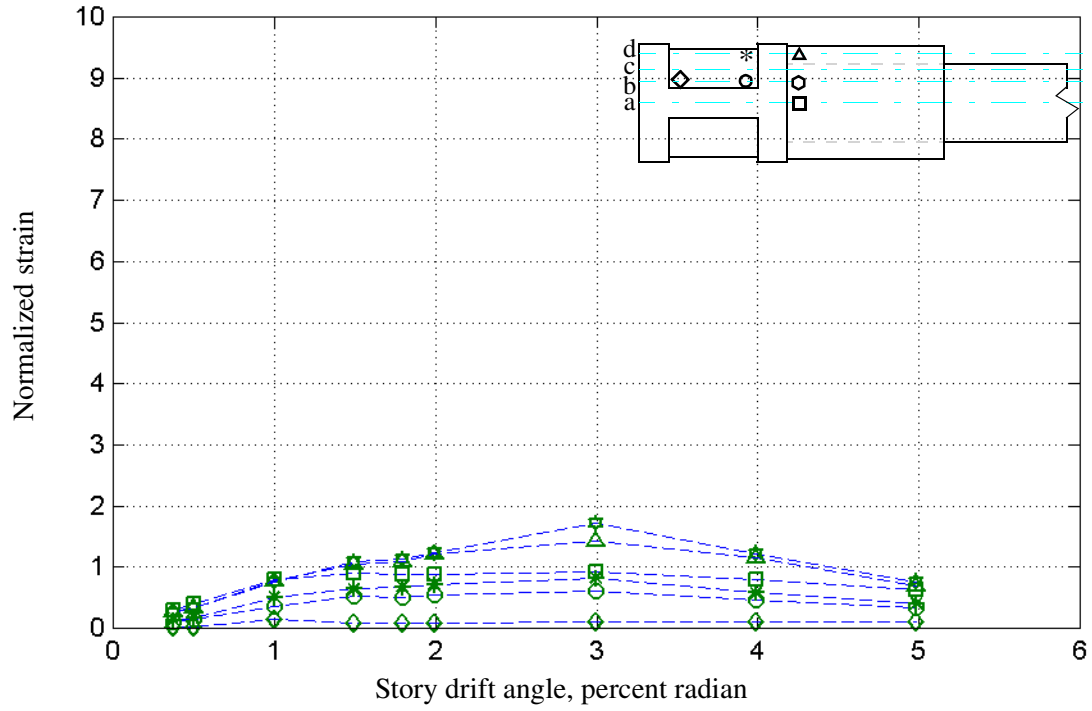


Figure 5-10 Cover-plate and continuity-plate strains for RC01

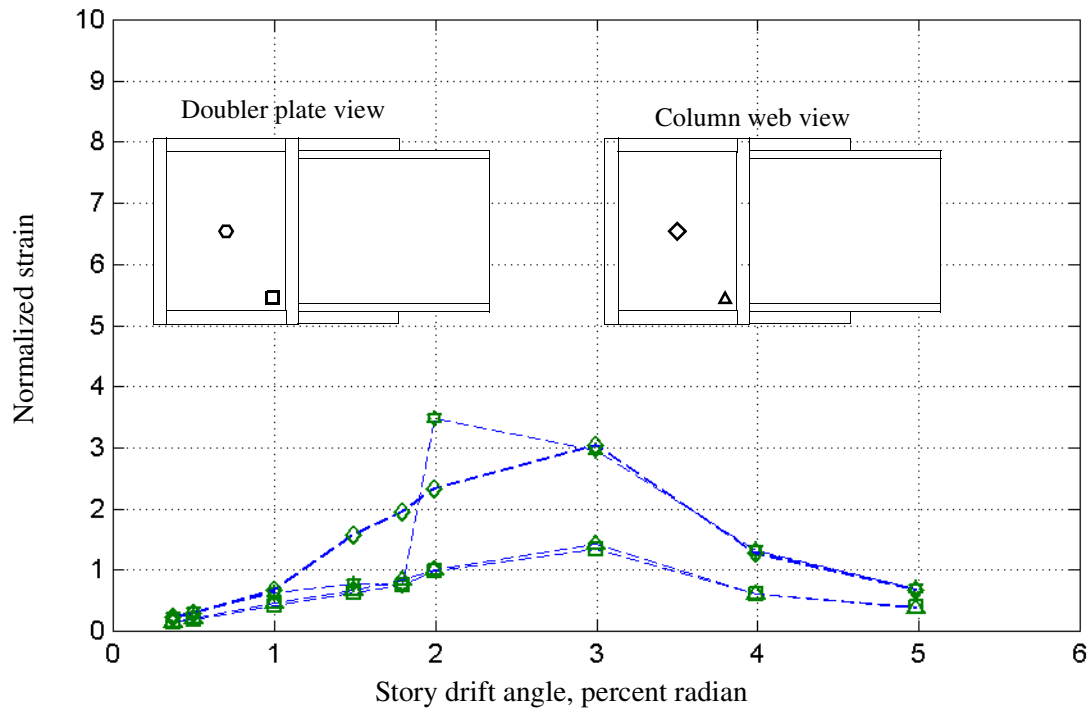


Figure 5-11 Column-web and the doubler-plate shear strains for RC01

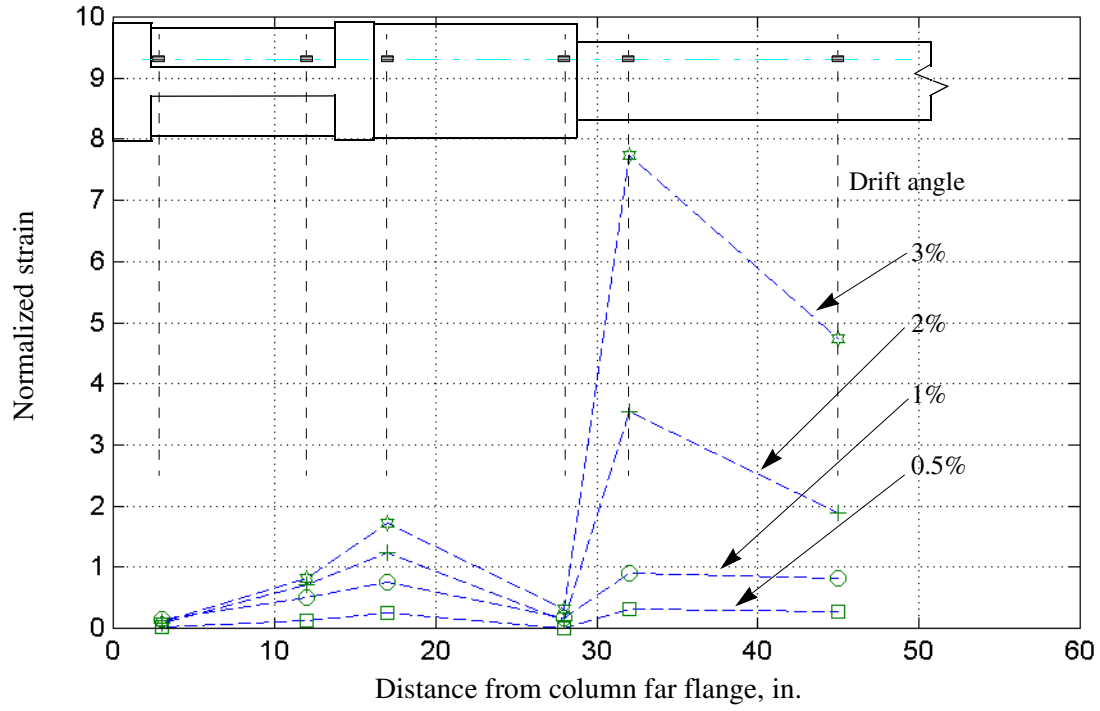


Figure 5-12 Strain response along line *b* for RC01

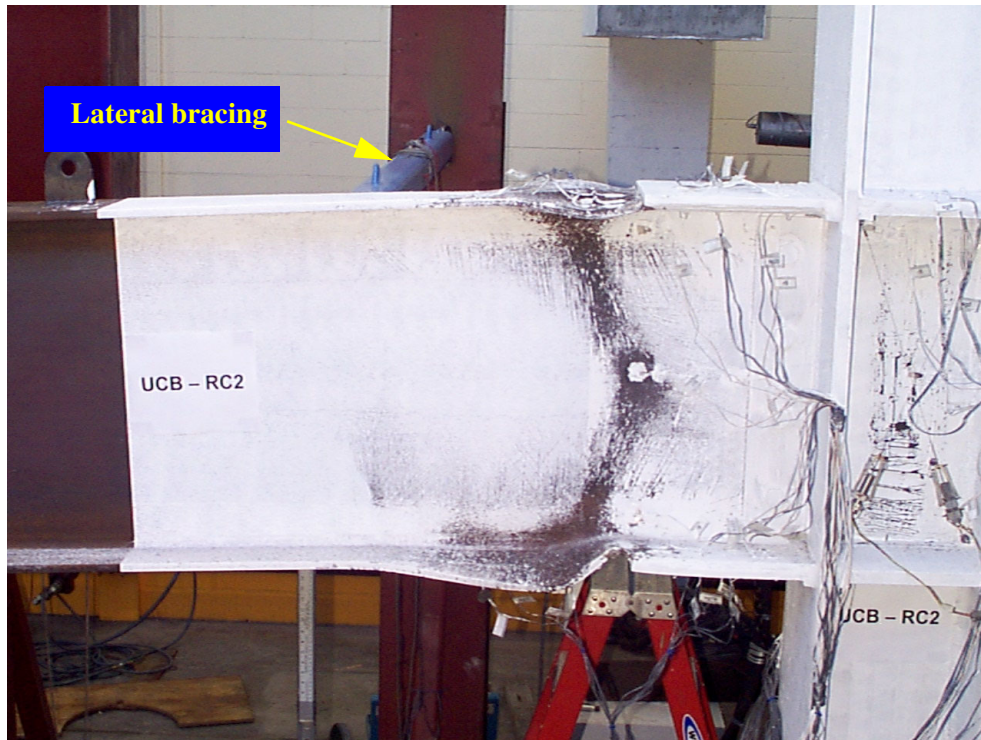


Figure 5-13 Beam FLB and WLB in RC02 at a drift angle of $0.03h$

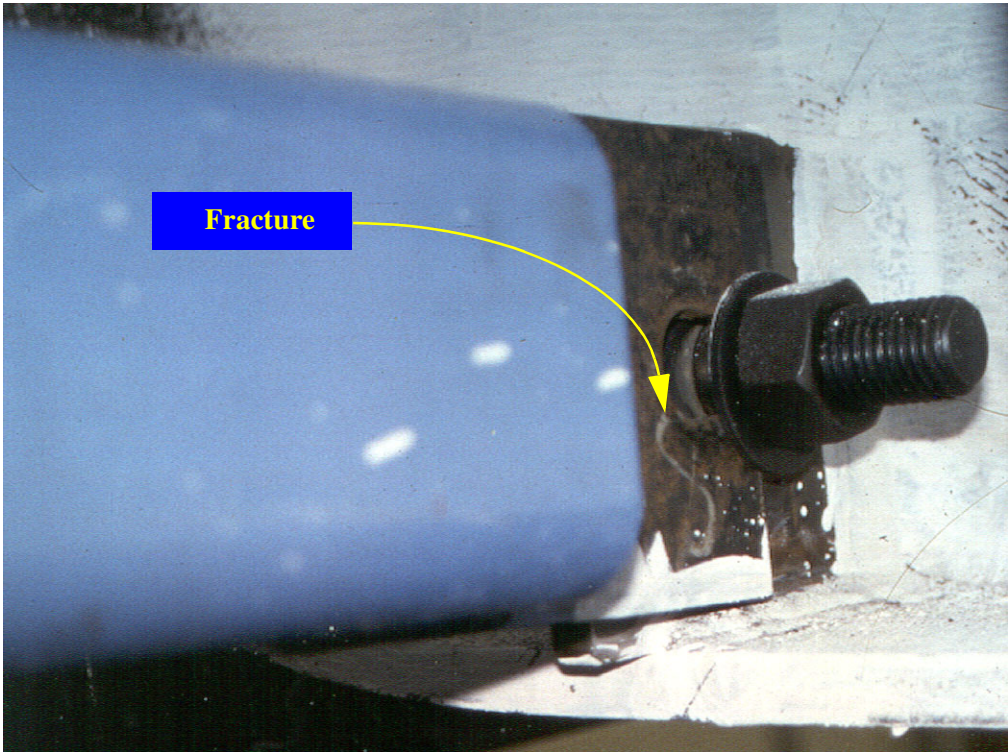


Figure 5-14 Fractured lateral brace web tabs in RC02

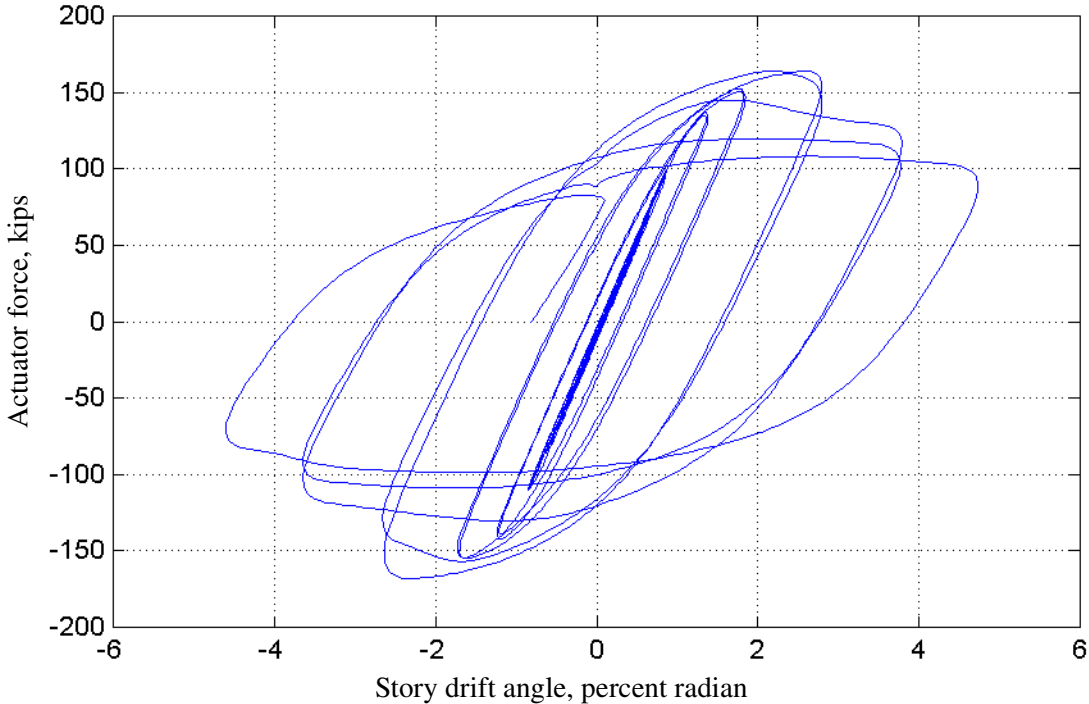


Figure 5-15 Actuator force versus drift angle for RC02

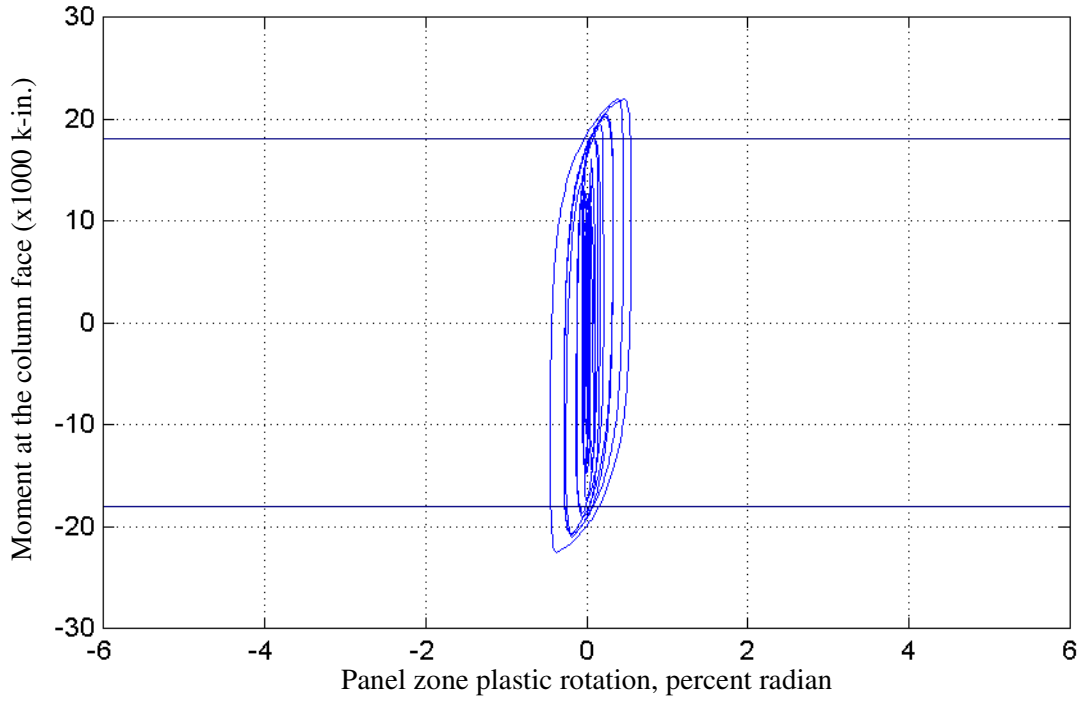


Figure 5-16 Moment at the column face versus panel zone plastic rotation for RC02

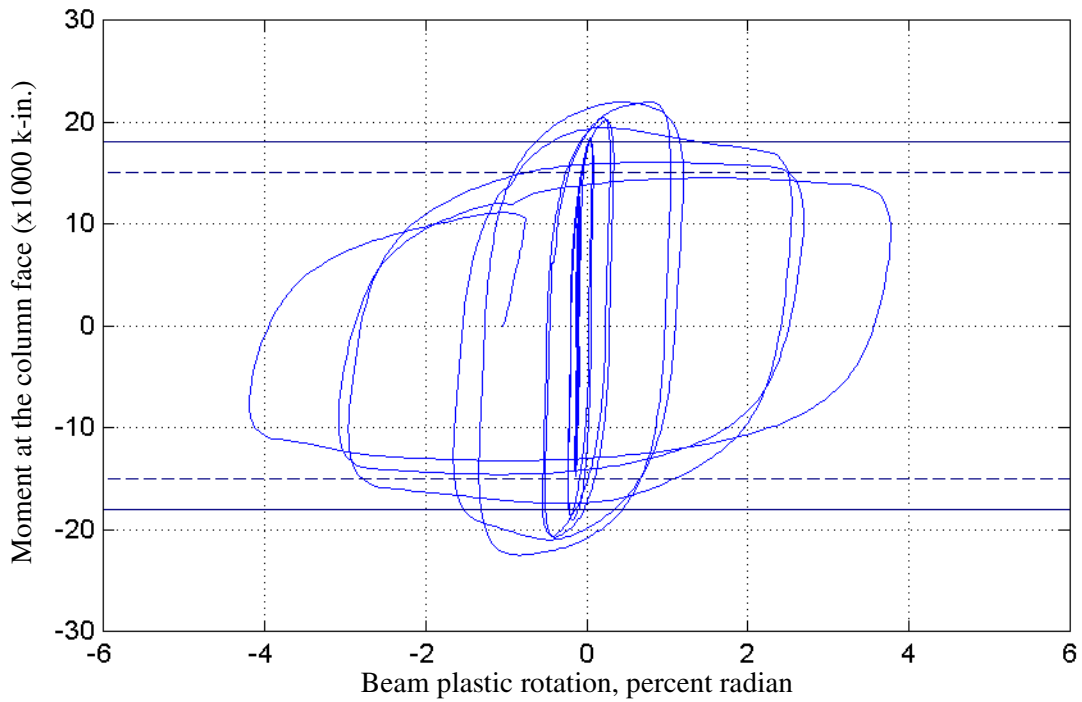


Figure 5-17 Moment at the column face versus beam plastic rotation for RC02

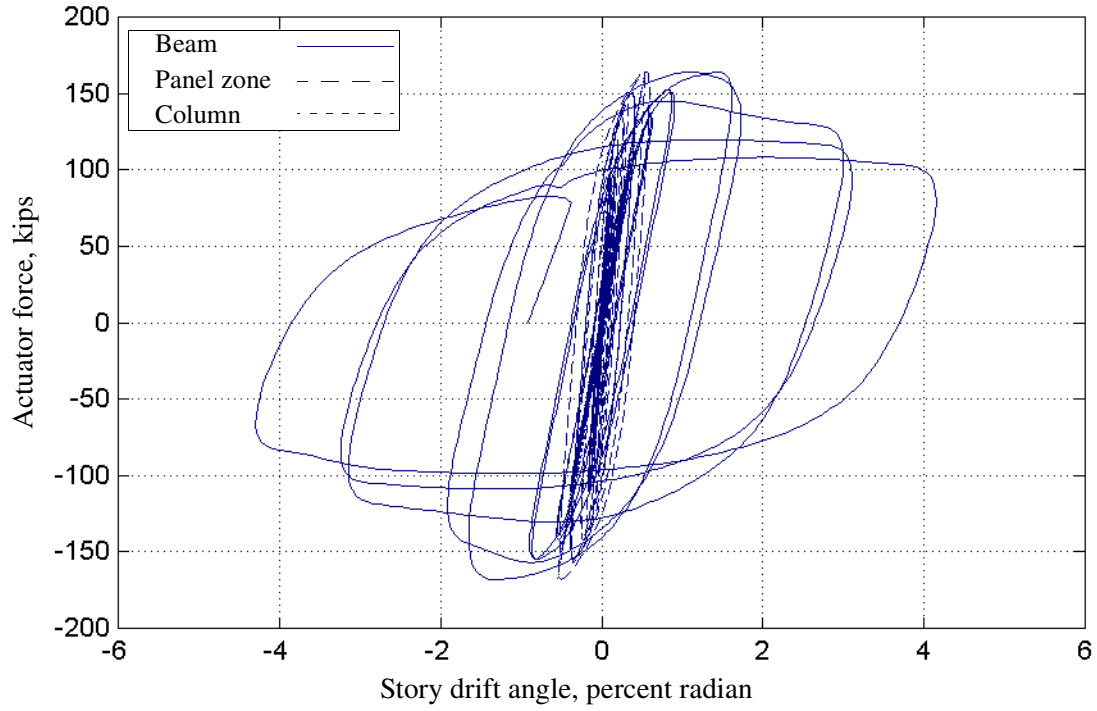


Figure 5-18 Components of drift angle for RC02

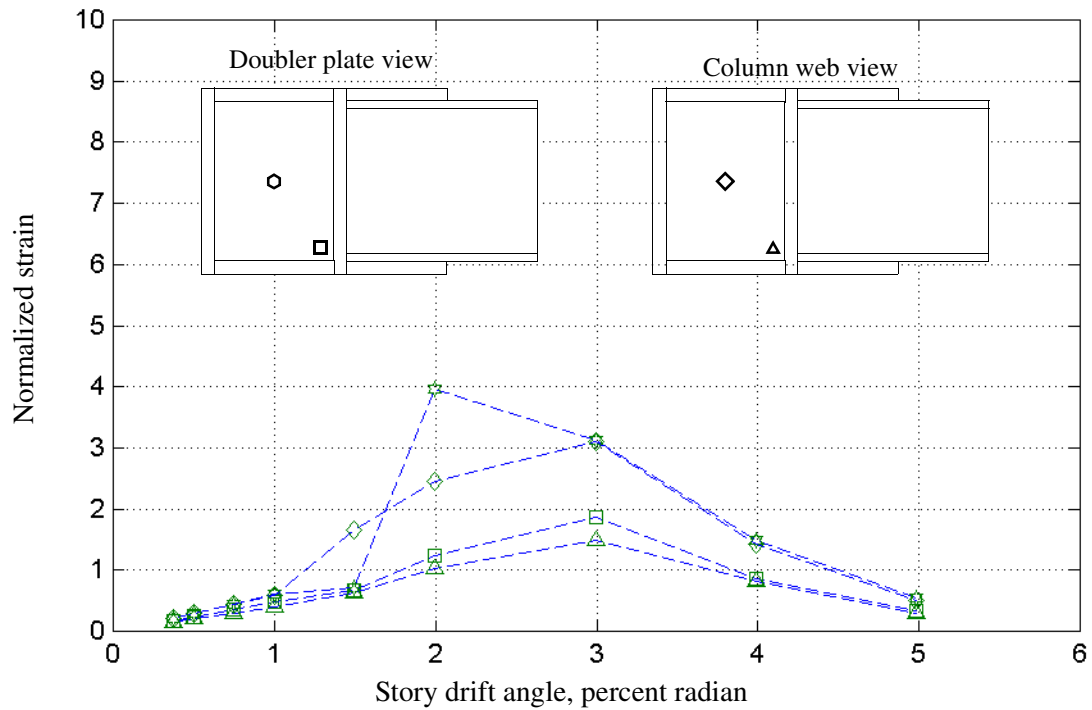


Figure 5-19 Column-web and the doubler-plate shear strains for RC02

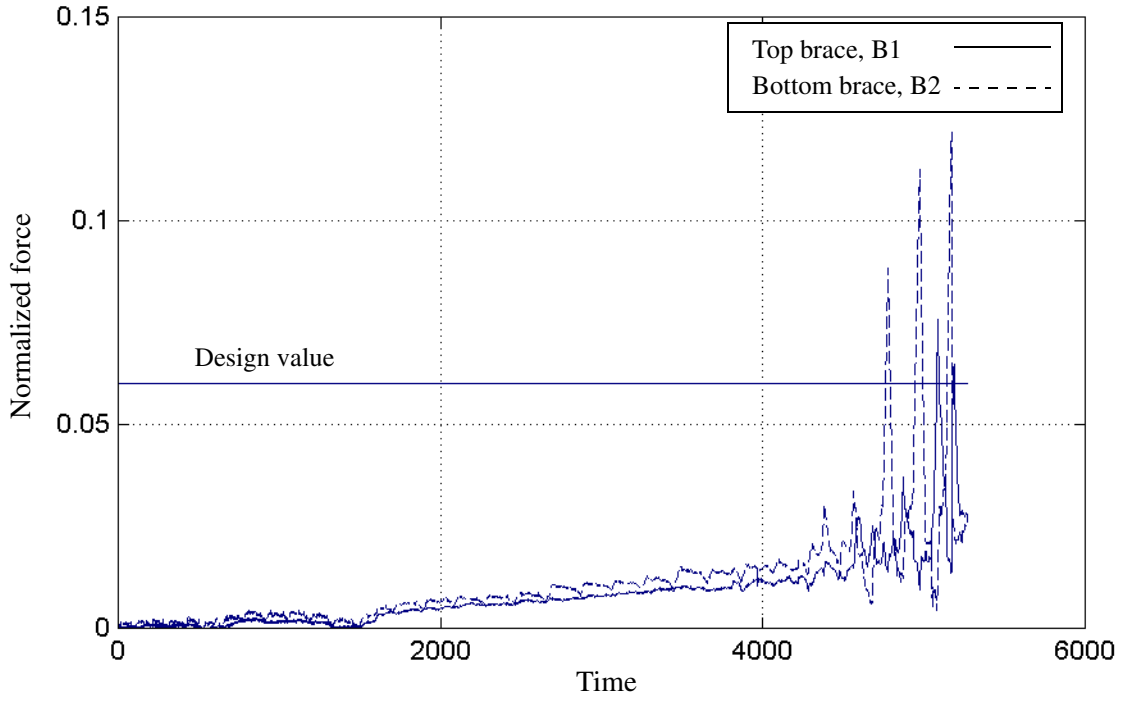


Figure 5-20 Normalized force history in lateral braces for RC02

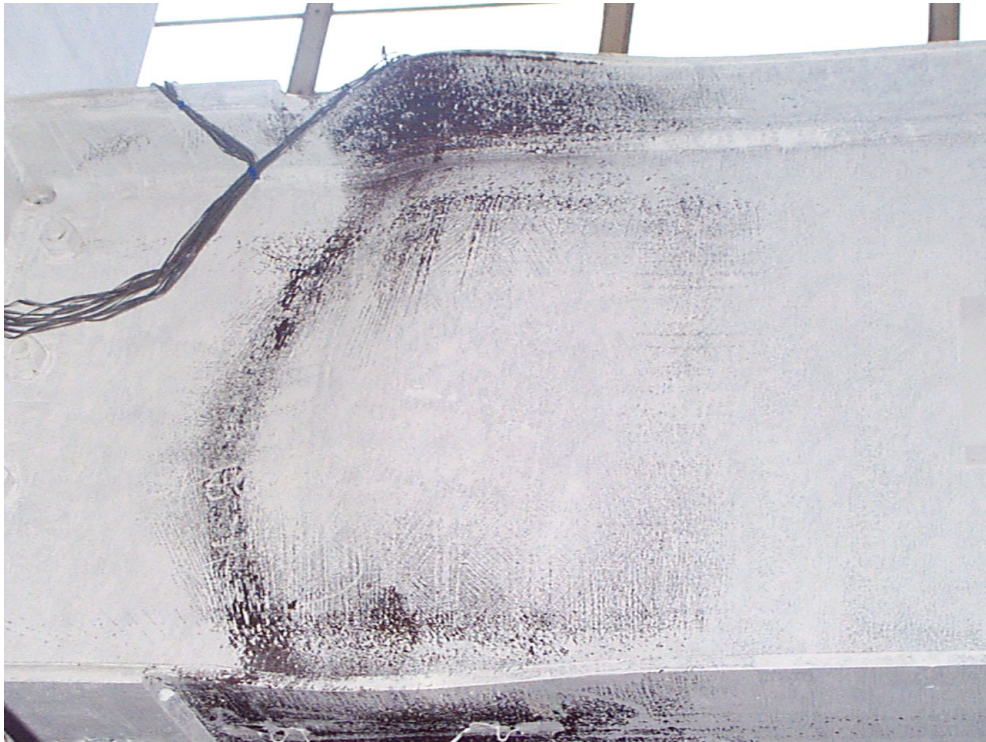


Figure 5-21 Beam FLB and WLB in RC03 at a drift angle of $0.03h$



Figure 5-22 Flange local buckling at nose of cover plate in RC03

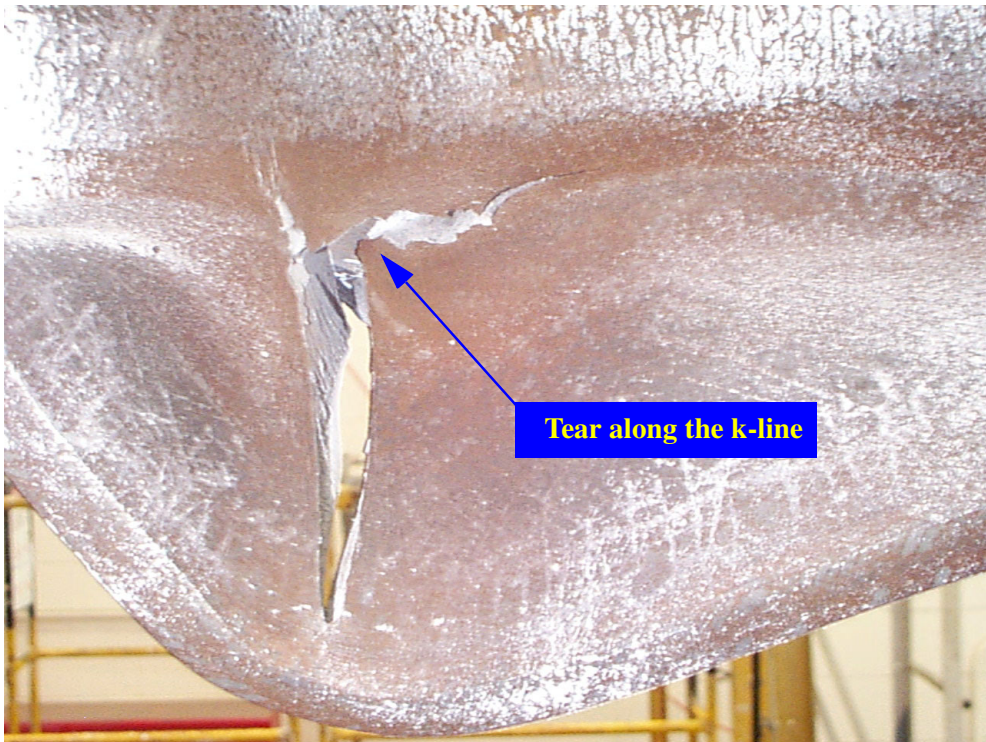


Figure 5-23 Tearing of k-line and beam bottom flange in RC03

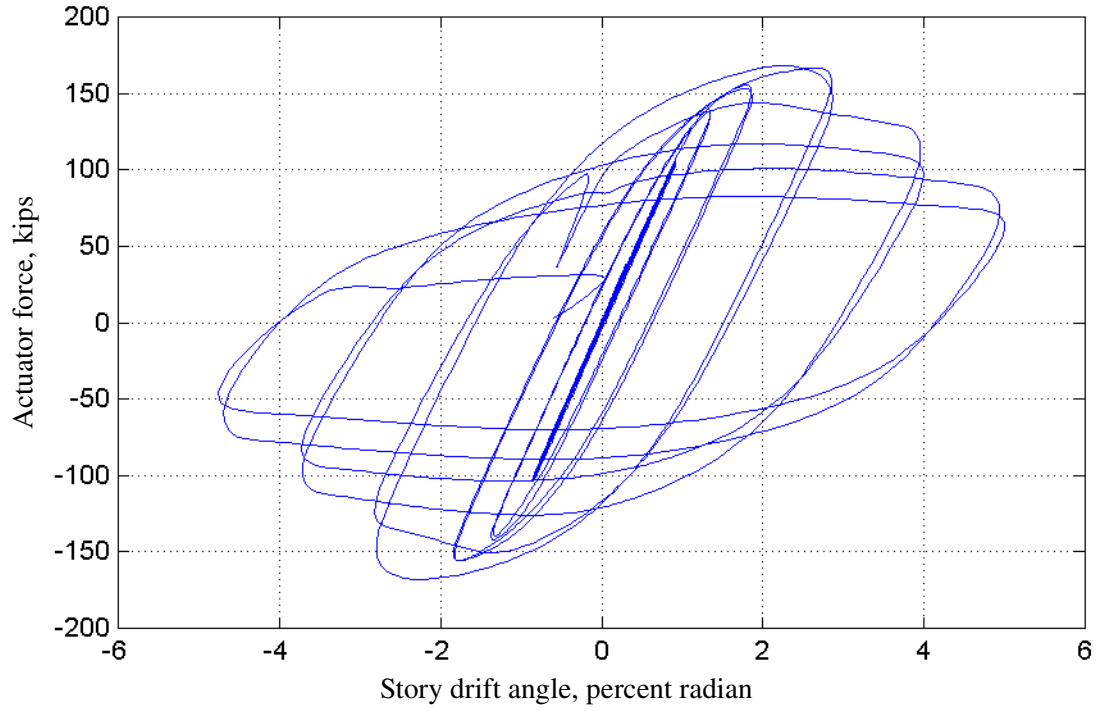


Figure 5-24 Actuator force versus drift angle for RC03

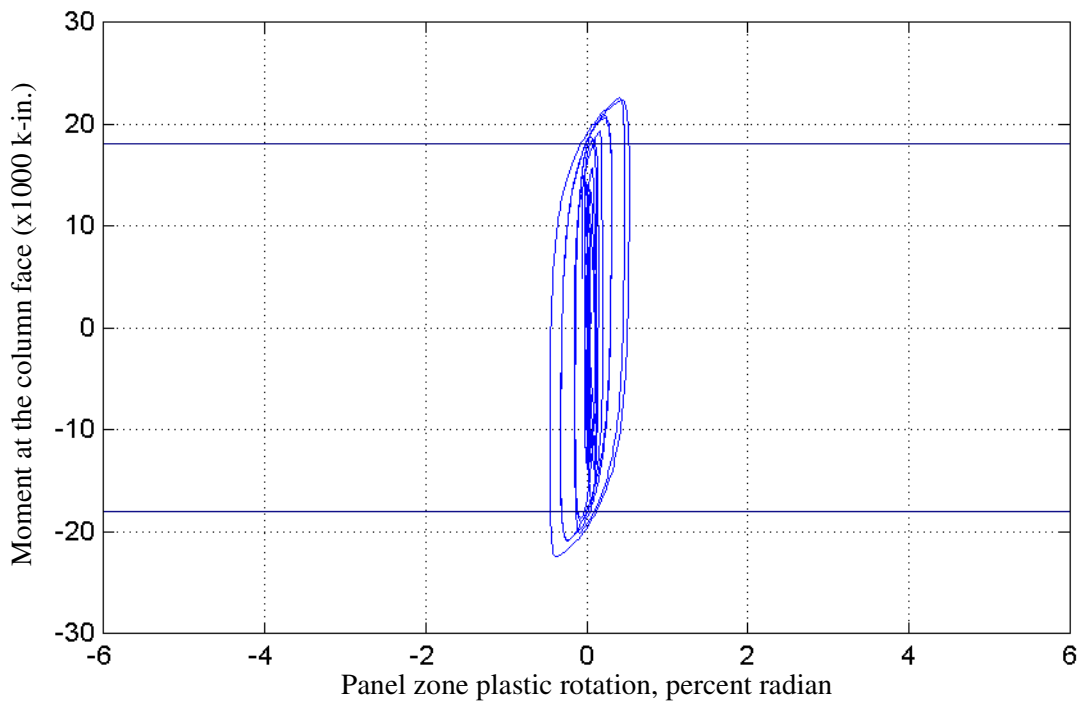


Figure 5-25 Moment at the column face versus panel zone plastic rotation for RC03

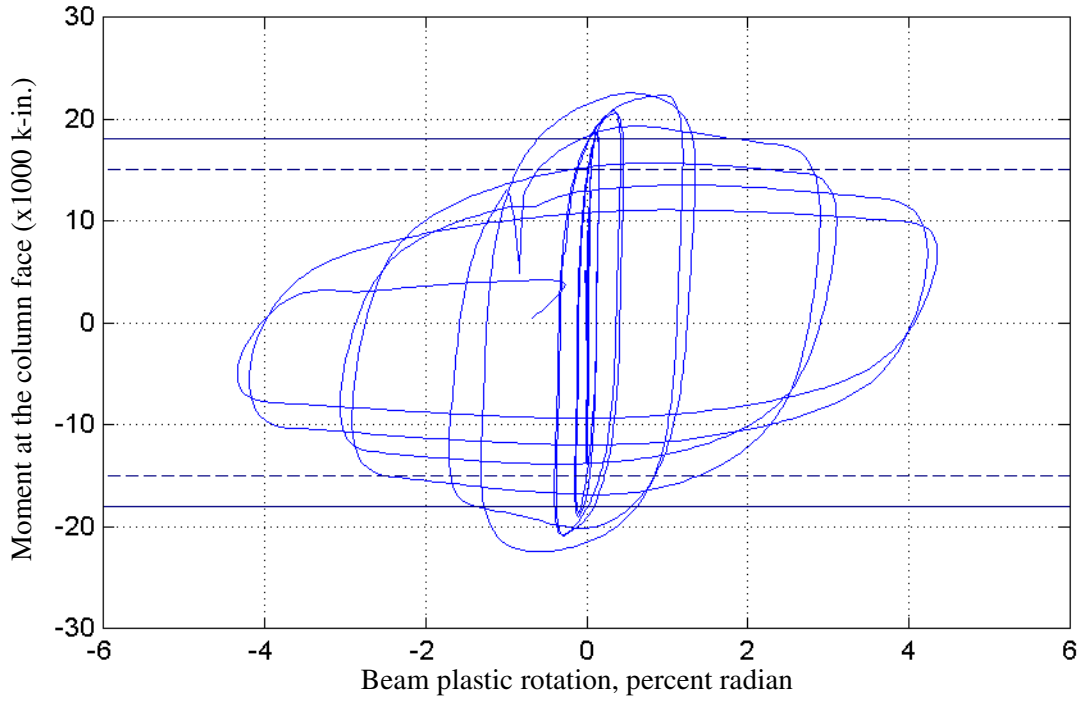


Figure 5-26 Moment at the column face versus beam plastic rotation for RC03

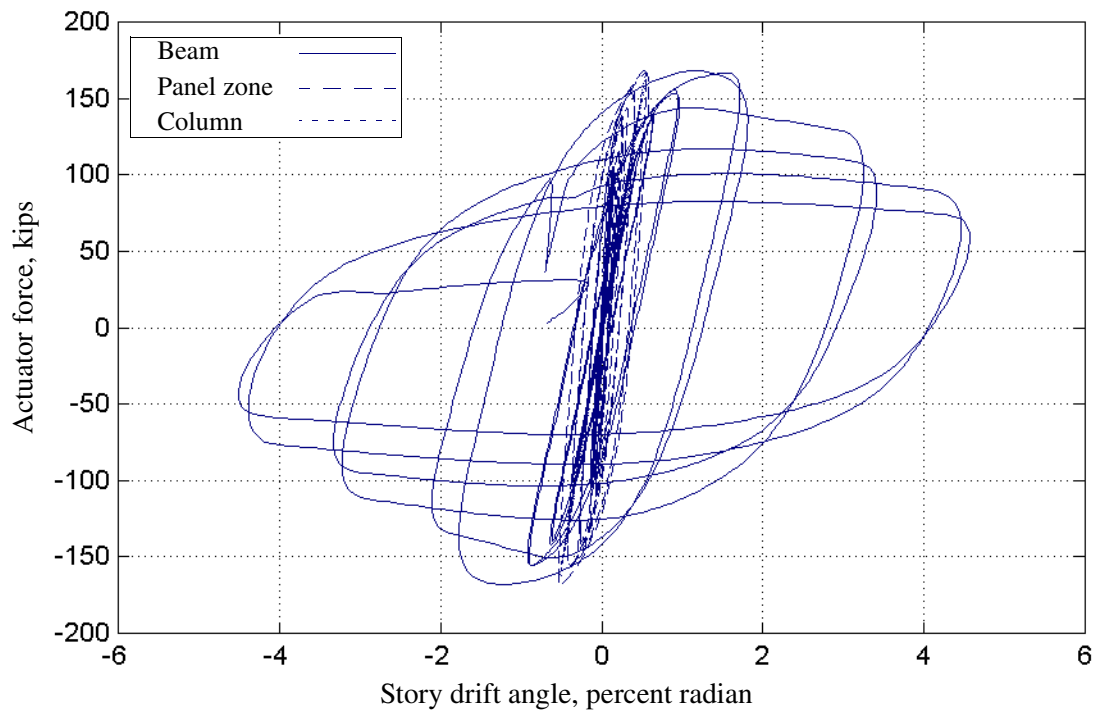


Figure 5-27 Components of drift angle for RC03

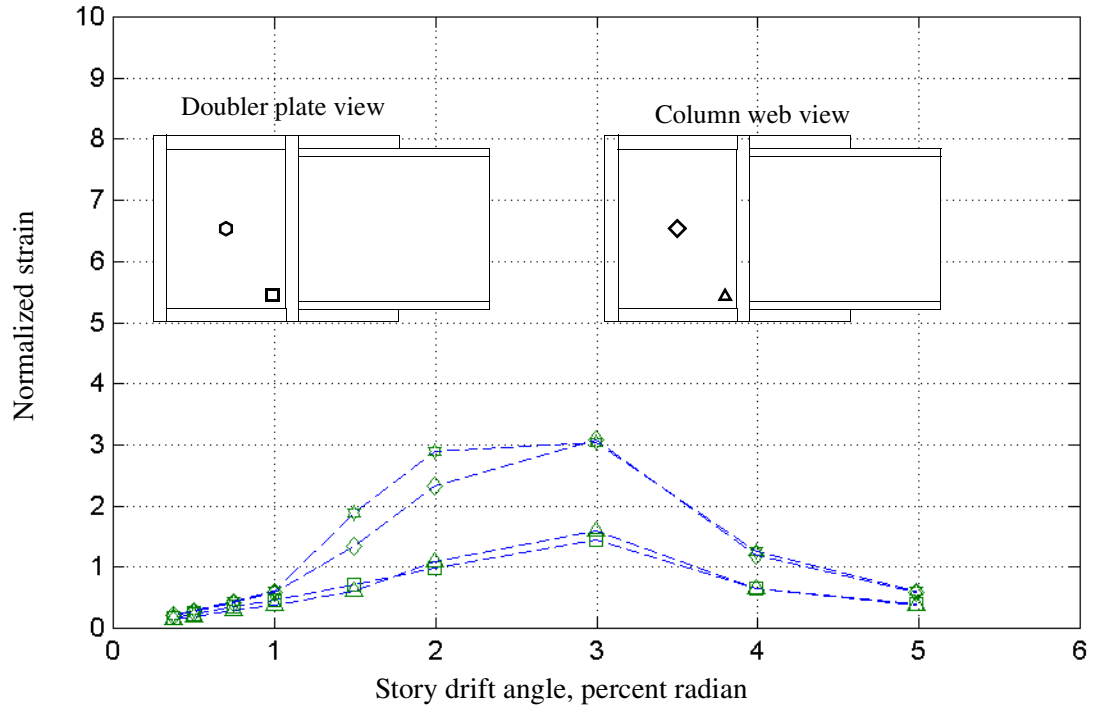


Figure 5-28 Column-web and the doubler-plate strains for RC03

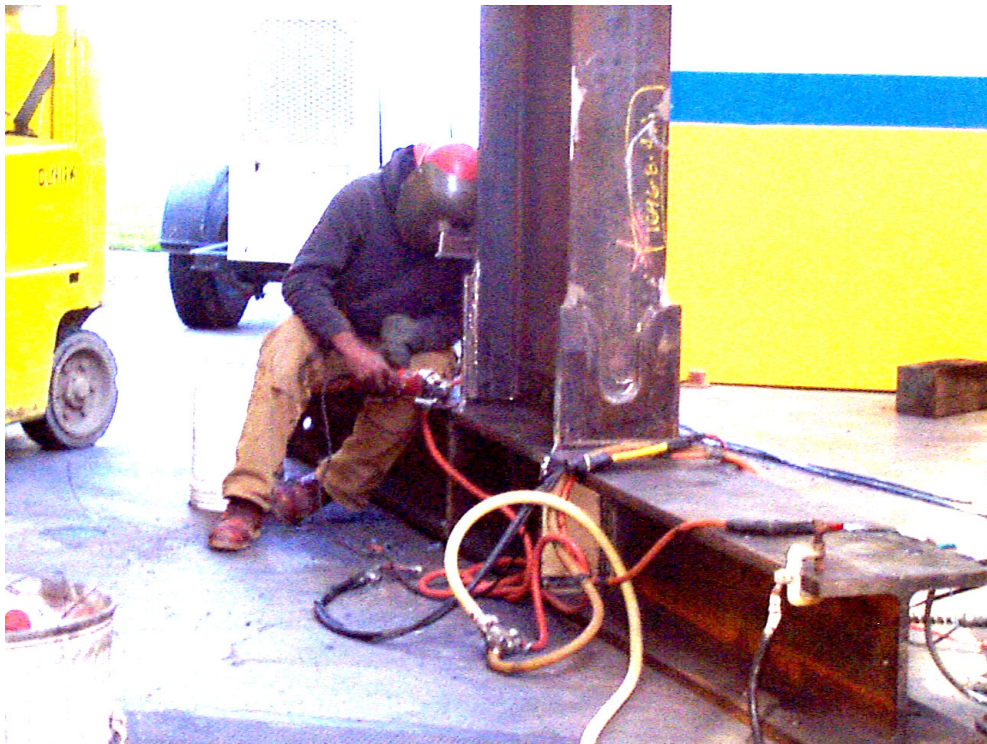


Figure 5-29 Swallowtail flange plate for RC04

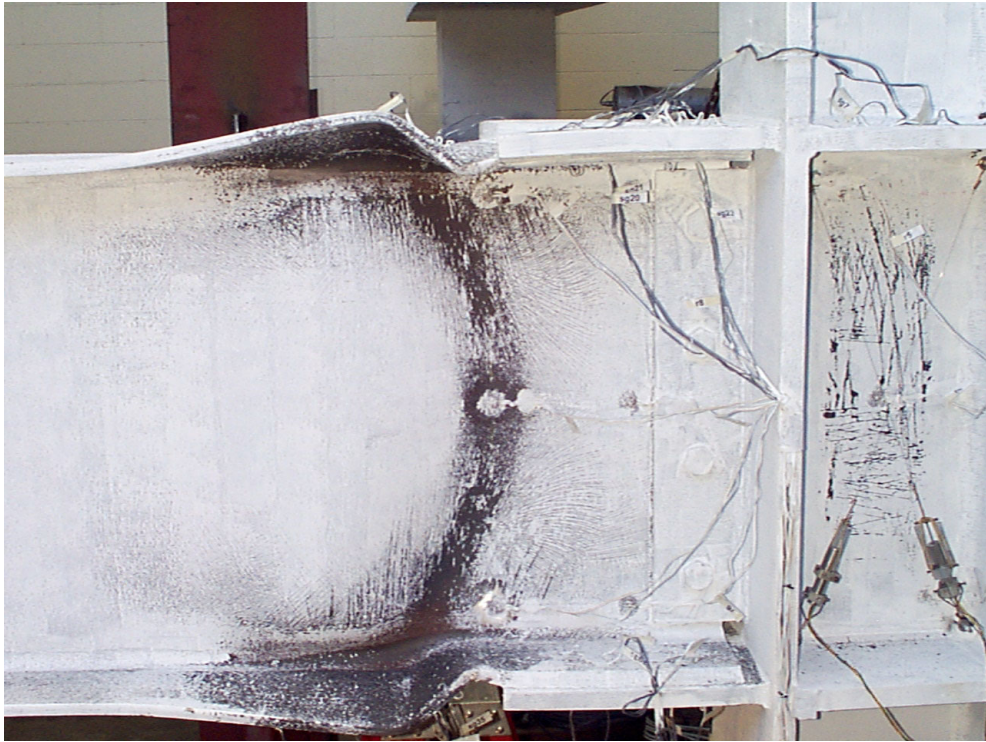


Figure 5-30 Beam FLB and WLB in RC04 at a drift angle of $0.03h$

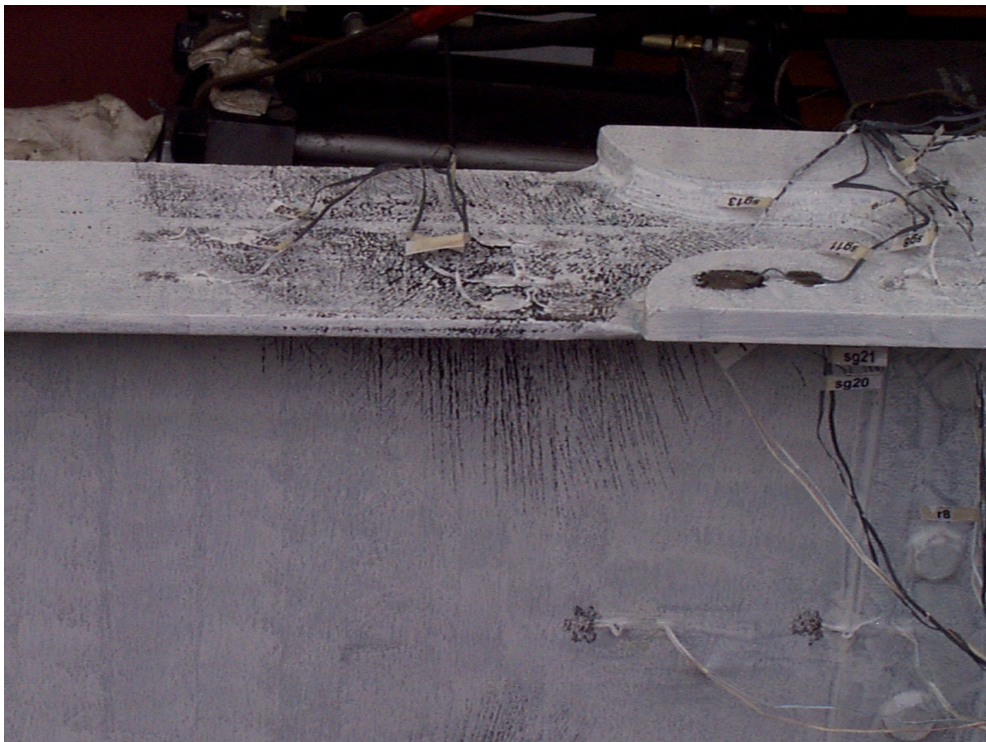


Figure 5-31 Beam top flange and flange plate in RC04 at a drift angle of $0.02h$

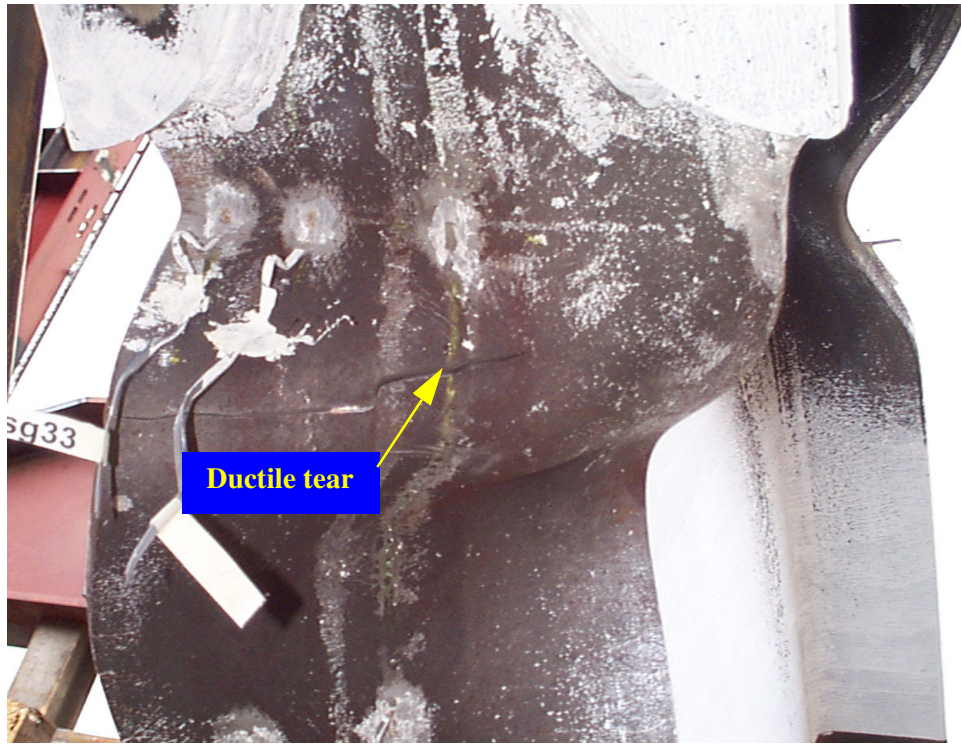


Figure 5-32 Fracture in bottom flange of beam in RC04

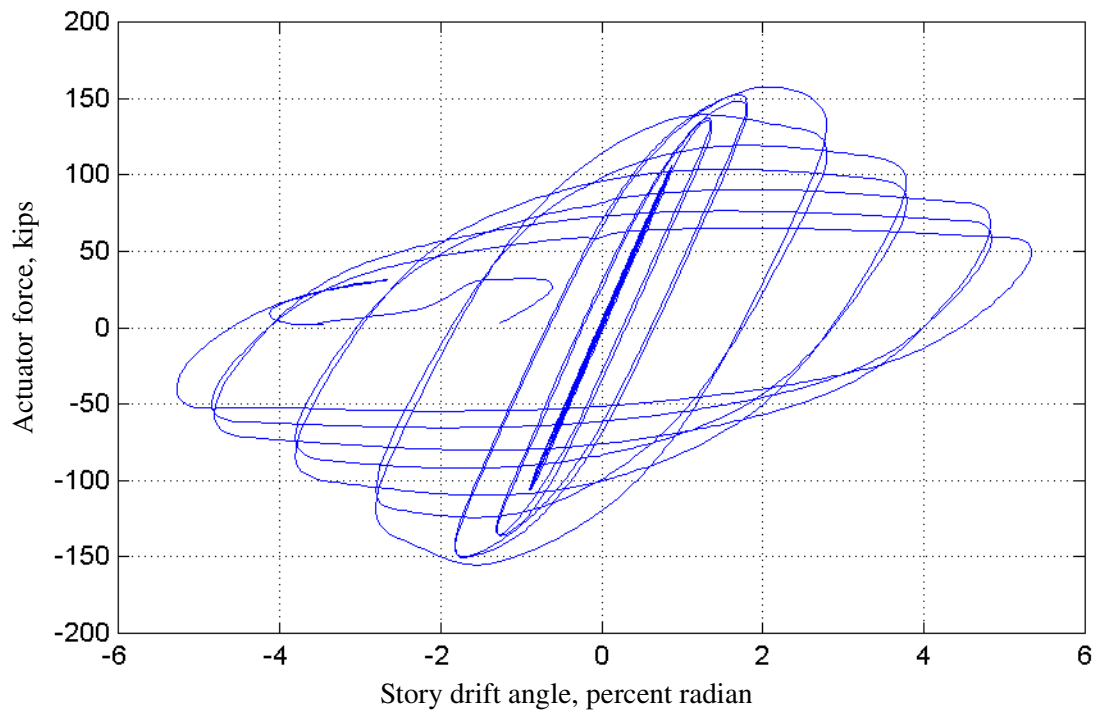


Figure 5-33 Actuator force versus drift angle for RC04

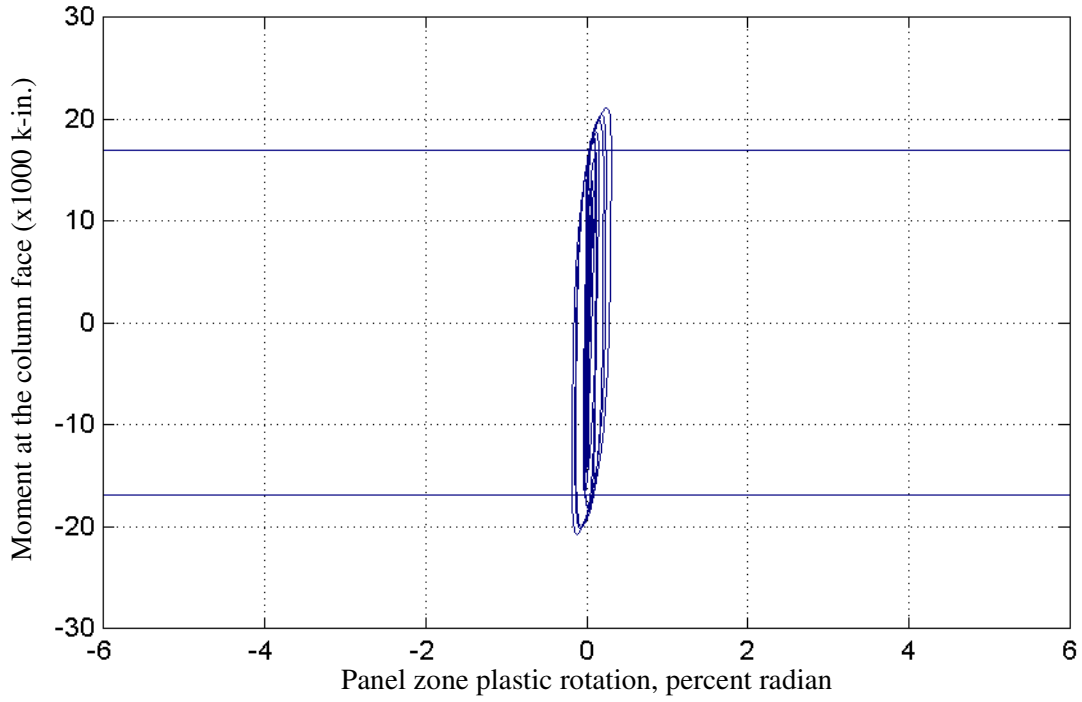


Figure 5-34 Moment at the column face versus panel zone plastic rotation for RC04

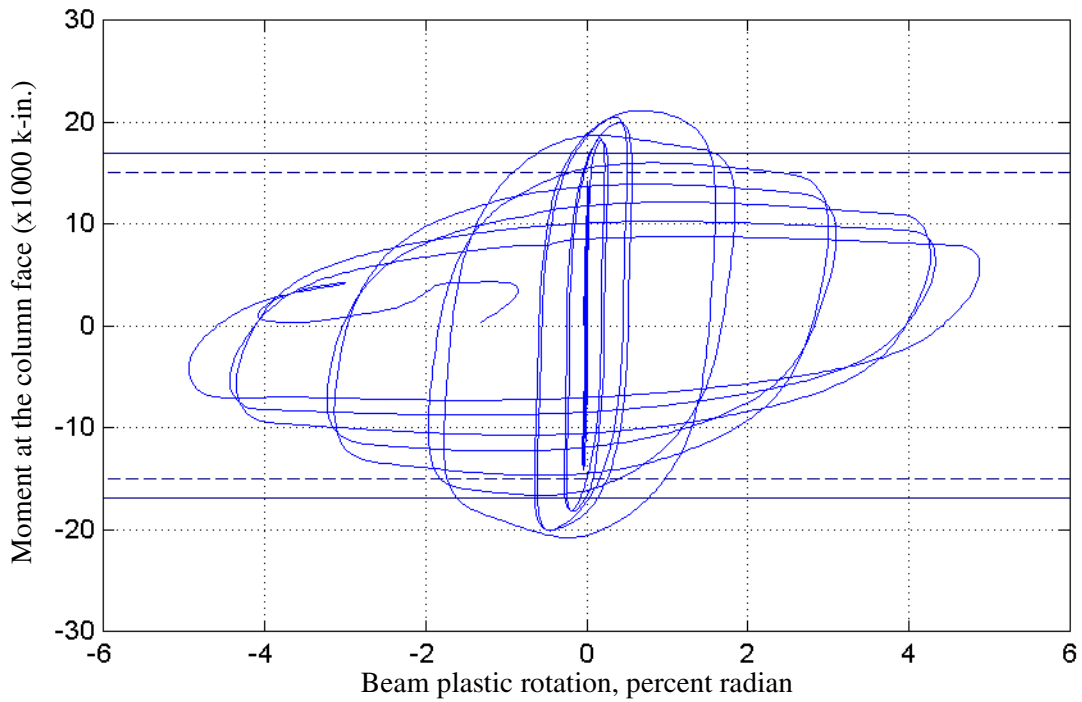


Figure 5-35 Moment at the column face versus beam plastic rotation for RC04

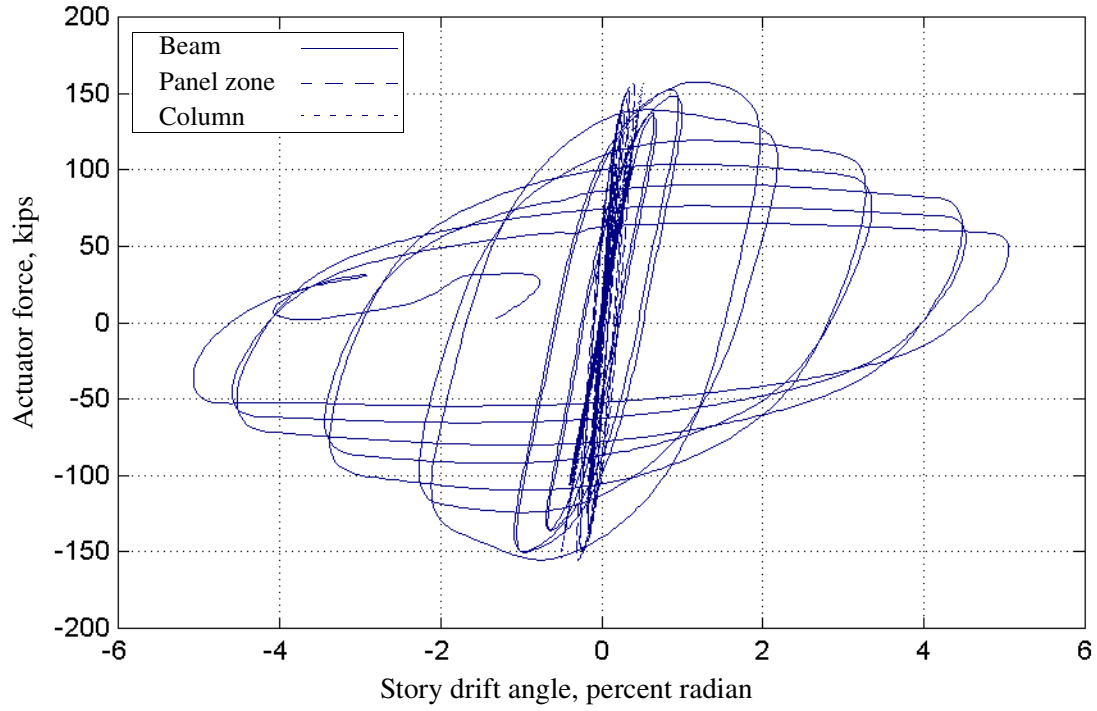


Figure 5-36 Components of drift angle for RC04

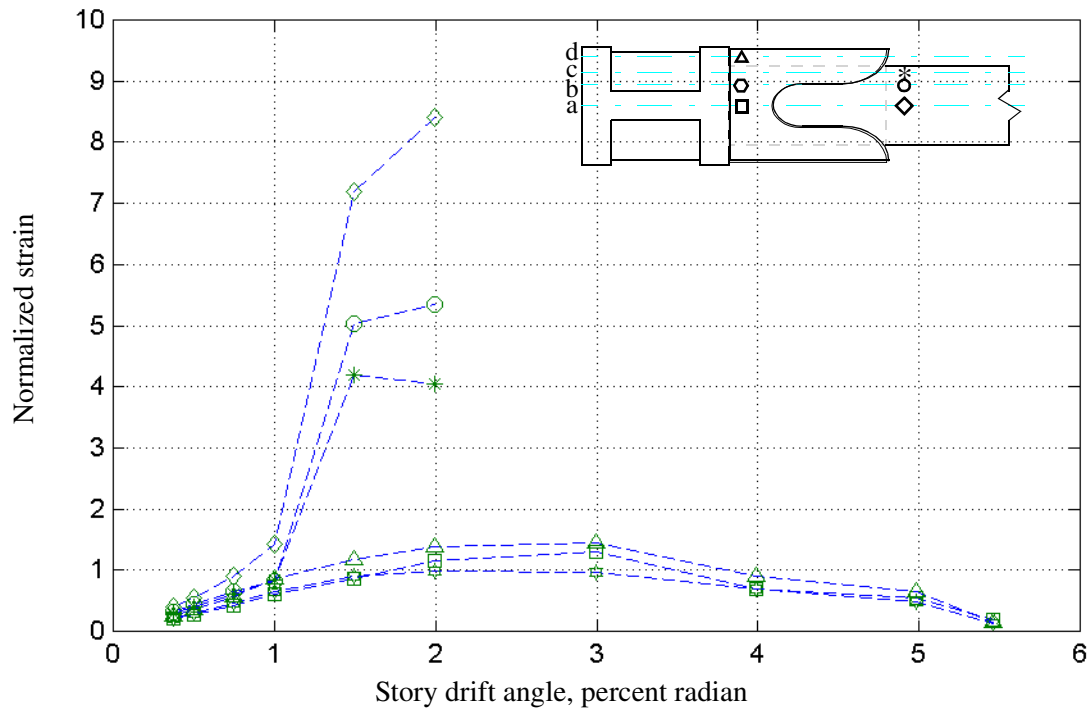


Figure 5-37 Beam and flange plate strains for RC04

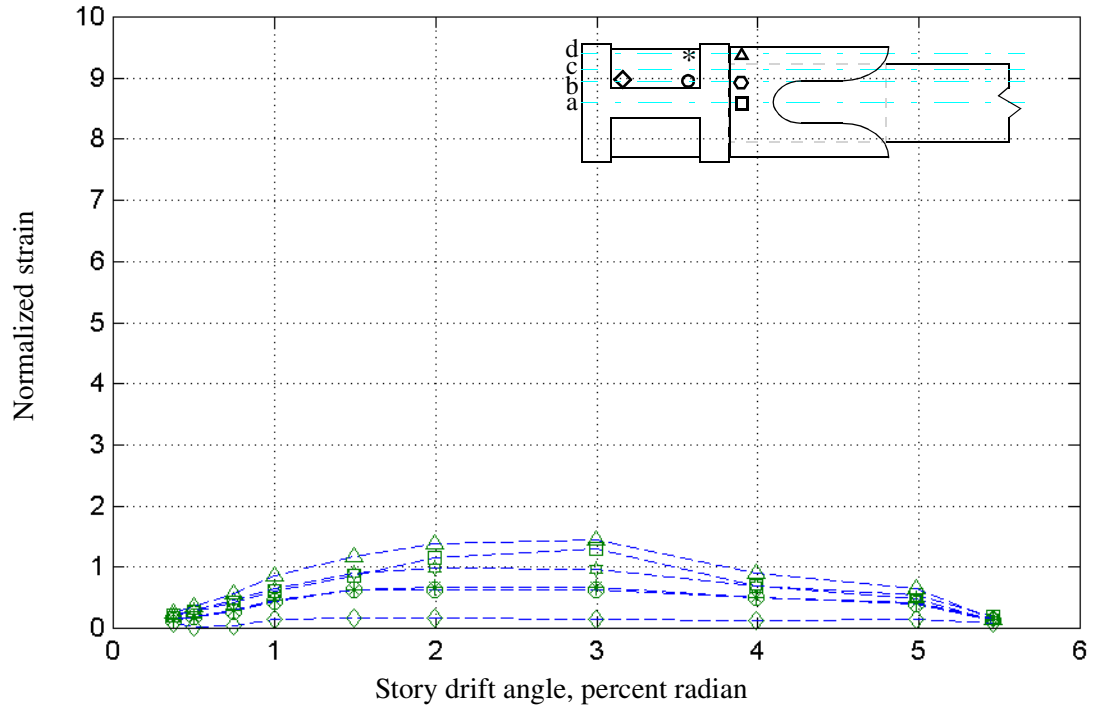


Figure 5-38 Flange plate and continuity plate strains for RC04

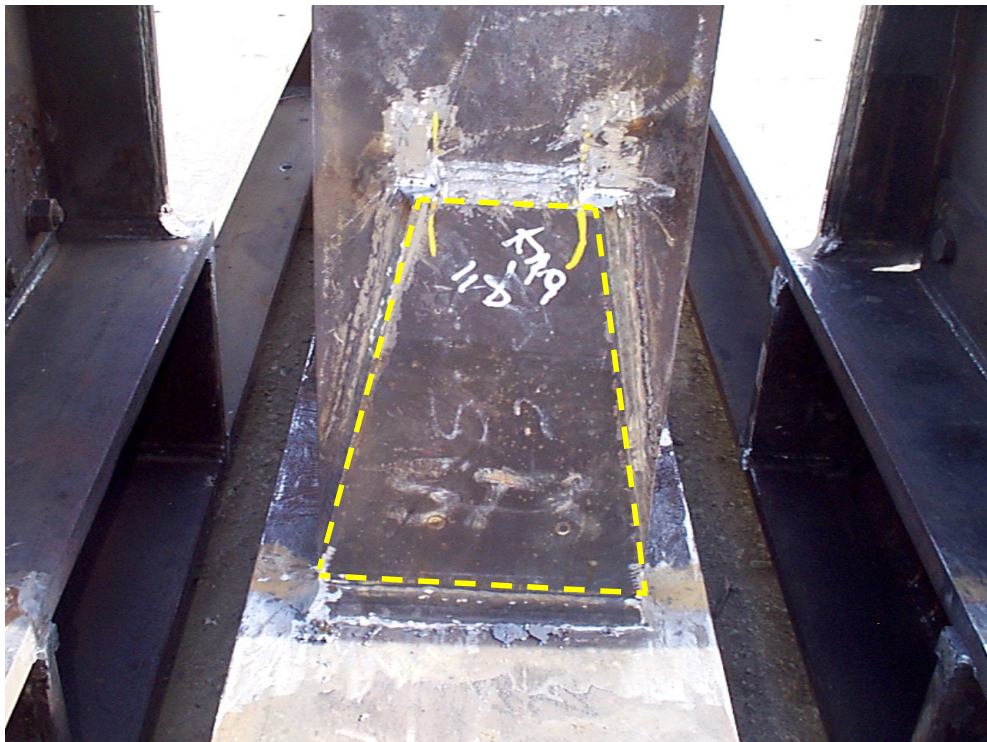


Figure 5-39 Trapezoidal cover plate of RC05

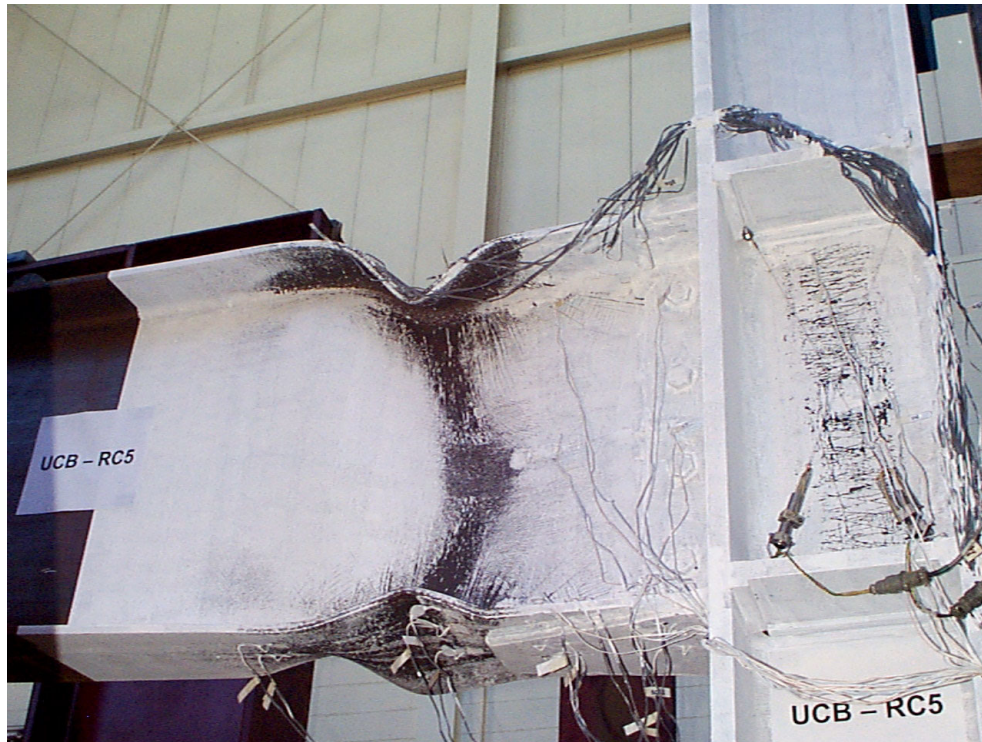


Figure 5-40 Beam FLB and WLB in RC05 at a drift angle of $0.05h$



Figure 5-41 Tear in bottom flange of beam in RC05

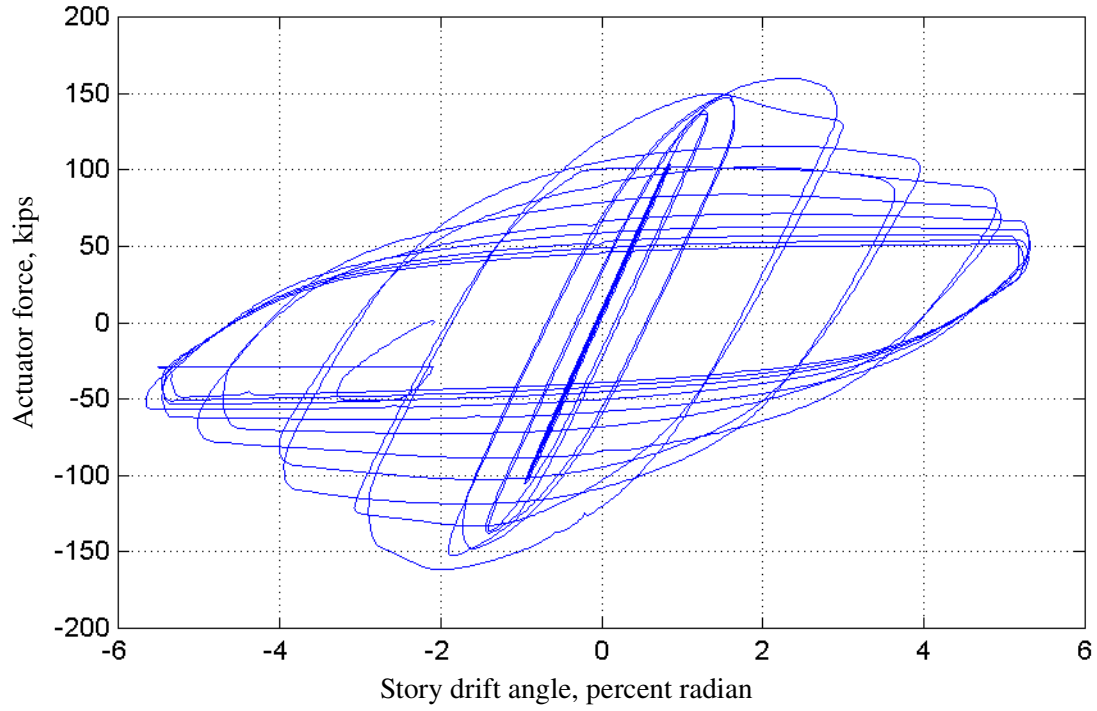


Figure 5-42 Actuator force versus drift angle for RC05

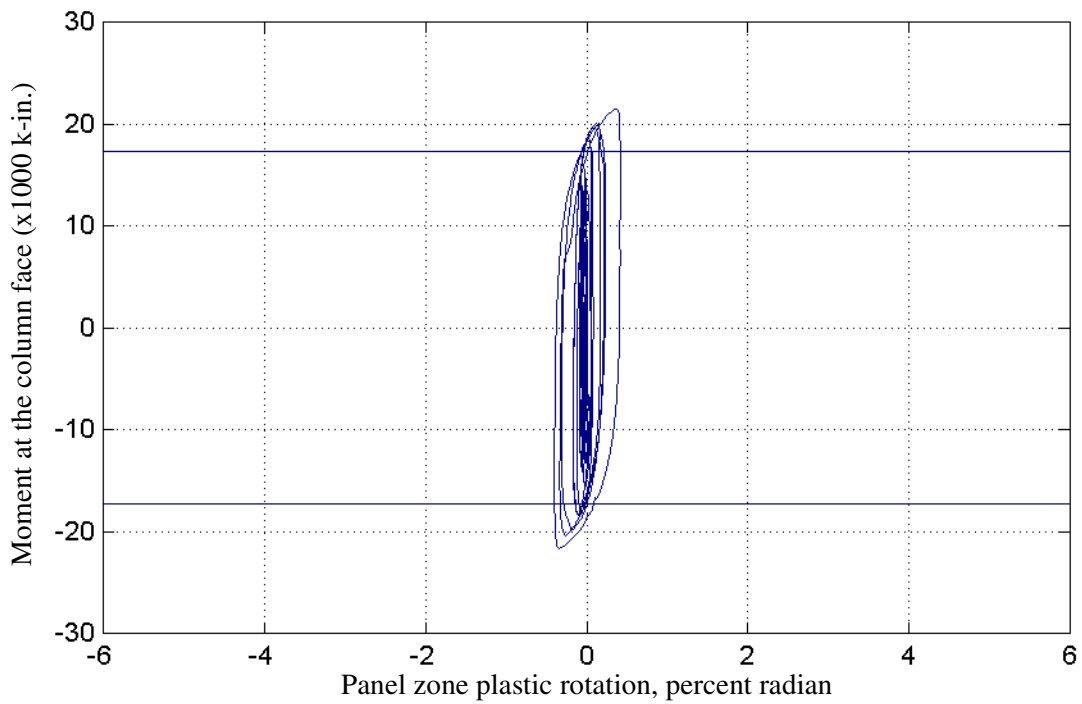


Figure 5-43 Moment at the column face versus panel zone plastic rotation for RC05

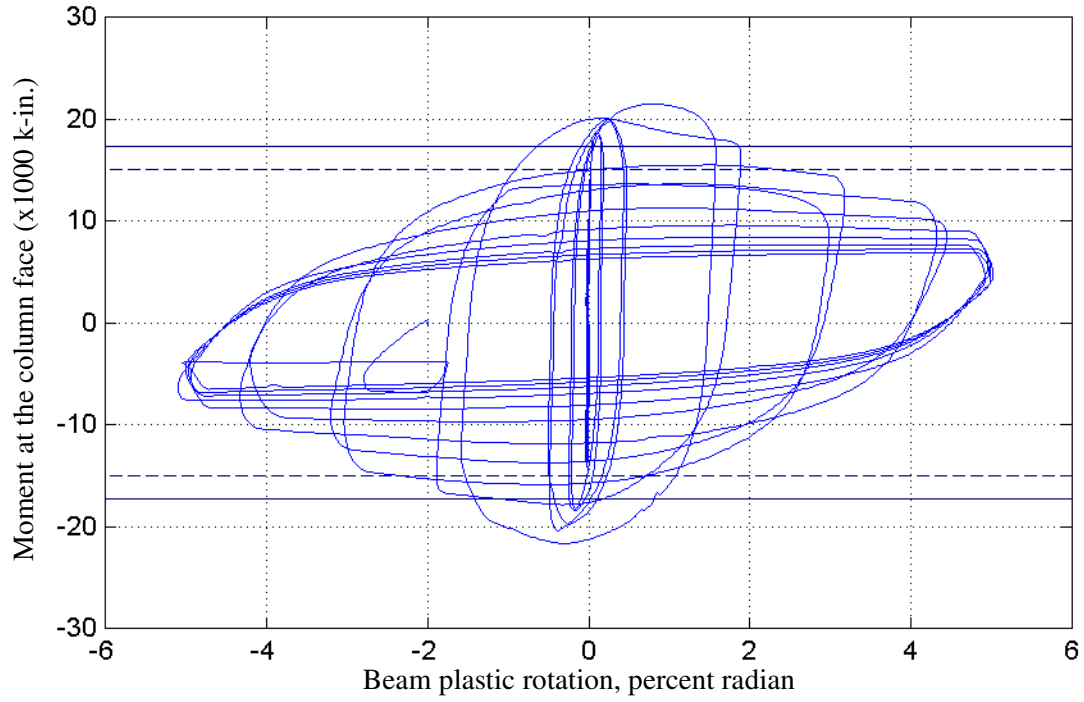


Figure 5-44 Moment at the column face versus beam plastic rotation for RC05

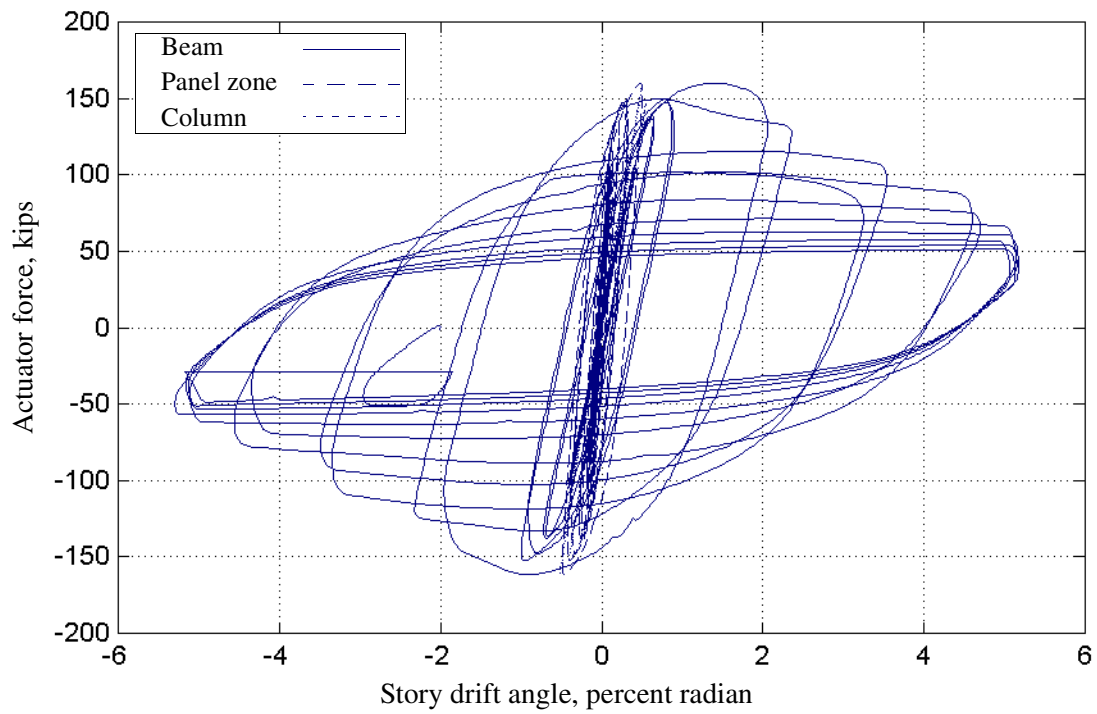


Figure 5-45 Components of drift angle for RC05

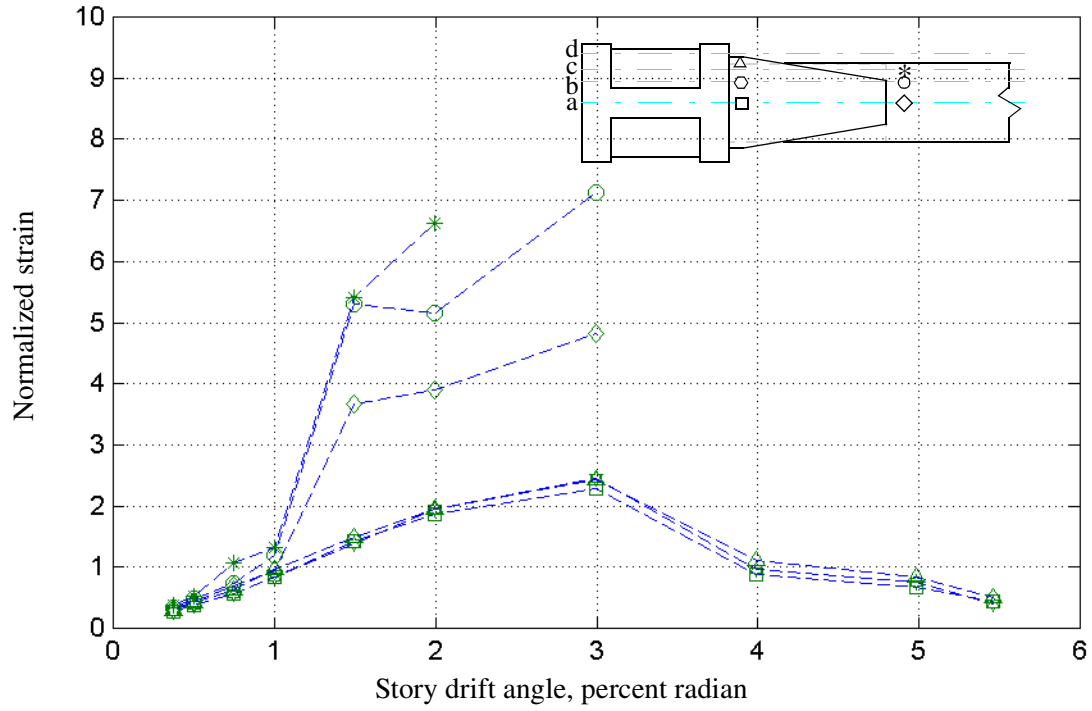


Figure 5-46 Beam and cover-plate strains for RC05

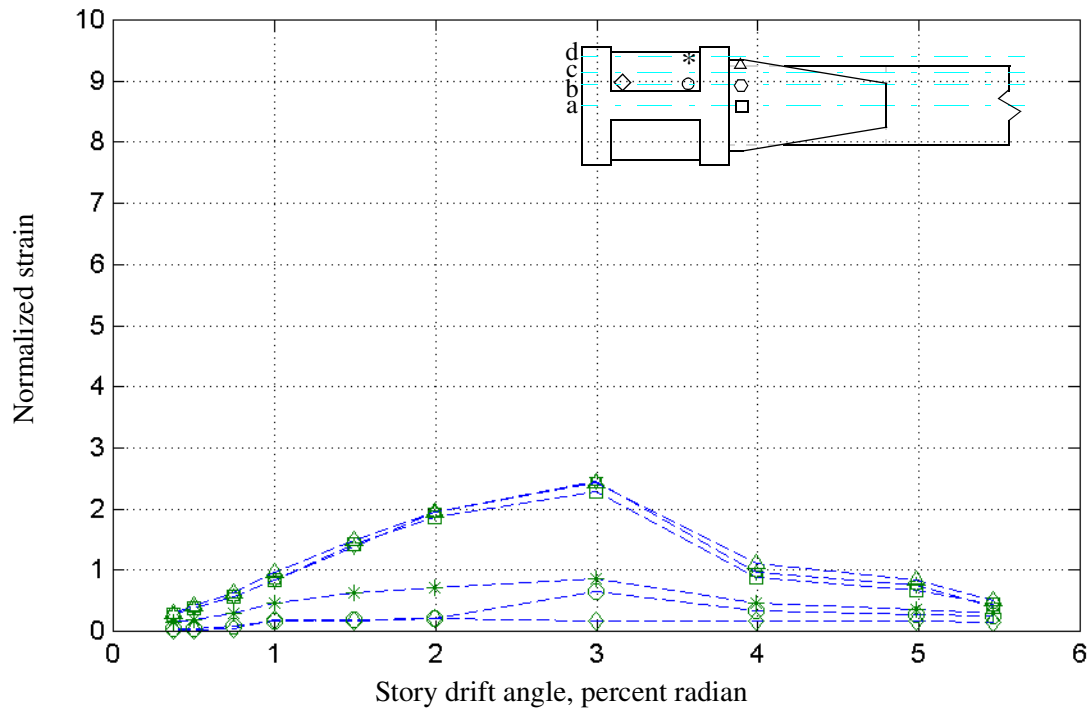


Figure 5-47 Cover-plate and continuity-plate strains for RC05

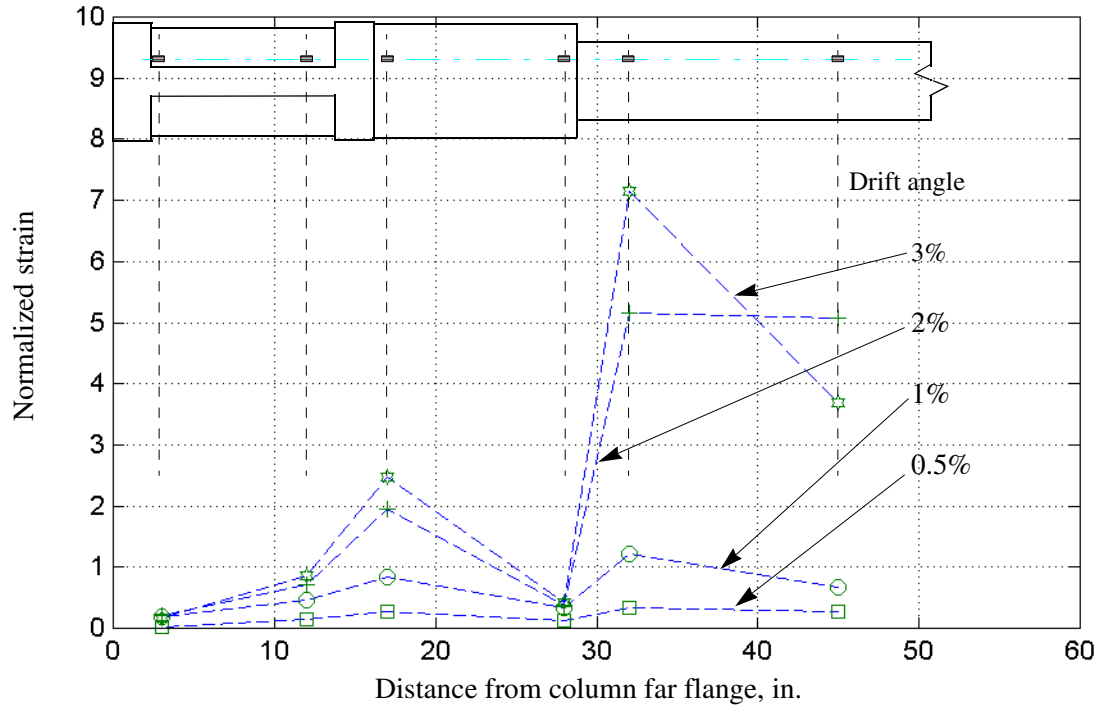


Figure 5-48 Strain response along line *b* for RC05

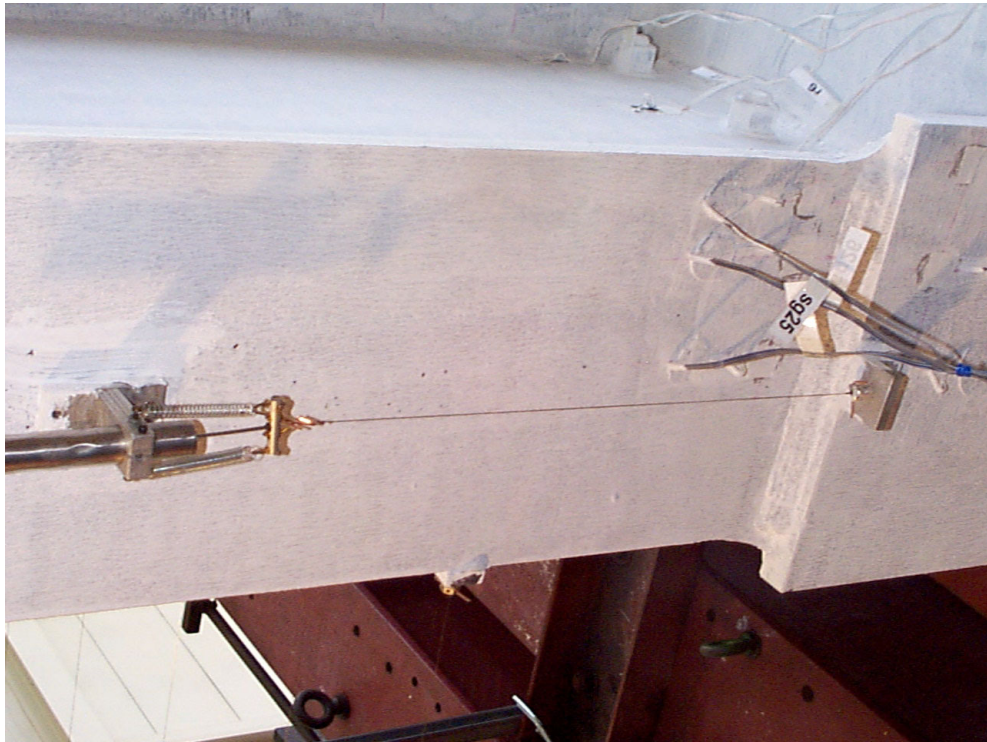


Figure 5-49 Rectangular flange plate of RC06

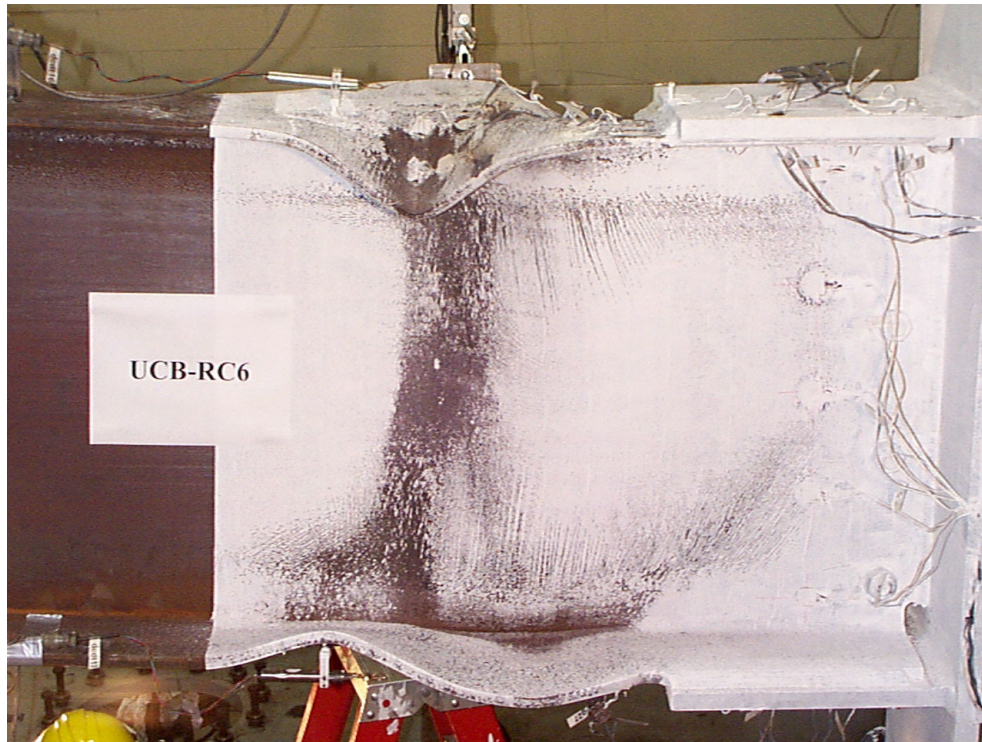


Figure 5-50 Beam FLB and WLB in RC06 at a drift angle of $0.04h$



Figure 5-51 Ductile tears in the beam top flange of RC06

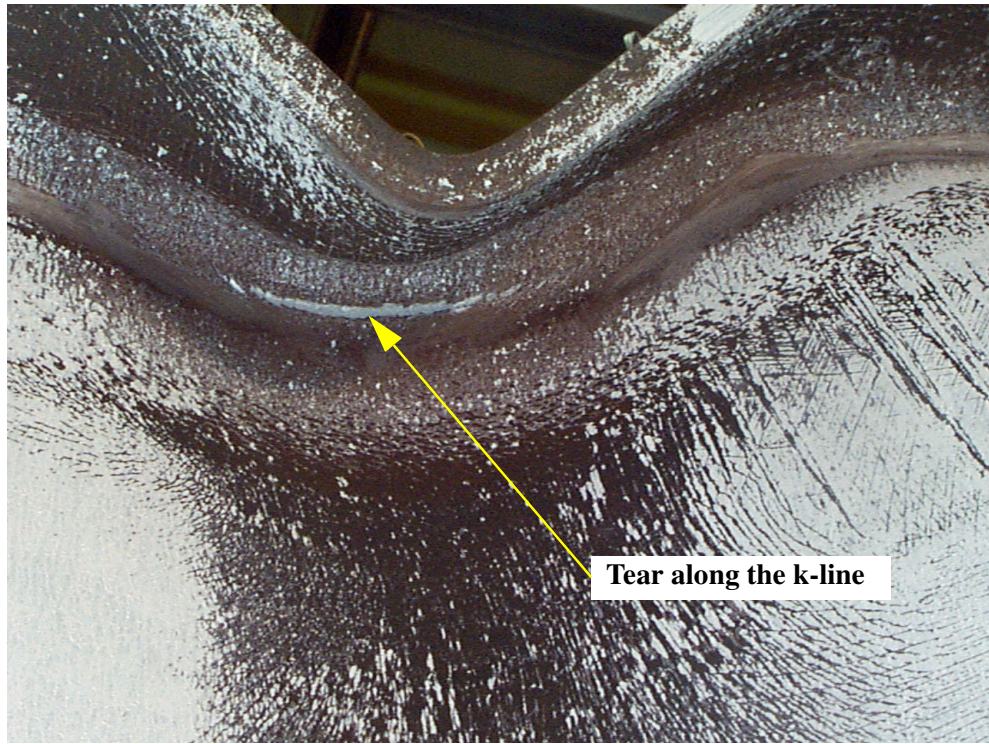


Figure 5-52 Fracture in the beam top flange k-line of RC06

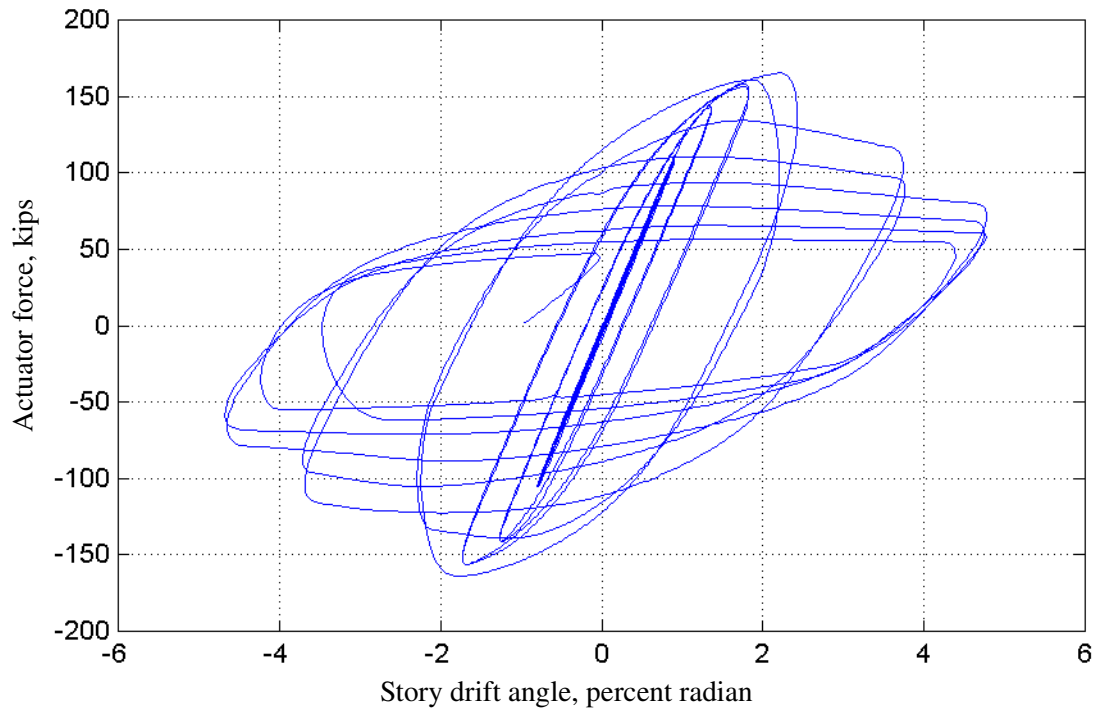


Figure 5-53 Actuator force versus drift angle for RC06

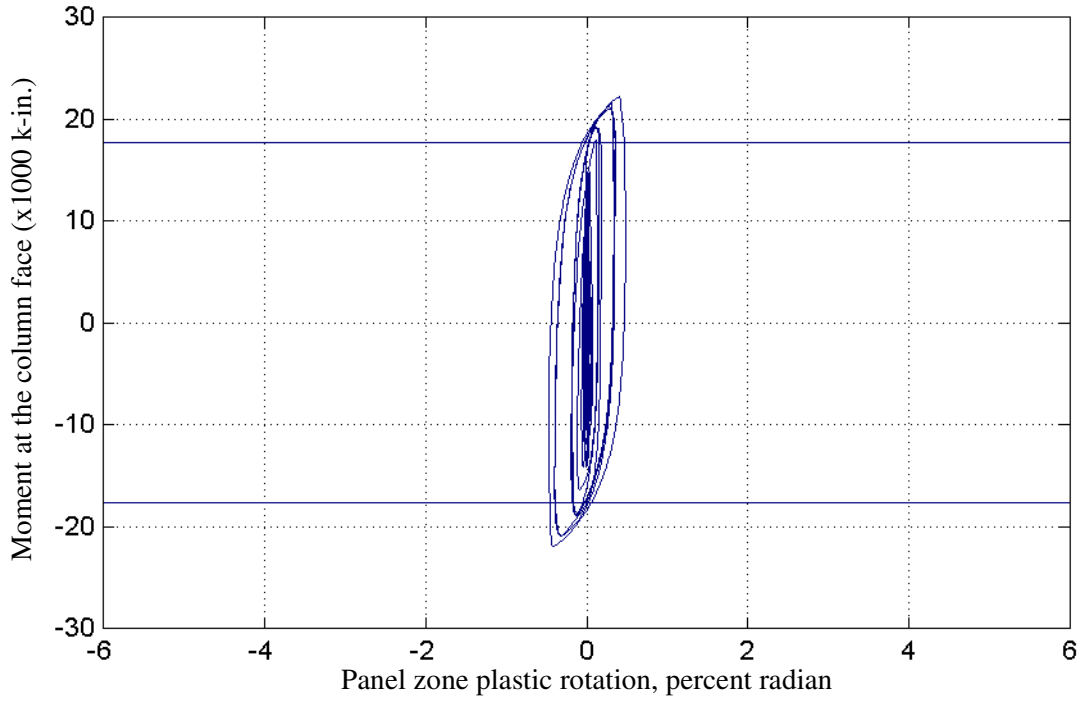


Figure 5-54 Moment at the column face versus panel zone plastic rotation for RC06

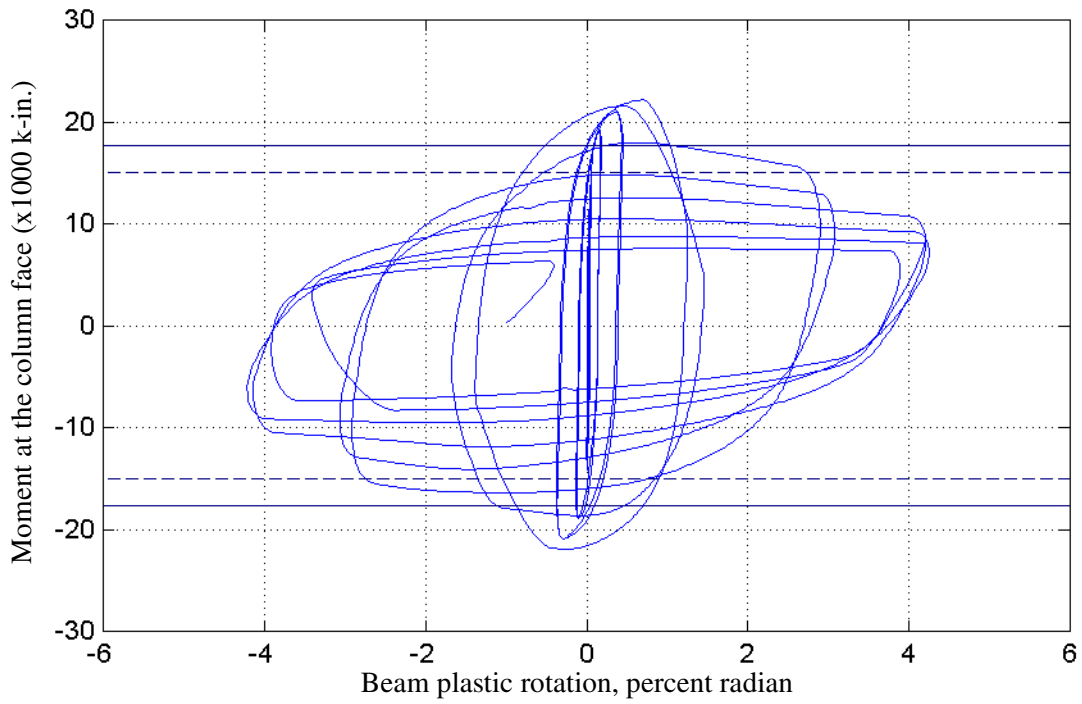


Figure 5-55 Moment at the column face versus beam plastic rotation for RC06

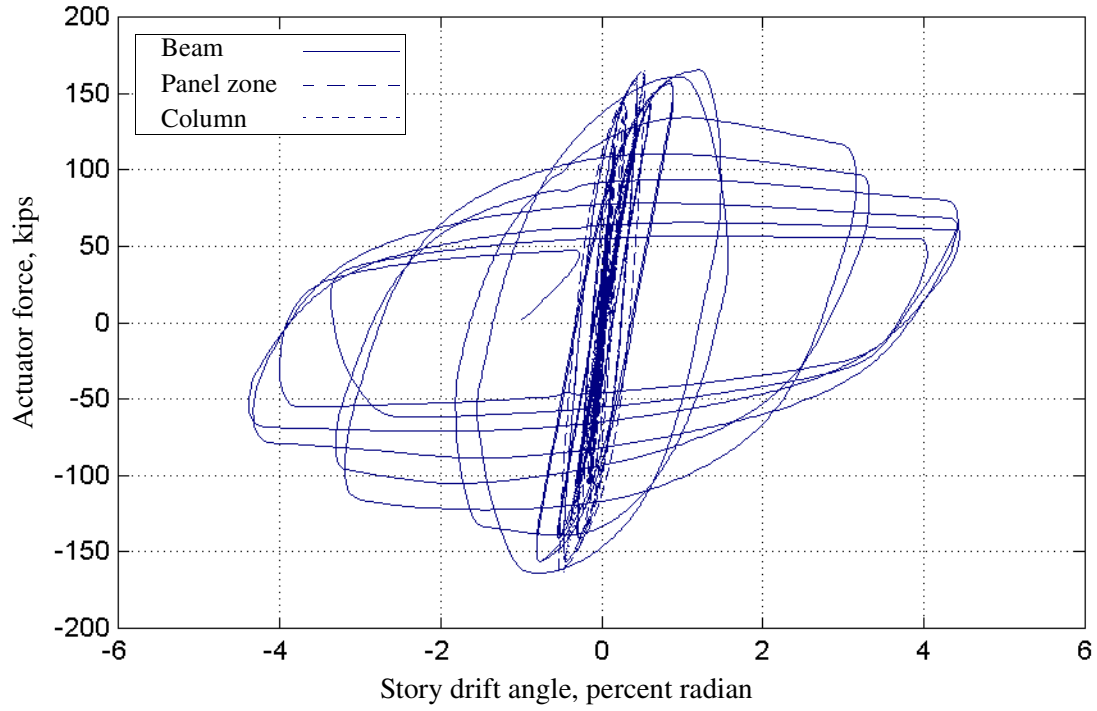


Figure 5-56 Components of drift angle for RC06

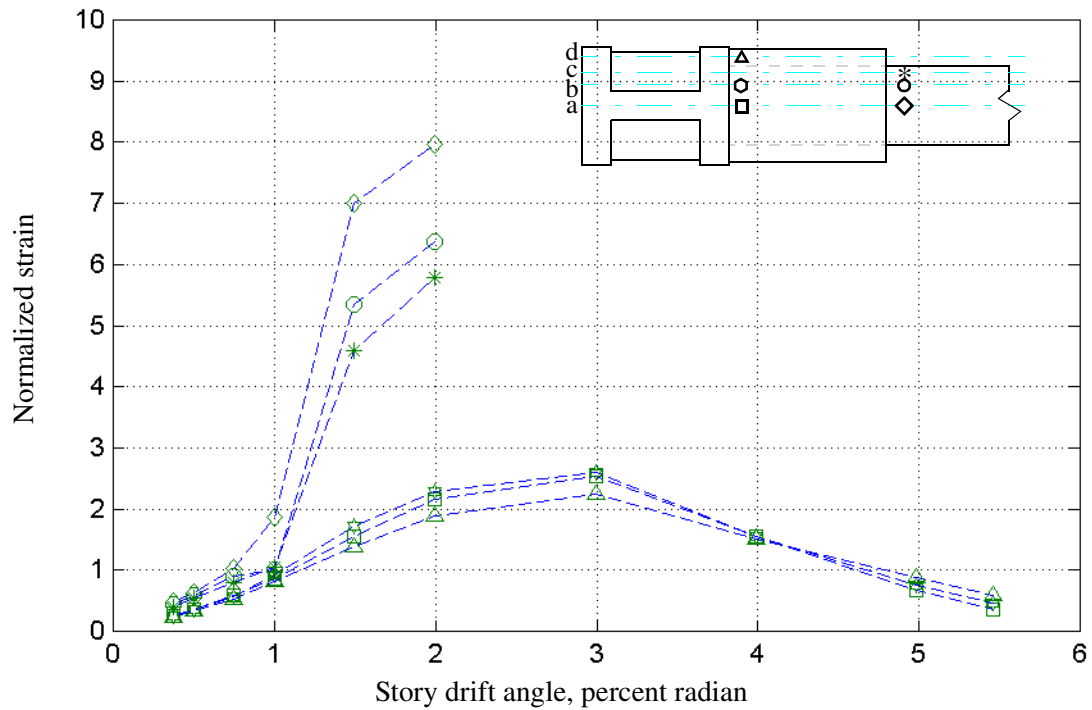


Figure 5-57 Beam and flange-plate strains for RC06

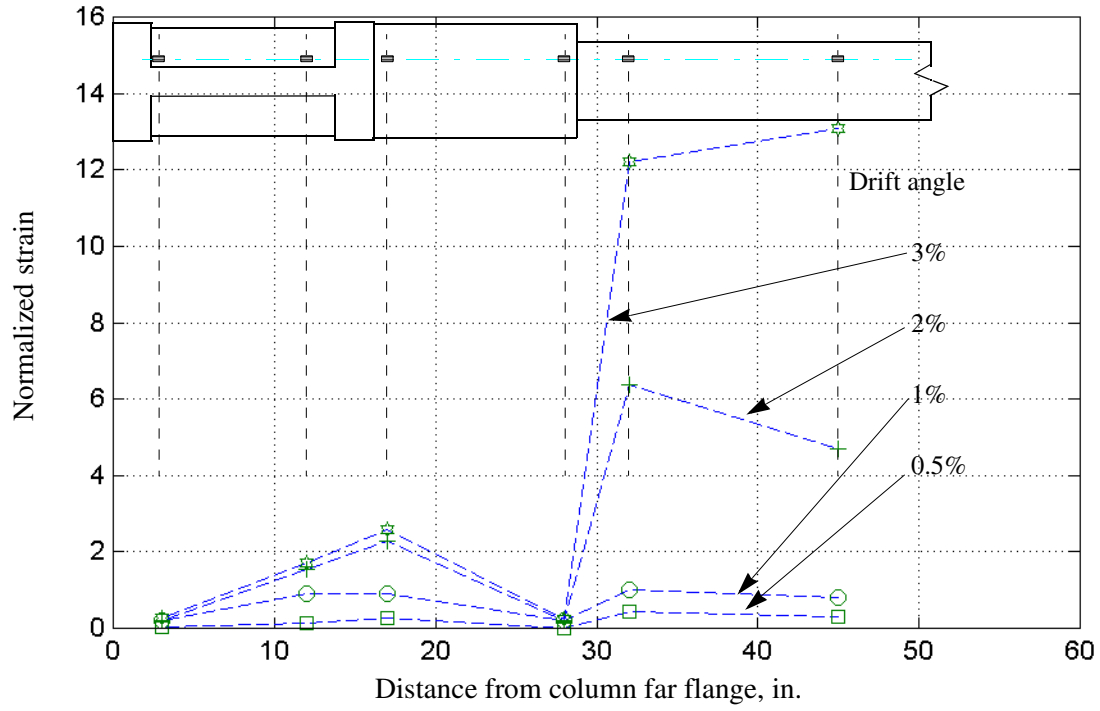


Figure 5-58 Strain response along line *b* for RC06

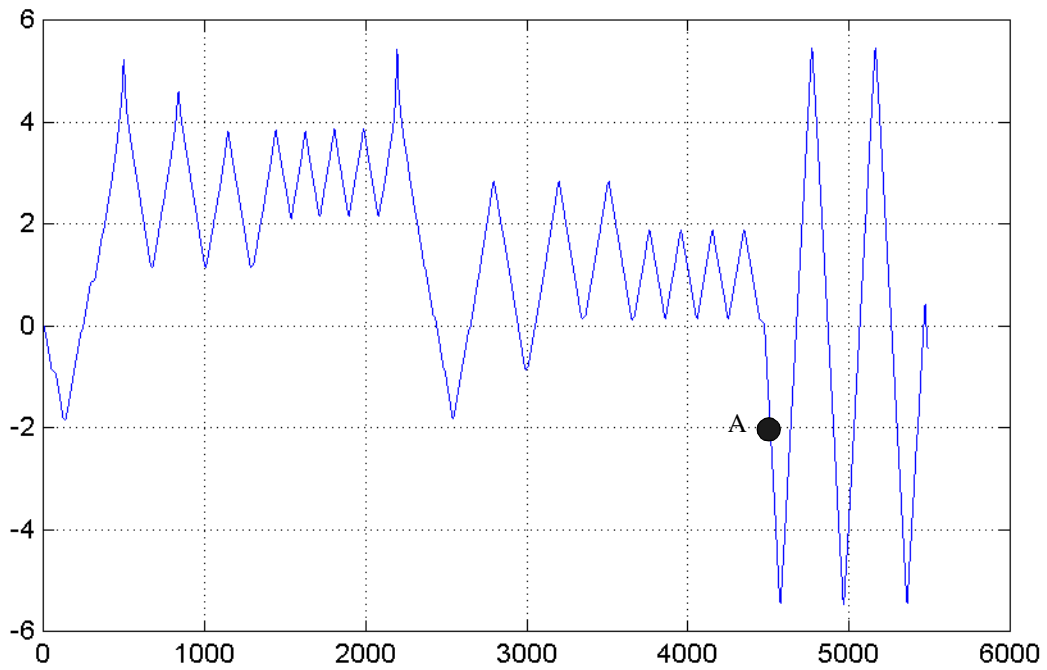


Figure 5-59 Near-field displacement history for RC07

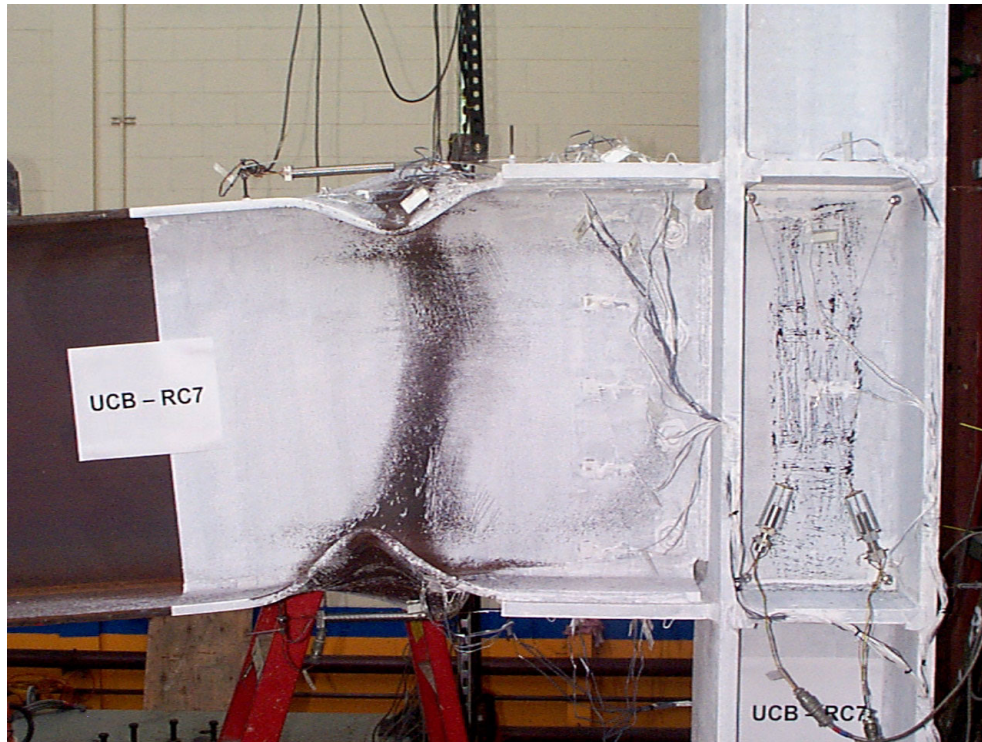


Figure 5-60 Beam FLB and WLB in RC07 at a drift angle of $0.04h$



Figure 5-61 Tearing of beam top flange in RC07

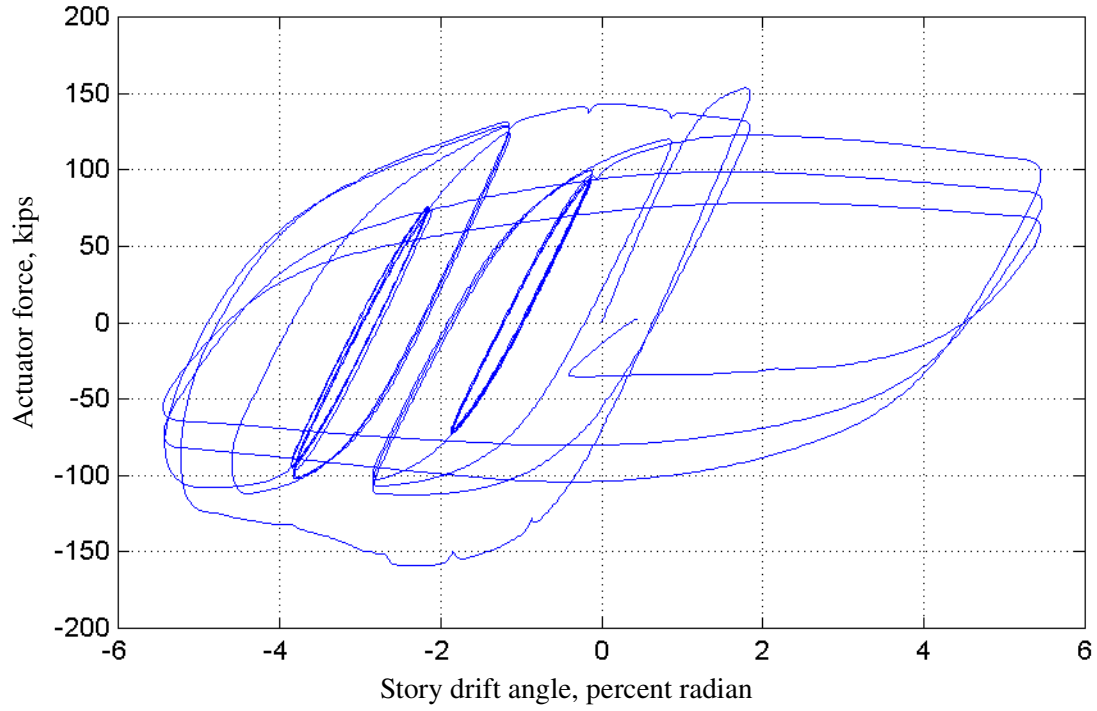


Figure 5-62 Actuator force versus drift angle for RC07

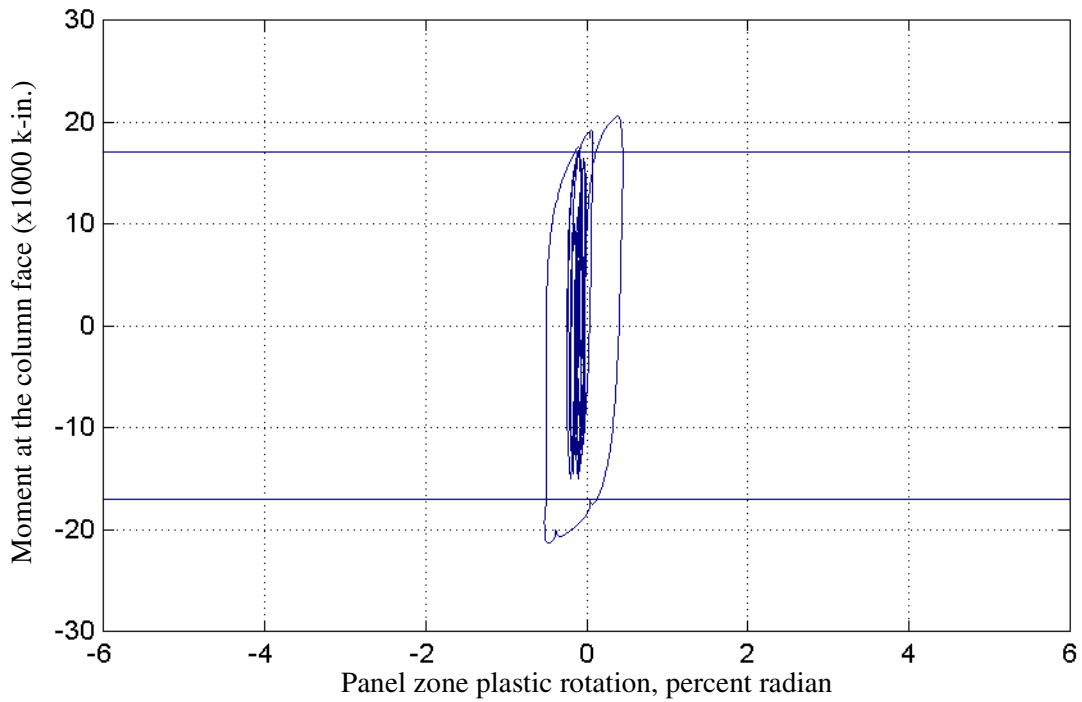


Figure 5-63 Moment at the column face versus panel zone plastic rotation for RC07

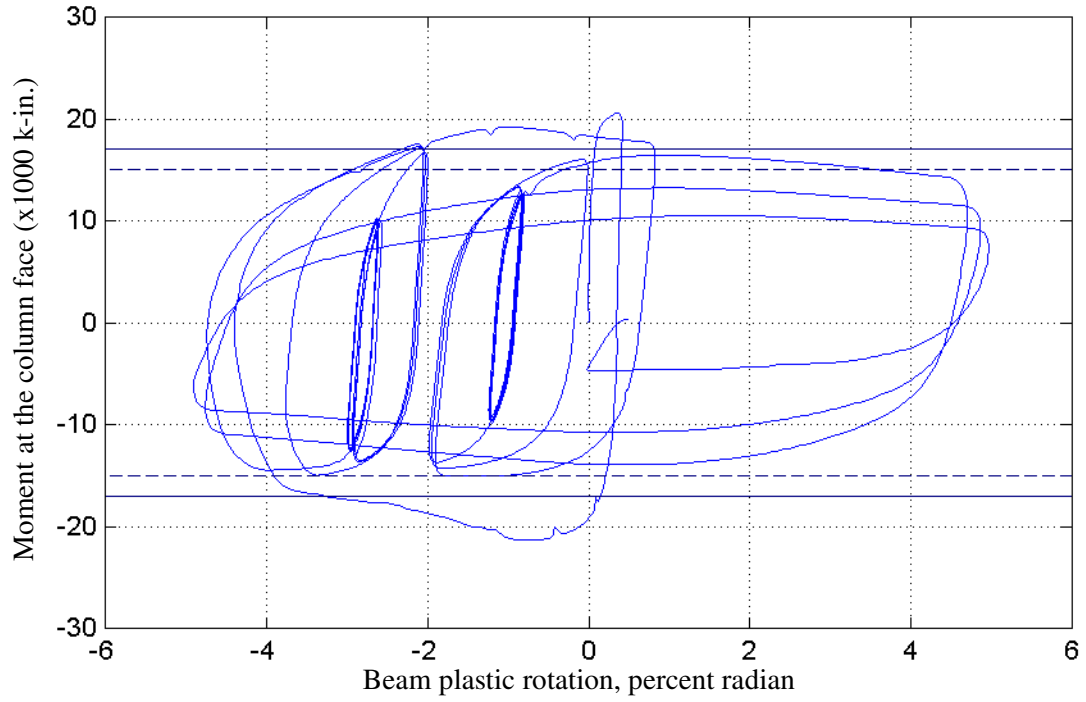


Figure 5-64 Moment at the column face versus beam plastic rotation for RC07

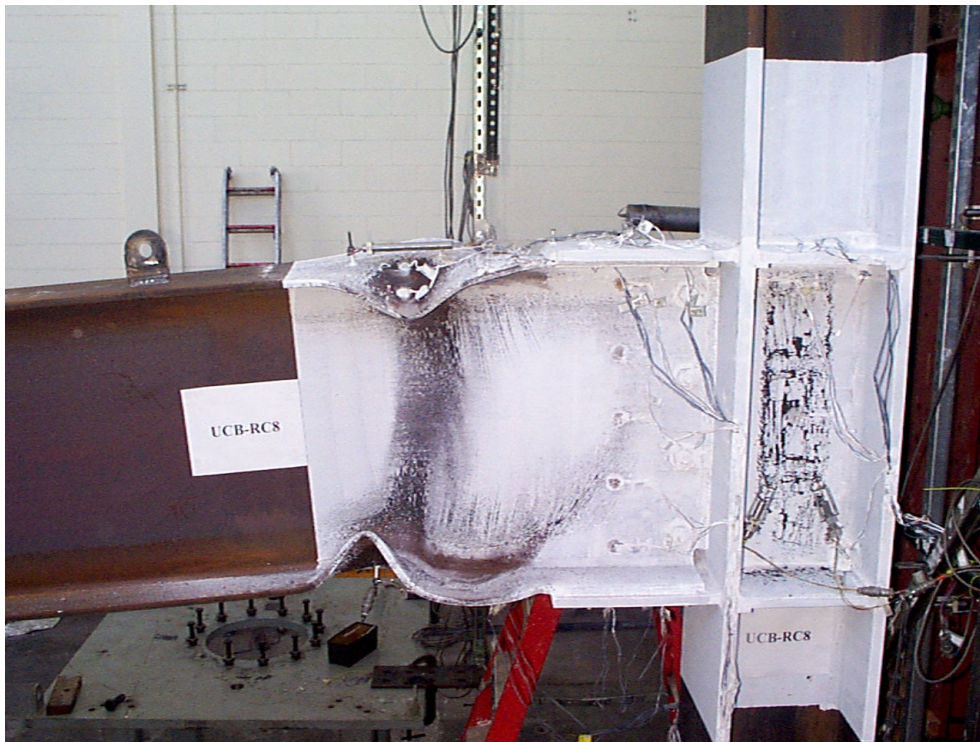


Figure 5-65 Beam FLB and WLB in RC08 at a drift angle of $0.05h$



Figure 5-66 Fracture in the beam top flange of RC08



Figure 5-67 Yielding of flange plate in RC08 at a drift angle of $0.04h$

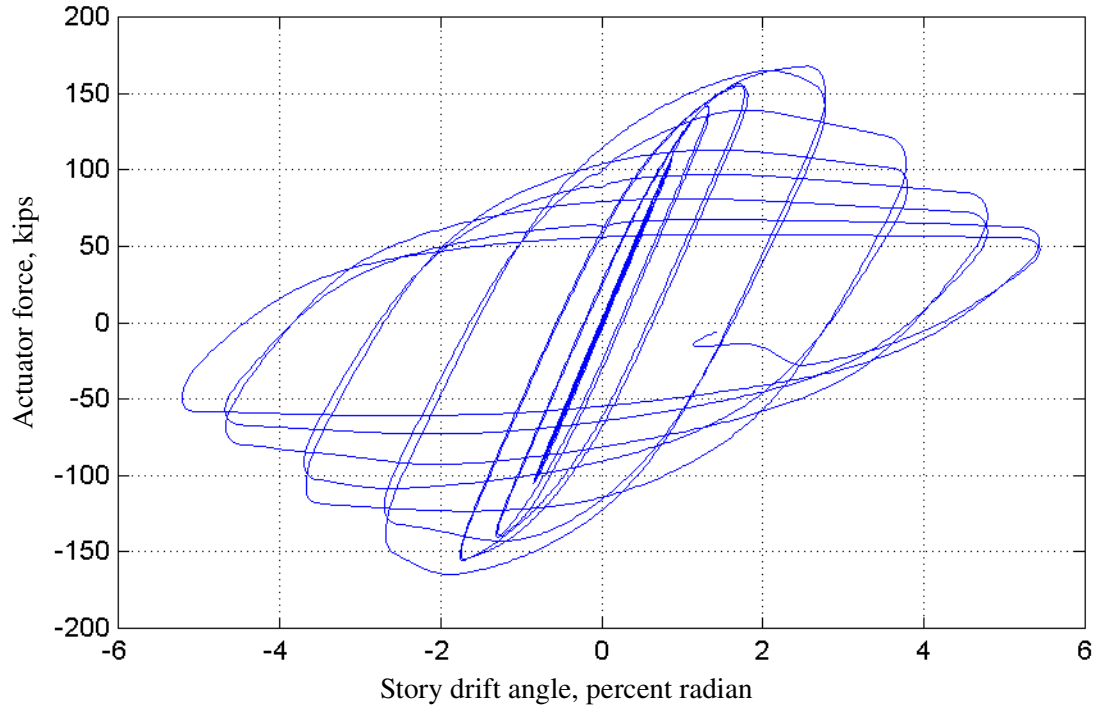


Figure 5-68 Actuator force versus drift angle for RC08

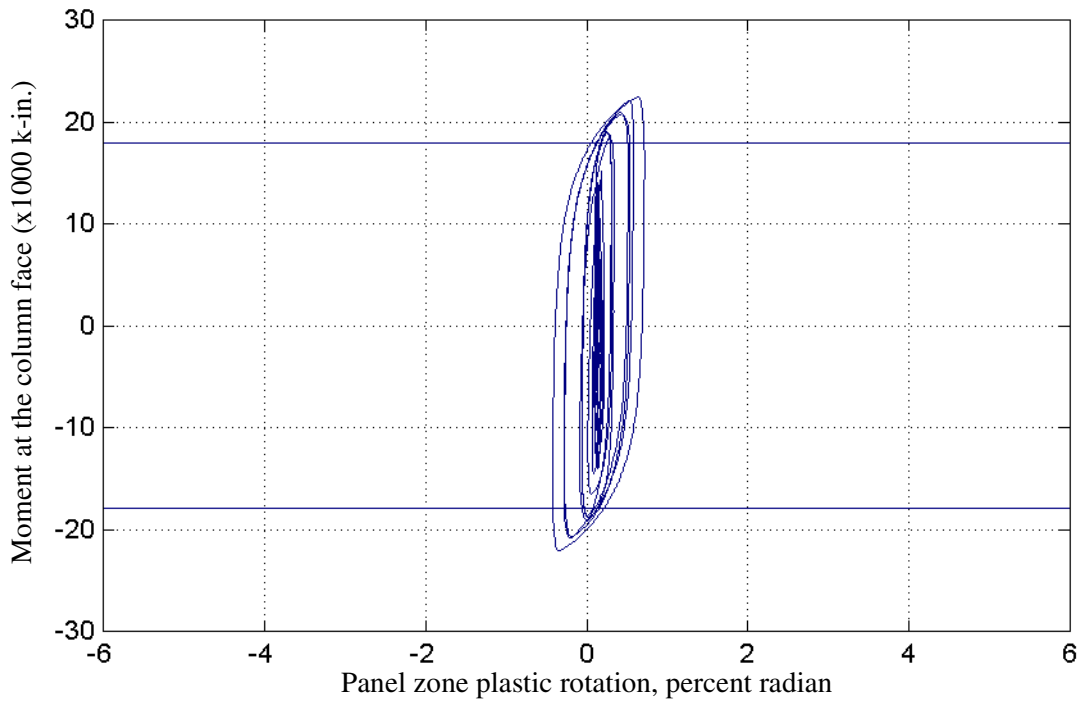


Figure 5-69 Moment at the column face versus panel zone plastic rotation for RC08

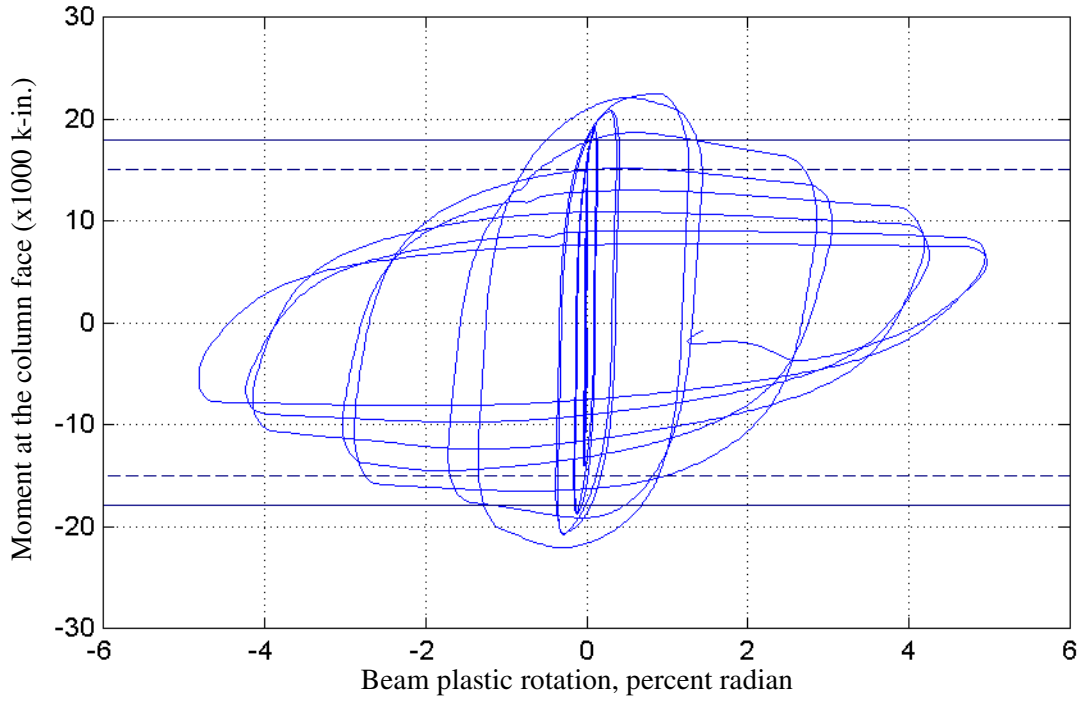


Figure 5-70 Moment at the column face versus beam plastic rotation for RC08

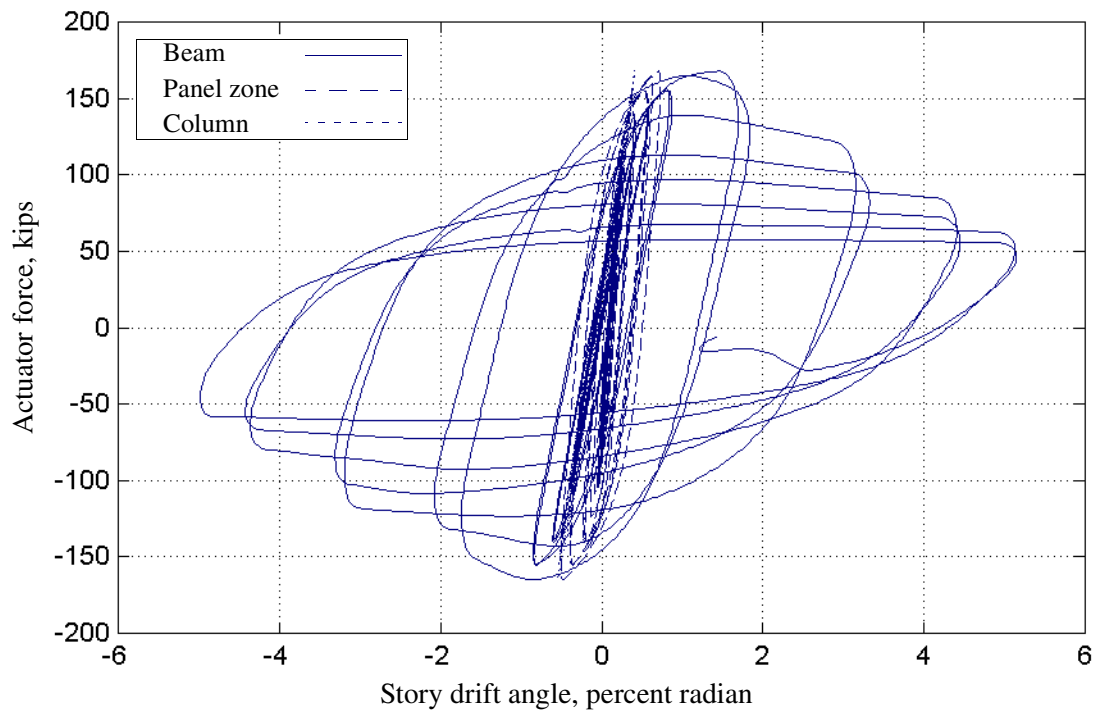


Figure 5-71 Components of drift angle for RC08

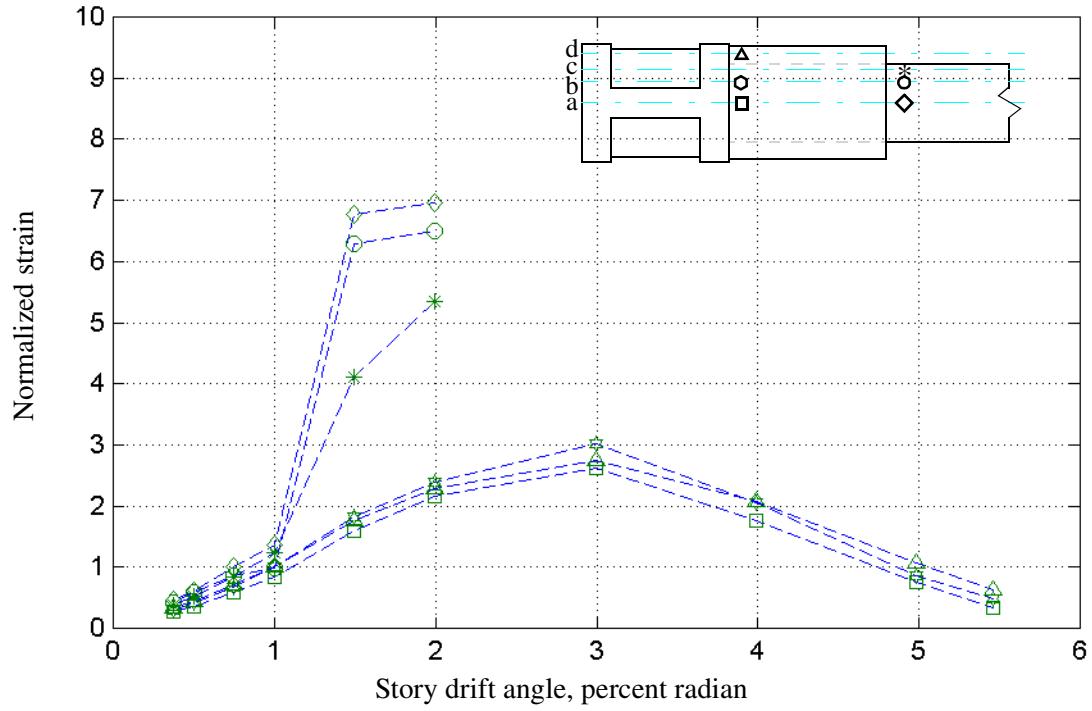


Figure 5-72 Beam and flange-plate strains for RC08

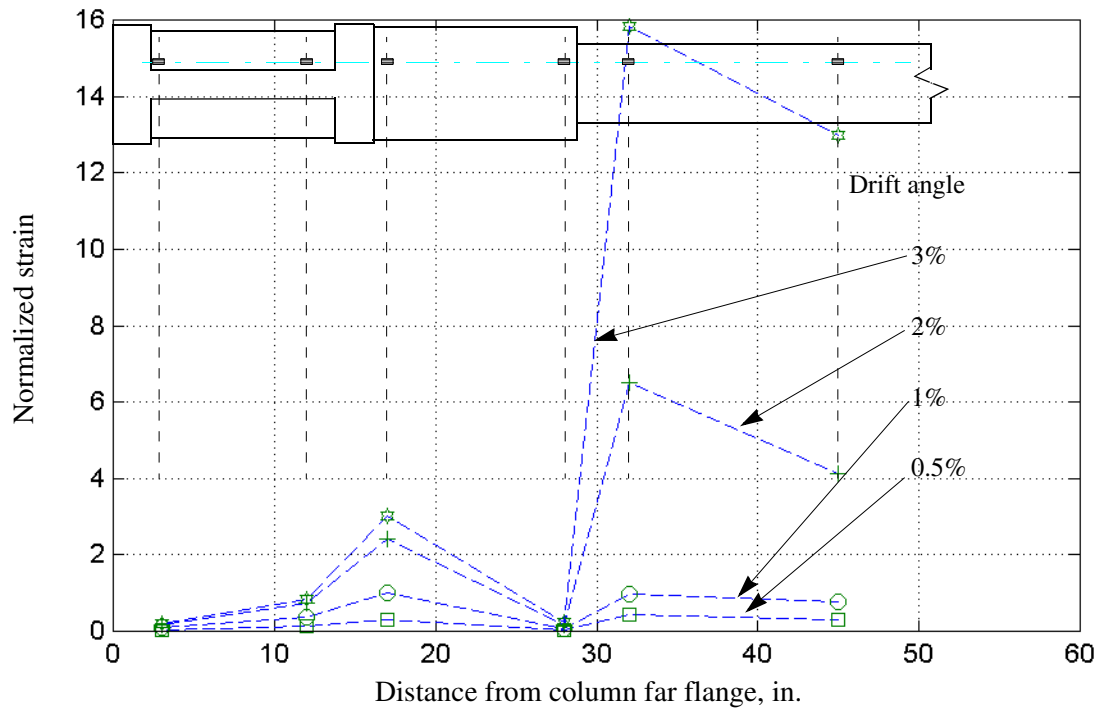


Figure 5-73 Strain response along line *b* for RC08

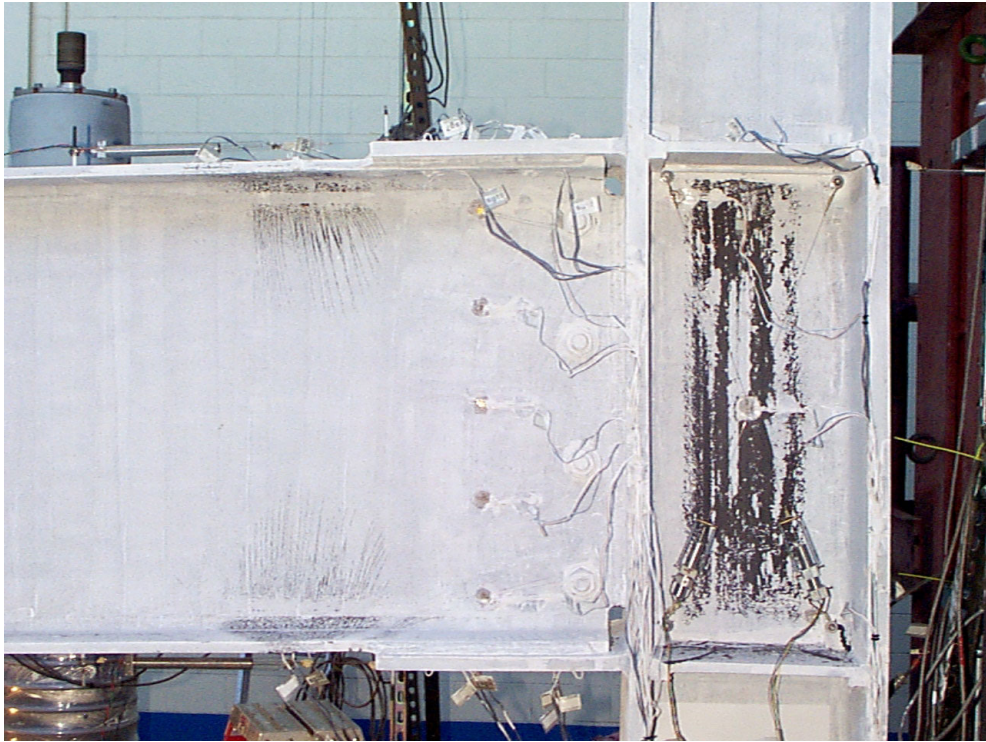


Figure 5-74 Yielding of the panel zone in RC09 at a drift angle of $0.015h$

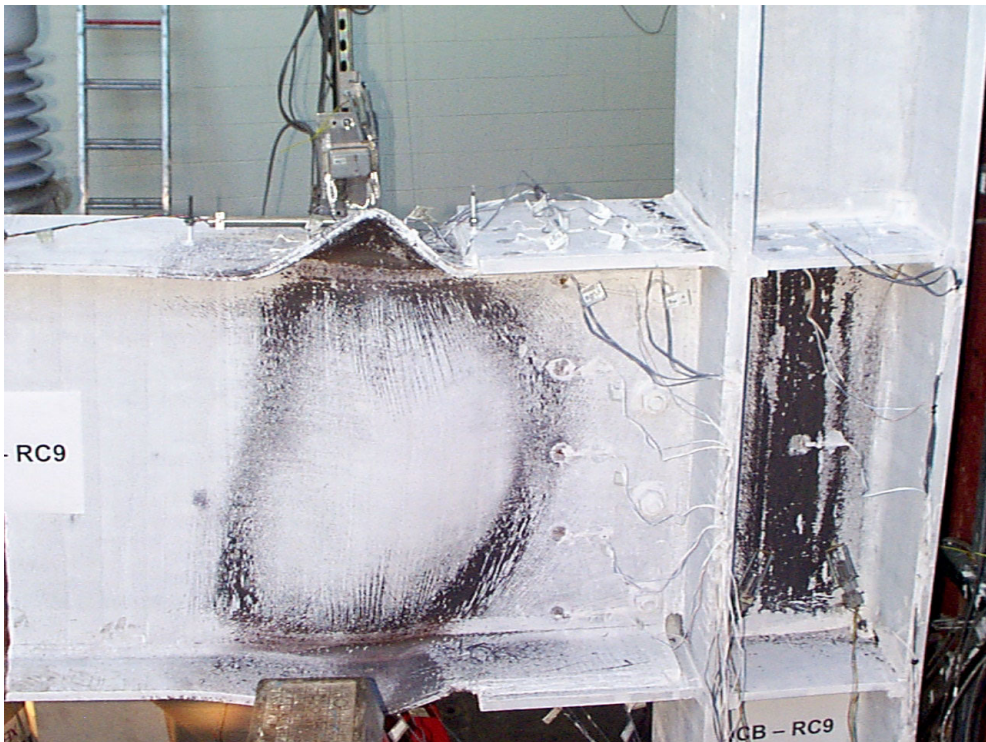


Figure 5-75 Beam FLB and WLB in RC09 at a drift angle of $0.05h$

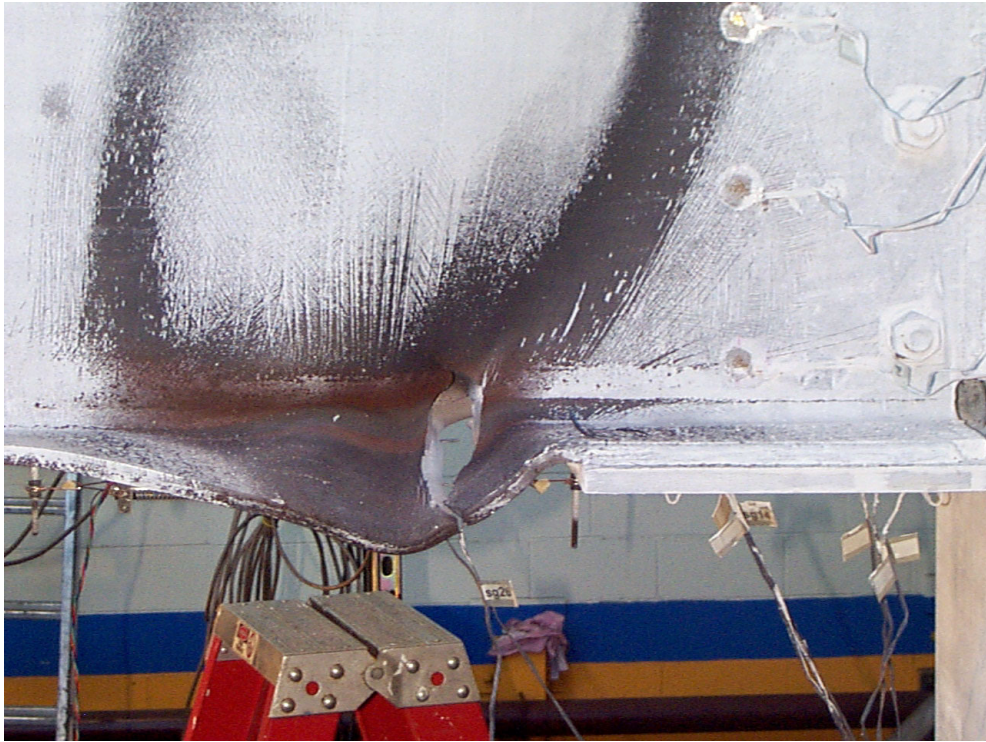


Figure 5-76 Fracture of beam bottom flange in RC09

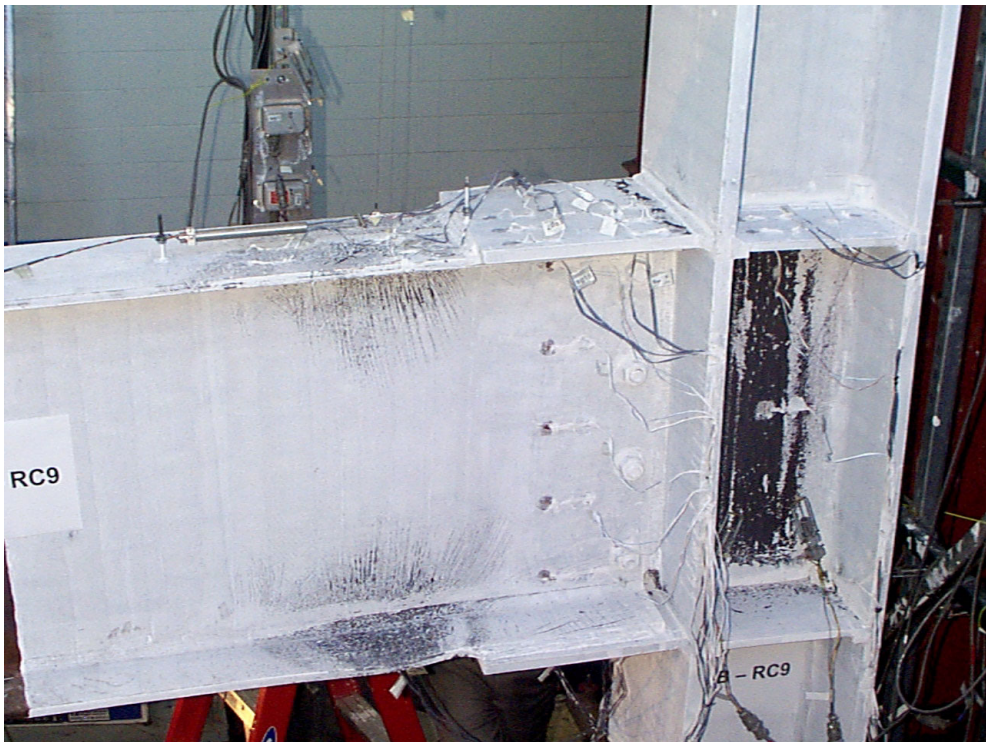


Figure 5-77 Yielding of top flange plate in RC09 at a drift angle of $0.03h$

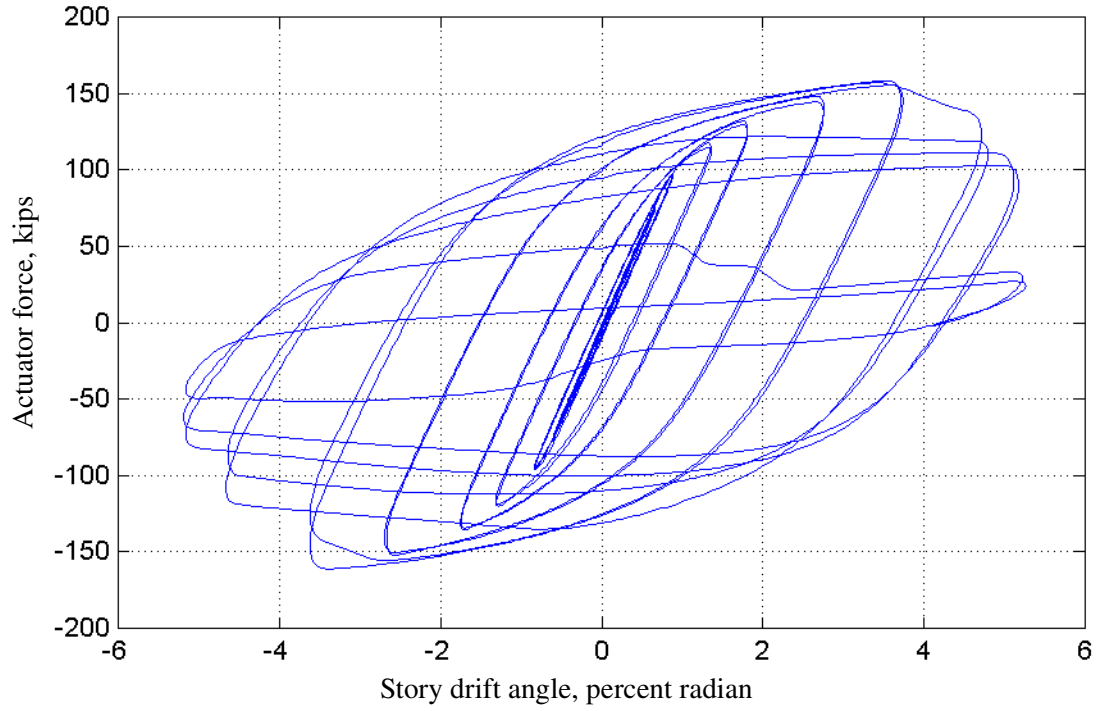


Figure 5-78 Actuator force versus drift angle for RC09

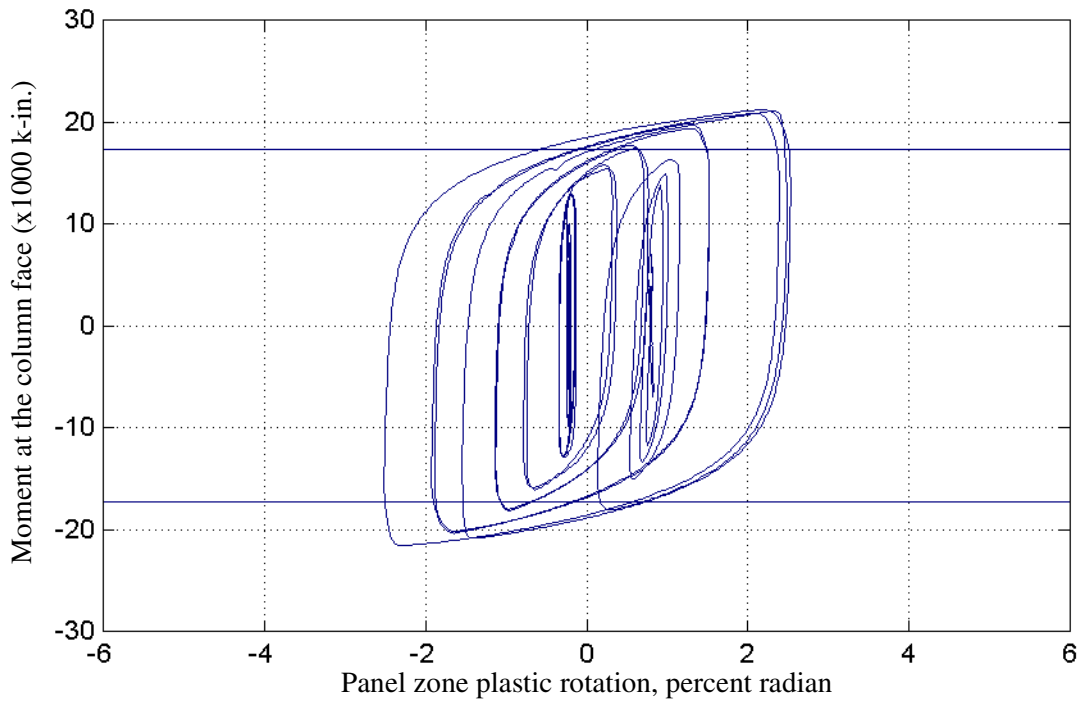


Figure 5-79 Moment at the column face versus panel zone plastic rotation for RC09

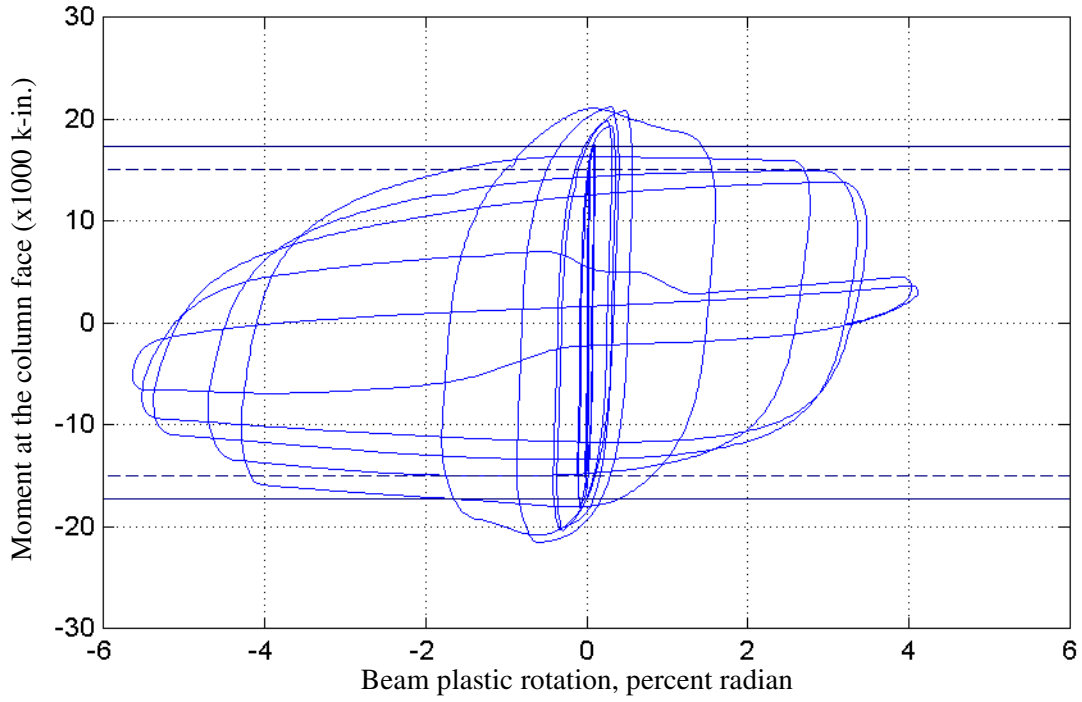


Figure 5-80 Moment at the column face versus beam plastic rotation for RC09

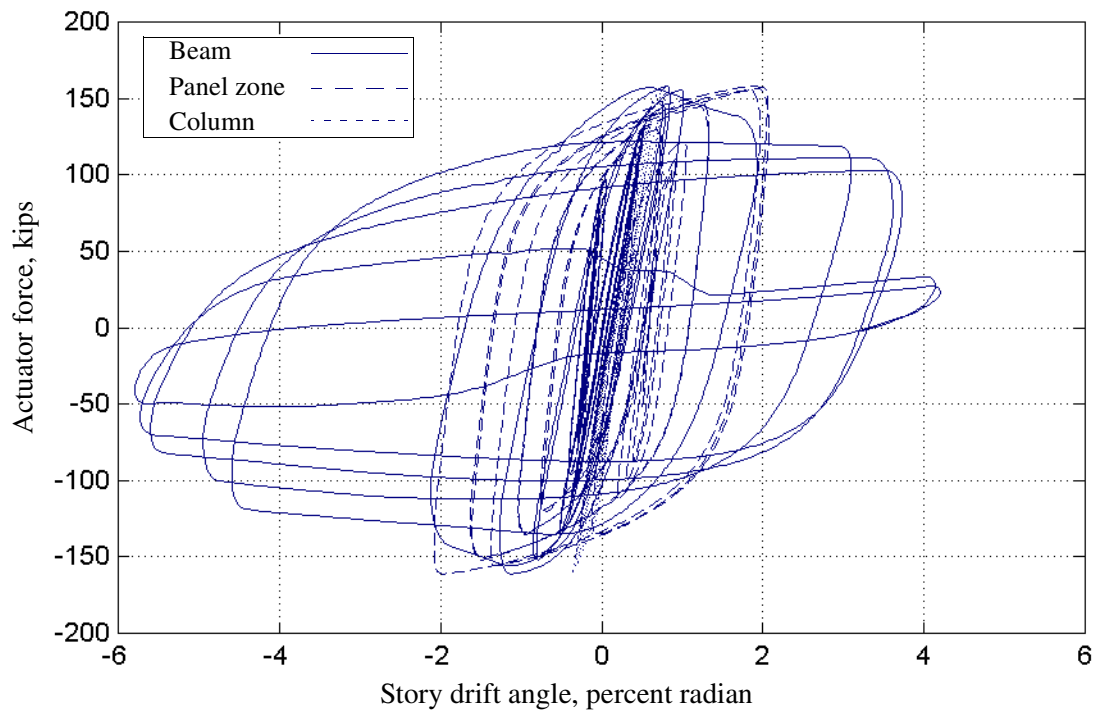


Figure 5-81 Components of drift angle for RC09

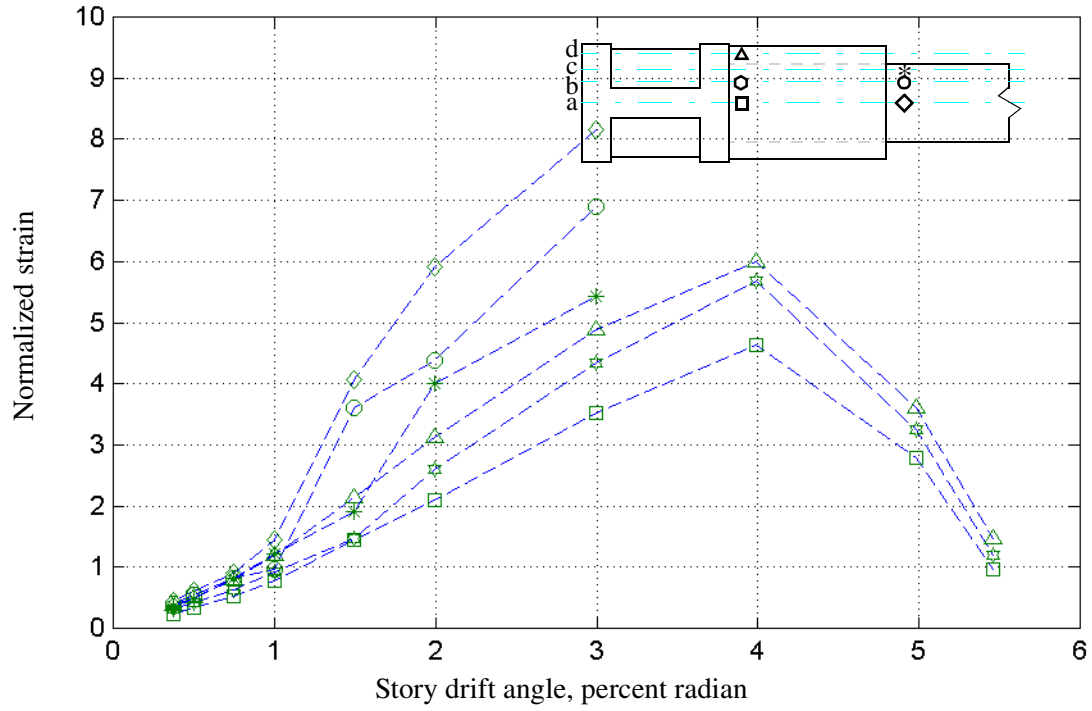


Figure 5-82 Beam and flange-plate strains in RC09

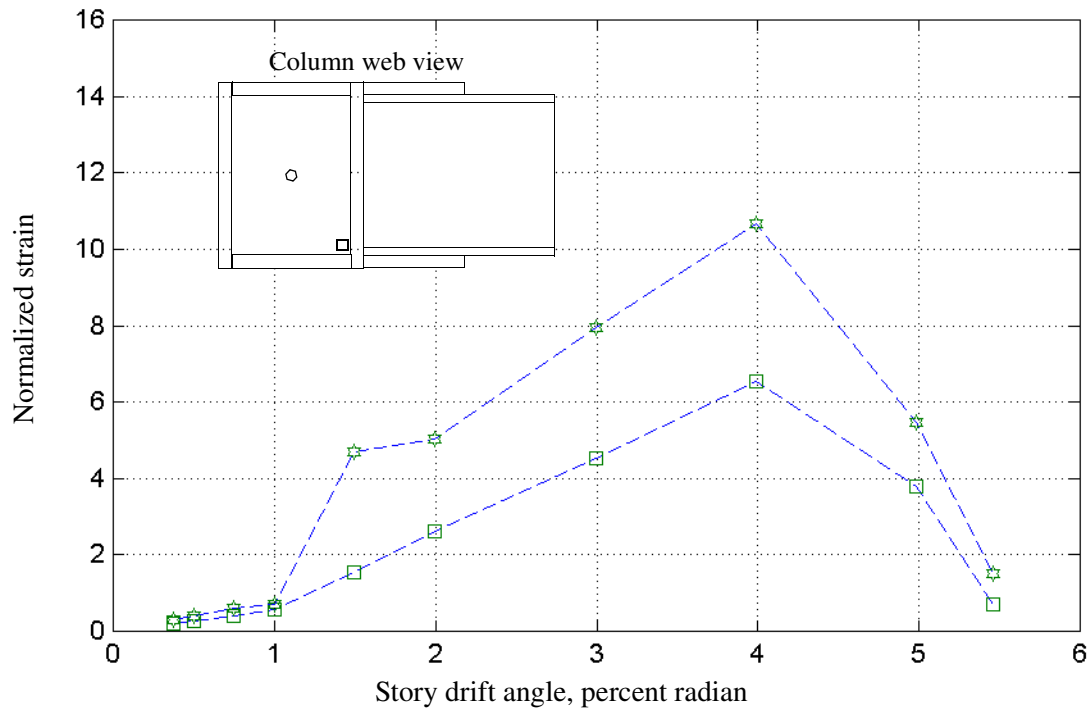


Figure 5-83 Column-web strains in panel zone of RC09

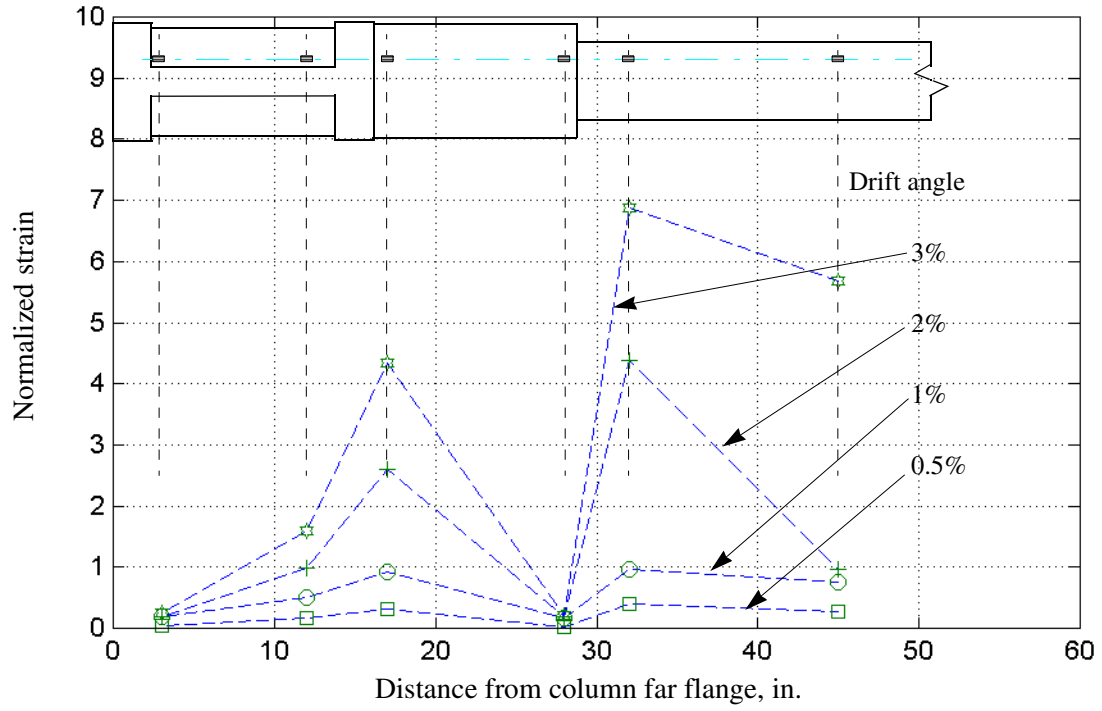


Figure 5-84 Strain response along line *b* in RC09



Figure 5-85 Horizontal stiffeners on RC10 to delay web local buckling

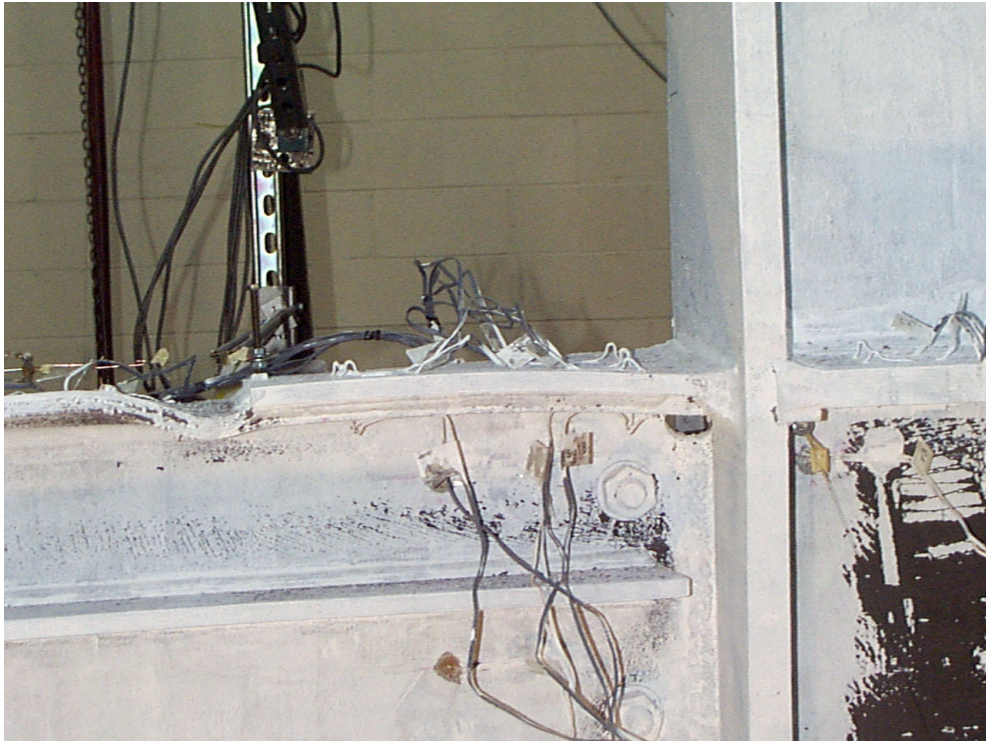


Figure 5-86 Beam flange local buckling in RC10 at a drift angle of $0.03h$

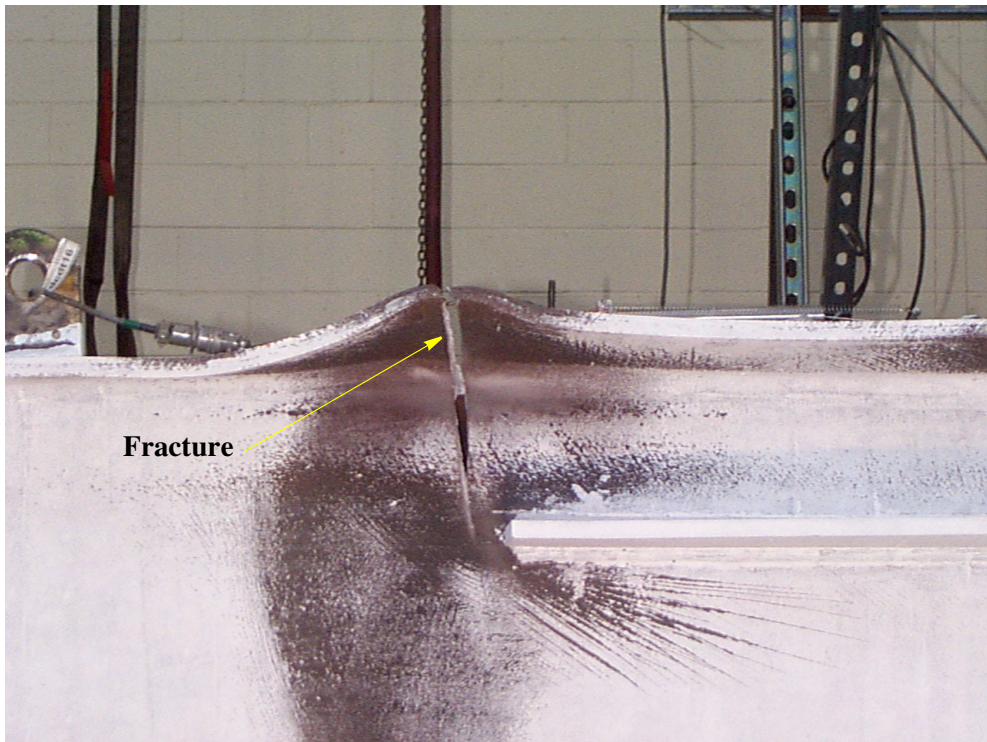


Figure 5-87 Fracture of top flange of RC10 outside horizontal stiffeners

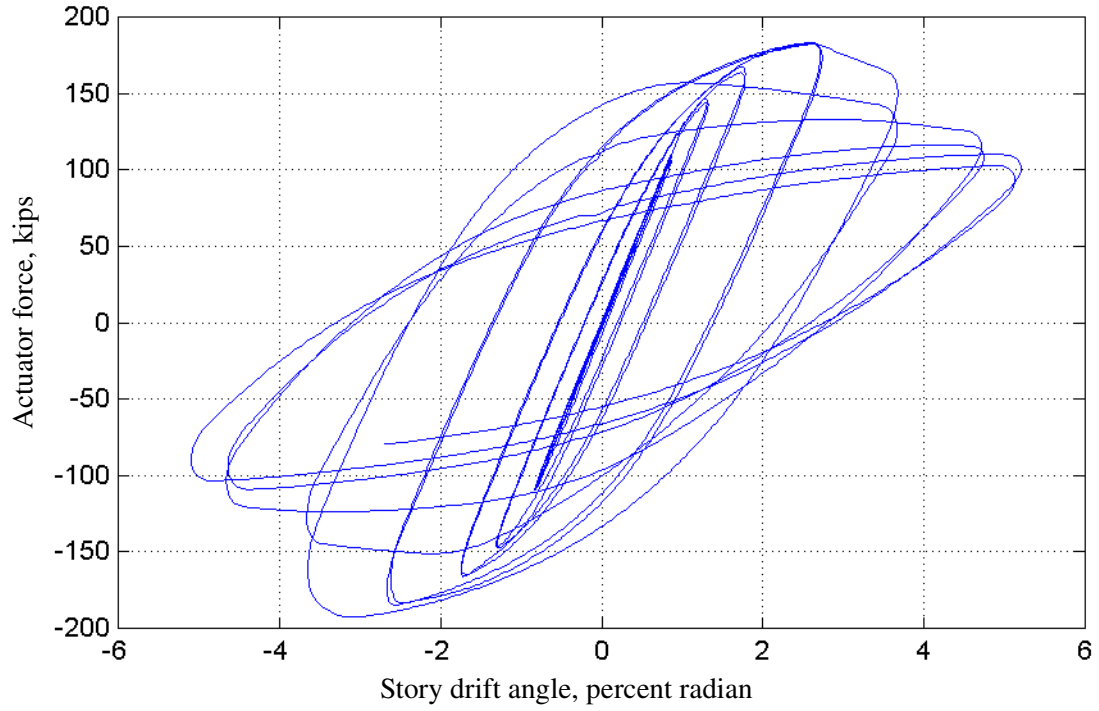


Figure 5-88 Actuator force versus drift angle for RC10

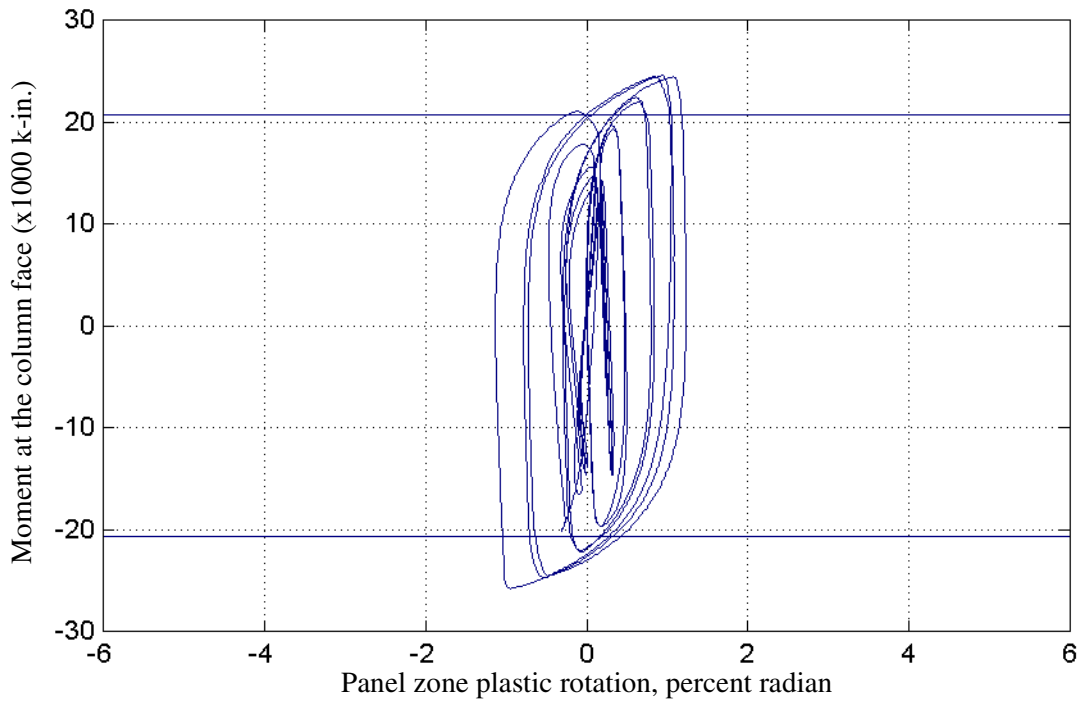


Figure 5-89 Moment at the column face versus panel zone plastic rotation for RC10

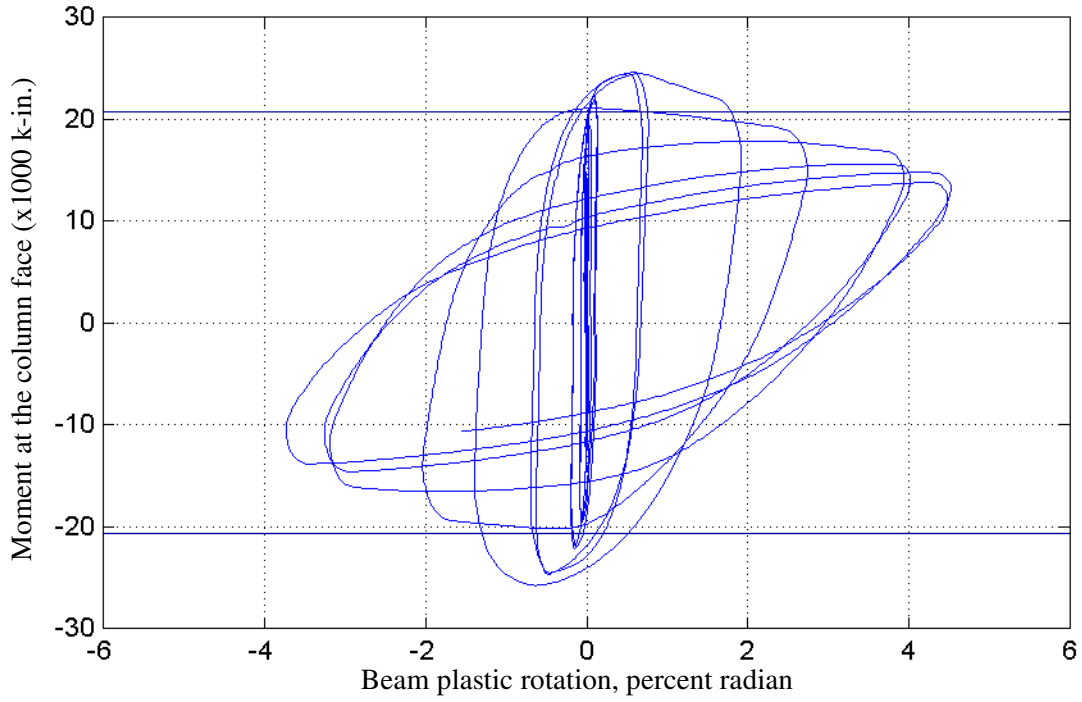


Figure 5-90 Moment at the column face versus beam plastic rotation for RC10

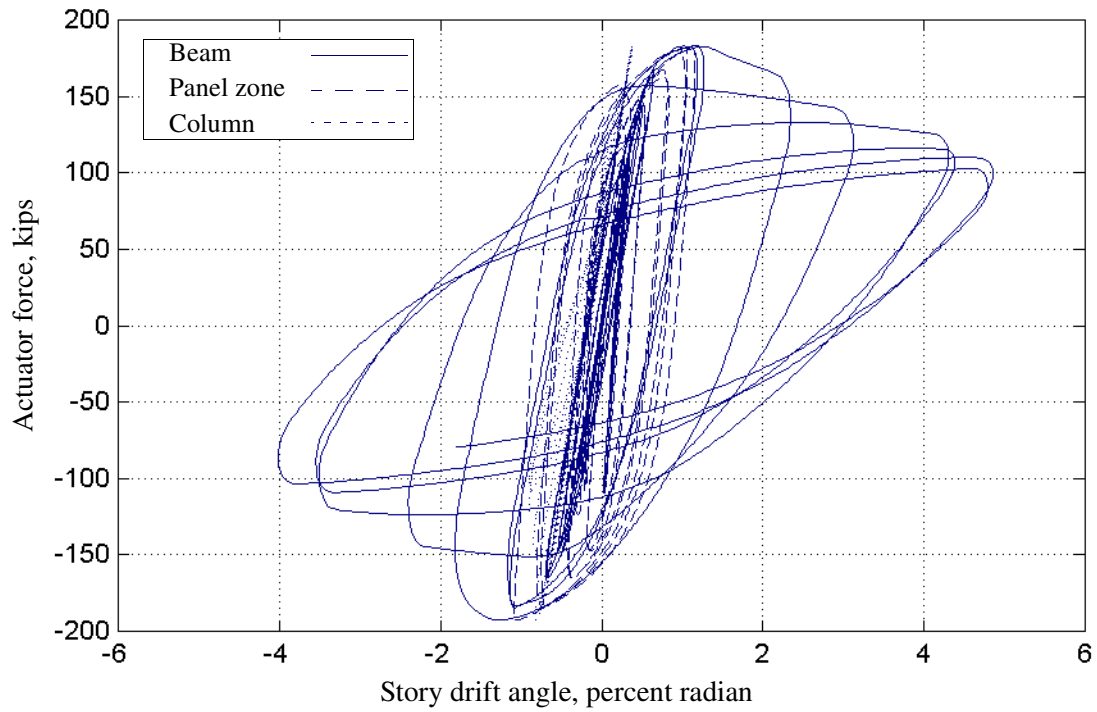


Figure 5-91 Components of drift angle for RC10

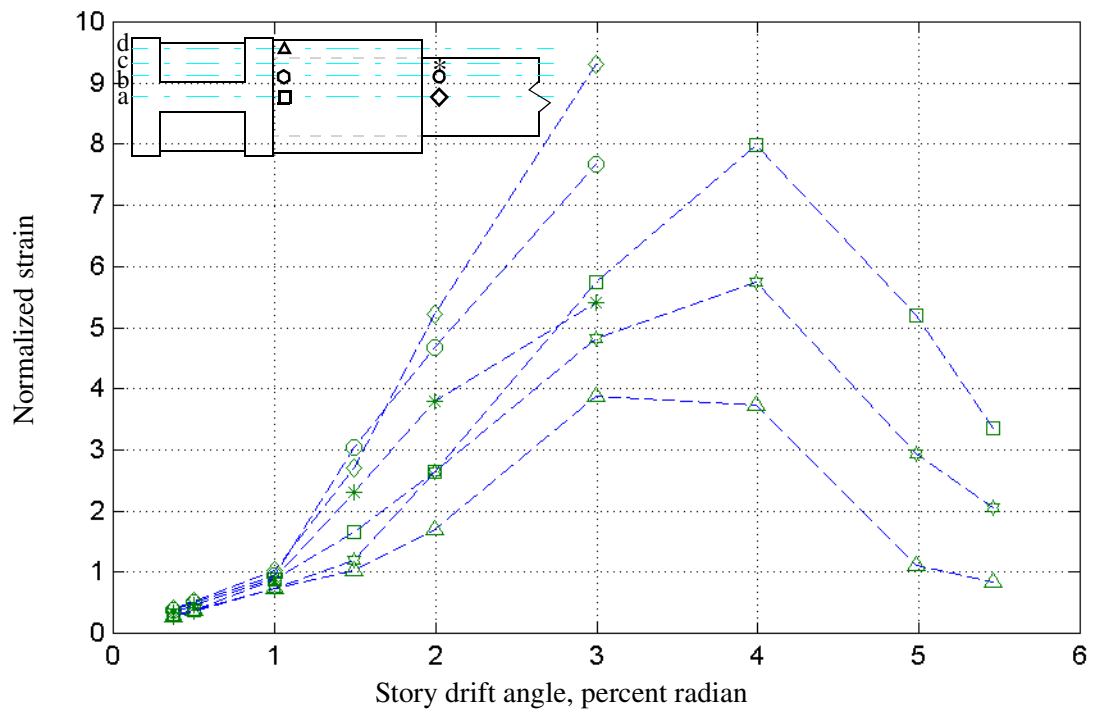


Figure 5-92 Beam and cover-plate strains for RC10

6 Evaluation of Analytical and Experimental Response Data

6.1 Introduction

This chapter serves to integrate the results of the analytical studies of Chapter 4 and the experimental studies of Chapter 5. Sections 6.2 through 6.10 present and evaluate the response of the ten specimens in terms of design variables identified in Chapter 3, namely, type of plate reinforcement (Section 6.2), plate geometry (Section 6.3), fillet weld geometry (Section 6.4), restraint of lateral-torsional buckling (Section 6.5), loading history (Section 6.6), influence of web-local buckling (Section 6.7), maximum strain in reinforcing plate (Section 6.8), and panel zone strength (Section 6.9). The results of studies of reinforced beam web connections and load-transfer mechanisms from the beam to the column are presented in Sections 6.10 and 6.11, respectively.

6.2 Plate Type Reinforcement

The perceived advantages and disadvantages of cover- and flange-plate reinforced connections have been widely discussed within the SAC Joint Venture. Consider the beam top flange/plate reinforcement-column flange connections shown in Figure 6-1; Figure 6-1a is a cover-plate connection and Figure 6-1b is the corresponding flange-plate connection. Two groove-weld options are shown for the cover-plate connection (A and B). One possible disadvantage of the cover-plate connection is that the connection geometry produces a stress riser near the face of the column flange at the interface of the reinforcing plate and the flange. This stress riser in conjunction with a triaxial state of tension at the face of the column could lead to unacceptable fractures of column flanges. For this reason, the flange-plate connection was considered by many to be the superior reinforcement detail of the two.

Of the two cover-plate groove weld options A and B, A uses less filler metal than B and produces smaller welding-induced residual stresses. However, the option A connection is composed of two groove welds, each with a root pass. Such root passes may include substantial defects that can trigger brittle fracture. Although the root pass of the flange-to-column weld can be inspected and replaced if necessary, the root pass of the plate-to-column flange groove weld can neither be easily inspected nor replaced. As such, any defect in this root pass would align with the stress riser identified in the previous paragraph, and potentially increase the likelihood of brittle fracture.

The global responses of cover-plate specimen RC03 and the flange-plate connection RC06 are presented in Figure 6-2 for the purpose of evaluating the influence of plate-reinforcement type on component response. This figure shows the relationship between the moment at the column face versus beam plastic rotation for each of the specimens. The maximum moment at the column face and beam plastic rotation of each connection were 22,000 kip-in. (2,500 kN-m) and 4.3 percent radian, respectively. These strength and rotation values were nearly identical because the properties of the beam (yield stress, tensile strength, flange compactness, and web compactness) controlled the global response of the connections and served to protect the plate reinforcement from substantial damage (yielding). As such, a comparison of the global responses of the two specimens does not provide substantial insight into the relative merits of the two connection details.

To gain further insight into the response of the cover-plate and flange-plate reinforcement details, the ABAQUS models of RC03 and RC06 presented in Chapter 4 were studied further. Figure 6-3 is a view of the displaced shapes of the cover plate and beam flange in RC03 along the beam web centerline near the face of the column at 1-percent story drift. The flange and cover plate are in tension. The groove welds were not modeled explicitly as shown in Figure 6-1a (option A or B). Note the separation of the flange and cover plate near the face of the column. The separation is likely due to the transfer of shear force through the beam flange to the column and produces tensile strains in the 3-direction at the column face (or in the welds of options A and B).

Consider the data presented in Figures 6-4, 6-5, and 6-6. Figures 6-4 and 6-5 present the distributions of Mises stress and hydrostatic pressure (PRESS in ABAQUS) in the beam top flange and the plate reinforcement at the face of the column at 1-percent story drift in RC03 and RC06, respectively. (At 1-percent story drift, the plastic strains at the face of the column in both RC03 and RC06 are negligible. As such, Mises stress and hydrostatic pressure distributions can be used to judge the relative likelihood of brittle fracture. See Chapter 4 for more information.) Figure 6-6 presents the distributions of equivalent plastic strain (PEEQ in ABAQUS) in the beam top flange and the plate reinforcement at the face of the column at 2-percent story drift for RC03 and RC06.

In RC03, the Mises stress at 1-percent story drift is largest at the top of the beam flange over beam web (point C in Figure 6-4a). Much of the beam flange at the column face is in triaxial tension (negative values of hydrostatic pressure in Figure 6-4b), with the largest values at point C. At point C, the values of S_{11} , S_{22} , and S_{33} are approximately +20 ksi (+138 MPa), +70 ksi (482 MPa), and +30 ksi (207 MPa), respectively. Of the four points identified in Figure 6-4a, point C is critical in terms of likelihood of brittle fracture. The maximum stresses in the cover plate (point A in Figure 6-4a) are smaller than the maximum stresses in the beam flange (e.g., point C) and counter to the trend predicted by beam theory, which was used to design the connection.

Figures 6-4a and 6-4b present Mises stress and hydrostatic pressure distributions for the top flange and cover plate of RC03. Point C lies at the top of the groove weld of the beam flange to the column flange where the weld quality is likely good. The stresses at point B at the bottom of the cover plate (immediately above point C) are substantially smaller than those at point C. The likelihood of brittle fracture at B is substantially smaller than at point C if the weld quality is

uniform throughout the depth of the beam flange-cover plate groove weld. If the sign of the shear force were reversed, Figures 6-4a and 6-4b would represent the distributions of Mises stress and hydrostatic pressure across the beam bottom flange and the bottom cover plate. In this instance, point C would lie in the root pass of the option A weld of Figure 6-1a.

The Mises and hydrostatic pressures in the top flange plate of RC06 at 1-percent story drift are presented in Figure 6-5. (The stresses in the beam flange beyond the face of the column are negligible because the flange is not welded to the column.) The flange plate is in tension. The maximum stresses in RC06 at this level of drift are significantly smaller than those in RC03.

The distributions of equivalent plastic strain in RC03 (cover plate and beam top flange) and RC06 (flange plate only) at 2-percent story drift are shown in Figure 6-6. The maximum values of equivalent plastic strain in RC06 and RC03 are approximately the same. The maximum value in RC03 is at point C (see Figure 6-6a). The maximum value in RC06 is at point A (see Figure 6-6b).

It is inappropriate to draw broad conclusions regarding the optimal type of reinforcement plate based on limited experimental and analytical data. However, on the basis of the data presented in the preceding paragraphs and in Chapter 4, the flange-plate connection appears marginally superior to the cover-plate connection, and the option B groove-weld detail of Figure 6-1a is superior to the option A detail.

6.3 Reinforcement Plate Geometry

Eight rectangular, one trapezoidal (RC05), and one swallowtail (RC04) shaped plates were evaluated in the experimental program. Only rectangular plates were used for the flange-plate connections. The swallowtail plate proved difficult to fabricate and is likely not an economical solution compared with other plate geometries. As such, the following discussion on plate geometry is limited to rectangular and trapezoidal plates. The responses of two specimens, RC03 (rectangular cover plate) and RC05 (trapezoidal cover plate), are compared below. Specimen RC03 was fabricated with reinforcing plates that were wider than the beam flange. The plates were shop welded to the beam flanges using downhand welds that required the beam to be rotated through 180 degrees midway through fabrication. Specimen RC05 was fabricated using trapezoidal plates with a maximum width equal to the width of the beam flange. The plates were shop welded to the beam flanges with downhand welds that also required the beam to be rotated 180 degrees midway through fabrication. (An alternative construction could involve the use of a trapezoidal top plate and a rectangular bottom plate that would eliminate the need to rotate the beam during fabrication. Such a construction was not considered as part of this research program.)

Figure 6-7 presents the relationships between moment at the column face versus beam plastic rotation relations for RC03 and RC05. The cross-sectional area of the beam flange-cover plate assembly for RC03 was slightly larger than that of RC05. The maximum resistance of the two specimens was virtually identical and the difference between the hysteresis loop shapes for the two specimens was small. Such an observation is not surprising because the properties of the beam (yield stress, tensile strength, flange compactness, and web compactness) controlled the global response of the two specimens and served to protect the plate reinforcement from substantial damage (yielding).

The reinforcement plates in RC03 and RC05 were welded to the beam flanges with longitudinal and transverse fillet welds. The transverse fillet welds of RC03 (10.5 in. [267 mm] in length) served to prevent penetration of flange local buckling beyond the nose of the rectangular plate. The transverse fillet welds of RC05 (5 in. in length) permitted some penetration of flange local buckling beyond the nose of the trapezoidal plate, but such buckling penetration appeared to have negligible impact on the response of the specimen.

The measured axial strains in the cover plates of RC03 and RC05 at story drift angles of 1-, 2-, 3-, and 4-percent radian are shown in Figure 6-8. The three strain gages were all located on one line 2 in. (51 mm) from the column face; the gages were located above the beam web, 2.75 in. (70 mm) from the beam web, and 5 in. (127 mm) for specimen RC03 and 4.2 in. (107 mm) for specimen RC05 from the beam web. Although the cover plates were designed to remain elastic at the face of the column for the maximum moment that could be delivered by the beam alone, the maximum axial strains exceeded the yield strain. Such inelastic strains had no apparent deleterious effect on the response of either specimen. The differences in strain response between RC03 and RC05 were insignificant; similar differences would not be unexpected for tests of two identical specimens.

The distribution of Mises stress in the cover plate and beam flange of RC05 at the face of the column at 1-percent story drift is presented in Figure 6-9. The maximum values of Mises stress in the cover plate and the beam flange are similar to those in RC03 at the same level of story drift. The maximum stress is located at the top of the beam flange immediately above the beam web (point C of Figure 6-9). The distribution of hydrostatic pressure in the cover plate and beam flange of RC05 at the face of the column is similar to that shown in Figure 6-4b for RC03.

The distributions of stress S_{22} (the 2-direction lies along the longitudinal axis of the beam) on the upper surface of the cover plates of RC03 and RC05 are presented in Figures 6-11a and 6-11b, respectively. Neither cover plate is effectively mobilized near the nose of the plate, and the S_{22} stresses in the beam flanges immediately below the cover plates typically exceed those in the cover plate at the same distance from the column face as seen in Figures 6-10a and 6-10b for RC03 and RC05, respectively.

Figures 6-12a and 6-12b present the distribution of Mises stress on the top surface of the beam flange at 1-percent story drift for RC03 and RC05, respectively. The maximum stresses are located at the nose of the cover plate and at the face of the column above the beam web in both specimens. The maximum values are similar. The distribution of Mises stress across the width of the beam flange at the nose of the cover plate is more uniform for RC03 (see Figure 6-12a) than RC05 (see Figure 6-12b). The hydrostatic pressures in the beam flanges at the nose of the plates exceed -35.7 ksi (-246 MPa) and -32.6 ksi (-225 MPa) for RC03 and RC05, respectively.

The distributions of equivalent plastic strain (PEEQ) on the top surface of the beam flange at 2-percent story drift are presented in Figures 6-13a and 6-13b for RC03 and RC05, respectively. The maximum values of PEEQ are similar in both specimens and are located at the intersection of the transverse and longitudinal fillet welds at the nose of the cover plates. Yielding of the beam flange penetrates beyond the nose of the trapezoidal plate (Figure 6-13b) but not at the wider rectangular plate (Figure 6-13a).

The differences in performance of reinforced connections fabricated using rectangular plates versus trapezoidal plates will likely be small provided that the width of the tapered nose of the trapezoidal plate is sufficient to prevent the formation of high triaxial tension at the nose of the plate. Assuming a given length of reinforcing plate and construction-related issues aside, the rectangular plate is likely superior to the trapezoidal plate for two reasons. First, the use of a rectangular plate similar to that adopted for RC03 provides a greater length for the placement of the plate-to-flange fillet welds than RC05, thus leading to a reduction in the size of the fillet welds. Second, the quality of the weld metal at the junction of the longitudinal and transverse fillet welds will likely be better for the rectangular plate because these welds are separated by the thickness of the plate and runoff tabs can be used to provide high quality weld metal at the end of the weld. Such tabs cannot be used at the junction of the welds for the trapezoidal plate because the welds are in the same plane.

6.4 Fillet Weld Geometry

Prior to the 1994 Northridge earthquake, connection-reinforcement plates such as cover plates were rarely used in steel moment-frame building construction but were routinely used in steel bridge construction to resist gravity-load effects. Conventional bridge construction practice involved joining the cover plates to the beam flanges with rows of bolts or longitudinal (parallel to beam axis) fillet welds. Although transverse fillet welds joining the noses of cover plates to beam flanges were not prohibited by the AWS Bridge Welding Code (AWS 1996), such welds were not encouraged because past failures of cover-plated steel bridge girders had been linked to *high-cycle fatigue* failures at the transverse fillet welds (e.g., Francis 1989).

Cover-plate steel moment-resisting connections in bridges and buildings vary substantially. Cover plates on bridge girders are typically of modest thickness and reasonable length (15 to 25 percent of the span) whereas cover plates in steel moment-resisting frames are typically thick and short (5 to 10 percent of the span). As such, the demands per unit length on welds or bolts joining the cover plate to the beam flange differ markedly for bridge and building construction. Also, the loading environments are substantially different for bridge and building construction, namely, high-cycle fatigue loading and elastic response for bridges, and low-cycle fatigue loading and modest inelastic response for buildings. These substantial differences between bridge and building construction led the authors to question whether the traditional joining details for cover plates in bridge girders were appropriate for building construction.

Tests of cover-plated connections for steel moment-frame buildings undertaken following the 1994 Northridge earthquake showed that rectangular cover plates tended to separate from the beam flanges at the line of the beam web. One cover-plate SAC Phase I test specimen (Whittaker et al. 1996) was detailed with two bolts that joined the cover plate to the beam flange, near the nose of the cover plate, to delay this separation. Figure 6-14 shows a photograph of this detail. An alternative to this bolted connection involved the use of a transverse fillet weld to join the cover plate to the beam flange. Although the welded detail was not studied during the SAC Phase I project, the authors deemed the welded detail to be most promising because fillet welding on three sides of the reinforcement plate rather than two permitted smaller fillet welds to be used to develop the strength of the reinforcing plate.

Setting aside the more complicated geometry of the fillet welds joining the RC04 flange plates to the beam flanges, three plate-to-flange fillet weld geometries were studied as part of the research program: 2- and 3-sided fillet welds for the rectangular cover plates, and the 3-sided fillet welds for the trapezoidal cover plates. The moment versus beam plastic rotation relations for RC01 (2-sided fillet weld, rectangular cover plates), RC03 (3-sided fillet weld, rectangular cover plates), and RC05 (3-sided fillet welds, trapezoidal cover plates) were very similar, and the small differences in global response could not be attributed to the use of different weld geometries. Figure 6-15 presents the maximum measured longitudinal (2-2) strains in the cover plates of RC01 and RC03, 13 in. (330 mm) from the face of the column. Maximum values are normalized to the nominal yield strain for the 50 ksi (345 MPa) cover plates at story drift angles of 1-, 2-, 3-, and 4-percent radian. For RC03, the axial strains were approximately equal across the half width of the beam flange, and substantially less than the yield strain; see Figure 6-15b. In contrast, the strain distribution across the half width of the RC01 beam flange was not uniform; see Figure 6-15a. The large strains at the edge of the beam flange outstand at 3- and 4- percent story drift were associated with local deformations in the cover plate due to beam flange local buckling.

Figures 6-16a and 6-16b are photographs of the beam flange and cover plate deformations at 4-percent story drift for RC01 and RC03, respectively. Although local buckling began in the beam flanges of RC01 outside the cover plate, the buckles penetrated back beyond the nose of the cover plate at 3- and 4-percent story drift, and tore the longitudinal fillet welds that joined the cover plate to the beam flange. Such tearing did not lead to failure because flange local buckling and web local buckling led to a loss of specimen strength and the consequent demand on the fillet welded connection. The transverse fillet welds in RC03 effectively prevented the buckle penetration observed in RC01 and no tearing of the fillet welds in RC03 was observed.

Crack propagation is influenced by the geometry of the affected region and the state of stress in that region. Consider the 2-sided fillet weld (longitudinal fillet welds only) and the end of the fillet weld at the nose of the reinforcing plate. The gap between the beam flange and the reinforcing plate at the bottom of the vertical leg of the fillet weld acts as an *initial defect*. Stress concentrations and a state of triaxial tension at the end of the longitudinal fillet weld substantially increase the likelihood of crack initiation and propagation. The addition of a transverse fillet weld reduces the stresses and triaxial tension at the end of the longitudinal fillet weld and eliminates the *defect* at the base of the vertical leg of the longitudinal fillet weld at its end.

Consider now the 2- and 3-sided fillet welds for the rectangular cover plates of RC01 and RC03, respectively, and only the stress distributions around the nose of the cover plate. Figures 6-17a and 6-17b present the distributions of Mises stress on half of the top flange of the beam for RC01 and RC03, respectively, at 1-percent story drift. Figures 6-18a and 6-18b present the distributions of hydrostatic pressure on one half of the top flange of the beam for RC01 and RC03, respectively, at 1-percent story drift. The maximum Mises stress in RC01 (Figure 6-17a) ranges between 50 and 55 ksi (345 and 379 MPa) and is located around the end of the longitudinal fillet weld; the maximum Mises stress at the beam web centerline is between 40 and 45 ksi (276 and 310 MPa). For reference, the Mises stress 6 in. (152 mm) away from the nose of the cover plate ranges between 40 and 45 ksi (276 and 310 MPa); this stress range is approximately that which would be calculated at the nose of the cover plate using beam theory. The maximum hydrostatic pressure at the end of the fillet weld is -30 ksi (-207 MPa); see Figure 6-18a. The normal (S) and

principal (σ) stresses at this location are $S11 = 23.4$ ksi (161 MPa), $S22 = 58.8$ ksi (405 MPa), $S33 = 7.8$ ksi (54 MPa), $\sigma_1 = 65.6$ ksi (452 MPa), $\sigma_2 = 17.9$ ksi (123 MPa), and $\sigma_3 = 6.6$ ksi (45 MPa). (For information, tensile stress is positive in ABAQUS. The orientation of the axes 1-1, 2-2, and 3-3 is shown in Figure 4-2.) All of these stresses are tensile. The maximum hydrostatic pressure at the beam web centerline below the nose of the cover plate is -11.9 ksi (82 MPa); only one of the principal stresses at this location is tensile. The maximum Mises stress in RC03 (Figure 6-17b) ranges between 55 and 60 ksi (379 and 414 MPa) in a band across the width of the flange immediately beyond the transverse fillet weld. The maximum hydrostatic pressure at the end of the fillet weld is -23 ksi (-158 MPa); see Figure 6-18b. The normal and principal stresses at this location are $S11 = 7.6$ ksi (52 MPa), $S22 = 55.8$ ksi (384 MPa), $S33 = 4.2$ ksi (29 MPa), $\sigma_1 = 57.9$ ksi (399 MPa), $\sigma_2 = 7.9$ ksi (54 MPa), and $\sigma_3 = 1.7$ ksi (12 MPa). The hydrostatic pressure at the beam web centerline below the nose of the cover plate is -35.7 ksi (-246 MPa); see Figure 6-18b. The normal and principal stresses at this location are $S11 = 19.9$ ksi (137 MPa), $S22 = 62.7$ ksi (432 MPa), $S33 = 25.2$ ksi (174 MPa), $\sigma_1 = 67.8$ ksi (467 MPa), $\sigma_2 = 24.9$ ksi (172 MPa), and $\sigma_3 = 14.4$ ksi (99 MPa). All of these stresses are tensile.

The maximum Mises stresses in RC01 and RC03 at 1-percent story drift are similar. These maximum values are dominated by the longitudinal normal stress, $S22$. Marked increases in Mises stress occur near the nose of the cover plate due to the stress concentrations in RC01 at the end of the longitudinal fillet weld, and the transverse fillet weld in RC03. In RC03, the stress gradient across the depth of the beam flange at the nose of the transverse fillet weld is substantial due to secondary ($S22$) flexural stresses that develop at the abrupt change in the effective thickness (stiffness) of the flange of the beam. The maximum hydrostatic pressure is larger in RC03 than RC01, albeit only by 20 percent. In both cases, the critical regions are in a state of triaxial tension. The largest difference between the two specimens is the value of $S33$ (stress in the 3-3 [vertical] direction) at the beam web centerline in RC03. The beam flange is highly constrained at this location by the beam web below and the welded cover plate above.

Figure 6-19 presents the distributions of equivalent plastic strain (PEEQ in ABAQUS) in half of the top flange of RC01 (Figure 6-19a) and RC03 (Figure 6-19b) at 2-percent story drift. The maximum value is twice as large in RC01. The distribution of PEEQ is more uniform across the width of the flange in RC03 than RC01, and extends further down the flange (away from the cover plate) in RC03.

The geometry of the fillet welds joining the reinforcement plate to the beam flange affects the distribution of stress and strain in the plate. Figure 6-20 presents the distribution of $S22$ in the cover plates of RC01 (Figure 6-20a) and RC03 (Figure 6-20b). Although the distribution and values of $S22$ are similar for the two fillet weld geometries close to the face of the column, the 3-sided weld mobilizes the cover plate more effectively than the 2-sided weld as evinced by the contour plots in the figure.

It is inappropriate to generalize the results of analyses and experimentation for one combination of beam flange and cover plate thickness and two weld geometries (2-sided and 3-sided) to all cover- and flange-plate connections. However, for beams, reinforcing plates, and weld sizes of similar proportions to those studied herein, the 3-sided fillet weld (2 longitudinal welds, 1 transverse weld) is preferred to the 2-sided fillet weld (2 longitudinal welds) for four reasons,

namely, (1) smaller fillet welds can be used to join the reinforcement plate to the beam flange, (2) the reinforcement plate is more effectively mobilized near the nose of the reinforcing plate, (3) the probability of tearing of the fillet welds due to flange local buckling is reduced because the transverse weld does not permit the buckling to penetrate beyond the nose of the reinforcing plate, and (4) the likelihood of fracture of the fillet welded connection is reduced. Regardless of whether 2- or 3-sided fillet welds are used, fabrication details should be adopted that maximize the quality of the weld metal at the ends of the longitudinal and transverse fillet welds. The runoff tabs used for such a purpose in this research program ensured that high quality weld metal of the correct throat thickness was placed at the nominal ends of the welds, where the strain demands are greatest.

Consider now the 3-sided fillet weld that joined the trapezoidal cover plate to the beam flange in RC05. The distributions of S_{22} and Mises stress on one half of the upper surface of the beam top flange beneath the cover plate at 1-percent story drift are shown in Figures 6-21a and 6-21b, respectively. The distribution of hydrostatic pressure at the same location is shown in Figure 6-22. The maximum Mises stress in RC05 (Figure 6-21b) ranges between 50 and 55 ksi (345 and 379 MPa) and is located in a band immediately beyond the transverse fillet weld at the nose of the cover plate. For reference, the normal stress, S_{22} , 6 in. (152 mm) away from the nose of the cover plate ranges between 45.5 and 47.1 ksi (313 and 324 MPa): approximately the stress range that would be calculated at the nose of the cover plate using beam theory. The maximum hydrostatic pressure at the edge of the transverse fillet weld on the beam web centerline at 1-percent story drift is -32.6 ksi (-225 MPa); see Figure 6-22. The normal and principal stresses at this location are $S_{11} = 16.2$ ksi (112 MPa), $S_{22} = 61.5$ ksi (424 MPa), $S_{33} = 20.1$ ksi (138 MPa), $\sigma_1 = 67.2$ ksi (463 MPa), $\sigma_2 = 20.6$ ksi (142 MPa), and $\sigma_3 = 10.0$ ksi (69 MPa). All of these stresses are tensile. The maximum hydrostatic pressure at the junction of the longitudinal and transverse fillet welds (point A in Figure 6-22) is -21.6 ksi (-149 MPa). The normal and principal stresses at this location are $S_{11} = 7.0$ ksi (48 MPa), $S_{22} = 53.8$ ksi (371 MPa), $S_{33} = 4.0$ ksi (28 MPa), $\sigma_1 = 55.0$ ksi (379 MPa), $\sigma_2 = 8.4$ ksi (58 MPa), and $\sigma_3 = 1.4$ ksi (10 MPa). All of these stresses are tensile. Two conclusions can be drawn from these data, namely (1) the fillet weld geometry of RC05 (3-sided fillet weld to a trapezoidal plate) is no worse than the fillet weld geometry of RC03 (3-sided fillet weld to a trapezoidal plate) for welds of identical quality, and (2) the beam web substantially constrains deformations in the 3-3 direction (compare the values of S_{33} at the beam web centerline and at the junction of the longitudinal and transverse welds), leading to a substantial increase in the hydrostatic pressure (-21.6 ksi to -32.6 ksi [-149 MPa to -225 MPa]) and increasing the probability of brittle fracture.

Figures 6-23, 6-24, and 6-25 present response data at the nose of the cover plate (or transverse fillet weld) for specimens RC01, RC03, and RC05 at 2-percent story drift. Figure 6-23 presents line plots of normal stresses S_{11} , S_{22} , and S_{33} as a function of distance from the beam web centerline. The distributions of S_{22} for all three specimens are similar, as expected. The largest values of S_{33} are recorded at the beam web centerline for RC03 and RC05 due to the constraint offered by the beam web. Figure 6-24 presents the distributions of hydrostatic pressure, Mises, and equivalent plastic strain (PEEQ) as a function of distance from the beam web centerline. The maximum hydrostatic pressures for the three specimens are similar (35 to 40 ksi or 241 to 276 MPa) but occur at different locations. The values are maximized at the beam web centerline for RC03 and RC05 and at the edge of the beam flange outstand for RC01. The maximum equivalent

plastic strains for RC03 and RC05 are approximately 0.012 (or $7\varepsilon_y$) and 0.018 for RC01 (or $10\varepsilon_y$), where ε_y is the assumed uniaxial yield strain equal to 0.0018. The maximum values were recorded at the end of the longitudinal fillet weld for RC01 and RC03, and at the junction of the longitudinal and transverse fillet welds for RC05. Figure 6-25 presents the distributions of Pressure Index, Triaxiality Ratio, and Rupture Index as a function of distance from the beam web centerline. (To recap from Chapter 4, the Pressure Index is defined as the hydrostatic pressure [stress] divided by the yield stress; the Triaxiality Ratio is defined as the hydrostatic stress divided by the Mises stress; and the Rupture Index is defined as the product of the equivalent plastic strain and a material constant divided by the product of the failure strain and the yield strain.) El-Tawil et al. (1998) note that high values of the Triaxiality Ratio (between 0.75 and 1.50) can cause a large reduction in the rupture strain of metals, and that larger values can result in brittle fracture; and that the Rupture Index can be used to compare different configurations for the potential for ductile fracture. The maximum values of the Triaxiality Ratio at 2-percent story drift ranged between 0.50 and 0.70: at the lower end of the range identified by El-Tawil et al. in which large reductions in rupture strain could occur. The maximum values of the Rupture Index in RC03 and RC05 were similar, and less than two-thirds of the maximum value in RC01, all at 2-percent story drift. On the basis of these data, the 3-sided weld configurations of RC03 and RC05 are superior to the 2-sided configuration of RC01.

6.5 Restraint of Lateral-Torsional Buckling

Three buckling modes can contribute to the instability of wide-flange sections: flange local buckling (FLB), web local buckling (WLB), and lateral-torsional buckling (LTB). Questions were raised early in the SAC Phase II project regarding the relative contributions of these three modes to the loss of strength and stiffness of wide flange sections. To delay FLB and WLB in wide-flange shapes strained into the inelastic range, the AISC *Seismic Provisions for Structural Steel Buildings* (AISC 1997) present limits on flange compactness and web compactness, respectively.

AISC writes that “Both flanges of beams [in Special Moment Frames] shall be laterally supported directly or indirectly. The unbraced length between lateral supports shall not exceed $2500r_y/F_y$ [in U.S. units]. In addition, lateral supports shall be placed near concentrated forces, changes in cross-section and other locations where analysis indicates that a plastic hinge will form during inelastic deformations...” For a Grade 50 W30x99 beam, the AISC limit is 105 in. (2.66 m).

To investigate the effect of delaying lateral-torsional buckling on the rotation capacity of a beam plastic hinge, specimen RC02 was detailed to accept two lateral bracing members located approximately 20 in. (508 mm) from the nose of the cover plate at the assumed far end of the plastic hinge. The braces were located at the level of the beam flanges. Specimen RC02 was identical in all other regards to RC01. Lateral bracing was provided to all ten specimens near the actuator to protect the actuator from damage due to horizontal translation and rotation of the beam following buckling. Also, the lateral stiffness of the reinforcing plates in all ten specimens served to prevent lateral-torsional buckling at the side of the plastic hinge closest to the column face.

The procedures used to design the lateral braces were described in Chapter 3. In summary, the braces were designed following normal practice for a lateral force equal to 6 percent of the squash load of the beam flange ($= 0.06 \times 7.25 \text{ in}^2 \times 55 \text{ ksi} = 24 \text{ kips}$ [108 kN]). The stiffness of each brace was selected to replicate that of a fly-brace spanning between the bottom flange of the (seismic) beam and the top flange of the adjacent (gravity) beam. This distance between the seismic and gravity beams was assumed to be 120 in. (3.0 m).

The backbone curves for RC01 and RC02 are presented in Figure 6-26. These curves were developed using data from the cyclic force-displacement relations presented in Chapter 5. There is no significant difference in the backbone curves for the two specimens. The restraint to lateral-torsional buckling provided to RC02 20 in. (508 mm) beyond the nose of the cover plate, at the assumed far end of the plastic hinge, did not delay the loss of strength in RC02 following FLB and WLB. The addition of the lateral braces did not improve the measured response of specimen RC02 with respect to that of specimen RC01. The shell-element analysis of Section 4.9.5 confirmed this observation. As such, there is no compelling reason to brace the bottom flange of beams in reinforced connections immediately beyond the plastic hinge zone.

The axial forces in the lateral braces of RC02 increased linearly with story drift until WLB of the RC02 led to a rapid loss of strength in the beam. At this point, the axial force in the top-flange brace increased markedly to a maximum of approximately 45 kips (200 kN). This axial force was composed of two components: (1) force due to elongation of the brace associated with the vertical displacement of the (seismic) beam with respect to the adjacent (gravity) beam and (2) force associated with preventing the lateral displacement of the beam top flange. Both force components will be developed in lateral braces in the field. The maximum measured brace axial force was equal to 12 percent of the calculated squash load of the beam flange: twice the force used to design the brace. The maximum brace force calculated using the Type SH models in Section 4.9.5 was 26 kips (118 kN). This force, which was equal to 7% of the squash load of the beam flange, served to prevent lateral displacement of the beam flanges, but did not include a component due to elongation of the brace. Further study of the design and detailing rules for lateral bracing of beam flanges is warranted.

6.6 Loading History

Two loading histories were used for the experimental studies: cyclic (see Figure 3-13a) and near-field (see Figure 3-13b). The cyclic history was used for nine of the ten specimens. The near-field history was used for RC07 only.

The effect of loading history on the behavior of plate-reinforced connections was studied by comparing the responses of two identical flange-plate specimens that were tested using the cyclic (RC06) and near-field (RC07) histories. Figure 6-27 presents the backbone curves for these specimens, which were developed using data from the positive drift excursions of RC06; and the first negative drift excursion to -0.02 radians and the first positive drift excursion from +0.02 to +0.06 radians for RC07. The difference between the maximum resistances of RC06 and RC07 was negligible. For story drift ratios of 0.03 radian and greater, the resistance of RC07 exceeded that of RC06, indicating that the near-field history was less damaging than the more traditional cyclic history.

The Park-Ang damage index (Park et al. 1987) is a useful tool for examining the behavior of steel and reinforced concrete components under “...repeated stress reversals and high-stress excursions.” The damage index, D , is given by

$$D = \frac{\delta_m}{\delta_u} + \frac{\beta}{Q_y \delta_u} \int dE \quad (6-1)$$

where δ_m is the maximum response deformation under earthquake (cyclic) loading, δ_u is the ultimate deformation capacity under monotonic loading, β is a non-negative constant, Q_y is the yield strength, and dE is the incremental dissipated hysteretic energy. A value of D equal or greater than 1.0 represents “...collapse or total damage.” Park et al. report a value of 0.025 for β based on tests of 132 steel specimens. None of the ten full-scale tests were monotonic tests to failure so the value of δ_u cannot be calculated directly from test data. (The loading protocol used for RC07 was the near-field protocol of Figure 3-13b and not a monotonic test to failure.) However, information from the cyclic tests to failure of RC06 can be used to estimate δ_u . (Data from the tests of RC06 are representative of the other data sets as evinced by the estimates of the variables in (6-1) presented in Tables 5-1 and 5-2.) For specimen RC06, δ_m is 6.7 in. (170 mm), β is 0.025, Q_y is 165 kips (734 kN), and dE is 11,663 kip-in (1318 kN-m) at failure (D equal to 1.0). The corresponding value of δ_u is 8.5 in. (216 mm). As such, the maximum monotonic displacement capacity of the flange-plate connection is equivalent to 6-percent story drift. The near-field deformation history (of RC07) is intuitively less damaging than the cyclic history (RC01-RC06, RC08-RC10) and it should likely be assigned a smaller value of β . For specimen RC07, δ_m is 7.6 in. (193 mm), β is 0.025, Q_y is 158 kips (703 kN), and dE is 9,982 kip-in (1127 kN-m) at failure. Assuming that δ_u is 8.5 in. (216 mm), the damage index is 1.08, which suggests that a smaller value of β should be used for evaluating the effects of near-field shaking on steel components.

6.7 Web Local Buckling

Table I-9-1 of the *AISC Seismic Provisions for Structural Steel Buildings* (AISC 1997) writes that the limiting width-to-thickness ratio for a beam web under zero axial load is

$$\frac{h_c}{t_w} \leq \frac{520}{\sqrt{F_y}} \quad (6-2)$$

where F_y is the yield strength in ksi. For a Grade 50 beam, this limit is equal to 74. The web compactness ratio for a W30x99 beam is 51.9 and substantially less than 74. Nonetheless, local buckling of the beam web in the plastic hinge zone led to a rapid loss of strength in the first nine specimens, RC01 through RC09. Such an unexpected loss of strength in the first five tests led the authors to recommend a reduction in the maximum width-to-thickness ratio to

$$\frac{h_c}{t_w} \leq \frac{350}{\sqrt{F_y}} \quad (6-3)$$

where F_y is the yield strength in ksi, to further delay web local buckling and the consequent loss of strength.

Specimen RC10 was designed specifically to study the effect of increasing web compactness on the rate of strength degradation in reinforced connections. Specimen RC10 was detailed in an identical manner to RC03 except that two pairs of longitudinal stiffeners were welded to the beam web of RC10. (This approach is likely not an economical strategy for increasing web compactness. Rather, an increase in the web thickness is recommended.) Information on these stiffeners is presented in Chapter 3. The maximum resistance of RC10 was 18 percent greater than that of RC03 due to the addition of the longitudinal stiffeners that increased the plastic section modulus of the beam from 312 in.³ (0.0051 m³) to 394 in.³ (0.0064 m³). To compare the hysteretic response of RC03 and RC10, the maximum moment at the face of the column was normalized to unity. The relationships between normalized moment and beam plastic rotation for RC03 and RC10 are presented in Figure 6-28. The rate of strength loss with increasing plastic rotation is smaller in RC10 than RC03 and it is evident that increased web compactness with respect to the current AISC limit is desirable.

6.8 Reinforcing Plate Strain

Specimens RC01 through RC07 were designed with the intent of limiting the maximum strain in the reinforcement plate to the yield strain. Section 3.2.1 outlines the design procedure that was based primarily on the procedures set forth in FEMA 267A (FEMA 1995b). Flange-plate specimen RC08 was identical to the benchmark flange-plate specimen RC06 in all regards except for the thickness of the flange-plate and fillet weld size. The flange-plate thickness in RC06 was 1 in. (25 mm). The thickness of the flange plate in RC08 was arbitrarily reduced to 7/8 in. (22 mm) to investigate the effect on global response of inelastic straining of the reinforcement plate. The fillet weld sizes in RC06 and RC08 were 5/8 in. and 9/16 in. (16 mm and 14 mm), respectively. Figure 6-29 presents a comparison of the global responses of RC06 and RC08. There is no significant difference in the moment-rotation response of the two specimens because flange and web local buckling in the beams of RC06 and RC08 prevented large strains being developed in the flange plates. The maximum measured strains in the flange plates of RC06 and RC08 as a function of the target story drift ratio are presented in Figure 6-30. The strains are normalized to the nominal yield strain. As expected, the flange plates of RC08 experienced larger axial strains than those of RC06, although the differences in maximum strain were relatively small. The use of yielding reinforcement plates did not result in poor or unexpected behaviors in this test program, but the levels of inelastic strain were modest. Further comments on the use of yielding reinforcement plates are presented in the following section.

6.9 Panel Zone Strength

Figures 6-31a and 6-31b present the relations between moment at the column face and story drift angle for specimens RC06 and RC09, respectively. Specimen RC09 was identical to RC06 in all regards except that no doubler plate was installed in RC09 and thinner flange plates and continuity plates were used in RC09. A comparison of the hysteresis loops in these figures shows that (1) the elastic stiffness of RC09 was slightly smaller than that of RC06 (as expected), and (2) RC09 dissipated substantially more energy than RC06. The maximum strengths of the two specimens are essentially identical, which is not surprising because the maximum strength is dictated by the strength of the W30x99 beam that was common to both specimens. The difference in global energy dissipation (and loop shape) between RC06 and RC09 is due to the substantial participation of the panel zone in the response of RC09 as seen in Figures 6-32a and 6-32b that

present the relation between moment at the column face and panel zone plastic rotation in RC06 and RC09, respectively. In RC06, the maximum panel zone plastic rotation was 0.5 percent radian; in RC09, the maximum rotation was 2.5 percent radian. Substantial strain hardening is evident in the RC09 panel zone. In both specimens the maximum panel zone plastic rotation was limited by flange local buckling (FLB) and web local buckling (WLB) in the W30x99 beam. In RC06, only modest yielding and strain-hardening of the panel zone preceded FLB and WLB of the beam. The yield strength of the RC09 panel zone was substantially less than that of RC06 due to the lack of a doubler plate in RC09. Substantial strain hardening (and yielding) in the RC09 panel zone was required to trigger FLB and WLB in the W30x99 beam. Once triggered, the maximum resistance and secant stiffness of RC09 degraded and the consequent demand on the panel zone dropped with cycling to larger displacements. Near elastic response (no plastic deformation) at a residual panel zone plastic rotation of approximately 1 percent radian (that followed FLB and WLB in the beam) can be clearly seen in Figure 6-32b.

Some expert engineers have recommended that connection plastic rotation be shared between the panel zone and the beam. Such a strategy is most appealing if (1) simultaneous yielding in the panel zone and the beam can be realized and (2) both components exhibit similar post-yield behaviors. If achieved, large connection rotations could be developed with modest contributions from the panel zone and the beam. A procedure for achieving simultaneous yielding in the panel zone and the beam (for cover-plate connections) is presented in Chapter 7. This procedure requires a priori knowledge of the likely yield stresses of the beam flange and the column web, which is impractical. Modest, yet acceptable (per the appropriate ASTM standards) variations in values of yield stress could render the procedure completely ineffective with all of the inelastic deformation being forced into either the panel zone or the beam. The requirement that both the panel zone and the beam exhibit similar post-yield behaviors ensures that yielding is shared in a predetermined (constant) manner over the likely range of inelastic response. However, such a requirement may be impractical because although the force-displacement relations for panel zones are bilinear over a wide range of inelastic deformation (see Figure 6-32b), most wide-flange beam sections lose strength after modest inelastic deformation due to FLB and WLB (see Figure 5-6 for example). In summary, it is most likely impractical to share large inelastic deformation demands between a panel zone and a beam section. Either the panel zone or the beam should be designed to accommodate the design inelastic deformations, and capacity design principles should be used to confine the inelastic deformations to the desired component.

Further insight into the behavior of reinforced steel connections with weak panel zones can be garnered by comparing the results of the ABAQUS analysis of specimens RC06 and RC09. Figure 6-33 presents the distribution of shear (S_{23}) stress in the panel zone of RC09 at 1-percent story drift. The values range from -30 ksi (-207 MPa) in the middle of the panel to -15 ksi (-104 MPa) in the corner of the panel: a factor of 2 difference. Similar differences were observed in this and other experimental programs. For reference, design procedures assume a constant value for shear stress in the calculation of the yield strength of a panel zone. Figure 6-34 shows the Mises stress distribution in the panel zone and the beam web at 1-percent story drift. Setting aside the flange plates at this time, the maximum values of Mises stress are recorded in the center of the panel zone and immediately below the cope hole in the beam.

Figures 6-35a and 6-35b show the distribution of Mises stress in the flange plates of RC09 and RC06, respectively, at 1-percent story drift. The maximum stresses in the two flange plates are nearly identical (53.6 ksi [369 MPa] in RC06 and 52.7 ksi [363 MPa] in RC09): the weaker and more flexible panel zone in RC09 reduces the demand on the flange-plate at 1-percent story drift, but the flange plate in RC09 is thinner than that in RC06, which results in higher strains in RC09 for the same demand. The maximum values of Mises stress in the flange plate, the beam flange at the face of the column, and the beam web immediately below the cope hole, of RC06 and RC09 differ by less than 10 percent.

The deformations of the RC09 beam web, flange plate, column flanges, and panel zone at 2-percent story drift are shown in Figure 6-36. The distortions of the flange plate at the column face, parallel and perpendicular to the longitudinal axis of the beam, are clearly evident. The localized vertical deformation of the flange plate over the cope is due to the transfer of shear force to the column flange through the flange plate. These distortions give rise to the complex states of strain in the flange plate at the face of the column, which cannot be predicted by beam theory. Figure 6-37 presents the distribution of equivalent plastic strain in the panel zone and the beam web at 2-percent story drift. Figures 6-38a and 6-38b present the distributions of equivalent plastic strain in flange plate and beam flange, respectively, at 2-percent story drift. Large values of equivalent plastic strain were recorded in the beam web immediately below the beam web cope. The maximum equivalent plastic strain in the flange plate at the face of the column ($= 0.0098$) is greater than that in the beam flange beyond the flange plate ($= 0.00062$) and greater than the maximum value in the panel zone ($= 0.0086$). Such a relationship is potentially problematic because yielding (plastic strain) will be concentrated in (a) the short free length of the flange plate between the face of the column and the edge of the beam flange and (b) the panel zone, rather than being shared between the panel zone and the beam beyond the flange plate. The inelastic deformation capacity of this reinforced connection would likely be limited by the strain (displacement) capacity of the flange plate.

Compare now the equivalent plastic strains in the flange plates and beam flanges of RC06 and RC09 at 2-percent story drift. Figures 6-39a and 6-39b present this data for RC06. For RC06, the maximum value of equivalent plastic strain in the flange plate at the face of the column ($= 0.008$) is substantially smaller than that in the beam flange beyond the flange plate ($= 0.024$). Ignoring plastic deformations in the panel zone and flange- and web-local buckling in the beam, this reinforced connection would likely develop larger plastic rotations than RC09 because most of the inelastic deformation would occur in a segment of the beam where yielding can spread over a relatively long length. That is, flange-plate connections should not be designed and detailed for large plastic straining in the flange plate at the column face as was the intent with RC09.

6.10 Reinforced Shear Tabs

For steel beam-column connections, it is well established (Lee et al. 1997) that the beam web transfers only part of the shear force in the beam to the column and that much of the shear force is transferred through the beam flanges. Section 4.5.2 of this report presented information on the distribution of shear stress in the W30x99 beam at different distances from the face of the column. Two key observations were made in that section: (1) in the elastic range of response (for story drifts less than 0.5 percent), approximately 50 percent of the shear force was transferred through

the beam flanges to the column—contrary to beam theory, and (2) in the elastic range of response, the distribution of shear stress in the beam web follows that predicted by beam theory only at a distance of $d_b/2$ from the face of the column, where d_b is the beam depth. The analysis of Section 4.5.2 is expanded in this section to investigate (1) distributions of shear force in the beam at the face of the column at story drift levels greater than 1 percent and (2) the effect of stiffening the beam web at the face of the column on these shear force distributions.

Table 6-1 presents information on the distribution of shear force in RC00 (unreinforced connection) at different levels of story drift. Also listed in the table are the calculated equivalent plastic strains in the beam flange at the face of the column, normalized by the estimated yield strain of 0.0018. It is evident that plastic straining of the beam flanges leads to a redistribution of shear stress at the face of the column, with a greater percentage of the shear force being passed through the beam web. However, the distribution is very sensitive to modest levels of plastic strain: compare the distributions in columns 2 and 3. Large plastic strains in the beam flanges would be needed for the shear force distribution to approach that of beam theory (97% in the beam web; 3% in the beam flanges). Such a result is somewhat intuitive. However, one design objective with reinforced connections is to limit or eliminate plastic straining at the column face by forcing yielding into the beam beyond the reinforcing plate and/or the beam-column panel zone. As such, increasing the percentage of the beam shear force transferred through the beam web as a result of plastification of the beam flange assembly at the column face is not a viable strategy for reinforced connections.

Table 6-1 Shear force transfer from RC00 W30x99 into W14x176 column

	<i>Story Drift Angle</i>		
	<i>0.5%</i>	<i>1%</i>	<i>2%</i>
Average equivalent plastic strain in beam flange/ ϵ_y ¹	0.0	0.4	5.1
Percentage of beam shear transferred via web	54	72	85
Percentage of beam shear transferred via flanges	46	28	15

1. Assumed yield strain = 0.0018

One strategy that has been proposed for increasing the percentage of the beam shear transferred through the beam web to the column involves the addition of welded web shear tabs to increase the stiffness of the beam web. This strategy was studied by analysis of five beam web configurations using the W30x99 beam and W14x176 column: (1) unreinforced web, (2) web reinforced with a 5 in. (127 mm) wide by 0.5 in. (13 mm) thick tab plate, (3) web reinforced with a 5 in. (127 mm) wide by 1.0 in. (25 mm) thick tab plate, (4) web reinforced with a 10 in. (254 mm) wide by 0.5 in. (12 mm) thick tab plate, and (5) web reinforced with a 10 in. (254 mm) wide by 1.0 in. (25 mm) thick tab plate. The depth of the tab plate configurations 2 through 5 was equal to the distance between the cope holes; see Figure 6-40. The reinforcement plate was assumed to be fully welded to the beam web, effectively increasing the thickness of the beam web over the elevation of the tab plate. Results are presented in Table 6-2.

Table 6-2 RC00 beam web reinforcement effectiveness at 0.5- and 2-percent story drift

Configuration	Web Tab Size		Story Drift Angle = 0.5%		Story Drift Angle = 2.0%	
	Width (mm)	Thickness (mm)	% beam web	% beam flange	% beam web	% beam flange
1 ¹	0	0	54	46	85	15
2	127	13	56	44	88	12
3	127	25	57	43	87	13
4	254	13	54	46	87	13
5	254	25	54	46	87	13

1. Thickness of beam web = 13 mm.

Configurations 2 through 5 represent bound the likely cost-effective sizes (width and thickness) of web reinforcement plates. For reference, the thickness of the W30x99 web is 0.5 in. (13 mm). The addition of a 25 mm thick tab plate to such a web represents a 200 percent increase in web thickness at the face of the column. The values listed in columns 4 through 7 of the table indicate that beam web reinforcement with welded web tab plates (installed between the weld access holes) serves no useful purpose.

6.11 Load Transfer to Column from Beam in Reinforced Connections

6.11.1 Cover-plate connections

The addition of flange reinforcement plates to an unreinforced connection will intuitively reduce the percentage of the beam shear transferred through the beam web to the column flange. Table 6-3 presents information on the percentage of the beam shear force transferred through the W30x99 beam web to the W14x176 column flange for three cover-plate thicknesses: 0 in. (unreinforced connection), 0.63 in. (16 mm), and 1.26 in. (32 mm). Both rectangular cover plates are 11.8 in. (300 mm) wide. The cover-plate thickness of 5/8 in. (16 mm) corresponds to that used for specimens RC01 through RC03.

An increase in cover-plate thickness from 0 mm to 32 mm has a significant effect on the percentage of the beam shear force transferred through the flange-plate assembly to the column. The trend evident in the table is clear: the thicker the cover plate, the greater the percentage of the beam shear transferred through the flange-plate assembly to the column. The use of cover plates in reinforced connections that are substantially thicker than those calculated using the simple procedures set forth in Chapter 3, ostensibly to reduce 2-2 strains in the flange-plate assembly, may not substantially improve connection performance.

Configurations 2 and 3 show a decrease in the percentage of shear force transferred through the beam web to the column with an increase in story drift. This trend is opposite to that of the unreinforced connection, RC00 (Configuration 1 in Table 6-3). Whereas much of the RC00 beam flange has yielded at 2-percent story drift, less than one half of the cover plate and one third of the

Table 6-3 Shear force transfer in cover-plate connection at 0.5- and 2-percent story drift

Configuration	Plate Size ¹		Story Drift Angle = 0.5%			Story Drift Angle = 2.0%		
	Width (mm)	Thickness (mm)	% beam web	% beam flange	% cover plate	% beam web	% beam flange	% cover plate
1 ²	0	0	54	46	0	85	15	0
2	300	16	52	31	17	46	37	17
3	300	32	31	25	44	12	34	54

1. Rectangular cover plates

2. Thickness of beam flange = 17 mm; width of beam flange = 267 mm.

beam flange have yielded. Beam web yielding is similar in both configurations at 2-percent story drift. As such, although large changes in the distribution of shear force are observed in Configuration 1 for an increase in story drift angle from 0.5 percent to 2.0 percent, there is only a small change in the distribution for Configuration 2.

For Configuration 2, the beam flange transfers more shear force to the column than the cover plate, although the area of the beam flange is less than (95 percent) that of the cover plate. Such a distribution of shear force is a result of the longer (more flexible) load path through the cover plate to the column. For shear force to be transferred through the cover plate to the column flange, the force must pass through the beam flanges in flexure to the cover plate via the fillet welds.

The cover-plate thickness of Configuration 3 is twice that of Configuration 2. In the elastic range (0.5-percent story drift), a much greater percentage of the shear force is transferred through the cover plate and beam flange of Configuration 3 than Configuration 2. Also, the cover plate transfers substantially more shear force to the column flange than the beam flange, which is likely a result of the significant increase in the stiffness of the cover plate with respect to that of the beam flange. As the story drift is increased from 0.5 percent to 2.0 percent, the percentage of the total shear force in the beam web at the face of the column is substantially reduced due to yielding of the beam web at the nose of the cover plate and the consequent transfer of shear force to the cover plate through the transverse fillet weld. The load-transfer mechanisms from the beam to the cover plate via the longitudinal and transverse fillet welds at 0.5- and 2-percent story drift are substantially different due in part to changes in the relative curvatures in the plate and the flange. (At 0.5-percent story drift, both the cover plate and the beam flange at the nose of the plate are elastic. At 2-percent story drift, the cover plate is elastic but the beam flange has yielded significantly.) Figure 6-41 shows the normalized cumulative shear force distribution in the cover plate at 0.5- and 2-percent story drift as a function of distance from the face of the column. The concentrated shear forces at a distance of 15 in. (381 mm) from the column face represent the shear forces transmitted through the transverse fillet welds. Note that contact between the beam flange and the plate was not modeled; such contact could modify the distributions.

The distribution of shear force between the beam web and plate-flange assembly was studied for thicker cover plates. As the plate thickness was increased to 2 in. (51 mm), the beam web at the face of the column resists a negligible percentage of the total shear force at 0.5-percent story drift, with approximately 80 percent of the total shear being transferred through the cover plates. As the story drift was increased to 2.0 percent, the plate-flange assembly resisted in excess of 110 percent of the total shear force (that is, the shear force in the beam web served to load the plate-flange assembly).

6.11.2 Flange-plate connections

Table 6-4 presents information on the percentage of the beam shear force transferred through the W30x99 beam web to the W14x176 column flange for two flange-plate thicknesses: 33 mm and 49 mm. Both rectangular flange plates are 300 mm wide. The flange-plate thickness of 33 mm is 30 percent greater than the thickness of the flange plate of RC06 (=25 mm) but was chosen to facilitate a comparison with Configuration 2 of Table 6-3. The trends of Table 6-4 are identical to those of Table 6-3 for cover-plate connections. A comparison of the results for cover-plate Configurations 2 and 3 and flange-plate Configurations 1 and 2 shows that a greater percentage of the total shear force is carried by the flange plate assembly. The load path for the flange-plate connections is less circuitous because the shear force in the reinforcing plate does not have to be transferred through the beam flanges and fillet welds.

Similar to the cover-plate connection of the previous section, the distribution of shear force between the beam web and flange plates assembly was studied for thicker flange plates. As the plate thickness was increased to 68 mm (for comparison with the cover-plate connection with a plate thickness of 51 mm), the flange plates resisted 116 percent of the total shear force at 0.5-percent story drift. This percentage increased marginally as the story drift was increased to 2.0 percent.

Table 6-4 Shear force transfer in flange-plate connection at 0.5- and 2-percent story drift

Configuration	Flange-plate dimensions ¹		Story Drift Angle					
			0.5 percent			2.0 percent		
	Width (mm)	Thickness (mm)	% beam web	% beam flange	% flange plate	% beam web	% beam flange	% flange plate
1	300	33	44	0	56	32	0	68
2	300	49	16	0	84	6	0	94

1. Rectangular flange plates

6.11.3 Summary remarks

The distributions of total shear force in reinforced connections between the beam web and the plate-flange assembly at different levels of story drift is substantially more complex than those of unreinforced connections. Factors that influence the distribution include level and distribution of plastic strain in the different components at the face of the column and the stiffness of the load path into the reinforcing plate. Evaluation of these factors is not possible using elementary theory similar in complexity to that used to design the reinforced connections.

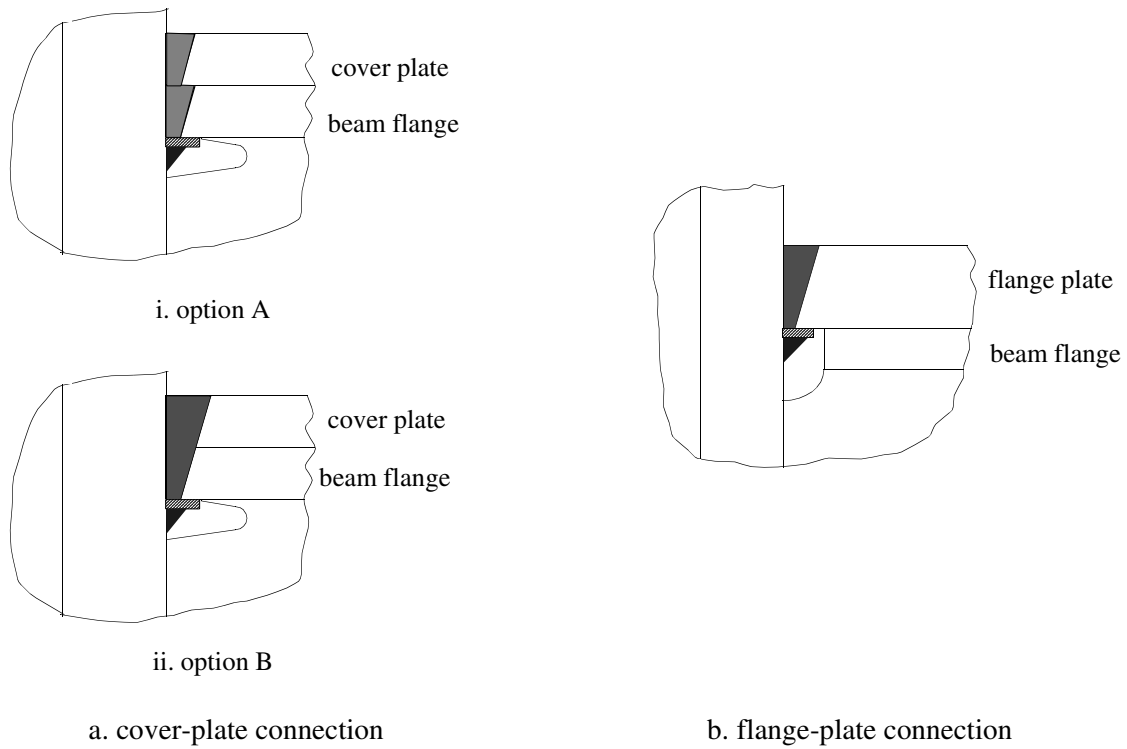


Figure 6-1 Reinforcement-plate groove weld geometries

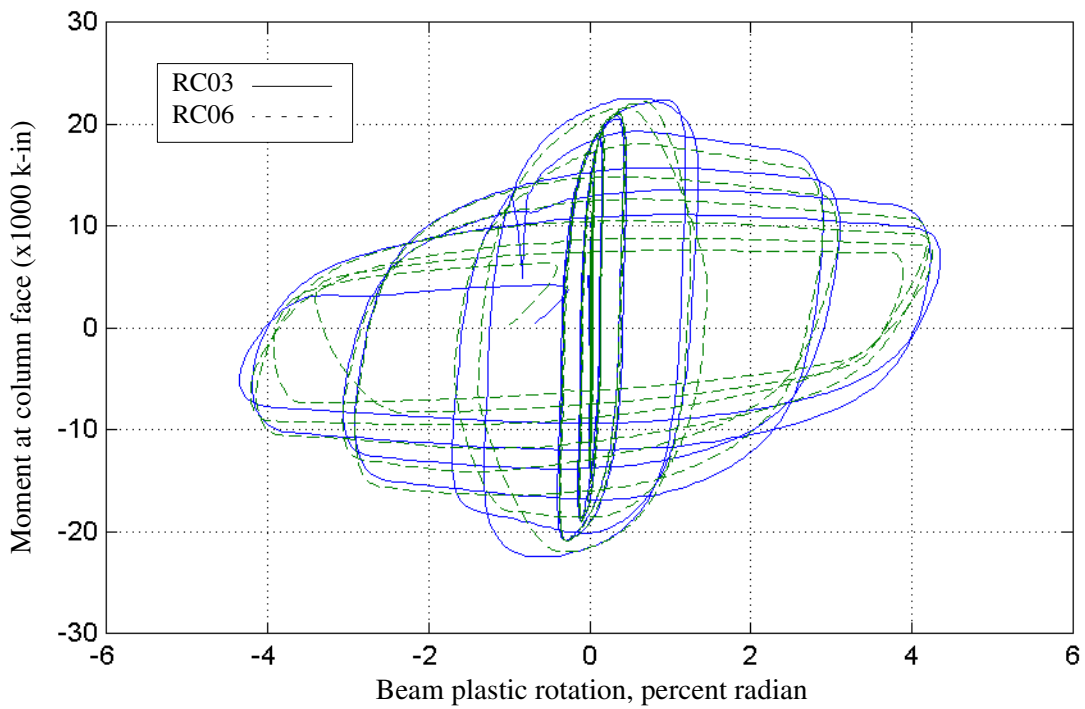


Figure 6-2 Comparison of response of cover-plated (RC03) and flange-plated (RC06) specimens

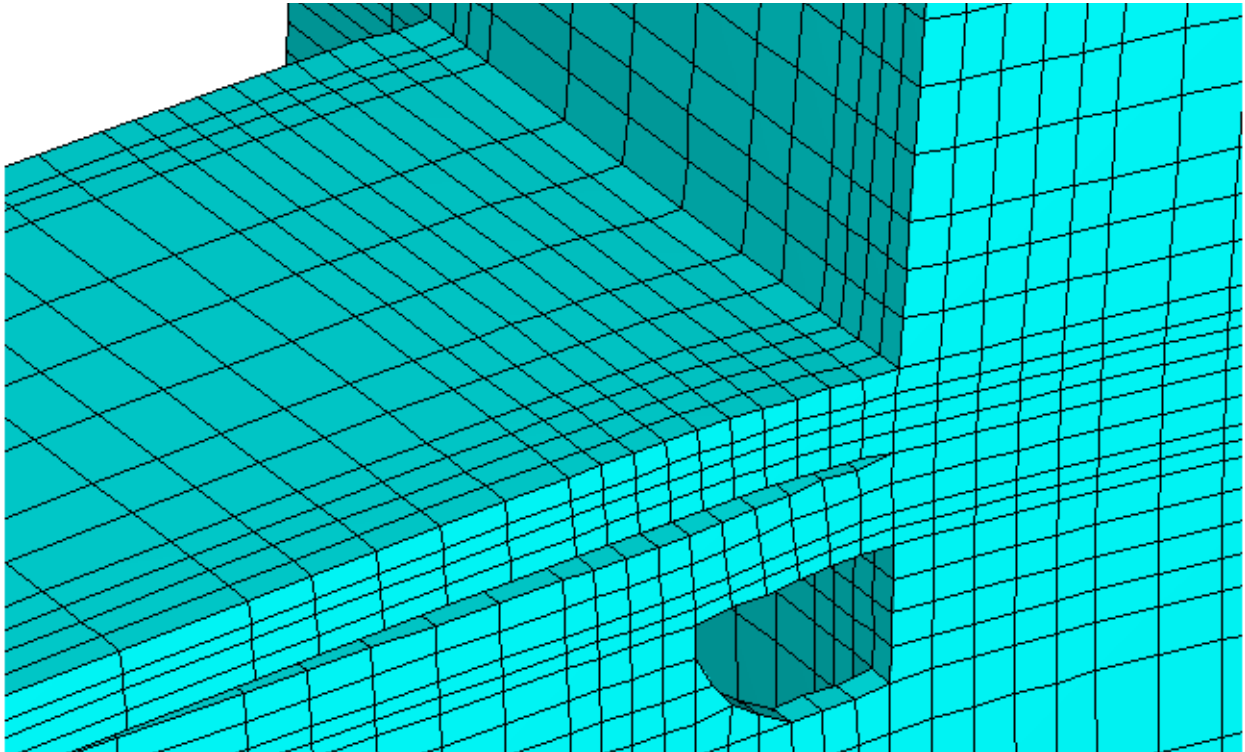
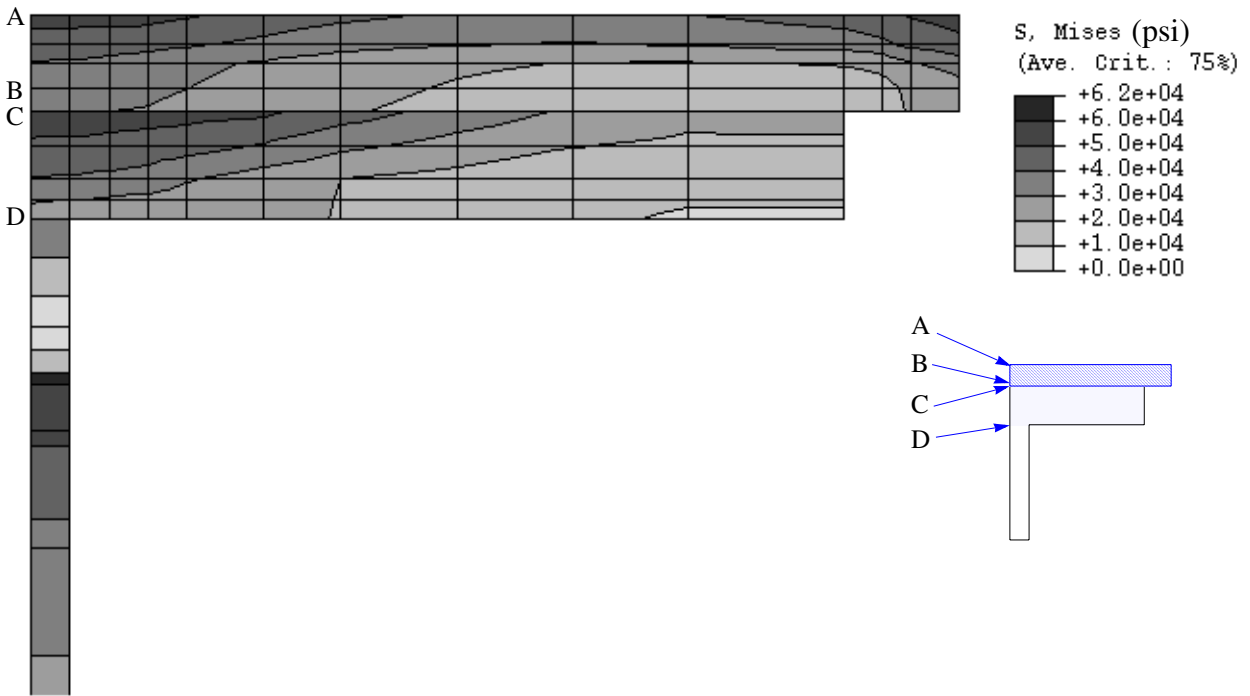
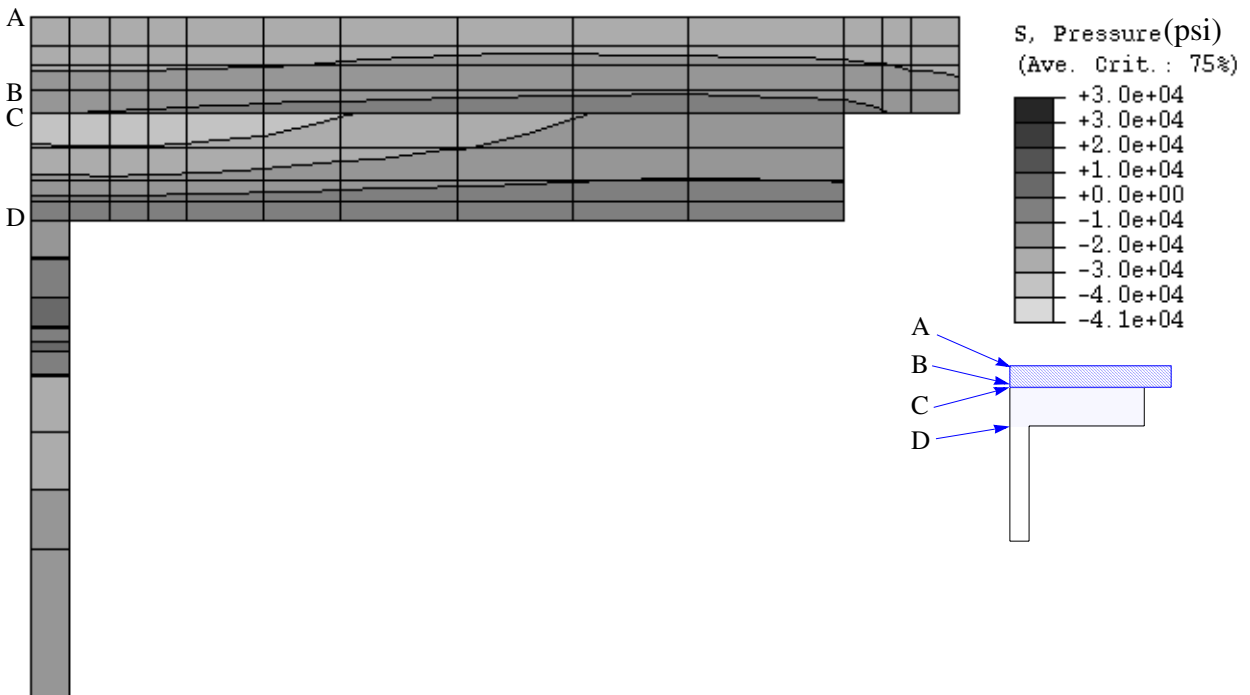


Figure 6-3 Deformed shape of cover plate and beam flange near face of column

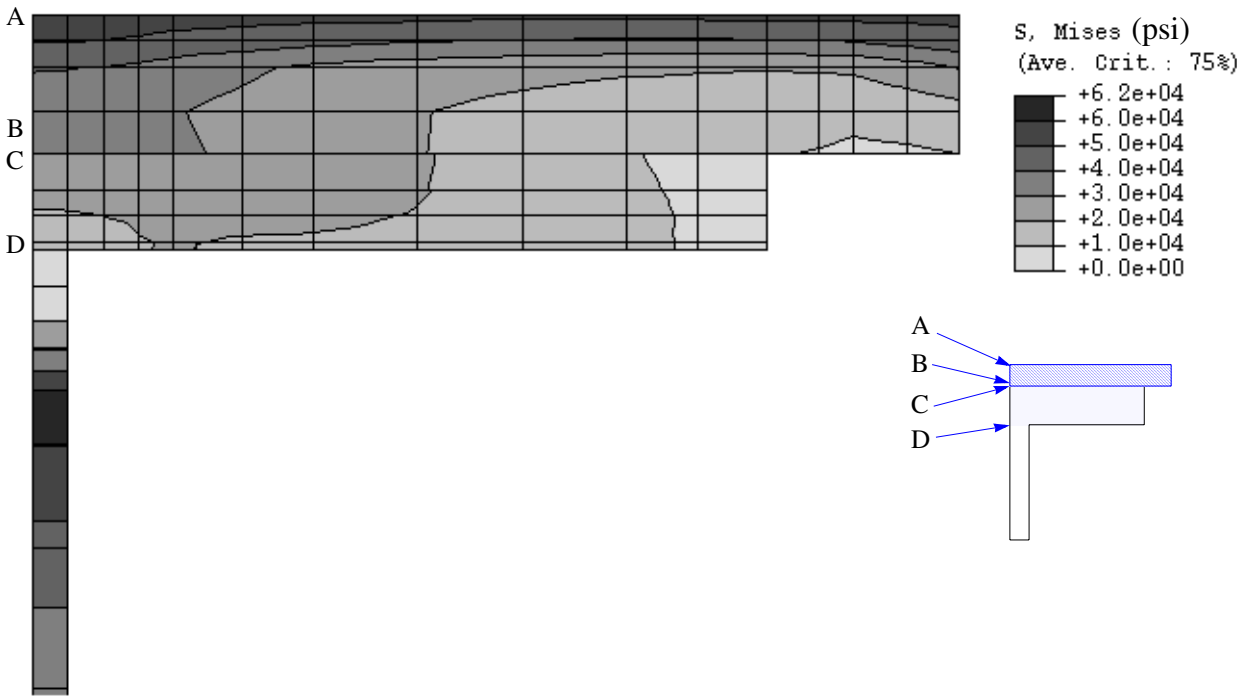


a. Mises distribution

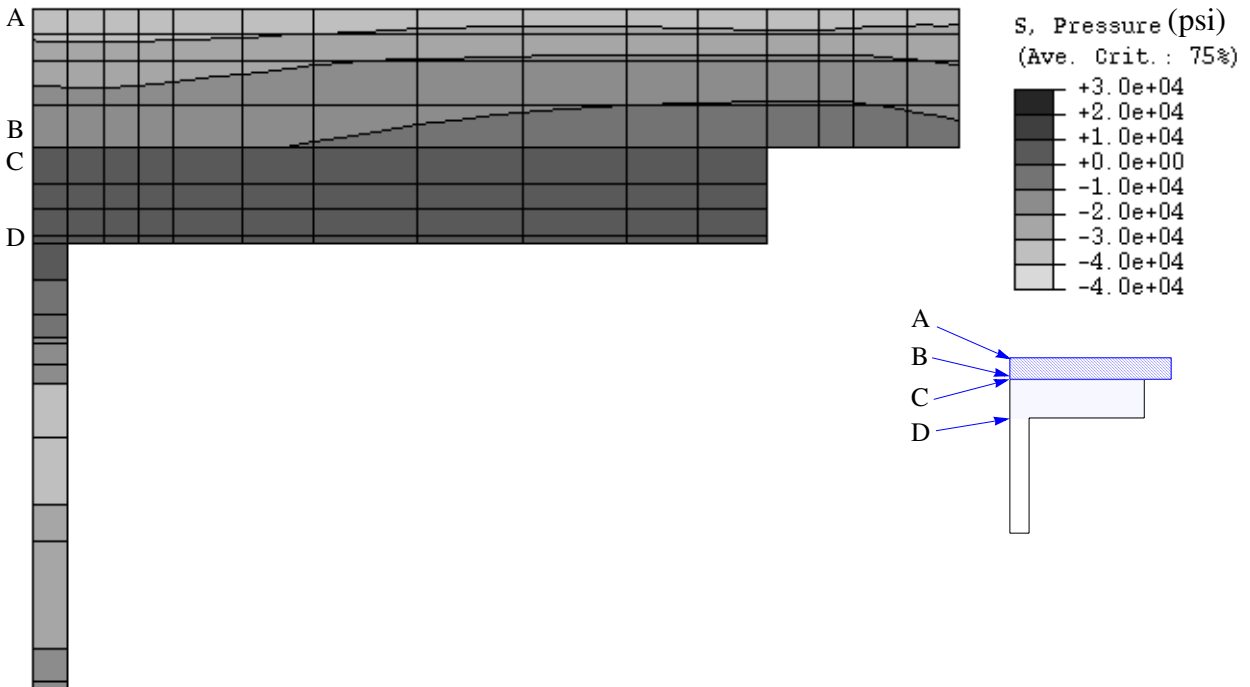


b. Hydrostatic pressure distribution

Figure 6-4 Mises and hydrostatic pressure distributions at column face in RC03 at 1-percent story drift

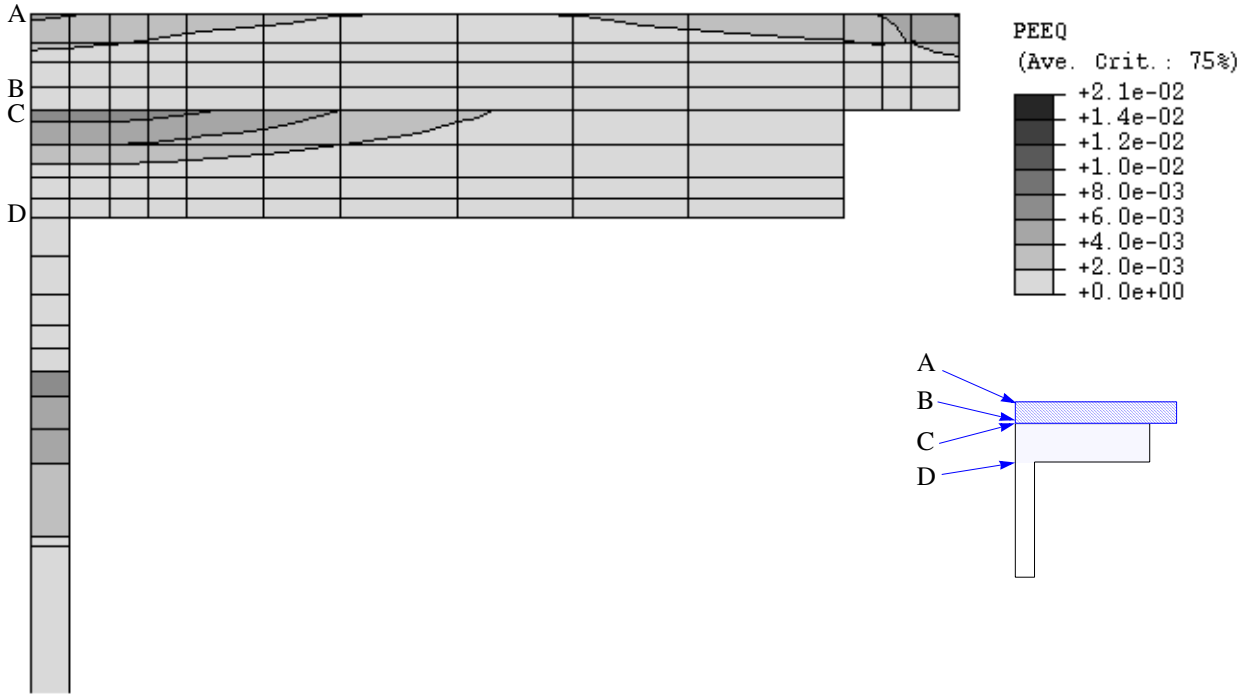


a. Mises distribution

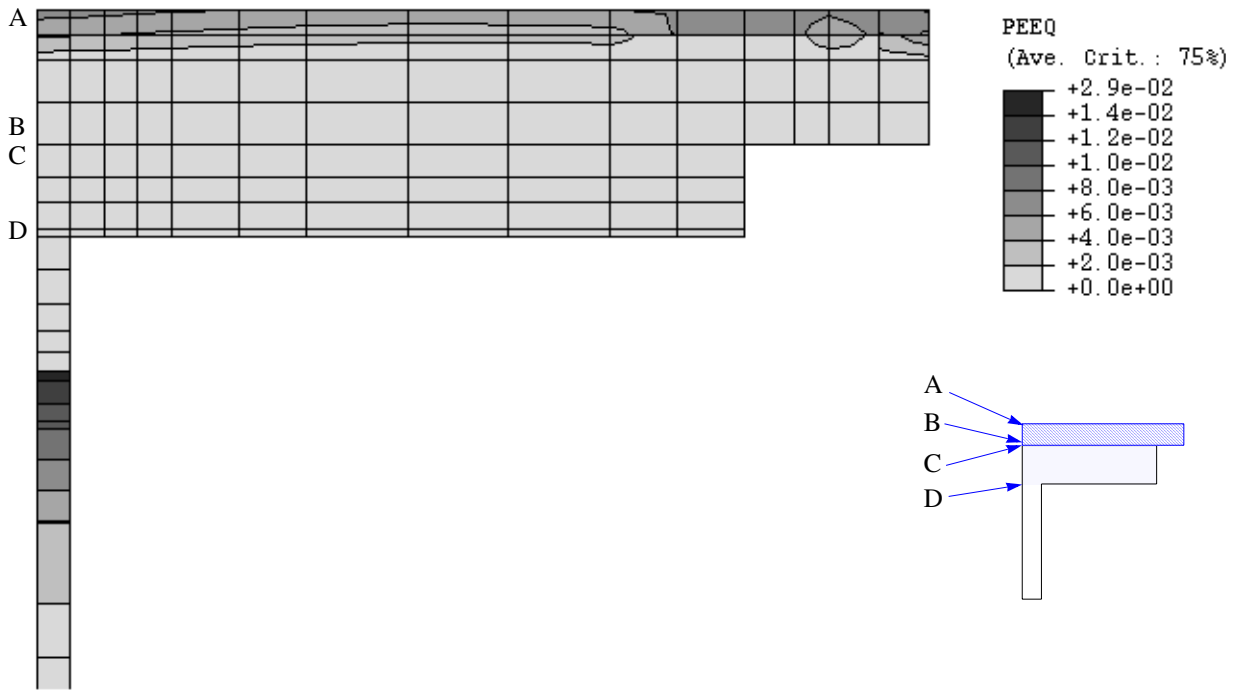


b. Hydrostatic pressure distribution

Figure 6-5 Mises and hydrostatic pressure distributions at column face in RC06 at 1-percent story drift



a. RC03 (cover-plate connection)



b. RC06 (flange-plate connection)

Figure 6-6 Equivalent plastic strain distribution at column face in RC03 and RC06 at 2-percent story drift

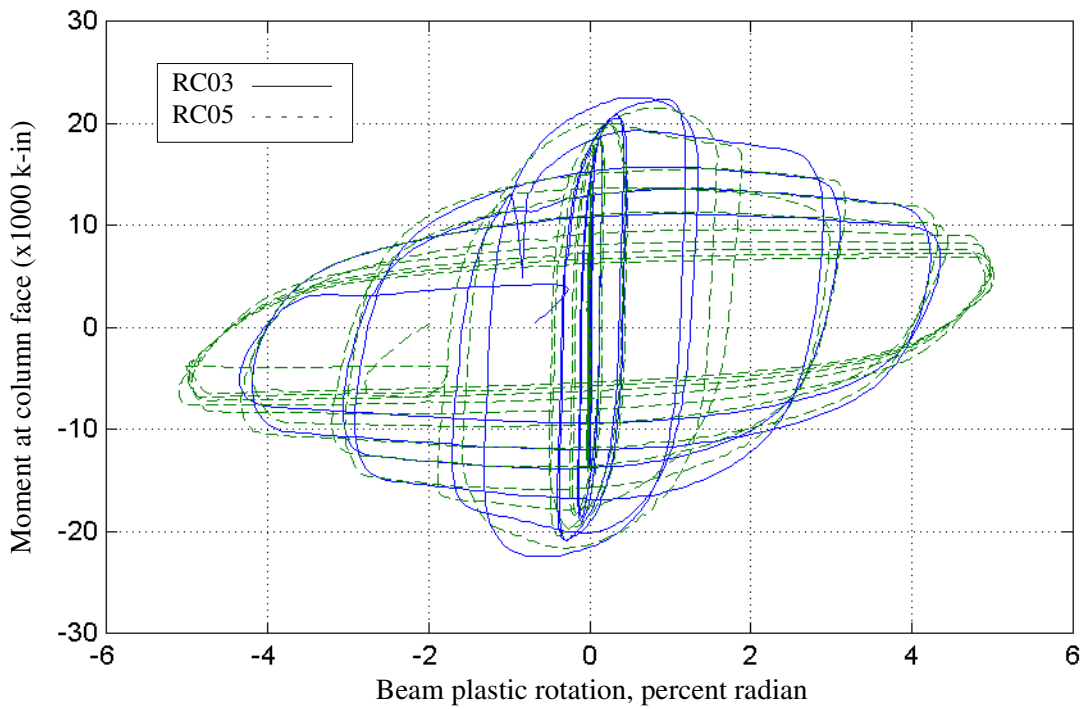


Figure 6-7 Moment at column face versus beam plastic rotation for RC03 and RC05

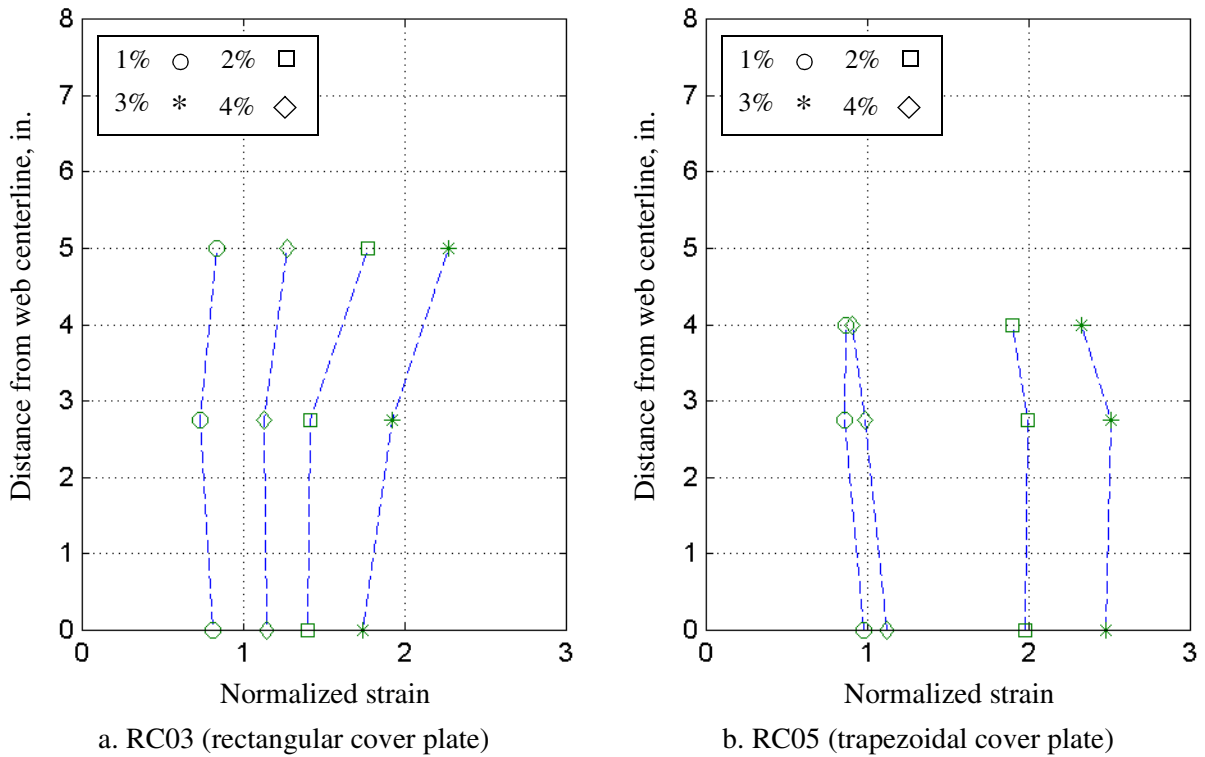


Figure 6-8 Strain response of cover plates in RC03 and RC05 as a function of story drift

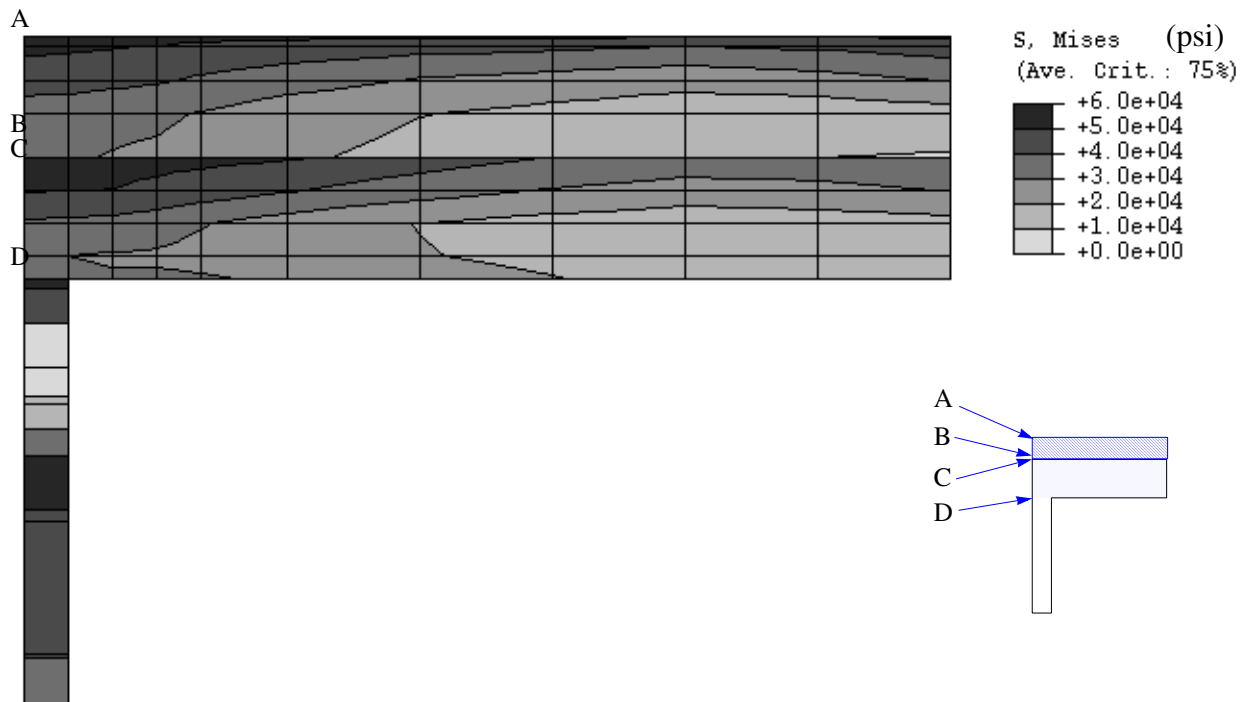
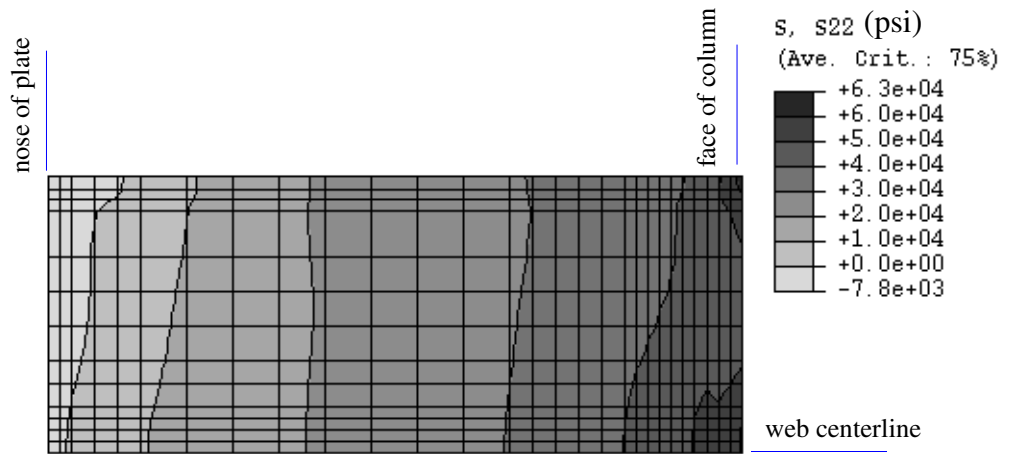
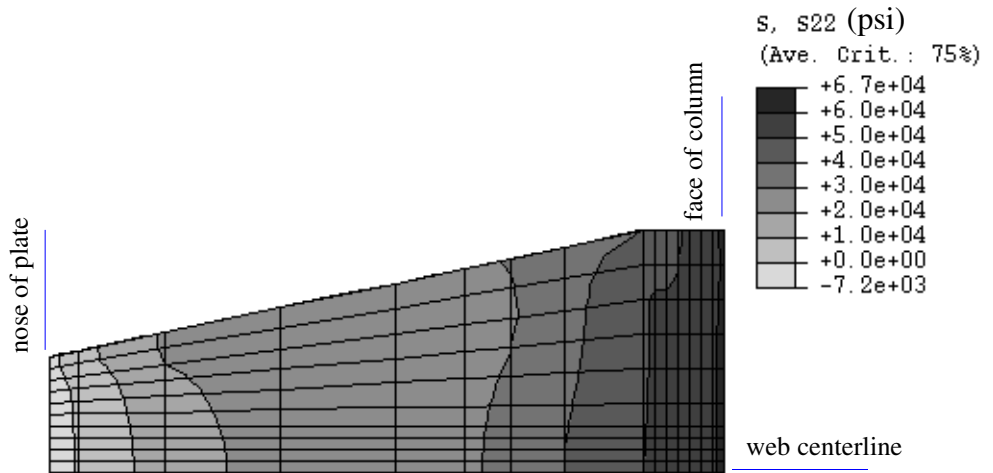


Figure 6-9 Mises stress distribution at column face in RC05 at 1-percent story drift

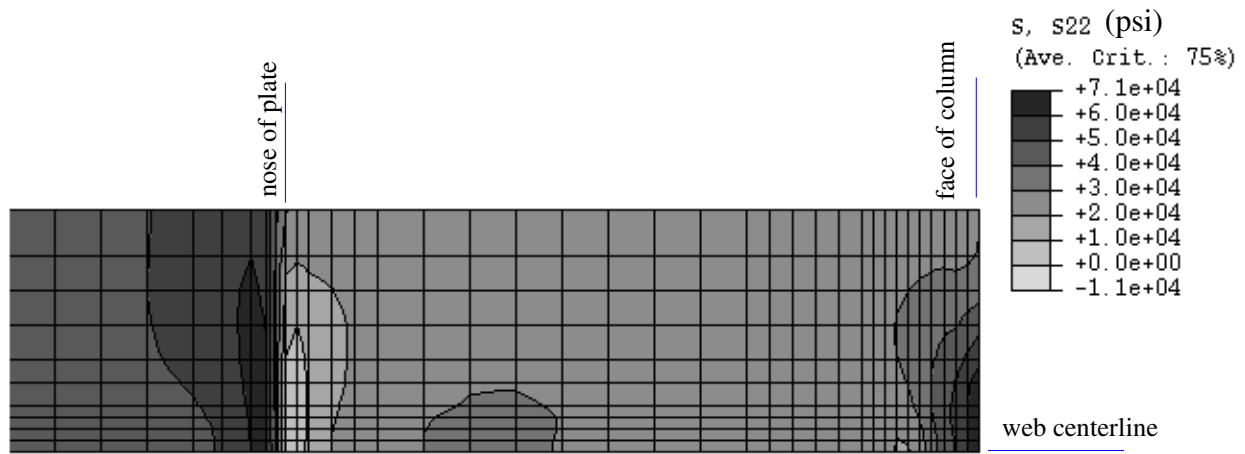


a. upper surface of RC03 cover plate

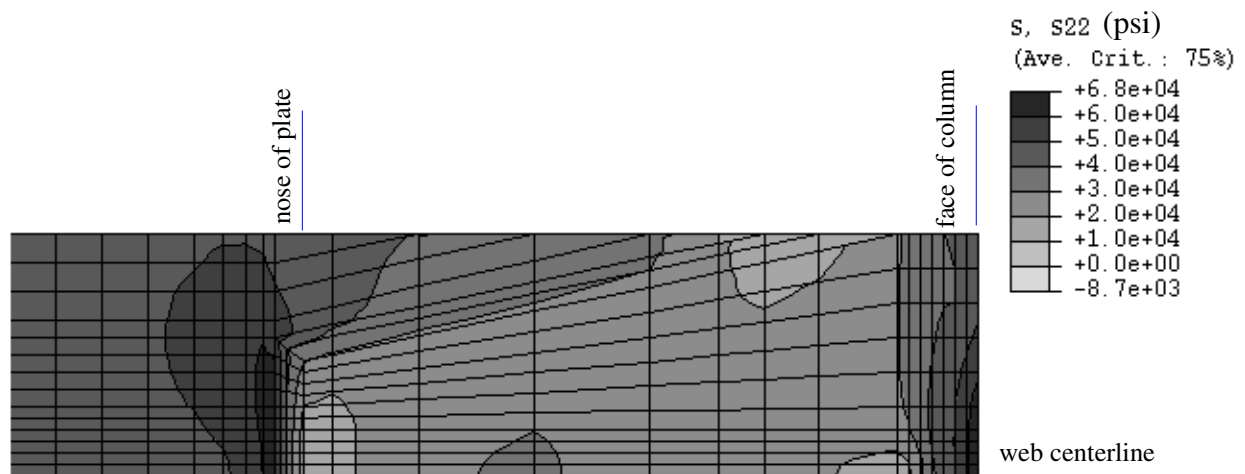


b. upper surface of RC05 cover plate

Figure 6-10 Stress S_{22} distribution along the cover plates of RC03 and RC05 at 1-percent story drift

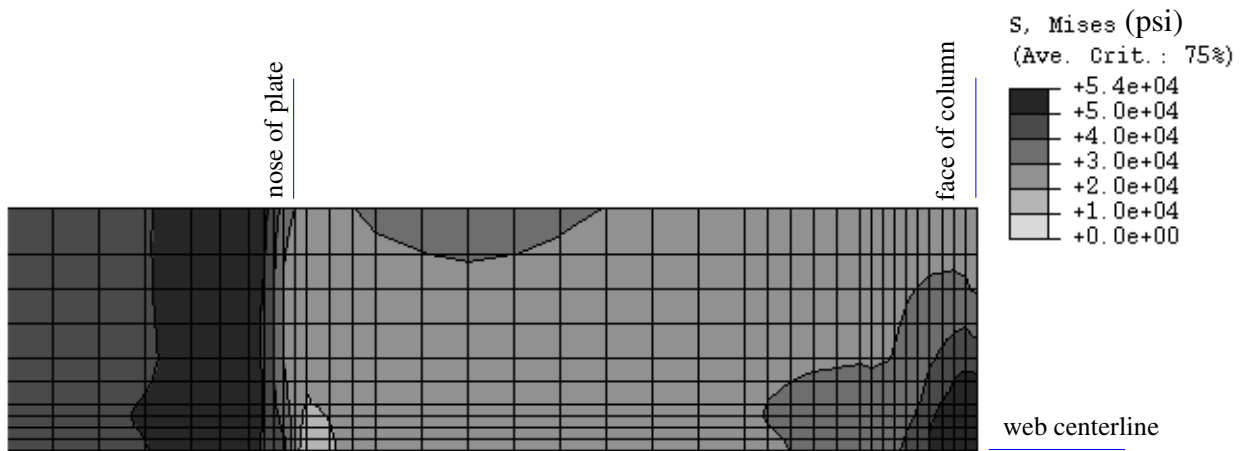


a. upper surface of RC03 beam flange

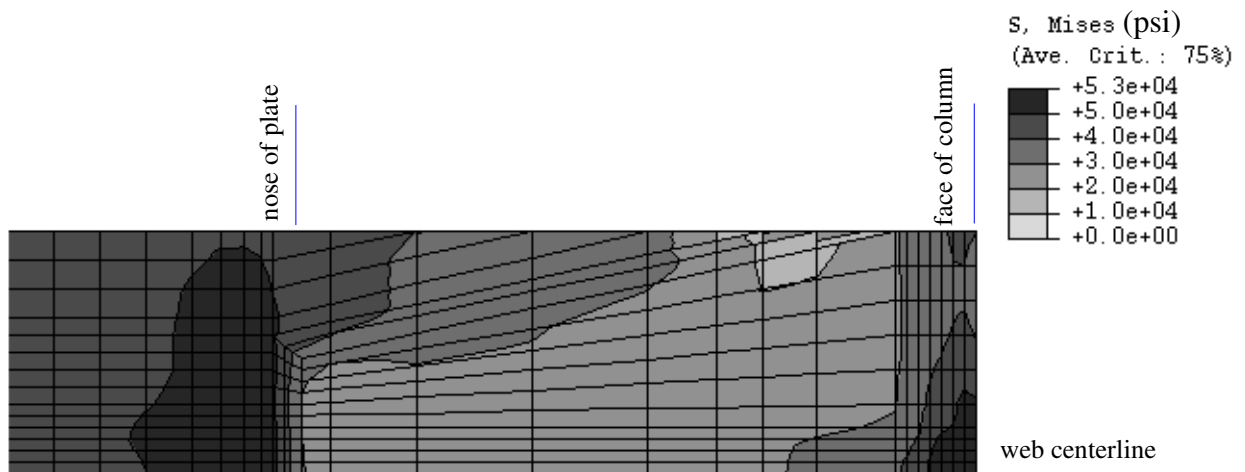


b. upper surface of RC05 beam flange

Figure 6-11 Stress S22 distribution along the beam flanges of RC03 and RC05 at 1-percent story drift

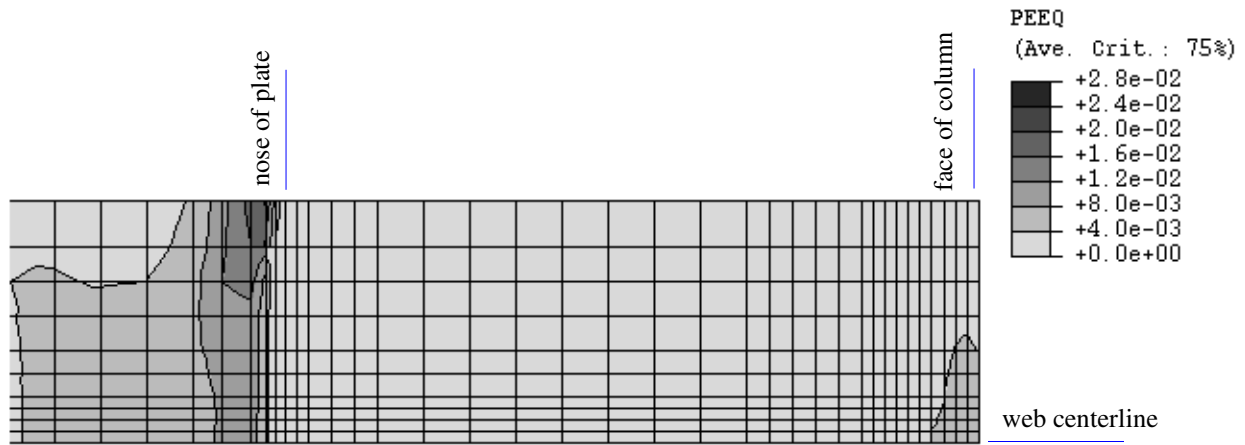


a. upper surface of RC03 beam flange

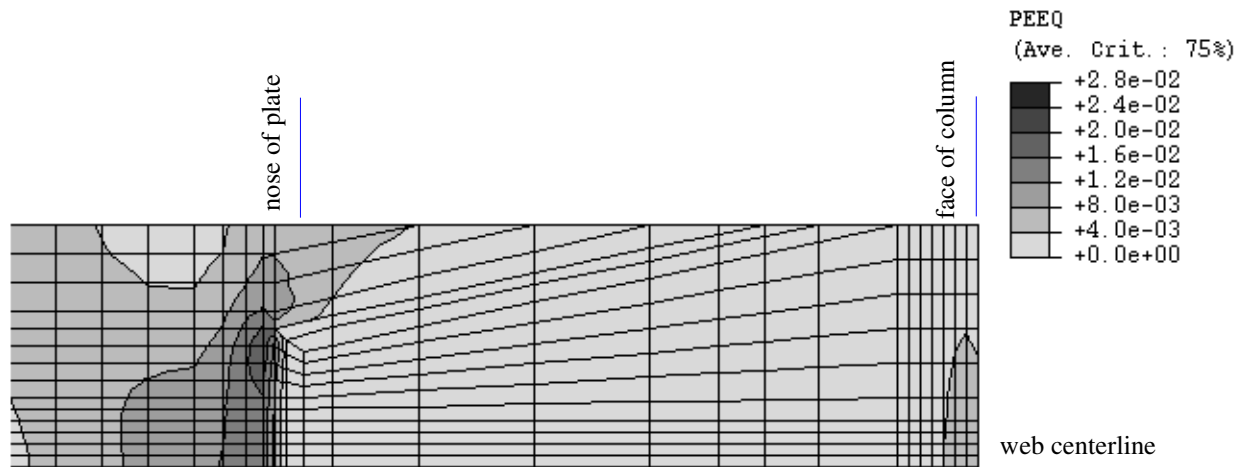


b. upper surface of RC05 beam flange

Figure 6-12 Mises stress distribution along the beam flanges of RC03 and RC05 at 1-percent story drift



a. upper surface of RC03 beam flange



b. upper surface of RC05 beam flange

Figure 6-13 Equivalent plastic strain distributions on the beam flanges of RC03 and RC06 at 2-percent story drift

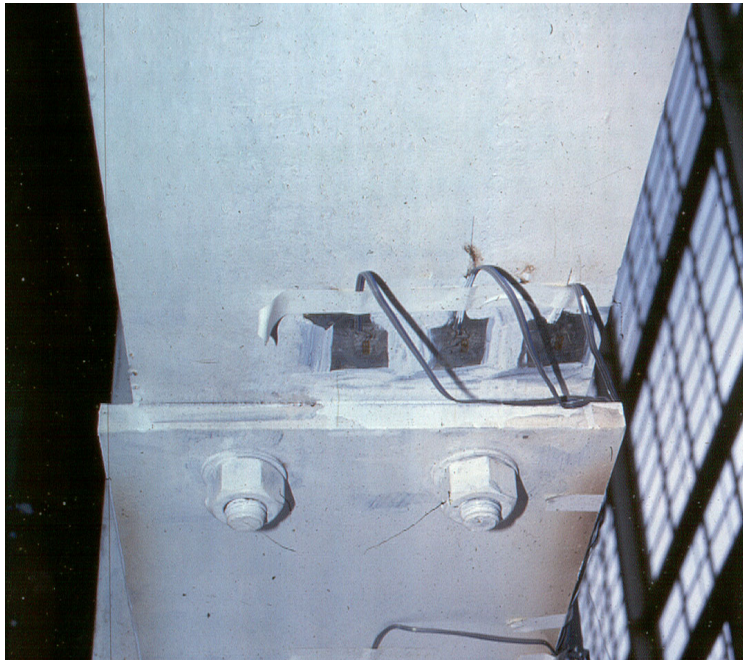


Figure 6-14 Photograph of SAC Phase I cover-plate specimen AN1 (Whittaker et al. 1996)

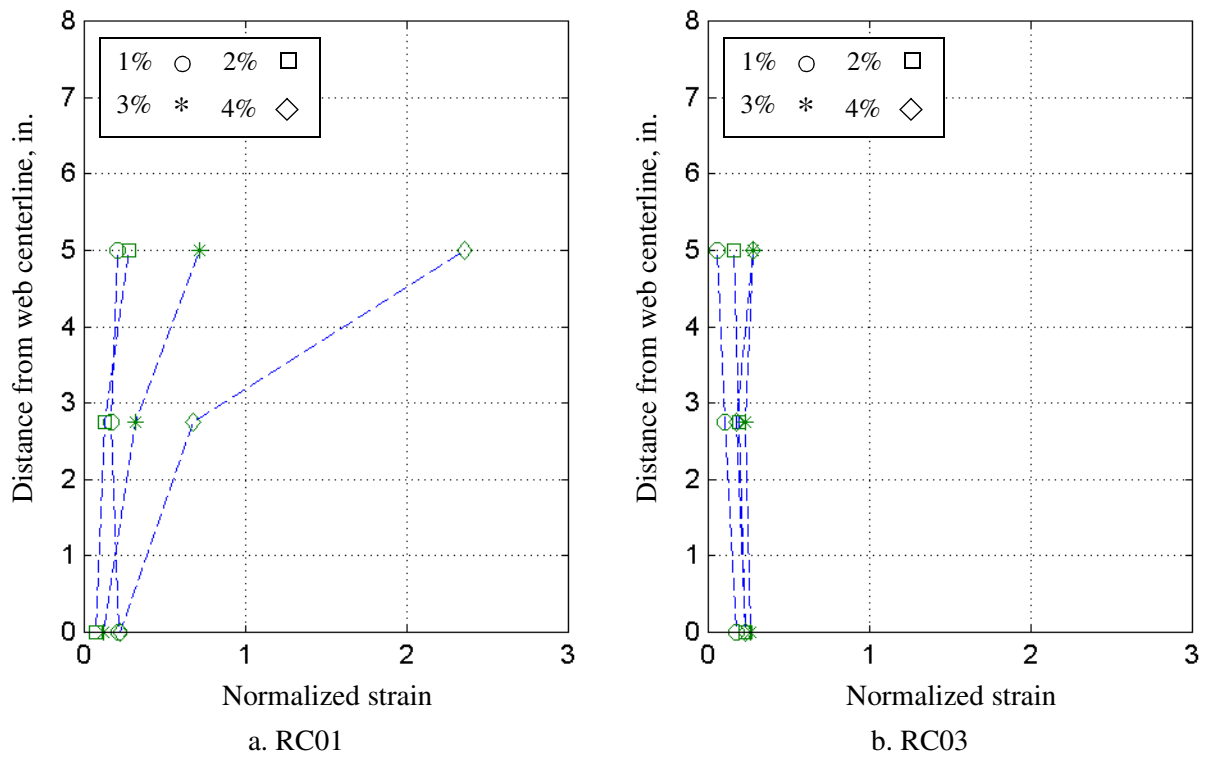
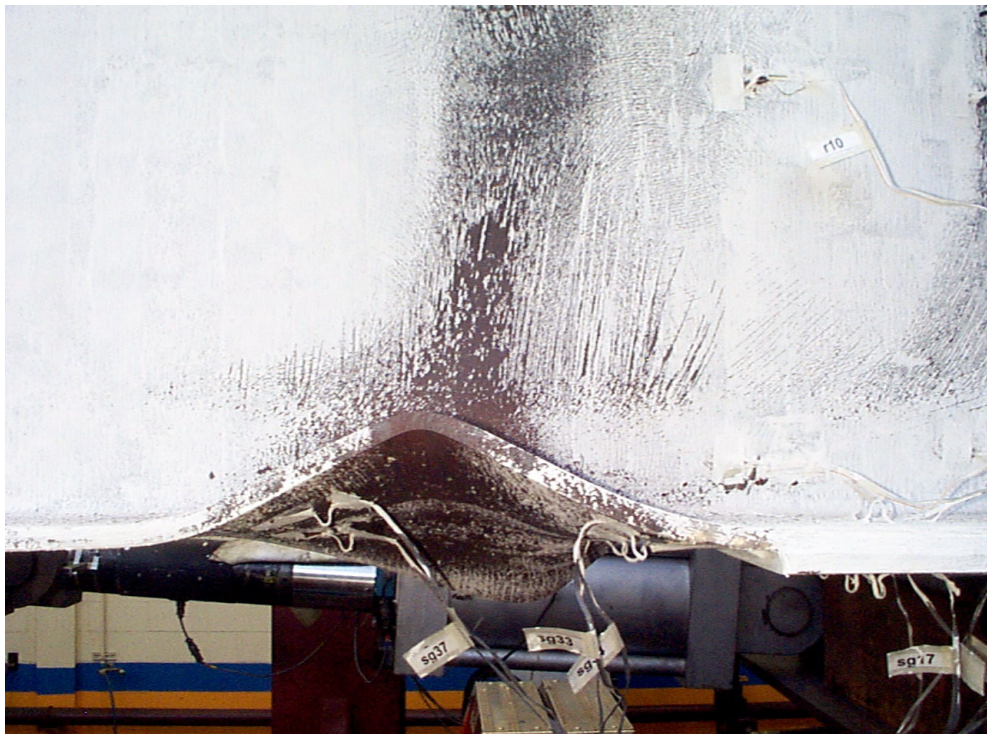


Figure 6-15 Measured longitudinal (2-2) strains in cover-plate specimens RC01 and RC03 at 13 in. (330 mm) from the column face

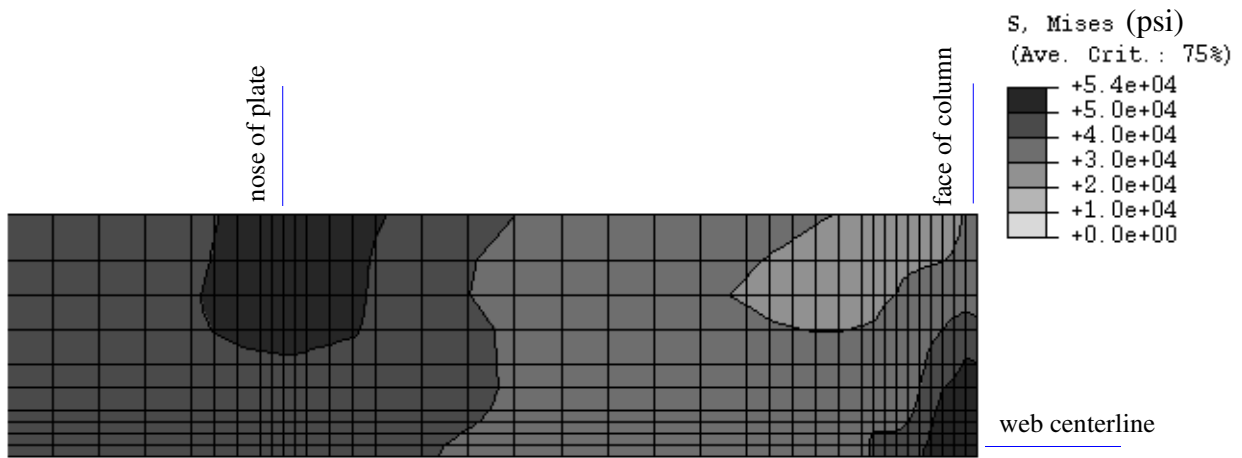


a. RC01 (2-sided fillet weld)

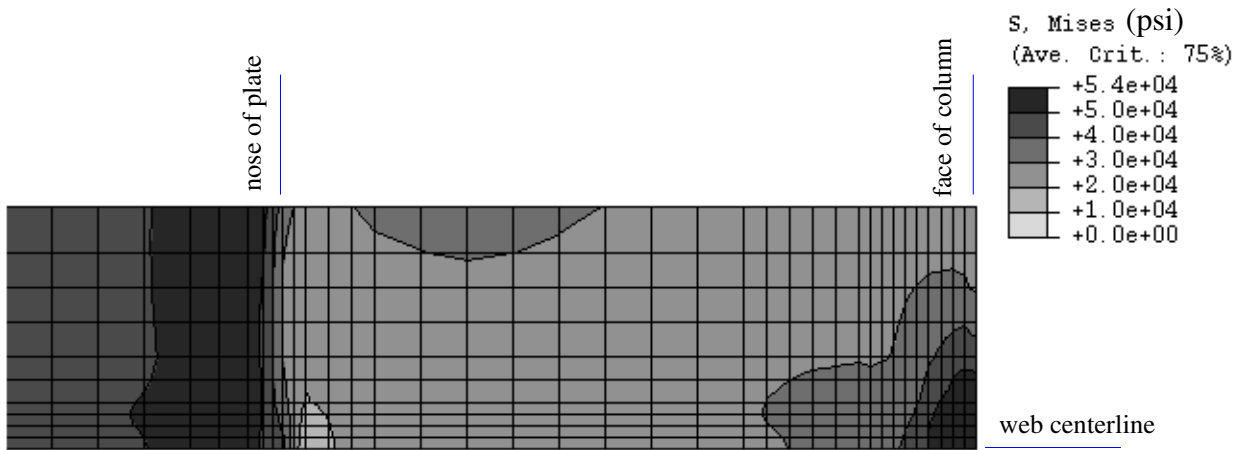


b. RC03 (3-sided fillet weld)

Figure 6-16 Deformations in cover plates and flanges of RC01 and RC03 at 4-percent story drift

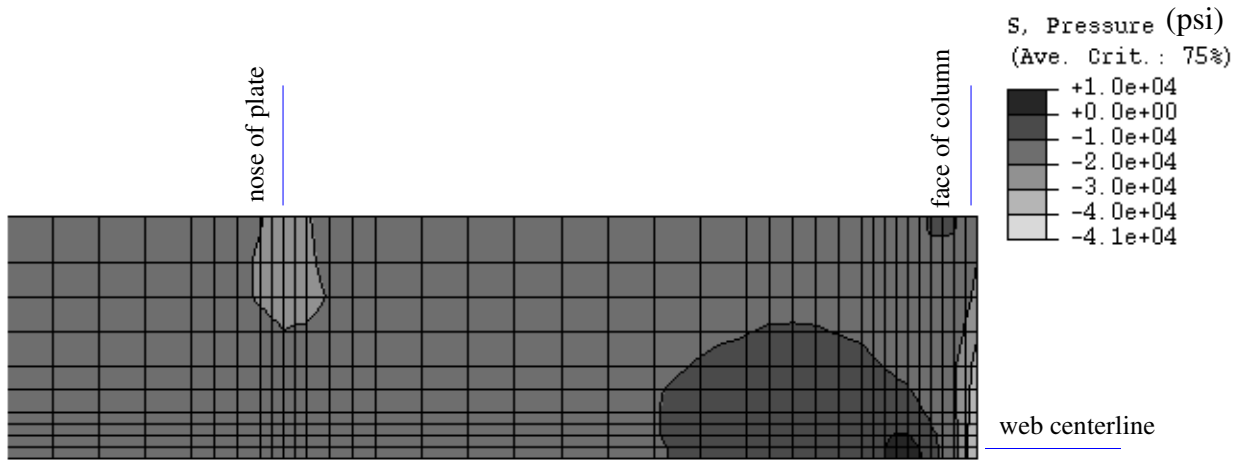


a. RC01 (2-sided fillet weld)

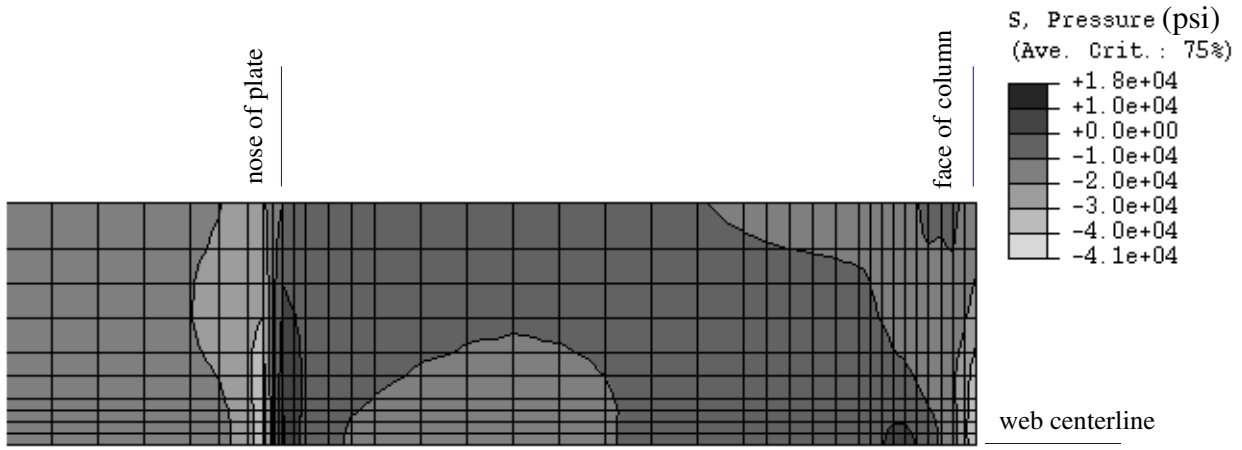


b. RC03 (3-sided fillet weld)

Figure 6-17 Mises stress distribution along the beam flanges of RC01 and RC03 at 1-percent story drift

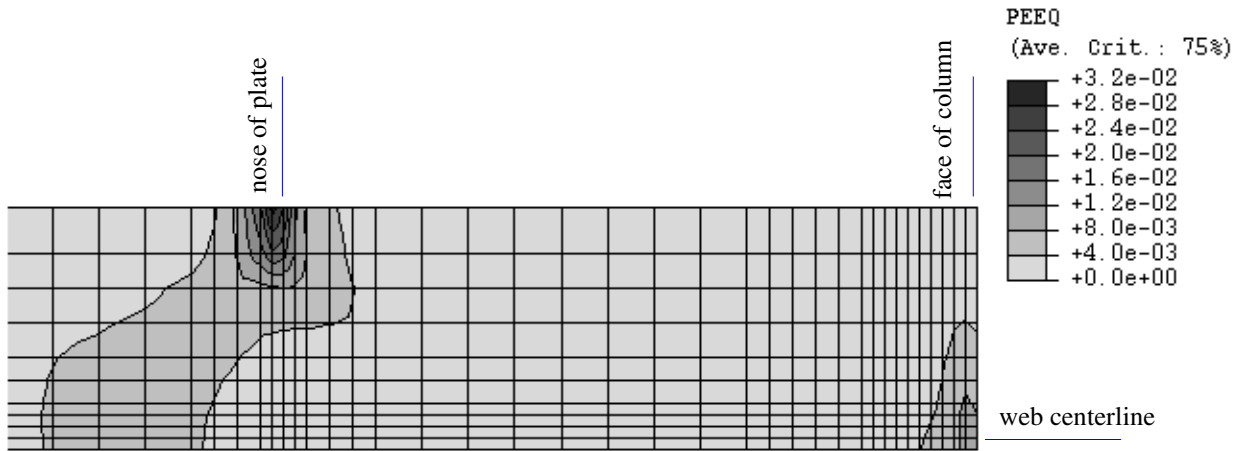


a. upper surface of RC01 (2-sided fillet weld)

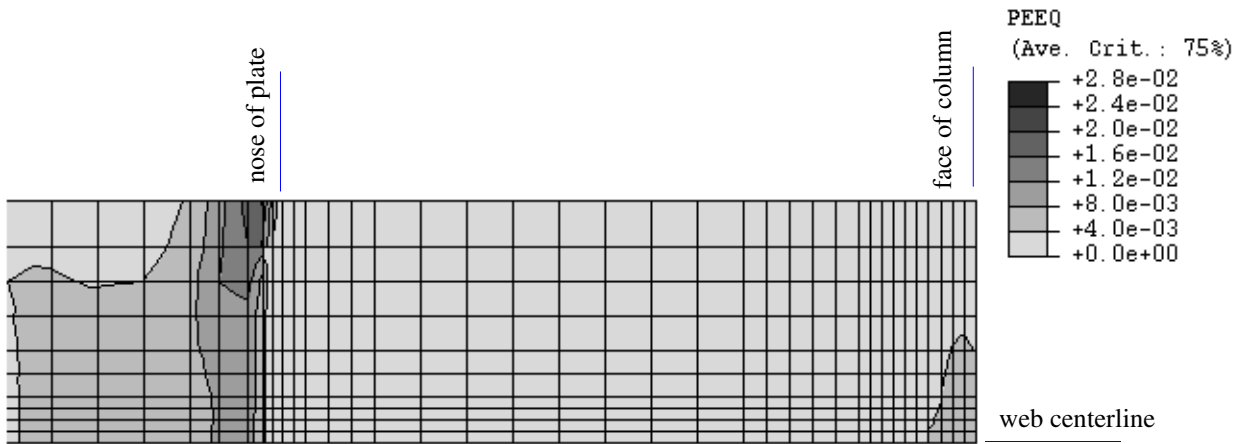


b. upper surface of RC03 (3-sided fillet weld)

Figure 6-18 Hydrostatic pressure distribution along the beam flanges of RC01 and RC03 at 1-percent story drift

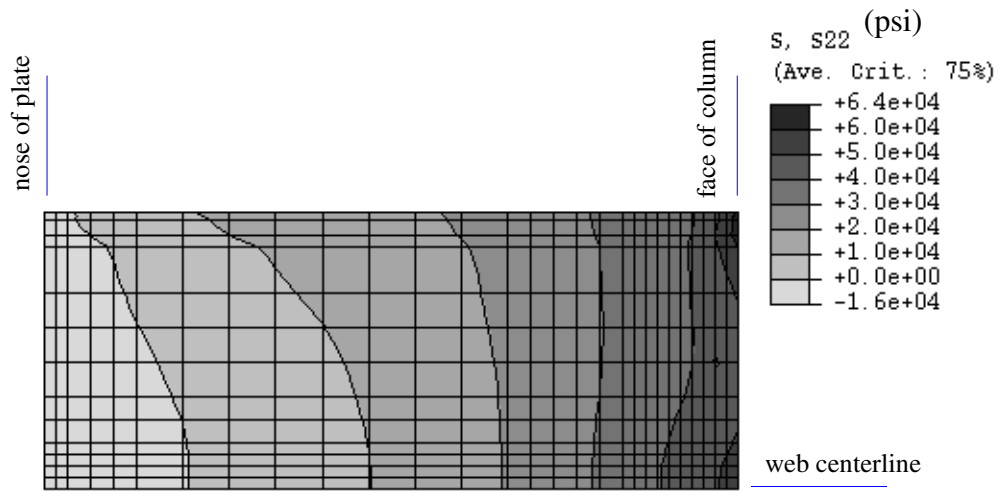


a. upper surface of RC01 (2-sided fillet weld)

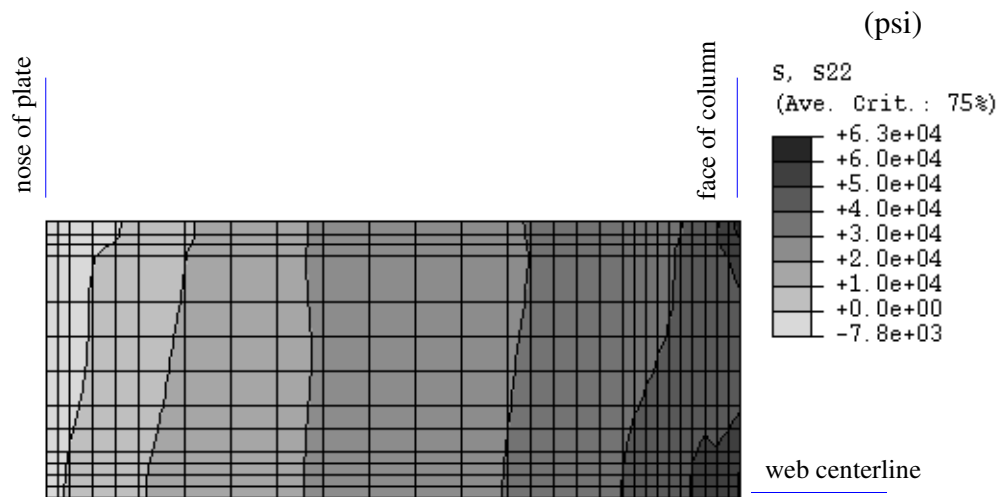


b. upper surface of RC03 (3-sided fillet weld)

Figure 6-19 Equivalent plastic strain distribution along the beam flanges of RC01 and RC03 at 2-percent story drift

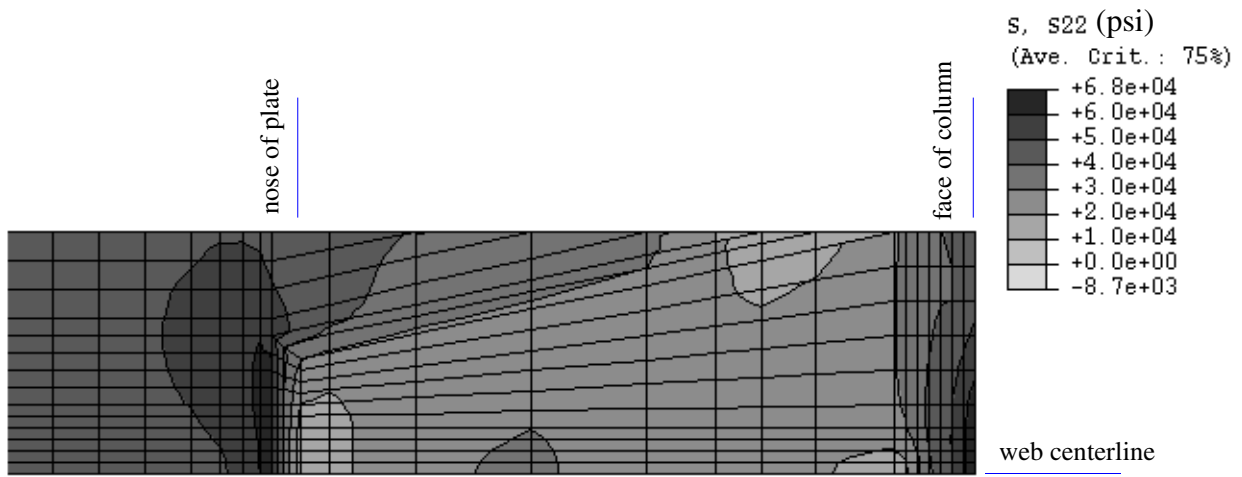


a. upper surface of RC01 (2-sided fillet weld)

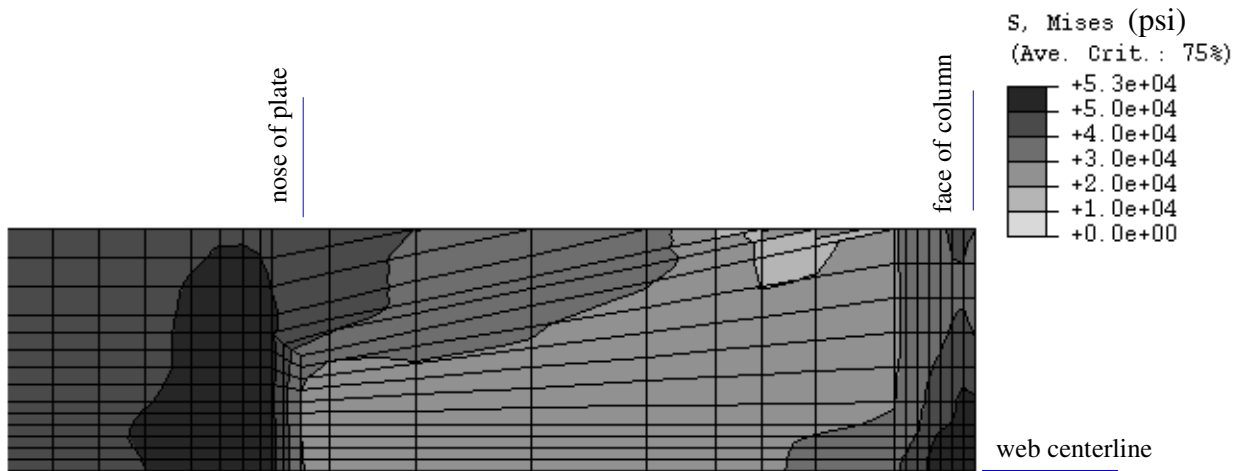


b. upper surface of RC03 (3-sided fillet weld)

Figure 6-20 Stress S_{22} distribution along the cover plates of RC01 and RC03 at 1-percent story drift



a. S22 distribution on upper surface of beam flange



b. Mises stress distribution on upper surface of beam flange

Figure 6-21 Stress S22 and Mises distributions along the beam flange of RC05 at 1-percent story drift

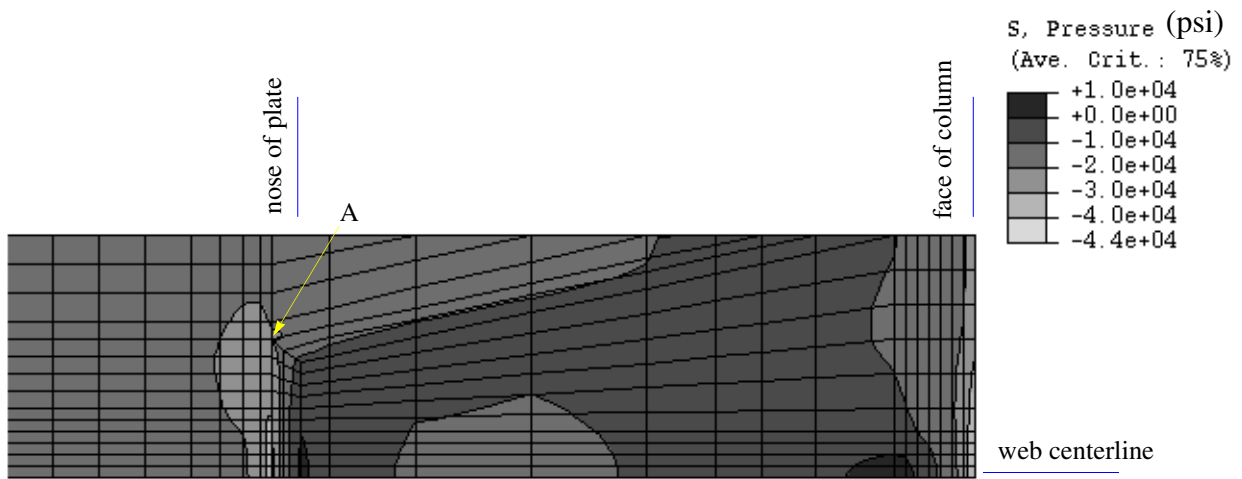
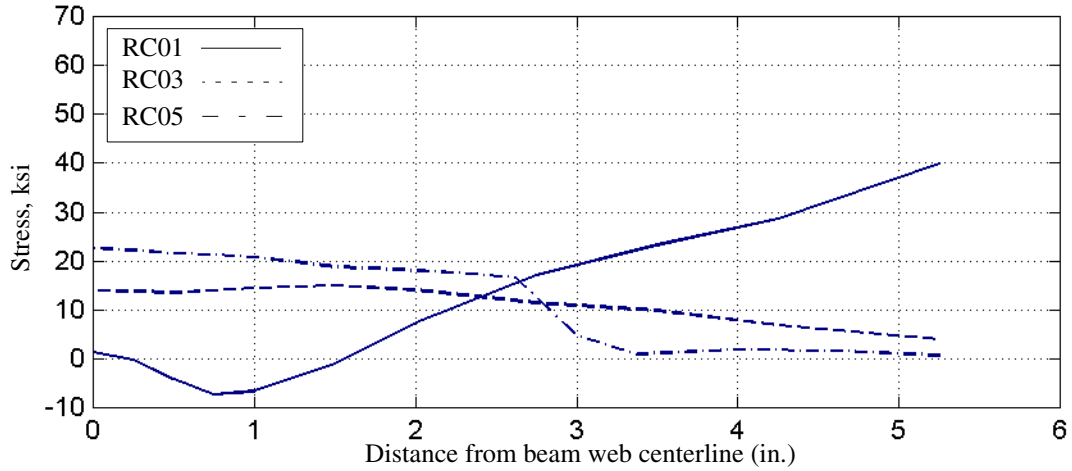
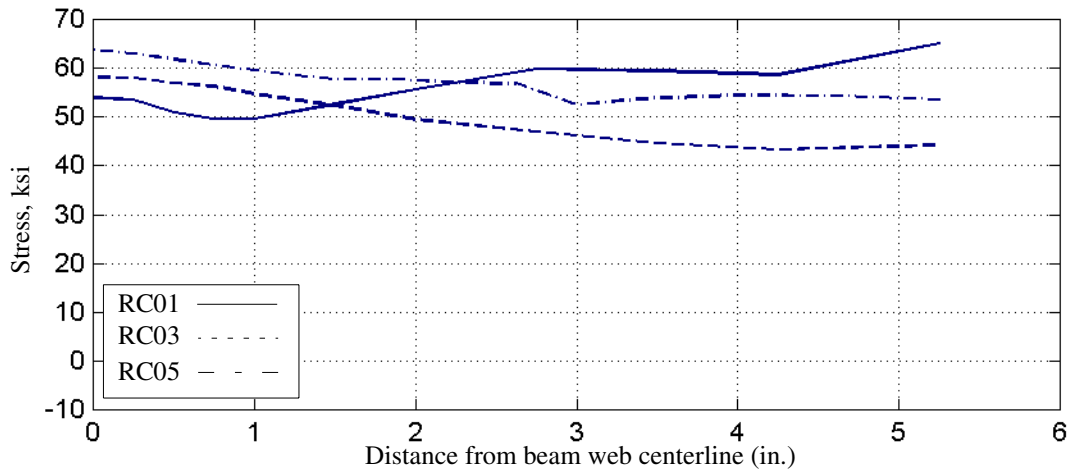


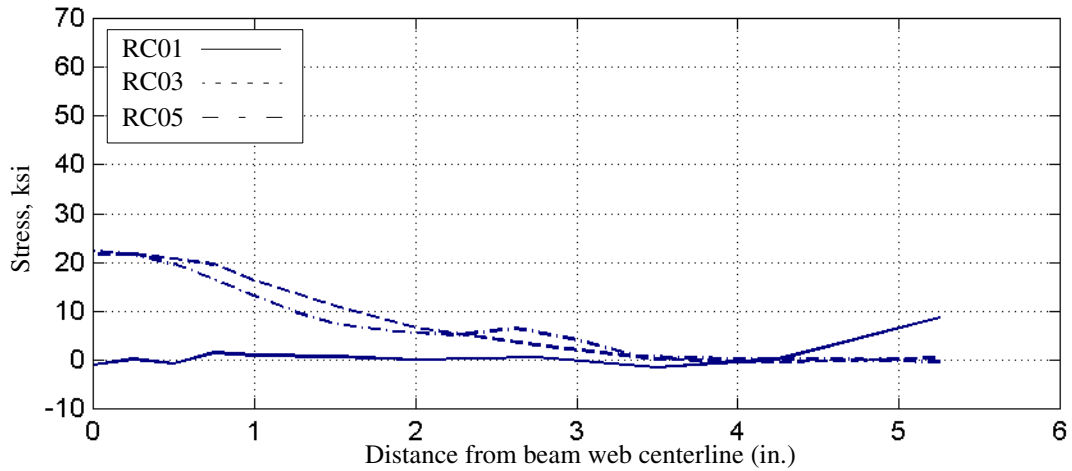
Figure 6-22 Hydrostatic pressure distribution along the upper surface of the beam flange of RC05 at 1-percent story drift



a. *S11*

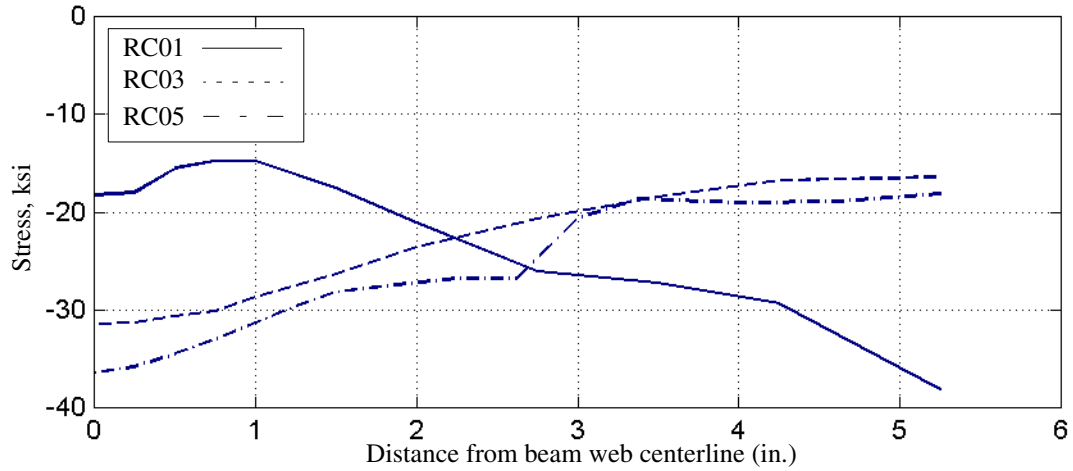


b. *S22*

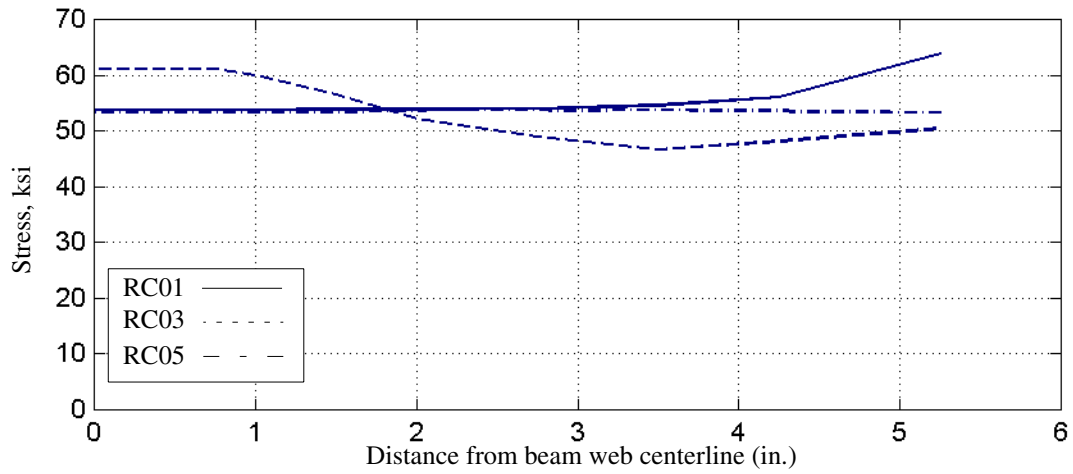


c. *S33*

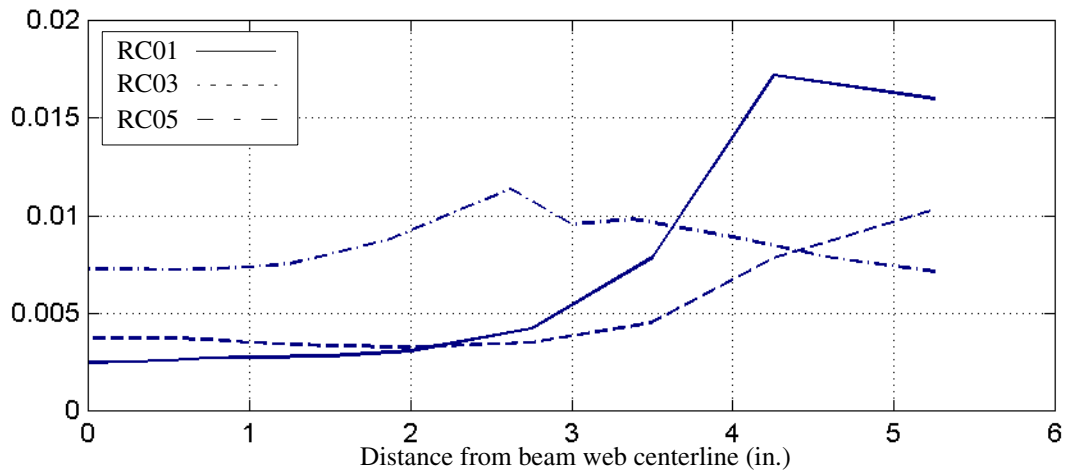
Figure 6-23 Normal stress distributions along the upper surface of the beam flanges for RC01, RC03, and RC05, at 2-percent story drift



a. Hydrostatic pressure

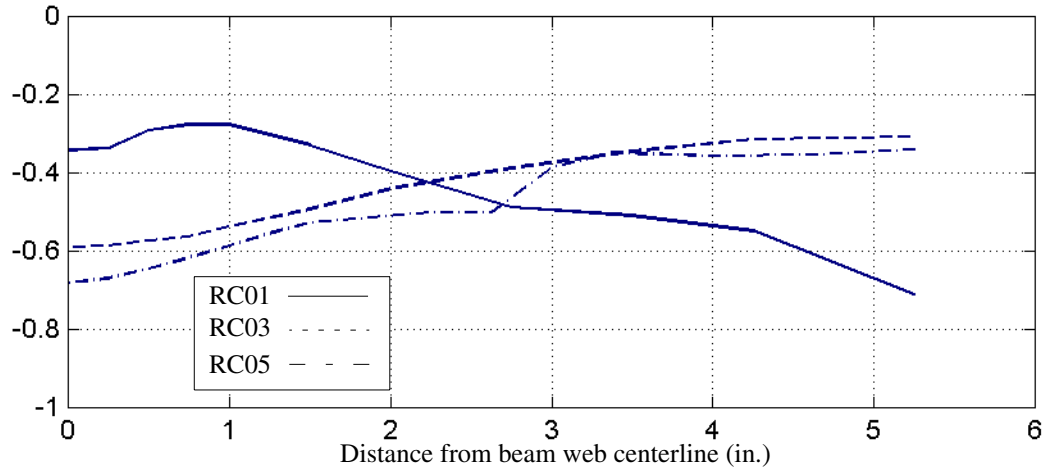


b. Mises stress

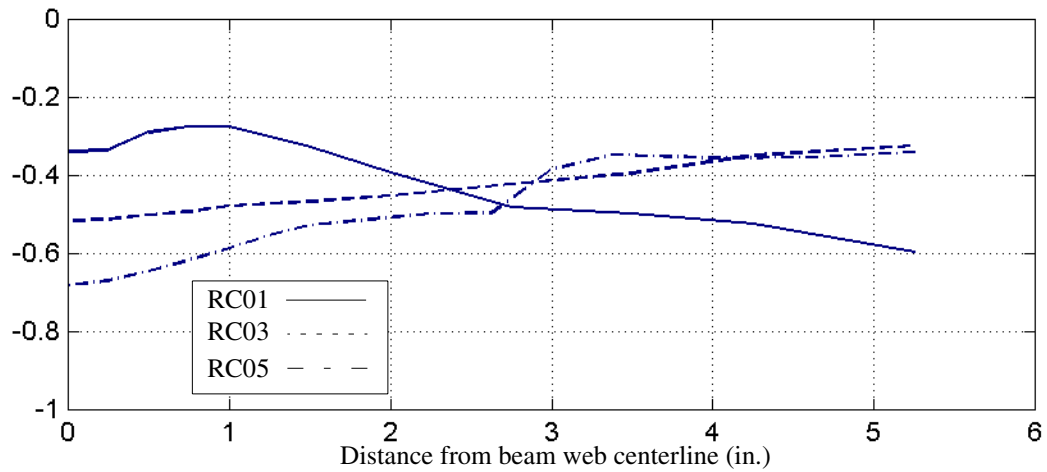


c. Equivalent plastic strain

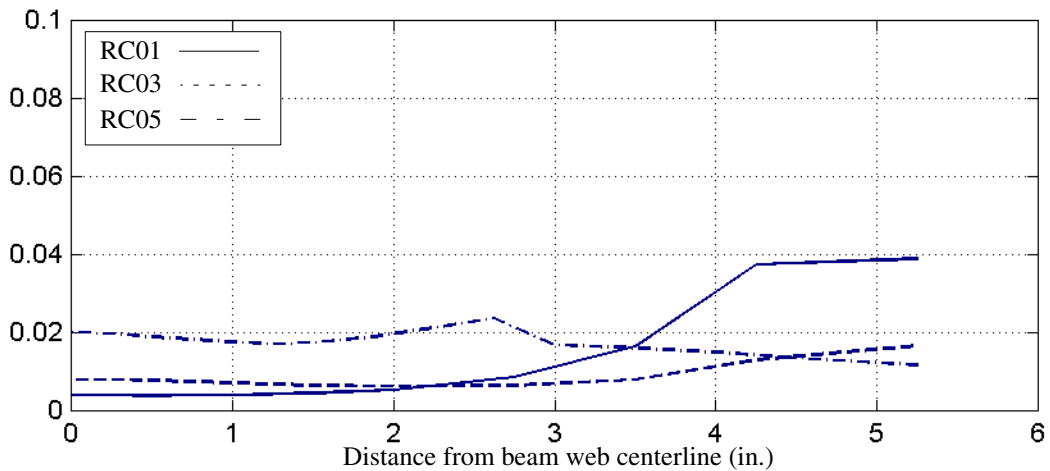
Figure 6-24 Response distributions along the upper surface of the beam flanges for RC01, RC03, and RC05, at 2-percent story drift



a. Pressure Index



b. Triaxiality Ratio



c. Rupture Index

Figure 6-25 Distributions on Pressure Index, Triaxiality Ratio, and Rupture Index along the upper surface of the beam flanges for RC01, RC03, and RC05, at 2-percent story drift

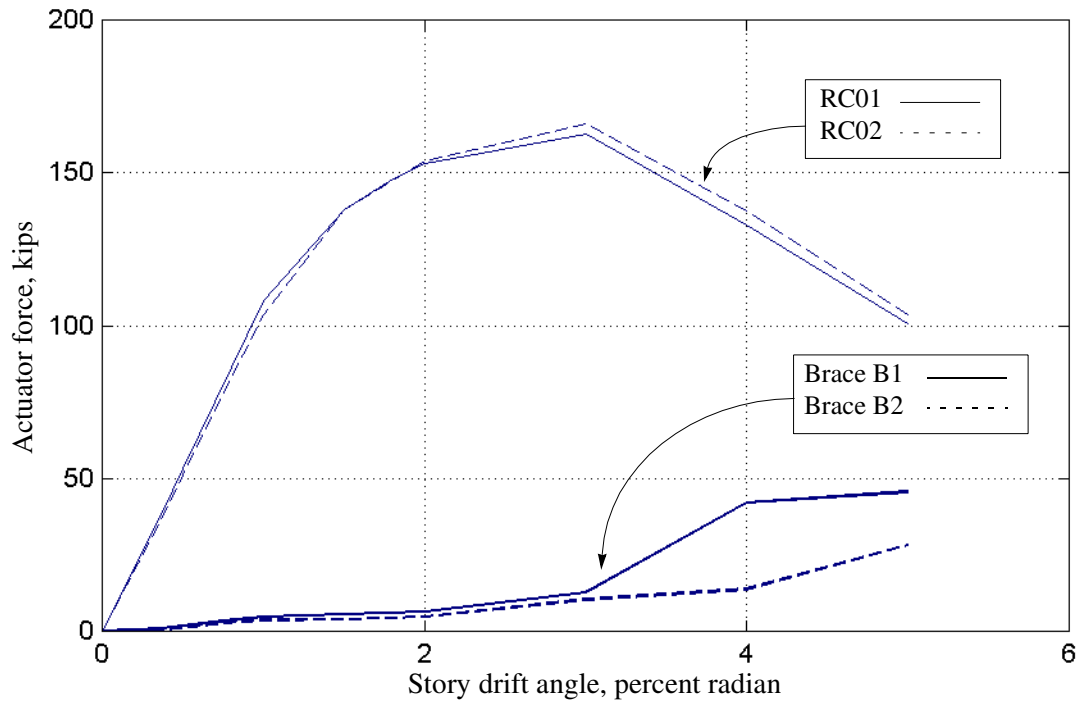


Figure 6-26 Backbone curves for RC01 and RC02 and forces in Braces B1 and B2 of RC02

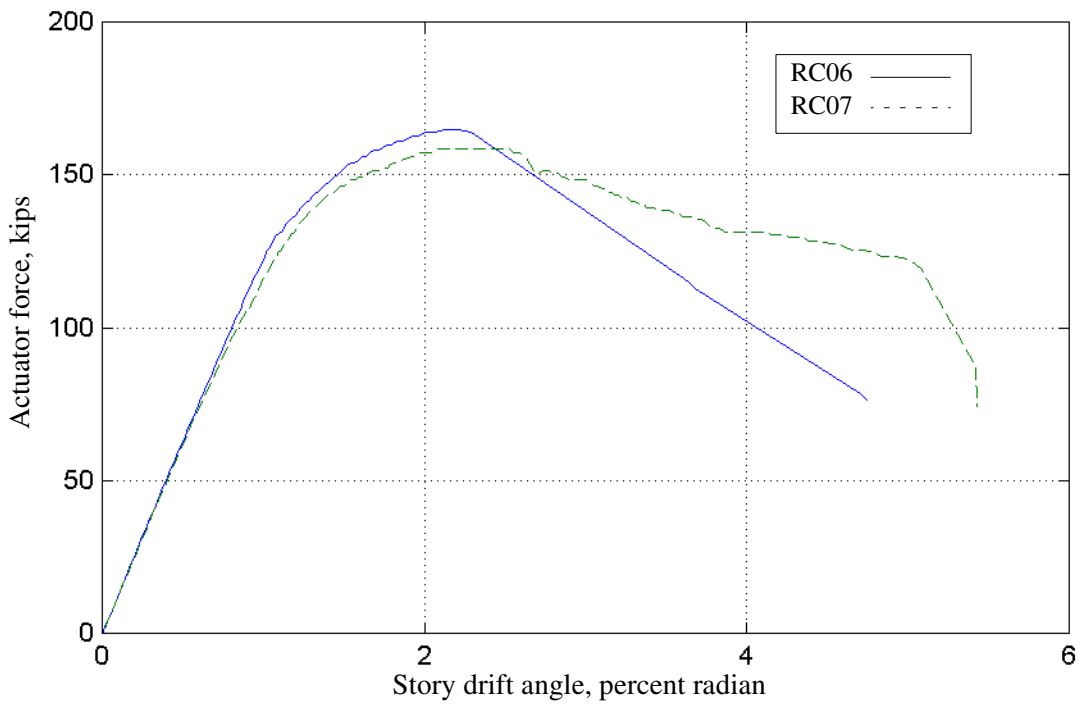


Figure 6-27 Backbone curves for RC06 and RC07

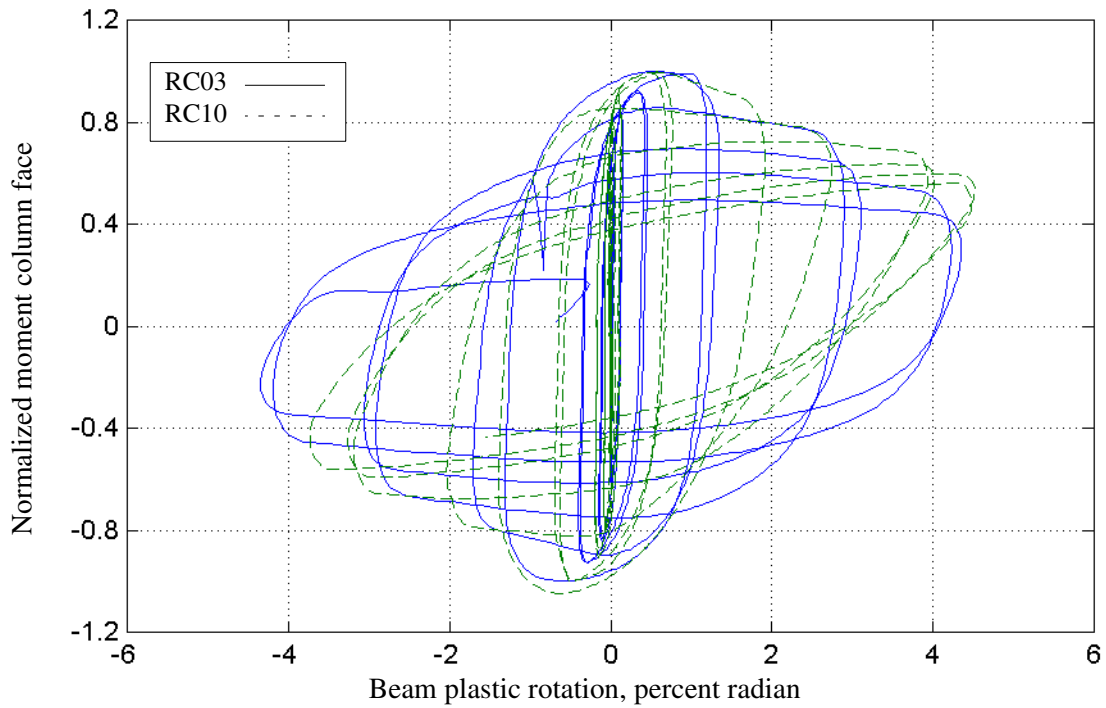


Figure 6-28 Normalized moment versus beam plastic rotation for RC03 and RC10

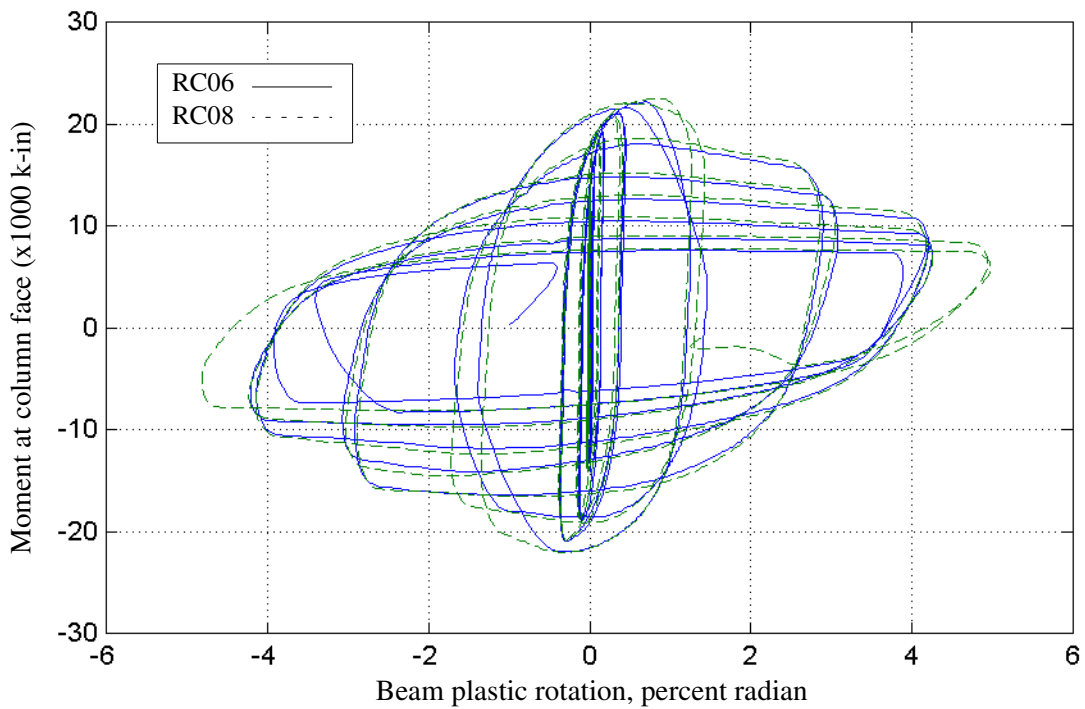


Figure 6-29 Comparison of global responses of RC06 and RC08

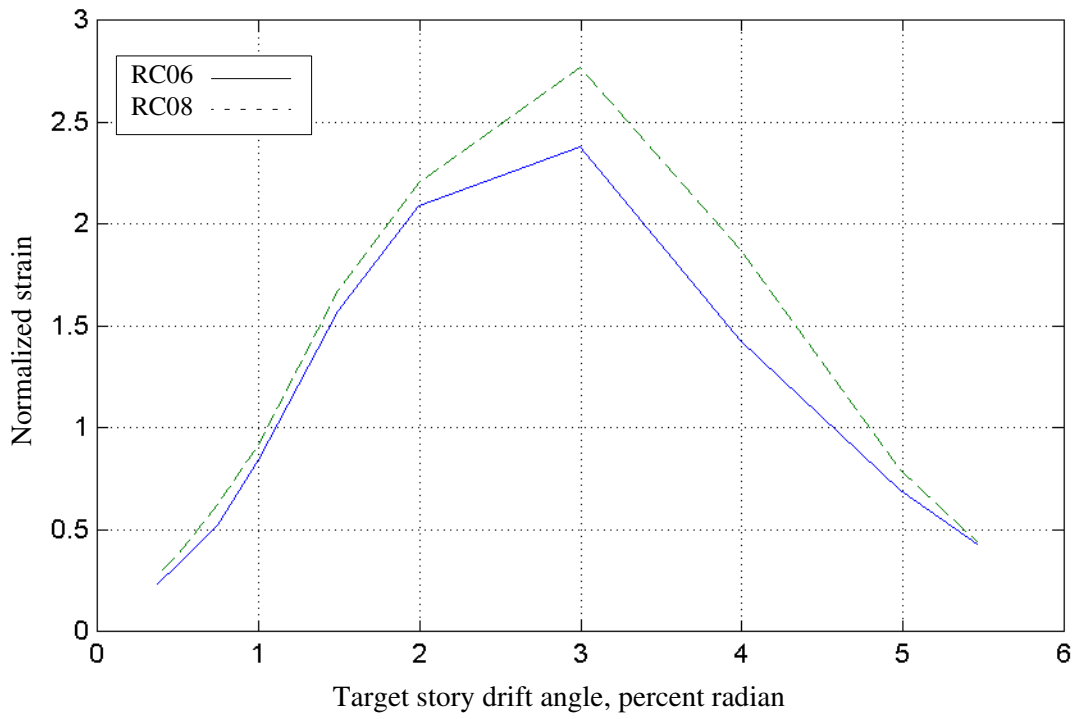


Figure 6-30 Measured strains in the flange plates of RC06 and RC08 at different story drift levels

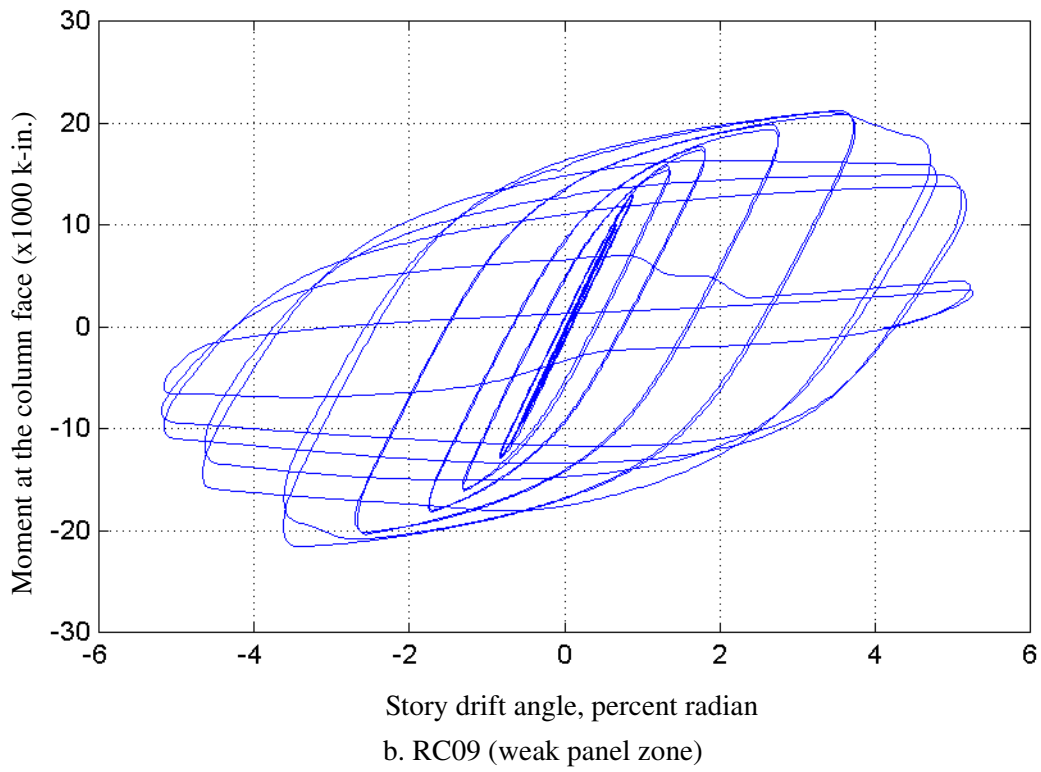
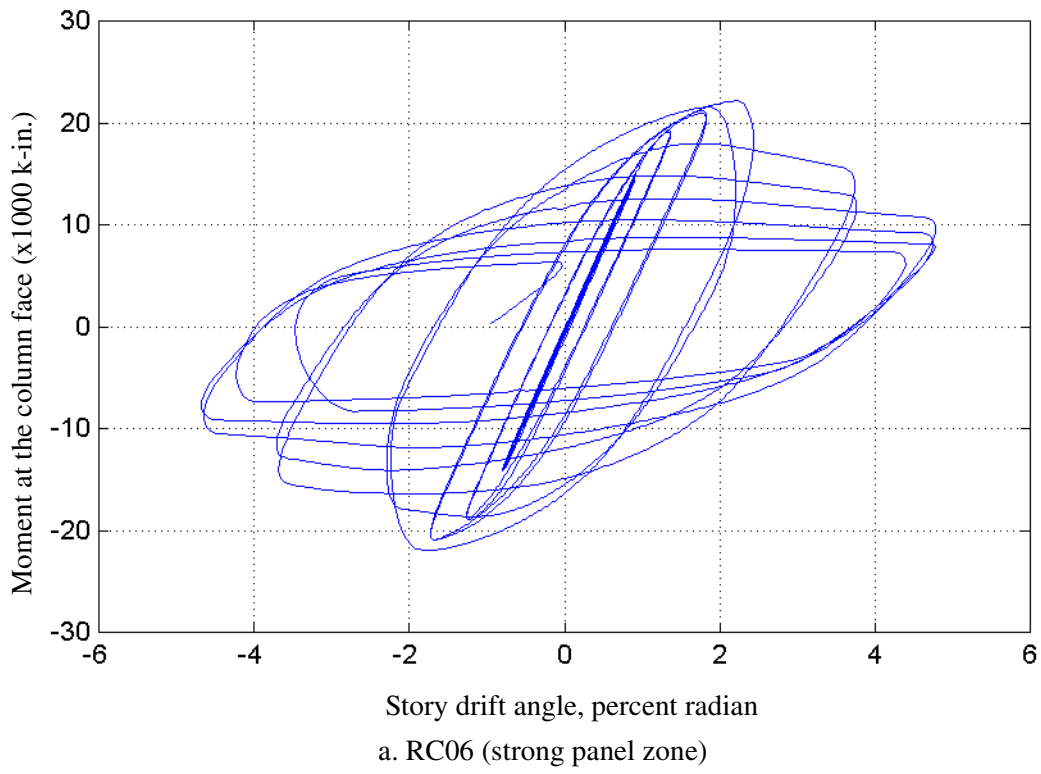


Figure 6-31 Moment versus story drift index relationships for RC06 and RC09

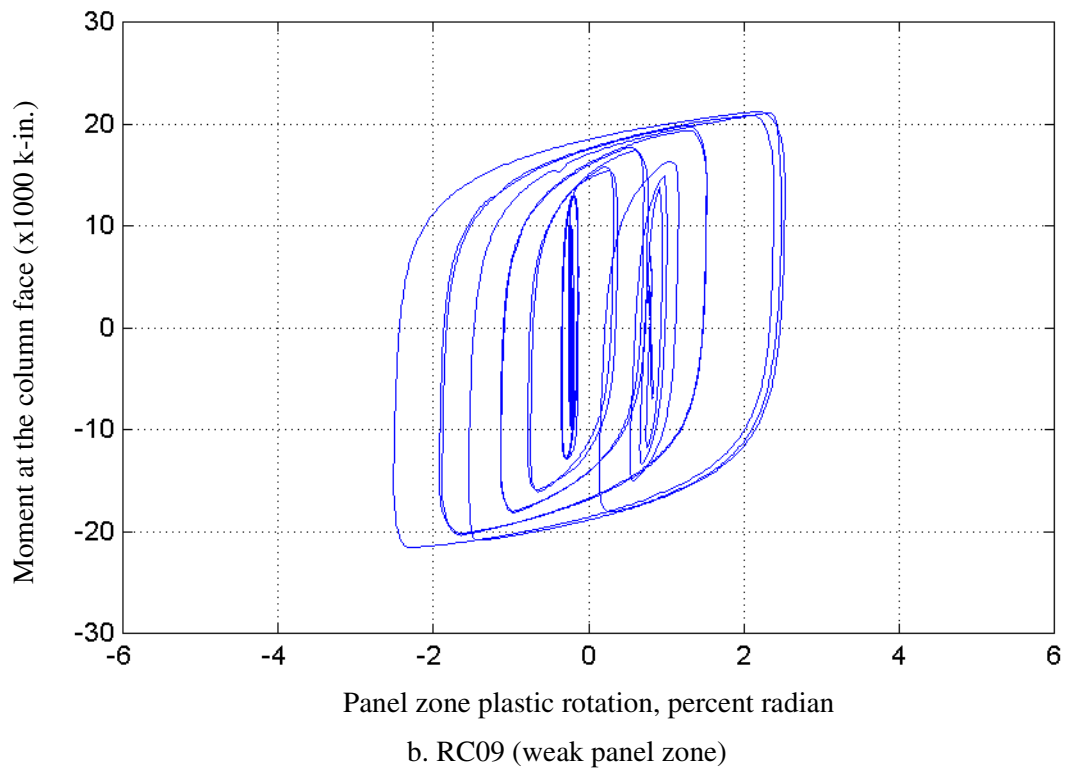
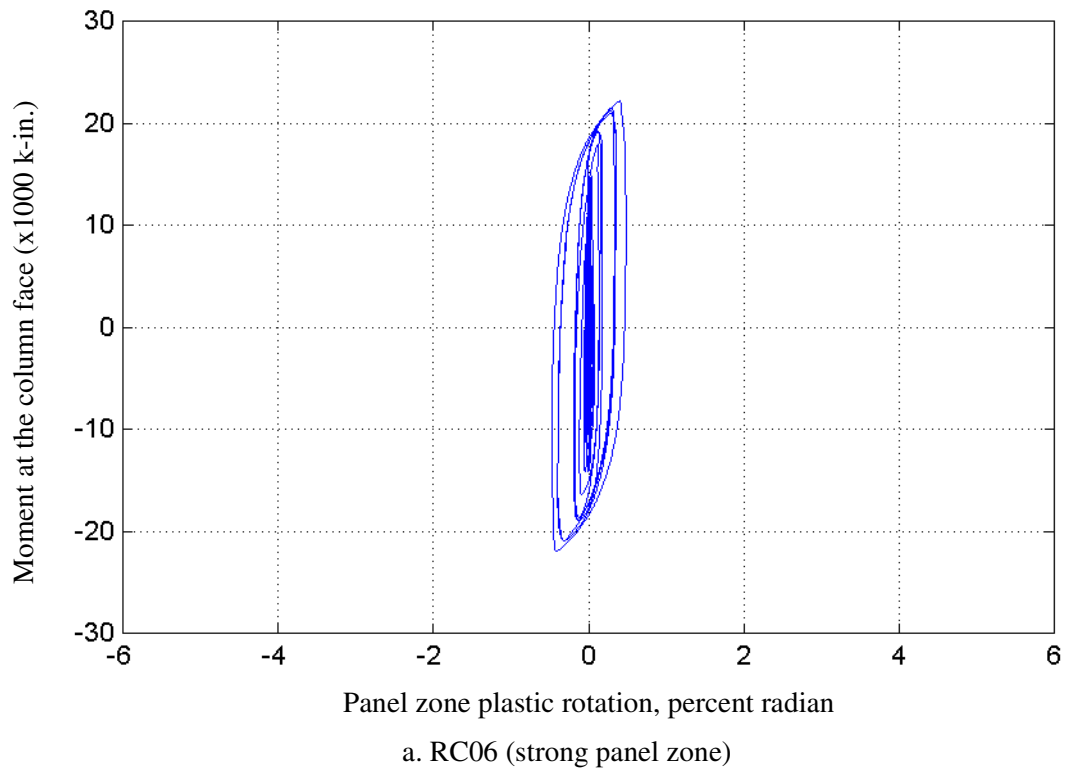


Figure 6-32 Moment versus panel zone plastic rotation relationships for RC06 and RC09

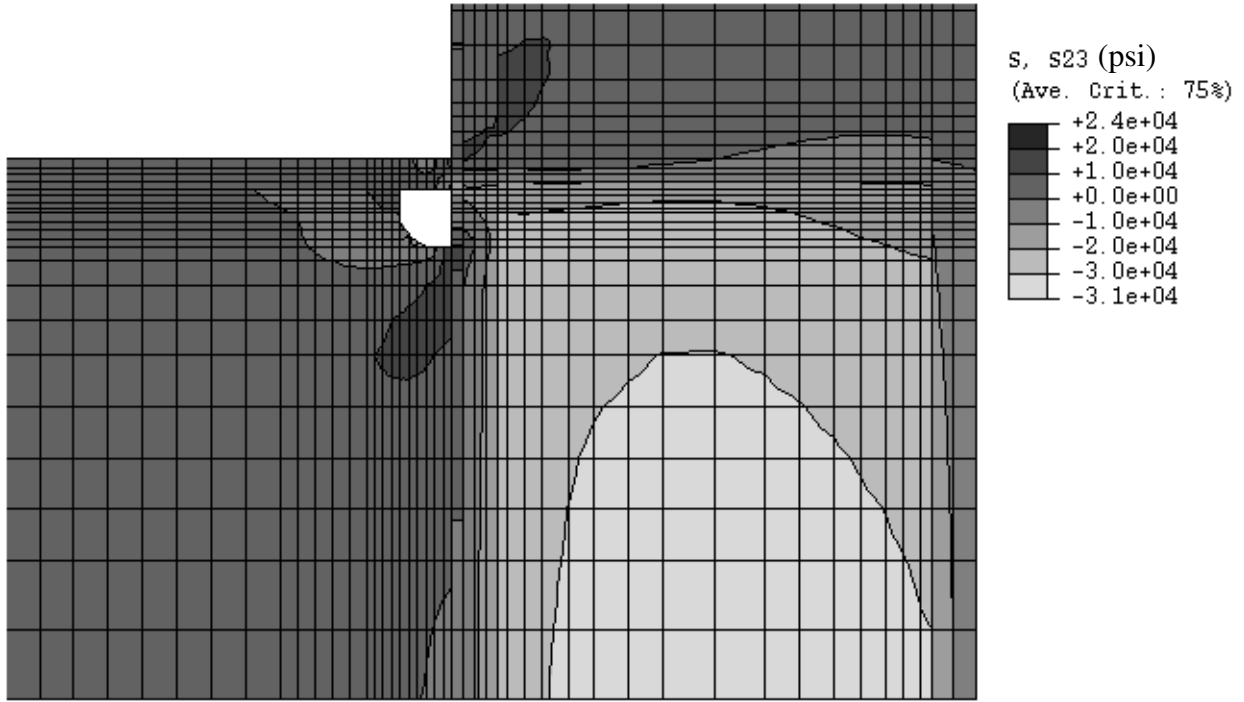


Figure 6-33 Stress (*S23*) distribution in panel zone of RC09 at 1-percent story drift

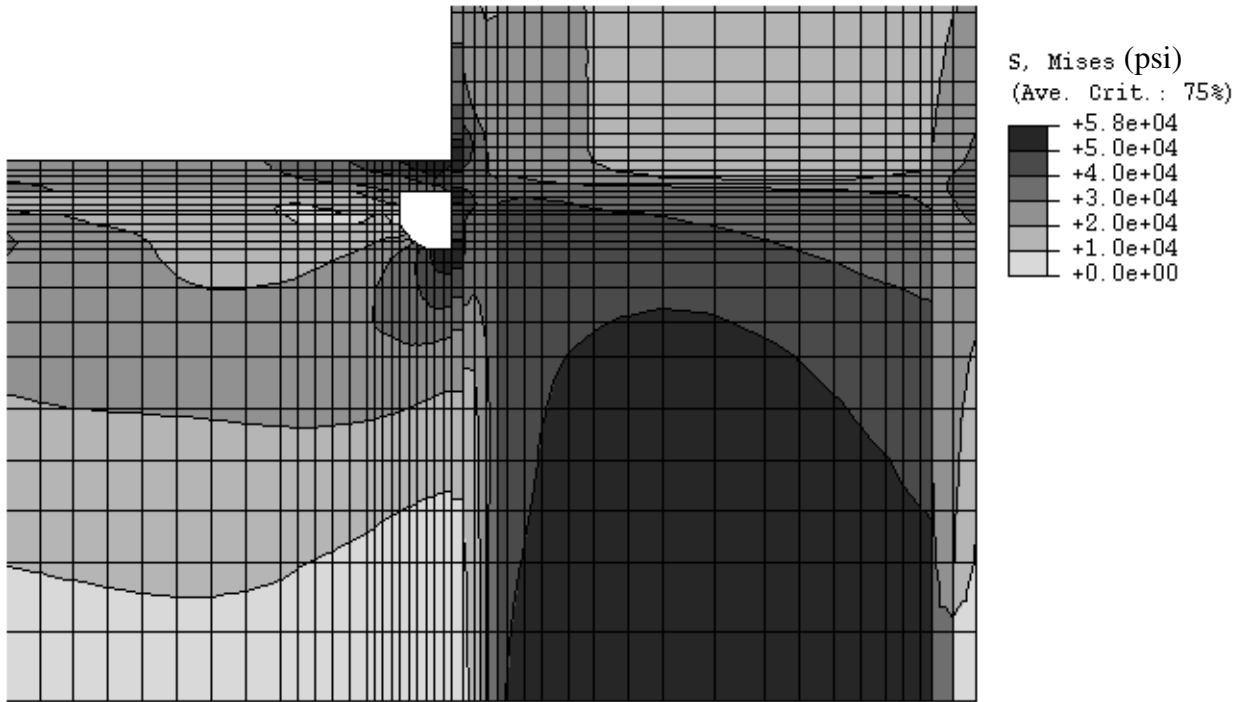
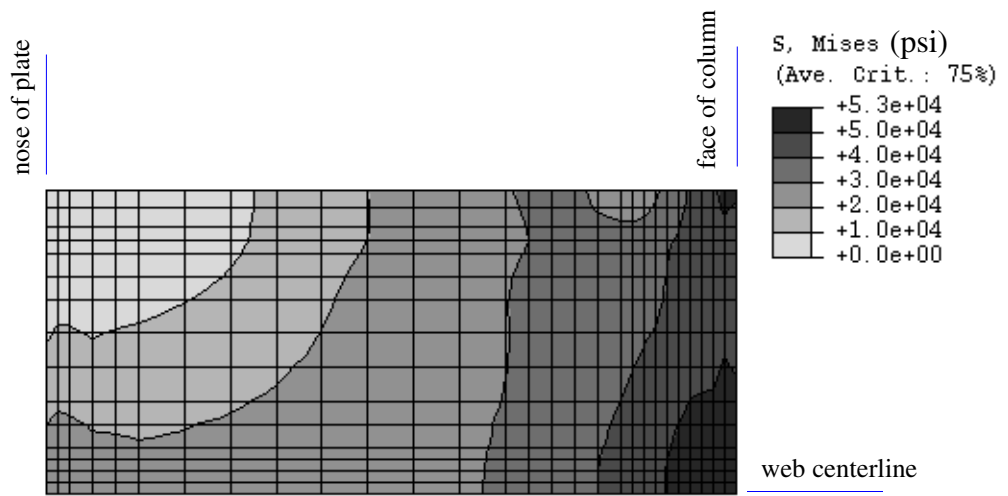
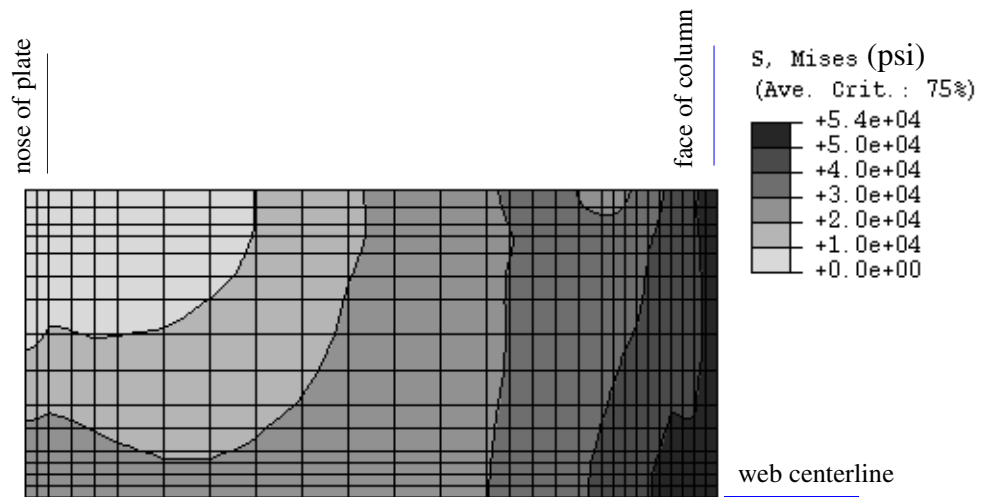


Figure 6-34 Mises stress distribution in panel zone of RC09 at 1-percent story drift

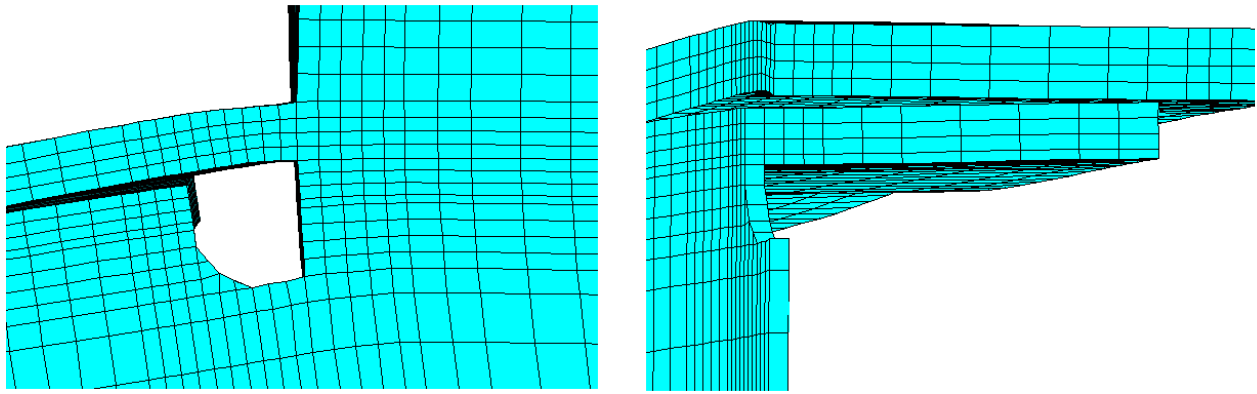


a. RC09 (weak panel zone)



b. RC06 (strong panel zone)

Figure 6-35 Mises stress distribution on upper surface of flange plates of RC09 and RC06 at 1-percent story drift



a. elevation

b. cross section

Figure 6-36 Deformations in RC09 at 2-percent story drift

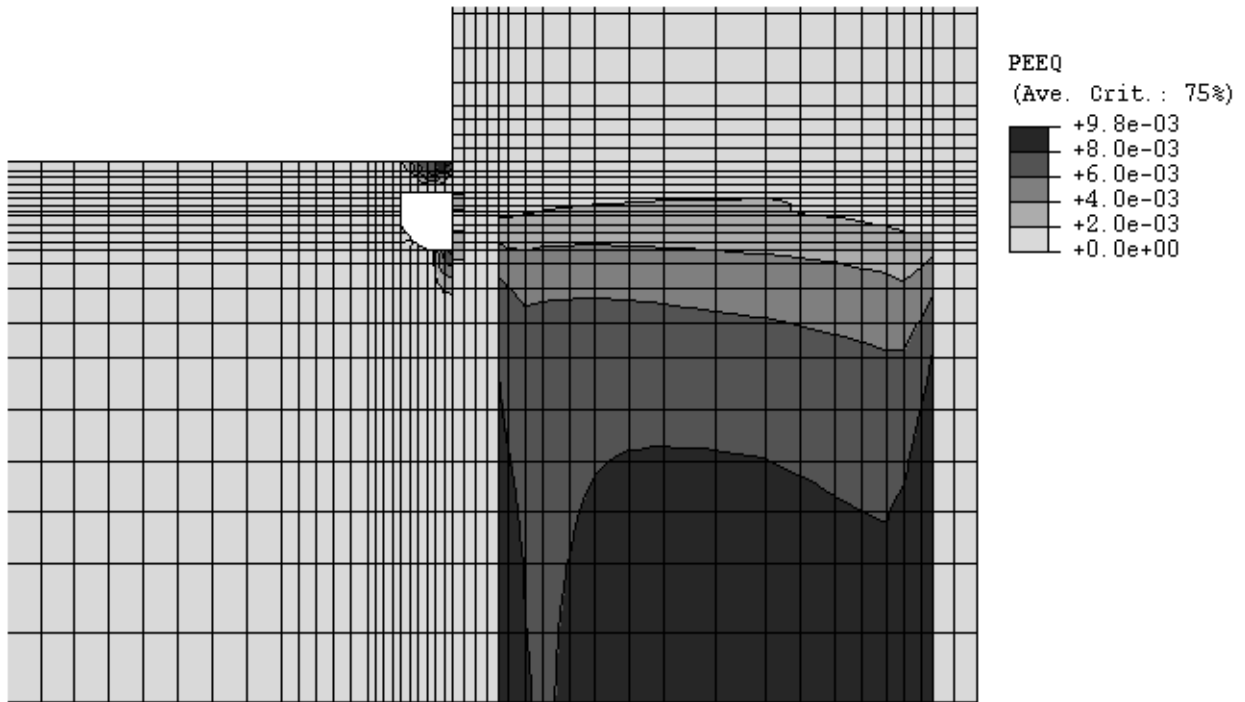
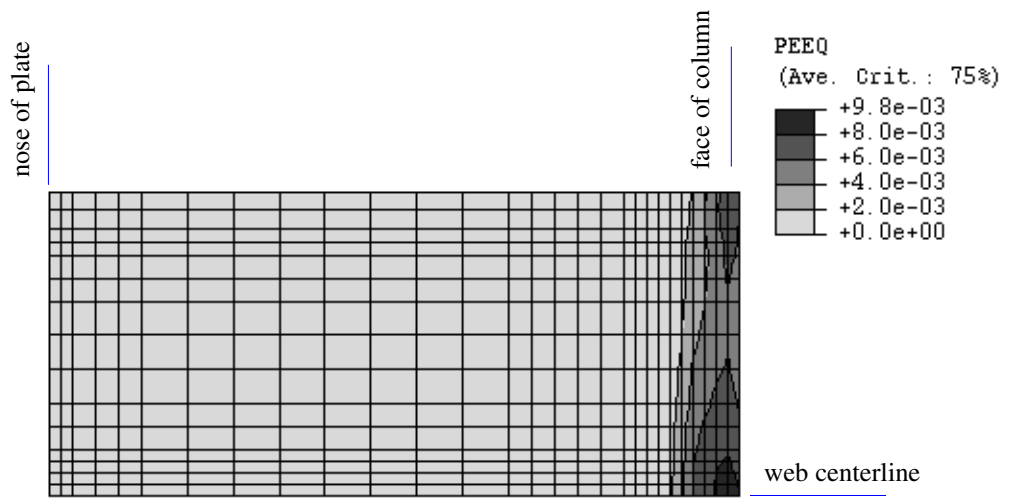
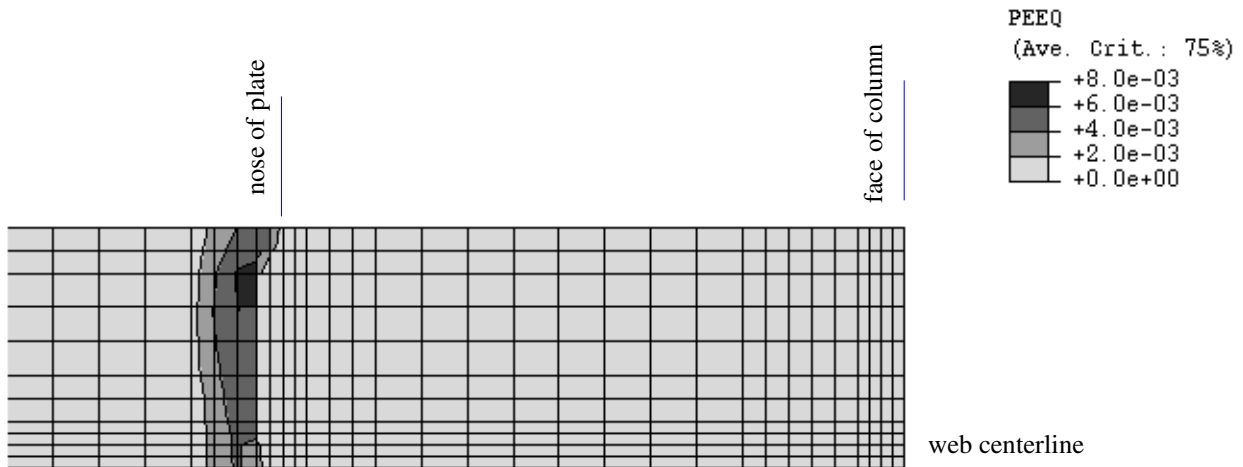


Figure 6-37 Equivalent plastic strain distribution in RC09 panel zone and beam web at 2-percent story drift

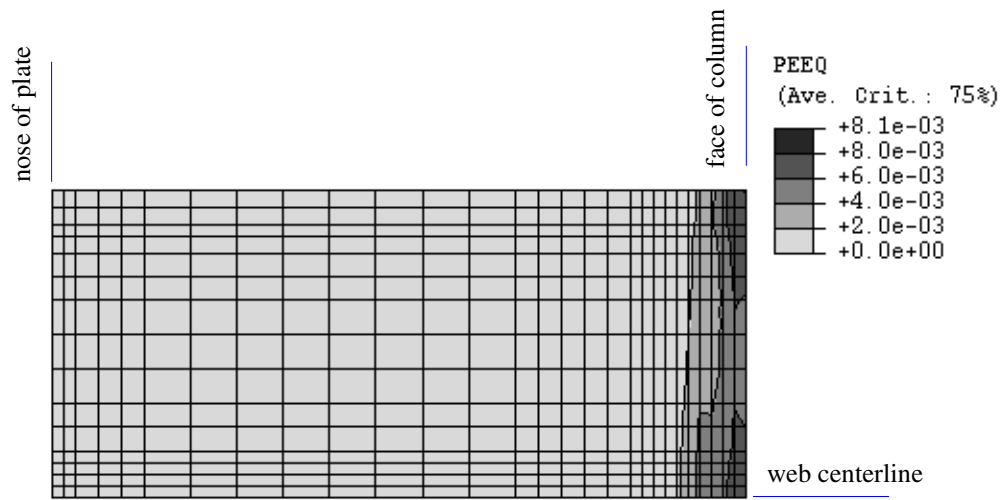


a. upper surface of flange plate

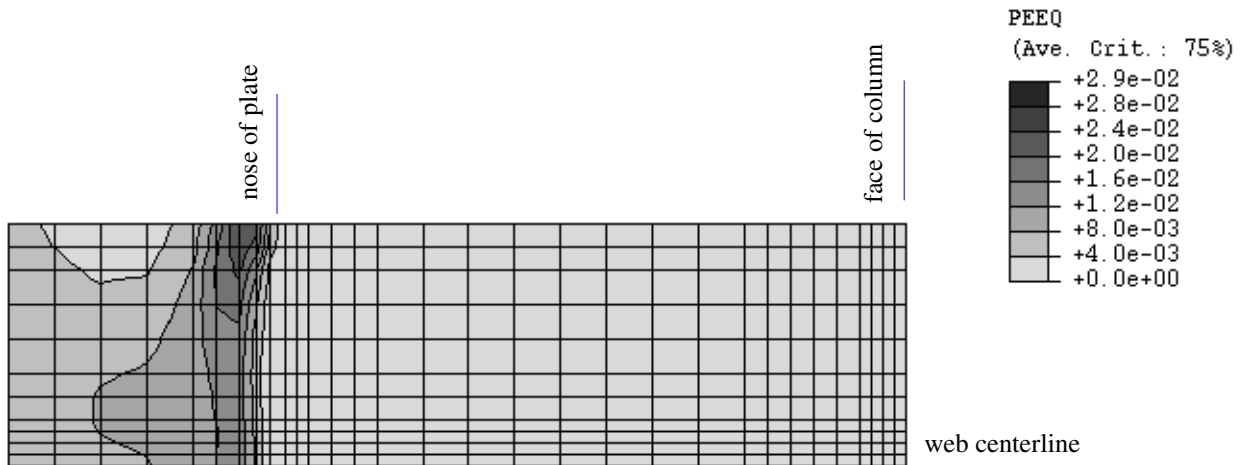


b. upper surface of beam flange

Figure 6-38 Equivalent plastic strain distributions in flange plate and beam flange of RC09 at 2-percent story drift



a. upper surface of flange plate



b. upper surface of beam flange

Figure 6-39 Equivalent plastic strain distributions in flange plate and beam flange of RC06 at 2-percent story drift

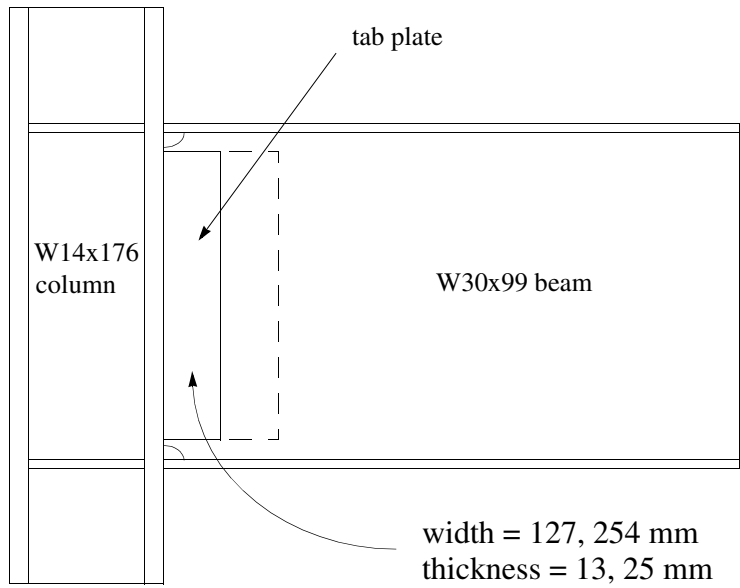


Figure 6-40 RC00 beam web reinforcement study

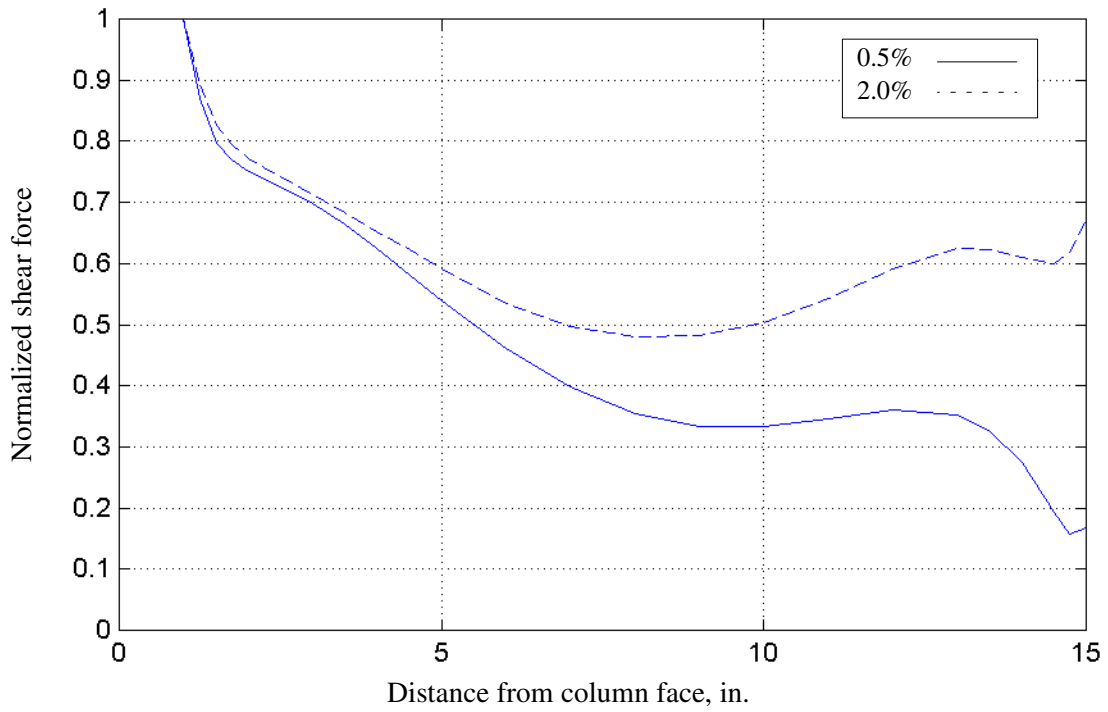


Figure 6-41 Normalized load transfer into cover plate of Configuration 3

7 Design Guidelines and Prequalified Reinforced Connections

7.1 Introduction

This chapter outlines design guidelines for cover-plate and flange-plate connections and presents requirements for prequalified reinforced connections that if followed should avoid the need for full-scale testing. The design guidelines and connection prequalification data are based on the results of this research program and prior studies on reinforced connections. Design guidelines are presented in Sections 7.2 and 7.3 for cover-plate and flange-plate connections, respectively. Connection prequalification data are listed in Section 7.4.

7.2 Design Guidelines for Cover-Plate Connections

7.2.1 Introduction

Design recommendations for Type FR (fully restrained) cover-plate connections are presented below. Design equations in U.S. units only are prepared for an interior beam-column connection. Figure 7-1a shows a sample frame. Figure 7-1b defines terms for the interior connection. The design objective for the cover-plate connection is to relocate inelastic action away from the face of the beam-column connection. Two sites for inelastic action are acceptable: the beam-column panel zone, and the beam section beyond the nose of the reinforcement plate. A combination of yielding in the panel zone and the beam section is acceptable although achieving an appropriate balance between the two may be most difficult. The preferred site for inelastic action is in the beam section for the reasons described in Section 6.9.

The following subsections provide guidelines for the design of Type FR cover-plate connections. These connections utilize cover plates to connect the beam flanges to the column flange, together with a direct connection of the beam flange to the column flange. The cover plates and beam flanges are CJP welded to the column flange with notch-tough electrodes (CVN greater than 20 ft-lbs at 0F). Cover plates are shop fillet welded to the beam flanges. Figure 7-2 provides typical details for this type of connection. These connections should be designed in accordance with the guidelines presented below. The geometry of the weld access hole should follow that of Figure 7-3a (FEMA 2000), which was first proposed by Ricles et al. (2000). All beams in Type FR cover-plate connections should meet the following compactness limits, that are presented in U.S. units.

$$\frac{b_f}{2t_f} \leq \frac{52}{\sqrt{F_{ye}}} \quad (7-1)$$

and

$$\frac{d_b}{t_w} \leq \frac{418}{\sqrt{F_{ye}}} \quad (7-2)$$

where b_f is the flange width, t_f is flange thickness, d_b is beam depth, and t_w is the web thickness. The expected value of the yield strength F_{ye} (in ksi) should be used to calculate the compactness limits and not the nominal value¹. The beam section² should be restrained against lateral-torsional buckling following the AISC equation, namely

$$L_b < \frac{2500r_y}{F_{ye}} \quad (7-3)$$

where L_b is the maximum unbraced length, and r_y is the radius of gyration of the beam about the y-y axis. For the purpose of this calculation, the beam flanges can be considered to be braced at the end of the reinforcement plates.

7.2.2 Cover-plate design

The cover plates should be designed to remain linearly elastic for flexural demands calculated assuming that a plastic hinge forms in the beam section a distance $d_b/3$ from the end of the cover plate. The maximum (plastic) moment in the beam shall be calculated as

$$M_{pb} = Z_b \frac{R_y(F_{yb} + F_{tb})}{2} \quad (7-4)$$

where Z_b is the plastic section modulus of the beam, R_y is the ratio of the expected yield strength to the specified minimum yield strength, F_{yb} is the specified minimum yield strength of the beam, and F_{tb} is the specified minimum tensile strength of the beam³. (For information, Section I.6.2 of the *AISC Seismic Provisions for Structural Steel Buildings* (AISC 1997) writes that R_y shall be set equal to 1.5 for rolled shapes and bars of ASTM A36 steel, 1.3 for rolled shapes and bars of A572 Grade 42 steel, 1.1 for rolled shapes and bars of other grades of steel, and 1.1 for plates of all grades of steel.) Ignoring gravity load effects for the purpose of this calculation⁴, the moment demand at the column face corresponding to M_{pb} is equal to

-
1. The limit of equation 7-2 is that proposed by the SAC Joint Venture and is more liberal than the limit identified in Chapter 6 (developed using W30x99 beam data only). The proposed SAC limit was based on the analysis of test data of different section sizes.
 2. Lateral bracing need not be provided on the other side of the plastic hinge from the reinforcement plates.
 3. Equation 6-4 provides a reasonable estimate of the maximum flexural resistance of a beam section.
 4. Equation 7-5 applies only if gravity load effects are small, that is, if the gravity-load shear force at the column face does not exceed 15 percent of the plastic shear force of the beam.

$$M_{cp} = M_{pb} \left(\frac{L \bar{D} d_c}{L \bar{D} d_c \bar{D} 2l_p \bar{D} \frac{2d_b}{3}} \right) \quad (7-5)$$

where M_{cp} is the design moment for the reinforced connection and other terms defined in Table 7-3. The elastic section modulus of the reinforced connection should be calculated as

$$S_{cp} = \frac{M_{cp}}{F_{yb}} \quad (7-6)$$

where it is assumed that the specified minimum yield strength of the reinforcement plate is no less than that of the beam. If the beam web is fully welded to the column web, the calculation of S_{cp} should include the contribution of the beam web¹.

Rectangular or trapezoidal cover plates may be used. Of the two plate geometries, the rectangular plate is preferred because the sizes of the fillet welds joining the cover plate to the beam flange can be minimized. The cross-sectional area of each cover plate at the face of the column should not exceed 125 percent of the area of the beam flange to which it is joined. The nominal yield stress of the cover plate material should closely match that of the beam.

7.2.3 Cover-plate joining

Beam flanges and cover plates shall be CJP welded to the column flange. The preferred CJP detail is shown in Figure 7-3b. The backing bar shall be removed from the underside of the bottom flange cover plate. The root pass shall be backgouged and rebuilt to the profile of a minimum 5/16 in. (8 mm) fillet weld. The backing bar need not be removed from the underside of the beam top flange provided that the backing bar is continuously welded to the column flange with a minimum 5/16 in. (8 mm) fillet weld. See Figure 7-3b for details. The access hole detail shall follow the details of Figure 7-3a.

Each cover plate shall be fillet welded to the beam flange to develop the yield strength of the cover plate calculated as R_y times the product of the cover plate area and the specified minimum yield strength of the plate. Three-sided fillet welds (2 longitudinal and 1 transverse) as shown in Figure 7-2 are preferred to two-sided fillet welds (2 longitudinal). Fillet welds of one size only should be placed parallel and perpendicular (3-sided weld only) to the beam web as shown in Figure 7-2. The fillet welds should be runoff onto backing so as to maintain the full throat thickness at the end of the plate. Backing shall be removed and the transition zone ground smooth.

1. This procedure will not prevent yielding of the cover plate but should limit the maximum strains to modest levels. Modest yielding of the reinforcement plates in the test specimens did not lead to premature fractures or undesirable behaviors.

7.2.4 Beam web connection

The shear connection is a CJP weld of the beam web to the column flange and a fillet weld of the beam web to the shear tab. Notch tough electrodes shall be used for the CJP and fillet welds. Runoff tabs shall be used at the ends of the CJP weld and removed. A shear tab of adequate thickness for erection purposes, with a minimum thickness of 0.25 in. (6 mm), shall be provided. The composite beam-web-shear-tab cross section should be designed to remain elastic for a flexural demand equal to the plastic moment of the beam web alone. If the gravity-load effects are small, the design shear force in the beam at the column face shall be calculated as

$$V_b = \frac{2M_{pb}}{\left(L \text{ } \text{ } d_c \text{ } \text{ } 2l_p \text{ } \text{ } \frac{2d_b}{3} \right)} \quad (7-7)$$

7.2.5 Panel zone design

The design of the panel zone shall consider requirements for continuity plates and doubler plates. Continuity plates should be provided opposite the geometric centroid of the composite plate-beam flange assembly; the thickness of the continuity plate should be no less than that of the beam flange. Continuity plates must be provided (FEMA 2000) if

$$t_{cf} \geq 0.4 \sqrt{\frac{P_{bf}}{F_{yc}}} \quad (7-8)$$

where t_{cf} is the column flange thickness, F_{yc} is the specified minimum yield strength of the column steel, and P_{bf} is the maximum axial force in the composite plate-beam-flange assembly, given by

$$P_{bf} = R_y(A_{bf}F_{yb} + A_{cp}F_{yp}) \quad (7-9)$$

where R_y is the ratio of expected yield strength to specified minimum yield strength, A_{bf} is the area of the beam flange, F_{yb} is the specified minimum yield strength of the beam steel, A_{cp} is the area of the cover plate, and F_{yp} is the specified minimum yield strength of the cover plate steel¹.

The yield strength of the panel zone can be calculated as

$$V_y = 0.55F_yd_ct_p \quad (7-10)$$

where F_y is the specified minimum yield strength of the panel zone steel, d_c is the depth of the column, and t_p is the thickness of the panel zone, including the doubler plates, if any. Subject to restrictions on the level of axial load in a column, the maximum strength of the panel zone in that column can be calculated using equation (9-1) of the AISC *Seismic Provisions for Structural Steel Buildings* (AISC 1997), namely,

1. The ratio of expected yield strength to the specified minimum yield strength, R_y , is applied to both the flange area and plate area for conservatism only.

$$R_v = 0.6F_y d_c t_p \left(1 + \frac{3b_{cf} t_{cf}^2}{d_b d_c t_p} \right) \quad (7-11)$$

where b_{cf} is the width of the column flange, t_{cf} is the thickness of the column flange, d_b is the depth of the beams framing into the column, and all other terms are defined above.

The shear force in the panel zone of the double-sided (interior) connection of Figure 7-1b can be calculated as

$$V_{pz} = \frac{\sum M_f}{d_b} \left(\frac{L}{L \text{ } \text{D} \text{ } d_c} \right) \left(\frac{h \text{ } \text{D} \text{ } d_b}{h} \right) \quad (7-12)$$

where M_f is the moment in the beam at the column face, h is the story height, and all other terms are defined above. The strength of the panel zone from (7-11) should exceed the maximum shear force from (7-12) where M_f is set equal to M_{cp} in (7-5).

Inelastic panel zone deformation can substantially increase the deformation capacity of beam-column connections. For example, the maximum inelastic deformation in the weak panel zone of Specimen RC09 was approximately 0.025 radian. As such, many expert structural engineers consider it desirable to share or balance the connection inelastic deformation between the beam section and the panel zone. FEMA (2000) proposed the following relationship as the basis for sharing the inelastic deformation between the beam section and the panel zone:

$$0.55F_y d_c t_p \cong \sum \frac{S_b F_{yb}}{d_b} \left(\frac{L}{L \text{ } \text{D} \text{ } d_c \text{ } \text{D} \text{ } 2l_p} \right) \left(\frac{L}{L \text{ } \text{D} \text{ } d_c} \right) \left(\frac{h \text{ } \text{D} \text{ } d_b}{h} \right) \quad (7-13)$$

where S_b is the elastic section modulus of the beam alone, F_{yb} is the specified minimum yield strength of the beam steel; L is the distance between the column centerlines, and l_p is the length of the reinforcement plate. If the beams that framed into the column were of different depths, d_b in (7-13) should be replaced by the average depth of the two beams. The shear force calculated on the right-hand side of (7-13) corresponds to initial yielding of the beam section at the nose of the reinforcement plate. This shear force will increase as the plastic hinge forms in the beam and the beam steel strain hardens in the plastic hinge zone. (For the W30x99 Grade 50 beams tested as part of this research program, the ratio of the maximum-to-yield moment demand at the column face is approximately 1.4.) Beam plastic deformations will accompany this increase in shear force. Likewise, the resistance of the panel zone will increase from the yield value calculated using (7-10) to the maximum value calculated using (7-11). (The ratio of the maximum-to-yield resistance of the panel zone of the W14x176 Grade 50 columns tested as part of this research program, including a 0.375-in. [10 mm] doubler plate, is 1.25.) Panel zone plastic deformations will also accompany the increase in shear force. The FEMA procedure may work well at *modest* levels of connection inelastic rotation if the specified minimum and actual values of the yield strengths in (7-13) are similar. At larger levels of connection inelastic deformation, web and flange local buckling in the beam can lead to a substantial loss of strength in the beam as exhibited in all ten W30x99 specimens tested in this research program. Such a loss of strength will reduce the shear force demands on the panel zone, likely to levels below that required to yield the panel zone. At this point, all of the inelastic deformation will occur in the beam section. (This

change in the balance of inelastic deformation between the beam section and the panel zone was clearly evident in the response of specimens RC08 and RC09.) For these reasons, sharing inelastic deformations between a panel zone and a wide-flange beam section in a reliable manner will be difficult to achieve in practice.

7.2.6 Column-beam flexural strength ratio

Equation (9-3) of the AISC *Seismic Provisions for Structural Steel Buildings* (AISC 1997) should be used to check the column-beam moment ratio, namely,

$$\frac{\sum M_{pc}^*}{\sum M_{pb}^*} > 1 \quad (7-14)$$

where the numerator is the sum of the moments in the column above and below the joint at the intersection of the beam and column centerlines, and the denominator is the sum of the moment(s) in the beam(s) at the intersection of the beam and column centerlines, which may be calculated as

$$\sum M_{pb}^* = \sum (M_{cp} + 0.5 V_b d_c) \quad (7-15)$$

where M_{cp} is given by (7-5), V_b is given by (7-7), and d_c is the depth of the column.

7.3 Design Guidelines for Flange-Plate Connections

7.3.1 Introduction

Design recommendations for Type FR (fully restrained) flange-plate connections are presented below. Design equations in U.S. units only are prepared for the interior beam-column connection of Figure 7-1. The design objective for the flange-plate connection, identical to that of the cover-plate connection, is to relocate inelastic action away from the face of the beam-column connection. Two sites for inelastic action are acceptable: the beam-column panel zone, and the beam section beyond the nose of the reinforcement plate. Sharing the connection inelastic deformation between the panel zone and the beam section would be ideal, but is most difficult to achieve for the reasons cited above. Substantial inelastic deformation in the flange plate near the face of the column is not acceptable. Large inelastic strains would have to be developed in the short free length of the plate between the column face and the beam flange to produce modest inelastic deformations in the frame. The preferred site for inelastic action in this connection is in the beam section beyond the flange plate.

The following subsections provide guidelines for the design of Type FR flange-plate connections. These connections utilize flange plates to connect the beam flanges to the column flange. There is no direct connection of the beam flange to the column flange. The flange plates are CJP welded to the column flange with notch-tough electrodes (CVN greater than 20 ft-lbs at 0F). Flange plates are shop fillet welded to the beam flanges. Figure 7-4 provides a typical detail for this type of connection. These connections should be designed in accordance with the guidelines presented below. The geometry of the weld access hole should follow that of Figure 7-5a. All beams in Type FR flange-plate connections should meet the compactness and bracing limits set forth in (7-1), (7-2), and (7-3) above.

7.3.2 Flange-plate design

The flange plates should be designed to remain linearly elastic for flexural demands calculated assuming that a plastic hinge forms in the beam section a distance $d_b/3$ from the end of the flange plate. The maximum (plastic) moment in the beam (M_{pb}) can be calculated using (7-4) if the gravity-load effects are small. The moment demand at the face of the column corresponding to M_{pb} shall be calculated using (7-5). The elastic section modulus of the reinforced flange-plate connection at the face of the column (S_{fp}) should be calculated as

$$S_{fp} = \frac{M_{cp}}{F_{yb}} \quad (7-16)$$

where it is assumed that specified minimum yield strength of the reinforcement plate is no less than that of the beam. (To do otherwise, would make little fiscal sense.) If the beam web is fully welded to the column web, the calculation of S_{fp} should include the contribution of the beam web.

Rectangular flange plates must be used. The cross-sectional area of each flange plate at the face of the column should not exceed 225 percent of the area of the beam flange to which it is joined. The nominal yield stress of the flange-plate material should closely match that of the beam.

7.3.3 Flange-plate joining

Flange plates shall be CJP welded to the column flange. The preferred CJP detail is shown in Figure 7-5. The backing bar shall be removed from the underside of the bottom flange plate. The root pass shall be backgouged and rebuilt to the profile of a minimum 5/16 in. (8 mm) fillet weld. The backing bar need not be removed from the underside of the top flange plate provided that the backing bar is continuously welded to the column flange with a minimum 5/16 in. (8 mm) fillet weld. See Figure 7-5 for details. The access hole detail shall follow the details of Figure 7-5a.

Each flange plate shall be fillet welded to the beam flange to develop the yield strength of the flange plate calculated as R_y times the product of the plate area and the specified minimum yield strength of the plate. Three-sided fillet welds (2 longitudinal and 1 transverse) as shown in Figure 7-4 are preferred to two-sided fillet welds (2 longitudinal). Fillet welds of one size only should be placed parallel and perpendicular (3-sided weld only) to the beam web as shown in Figure 7-4. The fillet welds should be run off onto backing so as to maintain the full throat thickness at the end of the plate. Backing shall be removed and the transition zone ground smooth.

7.3.4 Beam web connection

The shear connection is a CJP weld of the beam web to the column flange and a fillet weld of the beam web to the shear tab. Notch tough electrodes shall be used for the CJP and fillet welds. Run-off tabs shall be used at the ends of the CJP weld and removed. A shear tab of adequate thickness for erection purposes, with a minimum thickness of 0.25 in. (6 mm), shall be provided. The composite beam-web-shear-tab cross section should be designed to remain elastic for a flexural demand equal to the plastic moment of the beam web alone. The design shear force in the beam at the column face can be calculated using (7-7) if the gravity-load effects are small.

7.3.5 Panel zone design

The design of the panel zone shall consider requirements for continuity plates and doubler plates. Continuity plates should be provided opposite the geometric centroid of the flange plate; the thickness of the continuity plate should be no less than one half of the flange-plate thickness. Continuity plates must be provided if the column flange thickness does not comply with (7-8), where P_{bf} is the maximum axial force in the flange-plate, given by

$$P_{bf} = R_y A_{fp} F_{yp} \quad (7-17)$$

where R_y is the ratio of the expected yield strength to the specified minimum yield strength, A_{fp} is the area of the cover plate, and F_{yp} is the specified minimum yield strength of the flange-plate steel¹.

The yield strength and the maximum strength of the panel zone can be calculated using (7-10) and (7-11), respectively. The shear force in the panel zone of the double-sided connection of Figure 7-1 can be calculated using (7-12). The strength of the panel zone from (7-11) should exceed the maximum shear force from (7-12) where M_f is set equal to M_{cp} in (7-5).

The guidelines for sharing inelastic deformation between the panel zone and the beam section in flange-plate connections are identical to those presented for cover-plate connections; see Section 7.2.5 for details.

7.3.6 Column-beam flexural strength ratio

The check on the column-beam flexural strength ratio for flange-plate connections is identical to that for cover-plate connections; see Section 7.2.6 for details.

7.4 Prequalified Cover- and Flange-Plate Connections

Preliminary information on prequalified cover- and flange-plate connections are presented in Tables 7-1 and 7-2, respectively. Connections composed of components that satisfy the limitations set forth in these tables may not need to be tested prior to field implementation. This information should be considered to be preliminary and mutable at the time of this writing. Definitions of the symbols used in these tables are presented in Table 7-3.

1. The ratio of expected yield strength to specified minimum yield strength, R_y , is applied to both the flange area and plate area for conservatism only.

Table 7-1 Prequalified cover-plate connections, U.S. units¹

General	
Applicable systems	Special Moment Frame (SMF)
Hinge location	$s_h = d_c/2 + l_p + d_b/3$
Critical beam parameters	
Depth and weight	Up to W36 and 150 lbs/ft.
Flange	$b_f/(2t_f) \leq 52/(\sqrt{F_{ye}})$
Flange thickness	Up to 1.0 in.
Web	$d_b/t_w \leq 418/(\sqrt{F_{ye}})$
Lateral bracing	$L_b/r_y < 2500/F_y$
Permissible material specifications	A36, A572 Grade 50; A913 Grade 50 or 65
Critical column parameters	
Depth	W14; Group 2 through Group 4 shapes
Permissible material specifications	A36, A572 Grade 50; A913 Grade 50 or 65
Beam-column-plate relationships	
Flange and cover plate to column	$(t_f + t_{cp})/t_{fc} \leq 1$
Panel zone strength	Section 7.2.5
Column-beam flexural strength ratio	Section 7.2.6
Connection details	
Beam flexural strength	Section 7.2.2
Cover plate geometry and thickness	Rectangular or trapezoidal; $A_{cp} \leq 1.25A_{bf}$; $t_{cp} > 0.5t_f$; $b_{cp} \leq 1.25b_f$
Cover plate material	Match material properties of beam section
Cover plate welding	See Section 7.2.3; Welding QC Level 1
Plate and flange welding electrodes	CVN 20 ft-lbs at 0F and 40 ft-lbs at 70F
Web connection	Fully welded; see Section 7.2.4; Welding QC Level 1
Web welding electrodes	CVN 20 ft-lbs at 0F and 40 ft-lbs at 70F
Continuity plate thickness	Section 7.2.5

1. See Table 7-3 for definition of terms; connections only prequalified if gravity load effects are small.

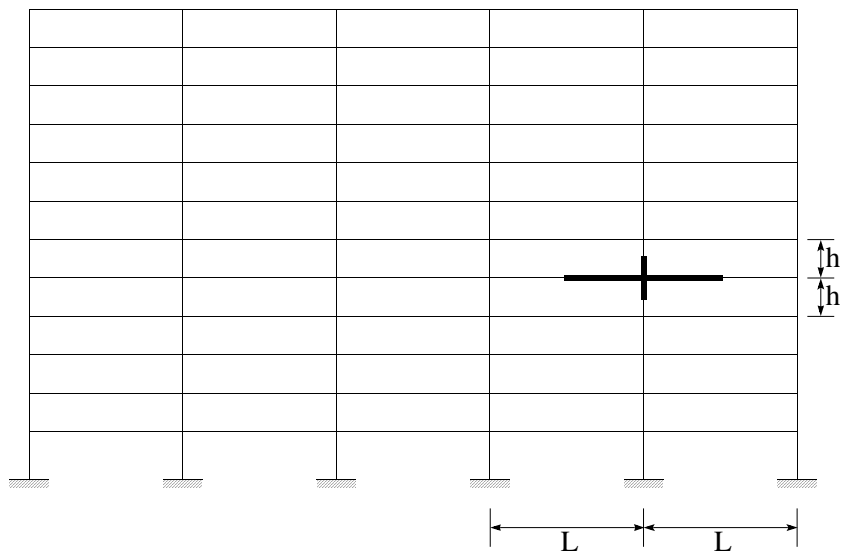
Table 7-2 Prequalified flange-plate connections, U.S. units¹

General	
Applicable systems	Special Moment Frame (SMF)
Hinge location	$s_h = d_c/2 + l_p + d_b/3$
Critical beam parameters	
Depth and weight	Up to W36 and 150 lbs/ft.
Flange	$b_f/(2t_f) \leq 52/(\sqrt{F_{ye}})$
Flange thickness	Up to 1.0 in.
Web	$d_b/t_w \leq 418/(\sqrt{F_{ye}})$
Lateral bracing	$L_b/r_y < 2500/F_y$
Permissible material specifications	A36, A572 Grade 50; A913 Grade 50 or 65
Critical column parameters	
Depth	W14; Group 2 through Group 4 shapes
Permissible material specifications	A36, A572 Grade 50; A913 Grade 50 or 65
Beam-column-plate relationships	
Flange plate to column	$t_p/t_{fc} \leq 1$
Panel zone strength	Section 7.3.5
Column-beam flexural strength ratio	Section 7.3.6
Connection details	
Beam flexural strength	Section 7.3.2
Flange plate geometry and thickness	Rectangular; $A_p \leq 2.25A_{bf}$; $b_p \leq 1.25b_f$
Flange plate material	Match material properties of beam section
Flange plate welding	See Section 7.3.3; Welding QC Level 1
Plate and flange welding electrodes	CVN 20 ft-lbs at 0F and 40 ft-lbs at 70F
Web connection	Fully welded; see Section 7.3.4; Welding QC Level 1
Web welding electrodes	CVN 20 ft-lbs at 0F and 40 ft-lbs at 70F
Continuity plate thickness	Section 7.3.5

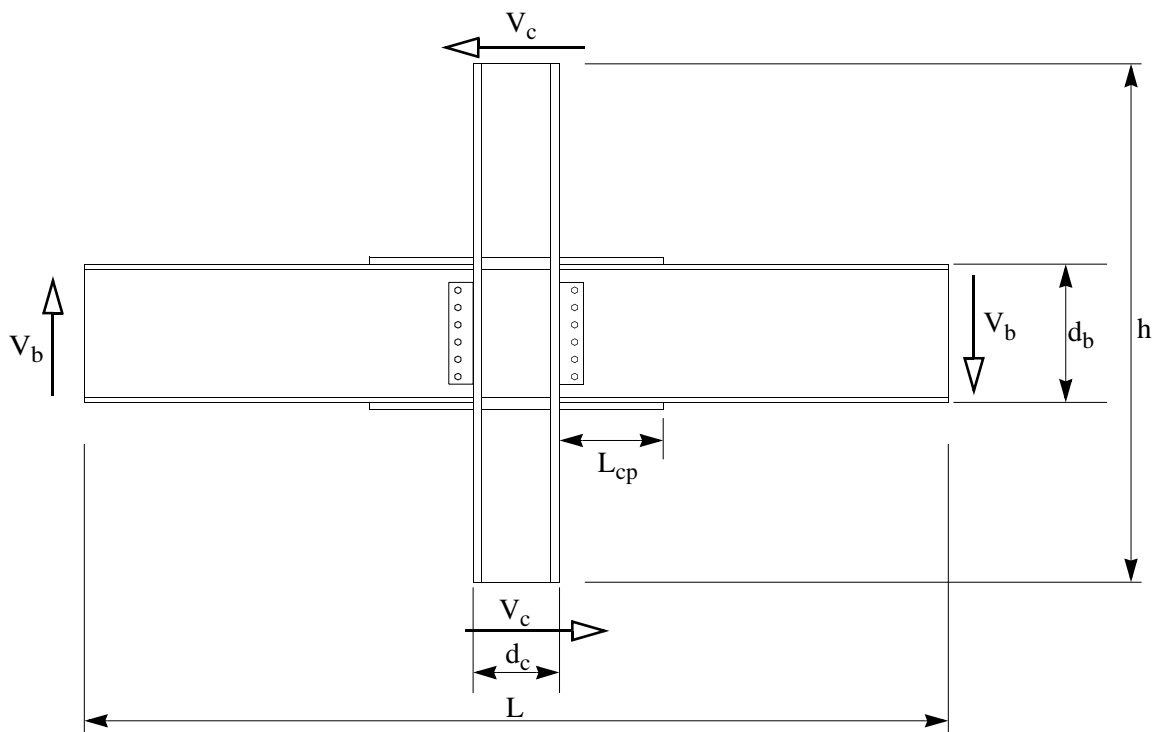
1. See Table 7-3 for definition of terms; connections only prequalified if gravity load effects are small.

Table 7-3 Definition of symbols for prequalified connections

<i>Symbol</i>	<i>Definition</i>
A_{bf}	Area of beam flange, in. ²
A_{cp}	Area of cover plate at face of column, in. ²
A_p	Area of flange plate, in. ²
b_{cp}	Width of cover plate, in.
b_f	Width of beam flange, in.
b_p	Width of flange plate, in.
d_b	Depth of beam, in.
d_c	Depth of column, in.
F_y	Specified minimum yield strength, ksi
F_{ye}	Expected yield strength, ksi
l_p	Length of reinforcing plate, in.
L_b	Unbraced length of beam, in.
r_y	Radius of gyration of beam about y-axis, in.
s_h	Distance to centerline of hinge from column centerline, in.
t_{cp}	Thickness of cover plate, in.
t_f	Thickness of beam flange, in.
t_{fc}	Thickness of column flange, in.
t_p	Thickness of flange plate, in.
t_w	Thickness of beam web, in.



a. sample frame elevation



b. design forces on an interior connection

Figure 7-1 Reinforced steel moment connections

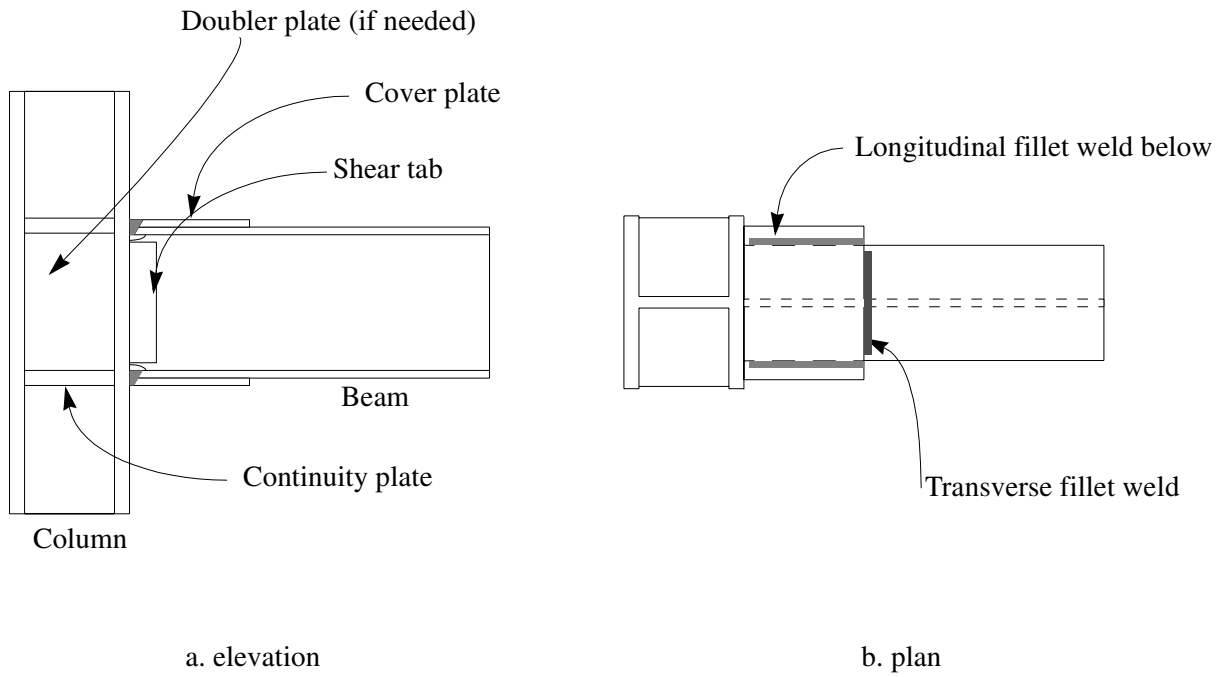


Figure 7-2 Typical details for cover-plate connection

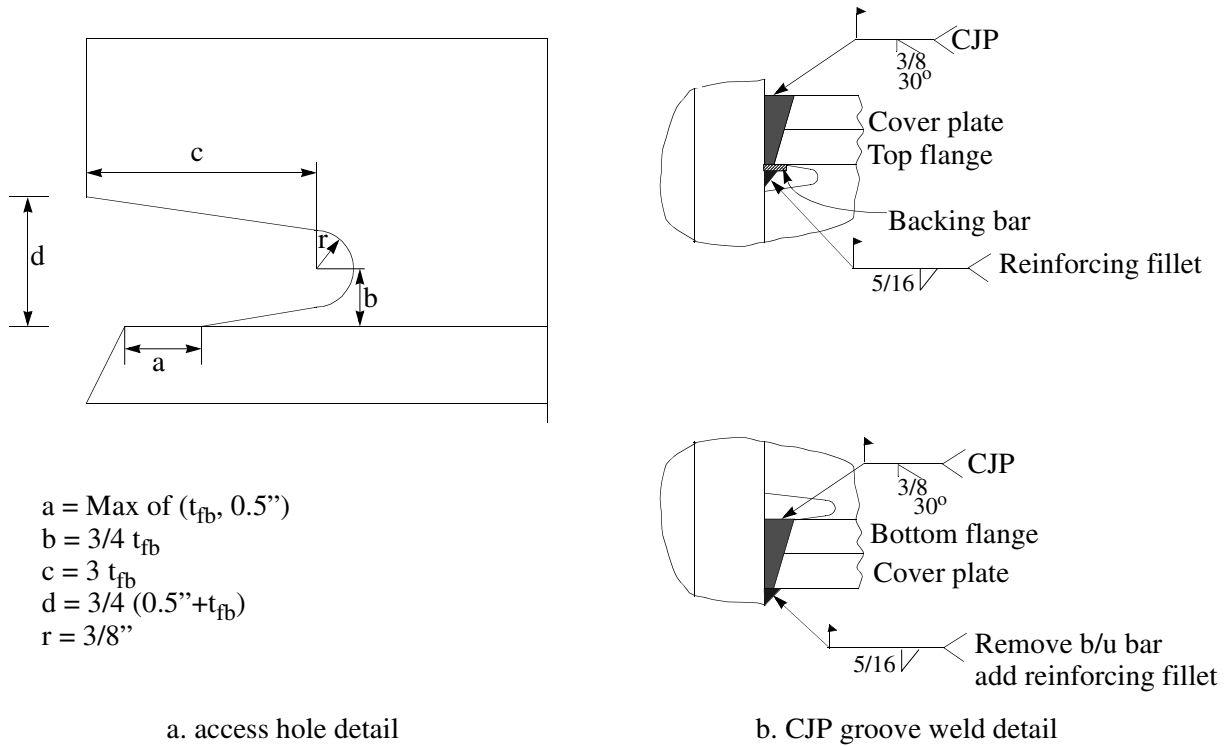


Figure 7-3 Preferred access hole and CJP groove weld details for cover-plate connections

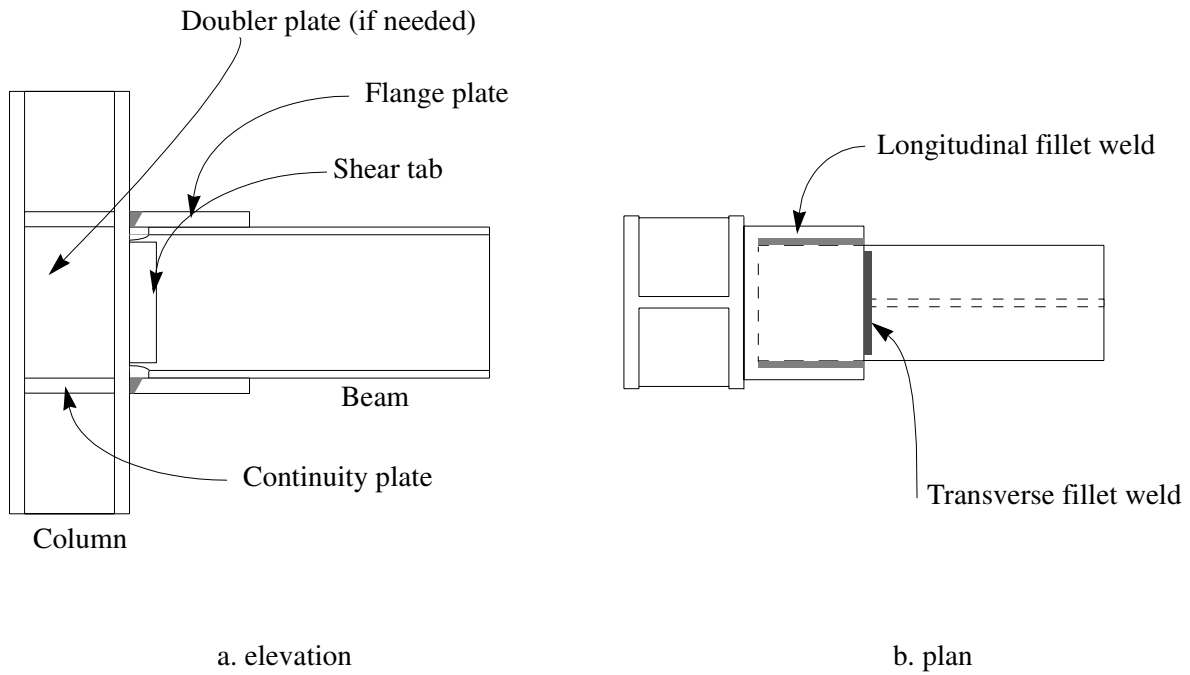


Figure 7-4 Typical details for flange-plate connection

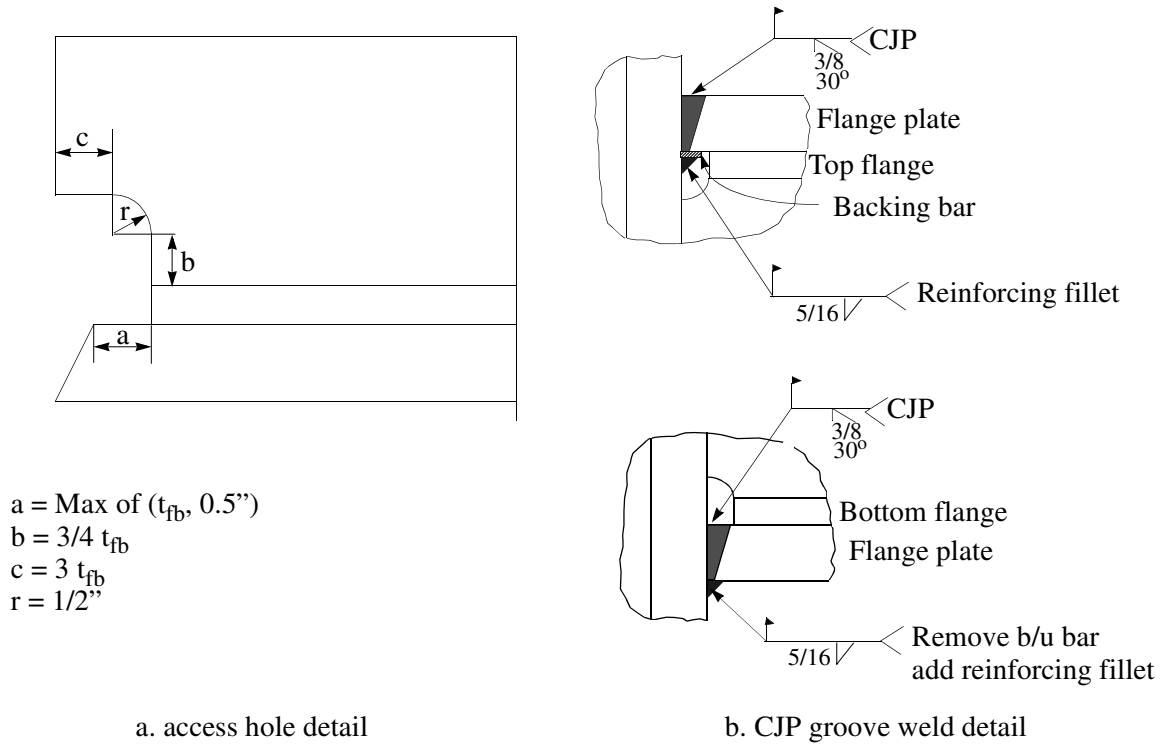


Figure 7-5 Preferred access hole and CJP groove weld details for flange-plate connections

8 Summary and Conclusions

8.1 Summary

8.1.1 Introduction

The performance of two plate-reinforced connections are discussed in this report: cover-plate and flange-plate connections. The major difference between the connection details is the welding of the beam flange to the column flange. For the cover-plate connection, the cover plate and the beam flange are groove welded to the column flange, whereas only the flange plate is groove welded to the column flange in the flange-plate connection.

The goal of the studies described in this report was to better understand the seismic response of large-scale steel moment-resisting connections reinforced with flat steel plates. The key objectives of the research program were five-fold, namely, (1) to identify the key design variables for reinforced steel moment-resisting connections and develop an experimental program to study such variables; (2) to design, detail, and construct ten full-size, single-sided specimens using the procedures of FEMA 267A for the purpose of static cyclic testing; (3) to prepare nonlinear finite element analysis models of each of the specimens to study the effect of weld and plate geometry on important elastic stress, plastic strain, and fracture-mechanics parameters prior to the construction of the specimens; (4) to test each single-sided specimen and report data in accordance with the procedures set forth by the SAC Joint Venture, and (5) to interpret the analytical and experimental data for the purpose of (a) writing guidelines for the design, detailing, and construction of plate-reinforced steel moment-resisting connections, and (b) developing prequalified plate-reinforced steel moment-resisting connections.

8.1.2 Plate-reinforced connections and test specimens

Five cover-plate and five flange-plate-reinforced steel moment-resisting connections were studied by analysis and experimentation. All ten were single-sided steel beam-column assemblies that are representative of exterior beam-column connections. The test specimens were fabricated from the same heat of W14x176 Grade 50 columns and W30x99 Grade 50 beams. Grade 50 reinforcing plates were used for both the cover-plate and the flange-plate specimens. Seven design variables for flat-plate reinforced connections were identified to focus the design and detailing of the ten

connections, namely, (1) reinforcing plate geometry, (2) maximum reinforcement-plate strain, (3) plate-to-flange fillet weld geometry, (4) loading history, (5) restraint to lateral-torsional buckling at the plastic hinge, (6) panel zone strength and stiffness, and (7) restraint to beam web local buckling.

The ten specimens were designed using the capacity-design procedures set forth in FEMA 267A (FEMA 1995b). Specimens RC01 and RC06 were designated as the benchmark cover-plate and flange-plate connections, respectively. Specimens RC01, RC02, RC03, RC05, and RC10 were cover-plate connections. Specimens RC04, RC06, RC07, RC08, and RC09 were flange-plate connections. Specimens RC01 through RC07, and RC10, were designed using elementary beam theory with the objective of limiting the strain in the reinforcing plates to the yield strain or less. Specimens RC08 and RC09 were designed with the intent of yielding the flange plate, and yielding the flange plate and beam-column panel zone, respectively. The key features of the ten specimens are listed in Table 8-1.

Table 8-1 Summary information on test specimens (SI units)

	<i>Specimen RC</i>									
	<i>01</i>	<i>02</i>	<i>03</i>	<i>04</i>	<i>05</i>	<i>06</i>	<i>07</i>	<i>08</i>	<i>09</i>	<i>10</i>
<i>Reinforcing plate</i> ¹	CP	CP	CP	FP	CP	FP	FP	FP	FP	CP
<i>Plate geometry</i> ²	R	R	R	S	Tr	R	R	R	R	R
<i>Width (mm)</i>	305	305	305	330	267	337	337	337	337	305
<i>Thickness (mm)</i>	16	16	16	29	17	25	25	22	22	16
<i>Fillet weld size</i> ³										
<i>Longitudinal (mm)</i>	14	14	11	14	16	16	16	14	14	11
<i>Transverse (mm)</i>	-	-	11	19	16	16	16	14	14	11
<i>Doubler plate (mm)</i>	10	10	10	10	10	10	10	10	0	10
<i>Continuity plate (mm)</i>	29	29	29	29	29	25	25	22	16	29
<i>Loading history</i> ⁴	Cy	Cy	Cy	Cy	Cy	Cy	Nf	Cy	Cy	Cy
<i>Restraint to LTB</i> ⁵	N	Y	N	N	N	N	N	N	N	N

1. CP = cover plate; FP = flange plate.

2. R = rectangular; S = swallowtail; Tr = trapezoidal.

3. Fillet welds joining the reinforcing plate to the beam flange.

4. Cy = cyclic; Nf = near-field.

5. Restraint to lateral-torsional buckling in the plastic hinge zone; N = no; Y = yes.

The steel used to fabricate the test specimens was supplied by the Nucor-Yamato Steel Company. The specimens were fabricated by the Gayle Manufacturing Company of Woodland, California, to details prepared by the authors, Mr. Rick Wilkinson of the Gayle Manufacturing Company, and the SAC Joint Venture. Fabrication inspection services were provided by Signet Testing Laboratories of Hayward, California.

The specimens were tested in the upright position. Axial loads were not applied to the columns. A composite slab was not included in any of the test specimens. The columns were attached to the strong floor (bottom) and the reaction frame (top) using short sections of W14x311 sections to simulate pinned (bottom) and roller supports. For all specimens, lateral restraint to the beam flanges was provided adjacent to the tip of the cantilever beam. For specimen RC02, lateral restraint against lateral-torsional buckling was also provided near the end of the plastic hinge. Displacements were imposed on the beam at a distance of 134 in. (3.4 m) from the column face. A 400 kip (1800 kN) actuator was used to load the specimens under displacement control. The testing protocol for the specimens was established by the authors and the SAC Joint Venture.

8.1.3 Analytical studies

Version 5.8 of the general purpose nonlinear finite element program ABAQUS (HKS 1998) was used to model eight of the ten beam-column reinforced connections: RC01, RC03, RC04, RC05, RC06, RC08, RC09, and RC10. These *preliminary* models were prepared and analyzed prior to the construction of the test specimens. Expected material properties were used for the models because mill certificate and coupon data were unavailable at that time. The primary objectives of the preliminary analyses were to (1) identify zones of high stress and strain in the test specimens, (2) understand the likely sequence of yielding in the test specimens, (3) ascertain whether the design procedures of FEMA 267A (FEMA 1995b) were appropriate for reinforced connections, and (4) determine if the strain conditions in reinforced connections were significantly better than those in unreinforced (pre-Northridge) connections. To address item (4), a mathematical model of an unreinforced connection, termed RC00, was prepared and analyzed. At the completion of the testing program, coupons were extracted from the test specimens, and accurate estimates of the beam and column material properties were established. Models of seven (RC01, RC03, RC05, RC06, RC08, RC09, and RC00) of the specimens were then updated and reanalyzed. Only the results of the reanalysis were reported in Chapter 4.

Solid-element (Type SOL) models were prepared for RC00, RC01, RC03, RC05, RC06, RC08, and RC09 for the purpose of calculating and comparing stresses, strains, and selected fracture indices. Shell-element (Type SH) models were prepared for RC01, RC02, RC03, and RC06 to characterize the force-displacement response of selected specimens, to better understand the relationship between flange- and web-local buckling and the effect of such buckling on strength degradation in wide-flange beams, and to study the effect of restraining lateral-torsional buckling in the plastic hinge zone on the force-displacement response of a single specimen. A vertical displacement history was imposed at the free end of the beam for both models using the displacement-control feature in ABAQUS. The history of the applied load for each analysis was then back-calculated from the support-reaction histories.

Five response indices were used for the analytical studies using the Type SOL models to identify potential sites of *brittle* and *ductile* fracture: Pressure Index, Mises Index, Equivalent Plastic Strain Index, Triaxiality Index, and Rupture Index. The responses of the models were compared at three values of story drift angle: 0.5 percent (elastic), 1.0 percent (minor inelastic response), and 2.0 percent (substantial inelastic response) because the addition of reinforcing plates will typically increase the stiffness of a steel moment-resisting frame only marginally and the drift demands on moment-resisting frames with unreinforced and reinforced connections would likely be similar.

Analysis of the unreinforced connection RC00 using solid elements showed that (1) approximately 50 percent of the beam shear force is transferred through the beam flanges to the column flange at 0.5-percent story drift; (2) the distribution of normal stress S_{22} along the beam flange at 0.5-percent story drift follows elementary beam theory beyond 10 in. (254 mm) from the column face but the values of S_{22} increase sharply near the face of the column, over the weld access hole, due to the transfer of shear force to the column through the beam flange; (3) the Equivalent Plastic Strain Index at 2-percent story drift is maximized at the edge of the beam flange at the face of the column; and (4) the maximum value of the Triaxiality Index at 2-percent story drift is computed at the beam web centerline. For RC00, initiation of *brittle* fracture is most likely in the beam flange above the beam web at the face of the column; the edge of the beam flange at the face of the column is the most likely initiation site for *ductile* fracture.

The utility of adding cover plates to steel moment-resisting connections to delay brittle and ductile fracture was assessed by comparing the peak values of the Pressure Index, Mises Index, Triaxiality Index, and Rupture Index in the unreinforced and reinforced connections. Summary data are presented in Table 8-2 at 2-percent story drift. At the face of the column, the maximum values of each index are larger in the beam flange than in the cover plate. As such, no cover-plate data are presented in the table. The maximum values of Pressure Index, Mises Index, and Triaxiality Index at the face of the column are similar for RC00, RC01, RC03, and RC05, but the maximum value of the Rupture Index in RC00 is 1.9 times greater than the maximum value in RC01 and 3.8 times greater than the maximum value in RC03 and RC05. The maximum values of the Triaxiality Index in all three cover-plate reinforced connections are greater at the face of the column than at the nose of the cover plate. The maximum values of the Rupture Index in all three reinforced connections at the nose of the cover plate are computed at the end of the longitudinal fillet weld that joins the cover plate to the beam flange; the maximum value for RC01 is 2+ times greater than the maximum values in RC03 and RC05.

Table 8-2 Cover-plate response indices at 2-percent story drift using Type SOL models

<i>Specimen</i>	<i>Beam Flange at Column Face</i>				<i>Beam Flange at Nose of Plate</i>			
	PI^1	MI^1	TI^1	RI^1	PI^1	MI^1	TI^1	RI^1
RC00	-0.82	1.11	-0.77	0.099	-	-	-	-
RC01	-0.86	1.02	-0.84	0.029	-0.71	1.20	-0.66	0.052
RC03	-0.86	1.02	-0.84	0.025	-0.66	1.14	-0.69	0.026
RC05	-0.84	1.00	-0.84	0.025	-0.68	1.01	-0.68	0.024

1. PI = Pressure Index; MI = Mises Index; TI = Triaxiality Index; RI = Rupture Index

The utility of adding flange plates to steel moment-resisting connections to delay brittle and ductile fracture was also assessed by comparing the peak values of the Pressure Index, Mises Index, Triaxiality Index, and Rupture Index in the unreinforced and flange-plate connections. Summary data are presented in Table 8-3 at 2-percent story drift. The maximum values of Pressure Index and Triaxiality Index at the face of the column are larger for the reinforced connections, but the maximum value of the Rupture Index in RC00 is 2.8 times greater than the maximum value in RC01 and 2.1 times greater than the maximum value in RC08. The maximum

values of the Triaxiality Index in all three flange-plate connections are greater at the face of the column than at the nose of the flange plate. The maximum values of the Rupture Index in all three reinforced connections at the nose of the flange plate are computed at the end of the longitudinal fillet weld that joins the flange plate to the beam flange; the maximum value for RC09 is small because much of the deformation in RC09 at 2-percent story drift is in the weak beam-column panel zone.

Table 8-3 Flange-plate response indices at 2-percent story drift using Type SOL models

<i>Specimen</i>	<i>Beam Flange or Plate at Column Face</i>				<i>Beam Flange at Nose of Plate</i>			
	<i>PI</i> ¹	<i>MI</i> ¹	<i>TI</i> ¹	<i>RI</i> ¹	<i>PI</i> ¹	<i>MI</i> ¹	<i>TI</i> ¹	<i>RI</i> ¹
RC00	-0.82	1.11	-0.77	0.099	-	-	-	-
RC06	-0.89	1.02	-0.88	0.025	-0.75	1.06	-0.81	0.035
RC08	-0.86	1.00	-0.87	0.023	-0.71	1.14	-0.78	0.046
RC09	-0.90	1.00	-0.90	0.028	-0.68	1.08	-0.88	0.0084

1. *PI* = Pressure Index; *MI* = Mises Index; *TI* = Triaxiality Index; *RI* = Rupture Index

Based on the results of the finite element analysis using Type SOL models, the use of any of the six reinforced connections listed in these two tables will reduce the likelihood of ductile and brittle fracture of steel moment-resisting connections with respect to the unreinforced connection, RC00. For story drift angles of up to 2-percent, RC03, RC05, and RC06 are the superior reinforced connections of the six listed in these tables.

Force-displacement relationships were computed for RC01 (cover plate), RC03 (cover plate), and RC06 (flange plate) using the Type SH models. Each model captured the loss of strength due to flange local buckling (FLB) and web local buckling (WLB) in the beam beyond the nose of the reinforcing plate. The differences between the computed responses were small because the beam load-beam tip displacement relationships were controlled by FLB and WLB in the beams, which were identical in each model. The responses of the Type SOL and Type SH models of RC03 were nearly identical for story drift angles of 2-percent radian and less. Because only the Type SH models accounted for FLB and WLB, the responses of the two models diverged at a drift angle of 2-percent radian.

The Type SH analysis of RC03 provided useful information on the relation between FLB and WLB, and the relation between such buckling and the force-displacement responses of steel moment-resisting connections. The Type SH analysis of RC03 showed that (1) increases in the amplitude of the flange buckles were accompanied by increases in the amplitude of the web buckles; (2) the rate of strength degradation in the connection is greatest when the rate of increase in the amplitudes of the flange and web buckles is the greatest; (3) the full wavelength of the flange buckles is equal to the yielded region of the flange as first proposed by Lay in 1965; and (4) plasticity spreads into the beam at a story drift angle of 2-percent radian and triggers substantial WLB.

Four conditions of lateral restraint to the beam flanges in the plastic hinge zone were considered to judge the effect on the global response of reinforced connections of delaying lateral-torsional buckling: no restraint, discrete (point) rigid bracing of the top and bottom flanges, and continuous restraint to the top flange and discrete rigid bracing of the bottom flange (2 loading cases). The Type SH analysis showed that little to no improvement in response was realized by adding lateral bracing to the beam bottom flange at the assumed far end of the plastic hinge zone. The addition of continuous restraint to the compression flange substantially delayed beam WLB and significantly reduced the loss of strength in the connection at drift angles greater than 2-percent radian.

8.1.4 Experimental studies

The global responses of the ten specimens are summarized in Table 8-4. This table lists the maximum actuator load, the maximum displacement in terms of story drift, the maximum moment in the beam at the nose of the reinforcing plate normalized by the plastic moment calculated as the product of the plastic section modulus ($=5112 \text{ cm}^3$) and the measured yield strength of beam flange ($=369 \text{ MPa}$ or 53.5 ksi), the maximum moment in the beam at the nose of the reinforcing plate normalized by the plastic moment calculated as the product of the plastic section modulus and the average of the measured yield and tensile ($=494 \text{ MPa}$ or 71.6 ksi) strengths of the beam flange, the maximum beam plastic rotation at the end of the test, the beam plastic rotation at which the maximum beam resistance dropped below 80 percent of the peak resistance, and the beam plastic rotation at which the moment in the beam at the nose of the reinforcing plate drops below 80 percent of the beam plastic moment calculated as the product of the plastic section modulus and the measured yield strength of the flange.

The maximum actuator loads for specimens RC01 through RC09 ranged between 158 kips (703 kN) and 168 kips (747 kN). The maximum load for RC10 was greater than that of the other specimens because the beam of RC10 was strengthened by the addition of longitudinal web stiffeners that were installed to delay beam web local buckling. The maximum moment developed in the beams of RC01 through RC09 ranged between

$$1.13 \leq \frac{M_b}{Z\sigma_y} \leq 1.20 \quad (8-1)$$

and

$$0.96 \leq \frac{M_b}{Z \frac{(\sigma_y + \sigma_u)}{2}} \leq 1.03 \quad (8-2)$$

where M_b is the maximum beam moment at the nose of the reinforcing plate, Z is the plastic section modulus, σ_y is the measured yield strength of the beam flange from coupon test data, and σ_u is the measured tensile strength of the beam flange from coupon test data. The maximum story drift in each specimen ranged between 4.8 and 5.5 percent of the story height. (For this calculation, the vertical displacement (drift) at the tip of the beam due to deflections in the reaction frame were removed.)

Table 8-4 Summary information for reinforced connections (SI units)

Response Quantity ¹	Specimen RC									
	01	02	03	04	05	06	07 ²	08	09	10
Q_m kN	729	747	747	703	721	734	707	747	716	854
θ_h %	4.8	4.8	5.0	5.3	5.5	4.8	5.4	5.5	5.3	5.2
$\frac{M_b}{Z\sigma_y}$	1.17	1.20	1.20	1.13	1.15	1.18	1.13	1.20	1.15	NA
$\frac{M_b}{Z \frac{(\sigma_y + \sigma_u)}{2}}$	1.00	1.03	1.03	0.96	0.99	1.00	0.97	1.03	0.99	NA
θ_p^m % rad	4.1	4.2	4.3	4.9	5.2	4.2	5.0	5.0	5.6	4.5
θ_p^{80} % rad	1.6	1.7	1.8	1.8	1.9	1.7	3.3	1.7	1.8	1.9
θ_p^{80b} % rad	2.6	2.5	2.8	2.4	2.3	2.7	3.9	2.8	2.7	3.9

1. Q_m = maximum actuator force; θ_h = maximum story drift; M_b = maximum moment in beam at nose of reinforcing plate; Z = plastic section modulus for

W30x99 beam; σ_y = measured yield strength of beam flanges; σ_u = measured ultimate strength of beam flanges; θ_p^m = maximum beam plastic rotation;

θ_p^{80} = maximum beam plastic rotation at 80 percent maximum resistance; θ_p^{80b} = maximum beam plastic rotation at 80 percent of beam plastic moment.

2. Near-field displacement history was used for Specimen RC07.

(8-3)

The maximum beam plastic rotation in each specimen varied between 4.1- and 5.6-percent radian. If the failure displacement is set equal to the displacement at which the maximum resistance in the cycle drops below 80 percent of the peak resistance, the maximum beam plastic rotation did not exceed 1.9 percent radian for the cyclically loaded connections. If the failure displacement is set equal to the displacement at which the moment in the beam at the nose of the reinforcing plate drops below 80 percent of the beam plastic moment, the maximum beam plastic rotation ranged between 2.3- and 2.8-percent radian for the cyclically loaded connections (with the exception of RC10 for which this failure descriptor was not used). For all ten specimens, the drop in maximum resistance was triggered by flange- and web-local buckling in the beam. Such buckling served to protect the reinforced connection from excessive straining. Summary remarks on each specimen follows.

Specimen RC01 was designed as the benchmark cover-plate connection. Rectangular cover plates were used to reinforce the connection, and these plates were joined to the beam flanges with longitudinal fillet welds only. The specimen was subjected to 32 displacement cycles at drifts up to $0.05h$, where h is the story height. RC01 failed during the second negative displacement excursion to $0.05h$. The beam top flange fractured near the tip of the cover plate due to severe flange local buckling and the resulting low cycle fatigue of the metal. The maximum measured strain in the reinforcement plates was less than twice the yield strain. Shear strains on the column web and doubler plate were measured at three locations. The strains in the web and doubler plate were most similar at story drift levels below 1 percent and greater than 3 percent of the story height.

Specimen RC02 was identical to RC01 except for the addition of lateral braces to the beam flanges, 35 in. (890 mm) from the column face. (Such lateral braces were added to RC02 only.) These braces were added to RC02 to prevent lateral movement (lateral-torsional buckling) of the beam flanges at the assumed far end of the beam plastic hinge. The specimen was subjected to 31 displacement cycles at drifts up to $0.05h$. The test of RC02 was terminated following fracture of the brace-to-flange tabs during the first negative displacement excursion to $0.05h$. The maximum axial load in the lateral braces was approximately equal to 12 percent of the product of the area of the beam flange and the measured yield strength of the beam flange. The maximum measured strain in the reinforcement plates was less than twice the yield strain. Modest yielding of the cover plate appeared to have no detrimental affect on the response of the connection.

Specimen RC03 was identical to RC01 except that each cover plate was joined to the beam flange with longitudinal and transverse fillet welds. The total volume of filler metal in the fillet welds of RC01 and RC03 was similar. The specimen was subjected to 32 displacement cycles at drifts up to $0.05h$. RC03 failed during the second negative displacement excursion to $0.05h$ due to fracture in the beam k-line due to severe local buckling of the beam flange and the beam web.

Specimen RC04 was the first flange-plate connection tested in this research program. Swallowtail-shaped plates were used to join the beam flanges to the column flange. The specimen was subjected to 33 displacement cycles at drifts up to $0.055h$. RC04 failed during the first negative displacement excursion to $0.055h$ due to fracture of the beam bottom flange due to severe flange local buckling. The maximum measured strain in the flange plates was less than 1.5 times the yield strain. Modest yielding of the flange plates appeared to have no detrimental effect on the response of the connection.

Specimen RC05 was fabricated with trapezoidal cover plates similar to that used to reinforce the top flange of specimen AN1 of the SAC Phase I project undertaken in the mid-1990s by some of the authors. Each cover plate was welded to the beam flange with two (inclined) longitudinal fillet welds and a transverse fillet weld. The specimen was subjected to 37 displacement cycles at drifts up to $0.055h$. RC05 failed during the second negative displacement excursion to $0.055h$ due to fracture of the beam bottom flange due to severe flange local buckling. The maximum measured strain in the cover plates ranged between 2 and 3 times the yield strain.

Specimen RC06 was designed as the benchmark flange-plate connection. The rectangular flange plates were joined to the beam flanges with two longitudinal and one transverse fillet welds. The fillet weld geometry of RC06 was similar to that of RC03 except that larger welds were used for RC06. The specimen was subjected to 34 displacement cycles at drifts up to $0.055h$. RC06 failed during the second negative displacement excursion to $0.055h$ due to fracture in the k-line of the beam, near the beam top flange, that resulted from severe flange and web local buckling. The maximum measured strains in the flange plates ranged between 2 and 3 times the yield strain.

Specimen RC07 was identical to RC06. RC07 was tested using the near-field displacement history described in Chapter 3. The objective of the RC07 test was to evaluate the effect of loading history (cyclic versus near-field) on the response of reinforced connections. Specimen RC07 failed during the third fully reversed displacement cycle to a drift level of $0.055h$ that was imposed following completion of the SAC near-field history. The top flange of the beam beyond the nose of the flange plate fractured due to severe flange local buckling and the resulting low cycle fatigue failure of the base metal. The rate of degradation of strength and stiffness of RC07 as a function of increasing story drift angle was substantially less than that of RC06, which provides clear evidence that the near-field loading protocol is less damaging than the cyclic loading protocol.

Specimen RC08 was identical to RC06 except for the thickness of the flange plates that was thinner in RC08. The objective of the RC08 test was to investigate the response of flange-plate connections with yielding flange plates. The specimen was subjected to 34 displacement cycles at drifts up to $0.055h$. RC08 failed during the second negative displacement excursion to $0.055h$ due to fracture of the beam top flange beyond the nose of the flange plate due to severe flange local buckling and the resulting low cycle fatigue failure of the base metal. The maximum measured strains in the flange plates ranged between 2 and 3 times the yield strain—similar to those recorded for RC06.

Specimen RC09 was identical to RC08 except that thinner continuity plates were used in RC09 and the doubler plate of RC08 was eliminated in RC09. As such, the panel zone of RC09 did not comply with current requirements (AISC 1997) for panel zone strength. The objective of this test was to study the effect of weak flange plates and a weak panel zone on the global response of plate-reinforced connections. RC09 was subjected to 34 displacement cycles at drifts up to $0.055h$. The specimen failed during the second positive displacement excursion to $0.055h$ due to fracture of the beam bottom flange beyond the nose of the flange plate due to the propagation of a crack that formed in the k-line of the beam. Testing was continued for another two cycles to a drift of $0.055h$ to investigate the post-fracture response of reinforced connections. The panel zone of RC09 yielded prior to the beam beyond the flange plate. Substantial strain hardening in the panel zone resulted in local buckling of the beam web and flanges at larger drift levels, which resulted in the loss of strength and stiffness in the specimen. The maximum measured strains in the flange plates ranged between 6 and 8 times the yield strain. Such yielding of the flange plates appeared to have no detrimental effect on the response of the connection.

Cover-plate specimen RC10 was designed to investigate the effect of delaying beam web local buckling on the global response of reinforced connections. RC10 was identical to cover-plate specimen RC03 except that two pairs of longitudinal stiffeners were welded to the beam web. Although these stiffeners were designed to delay web local buckling, they also increased the strength of the specimen, and placed greater strength demands on the cover-plate connection at the face of the column. RC10 was subjected to 32 displacement cycles at drifts up to $0.055h$. The specimen failed during the second negative displacement excursion to $0.055h$ due to fracture of the beam top flange beyond the end of the longitudinal stiffeners. The maximum measured strains in the flange plates ranged between 4 and 8 times the yield strain at a drift level of $0.03h$.

8.1.5 Response evaluation

The perceived advantages and disadvantages of cover- and flange-plate reinforced connections have been widely discussed within the SAC Joint Venture. One possible disadvantage of the cover-plate connection is that the connection geometry produces a stress riser near the face of the column flange at the interface of the reinforcing plate and the flange. This stress riser in conjunction with a triaxial state of tension at the face of the column could lead to unacceptable fractures of column flanges. For this reason, the flange-plate connection was considered by many to be the superior reinforcement detail of the two. The results of the experimental program did not serve to identify the superior connection because local instabilities in the beam limited the demand at the reinforced connection of the beam to the column. The nonlinear finite element analysis predicted smaller values of Mises stress and hydrostatic pressure in the flange-plate connection. Two cover-plate groove weld options, A and B, were considered; see Figure 6-1a. The option A connection is composed of two groove welds, each with a root pass. Such root passes may include substantial defects that can trigger brittle fracture. Although the root pass of the flange-to-column weld can be inspected and replaced if necessary, the root pass of the plate-to-column flange groove weld can neither be easily inspected nor replaced. As such, any defect in this root pass would align with the stress riser identified in the previous paragraph, and potentially increase the likelihood of brittle fracture. The ABAQUS analysis predicted maximum values of the fracture indices at the top of the beam flange-column flange groove weld—in the root pass of the cover plate-column flange groove weld, which can neither be inspected nor easily replaced.

Although broad conclusions should not be drawn from the analysis of one connection geometry, it appears that the flange-plate connection is marginally superior to the cover-plate connection, but that for cover-plate connections, the single-bevel groove weld detail (option B) is superior to the dual single-bevel groove weld (option A).

Three reinforcement-plate geometries were studied in this research program: rectangular, swallowtail, and trapezoidal. The swallowtail plate is not considered to be economical and is not considered further. The differences in performance of connections reinforced using rectangular plates versus trapezoidal plates will likely be small provided that the width of the tapered nose of the trapezoidal plate is sufficient to prevent the formation of high triaxial tension at the nose of the plate. Assuming a given length of reinforcing plate, and construction-related issues aside, the rectangular plate is likely superior to the trapezoidal plate for two reasons. First, the use of a rectangular plate similar to that adopted for RC03 provides a greater length for the placement of the plate-to-flange fillet welds than RC05, thus leading to a reduction in the size of the fillet welds. Second, the quality of the weld metal at the junction of the longitudinal and transverse fillet welds will likely be better for the rectangular plate because these welds are separated by the thickness of the plate and runoff tabs can be used to provide high quality weld metal at the end of the weld. Such tabs cannot be used at the junction of the welds for the trapezoidal plate because the welds are in the same plane.

Two geometries of the fillet welds joining the beam flange to the reinforcing plate were evaluated by analysis and experimentation: two longitudinal fillet welds only; and two longitudinal and one transverse fillet weld. The results of the experimental program did not serve to identify the superior geometry because flange and web local buckling in the beam limited the demand at the reinforced connection of the beam to the column. Finite element analysis of the two fillet weld geometries indicate that the 3-sided fillet weld (2 longitudinal welds, 1 transverse weld) is superior to the 2-sided fillet weld (2 longitudinal welds) for four reasons, namely, (1) smaller fillet welds can be used to join the reinforcement plate to the beam flange, (2) the reinforcement plate is more effectively mobilized near the nose of the reinforcing plate, (3) the probability of tearing of the fillet welds due to flange local buckling is reduced because the transverse weld does not permit the buckling to penetrate beyond the nose of the reinforcing plate, and (4) the likelihood of ductile fracture of the fillet welded connection is reduced. Regardless of whether 2- or 3-sided fillet welds are used, fabrication details should be adopted that maximize the quality of the weld metal at the ends of the longitudinal and transverse fillet welds. The runoff tabs used for such a purpose in this research program ensured that high quality weld metal of the correct throat thickness was placed at the nominal ends of the welds, where the strain demands are greatest.

The influence of delaying lateral-torsional buckling on the rotation capacity of a beam plastic hinge was studied using (a) response data from specimens RC01 and RC02 and (b) analysis using shell elements. Lateral bracing to the beam flanges of specimen RC02 was provided approximately 20 inches (508 mm) from the nose of the cover plate at the assumed far end of the plastic hinge; no such bracing was provided for RC01. Based on the force-displacement backbone curves for RC01 and RC02, there is no significant difference in the response of the two specimens. The restraint to lateral-torsional buckling provided to RC02 did not delay the loss of strength in RC02 following flange local buckling and web local buckling. The ABAQUS shell-

element analysis of four conditions of lateral restraint confirmed these experimental observations, namely, that provision of lateral bracing to the beam bottom flange at the far end of the plastic hinge zone will not lead to significant improvements in the cyclic response of reinforced connections.

The effect of loading history on the response of reinforced connections was studied using response data from specimens RC06 and RC07. Specimen RC06 was tested using the SAC cyclic displacement history. Specimen RC07, which was identical to RC06, was tested with the SAC near-field displacement history. The near-field displacement history is less damaging than the cyclic history as measured (a) experimentally using the force-displacement backbone curves for RC06 and RC07 and (b) analytically using the Park-Ang damage index. Specimen RC07 survived the displacement excursion to a drift level of $0.06h$, although the maximum resistance at such drift was much smaller than the peak resistance.

The effect of the beam web compactness ratio on the rotation capacity of reinforced connections was studied by comparing the normalized force-displacement backbone curves for specimens RC03 and RC10. (These two specimens were identical except for the two pairs of longitudinal stiffeners that were welded to the web of RC10 in the plastic hinge zone to delay web local buckling.) The rate of strength loss with increasing story drift angle was smaller in RC10 than in RC03.

Specimens RC08 and RC09 were detailed to promote modest yielding in the reinforcing plate. Maximum strains of 3 to 5 times the yield strain were measured in the flange plates of these specimens at a story drift angle of 3-percent radian. These strains were measured in the flange plate between the end of the beam and the face of the column: a distance of less than 2 in. (51 mm). Larger strains were not recorded because FLB and WLB in the beam at story drift angles greater than 3-percent radian led to a loss of strength in the beam and a consequent reduction in the flange-plate strains. Although strains of 3 to 5 times the yield strain had no apparent deleterious effect on the response of these two flange-plate specimens, the plastic rotations associated with these localized plastic strains will be small.

The utility and practicality of sharing joint plastic rotation between the panel zone and the beam in a reinforced connection were studied experimentally and analytically using specimens RC06 and RC09. Specimen RC09 was similar to RC06 except that thinner continuity plates were used in RC09 and the doubler plate was eliminated in RC09. The panel zones of RC06 and RC09 would be considered strong and weak, respectively, by current standards. The weak panel zone of RC09 yielded before the beam, and substantial strain hardening in the panel zone was required to initiate beam yielding. At this stage, all of the plastic deformation was in the panel zone. As the imposed displacements were increased further, the flange and web of the beam buckled and the resistance of the beam dropped. As the beam strength degraded, the strength demand on the panel zone dropped, and the panel zone responded elastically. At this stage, all of the plastic deformation was in the beam. These experiments clearly illustrate the difficulty of sharing joint plastic rotation between the panel zone and beams in reinforced connections over a wide range of story drift angles.

The load paths for the transfer of shear force from unreinforced and reinforced beams to the column were studied by analysis using Type SOL models. Design per FEMA 267A follows elementary beam theory and assumes that nearly 100 percent of the shear force in the beam is passed through the beam web to the column flange. Analysis of the unreinforced beam RC00 showed that the percentage of the shear force transferred through the beam flanges to the column is most different from that predicted by beam theory, and that the percentage varies as a function of the equivalent plastic strain in the beam flange: from 46 percent for beams with elastic flanges to 15 percent for flanges with an average equivalent plastic strain of 5.1 times the yield strain. Such differences from elementary beam theory make it difficult to design unreinforced and reinforced connections. The web of RC00 was reinforced with welded shear tabs of different thicknesses and widths to study analytically whether the addition of such plates substantially changed the beam-shear-force load path. The tabs included in the model of RC00 were installed between the weld access holes. The analytical studies showed no substantial change in the distribution between the flanges and the web at story drifts of 0.5- and 2-percent radian, even if the web thickness was increased by a factor of 3 for a distance of 10 in. (254 mm) from the column face. The load paths for the transfer of shear force in cover-plate and flange-plate connections were studied for different thicknesses of reinforcing plate. For both the cover-plate and flange-plate connections, the thicker the reinforcing plate, the greater the percentage of the beam shear force that is passed through the beam flanges and/or reinforcing plates.

8.1.6 Guidelines

Design guidelines and prequalified connections were presented in Chapter 7 based on the analytical and experimental studies presented in this report. The design guidelines make use of capacity design and elementary (elastic) beam theory. Such practices will neither preclude inelastic action at the face of the column nor accurately predict distributions of stress and strain over the length of the reinforced connection. Nonetheless, if the beam sizes are modest and the reinforcing plates are not overly thick, the use of the design guidelines should produce connections capable of developing plastic hinge rotations in excess of 2.5-percent radian. Reinforced connections that are required to develop plastic rotations that are substantially larger than 2.5-percent radian should be evaluated by full-scale testing.

8.2 Conclusions

Many conclusions can be drawn from the experimental and analytical studies described in this report. The key conclusions are listed below. Extrapolation of these conclusions to reinforced connections of a substantially different size or configuration should be undertaken with care.

1. None of the eight connections designed using FEMA 267A failed in a catastrophic manner; that is, the design procedures of FEMA 267A produced robust reinforced connections.
2. Connections reinforced with cover plates and flange plates will perform substantially better than unreinforced connections and are technically viable alternatives to moment-resisting connections reinforced with haunches or connections utilizing reduced beam sections.
3. Flange-plate connections are marginally less likely to suffer brittle or ductile fracture than

cover-plate connections. The beam-plate assembly of the cover-plate connection should be welded to the column flange with a single-bevel groove weld. Beam web connections should be groove welded to the column flange.

4. Rectangular reinforcing plates are preferable to trapezoidal or swallowtail shaped plates.
5. Reinforcing plates should be joined to beam flanges using three-sided fillet welds.
6. Bracing the bottom flange of beams in reinforced connections immediately beyond the plastic hinge zone will not lead to significant improvements in connection hysteresis.
7. The cyclic displacement history is more damaging for reinforced connections than the near-field displacement history.
8. Increased beam web compactness with respect to the current AISC limit is desirable. The new limit proposed by the SAC Joint Venture is most reasonable.
9. The use of yielding reinforcing plates will likely not lead to unacceptable connection performance if the maximum strains are modest. However, elastic-beam-theory design procedures for limiting the maximum strain to this value are unavailable at this time and the benefits gained in terms of increased beam plastic rotation will typically be small. Reinforcing plates should be detailed to remain elastic if the procedures of FEMA 267A are used for design.
10. It is impractical to share large plastic rotations between a panel zone and a beam section across a wide range of story drifts. Either the panel zone or the beam should be design to develop the design inelastic deformations, and capacity design principles should be used to confine the inelastic deformations to the selected component. Full-scale testing of prototype connections is recommended if the inelastic deformation is to be confined to the panel zone, especially for columns with relatively thin flanges.
11. The effectiveness of beam web reinforcement in the form of plates welded to the beam web and the column flange is likely most limited, especially if the web reinforcement is added between the weld access holes only.
12. The use of overly thick reinforcing plates in either cover- or flange-plate connections may not be advantageous because (1) much (all) of the shear force in the beam may be transferred to the column via the reinforcing plates and (2) large fillet welds will be needed to join the beam flange to the reinforcing plate. The effect of large shearing forces in the reinforcing plate and the beam flange (cover-plate connections only) cannot be captured by elementary beam theory. Either nonlinear finite element analysis or full-scale testing should be undertaken to evaluate the effects of such large shearing forces.
13. The maximum resistance of wide-flange beams can be estimated as the product of the plastic section modulus and the average of the expected yield and tensile strengths of the beam flange.

References

- Anderson, J. C., and Duan, X. 1998. *Repair/upgrade procedures for welded beam to column connections*. PEER 1998/03. Berkeley, Calif.: Pacific Earthquake Engineering Research Center, University of California.
- AISC. 1997. *Seismic provisions for structural steel buildings*. AISC Publication No. S341. Chicago: American Institute of Steel Construction, Inc.
- ATC. 1992. *Guidelines for cyclic testing of components of steel structures*. Report No. ATC-24. Redwood City, Calif.: Applied Technology Council.
- AWS 1996. *Bridge Welding Code*, Report No. ANSI/AASHTO/AWS D1.5-96. American Welding Society, Miami, FL.
- Barsom, J. M., and Rolfe, S. T. 1999. *Fracture and fatigue control in structures*. 3rd ed. Woburn, Mass.: Butterworth & Heinemann.
- Blackman, B., and Popov, E. P. 1995. *Studies in steel moment resisting beam-to-column connections for seismic design*. EERC 1995/11. Berkeley, Calif.: Earthquake Engineering Research Center, University of California at Berkeley.
- Bjorhovde, R., Goland, L. J., and Benac, D. J. 1999. *Tests of full-scale beam-to-column connections*. Tuscon, Ariz.: The Bjorhovde Group.
- El-Tawil, S., Mikesell, T., Vidarsson, E., and Kunnath, S. 1998. *Strength and ductility of FR welded-bolted connections*. SAC Report 98-01. Sacramento, Calif.: SAC Joint Venture.
- Engelhardt, M. D., and Sabol, T. A. 1995. *Testing of welded steel moment connections in response to the Northridge earthquake in Northridge steel update I*. American Institute of Steel Construction, October 1994. Available from AISC:312-670-2400. Also presented in *Modern Steel Construction* (May 1995) and in proceedings of *1995 AISC National Steel Construction Conference* (San Antonio, May 1995).
- FEMA. 1995a. *Interim guidelines: evaluation, repair, modification, and design of welded steel moment frame structures*. FEMA Report No. 267. Washington, D. C.: Federal Emergency Management Agency.

- FEMA. 1995b. *Interim guidelines: advisory no. 1, supplement to FEMA-276*. FEMA Report No. 267. Washington, D.C.: Federal Emergency Management Agency.
- FEMA. 2000. *State of the art report connection performance*. FEMA Report No. 355D. Washington, D.C.: Federal Emergency Management Agency.
- Francis, A. J. 1989. *Introducing Structures: Civil and Structural Engineering, Building and Architecture*, Ellis Horwood, UK.
- Gaylord, E. H., Gaylord, C., and Stallmeyer, J. E. 1992. *Design of steel structures*. 3rd ed. New York: McGraw Hill.
- Hancock, J. W., and Mackenzie, A. C. 1976. On the mechanism of ductile fracture in high-strength steels subjected to multi-axial stress states. *J. of Mech. Phys. Solids* 24:147–69.
- HKS. 1998. *ABAQUS theory manual*. Pawtucket, RI.: Hibbit, Karlsson, and Sorenson, Inc.
- Kaufmann, E. J. 1997. *Dynamic tension tests of simulated moment resisting frame weld joints*. Chicago: Steel Tips, Structural Steel Education Council, American Institute of Steel Construction, Inc.
- Krawinkler, H. 1998. *SAC testing program and loading histories*. Report to the SAC Joint Venture. Sacramento, Calif.: SAC Joint Venture.
- Lay, M. 1965. “Flange local buckling in wide-flange shapes.” *Journal of the Structural Division*, Vol. 91, No. ST6, pp. 95-116, American Society of Civil Engineers, Reston, Virginia.
- Lee, K-H., Goel, S. C., and Stojadinovic, B. 1997. *Boundary effects in welded steel moment connections*. UMCEE 97-20. Ann Arbor, Mich.: Department of Civil and Environmental Engineering, University of Michigan at Ann Arbor.
- Lemaitre, J. 1996. *A course of damage mechanics*. Berlin: Springer-Verlag.
- Mathworks. 1999. *The language of technical computing*. Natick, Mass.: The Mathworks, Inc.
- Noel, A., and Uang, C-M. 1996. *Cyclic testing of steel moment connections for the San Francisco Civic Center Complex*. TR-96/07. La Jolla, Calif.: Structural Systems Research Project, University of California at San Diego.
- Park, Y. J., Ang, A. H.-S., and Wen, Y. K., 1987. Damage-limiting aseismic design of buildings. *Earthquake Spectra* 3(1) 1–26. Oakland, Calif.: Earthquake Engineering Research Institute.
- Popov, E. P., and Stephen, R. M. 1970. *Cyclic loading of full-size steel connections*. EERC 1970/03. Berkeley, Calif.: Earthquake Engineering Research Center, University of California at Berkeley.

Popov, E. P., and Jakerst, M. 1995. *Lawrence Berkeley National Laboratory Human Genome Laboratory steel joint test: Technical Brief*. Forell/Elsesser Engineers, Inc. July 20, 1995. Unpublished report.

Popov, E. P., Blondet, M., and Stepanov, L. 1996. *Application of “dog bones” for improvement of seismic behavior of steel connections*. EERC 1996/05. Berkeley, Calif.: Earthquake Engineering Research Center, University of California at Berkeley.

Ricles, J. M., Mao, C., Lu, L. W., and Fisher, J. W. 2000. *Development and evaluation of improved details for ductile welded unreinforced flange connections*. SAC Report BD 00-24. Sacramento, Calif. SAC Joint Venture.

SAC. 1996. *Technical report: experimental investigations of beam-column subassemblages*. SAC Report 96-01, parts 1 and 2. Sacramento, Calif.: SAC Joint Venture.

Thomason, P. F. 1990. *Ductile fracture of metals*. New York: Pergamon Press.

Whittaker, A., and Gilani, A. 1996. *Cyclic testing of steel beam-column connections*. EERC-STI 1996/04. Berkeley, Calif.: Earthquake Engineering Research Center, University of California at Berkeley.

Whittaker, A. S. Bertero, V. V., and Gilani, A. S. 1996. *Experimental investigations of beam-column subassemblages*. SAC-96-01, part 1. Sacramento, Calif.: SAC Joint Venture.

Appendix A Fabrication Details

A.1 Mill Certificate Data

A.2 Welding Procedure Specifications

A.3 Stress-Strain Relations from Coupon Tests

A.4 Charpy Test Data

Mill Certificate Data

DATE	9/01/98
INVOICE NO.	439255
BILL OF LADING	369764
CUSTOMER NO.	2997
CUSTOMER PO.	TASK 7.08

NUCOR-YAMATO STEEL CO.
P.O. BOX 1228 • BLYTHEVILLE, AR 72316

CERTIFIED MILL TEST REPORT
100% MELTED AND MANUFACTURED IN U.S.A.

All beams produced by Nucor-Yamato Steel are cast and rolled to a fully killed and fine grain practice.

S H I P T O
GAYLE MANUFACTURING CO.
C/O RIK WILKINSON
S.P. SPUR 3767
WOODLAND CA 95695

S P E C I F I C A T I O N S
GRADE: ASTM A572GR50-97
GRADE: ASTM A709-97a GR50

(*)ASTM A572-50 Special requirements per
AISC Technical Bulletin #3 March, 1997.
GRADE: ASTM A6/A6M-97

S O L D T O
UNIV. OF CAL, BERKELEY 501-231-5627
EARTHQUAKE ENG. RESEARCH CTR
1301 S 46TH ST -- ANDREW WHITTAKER
BERKELEY CA 94804-4698

ITEM #	ITEM DESCRIPTION	QTY	HEAT #	MECHANICAL PROPERTIES						CHEMICAL PROPERTIES													
				YIELD TO TENSILE RATIO	YIELD STRENGTH	TENSILE STRENGTH	ELONG	CHARPY IMPACT		C	Mn	P	S	Si	Cu	Ni	Cr	Mo	V	Cb	CE1		
					PSI	PSI		%	TEMP °F													IMPACT ENERGY FT-LBS	Sn
1	WS14 -176.0 45' 4" W360 x262.0 13.818 #	4	122919	.76	55000	72000	23					.07	1.31	.013	.015	.24	.28	.11	.10	.03	.05	.002	.36
				.73	52000	71000	22													.01	.18	.0005	.40
					379	496	23																
					359	490	22																
2	WS30 - 99.0 45' W760 x147.0 13.716 #	3	121046	.76	50000	66000	20					.08	1.19	.014	.024	.21	.33	.10	.09	.02	.03	.004	.34
				.77	55000	71000	20													.01	.17	.0005	.37
					345	455	20																
					379	490	20																

RECEIVED
SEP 08 1998
Earthquake Engineering

ELONGATION BASED ON 8.00 INCH GAUGE LENGTH
 $CE1 = CE(IIW) = C + Mn/6 + (Cr+Mo+V)/5 + (Ni + Cu)/15$
 $CE2 = CE(SS0) = C + (Mn+Si)/6 + (Cu+Ni)/15 + (Cr+Mo+V+Cb)/5$

I hereby certify that the contents of this report are accurate and correct. All test results and operations performed by this material manufacturer are in compliance with the requirements of the material specifications, and when designated by the purchaser, meet the applicable specifications.

Gary Daph

QUALITY ASSURANCE
CUSTOMER COPY

STATE OF ARKANSAS COUNTY OF MISSISSIPPI
SWORN TO AND SUBSCRIBED BEFORE ME THIS _____ Day of _____
Charlene Washburn

NOTARY PUBLIC
MY COMMISSION EXPIRES _____

Welding Procedure Specifications

04/14/99 5:11 PM GAYLE MFG. COMPANY

NO.259 P.1/11

GAYLE

530 - 662 - 0284
FAX: 7841

MANUFACTURING COMPANY

FAX TRANSMITTAL

Company: EERC

Date: 04/14/99

Attention: Andrew Whittaker

Time: 2:46 AM

From: Rick Wilkinson

Subject: SAC Phase II Tests

Job#:WO 1696

Message:

The welding procedures we intend to use are attached for your use. Let me know if you need anything more.

FCAW 7-0 CJP charpy welds in the horizontal position (2G)

FCAW 15-0 Plug welds

FCAW 19-10 Non-charpy fillet welds (w/PQR's)

FCAW 21-0 CJP charpy welds in the flat position (1G)

FCAW 26-0 Charpy fillet welds

HD70 DBLR PL PJP fill gap welds at the edge of doubler plates

cc: Signet - Vicki @ (510) 783-4295
Mike Johnson @ GMC plant

PERFORMANCE THROUGH INNOVATION

PAGE 1 OF 1 PAGES SENT

EERC weld procedures

Welding Procedure Specifications

Gayle Manufacturing Co. Welding Procedure Specification

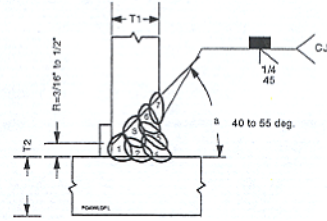
Page 1

FCAW7-0

WPS No. FCAW7-0 Date 6/2/97 By Bruce Cunningham Type Manual Machine
 Authorized By Bruce Cunningham Date 9/23/97 Revision 2 Semi-Auto Auto
 Welding Process(es) FCAW Prequalified
 Supporting PQR(s) N/A N/A N/A N/A

JOINT
 Type T-joint-TC-U4a-GF
 Backing Yes No Single Weld Double Weld
 Backing Material A36
 Root Opening 3/16 to 1/2" Root Face Dimension 0"
 Groove Angle 40to55 Radius (J-U) N/A
 Back Gouge Yes No
 Method N/A

Joint Detail



BASE METALS
 Material Spec. D1.1 Tbl 3.2 to D1.1 Tbl 3.2
 Type or Grade Category B to Category B
 Thickness: Groove (in) Unlimited - Unlimited
 Fillet (in) _____
 Diameter (Pipe, in) _____

POSITION
 Position of Groove 2G Fillet _____
 Vertical Progression: Up Down

FILLER METALS
 AWS Specification A5.20 Charpy V-notch
 AWS Classification E70T-1 & -9 @ -20 deg. F:
LCN Otshld HD70 20 ft-lbs min.

ELECTRICAL CHARACTERISTICS
 Transfer Mode (GMAW):
 Short-Circuiting Globular Spray
 Current: AC DCEP DCEN Pulsed
 Other N/A
 Tungsten Electrode (GTAW):
 Size N/A Type N/A

SHIELDING
 Flux Gas C02
Cored Composition 100%
 Electrode-Flux (Class) Flow Rate 50 CFH
N/A Gas Cup Size 3/4in.

TECHNIQUE
 Stringer or Weave Bead Stringer
 Multi-pass or Single Pass (per side) Multiple
 Number of Electrodes 1
 Electrode Spacing: Longitudinal N/A
 Lateral N/A
 Angle Pull 5 W 10
 Contact Tube to Work Distance 1 1/4in.
 Peening None
 Interpass Cleaning D1.1-96 Sec. 5.30.1 NOTES

PREHEAT
 Preheat Temp., Min. Table 3.2
 Thickness Up to 3/4" Temperature Note 1
 Over 3/4" to 1-1/2" 50 Deg. F
 Over 1-1/2" to 2-1/2" 150 Deg. F
 Over 2-1/2" 225 Deg. F
 Interpass Temp., Min. Table 3.2 Max. 550 Deg. F

POSTWELD HEAT TREATMENT PWHT Required
 Temp. N/A Time N/A

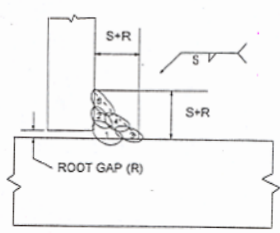
WELDING PROCEDURE

Layer/Pass	Process	Filler Metal Class	Diameter	Cur. Type	Amps or WFS	Volts	Travel Speed	Other Notes
Root	FCAW	E70T-1 & -9	3/32"	DCEP	475/250	29.5	9-14(12)	
2-5(2)	FCAW	E70T-1 & -9	3/32"	DCEP	475/250	29.5	13-21(13)	T1=3/8"
2-7(3)	FCAW	E70T-1 & -9	3/32"	DCEP	475/250	29.5	9-13(13)	T1=1/2"
3-9(4)	FCAW	E70T-1 & -9	3/32"	DCEP	475/250	29.5	9-14(12)	T1=5/8"
4-11(5)	FCAW	E70T-1 & -9	3/32"	DCEP	475/250	29.5	9-14(11)	T1=3/4"
5-13(7)	FCAW	E70T-1 & -9	3/32"	DCEP	475/250	29.5	9-14(12)	T1=7/8"
7-15(8)	FCAW	E70T-1 & -9	3/32"	DCEP	475/250	29.5	9-15(11)	T1=1"
8-18(10)	FCAW	E70T-1 & -9	3/32"	DCEP	475/250	29.5	9-14(12)	T1=1 1/8"

Welding Procedure Specifications

Gayle Manufacturing Co. Welding Procedure Specification

Page 1 of 1
FCAW 19-10

WPS No. <u>FCAW 19-10</u> Date <u>12/5/97</u> By <u>Keith Davey</u> Type Manual <input type="checkbox"/> Machine <input type="checkbox"/>																																																																																																				
Authorized By <u>Keith Davey</u> Date <u>12/5/97</u> Revision <u>0</u> Semi-Auto <input checked="" type="checkbox"/> Auto <input type="checkbox"/>																																																																																																				
Welding Process(es) <u>FCAW</u> <u>N/A</u> Prequalified <input type="checkbox"/>																																																																																																				
Supporting PQR(s) <u>FCAW 19S</u> <u>FCAW 19M</u> <u>N/A</u> <u>N/A</u>																																																																																																				
JOINT Type <u>T-Joint</u> Backing Yes <input type="checkbox"/> No <input checked="" type="checkbox"/> Single Weld <input checked="" type="checkbox"/> Double Weld <input type="checkbox"/> Backing Material <u>N/A</u> Root Opening <u>0 to 3/16"</u> Root Face Dimension <u>N/A</u> Groove Angle <u>N/A</u> Radius (J-U) <u>N/A</u> Back Gouge Yes <input type="checkbox"/> No <input checked="" type="checkbox"/> Method <u>N/A</u>	Joint Detail 																																																																																																			
BASE METALS Material Spec. <u>D1.1-98Tb13.1</u> to <u>D1.1-98Tb13.1</u> Type or Grade <u>Group I & II</u> to <u>Group I & II</u> Thickness: Groove (in) _____ - _____ Fillet (in) <u>1/8</u> - <u>Unlimited</u> Diameter (Pipe, in) <u>24</u> - <u>Unlimited</u>	POSITION Position of Groove <u>N/A</u> Fillet <u>1F and 2F</u> Vertical Progression: <input type="checkbox"/> Up <input type="checkbox"/> Down																																																																																																			
FILLER METALS AWS Specification <u>A5.20</u> <u>N/A</u> AWS Classification <u>E70T-7</u> <u>N/A</u> <u>Lincoln NR311</u> <u>N/A</u>	ELECTRICAL CHARACTERISTICS Transfer Mode (GMAW): Short-Circuiting <input type="checkbox"/> Globular <input type="checkbox"/> Spray <input type="checkbox"/> Current: AC <input type="checkbox"/> DCEP <input type="checkbox"/> DCEN <input checked="" type="checkbox"/> Pulsed <input type="checkbox"/> Other <u>N/A</u> Tungsten Electrode (GTAW): Size <u>N/A</u> Type <u>N/A</u>																																																																																																			
SHIELDING Flux Gas <u>N/A</u> Cored _____ Composition <u>N/A</u> Electrode-Flux (Class) Flow Rate <u>N/A</u> N/A Gas Cup Size <u>N/A</u>	TECHNIQUE Stringer or Weave Bead <u>Stringer</u> Multi-pass or Single Pass (per side) <u>Multiple</u> Number of Electrodes <u>1</u> Electrode Spacing: Longitudinal <u>N/A</u> Lateral <u>N/A</u> Angle <u>Variable</u> Contact Tube to Work Distance <u>2 1/4"</u> Peening <u>None</u> Interpass Cleaning <u>D1.1-98 Sec. 5.30.1</u>																																																																																																			
PREHEAT Preheat Temp., Min. <u>Table 3.2</u> Thickness Up to 3/4" Temperature <u>Note 1</u> Over 3/4" to 1-1/2" <u>50 Deg. F</u> Over 1-1/2" to 2-1/2" <u>150 Deg. F</u> Over 2-1/2" <u>225 Deg. F</u> Interpass Temp., Min. <u>Table 3.2</u> Max. <u>550 Deg. F</u>	POSTWELD HEAT TREATMENT PWHT Required <input type="checkbox"/> Temp. <u>N/A</u> Time <u>N/A</u>																																																																																																			
WELDING PROCEDURE																																																																																																				
<table border="1" style="width: 100%; border-collapse: collapse;"> <thead> <tr> <th>Layer/Pass</th> <th>Process</th> <th>Filler Metal Class</th> <th>Diameter</th> <th>Cur. Type</th> <th>Amps or WFS</th> <th>Volts</th> <th>Travel Speed</th> <th>Other Notes</th> </tr> </thead> <tbody> <tr> <td>1)</td> <td>FCAW</td> <td>E70T-7</td> <td>7/64"</td> <td>DCEN</td> <td>525 / 260</td> <td>32</td> <td>17-26(21)</td> <td>5/16 in.</td> </tr> <tr> <td>2-3(2)</td> <td>FCAW</td> <td>E70T-7</td> <td>7/64"</td> <td>DCEN</td> <td>525 / 260</td> <td>32</td> <td>13-19(16)</td> <td>3/8 in.</td> </tr> <tr> <td>3-6(3)</td> <td>FCAW</td> <td>E70T-7</td> <td>7/64"</td> <td>DCEN</td> <td>525 / 260</td> <td>32</td> <td>12-20(16)</td> <td>1/2 in.</td> </tr> <tr> <td>4-7(4)</td> <td>FCAW</td> <td>E70T-7</td> <td>7/64"</td> <td>DCEN</td> <td>525 / 260</td> <td>32</td> <td>11-17(12)</td> <td>5/8 in.</td> </tr> <tr> <td>6-10(6)</td> <td>FCAW</td> <td>E70T-7</td> <td>7/64"</td> <td>DCEN</td> <td>525 / 260</td> <td>32</td> <td>12-19(14)</td> <td>3/4 in.</td> </tr> <tr> <td>8-12(8)</td> <td>FCAW</td> <td>E70T-7</td> <td>7/64"</td> <td>DCEN</td> <td>525 / 260</td> <td>32</td> <td>12-18(14)</td> <td>7/8 in.</td> </tr> <tr> <td>10-15(10)</td> <td>FCAW</td> <td>E70T-7</td> <td>7/64"</td> <td>DCEN</td> <td>525 / 260</td> <td>32</td> <td>12-18(14)</td> <td>1 in.</td> </tr> <tr> <td>13-19(13)</td> <td>FCAW</td> <td>E70T-7</td> <td>7/64"</td> <td>DCEN</td> <td>525 / 260</td> <td>32</td> <td>13-19(15)</td> <td>1 1/8 in.</td> </tr> <tr> <td> </td> </tr> <tr> <td> </td> </tr> </tbody> </table>		Layer/Pass	Process	Filler Metal Class	Diameter	Cur. Type	Amps or WFS	Volts	Travel Speed	Other Notes	1)	FCAW	E70T-7	7/64"	DCEN	525 / 260	32	17-26(21)	5/16 in.	2-3(2)	FCAW	E70T-7	7/64"	DCEN	525 / 260	32	13-19(16)	3/8 in.	3-6(3)	FCAW	E70T-7	7/64"	DCEN	525 / 260	32	12-20(16)	1/2 in.	4-7(4)	FCAW	E70T-7	7/64"	DCEN	525 / 260	32	11-17(12)	5/8 in.	6-10(6)	FCAW	E70T-7	7/64"	DCEN	525 / 260	32	12-19(14)	3/4 in.	8-12(8)	FCAW	E70T-7	7/64"	DCEN	525 / 260	32	12-18(14)	7/8 in.	10-15(10)	FCAW	E70T-7	7/64"	DCEN	525 / 260	32	12-18(14)	1 in.	13-19(13)	FCAW	E70T-7	7/64"	DCEN	525 / 260	32	13-19(15)	1 1/8 in.																		
Layer/Pass	Process	Filler Metal Class	Diameter	Cur. Type	Amps or WFS	Volts	Travel Speed	Other Notes																																																																																												
1)	FCAW	E70T-7	7/64"	DCEN	525 / 260	32	17-26(21)	5/16 in.																																																																																												
2-3(2)	FCAW	E70T-7	7/64"	DCEN	525 / 260	32	13-19(16)	3/8 in.																																																																																												
3-6(3)	FCAW	E70T-7	7/64"	DCEN	525 / 260	32	12-20(16)	1/2 in.																																																																																												
4-7(4)	FCAW	E70T-7	7/64"	DCEN	525 / 260	32	11-17(12)	5/8 in.																																																																																												
6-10(6)	FCAW	E70T-7	7/64"	DCEN	525 / 260	32	12-19(14)	3/4 in.																																																																																												
8-12(8)	FCAW	E70T-7	7/64"	DCEN	525 / 260	32	12-18(14)	7/8 in.																																																																																												
10-15(10)	FCAW	E70T-7	7/64"	DCEN	525 / 260	32	12-18(14)	1 in.																																																																																												
13-19(13)	FCAW	E70T-7	7/64"	DCEN	525 / 260	32	13-19(15)	1 1/8 in.																																																																																												
Per AWS D1.1																																																																																																				

Welding Procedure Specifications

PROCEDURE QUALIFICATION RECORD (PQR) Gayle Manufacturing Company

Identification: FCAW 19S-PQR

Welding Process: Semi-Automatic FCAW

JOINT DESIGN USED

Type: Fillet
Root Opening: 0 in.

PREHEAT

Preheat Temperature: 50 F. Deg.
Interpass Temperature: 100 F. Deg. to 400 F. Deg.

BASE METAL

Material Specification: ASTM A36
Thickness: 3/8 in. to 1 in.

POSITION

Position of Groove: 2F

FILLER METAL

AWS Specification: A5.20
AWS Classification: E70T-7 (Lincoln NR311)
Diameter: 7/64 in.

ELECTRICAL CHARACTERISTICS

Voltage: Constant Current: DCEN

SHIELDING

Flux: Cored

TECHNIQUE

Bead: Stringer
Pass: Single-pass
ESO: 2 1/4 in.
Interpass Cleaning: AWS D1.1-94 Sec. 3.11.1

TEST RESULTS

Visual Inspection:

Appearance: Satisfactory
 Undercut: Satisfactory
 Porosity: Satisfactory

Macroetch Test: See Attached Test Report
1. Satisfactory 2. Satisfactory 3. Satisfactory

Test date: 1/9/96
Conducted by: Mike Johnson/STL
Laboratory: Signet Testing Laboratories, Inc.

WELDING PROCEDURE

SIZE	PASSES	TRAVEL (IPM)	AMPS	WFS (IPM)	VOLTS
5/16 in.	1	20	525	240	32

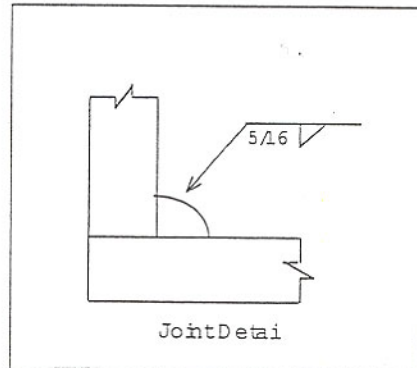
WELDER

Name: Alfredo Pineda
Identification Stamp: L

We the undersigned, certify that the statements in this record are correct and that the test welds were prepared, welded, and tested in accordance with the requirements of section 5, Part B of AWS D1.1-94 Structural Welding Code-Steel.

Signed: Gayle Manufacturing Company
By:

 Bruce Cunningham
Title: Quality Control Manager
Date: 2/20/96



Welding Procedure Specifications

SIGNET
Testing Labs

February 13, 1996

Mr. Gary Glenn
GAYLE MANUFACTURING COMPANY
P.O. Box 1365
1455 E. Kentucky Avenue
Woodland, CA 95776

STL NO.: 1219-001
LAB NO.: M11717-2

RE: **Fillet Weld Welding Procedure Qualification Test Record (PQR) #FCAW 19S-PQR**

Dear Gary:

Please find listed below, the procedure specifications and test results for the fillet weld procedure qualification test, performed at your facilities on January 9, 1996.

Gayle Mfg. Co. PQR No. : FCAW 19S-PQR
Joint Design : T-Joint / 5/16" Fillet Weld
Base Material : ASTM A36 (Base Thickness - 1" & Stem Thickness - 3/8")
Position : 2F - Horizontal
Filler Metal Specification : A5.20
Filler Metal Classification : E70T-7 (Lincoln NR311)
Wire Diameter : 7/64"
Electrical Stickout : 2-1/4"
Voltage : 32
Amperage : 525
Wire Feed Speed : 240 IPM
Travel Speed : 20 IPM
Preheat Temperature : 50°F
Interpass Temperature : 100°F to 400°F
Technique : Single-Pass Stringer Bead
Welder : Alfredo Pineda, Stamp L

Qualification Test Results

Visual Inspection : Satisfactory
Conducted By : Mike Johnson / Signet Testing Labs
Test Date : January 9, 1996
Macroetch Tests : Satisfactory (a total of 3 required)

We, the undersigned, certify that the statements in this record are correct, and that the test welds were prepared, welded and tested in accordance with the requirements of Section 5 of AWS D1.1-94 - Structural Welding Code - Steel.

Respectfully Submitted,

SIGNET TESTING LABORATORIES



Michael F. Everson
Manager, Structural Dept.

MFE/dd

Corporate Office: 25064 Viking St. □ Hayward, CA 94545 □ 510-887-8484 □ FAX 510-783-4295
Other Locations: Oakland □ San Francisco □ Sacramento □ Santa Ana

Welding Procedure Specifications

PROCEDURE QUALIFICATION RECORD (PQR) Gayle Manufacturing Company

Identification: FCAW 19M-PQR

Welding Process: Semi-Automatic FCAW

JOINT DESIGN USED

Type: Fillet
Root Opening: 0 in.

PREHEAT

Preheat Temperature: 50 F. Deg.
Interpass Temperature: 100 F. Deg. to 400 F. Deg.

BASE METAL

Material Specification: ASTM A36
Thickness: 3/8 in. to 1 in.

POSITION

Position of Groove: 2F

FILLER METAL

AWS Specification: A5.20
AWS Classification: E70T-7 (Lincoln NR311)
Diameter: 7/64 in.

ELECTRICAL CHARACTERISTICS

Voltage: Constant Current: DCEN

SHIELDING

Flux: Cored

TECHNIQUE

Bead: Stringer
Pass: Multi-pass
ESO: 2 1/4 in.
Interpass Cleaning: AWS D1.1-94 Sec. 3.11.1

TEST RESULTS

Visual Inspection:

Appearance: Satisfactory
Undercut: Satisfactory
Porosity: Satisfactory

Macroetch Test: See Attached Test Report
1. Satisfactory 2. Satisfactory 3. Satisfactory

Test date: 1/5/96
Conducted by: Mike Johnson/STL
Laboratory: Signet Testing Laboratories, Inc.

WELDING PROCEDURE

SIZE	PASSES	TRAVEL (IPM)	AMPS	WFS (IPM)	VOLTS
3/8 in.	2	16	525	240	32

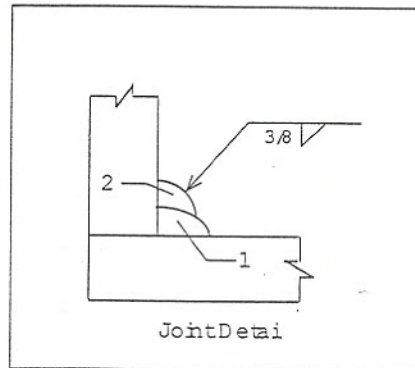
WELDER

Name: Paul Truit
Identification Stamp: T

We the undersigned, certify that the statements in this record are correct and that the test welds were prepared, welded, and tested in accordance with the requirements of section 5, Part B of AWS D1.1-94 Structural Welding Code-Steel.

Signed: Gayle Manufacturing Company
By:

Bruce Cunningham
Title: Quality Control Manager
Date: 2/20/96



Welding Procedure Specifications

SIGNET
Testing Labs

February 13, 1996

Mr. Gary Glenn
GAYLE MANUFACTURING COMPANY
P.O. Box 1365
1455 E. Kentucky Avenue
Woodland, CA 95776

STL NO.: 1219-001
LAB NO.: M11717-1

RE: **Fillet Weld Welding Procedure Qualification Test Record (PQR) #FCAW 19M-PQR**

Dear Gary:

Please find listed below, the procedure specifications and test results for the fillet weld procedure qualification test, performed at your facilities on January 5, 1996.

Gayle Mfg. Co. PQR No. : FCAW 19M-PQR
Joint Design : T-Joint / 3/8" Fillet Weld
Base Material : ASTM A36 (Base Thickness - 1" & Stem Thickness - 3/8")
Position : 2F - Horizontal
Filler Metal Specification : A5.20
Filler Metal Classification : E70T-7 (Lincoln NR311)
Wire Diameter : 7/64"
Electrical Stickout : 2-1/4"
Voltage : 32
Amperage : 525
Wire Feed Speed : 240 IPM
Travel Speed : 16 IPM
Preheat Temperature : 50°F
Interpass Temperature : 100°F to 400°F
Technique : Multiple-Pass Stringer Bead
Welder : Paul Truit, Stamp T

Qualification Test Results

Visual Inspection : Satisfactory
Conducted By : Mike Johnson / Signet Testing Labs
Test Date : January 5, 1996
Macroetch Tests : Satisfactory (a total of 3 required)

We, the undersigned, certify that the statements in this record are correct, and that the test welds were prepared, welded and tested in accordance with the requirements of Section 5 of AWS D1.1-94 - Structural Welding Code - Steel.

Respectfully Submitted,

SIGNET TESTING LABORATORIES



Michael F. Everson
Manager, Structural Dept.

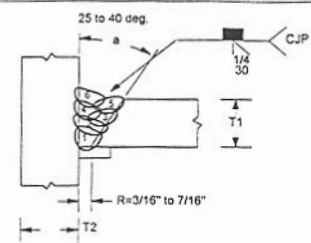
MFE/dd

Corporate Office: 25064 Viking St. □ Hayward, CA 94545 □ 510-887-8484 □ FAX 510-783-4295
Other Locations: Oakland □ San Francisco □ Sacramento □ Santa Ana

Welding Procedure Specifications

Gayle Manufacturing Co. Welding Procedure Specification

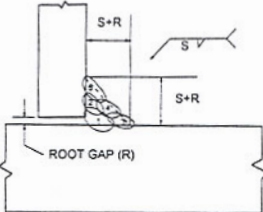
Page 1 of 1
FCAW21-0

WPS No. <u>FCAW21-0</u> Date <u>9/23/97</u> By <u>Bruce Cunningham</u> Type Manual <input type="checkbox"/> Machine <input type="checkbox"/>																																																																																		
Authorized By <u>Bruce Cunningham</u> Date <u>9/23/97</u> Revision <u>15</u> Semi-Auto <input checked="" type="checkbox"/> Auto <input type="checkbox"/>																																																																																		
Welding Process(es) <u>FCAW</u> Prequalified <input checked="" type="checkbox"/>																																																																																		
Supporting PQR(s) <u>N/A</u> <u>N/A</u> <u>N/A</u> <u>N/A</u>																																																																																		
JOINT Type <u>T-joint-TC-U4a-GF</u> Backing Yes <input checked="" type="checkbox"/> No <input type="checkbox"/> Single Weld <input checked="" type="checkbox"/> Double Weld <input type="checkbox"/> Backing Material <u>A36</u> Root Opening <u>3/16 to 7/16</u> Root Face Dimension <u>0"</u> Groove Angle <u>25 TO 40</u> Radius (J-U) <u>N/A</u> Back Gouge Yes <input type="checkbox"/> No <input checked="" type="checkbox"/> Method <u>N/A</u>	Joint Detail 																																																																																	
BASE METALS Material Spec. <u>D1.1 Tbl 3.1</u> to <u>D1.1 Tbl 3.1</u> Type or Grade <u>Group I & II</u> to <u>Group I & II</u> Thickness: Groove (in) <u>Unlimited</u> - <u>Unlimited</u> Fillet (in) _____ - _____ Diameter (Pipe, in) _____ - _____	POSITION Position of Groove <u>1G</u> Fillet _____ Vertical Progression: <input type="checkbox"/> Up <input type="checkbox"/> Down ELECTRICAL CHARACTERISTICS Transfer Mode (GMAW): Short-Circuiting <input type="checkbox"/> Globular <input type="checkbox"/> Spray <input type="checkbox"/> Current: AC <input type="checkbox"/> DCEP <input checked="" type="checkbox"/> DCEN <input type="checkbox"/> Pulsed <input type="checkbox"/> Other <u>N/A</u> Tungsten Electrode (GTAW): Size <u>N/A</u> Type <u>N/A</u>																																																																																	
FILLER METALS AWS Specification <u>A5.20</u> Charpy V-notch _____ AWS Classification <u>E70T-1 & -9</u> LCN Otshld HD70 _____ @ -20 deg. F: <u>20 ft-lbs min.</u>	TECHNIQUE Stringer or Weave Bead <u>Stringer</u> Multi-pass or Single Pass (per side) <u>Table 3.7</u> Number of Electrodes <u>1</u> Electrode Spacing: Longitudinal <u>N/A</u> Lateral <u>N/A</u> Angle <u>Pull 5 W 10</u> Contact Tube to Work Distance <u>1 1/4in.</u> Peening <u>None</u> Interpass Cleaning <u>D1.1-96 Sec. 5.30.1 NOTES</u>																																																																																	
SHIELDING Flux _____ Gas <u>C02</u> Cored _____ Composition <u>100%</u> Electrode-Flux (Class) _____ Flow Rate <u>60 CFH</u> N/A _____ Gas Cup Size <u>3/4in.</u>	POSTWELD HEAT TREATMENT PWHT Required <input type="checkbox"/> Temp. <u>N/A</u> Time <u>N/A</u>																																																																																	
PREHEAT Preheat Temp., Min. <u>Table 3.2</u> Thickness Up to 3/4" Temperature <u>Note 1</u> Over 3/4" to 1-1/2" <u>50 Deg. F</u> Over 1-1/2" to 2-1/2" <u>150 Deg. F</u> Over 2-1/2" <u>225 Deg. F</u> Interpass Temp., Min. <u>Table 3.2</u> Max. <u>550 Deg. F</u>																																																																																		
WELDING PROCEDURE																																																																																		
<table border="1" style="width: 100%; border-collapse: collapse;"> <thead> <tr> <th>Layer/Pass</th> <th>Process</th> <th>Filler Metal Class</th> <th>Diameter</th> <th>Cur. Type</th> <th>Amps or WFS</th> <th>Volts</th> <th>Travel Speed</th> <th>Other Notes</th> </tr> </thead> <tbody> <tr> <td>Root</td> <td>FCAW</td> <td>E70T-1 & -9</td> <td>3/32"</td> <td>DCEP</td> <td>475/250</td> <td>29.5</td> <td>10-16(13)</td> <td></td> </tr> <tr> <td>1-5(2)</td> <td>FCAW</td> <td>E70T-1 & -9</td> <td>3/32"</td> <td>DCEP</td> <td>475/250</td> <td>29.5</td> <td>15-23(14)</td> <td>T1=3/8"</td> </tr> <tr> <td>2-6(2)</td> <td>FCAW</td> <td>E70T-1 & -9</td> <td>3/32"</td> <td>DCEP</td> <td>475/250</td> <td>29.5</td> <td>14-21(14)</td> <td>T1=1/2"</td> </tr> <tr> <td>2-7(3)</td> <td>FCAW</td> <td>E70T-1 & -9</td> <td>3/32"</td> <td>DCEP</td> <td>475/250</td> <td>29.5</td> <td>13-20(14)</td> <td>T1=5/8"</td> </tr> <tr> <td>3-9(4)</td> <td>FCAW</td> <td>E70T-1 & -9</td> <td>3/32"</td> <td>DCEP</td> <td>475/250</td> <td>29.5</td> <td>13-20(16)</td> <td>T1=3/4"</td> </tr> <tr> <td>4-11(5)</td> <td>FCAW</td> <td>E70T-1 & -9</td> <td>3/32"</td> <td>DCEP</td> <td>475/250</td> <td>29.5</td> <td>12-19(15)</td> <td>T1=7/8"</td> </tr> <tr> <td>4-12(6)</td> <td>FCAW</td> <td>E70T-1 & -9</td> <td>3/32"</td> <td>DCEP</td> <td>475/250</td> <td>29.5</td> <td>12-19(15)</td> <td>T1=1"</td> </tr> <tr> <td>4-18(18)</td> <td>FCAW</td> <td>E70T-1 & -9</td> <td>3/32"</td> <td>DCEP</td> <td>475/250</td> <td>29.5</td> <td>12-19(15)</td> <td>T1=1 1/8"</td> </tr> </tbody> </table>		Layer/Pass	Process	Filler Metal Class	Diameter	Cur. Type	Amps or WFS	Volts	Travel Speed	Other Notes	Root	FCAW	E70T-1 & -9	3/32"	DCEP	475/250	29.5	10-16(13)		1-5(2)	FCAW	E70T-1 & -9	3/32"	DCEP	475/250	29.5	15-23(14)	T1=3/8"	2-6(2)	FCAW	E70T-1 & -9	3/32"	DCEP	475/250	29.5	14-21(14)	T1=1/2"	2-7(3)	FCAW	E70T-1 & -9	3/32"	DCEP	475/250	29.5	13-20(14)	T1=5/8"	3-9(4)	FCAW	E70T-1 & -9	3/32"	DCEP	475/250	29.5	13-20(16)	T1=3/4"	4-11(5)	FCAW	E70T-1 & -9	3/32"	DCEP	475/250	29.5	12-19(15)	T1=7/8"	4-12(6)	FCAW	E70T-1 & -9	3/32"	DCEP	475/250	29.5	12-19(15)	T1=1"	4-18(18)	FCAW	E70T-1 & -9	3/32"	DCEP	475/250	29.5	12-19(15)	T1=1 1/8"
Layer/Pass	Process	Filler Metal Class	Diameter	Cur. Type	Amps or WFS	Volts	Travel Speed	Other Notes																																																																										
Root	FCAW	E70T-1 & -9	3/32"	DCEP	475/250	29.5	10-16(13)																																																																											
1-5(2)	FCAW	E70T-1 & -9	3/32"	DCEP	475/250	29.5	15-23(14)	T1=3/8"																																																																										
2-6(2)	FCAW	E70T-1 & -9	3/32"	DCEP	475/250	29.5	14-21(14)	T1=1/2"																																																																										
2-7(3)	FCAW	E70T-1 & -9	3/32"	DCEP	475/250	29.5	13-20(14)	T1=5/8"																																																																										
3-9(4)	FCAW	E70T-1 & -9	3/32"	DCEP	475/250	29.5	13-20(16)	T1=3/4"																																																																										
4-11(5)	FCAW	E70T-1 & -9	3/32"	DCEP	475/250	29.5	12-19(15)	T1=7/8"																																																																										
4-12(6)	FCAW	E70T-1 & -9	3/32"	DCEP	475/250	29.5	12-19(15)	T1=1"																																																																										
4-18(18)	FCAW	E70T-1 & -9	3/32"	DCEP	475/250	29.5	12-19(15)	T1=1 1/8"																																																																										
Per AWS D1.1																																																																																		

Welding Procedure Specifications

Gayle Manufacturing Co. Welding Procedure Specification

Page 1 of 1
FCAW 26-0

WPS No. <u>FCAW 26-0</u> Date <u>1/30/98</u> By <u>Keith Davey</u> Type Manual <input type="checkbox"/> Machine <input type="checkbox"/>																																																																																																				
Authorized By <u>Keith Davey</u> Date <u>1/30/98</u> Revision <u>0</u> Semi-Auto <input checked="" type="checkbox"/> Auto <input type="checkbox"/>																																																																																																				
Welding Process(es) <u>FCAW</u> <u>N/A</u> Prequalified <input checked="" type="checkbox"/>																																																																																																				
Supporting PQR(s) <u>N/A</u> <u>N/A</u> <u>N/A</u> <u>N/A</u>																																																																																																				
JOINT Type <u>T-Joint</u> Backing Yes <input type="checkbox"/> No <input checked="" type="checkbox"/> Single Weld <input checked="" type="checkbox"/> Double Weld <input type="checkbox"/> Backing Material <u>N/A</u> Root Opening <u>0 to 3/16"</u> Root Face Dimension <u>N/A</u> Groove Angle <u>N/A</u> Radius (J-U) <u>N/A</u> Back Gouge Yes <input type="checkbox"/> No <input checked="" type="checkbox"/> Method <u>N/A</u>	Joint Detail 																																																																																																			
BASE METALS Material Spec. <u>D1.1-98 Tbl3.1</u> to <u>D1.1-98 Tbl3.1</u> Type or Grade <u>Group I & II</u> to <u>Group I & II</u> Thickness: Groove (in) _____ - _____ Fillet (in) <u>1/8</u> - <u>Unlimited</u> Diameter (Pipe, in) <u>24</u> - <u>Unlimited</u>	POSITION Position of Groove <u>N/A</u> Fillet <u>1F and 2F</u> Vertical Progression: <input type="checkbox"/> Up <input type="checkbox"/> Down ELECTRICAL CHARACTERISTICS Transfer Mode (GMAW): Short-Circuiting <input type="checkbox"/> Globular <input type="checkbox"/> Spray <input type="checkbox"/> Current: AC <input type="checkbox"/> DCEP <input checked="" type="checkbox"/> DCEN <input type="checkbox"/> Pulsed <input type="checkbox"/> Other <u>N/A</u> Tungsten Electrode (GTAW): Size <u>N/A</u> Type <u>N/A</u>																																																																																																			
FILLER METALS AWS Specification <u>A5.20</u> Charpy V-Notch _____ AWS Classification <u>E70T-1 & -9</u> 20 Ft-Lbs _____ <u>LCN O.S. HD70</u> @ -20 deg. F. _____	TECHNIQUE Stringer or Weave Bead <u>Stringer</u> Multi-pass or Single Pass (per side) <u>Multiple</u> Number of Electrodes <u>1</u> Electrode Spacing: Longitudinal <u>N/A</u> Lateral <u>N/A</u> Angle <u>Pu 0-5 W 0/50</u> Contact Tube to Work Distance <u>1 to 1 1/4"</u> Peening <u>None</u> Interpass Cleaning <u>D1.1-98 Sec. 5.30.1</u>																																																																																																			
SHIELDING Flux Gas <u>Carbon Dioxide</u> Cored Composition <u>100%</u> Electrode-Flux (Class) Flow Rate <u>40-50 cfh</u> <u>N/A</u> Gas Cup Size <u>3/4 in</u>	POSTWELD HEAT TREATMENT PWHT Required <input type="checkbox"/> Temp. <u>N/A</u> Time <u>N/A</u>																																																																																																			
PREHEAT Preheat Temp., Min. <u>Table 3.2</u> Thickness Up to 3/4" Temperature <u>Note 1</u> Over 3/4" to 1-1/2" <u>50 Deg. F</u> Over 1-1/2" to 2-1/2" <u>150 Deg. F</u> Over 2-1/2" <u>225 Deg. F</u> Interpass Temp., Min. <u>Table 3.2</u> Max. <u>550 Deg. F</u>																																																																																																				
WELDING PROCEDURE																																																																																																				
<table border="1" style="width: 100%; border-collapse: collapse;"> <thead> <tr> <th>Layer/Pass</th> <th>Process</th> <th>Filler Metal Class</th> <th>Diameter</th> <th>Cur. Type</th> <th>Amps or WFS</th> <th>Volts</th> <th>Travel Speed</th> <th>Other Notes</th> </tr> </thead> <tbody> <tr> <td>1-2 (1)</td> <td>FCAW</td> <td>E70T-1</td> <td>3/32 in</td> <td>DCEP</td> <td>475 / 250</td> <td>29</td> <td>15-21 (21)</td> <td>1/4 in.</td> </tr> <tr> <td>1-3 (1)</td> <td>FCAW</td> <td>E70T-1</td> <td>3/32 in</td> <td>DCEP</td> <td>475 / 250</td> <td>29</td> <td>11-15 (11)</td> <td>3/8 in.</td> </tr> <tr> <td>2-4 (2)</td> <td>FCAW</td> <td>E70T-1</td> <td>3/32 in</td> <td>DCEP</td> <td>475 / 250</td> <td>29</td> <td>11-16 (13)</td> <td>1/2 in.</td> </tr> <tr> <td>3-5 (3)</td> <td>FCAW</td> <td>E70T-1</td> <td>3/32 in</td> <td>DCEP</td> <td>475 / 250</td> <td>29</td> <td>11-16 (14)</td> <td>5/8 in.</td> </tr> <tr> <td>4-6 (4)</td> <td>FCAW</td> <td>E70T-1</td> <td>3/32 in</td> <td>DCEP</td> <td>475 / 250</td> <td>29</td> <td>11-15 (13)</td> <td>3/4 in.</td> </tr> <tr> <td>5-7 (5)</td> <td>FCAW</td> <td>E70T-1</td> <td>3/32 in</td> <td>DCEP</td> <td>475 / 250</td> <td>29</td> <td>10-14 (12)</td> <td>7/8 in.</td> </tr> <tr> <td>6-9 (6)</td> <td>FCAW</td> <td>E70T-1</td> <td>3/32 in</td> <td>DCEP</td> <td>475 / 250</td> <td>29</td> <td>10-14 (12)</td> <td>1 in.</td> </tr> <tr> <td>7-11 (7)</td> <td>FCAW</td> <td>E70T-1</td> <td>3/32 in</td> <td>DCEP</td> <td>475 / 250</td> <td>29</td> <td>10-14 (11)</td> <td>1 1/8 in.</td> </tr> <tr> <td> </td> </tr> <tr> <td> </td> </tr> </tbody> </table>		Layer/Pass	Process	Filler Metal Class	Diameter	Cur. Type	Amps or WFS	Volts	Travel Speed	Other Notes	1-2 (1)	FCAW	E70T-1	3/32 in	DCEP	475 / 250	29	15-21 (21)	1/4 in.	1-3 (1)	FCAW	E70T-1	3/32 in	DCEP	475 / 250	29	11-15 (11)	3/8 in.	2-4 (2)	FCAW	E70T-1	3/32 in	DCEP	475 / 250	29	11-16 (13)	1/2 in.	3-5 (3)	FCAW	E70T-1	3/32 in	DCEP	475 / 250	29	11-16 (14)	5/8 in.	4-6 (4)	FCAW	E70T-1	3/32 in	DCEP	475 / 250	29	11-15 (13)	3/4 in.	5-7 (5)	FCAW	E70T-1	3/32 in	DCEP	475 / 250	29	10-14 (12)	7/8 in.	6-9 (6)	FCAW	E70T-1	3/32 in	DCEP	475 / 250	29	10-14 (12)	1 in.	7-11 (7)	FCAW	E70T-1	3/32 in	DCEP	475 / 250	29	10-14 (11)	1 1/8 in.																		
Layer/Pass	Process	Filler Metal Class	Diameter	Cur. Type	Amps or WFS	Volts	Travel Speed	Other Notes																																																																																												
1-2 (1)	FCAW	E70T-1	3/32 in	DCEP	475 / 250	29	15-21 (21)	1/4 in.																																																																																												
1-3 (1)	FCAW	E70T-1	3/32 in	DCEP	475 / 250	29	11-15 (11)	3/8 in.																																																																																												
2-4 (2)	FCAW	E70T-1	3/32 in	DCEP	475 / 250	29	11-16 (13)	1/2 in.																																																																																												
3-5 (3)	FCAW	E70T-1	3/32 in	DCEP	475 / 250	29	11-16 (14)	5/8 in.																																																																																												
4-6 (4)	FCAW	E70T-1	3/32 in	DCEP	475 / 250	29	11-15 (13)	3/4 in.																																																																																												
5-7 (5)	FCAW	E70T-1	3/32 in	DCEP	475 / 250	29	10-14 (12)	7/8 in.																																																																																												
6-9 (6)	FCAW	E70T-1	3/32 in	DCEP	475 / 250	29	10-14 (12)	1 in.																																																																																												
7-11 (7)	FCAW	E70T-1	3/32 in	DCEP	475 / 250	29	10-14 (11)	1 1/8 in.																																																																																												

Per AWS D1.1

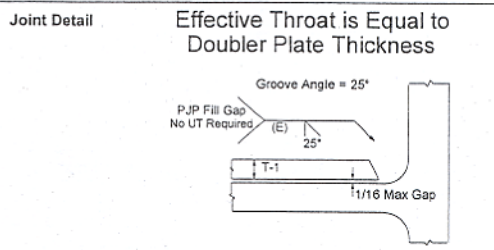
Welding Procedure Specifications

Gayle Manufacturing Co. Welding Procedure Specification

Page 1 of 1
HD70 DBLR PL

WPS No. HD70 DBLR PL Date 3/8/99 By Keith Davey Type Manual Machine
 Authorized By Keith Davey Date 3/8/99 Revision 0 Semi-Auto Auto
 Welding Process(es) FCAW Prequalified
 Supporting PQR(s) N/A N/A N/A

JOINT
 Type Doublers Plate PJP
 Backing Yes No Single Weld Double Weld
 Backing Material N/A
 Root Opening N/A Root Face Dimension N/A
 Groove Angle 25 Deg Radius (J-U) N/A
 Back Gouge Yes No
 Method N/A



BASE METALS
 Material Spec. D1.1 98 Tbl 3.1 to D1.1 98 Tbl 3.1
 Type or Grade Group I & II to Group I & II
 Thickness: Groove (in) 1/8 - Unlimited
 Fillet (in) _____ - _____
 Diameter (Pipe, in) _____ - _____

POSITION
 Position of Groove 1G Fillet N/A
 Vertical Progression: Up Down

FILLER METALS
 AWS Specification A5.20 Charpy V-notch _____
 AWS Classification E70T-1 & -9 20 Ft Lbs min _____
Lincoln OS HD70 @-20 deg F.

ELECTRICAL CHARACTERISTICS
 Transfer Mode (GMAW):
 Short-Circuiting Globular Spray
 Current: AC DCEP DCEN Pulsed
 Other N/A
 Tungsten Electrode (GTAW):
 Size N/A Type N/A

SHIELDING
 Flux _____ Gas CO2
 Cored _____ Composition 100%
 Electrode-Flux (Class) _____ Flow Rate 85 CFH
N/A Gas Cup Size 3/4 in

TECHNIQUE
 Stringer or Weave Bead Stringer
 Multi-pass or Single Pass (per side) As Needed
 Number of Electrodes 1
 Electrode Spacing: Longitudinal N/A
 Lateral N/A
 Angle Pull
 Contact Tube to Work Distance 1 to 1-1/4
 Peening None
 Interpass Cleaning D1.1-98 Sec. 5.30.1

PREHEAT
 Preheat Temp., Min. Table 3.2
 Thickness Up to 3/4" Temperature Table 3.2
 Over 3/4" to 1-1/2" 50 Deg. F
 Over 1-1/2" to 2-1/2" 150 Deg. F
 Over 2-1/2" 225 Deg. F
 Interpass Temp., Min. Table 3.2 Max. 550 Deg. F

POSTWELD HEAT TREATMENT PWHT Required
 Temp. N/A Time N/A

WELDING PROCEDURE								
Layer/Pass	Process	Filler Metal Class	Diameter	Cur. Type	Amps or WFS	Volts	Travel Speed	Other Notes
2-4	FCAW	E70T-1 & -9	3/32	DCEP	530 / 300	31 +/- 2	12-20 IPM	T-1 = 3/8
3-6	FCAW	E70T-1 & -9	3/32	DCEP	530 / 300	31 +/- 2	12-20 IPM	T-1 = 1/2
4-8	FCAW	E70T-1 & -9	3/32	DCEP	530 / 300	31 +/- 2	12-20 IPM	T-1 = 5/8
5-10	FCAW	E70T-1 & -9	3/32	DCEP	530 / 300	31 +/- 2	12-20 IPM	T-1 = 3/4

Per AWS D1.1

Stress-Strain Relations from Coupon Tests

MAR- 2-00 THU 10:13

P. 01

SIGNET TESTING LABORATORIES, INC.
3121 DIABLO AVENUE
HAYWARD, CA 94545

Fax Cover Sheet

DATE: March 2, 2000 TIME: 10:05 AM
TO: Amir Gilliani PHONE: 510-231-9563
UC Berkeley FAX: 510-231-9572
FROM: Robert Tongson PHONE: 510-887-8484
Signet Testing/Hayward FAX: 510-783-4295
RE: Test Results
CC:

Number of pages including cover sheet: 1

Message

Subject: Test results for the beam sample delivered on February 24, 2000.

STL #:

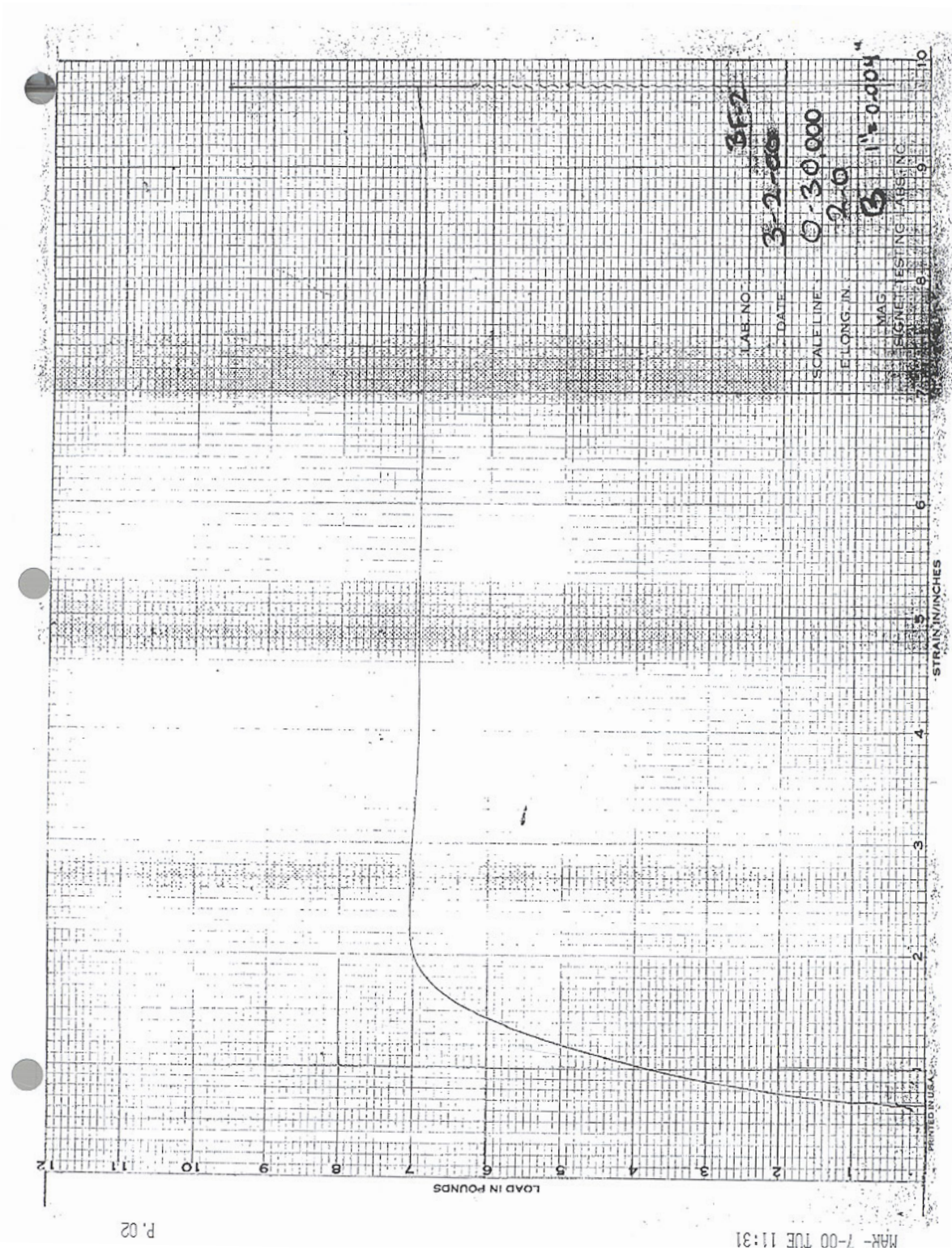
Test Date: 3/2/00

The test results for the two (2) tensiles on the flange and the two (2) tensiles on the web of the beam sample are listed below.

Sample Identification	Dimensions, in.	Area, sq.in.	Yield Point, psi	Tensile Strength, psi	Elongation in 2 in., %
Beam Flange-1	0.652 x 0.501	0.327	52000	70600	39.0
Beam Flange-2	0.655 x 0.499	0.327	53800	73400	39.0
Beam Web-1	0.528 x 0.496	0.262	59500	72900	38.5
Beam Web-2	0.529 x 0.499	0.264	66700	74600	38.5

The test coupons were flat tensiles with a 2 1/2 x 1/2 inch reduced section.

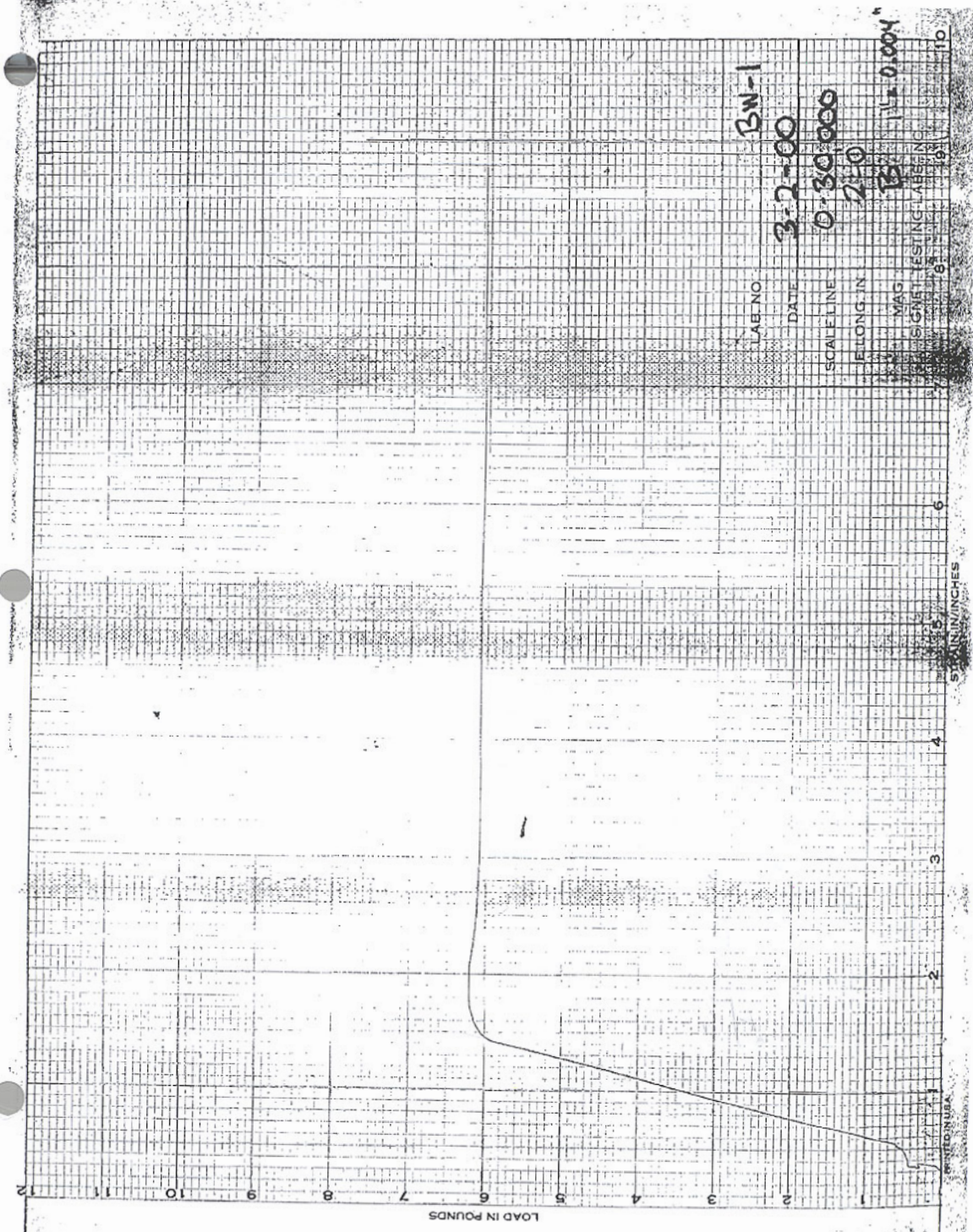
Stress-Strain Relations from Coupon Tests



MARK-7-00 TUE 11:31

P.02

Stress-Strain Relations from Coupon Tests

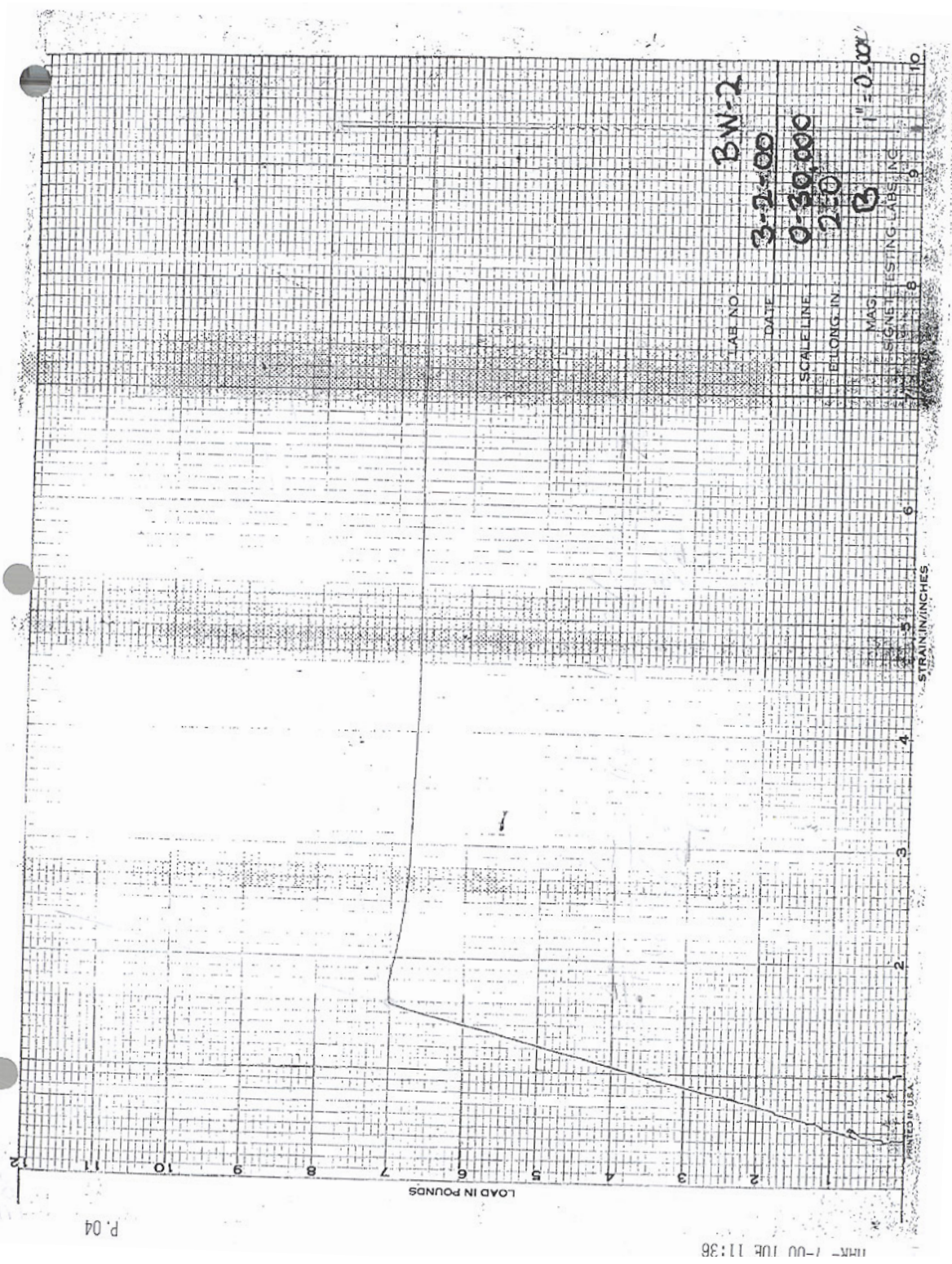


LAB NO 3N-1
DATE 3-2-00
SCALE LINE 0-30,000
GAGE LENGTH 2.0
MAG 15X
TESTING LAB ENG

MAR-7-00 TUE 11:34

P.03

Stress-Strain Relations from Coupon Tests



Stress-Strain Relations from Coupon Tests

MAR- 8-00 WED 14:47

P. 01

SIGNET TESTING LABORATORIES, INC.

3121 DIABLO AVENUE
HAYWARD, CA 94545

Fax Cover Sheet

DATE: March 8, 2000 TIME: 2:15 PM
TO: Amir Gillani PHONE: 510-231-9563
UC Berkeley FAX: 510-231-9572
FROM: Robert Tongson PHONE: 510-887-8484
Signet Testing/Hayward FAX: 510-783-4295
RE: Test Results
CC:

Number of pages including cover sheet: ~~4~~ 3

Message

Subject: Test results and stress-strain curves for the beam sample delivered on February 24, 2000.

STL #:

Test Date: 3/8/00

As requested, please find in this fax transmission the test results for the additional tensile tests for the Beam-Web and Beam-Flange with two (2) stress-strain curves with the following sample identification, BF-3, BW-3.

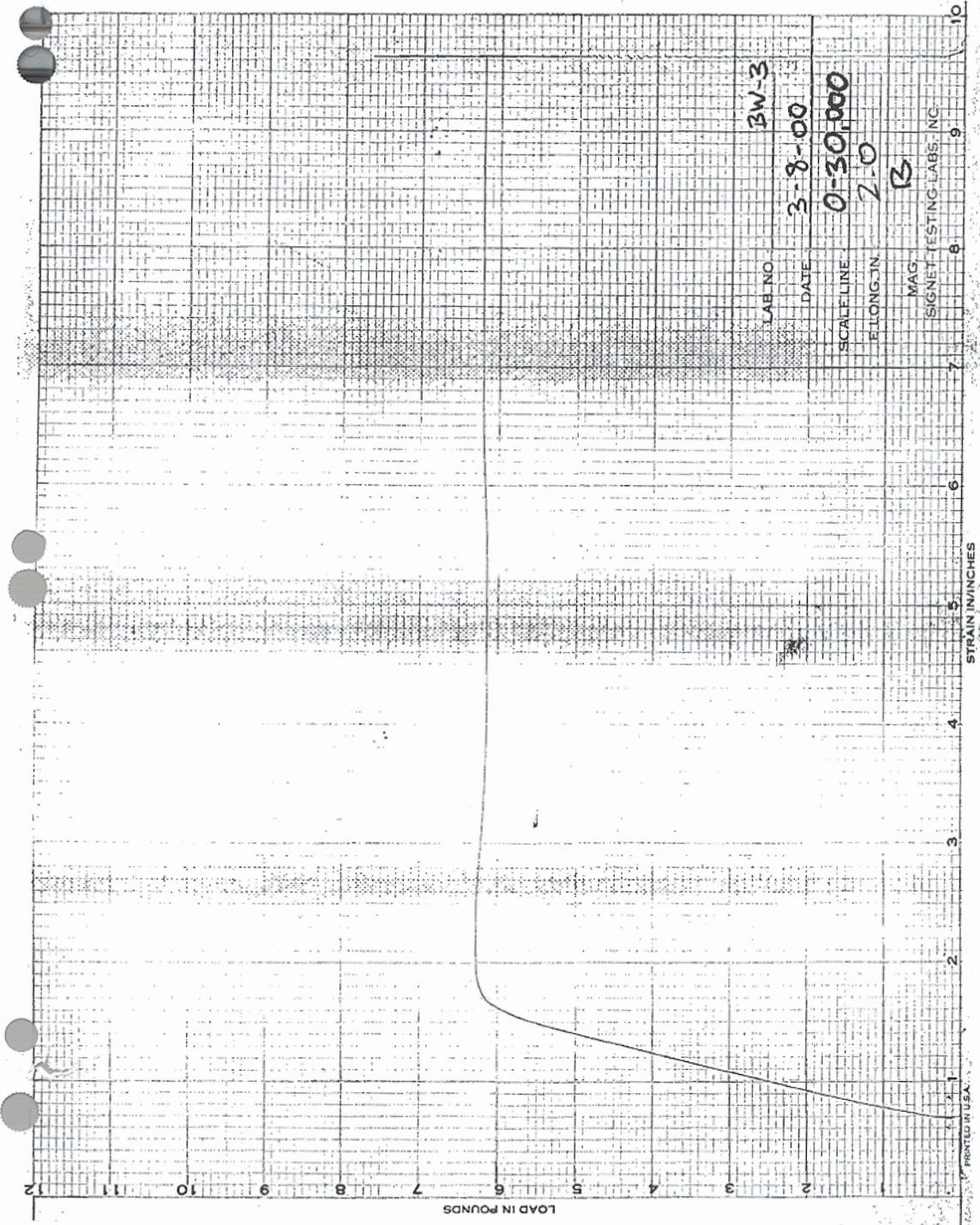
Sample Identification	Dimensions, in.	Area, sq. in.	Yield Point, psi	Tensile Strength, psi	Elongation in 2 in., %
Beam Flange-3	0.642 x 0.500	0.321	54800	70700	39.0
Beam Web-3	0.527 x 0.501	0.264	59800	72700	38.0

The test coupons were flat tensiles with a 2 1/2 x 1/2 inch reduced section.

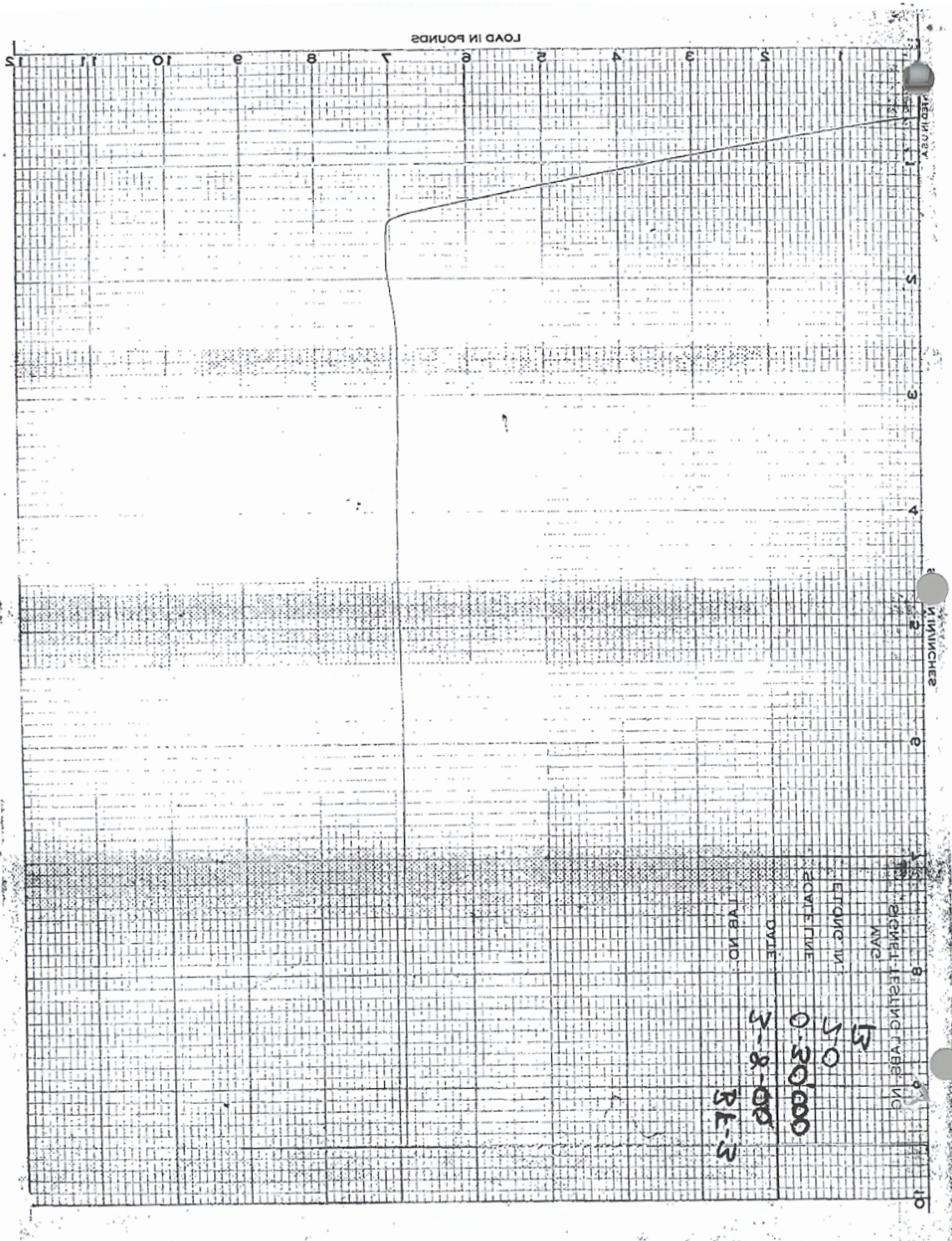
Stress-Strain Relations from Coupon Tests

MAR- 8-00 WED 14:50

P. 03



Stress-Strain Relations from Coupon Tests



8A:41 00-8-KAM

50 9'

Stress-Strain Relations from Coupon Tests

SIGNET TESTING LABORATORIES, INC.
3121 DIABLO AVENUE
HAYWARD, CA 94545

Fax Cover Sheet

DATE: March 8, 2000 TIME: 3:15 PM
TO: Amir Giliani PHONE: 510-231-9563
UC Berkeley FAX: 510-231-9572
FROM: Robert Tongson PHONE: 510-887-8484
Signet Testing/Hayward FAX: 510-783-4295
RE: Test Results
CC:

Number of pages including cover sheet:5

Message

Subject: Test results for the column sample delivered on February 24, 2000.

STL #:

Test Date: 3/8/00

The test results for the two (2) tensiles on the flange and the two (2) tensiles on the web of the beam sample are listed below. Also included in this fax transmission are four (4) stress-strain curves with the following sample identification, CF-1, CF-2, CW-1, CW-2.

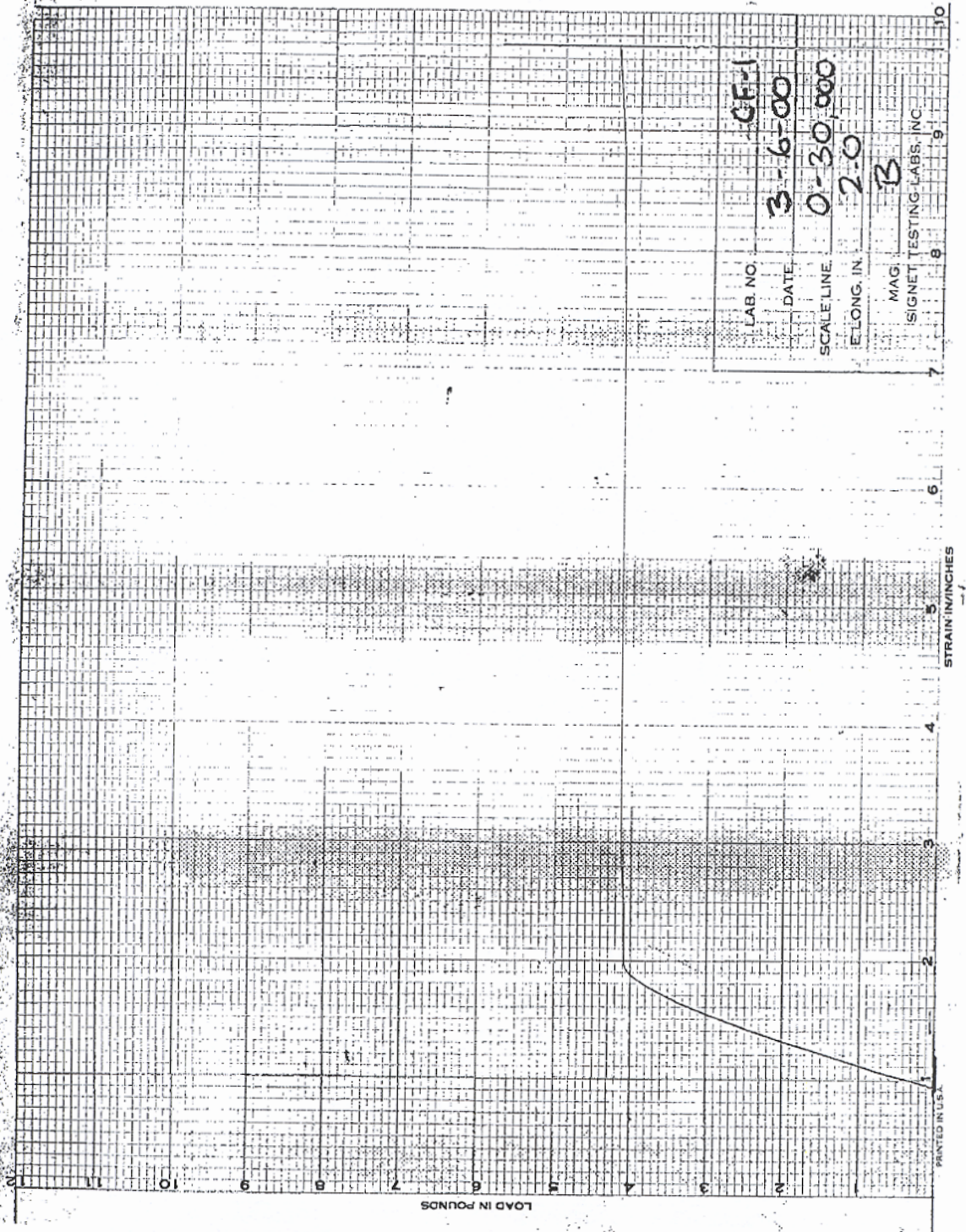
Sample Identification	Dimensions, in.	Area, sq. in.	Yield Point, psi	Tensile Strength, psi	Elongation in 2 in., %
Column Flange-1	0.500	0.196	52000	74000	32.0
Column Flange-2	0.500	0.196	49500	71900	31.0
Column Web-1	0.499	0.196	55100	71400	35.5
Column Web-2	0.496	0.193	57000	73100	31.5

The test coupons were 0.505 diameter x 2 1/2-inch reduced section.

Stress-Strain Relations from Coupon Tests

MAR- 8-00 WED 16:34

P. 02

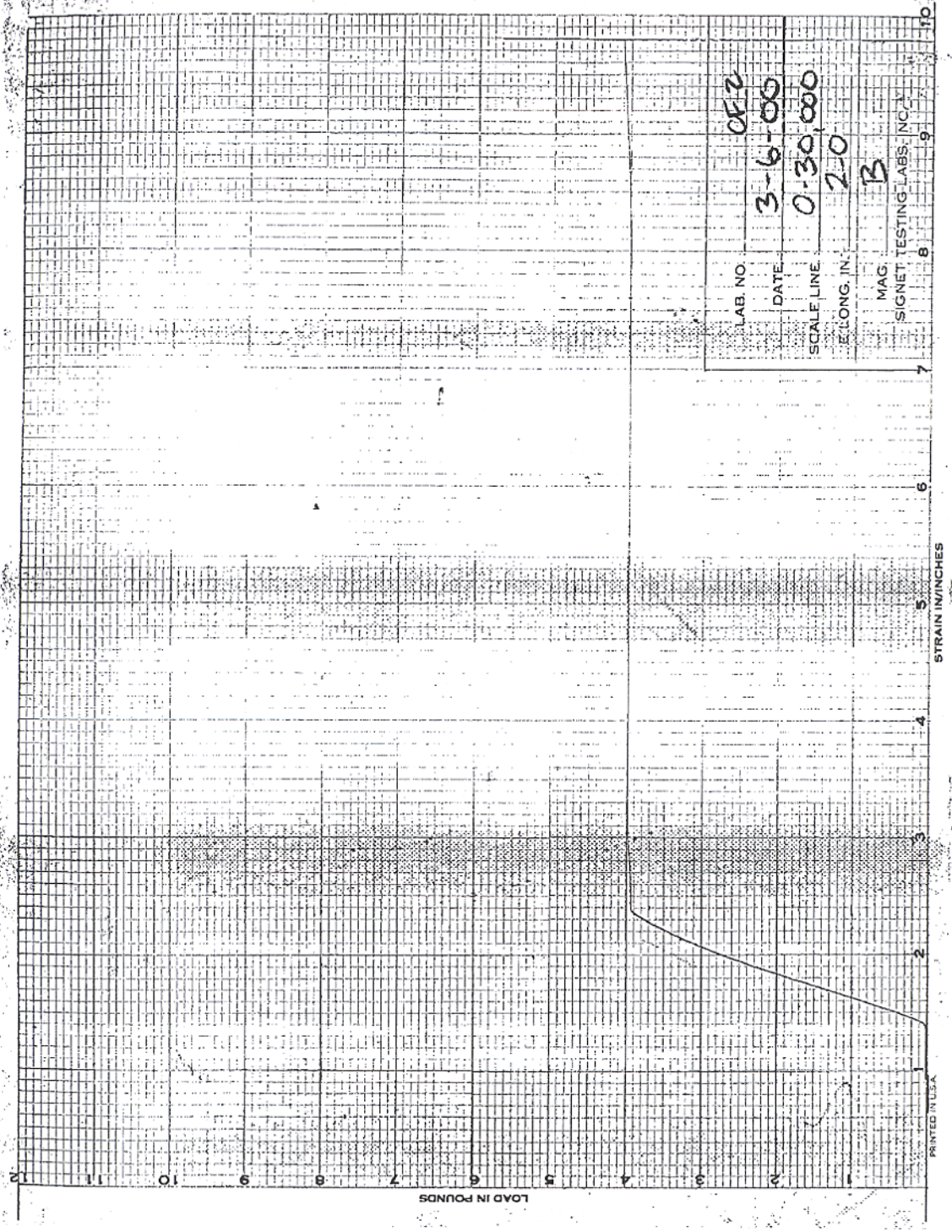


LAB. NO. **CF-1**
DATE **3-6-00**
SCALE LINE **0-30,000**
ELONG. IN. **2.0**
MAG. **B**
SIGNET TESTING LABS., INC.

Stress-Strain Relations from Coupon Tests

MAR- 8-00 WED 16:36

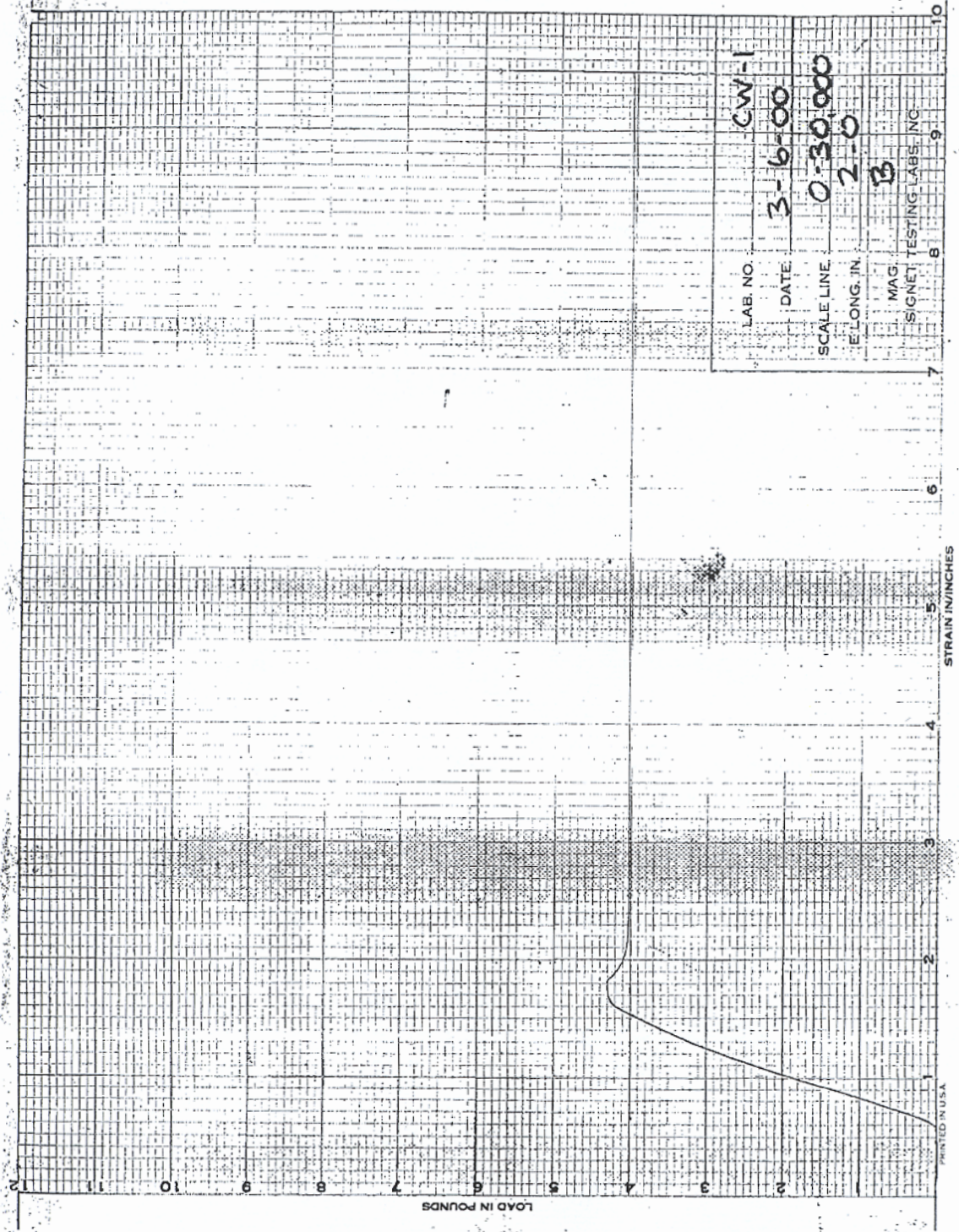
P.03



Stress-Strain Relations from Coupon Tests

MAR- 8-00 WED 16:38

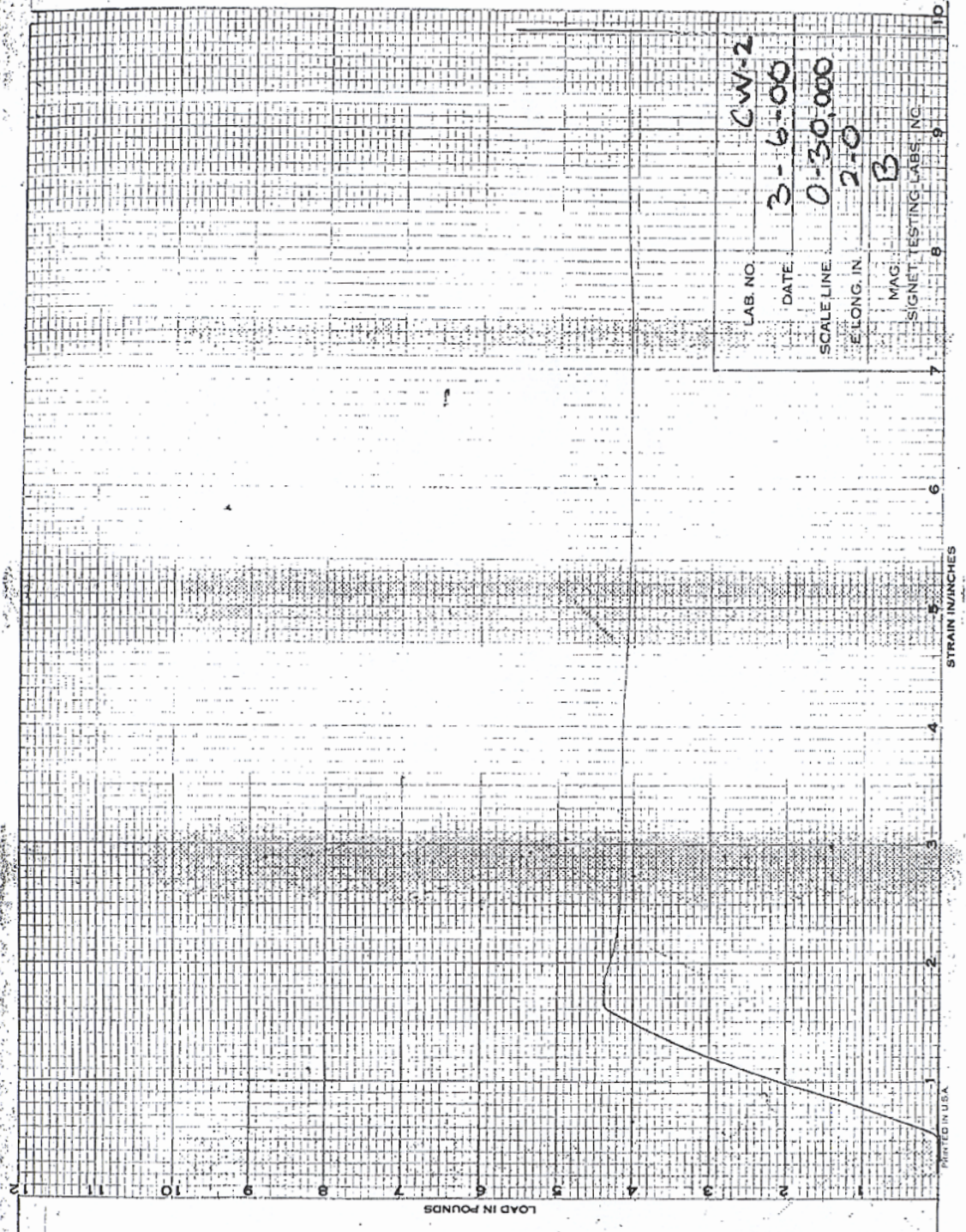
P. 04



Stress-Strain Relations from Coupon Tests

MAR- 8-00 WED 16:40

P. 05



Charpy Test Data

Signet Testing Laboratories
3121 Diablo Avenue
Hayward, CA 94545
Phone: 510-887-8484
Fax: 510-783-4295

facsimile transmittal

To: Amir Giliani/UC Berkeley Fax: 510-231-9572
From: Robert Tongson/Signet Testing Date: 03/13/00
Re: Test Results Pages: 1
CC:

Urgent For Review Please Comment Please Reply Please Recycle

Subject: The test results for the beam and column samples delivered on February 24, 2000.

STL#:

Test Date: 3/13/00

The results for the impact tests on the beam and column samples taken from the flange and K-section are listed below.

Specimen Size: 10 x 10 x 55 mm
Notch: 45 degree V
Orientation: Longitudinal
Test Temperature: +70 degrees Fahrenheit

Sample Identification	Impact Value, ft-lbf	Lateral Expansion, mils	Shear, Percent
BF-1	127.9	108	100
BF-2	128.3	101	100
BK-1	126.9	106	100
BK-2	128.3	106	100
CF-1	125.3	106	100
CF-2	128.3	107	100
CK-1	128.3	110	100
CK-2	128.3	108	100

Appendix B Summary of Test Data

Pertinent test results from the testing of nine specimens for all displacement excursions are presented in Table 1 through Table 9. The format of these tables is that specified by the SAC Joint Venture for reporting experimental data from full-scale connection tests. The format of the tables was prepared for cyclic test data and is not suitable for reporting data from tests using a near-field displacement history. For this reason, data are not presented for specimen RC07.

Table B-1 Experimental results for specimen RC01

<i>Excursion</i>	$D1 (in.)^1$	$D2 (in.)^1$	$D3 (in.)^1$	$D4 (in.)^1$	$Q1 (kips)^1$	$Q2 (kips)^1$	$K (kips/in.)^1$	$E (kips-in.)^1$
1+	0.53	0.17	0.00	0.00	39	39	233	0
1-	-0.53	-0.14	0.01	0.01	-38	-38	278	0
7+	0.71	0.24	0.08	0.00	55	55	227	1
7-	-0.71	-0.22	0.08	0.01	-51	-51	234	1
13+	1.42	0.54	0.17	0.04	107	107	200	4
13-	-1.42	-0.53	0.17	0.07	-109	-109	205	8
14+	1.42	0.50	0.17	0.04	106	106	211	3
14-	-1.42	-0.50	0.17	0.03	-104	-104	210	4
15+	1.42	0.51	0.16	0.03	107	107	213	3
15-	-1.42	-0.50	0.16	0.03	-105	-105	211	4
16+	1.42	0.51	0.15	0.04	107	108	213	3
16-	-1.42	-0.50	0.15	0.03	-106	-106	209	4
17+	2.12	0.80	0.14	0.25	134	138	168	32
17-	-2.12	-0.92	0.13	0.51	-131	-138	143	61
18+	2.12	0.79	0.12	0.46	139	141	177	48
18-	-2.12	-0.90	0.12	0.43	-132	-135	147	46
19+	2.55	1.02	0.11	0.64	143	150	140	81
19-	-2.55	-1.09	0.10	0.76	-140	-146	128	93
20+	2.83	1.17	0.10	0.88	145	154	124	117
20-	-2.83	-1.32	0.09	1.08	-139	-151	105	143
21+	2.83	1.15	0.08	1.03	148	155	129	132
21-	-2.83	-1.32	0.07	1.03	-144	-151	109	134
22+	4.25	2.31	0.07	2.21	142	164	62	384
22-	-4.25	-2.50	0.06	2.97	-133	-161	53	502
23+	4.25	2.58	0.05	3.20	126	159	49	517
23-	-4.25	-2.74	0.05	3.20	-120	-152	44	521
24+	5.66	4.26	0.04	4.96	101	139	24	812
24-	-5.66	-4.41	0.03	5.21	-95	-127	21	849
25+	5.66	4.49	0.03	5.24	89	116	20	720

Table B-1 Experimental results for specimen RC01

Excursion	$D1$ (in.) ¹	$D2$ (in.) ¹	$D3$ (in.) ¹	$D4$ (in.) ¹	$Q1$ (kips) ¹	$Q2$ (kips) ¹	K (kips/in.) ¹	E (kips-in.) ¹
25-	-5.66	-4.54	0.02	5.12	-92	-109	20	736
26+	7.08	5.97	0.02	6.62	70	100	12	843
26-	-7.08	-5.94	0.01	6.46	-80	-101	13	919
27+	7.08	6.11	0.01	6.82	57	89	9	705
27-	-7.08	-6.03	0.00	6.33	-70	-90	12	769

1. $D1$ = target beam displacement;

$D2$ = Peak beam deflection;

$D3$ = Beam deflection at start of excursion;

$D4$ = beam plastic deformation range;

$Q1$ = load at peak beam deflection;

$Q2$ = maximum load in excursion;

K = effective stiffness;

E = beam hysteresis area.

Table B-2 Experimental results for specimen RC02

Excursion	$D1$ (in.) ¹	$D2$ (in.) ¹	$D3$ (in.) ¹	$D4$ (in.) ¹	$Q1$ (kips) ¹	$Q2$ (kips) ¹	K (kips/in.) ¹	E (kips-in.) ¹
1+	0.53	0.16	0.16	0	33	33	202	-3
1-	-0.53	-0.16	0.15	0	-38	-38	237	0
7+	0.71	0.22	0.07	0.01	45	45	207	0
7-	-0.71	-0.24	0.07	0	-54	-54	225	0
13+	1.06	0.35	-0.01	0.01	69	69	197	1
13-	-1.06	-0.42	-0.02	0.04	-86	-86	204	2
19+	1.42	0.47	-0.09	0.04	94	94	200	2
19-	-1.42	-0.56	-0.1	0.06	-111	-111	199	4
20+	1.42	0.47	-0.11	0.03	97	97	205	1
20-	-1.42	-0.54	-0.11	0.04	-108	-109	200	2
21+	1.42	0.48	-0.12	0.03	98	98	206	1
21-	-1.42	-0.55	-0.13	0.04	-109	-109	199	2
22+	1.42	0.48	-0.14	0.03	98	98	206	1
22-	-1.42	-0.54	-0.14	0.04	-109	-109	200	1
23+	2.12	0.88	-0.15	0.26	131	134	149	28
23-	-2.12	-0.79	-0.16	0.39	-138	-142	175	41
24+	2.12	0.87	-0.16	0.37	136	137	155	38
24-	-2.12	-0.78	-0.16	0.35	-136	-139	176	33
25+	2.83	1.28	-0.16	0.75	145	151	113	102
25-	-2.83	-1.27	-0.16	1.06	-145	-155	114	139
26+	2.83	1.23	-0.16	1.02	146	153	119	130
26-	-2.83	-1.22	-0.16	0.96	-147	-155	121	120
27+	4.25	2.28	-0.15	2.04	147	164	65	359
27-	-4.25	-2.33	-0.14	2.72	-140	-168	60	451
28+	4.25	2.44	-0.14	2.96	131	164	54	497
28-	-4.25	-2.69	-0.13	3.17	-117	-157	43	507
29+	5.66	4.23	-0.13	4.9	106	145	25	862
29-	-5.66	-4.43	-0.12	5.17	-96	-130	22	815
30+	5.66	4.38	-0.11	5.24	96	120	22	800

Table B-2 Experimental results for specimen RC02

30-	-5.66	-4.57	-0.11	5.08	-83	-109	18	714
31+	7.08	5.85	-0.1	6.59	79	108	14	974
31-	-7.08	-6.05	-0.09	6.68	-67	-99	11	871

1. $D1$ = target beam displacement;

$D2$ = Peak beam deflection;

$D3$ = Beam deflection at start of excursion;

$D4$ = beam plastic deformation range;

$Q1$ = load at peak beam deflection;

$Q2$ = maximum load in excursion;

K = effective stiffness;

E = beam hysteresis area.

Table B-3 Experimental results for specimen RC03

Excursion	$D1$ (in.) ¹	$D2$ (in.) ¹	$D3$ (in.) ¹	$D4$ (in.) ¹	$Q1$ (kips) ¹	$Q2$ (kips) ¹	K (kips/in.) ¹	E (kips-in.) ¹
1+	0.53	0.17	0	0	37	37	223	0
1-	-0.53	-0.16	0	0.01	-37	-37	223	0
7+	0.71	0.29	0.02	0	53	53	185	0
7-	-0.71	-0.23	0.03	-0.01	-47	-47	206	0
13+	1.06	0.42	0.1	0.01	76	76	181	0
13-	-1.06	-0.4	0.11	0	-78	-78	194	0
19+	1.42	0.6	0.16	0.03	105	105	175	2
19-	-1.42	-0.53	0.16	0.02	-104	-104	194	2
20+	1.42	0.6	0.15	0.03	105	105	176	1
20-	-1.42	-0.52	0.15	0.01	-102	-102	196	1
21+	1.42	0.6	0.14	0.03	105	105	176	1
21-	-1.42	-0.53	0.14	0.01	-103	-103	194	1
22+	1.42	0.61	0.13	0.03	106	106	176	1
22-	-1.42	-0.53	0.12	0.02	-103	-103	196	1
23+	2.12	0.89	0.11	0.19	136	138	152	22
23-	-2.12	-0.9	0.11	0.35	-140	-142	155	40
24+	2.12	0.91	0.1	0.35	139	140	153	36
24-	-2.12	-0.87	0.09	0.33	-137	-139	158	34
25+	2.83	1.36	0.08	0.75	146	153	107	109
25-	-2.83	-1.3	0.08	1.04	-148	-156	114	138
26+	2.83	1.33	0.07	0.98	149	155	112	128
26-	-2.83	-1.27	0.06	0.95	-149	-156	117	124
27+	4.25	2.41	0.05	2.03	154	167	64	363
27-	-4.25	-2.5	0.04	2.93	-137	-168	55	494
28+	4.25	2.56	0.04	3.05	137	168	53	512
28-	-4.25	-2.97	0.03	3.52	-114	-151	38	552
29+	5.66	4.58	0.02	5.17	98	144	21	914

Table B-3 Experimental results for specimen RC03

29-	-5.66	-4.54	0.02	5.41	-88	-126	19	824
30+	5.66	4.82	0.01	5.56	87	117	18	834
30-	-5.66	-4.69	0	5.31	-77	-104	17	698
31+	7.08	6.29	0	7.05	65	101	10	979
31-	-7.08	-6.18	-0.01	6.8	-52	-90	8	812
32+	7.08	6.45	-0.02	7.1	57	83	9	812
32-	-7.08	-6.35	-0.02	6.72	-41	-70	7	549

1. $D1$ = target beam displacement;

$D2$ = Peak beam deflection;

$D3$ = Beam deflection at start of excursion;

$D4$ = beam plastic deformation range;

$Q1$ = load at peak beam deflection;

$Q2$ = maximum load in excursion;

K = effective stiffness;

E = beam hysteresis area.

Table B-4 Experimental results for specimen RC04

Excursion	$D1 (in.)^1$	$D2 (in.)^1$	$D3 (in.)^1$	$D4 (in.)^1$	$Q1 (kips)^1$	$Q2 (kips)^1$	$K (kips/in.)^1$	$E (kips-in.)^1$
1+	0.53	0.15	0	0	35	35	231	0
1-	-0.53	-0.18	0	0	-40	-40	218	0
7+	0.71	0.24	0.02	0	50	50	210	0
7-	-0.71	-0.25	0.03	0	-53	-53	211	0
13+	1.06	0.38	0.1	0.01	77	77	203	0
13-	-1.06	-0.39	0.11	0.02	-79	-79	200	1
19+	1.42	0.52	0.15	0.04	101	101	196	2
19-	-1.42	-0.56	0.14	0.08	-106	-106	190	5
20+	1.42	0.51	0.14	0.05	105	105	204	3
20-	-1.42	-0.56	0.13	0.05	-106	-106	188	2
21+	1.42	0.52	0.13	0.05	106	106	203	2
21-	-1.42	-0.55	0.12	0.05	-104	-104	188	2
22+	1.42	0.51	0.11	0.05	105	105	203	2
22-	-1.42	-0.56	0.11	0.05	-105	-105	188	2
23+	2.12	0.95	0.1	0.37	128	135	134	44
23-	-2.12	-0.98	0.09	0.67	-127	-136	130	77
24+	2.12	0.92	0.09	0.63	132	137	144	66
24-	-2.12	-0.94	0.08	0.58	-130	-136	138	63
25+	2.83	1.41	0.07	1.07	136	148	97	145
25-	-2.83	-1.53	0.07	1.52	-135	-150	88	204
26+	2.83	1.34	0.06	1.39	141	152	105	180
26-	-2.83	-1.49	0.05	1.38	-138	-150	93	181
27+	4.25	2.77	0.05	2.89	120	158	43	503
27-	-4.25	-2.98	0.04	3.69	-106	-155	36	599
28+	4.25	3.08	0.03	3.84	105	139	34	573
28-	-4.25	-3.19	0.03	3.82	-97	-124	30	543
29+	5.66	4.62	0.02	5.3	85	119	18	789
29-	-5.66	-4.76	0.01	5.48	-74	-110	16	774
30+	5.66	4.72	0.01	5.43	74	104	16	704

Table B-4 Experimental results for specimen RC04

30-	-5.66	-4.84	0	5.4	-62	-92	13	668
31+	7.08	6.31	-0.01	6.91	63	91	10	845
31-	-7.08	-6.38	-0.01	6.93	-51	-80	8	783
32+	7.08	6.37	-0.02	6.93	53	76	8	708
32-	-7.08	-6.47	-0.02	6.89	-45	-65	7	654
33+	7.75	7.12	-0.03	7.55	48	65	7	663
33-	-7.75	-7.15	-0.04	7.5	-34	-55	5	469

1. $D1$ = target beam displacement;

$D2$ = Peak beam deflection;

$D3$ = Beam deflection at start of excursion;

$D4$ = beam plastic deformation range;

$Q1$ = load at peak beam deflection;

$Q2$ = maximum load in excursion;

K = effective stiffness;

E = beam hysteresis area.

Table B-5 Experimental results for specimen RC05

<i>Excursion</i>	$D1 (in.)^1$	$D2 (in.)^1$	$D3 (in.)^1$	$D4 (in.)^1$	$Q1 (kips)^1$	$Q2 (kips)^1$	$K (kips/in.)^1$	$E (kips-in.)^1$
1+	0.53	0.13	0	0	34	34	255	0
1-	-0.53	-0.19	0.01	0.01	-34	-34	178	0
7+	0.71	0.24	0.13	0	52	52	216	0
7-	-0.71	-0.28	0.13	0.01	-49	-49	178	0
13+	1.06	0.38	0.02	0.01	73	73	191	0
13-	-1.06	-0.47	0	0.02	-83	-83	176	2
19+	1.42	0.56	-0.16	0.04	104	104	184	2
19-	-1.42	-0.59	-0.17	0.05	-106	-106	180	4
20+	1.42	0.55	-0.18	0.04	104	104	188	1
20-	-1.42	-0.58	-0.18	0.03	-104	-104	181	2
21+	1.42	0.54	-0.19	0.03	103	103	190	0
21-	-1.42	-0.58	-0.19	0.03	-104	-104	180	2
22+	1.42	0.55	-0.19	0.03	103	103	188	1
22-	-1.42	-0.58	-0.19	0.03	-105	-105	180	2
23+	2.12	0.92	-0.18	0.27	132	137	144	32
23-	-2.12	-1.02	-0.18	0.56	-133	-138	130	66
24+	2.12	0.91	-0.17	0.49	135	139	150	50
24-	-2.12	-0.97	-0.16	0.46	-133	-136	137	50
25+	2.83	1.27	-0.15	0.89	128	148	101	119
25-	-2.83	-1.29	-0.14	1.25	-120	-148	93	164
26+	2.83	1.23	-0.13	1.17	130	150	106	146
26-	-2.83	-1.41	-0.12	1.16	-146	-152	104	155
27+	4.25	2.91	-0.11	2.69	131	160	45	468
27-	-4.25	-2.76	-0.1	3.59	-104	-162	38	603
28+	4.25	3.32	-0.08	3.78	127	149	38	587
28-	-4.25	-3.27	-0.07	3.93	-120	-133	37	631
29+	5.66	4.58	-0.06	4.48	73	101	16	637
29-	-5.66	-4.72	-0.05	5.69	-86	-118	18	872
30+	5.66	4.99	-0.04	5.56	97	116	19	802

Table B-5 Experimental results for specimen RC05

30-	-5.66	-4.91	-0.02	5.73	-77	-103	16	764
31+	7.08	6.48	-0.01	6.99	74	102	11	938
31-	-7.08	-6.43	0.01	7.19	-60	-89	9	870
32+	7.08	6.63	0.02	7.03	66	84	10	773
32-	-7.08	-6.13	0.03	6.85	-36	-73	6	716
33+	7.75	7.25	0.05	7.58	46	71	6	739
33-	-7.75	-7.21	0.06	7.79	-42	-63	6	717
34+	7.75	7.28	0.08	7.53	46	63	6	644
34-	-7.75	-7.47	0.09	7.92	-51	-57	7	640
35+	7.75	7.15	0.1	7.36	39	57	5	579
35-	-7.75	-7.22	0.12	7.69	-38	-54	5	585
36+	7.75	7.3	0.13	7.49	39	54	5	544
36-	-7.75	-7.27	0.14	7.66	-37	-51	5	548
37+	7.75	7.24	0.15	7.38	36	52	5	506
37-	-7.75	-7.29	0.16	7.71	-29	-51	4	257

1. $D1$ = target beam displacement;

$D2$ = Peak beam deflection;

$D3$ = Beam deflection at start of excursion;

$D4$ = beam plastic deformation range;

$Q1$ = load at peak beam deflection;

$Q2$ = maximum load in excursion;

K = effective stiffness;

E = beam hysteresis area.

Table B-6 Experimental results for specimen RC06

Excursion	$D1 (in.)^1$	$D2 (in.)^1$	$D3 (in.)^1$	$D4 (in.)^1$	$Q1 (kips)^1$	$Q2 (kips)^1$	$K (kips/in.)^1$	$E (kips-in.)^1$
1+	0.53	0.18	0	0	39	39	222	0
1-	-0.53	-0.13	0	0	-36	-36	275	0
7+	0.71	0.25	0.06	-0.01	55	55	217	0
7-	-0.71	-0.18	0.07	0	-47	-47	262	0
13+	1.06	0.4	0.15	0.02	82	82	206	1
13-	-1.06	-0.32	0.16	0.01	-78	-78	246	1
19+	1.42	0.54	0.16	0.05	108	108	199	3
19-	-1.42	-0.45	0.15	0.05	-106	-106	237	3
20+	1.42	0.55	0.15	0.04	110	110	201	2
20-	-1.42	-0.45	0.14	0.04	-105	-105	235	2
21+	1.42	0.55	0.13	0.04	110	110	202	2
21-	-1.42	-0.44	0.13	0.04	-105	-105	236	2
22+	1.42	0.55	0.12	0.04	111	111	201	2
22-	-1.42	-0.44	0.11	0.03	-105	-105	238	2
23+	2.12	0.84	0.11	0.21	141	143	168	25
23-	-2.12	-0.77	0.1	0.37	-139	-142	180	39
24+	2.12	0.85	0.09	0.37	142	144	166	39
24-	-2.12	-0.76	0.08	0.35	-140	-141	184	35
25+	2.83	1.25	0.07	0.74	149	156	120	106
25-	-2.83	-1.14	0.07	0.99	-149	-156	132	130
26+	2.83	1.24	0.06	0.97	152	158	123	128
26-	-2.83	-1.14	0.05	0.93	-148	-156	130	120
27+	4.25	2.09	0.04	2.11	91	165	43	365
27-	-4.25	-2.18	0.03	3.09	-55	-164	25	489
28+	4.25	2.21	0.03	3.13	38	161	17	485
28-	-4.25	-2.56	0.02	3.49	-53	-139	21	517
29+	5.66	4.46	0.01	5.15	89	134	20	845
29-	-5.66	-4.5	0.01	5.24	-94	-122	21	815
30+	5.66	4.68	0	5.44	84	110	18	744

Table B-6 Experimental results for specimen RC06

30-	-5.66	-4.66	-0.01	5.21	-81	-105	17	707
31+	7.08	6.23	-0.01	6.84	66	94	11	835
31-	-7.08	-6.1	-0.02	6.65	-57	-89	9	810
32+	7.08	6.26	-0.02	6.75	59	78	10	684
32-	-7.08	-6.18	-0.03	6.53	-55	-71	9	658
33+	7.75	6.19	-0.03	6.58	61	65	10	585
33-	-7.75	-4.73	-0.04	5.3	11	-62	-2	477
34+	7.75	5.69	-0.04	6.07	44	57	8	489
34-	-7.75	-5.64	-0.05	5.92	-27	-55	5	490

1. $D1$ = target beam displacement;

$D2$ = Peak beam deflection;

$D3$ = Beam deflection at start of excursion;

$D4$ = beam plastic deformation range;

$Q1$ = load at peak beam deflection;

$Q2$ = maximum load in excursion;

K = effective stiffness;

E = beam hysteresis area.

Table B-7 Experimental results for specimen RC08

Excursion	$D1 (in.)^1$	$D2 (in.)^1$	$D3 (in.)^1$	$D4 (in.)^1$	$Q1 (kips)^1$	$Q2 (kips)^1$	$K (kips/in.)^1$	$E (kips-in.)^1$
1+	0.53	0.16	0	0	37	37	240	0
1-	-0.53	-0.17	0.01	0	-37	-37	221	0
7+	0.71	0.22	0.08	0	52	52	234	0
7-	-0.71	-0.24	0.09	-0.01	-49	-49	206	0
13+	1.06	0.36	0.16	0	79	79	217	1
13-	-1.06	-0.39	0.16	0.01	-78	-78	200	1
19+	1.42	0.5	0.08	0.03	105	105	208	2
19+	-1.42	-0.55	0.07	0.04	-104	-105	190	4
20+	1.42	0.52	0.06	0.03	108	108	209	2
20-	-1.42	-0.54	0.05	0.03	-104	-104	194	2
21+	1.42	0.52	0.04	0.03	108	108	209	2
21-	-1.42	-0.54	0.04	0.03	-104	-104	194	2
22+	1.42	0.52	0.03	0.03	108	108	209	3
22-	-1.42	-0.54	0.02	0.03	-105	-105	195	2
23+	2.12	0.82	0.01	0.21	138	141	168	27
23-	-2.12	-0.85	0	0.35	-138	-140	162	39
24+	2.12	0.82	-0.01	0.33	141	142	171	35
24-	-2.12	-0.84	-0.02	0.31	-138	-139	164	32
25+	2.83	1.23	-0.02	0.71	146	155	119	105
25-	-2.83	-1.19	-0.03	0.95	-147	-155	123	126
26+	2.83	1.18	-0.04	0.91	149	156	126	118
26-	-2.83	-1.19	-0.05	0.87	-152	-156	128	111
27+	4.25	2.39	-0.06	2.14	137	168	57	389
27-	-4.25	-2.46	-0.07	3.01	-124	-165	50	504
28+	4.25	2.59	-0.08	3.08	127	165	49	519
28-	-4.25	-2.93	-0.09	3.5	-108	-143	37	533
29+	5.66	4.44	-0.1	5.12	96	139	22	867
29-	-5.66	-4.5	-0.11	5.22	-97	-123	22	810
30+	5.66	4.69	-0.11	5.46	82	113	18	758

Table B-7 Experimental results for specimen RC08

30-	-5.66	-4.67	-0.12	5.16	-85	-108	18	713
31+	7.08	6.21	-0.13	6.92	65	97	11	876
31-	-7.08	-6.15	-0.14	6.65	-62	-93	10	837
32+	7.08	6.27	-0.15	6.84	56	81	9	717
32-	-7.08	-6.24	-0.15	6.55	-54	-73	9	668
33+	7.75	7.23	-0.16	7.71	52	67	7	692
33-	-7.75	-7.03	-0.16	7.25	-47	-61	7	656
34+	7.75	7.25	-0.17	7.61	46	58	6	477

1. $D1$ = target beam displacement;

$D2$ = Peak beam deflection;

$D3$ = Beam deflection at start of excursion;

$D4$ = beam plastic deformation range;

$Q1$ = load at peak beam deflection;

$Q2$ = maximum load in excursion;

K = effective stiffness;

E = beam hysteresis area.

Table B-8 Experimental results for specimen RC09

Excursion	$D1 (in.)^1$	$D2 (in.)^1$	$D3 (in.)^1$	$D4 (in.)^1$	$Q1 (kips)^1$	$Q2 (kips)^1$	$K (kips/in.)^1$	$E (kips-in.)^1$
1+	0.53	0.16	0	0	32	33	199	0
1-	-0.53	-0.12	0	0	-34	-34	280	0
7+	0.71	0.23	0.07	0	45	46	201	0
7-	-0.71	-0.19	0.08	0	-49	-49	256	-1
13+	1.06	0.38	0.16	0.01	74	74	196	0
13-	-1.06	-0.32	0.16	-0.01	-75	-75	235	0
19+	1.42	0.48	0.11	0.01	96	96	198	0
19-	-1.42	-0.44	0.1	0.01	-96	-96	221	1
20+	1.42	0.49	0.1	0.02	96	96	198	-1
20-	-1.42	-0.43	0.09	0	-96	-96	222	-1
21+	1.42	0.48	0.08	0.01	97	97	201	0
21-	-1.42	-0.43	0.07	0	-96	-96	221	0
22+	1.42	0.49	0.07	0.02	98	98	200	-1
22-	-1.42	-0.43	0.06	0	-95	-96	220	0
23+	2.12	0.58	0.05	0.03	114	115	199	3
23-	-2.12	-0.56	0.05	0.02	-119	-119	212	0
24+	2.12	0.58	0.04	0.02	117	118	202	-1
24-	-2.12	-0.57	0.03	0.03	-120	-120	211	0
25+	2.83	0.71	0.02	0.1	129	130	183	20
25-	-2.83	-0.74	0.02	0.22	-134	-134	181	25
26+	2.83	0.73	0.01	0.2	131	132	179	24
26-	-2.83	-0.74	0	0.21	-135	-136	183	22
27+	4.25	1.11	-0.01	0.54	141	145	127	97
27-	-4.25	-1.19	-0.01	0.83	-141	-151	118	127
28+	4.25	1.07	-0.02	0.7	144	148	135	106
28-	-4.25	-1.14	-0.03	0.67	-146	-152	128	103
29+	5.66	1.42	-0.03	0.98	150	156	105	188
29-	-5.66	-1.78	-0.04	1.49	-131	-161	74	264
30+	5.66	1.19	-0.05	1.14	152	158	128	200

Table B-8 Experimental results for specimen RC09

30-	-5.66	-2.99	-0.05	2.57	-106	-156	36	453
31+	7.08	2.72	-0.06	3.51	108	157	40	668
31-	-7.08	-6.47	-0.07	6.46	-99	-135	15	1064
32+	7.08	4.37	-0.07	6.37	102	122	23	1064
32-	-7.08	-6.97	-0.08	6.73	-77	-112	11	984
33+	7.75	5.09	-0.09	7.07	81	111	16	1131
33-	-7.75	-7.9	-0.09	7.51	-69	-100	9	964
34+	7.75	5.26	-0.1	7.06	82	103	16	1039
34-	-7.75	-8.07	-0.11	7.5	-60	-87	7	770
35+	7.75	5.84	-0.11	7.48	29	52	5	317
35-	-7.75	-8.17	-0.12	6.94	-42	-52	5	323
36+	7.75	5.93	-0.12	7.09	24	27	4	113

1. $D1$ = target beam displacement;

$D2$ = Peak beam deflection;

$D3$ = Beam deflection at start of excursion;

$D4$ = beam plastic deformation range;

$Q1$ = load at peak beam deflection;

$Q2$ = maximum load in excursion;

K = effective stiffness;

E = beam hysteresis area.

Table B-9 Experimental results for specimen RC10

Excursion	$D1$ (in.) ¹	$D2$ (in.) ¹	$D3$ (in.) ¹	$D4$ (in.) ¹	$Q1$ (kips) ¹	$Q2$ (kips) ¹	K (kips/in.) ¹	E (kips-in.) ¹
1+	0.53	0.15	0	0	39	39	266	0
1-	-0.53	-0.16	0	-0.01	-37	-37	233	0
7+	0.71	0.21	0.05	0	53	53	250	0
7-	-0.71	-0.22	0.06	0	-50	-50	232	0
13+	1.42	0.49	0.14	0.02	106	106	218	3
13-	-1.42	-0.5	0.14	0.03	-109	-109	219	4
14+	1.42	0.49	0.14	0	110	110	226	2
14-	-1.42	-0.51	0.15	0.01	-109	-109	217	2
15+	1.42	0.49	0.15	0	110	110	227	1
15-	-1.42	-0.5	0.14	0	-108	-108	217	2
16+	1.42	0.49	0.14	0	111	111	226	2
16-	-1.42	-0.5	0.14	0.01	-108	-108	217	2
17+	2.12	0.72	0.13	0.11	144	144	200	17
17-	-2.12	-0.76	0.13	0.17	-146	-147	192	23
18+	2.12	0.7	0.12	0.12	146	147	210	14
18-	-2.12	-0.76	0.11	0.12	-146	-147	192	16
19+	2.83	0.89	0.11	0.26	161	164	181	45
19-	-2.83	-0.96	0.1	0.39	-161	-165	168	56
20+	2.83	0.9	0.09	0.37	165	167	183	49
20-	-2.83	-0.98	0.09	0.37	-164	-166	167	51
21+	4.25	1.67	0.08	1.15	169	182	101	231
21-	-4.25	-1.64	0.07	1.57	-157	-184	96	282
22+	4.25	1.79	0.07	1.66	167	183	93	293
22-	-4.25	-1.61	0.06	1.47	-168	-185	105	259
23+	5.66	3.3	0.05	3.19	139	182	42	627
23-	-5.66	-2.56	0.05	3.05	-144	-192	56	634
24+	5.66	4.41	0.04	4.67	119	157	27	733
24-	-5.66	-3.39	0.03	4.29	-115	-151	34	729
25+	7.08	6.07	0.03	6.13	110	133	18	860

Table B-9 Experimental results for specimen RC10

25-	-7.08	-4.94	0.02	6.03	-98	-124	20	842
26+	7.08	6.17	0.01	6.06	108	116	17	673
26-	-7.08	-5	0	5.88	-89	-109	18	673
27+	7.75	6.85	0	6.66	100	110	15	684
27-	-7.75	-5.67	-0.01	6.5	-88	-103	15	686
28+	7.75	6.76	-0.02	6.54	93	103	14	599
28-	-7.75	-2.48	-0.02	3.19	-79	-79	32	230

1. $D1$ = target beam displacement;

$D2$ = Peak beam deflection;

$D3$ = Beam deflection at start of excursion;

$D4$ = beam plastic deformation range;

$Q1$ = load at peak beam deflection;

$Q2$ = maximum load in excursion;

K = effective stiffness;

E = beam hysteresis area.

PEER REPORTS

PEER reports are available from the National Information Service for Earthquake Engineering (NISEE). To order PEER reports, please contact the Pacific Earthquake Engineering Research Center, 1301 South 46th Street, Richmond, California 94804-4698. Tel.: (510) 231-9468; Fax: (510) 231-9461.

- PEER 2000/07** *Cover-Plate and Flange-Plate Reinforced Steel Moment-Resisting Connections.* Taejin Kim, Andrew S. Whittaker, Amir S. Gilani, Vitelmo V. Bertero, and Shakhzod M. Takhirov. September 2000. \$33.00
- PEER 2000/06** *Seismic Evaluation and Analysis of 230-kV Disconnect Switches.* Amir S. J. Gilani, Andrew S. Whittaker, Gregory L. Fenves, Chun-Hao Chen, Henry Ho, and Eric Fujisaki. July 2000. \$26.00
- PEER 2000/05** *Performance-Based Evaluation of Exterior Reinforced Concrete Building Joints for Seismic Excitation.* Chandra Clyde, Chris P. Pantelides, and Lawrence D. Reaveley. July 2000. \$15.00
- PEER 2000/04** *An Evaluation of Seismic Energy Demand: An Attenuation Approach.* Chung-Che Chou and Chia-Ming Uang. July 1999. \$20.00
- PEER 2000/03** *Framing Earthquake Retrofitting Decisions: The Case of Hillside Homes in Los Angeles.* Detlof von Winterfeldt, Nels Roselund, and Alicia Kitsuse. March 2000. \$13.00
- PEER 2000/01** *Further Studies on Seismic Interaction in Interconnected Electrical Substation Equipment.* Armen Der Kiureghian, Kee-Jeung Hong, and Jerome L. Sackman. November 1999. \$20.00
- PEER 1999/14** *Seismic Evaluation and Retrofit of 230-kV Porcelain Transformer Bushings.* Amir S. Gilani, Andrew S. Whittaker, Gregory L. Fenves, and Eric Fujisaki. December 1999. \$26.00
- PEER 1999/12** *Rehabilitation of Nonductile RC Frame Building Using Encasement Plates and Energy-Dissipating Devices.* Mehrdad Sasani, Vitelmo V. Bertero, James C. Anderson. December 1999. \$26.00
- PEER 1999/11** *Performance Evaluation Database for Concrete Bridge Components and Systems under Simulated Seismic Loads.* Yael D. Hose and Frieder Seible. November 1999. \$20.00
- PEER 1999/10** *U.S.-Japan Workshop on Performance-Based Earthquake Engineering Methodology for Reinforced Concrete Building Structures.* December 1999. \$33.00
- PEER 1999/09** *Performance Improvement of Long Period Building Structures Subjected to Severe Pulse-Type Ground Motions.* James C. Anderson, Vitelmo V. Bertero, and Raul Bertero. October 1999. \$26.00

- PEER 1999/08** *Envelopes for Seismic Response Vectors.* Charles Menun and Armen Der Kiureghian. July 1999. \$26.00
- PEER 1999/07** *Documentation of Strengths and Weaknesses of Current Computer Analysis Methods for Seismic Performance of Reinforced Concrete Members.* William F. Cofer. November 1999. \$15.00
- PEER 1999/06** *Rocking Response and Overturning of Anchored Equipment under Seismic Excitations.* Nicos Makris and Jian Zhang. November 1999. \$15.00
- PEER 1999/05** *Seismic Evaluation of 550 kV Porcelain Transformer Bushings.* Amir S. Gilani, Andrew S. Whittaker, Gregory L. Fenves, and Eric Fujisaki. October 1999. \$15.00
- PEER 1999/04** *Adoption and Enforcement of Earthquake Risk-Reduction Measures.* Peter J. May, Raymond J. Burby, T. Jens Feeley, and Robert Wood. \$15.00
- PEER 1999/03** *Task 3 Characterization of Site Response General Site Categories.* Adrian Rodriguez-Marek, Jonathan D. Bray, and Norman Abrahamson. February 1999. \$20.00
- PEER 1999/02** *Capacity-Demand-Diagram Methods for Estimating Seismic Deformation of Inelastic Structures: SDF Systems.* Anil K. Chopra and Rakesh Goel. April 1999. \$15.00
- PEER 1999/01** *Interaction in Interconnected Electrical Substation Equipment Subjected to Earthquake Ground Motions.* Armen Der Kiureghian, Jerome L. Sackman, and Kee-Jeung Hong. February 1999. \$20.00
- PEER 1998/08** *Behavior and Failure Analysis of a Multiple-Frame Highway Bridge in the 1994 Northridge Earthquake.* Gregory L. Fenves and Michael Ellery. December 1998. \$20.00
- PEER 1998/07** *Empirical Evaluation of Inertial Soil-Structure Interaction Effects.* Jonathan P. Stewart, Raymond B. Seed, and Gregory L. Fenves. November 1998. \$26.00
- PEER 1998/06** *Effect of Damping Mechanisms on the Response of Seismic Isolated Structures.* Nicos Makris and Shih-Po Chang. November 1998. \$15.00
- PEER 1998/05** *Rocking Response and Overturning of Equipment under Horizontal Pulse-Type Motions.* Nicos Makris and Yiannis Roussos. October 1998. \$15.00
- PEER 1998/04** *Pacific Earthquake Engineering Research Invitational Workshop Proceedings, May 14–15, 1998: Defining the Links between Planning, Policy Analysis, Economics and Earthquake Engineering.* Mary Comerio and Peter Gordon. September 1998. \$15.00
- PEER 1998/03** *Repair/Upgrade Procedures for Welded Beam to Column Connections.* James C. Anderson and Xiaojing Duan. May 1998. \$33.00

PEER 1998/02 *Seismic Evaluation of 196 kV Porcelain Transformer Bushings.* Amir S. Gilani, Juan W. Chavez, Gregory L. Fenves, and Andrew S. Whittaker. May 1998. \$20.00

PEER 1998/01 Unassigned.